



Geological Fieldwork 2017

A Summary of Field Activities and Current Research



Ministry of
Energy, Mines and
Petroleum Resources



Ministry of Energy, Mines and Petroleum Resources
British Columbia Geological Survey
Paper 2018-1

British Columbia Geological Survey
Ministry of Energy, Mines and Petroleum Resources
www.empr.gov.bc.ca/geology





Ministry of
Energy, Mines and
Petroleum Resources



Geological Fieldwork 2017

A Summary of Field Activities and Current Research

Ministry of Energy, Mines and Petroleum Resources
British Columbia Geological Survey

Paper 2018-1

Ministry of Energy, Mines and Petroleum Resources

Mines and Mineral Resources Division

British Columbia Geological Survey

Recommended citation format for individual papers:

Nelson, J., Waldron, J., van Straaten, B., Zagorevski, A., and Rees, C., 2018. Revised stratigraphy of the Hazelton Group in the Iskut River region, northwestern British Columbia. In: *Geological Fieldwork 2017*, British Columbia Ministry of Energy, Mines and Petroleum Resources, British Columbia Geological Survey Paper 2018-1, pp. 15-38.

Front Cover: Examining an outcrop of folded marble in the Tally-Ho shear zone, the possible Yukon extension of the Llewellyn fault in northwestern British Columbia. The marble is part of the Lewes River Group (Upper Triassic) of Stikine terrane. The Lewes River Group and Tally-Ho shear zone can be traced from the photograph location to the plateau across the valley (upper left of geologist), straight until the distant ridge in the upper-central part of the photograph. The view is north from Tally-Ho Mountain; the Wheaton River is in the lower left.

See Ootes, L., Castonguay, S., Friedman, R., Devine, F., and Simmonds, R., 2018. Testing the relationship between the Llewellyn fault, Tally-Ho shear zone, and gold mineralization in northwest British Columbia, this volume. **Photo by Luke Ootes.**

Back Cover: Mapping the Stuhini Group-Hazelton Group contact on the north ridge of Bromley Peak, 16 km east of Stewart. Looking north-northeast at the Cambria Icefield, with the Red Mountain gold deposit on the left.

See: Nelson, J., Waldron, J., van Straaten, B., Zagoresvski, A., and Rees, C., 2018. Revised stratigraphy of the Hazelton Group in the Iskut River region, northwestern British Columbia, this volume. **Photo by Bram van Straaten.**

This publication is available, free of charge, from the British Columbia Geological Survey website:
<http://www.empr.gov.bc.ca/Mining/Geoscience/PublicationsCatalogue/Fieldwork>

British Columbia Cataloguing in Publication Data

Main entry under title:

Geological Fieldwork: - 1974 -

Annual.

Issuing body varies

Vols. for 1978-1996 issued in series: Paper / British Columbia. Ministry of Energy, Mines and Petroleum Resources; vols. for 1997 - 1998, Paper / British Columbia. Ministry of Employment and Investment; vols. for 1999-2004, Paper / British Columbia. Ministry of Energy and Mines; vols. for 2005-2009, Paper / British Columbia. Ministry of Energy, Mines and Petroleum Resources; vols. for 2010, Paper / British Columbia. Ministry of Forests, Mines and Lands; vols. for 2011, Paper / British Columbia. Ministry of Energy and Mines; vols. for 2012- , Paper / British Columbia. Ministry of Energy, Mines and Natural Gas; vols. for 2014- , Paper / British Columbia. Ministry of Energy and Mines.

Includes Bibliographical references.

ISSN 0381-243X=Geological Fieldwork

1. Geology - British Columbia - Periodicals. 2. Mines and mineral resources - British Columbia - Periodicals. 3. Geology - Fieldwork - Periodicals. 4. Geology, Economic - British Columbia - Periodicals. 5. British Columbia. Geological Survey Branch - Periodicals. I. British Columbia. Geological Division. II. British Columbia. Geological Survey Branch. III. British Columbia. Geological Survey Branch. IV. British Columbia. Dept. of Mines and Petroleum Resources. V. British Columbia. Ministry of Energy, Mines and Petroleum Resources. VI. British Columbia. Ministry of Employment and Investment. VII. British Columbia Ministry of Energy and Mines. VIII. Series: Paper (British Columbia. Ministry of Energy, Mines and Petroleum Resources). IX. Series: Paper (British Columbia. Ministry of Employment and Investment). X. Series: Paper (British Columbia Ministry of Energy and Mines). XI. Series: Paper (British Columbia Ministry of Energy, Mines and Petroleum Resources). XII. Series: Paper (British Columbia Ministry of Forests, Mines and Lands). XIII. Series: Paper (British Columbia Ministry of Energy and Mines). XIV. Series: Paper (British Columbia Ministry of Energy, Mines and Natural Gas). XV. Series: Paper (British Columbia Ministry of Energy and Mines).

QE187.46 622.1'09711 C76-083084-3 (Rev.)

Victoria
British Columbia
Canada

January 2018

Preface

Geological Fieldwork 2017

The 43rd edition of **Geological Fieldwork** is a volume of peer-reviewed papers that presents the results of geological research conducted by the **British Columbia Geological Survey** (BCGS) and its partners in 2017. The volume provides new geoscience information at no cost to the public. Many geoscience projects in 2017 were collaborations with partners including the Geological Survey of Canada (GSC), the University of Victoria, and the University of British Columbia.

Papers in the volume address various aspects of British Columbia's geology, with an emphasis on regional geological studies and mineral systems. Papers also include method development studies related to field mapping and online digital delivery, indicator mineral surveys, and 3D computer models for estimating depth to bedrock in areas of thick glacial cover. Collaboration between the BCGS and the GSC focused on the second iteration of the five-year Geo-mapping for Energy and Minerals program (GEM 2) and the fifth iteration of the Targeted Geoscience Initiative (TGI-5) program. The GEM 2 program saw Survey geologists investigating the bedrock geology and crustal architecture of northern BC to better understand the genesis and distribution of Jurassic and Triassic porphyry copper-gold-molybdenum deposits. The TGI-5 projects continued in 2017, with an investigation of the relationship between the Llewellyn fault, Tally-Ho shear zone, and gold mineralization in northwest BC and Yukon. The BCGS also expanded its field mapping program in 2017, with investigations in the Spanish Lake, McBride River, Trembleur Lake (Decar) and Iskut River areas.

Survey staff delivered MapPlace 2 workshops at the Mineral Exploration Roundup conference and the Kamloops Exploration Group (KEG) meeting in 2017, following the launch of MapPlace 2 at the 2016 BCGS Open House. In addition, Survey staff took the lead in publishing a special volume titled 'Indicator Minerals in Till and Stream Sediments of the Canadian Cordillera'. This volume stems from a workshop given at the 2016 Geological Association of Canada–Mineralogical Association of Canada (GAC-MAC) annual meeting in Whitehorse, Yukon. The publication fills a notable knowledge gap on the use of indicator minerals in the Canadian Cordillera. We hope that it serves as a user guide and encourages the wider application of indicator minerals by the exploration community.

In November, the BCGS held its annual Open House in Victoria, featuring technical talks and posters by research scientists from the BCGS, GSC and the University of Victoria. A highlight of 2017 was the formal recognition of research done by BCGS staff with two awards. Drs. Mao Mao, Alexei Rukhlov and Steve Rowins, together with Jody Spence and Laurence Coogan from the University of Victoria, won the Brian J. Skinner Award for the 'Best Paper' published in *Economic Geology* in 2016. The award was presented to Mao in September at the Society of Economic Geologists annual meeting in Beijing, China. Another award went to JoAnne Nelson who received the 2017 Provincial and Territorial Geologists Medal. The Medal is presented annually by the Committee of Provincial and Territorial Geologists to an individual for outstanding work at one of Canada's provincial or territorial geological surveys. JoAnne accepted her medal at the annual Energy and Mines Ministers meeting in St. Andrews, New Brunswick, and will be embarking on a nationwide lecture tour in 2018.

Finally, the past year saw a change in government and an expansion of the Ministry from 'Energy and Mines' to 'Energy, Mines and Petroleum Resources', a name familiar to many both inside and outside of government. The role of the BCGS, however, remains the same.



Stephen M. Rowins
Chief Geologist and Executive Director
British Columbia Geological Survey

Table of Contents

Hickin, A.S., Jones, L.D., and Clarke, G.: British Columbia Geological Survey annual program review 2017-2018	1	Rukhlov, A.S., Mao, M., and Rippon, C.: Rapid identification of sand-size mineral grains using portable XRF: A new method for indicator mineral surveys	167
Nelson, J., Waldron, J., van Straaten, B., Zagorevski, A., and Rees, C.: Revised stratigraphy of the Hazelton Group in the Iskut River region, northwestern British Columbia	15	Cui, Y., Zhao, S., Fortin, G., Meredith-Jones, S., and Jones, L.D.: Development of MapPlace 2 geospatial web service to disseminate geoscience in British Columbia.....	183
van Straaten, B.I., and Bichlmaier, S.: Late Early to Middle Jurassic Hazelton Group volcanism and its tectonic setting, McBride River area, northwest British Columbia.....	39	Cui, Y., Hickin, A.S., Schiarizza, P., Diakow, L.J., Miller, D., Nixon, G.T., Nelson, J.L., and Ferri, F.: Methods to update the digital geology of British Columbia and synopses of recently integrated mapping programs	197
Ootes, L., Castonguay, S., Friedman, R., Devine, F., and Simmonds, R.: Testing the relationship between the Llewellyn fault, Tally-Ho shear zone, and gold mineralization in northwest British Columbia.....	67	Rowins, S.M., Miller, D.R., and Cui, Y.: Estimating the thickness of drift using a 3D depth-to-bedrock GOCAD model in the Ootsa Lake porphyryCu-Mo-Au district of west-central British Columbia.....	217
Mihalynuk, M.G., Zagorevski, A., Milidragovic, D., Tsekhmistrenko, M., Friedman, R.M., Joyce, N., Camacho, A., and Golding, M.: Geologic and geochronologic update of the Turtle Lake area, NTS 104M/16, northwest British Columbia.....	83	Appendix: British Columbia Geological Survey publications and peer-reviewed journal papers authored by BCGS staff and released in 2017	229
Milidragovic, D., Grundy, R., and Schiarizza, P.: Geology of the Decar area north of Trembleur Lake, NTS 93K/14.....	129		
Schiarizza, P.: Geology of the Spanish Lake area, south-central British Columbia.....	143		
Hora, Z.D., Stein, H., Žák, K., and Dobeš, P.: Eaglet property, southeastern British Columbia: Re-Os geochronology, sulphur isotopes, and thermobarometry	157		

British Columbia Geological Survey annual program review 2017-2018



Adrian S. Hickin^{1, a}, Larry D. Jones¹, and Gordon Clarke²

¹ British Columbia Geological Survey, Ministry of Energy, Mines and Petroleum Resources, Victoria, BC, V8W 9N3

² British Columbia Geological Survey, Ministry of Energy, Mines and Petroleum Resources, Vancouver, BC, V6Z 2G3

^a corresponding author: Adrian.Hickin@gov.bc.ca

Recommended citation: Hickin, A.S., Jones, L.D., and Clarke, G., 2018. British Columbia Geological Survey annual program review 2017-2018. In: *Geological Fieldwork 2017*, Ministry of Energy, Mines and Petroleum Resources, British Columbia Geological Survey Paper 2018-1, pp. 1-13.

1. Introduction

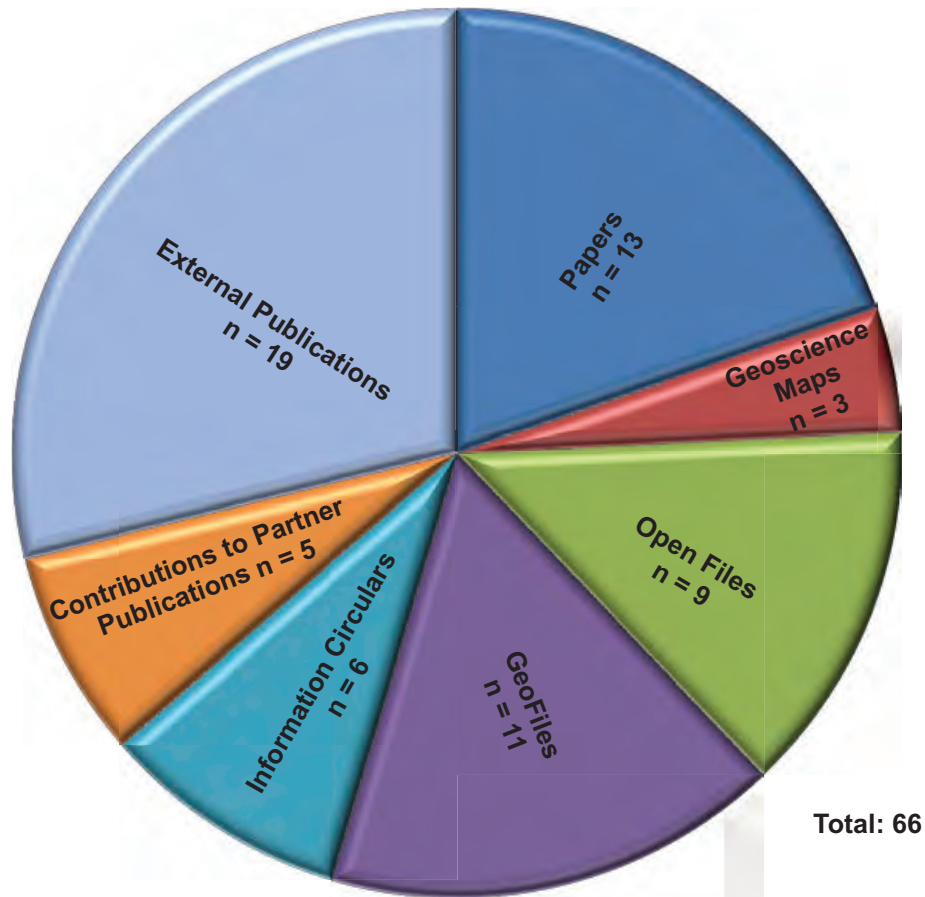
The British Columbia Geological Survey (BCGS) annual program review highlights the activities of the Survey and provides a summary of the activities, events, and accomplishments. BCGS links government, the minerals industry, and communities to the province's geology and mineral resources. The BCGS generates, disseminates, and archives British Columbia's geoscience data to stimulate investment and provide knowledge to society's decision makers for responsible land and resource management. The Survey strives to be a leader in public government geoscience, providing geological and geomorphological information to all through traditional reports, maps, and databases (Fig. 1), which can be freely accessed online. The BCGS is part of the Mines and Mineral Resources Division of the Ministry of Energy, Mines and Petroleum Resources and operates from two offices, the headquarters in Victoria and the Mineral Development Office in Vancouver. The Survey has a permanent staff of 29 people (Fig. 2) in three sections: 1) Cordilleran Geoscience; 2) Resource Information; and 3) the Mineral Development Office (MDO). The Cordilleran Geoscience Section is responsible for generating new geoscience knowledge, largely through field-based studies and surveys. The Resource Information Section is responsible for maintaining and developing the provincial geoscience databases and disseminating geoscience data online through MapPlace 2. This section is also responsible for evaluating, approving, and archiving mineral and coal exploration assessment reports filed by the exploration and mining industry. The MDO links the province's mineral and coal resources to the investment community, distributes and promotes BCGS technical data, and coordinates the technical outputs of the Regional Geologists Program.

Although the mineral exploration sector continues to struggle against difficult market conditions, some relief may be forthcoming as highlighted in the 2017 British Columbia Mineral and Coal Exploration Survey, a joint initiative amongst EY (formerly Ernst & Young), the Government of British Columbia's Ministry of Energy, Mines and Petroleum Resources, and the Association for Mineral Exploration

(AME). The survey, conducted in the fall of 2016, provides an overview of the mineral and coal exploration sector in British Columbia and examines a range of economic and sociopolitical topics that affect exploration and prospecting in British Columbia. Analysis presented in the 2017 report are based on data collected directly from 30 prospectors and 177 companies. This survey, which the BCGS helped coordinate, suggests that the outlook for the exploration sector in British Columbia will largely be influenced by the level of investment in grassroots and early-stage exploration that, in turn, will be determined by commodity prices and the ability of exploration companies to raise capital. Expenditure trends suggest that exploration in British Columbia may be experiencing an exploration lifecycle 'reset' as the province has benefitted from large-scale mine development projects that were approved and fully funded before the 2012 exploration downturn. Another survey was conducted in 2017, the results of which will be released in spring 2018.

BCGS staff received two significant acknowledgements from the geoscience community in 2017. We are proud to announce that geoscientist JoAnne Nelson was awarded the 2017 Provincial and Territorial Geologists Medal by the Committee of Provincial and Territorial Geologists (CPTG). The Medal is presented annually to an individual who has produced outstanding work at one of Canada's provincial or territorial geological surveys. The award recognizes major contributions in the areas of geoscience research and related developments or applications that serve to meet the mandates of Canada's geological surveys. JoAnne received her medal at the Energy and Mines Ministers Conference in St. John New Brunswick from the Federal Minister of Natural Resources Jim Carr and the New Brunswick Minister of Energy and Resource Development Rick Doucet (Fig. 3). The citation from JoAnne's nomination states:

"JoAnne Nelson is an exceptional scientist, mentor, and teacher who synthesizes research at many scales. This has led to a career of innovative and insightful studies on the tectonics and metallogeny of the northern Cordillera, as related through more than 125 publications that include



Types of Publications by the British Columbia Geological Survey

Papers*: This series is reserved for reviews and final thematic or regional works. Geological Fieldwork, our annual review of field activities and current research, is released as the first Paper of each year.

Geoscience Maps: This series is the BCGS vehicle for publishing final maps.

Open Files: These maps and reports present the interim results of ongoing research, particularly mapping projects.

GeoFiles: These publications enable rapid release of extensive data tables from ongoing geochemical, geochronologic, and geophysical work. As such, they serve the same function as data repositories provided by many journals, providing immediate access to raw data from specific projects.

Information Circulares: These publications provide accessible geoscience information to a broad audience in government, industry, and the general public. Included in the Information Circular series are the annual Provincial Overview of Mining and Exploration, **Exploration and Mining in British Columbia, and the Coal Industry Overview.

Contributions to partner publications: This category includes reports, maps, and other products published by another agency such as the Geological Survey of Canada or Geoscience BC, but have received contributions from British Columbia Geological Survey staff.

External publications: These are contributions to the peer reviewed literature and published in a recognized national or international scientific journal.

*The count refers to the total number of articles authored by BCGS personnel in a volume.

**Although five articles are included in Exploration and Mining in British Columbia, it is counted as a single volume.

Fig. 1. British Columbia Geological Survey Publications in 2017.



Fig. 2. Members of the British Columbia Geological Survey at Mystic Beach, British Columbia.



Fig. 3. JoAnne Nelson receiving her Provincial and Territorial Geologists Medal from Federal Minister of Natural Resources Jim Carr (left) and New Brunswick Minister of Energy and Resource Development Rick Doucet (right) at the Energy and Mines Ministers Conference in St. John New Brunswick.

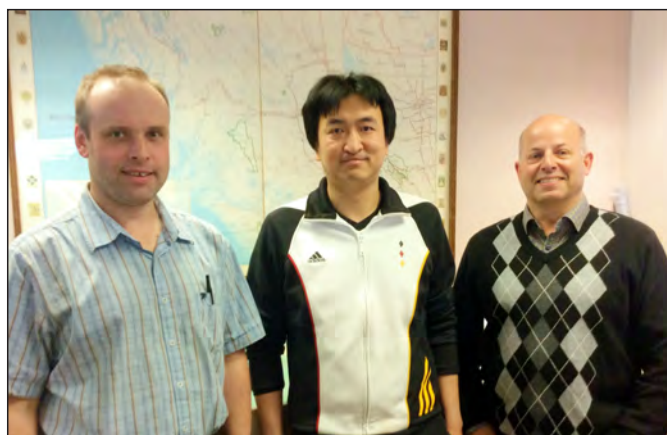


Fig. 4. Alexei Rukhlov (left), Mao Mao (centre), and Stephen Rowins (right) of the BCGS and colleagues at the University of Victoria received the 2017 Brian J. Skinner award from the Society of Economic Geologists for the best paper in the journal *Economic Geology*.

geological maps, bulletins, and peer-reviewed papers. In 1986, JoAnne joined the British Columbia Geological Survey where she undertook bedrock mapping and the study of mineral deposits in the northwestern part of the Province. In addition to her many scientific contributions maps, she is the co-author of a book aimed at the general public titled “The Geology of British Columbia: A Journey through Time”.

JoAnne is embarking on a cross-country lecture tour in the New Year to tell her remarkable stories of mapping in the Canadian Cordillera.

We also recognize geoscientists Drs. Mao Mao, Alexei Rukhlov, and Stephen Rowins (Fig. 4), and University of Victoria colleagues Drs. Jody Spence and Laurence Coogan as recipients of the Brian J. Skinner award from the Society of Economic Geologists for their paper “Apatite Trace Element Compositions: A Robust New Tool for Mineral Exploration”

(Mao et al., 2016). The Brian J. Skinner Award is presented annually to the authors of the most innovative and original paper appearing in the journal *Economic Geology* as selected by the editorial board. Papers are judged on technical excellence, innovation, and impact on the science of economic geology. Mao accepted the award on behalf of his colleagues at the Society of Economic Geologists annual meeting in Beijing, China.

BCGS is a technical partner for the Resources for Future Generations 2018 (RFG 2018) conference being held in Vancouver in June 2018 under the auspices of the International Union of Geological Sciences (IUGS). The Survey has been organizing sessions, preparing presentations, and planning two fieldtrips. More than 30 technical societies and geological surveys are partnering to mobilize industry, academia, and governments to address the availability and responsible use of Earth’s finite resources. The RFG 2018 program will explore

six themes: the Earth, education and youth, energy, minerals, resources, and water. We invite the British Columbia geoscience community to participate in the conference.

2. Partnerships

The BCGS is a collaborative agency and partners with federal, provincial, and territorial governments, other national and international organizations, and the mineral exploration industry to develop and deliver geoscience projects. Based on a relationship that is embedded in the terms of British Columbia's entry into confederation, the Geological Survey of Canada (GSC) and the BCGS continue to benefit from strong partnerships. In 2017, this collaboration included two main programs, the Cordilleran Project in the second iteration of the Geo-mapping for Energy and Minerals (GEM 2) Program, and the fifth iteration of the Targeted Geoscience Initiative (TGI-5). The Survey is continuing its partnership with the Geological Survey of Japan to advance studies on critical and strategic material. Several projects are co-operations with the Department of Earth, Ocean, and Atmospheric Science at the University of British Columbia, supported by TGI-5 grants from the GSC. Since 2003, the Ministry has maintained a formal partnership with the University of Victoria that supports joint research projects and student training of benefit to the School of Earth and Ocean Science, the Ministry of Energy, Mines, and Petroleum Resources, and the mineral exploration sector.

3. Cordilleran Geoscience Section

Cordilleran Geoscience Section geologists have expertise in regional bedrock mapping, tectonics, mineral deposits, coal, Quaternary and surficial geology, geochemistry, petrology, mineral exploration methods, copper, gold, and nickel metallogeny, and geoscience data management. BCGS undertakes a variety of field-based, long-term initiatives and short-term projects that include mapping, mineral deposit studies, and developing exploration methods (Fig. 5). Many current projects are continuations of multi-year efforts, whereas others are new.

In addition to the typical projects executed in 2017, BCGS staff also contributed to, and edited a volume entitled "Indicator Minerals in Till and Stream Sediments of the Canadian Cordillera", a Special Paper of the Geological Association of Canada (GAC) and the inaugural contribution to the Mineralogical Association of Canada (MAC)'s new Topics in Mineral Sciences series (Fig. 6; Ferbey et al., 2017). The volume is the first joint publication of the GAC and the MAC and stems from a workshop given in 2016 at the annual GAC-MAC meeting in Whitehorse, Yukon. The workshop was led by the BCGS with support from the Yukon Geological Survey and the GSC. It was designed to address a subject of importance to the mineral exploration community: the use of indicator minerals in the Canadian Cordillera. With samples now routinely collected for mineral separations during regional till and stream-sediment surveys, indicator minerals

are an efficient and cost-effective exploration tool. BCGS has delivered indicator mineral programs for many years and these approaches are becoming important as exploration is forced to consider covered terrain. The volume includes papers on the glacial history of the Cordillera Ice Sheet, drift prospecting methods, the evolution of survey sampling strategies, new analytical methods, and recent advances in applying indicator minerals to exploration in British Columbia.

3.1. Mapping, regional synthesis, and compilation

3.1.1. Porphyry transitions (BCGS-GSC-GEM 2)

The Porphyry Environment Transitions project is in collaboration with the GSC through the GEM 2 program and includes both topical studies and focused mapping. The project addresses the continuity of the prospective Triassic-Jurassic magmatic belt and assess porphyry potential in northern Stikinia and other prospective deposits in adjacent terranes. In 2015, BCGS activities focused in the Sinwa Creek area (Mihalynuk et al., 2017), and in 2016 mapping was completed in the Turtle Lake map area. The field mapping component of the project is now complete and activities in 2017 focused on synthesising data and updating the provincial geology compilation.

3.1.2. Stikinia magmatism

This program is an ongoing multi-year 1:50,000-scale mapping project aimed at late Early to Middle Jurassic rocks in the Dease Lake region (Fig. 7). Mapping, which incorporates the interpretation of regional airborne geophysical data (Aeroquest Airborne, 2012), is accompanied by geochronological studies that constrain key magmatic and mineralizing events, and litho-geochemical analyses for evaluating magma sources, melt evolution, and tectonic setting. The 2017 program was the second full field season and a third year of fieldwork is planned. These regional studies will help develop northern Stikinia-wide tectonic and metallogenic models and provide insight into the accretion of the Cache Creek and Stikine terranes. The project will also provide a much-needed regional update of the geology east of the Hotailuh batholith.

3.1.3. SeArch (BCGS-MDRU-GBC)

Building on mapping completed by the BCGS between 2005 and 2009 (Nelson et al., 2006, 2007, 2008), this mapping project, north of Smithers and Terrace, was led by Mineral Deposits Research Unit (University of British Columbia), and completed in collaboration with BCGS, with funding from Geoscience BC. Economically significant porphyry and related mineralization is genetically related to Late Cretaceous and Eocene intrusions in a northeast-trending paleotopographic high (Skeena arch). Angen et al. (2017) provided an update of the project; final maps will be released in 2018, along with an update to the provincial geology compilation.

3.1.4. Trembleur Ultramafic Complex

The Trembleur ultramafic unit, host to the Decar aaurite prospect (Britten, 2017), was the focus of a one-year mapping

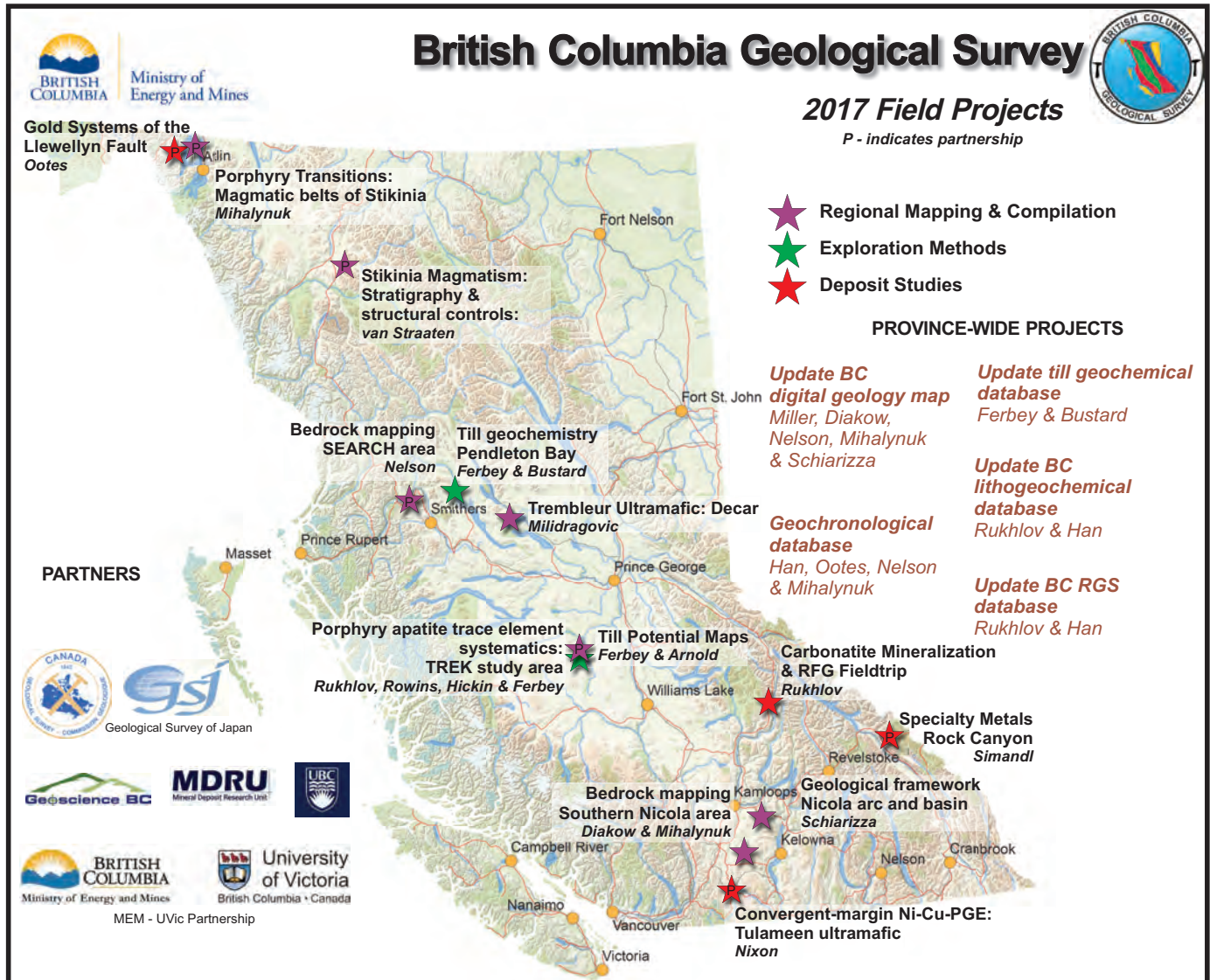


Fig. 5. British Columbia Geological Survey field projects in 2017.

project in 2017 (Fig. 8). The unit, forming a series of tectonic panels in the Cache Creek complex, is interpreted as obducted mantle that is overlain by massive to pillowed basalt flows, and intruded by sheeted diabase dikes. Formation of awaruite is intimately linked to hydrothermal alteration (serpentinization) of Ni-bearing Fe-Mg silicate minerals (olivine+pyroxene), and is therefore critically dependent on fluid chemistry and deformation history. At present, both the age and geochemical affinity of the unit are poorly constrained. Geochemical and isotopic characterization of the Trembleur ultramafic unit and overlying successions will be used to improve the petrological and tectonic framework of the Cache Creek complex and provide a better understanding of its Ni potential.

3.1.5. Till potential (BCGS-GBC)

Basal till potential maps are derived from surficial geology, terrain, or soils and landform data. The purpose of the basal

till potential map series is to assist designing surface-sediment exploration programs by identifying areas where basal till is most likely to occur. Basal till is ideal for assessing bedrock-hosted mineral potential in areas covered by Quaternary sediments because it is commonly a first derivative of bedrock (Shilts, 1993), has a relatively simple and predictable transport history, and produces a geochemical and mineralogical signature that is more extensive than its bedrock source (Levson, 2001). Glacial transport and deposition of basal till produces a dispersal train elongated down ice from its bedrock source. In 2017, the BCGS and Geoscience BC released six new maps for the Targeting Resources for Exploration and Knowledge (TREK) project area of central British Columbia, complementing the 12 that were published in 2014.

3.1.6. Geological framework of the Nicola arc

Quesnel terrane is an important metallogenic belt that hosts

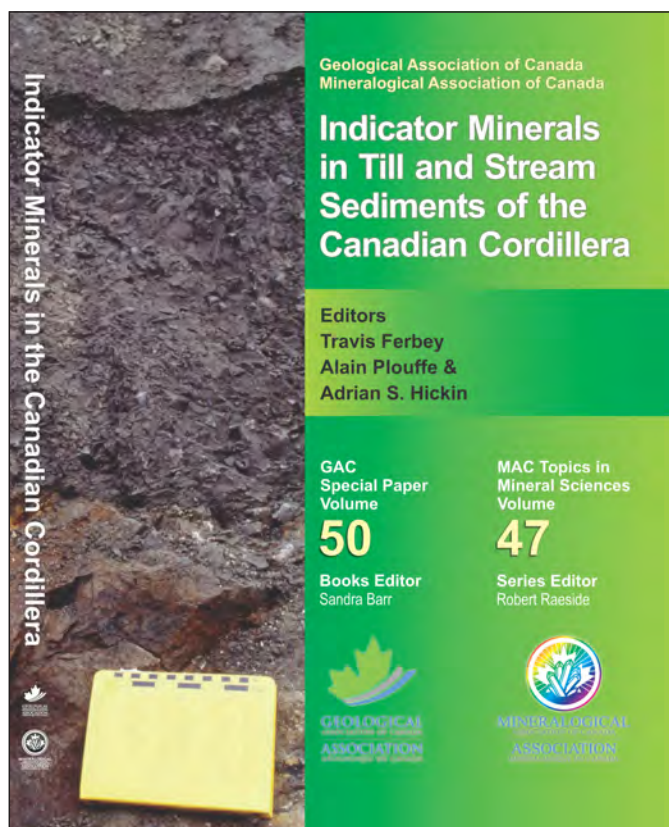


Fig. 6. Cover of the first joint GAC-MAC publication. The Minerals in Till and Stream Sediments of the Canadian Cordillera volume was coordinated by the BCGS with support from GSC.



Fig. 7. Horn Mountain Formation (Lower to Middle Jurassic) from the Dease Lake area.

most of British Columbia’s producing porphyry Cu-Au-Mo mines. This Mesozoic arc complex includes Triassic to Jurassic volcanic and sedimentary rocks and related calc-alkaline and alkalic intrusions. In south-central British Columbia, the Nicola Group represents the supracrustal part of the arc and was originally named for exposures of volcanic rock and limestone on the south side of Nicola Lake. The Nicola Group



Fig. 8. Trembleur ultramafic rocks at the top of Mount Sidney-Williams, central British Columbia.

has not been formally defined or subdivided on a regional scale. Ages, typically Carnian or Norian, are known only locally, and syndepositional faults are known to control the distribution of some facies.

In 2015, the BCGS started a multi-year field-based program to establish a regional stratigraphic framework for the Nicola Group. The study aims to define the characteristics and ages of individual volcano-sedimentary facies, and establish their stratigraphic and structural relationships. Initial investigations were carried out in the Bridge Lake-Quesnel River area in 2015. The preliminary results included separation of Triassic rocks into the Nicola and Slokan groups, and dividing Nicola Group rocks into four stratigraphic assemblages (Schiarizza, 2016). The 2016 mapping covered the eastern part of the Nicola belt in the Stump Lake-Salmon River area, southeast of Kamloops (Schiarizza, 2017). The youngest Nicola rocks in this area correlate to assemblage four of the Bridge Lake-Quesnel River area, and older Nicola rocks were tentatively assigned to assemblages two and three, suggesting that the stratigraphic scheme may have general applicability. Easternmost exposures of Triassic rocks, along the Salmon River, were assigned to the Slokan Group, which highlighted the need for a better understanding of the relationships between the Slokan basin and the coeval Nicola arc to the west. Fieldwork in 2017, near the town of Likely, focused on an eastern siltstone-rich component of the Nicola Group and its relationship to the main part of the Nicola arc to the west, and the Slokan Group to the east.

3.1.7. Southern Nicola arc

The Southern Nicola Arc Project (SNAP), between Merritt and Princeton was a mapping project conducted from 2012 to 2015 (Mihalynuk et al., 2016). Ongoing work complements the Nicola arc project described above, refining stratigraphic subdivisions along a segment of the Late Triassic Nicola magmatic arc axis in southern Quesnel terrane. Recent results provide time-space relationships in three northerly trending

stratigraphic belts that were originally proposed to subdivide stratigraphy of the Nicola Group (Preto, 1979). Nicola arc magmatism occurred during a 37 million year interval, spanning the Middle Triassic to end of the Late Triassic. Stratigraphic ties, supported by conodont-biostratigraphy and radiometric ages, suggest the western and central belts evolved as a solitary block between 238 and 224 Ma, and that the central and eastern belts were stratigraphically linked before 202 Ma. The southern Nicola magmatic arc segment evolved during two major constructional stages, the first between 238 to 223 Ma, the second between 212 to 202 Ma. The economically significant calc-alkaline and alkalic intrusions spatially associated with the Nicola Group apparently coincide in age with the younger stage in southern Quesnellia. A 1:50,000-scale geoscience-series map that revises the stratigraphic and structural framework will be released and incorporated into the provincial geology compilation. Brief follow-up fieldwork in 2017 was aimed at: 1) infill mapping for selected areas; 2) targeted assessment of intra-arc stratigraphic relationships; and 3) geochronologic sampling to validate and constrain late-arc incision and erosion. These data will be incorporated into a depositional and tectonic reconstruction for the basin east of the Nicola arc.

3.2. Deposit studies

3.2.1. Gold and the Llewellyn fault (BCGS-GSC-TGI-5)

The Llewellyn Fault gold project is a collaboration between the GSC and BCGS, under the TGI-5 program (Ootes et al., 2017). The Llewellyn fault is a southeast-striking, steeply dipping brittle dextral strike-slip structure that overprints 'early' ductile deformation (Fig. 9). The Tally-Ho shear zone, Yukon, shares similar early ductile deformation and is overprinted by the Llewellyn fault. Previous work and this study demonstrate that brittle strike-slip deformation along the Llewellyn fault occurred between ca. 56 and 50 Ma (Love et al., 1998; Millonig et al., 2017). Results suggest that the early ductile fabrics formed before ca. 75 Ma and, potentially, after ca. 120 Ma. This study demonstrates that, although the early ductile and

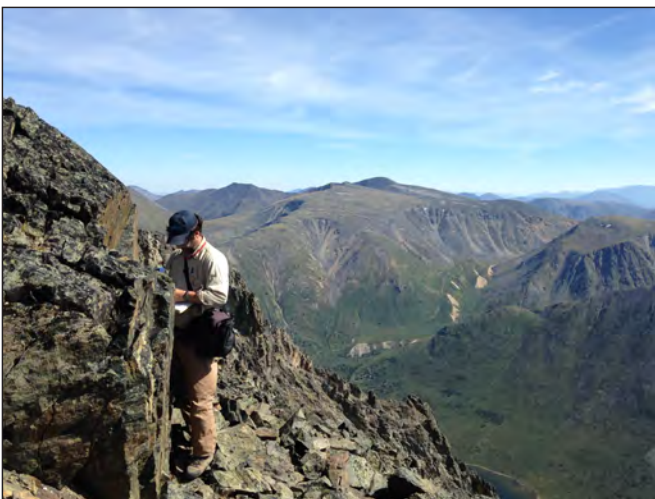


Fig. 9. Investigating the Tally-Ho shear zone and Llewellyn fault at Mount Hodnett, Yukon.

late brittle deformation share the same space, they developed at least ca. 20 Ma apart and are not part of a structural continuum. The various styles of gold mineralization developed during temporally distinct tectonic events.

3.2.2. Blue River Carbonatite

Carbonatites, such as those in the Blue River area of east-central British Columbia, continue to be of interest as potential sources of REE, Ta, Nb and other commodities. The area is in the Omineca belt, at the northeastern margin of the Shuswap metamorphic complex in the Monashee Mountains. Much of the area is underlain by Neoproterozoic supracrustal rocks and mafic intrusions that formed during rifting of western Laurentia. Several alkaline-ultramafic and carbonatite complexes were emplaced into these rocks during the Cambrian and Late Devonian-Mississippian (mostly ca. 330 Ma; Pell, 1994; Rukhlov and Bell, 2010; Millonig and Groat, 2013). The origin of carbonatite magmas, their mantle sources, and controls of their mineralization are not well understood. For example, the origin of the unusual Nb-Ta and Mo mineralization of the Blue River carbonatites remains ambiguous. This project examines the petrography, mineral chemistry, and isotope geochemistry of the Blue River carbonatites to better understand their petrogenesis and mineralization, and will be featured in a RFG 2018 conference fieldtrip to the Upper Fir deposit.

3.2.3. Specialty metals (BCGS-GSC-TGI-5)

Building on the collaborative work completed under the joint BCGS-GSC TGI-4 Specialty Metals project, the BCGS and GSC are advancing a multi-year partnership under the TGI-5 program. The continued availability of 'specialty metals', also referred to as high-technology metals or rare metals, is essential to the growth of the electronics and green-energy sectors. Specialty metals are informally defined as a group of materials considered critical or strategic for technologically advanced devices and industrial processes but are produced in quantities of less than 150,000 tonnes/year. Examples include rare earth elements (REE), Li, Ta, Nb, Ga, Ge, In, Co, W, Mg, Cs, Rb, Rh, Be, Zr, Hf, V, Sb and Sc. Canada has a specialty metals resource potential to support domestic use, but remains underexplored. To help with the efficient search for, and extraction of, specialty metals, this project investigates the ore-forming mineralizing systems and geological conditions.

3.2.4. Convergent margin Ni-Cu-PGE

This project will advance the understanding of the metallogeny and potential of Ni-Cu-PGE deposits at convergent margins by investigating precious metal-enriched magmatic sulphide mineralization in late-stage differentiates of an Alaskan-type ultramafic-mafic intrusion. High-tenor Cu-PGE magmatic sulphides have recently been discovered in the Tulameen ultramafic-mafic intrusion, a classically zoned Alaskan-type complex. These discoveries led to establishing a new subclass of magmatic Ni-Cu-PGE deposit formed at convergent margins, and prompted re-evaluating the mineral potential

of ultramafic-mafic intrusions in the Cordillera and possible genetic links to porphyry Cu-Au systems (Fig. 10). This study complements a BCGS-University of British Columbia-TGI-5-funded project of broader scope that investigates the physical and chemical controls on the emplacement and contrasting metallogenic evolution of two Alaskan-type ultramafic-mafic intrusions in British Columbia: the Turnagain intrusion with its unusual endowment of Ni-Cu-PGE mineralization; and the Tulameen intrusion with early chromitite-PGE mineralization. Fieldwork in 2017 defined the mineralogical and geochemical characteristics of high-tenor Cu-PGE mineralization in late-stage differentiates of the Tulameen intrusion.



Fig. 10. Sampling pyroxenite and dunite exposed in bed of Tulameen River.

3.3. Exploration methods

3.3.1. Till geochemistry of the Pendleton Bay map area (93K/12)

Subglacial till geochemical surveys conducted in British Columbia have been effective at identifying covered mineralized bedrock sources, including both known and new mineral occurrences (Bustard and Ferbey, 2016). The Pendleton Bay map area (93K/12) is relatively underexplored compared to other areas of the Interior Plateau. In 1998, as part of the NATMAP Nechako Project, 182 subglacial till samples were collected and analyzed to assess the area's mineral potential. Geochemical results will be released in 2018 and preliminary interpretation shows that the most pronounced anomaly in the area is related to the Fort porphyry Cu±Mo±Au showing (MINFILE 093K 093). Here, elevated concentrations of Cu, Mo, Ni, Cr, As, and Zn occur in subglacial tills for up to 2 km to the southeast. This dispersal direction is consistent with the predominant ice-flow direction through the area during the Late Wisconsinan glacial maximum. Three new areas of geochemical interest were also identified from this data set, possibly related to porphyry-style mineralized systems.

3.3.2. Porphyry apatite

As a contribution to the GAC-MAC volume 'Indicator Minerals in Till and Stream Sediments of the Canadian Cordillera', this project applies the step-wise discrimination

approach developed by Mao et al. (2016) that enables the subdivision of apatites by origin. Detrital apatite grains recovered from till in ten glaciated and underexplored study areas of the Nechako Plateau in central British Columbia were analyzed by electron probe microanalysis and laser ablation-inductively coupled plasma mass spectrometry. Based in previous BCGS-UVic work, the apatite grain trace element chemistry discriminated the major types of mainly magmatic-hydrothermal mineral deposits. Aided by till geochemistry, detrital chalcopyrite and gold grain counts, and airborne geophysics, the interpretation of these apatite data, enabled 342 apatite grains (344 analyses) to be classified as associated with mineralization, whereas 41 apatite grains were classified as derived from barren rocks. Mineralization-related apatite grains were classified as alkalic porphyry Cu-Au (80), porphyry Cu-Mo-Au (28), porphyry Mo (72), porphyry-related Cu-Au breccia (16), W skarn (112), orogenic Au (26), orogenic Ni-Cu (7), and Kiruna-type IOA (3) deposit-types. Detrital apatite grains in till down-ice from developed mineral prospects in brownfield areas were correctly identified by the discriminant method. Detrital apatites also helped to generate several new exploration targets in greenfield areas lacking known mineralization or hosting only minor mineral occurrences, demonstrating that the method is beneficial for exploring covered terrain.

3.3.3. Single grain XRF

Qualitative portable X-ray fluorescence (pXRF) offers a novel method of rapid, non-destructive identification of sand-size, single mineral grains. Using a (pXRF) instrument on 60 single-grain (0.5-1.0 mm) samples comprising 17 different rock-forming and accessory minerals, results of this study show that the essential constituents can be detected and used to identify ambiguous grains recovered from concentrates (e.g., Ca-P for apatite, Ca-Ti-Si for titanite, Ca-Nb-Ta for pyrochlore). Thus real-time readings (30-150 s) from a factory-calibrated instrument can cost effectively help identify separated sand-sized single mineral grains in the field or laboratory.

4. Resource Information Section

The BCGS creates, delivers, and archives geoscience data to help the mineral industry, resource planners, public safety agencies, communities, First Nations, government, research organizations, and the general public make decisions related to the Earth sciences. In particular, the data and derived products increase exploration effectiveness by enabling users to efficiently gather regional information for property-scale evaluation, and help explorers advance projects without duplicating previous work. To accomplish this mandate, the Resource Information Section continues to update databases and disseminate information through MapPlace 2.

4.1. MapPlace 2

Since 1995, MapPlace has provided web map services to help clients browse, visualize, and analyze geoscience and

mineral resource data, such as geology, mineral occurrences, regional geochemical survey, assessment reports, surficial geology, geophysical survey, and mineral tenures. Building on its predecessor, MapPlace 2 available on the BCGS website, continues to offer tools to query and generate custom results from data connected to many sources (Cui et al., 2017a, 2018).

MapPlace 2 works in commonly available web browsers, requires no plug-ins, and has a quicker, simpler, more intuitive interface that accesses third-party base maps and imagery from sources such as Google Maps and OpenStreetMap. MapPlace 2 is designed for anyone who wants to reduce the costs of accessing and analyzing geoscience data in British Columbia, including the mineral industry, resource planners, public safety agencies, communities, First Nations groups, government, research organizations, and the general public. Based on the MapPlace 2 (beta) Workshop notes (Cui et al., 2017a), the BCGS offers workshops on how to use MapPlace 2. BCGS will continue to improve MapPlace 2 with advanced applications and access to more databases.

4.2. Databases

ARIS is the searchable database of over 35,800 assessment reports submitted to the Ministry of Energy, Mines and Petroleum Resources, in compliance with Mineral Tenure Act Regulations. These reports summarize results from exploration programs on mineral claims. After a one-year confidentiality period, the reports become an open resource for planning mineral exploration, investment, research, land use, and resource management. Between 1967 and 2017, ARIS stored work representing expenditures of about \$2.8 billion. Digital data are available for download from 480 assessment reports through the ARIS search application and monthly tables. The BCGS has been digitally capturing surface-sediment geochemistry data from reports in the Interior Plateau (Fig. 11). In early 2018, MapPlace will display more than 30,000 sample sites with over 1 million analyses from over 100 assessment reports dating between 2000 and 2015.

COALFILE is a library of 1000 Coal Assessment Reports submitted by exploration companies since 1900. It includes data from more than 15,400 boreholes, 540 bulk samples, 5500 maps, and 3600 trenches. MINFILE is an inventory documenting metallic mineral, industrial mineral, and coal occurrences in the province. With more than 14,650 entries, the database is being updated continuously. Users can query MINFILE by location, identification number, mineralogy, commodity, host rock, deposit type, geological setting, age, production, and references. Property File is a collection of more than 66,500 documents donated by people from government, universities, and industry dating from the late 1800s. Previously available only in hard copy, these documents can now be searched for, and downloaded from, the Property File database. Property File contains: unpublished reports; theses; field notes; company prospectuses; correspondence; hand-drawn maps; claim maps; mine plans; photographs; and geological, geochemical,

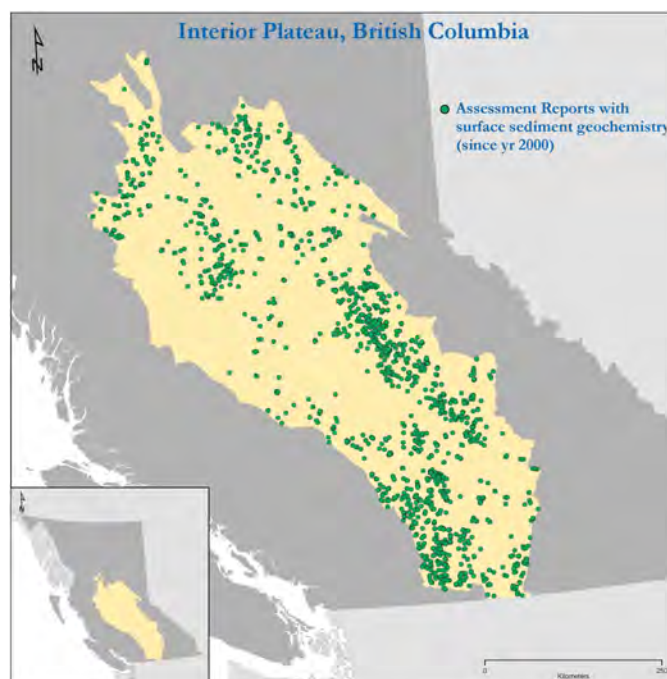


Fig. 11. Location of ARIS reports with surface-sediment geochemical sampling from the Interior Plateau since 2000.

geophysical, and drill data. The BCGS accepts donations to Property File.

The provincial geochemical databases hold field and geochemical data from multi-media surveys by the GSC, the BCGS, and Geoscience BC. The databases are updated regularly and contain results from: 1) the Regional Geochemical Survey program (RGS), including analyses from stream-sediment, lake-sediment, moss, and water samples; 2) till surveys; and 3) rock samples. The current version of the RGS database of about 65,000 samples is compiled from 111 original sources (Han and Rukhlov, 2017) and is delivered in flat tabular XLS format for ease of use and consistency with previously published data. The till index and till database were updated in 2017. The till index is available in various formats and links to 56 regional-scale and 78 property-scale subglacial till geochemical and mineralogical surveys (Bustard and Ferbey, 2016). The till database, a compilation from 39 reports released between 1992 and 2017, includes geochemical data from 10,450 samples and is released in XLS format (Bustard, et al., 2017). Han et al. (2016) published an update to the provincial litho-geochemical database, which includes a new data model and rigorous quality control. This database includes data from about 2000 papers and reports published by the BCGS, GSC, and universities between 1986 and 2015. The data set consists of about 11,000 samples, including a quarter million determinations analyzed by 26 different methods in 21 laboratories. New in 2017, is a coal ash chemistry database that will be of value to those seeking information on coal quality and coke strength (Riddell and Han, 2017).

Ice-flow indicator data were compiled from published and

unpublished surficial geology, terrain, and glacial feature maps. New data were generated using digital stereo airphotos, digital derived-stereo orthophoto mosaics, and digital derived-stereo SPOT imagery (Arnold et al., 2016). Using the geochemical database with ice-flow indicator data helps to target the location of mineral deposits. The geochemical databases and ice-flow indicators are available on MapPlace 2.

4.3. British Columbia digital geology map

BCGS provides digital coverage of British Columbia's bedrock geology, integrating details from compilations of field mapping at scales from 1:50,000 to 1:250,000. The bedrock geology of the entire province is held in a database, and people can download shapefiles to conduct computations and generate customized products. People can work in GIS software or MapPlace 2 (Fig. 12). A new 'geospatial frame data' model simplifies integration and reduces the time needed to move from field mapping to data delivery. The current edition (Cui et al., 2017b) includes updates to the Chilcotin-Bonaparte, northern Vancouver Island, North Coast, Kutcho, QUEST, and Terrace areas; updates to Nicola South and Bowser-Sustut basins are coming soon.

4.4. Three-dimension geological modelling

The BCGS conducted two 3D modeling exercises using GOCAD, one on the Turnagain intrusion and the other in the Ootsa Lake area. The Turnagain intrusion is an ultramafic-mafic Alaskan-type body that was emplaced in four discrete stages during a period of at least 3 million years (ca. 188-185 Ma).

Nixon et al. (2017) generated a model (Fig. 13) based on field mapping aided by drill and structural data provided by Giga Metals Corporation (formerly Hard Creek Nickel Corporation). At Ootsa Lake, digital datasets were used to build a three-dimensional (3D) GOCAD model that estimated the thickness of unconsolidated sediments covering bedrock. The area hosts several porphyry Cu±Mo±Au deposits and the past-producing Huckleberry Cu-Mo mine. Estimates of drift thickness in the depth-to-bedrock model were based on bedrock surfaces identified in diamond drill holes, bedrock outcrop, and surface topography derived from aerial Light Detection and Ranging survey (LiDAR) data. Where combined with geophysical data, structural data, and geochemical anomalies identified in sediment from Regional Geochemical Survey (RGS) data, the depth-to-bedrock model is a useful aid in ranking exploration targets.

5. Mineral Development Office

The British Columbia Mineral Development Office (MDO) in Vancouver provides mineral and coal resource information and is a point of contact on issues affecting the exploration and mining industries. Through formal and informal activities including conferences, business meetings, investment missions, and over the counter contacts, the MDO promotes the province's mineral and coal industries both domestically and abroad.

A primary output is the delivery of a technical marketing campaign that highlights the province's mineral and coal potential, geoscience resources, global expertise, and attractive

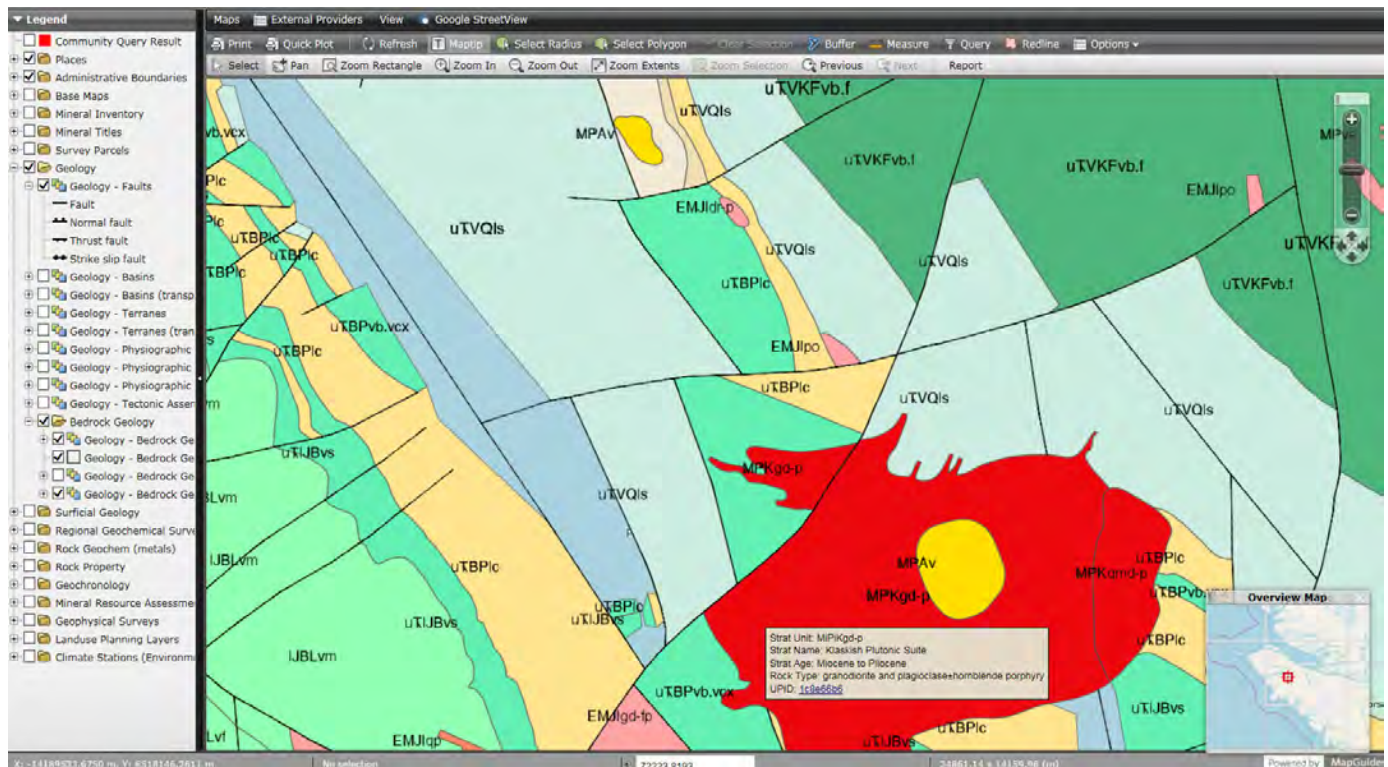


Fig. 12. Screen capture from MapPlace 2.

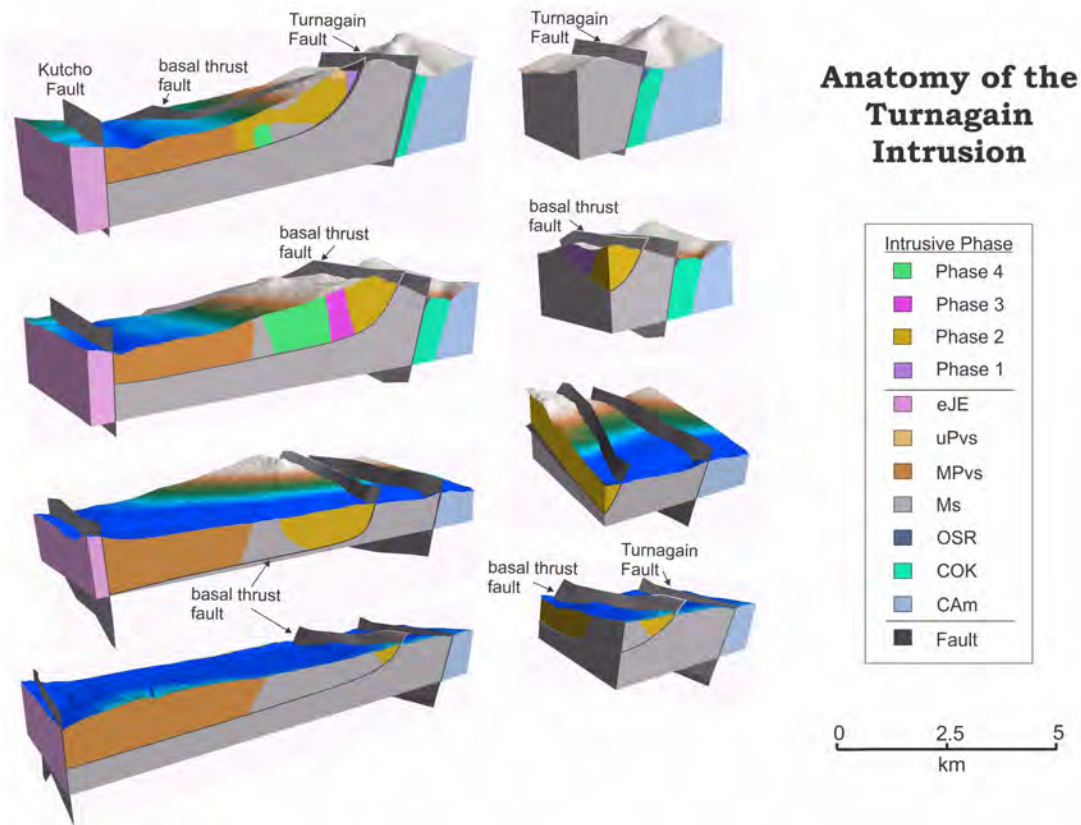


Fig. 13. 3D model of the geology in the Turnagain area from Nixon et al. (2017).

business climate. This includes developing publications aimed at audiences from large foreign investors through to independent domestic entrepreneurs. These publications are distributed widely at conferences, business meetings, over the counter, and online.

In September of 2017, the MDO supported the Ministry of Jobs, Trade and Technology at events in Asia. The MDO provided materials to raise British Columbia's profile at the Canada Mineral Investment Forum in Beijing and the Canada Mineral Investment Forum in Tokyo.

The MDO oversees publication of the 'Provincial Overview of Exploration and Mining in British Columbia' a document containing an overview of mineral exploration and mining activities in the different regions of BC written by the Regional Geologists and the MDO. The most recent annual summaries can be found in Clarke et al. (2018) and BCGS (2018).

6. Regional geologists

The British Columbia Regional Geologists (Table 1) represent the provincial government on geological matters at a regional level and capture information on industry activity in their jurisdictions. Within their communities, they provide information on exploration trends, possible investment opportunities, land use processes, First Nation capacity building, and public outreach.

7. Staff

After more than 30 years with the BCGS, JoAnne Nelson (Fig. 14), Senior Project Geologist and Northwestern British Columbia Manager, retired at the close of 2017. JoAnne's insightful scientific contributions and commitment to public service have made her a role model and leader in Cordilleran geoscience. JoAnne has influenced several generations of Cordilleran geologists and has published in national and international journals on topics that have strongly shaped our current understanding of Cordilleran tectonics. In addition to her research excellence, JoAnne has remained extremely active and enthusiastic member of the BCGS, organizing conferences, special sessions, and fieldtrips. JoAnne's accomplishments were formally recognized in 2013 when she was listed in the top '100 Global Inspirational Women in Mining' by the United Kingdom's Standard Bank. In 2015, she was awarded the 'Gold Pick' award by the Kamloops Exploration Group (KEG) in recognition of "outstanding services and contributions to the minerals industry". In 2017, she was given a 'Special tribute' by the Association of Mineral Exploration (AME) at the 2017 Mineral Exploration Roundup conference in recognition of her distinguished career in geoscience focused on the tectonics and metallogeny of the Northern Cordillera. JoAnne's decades of outstanding work in Canadian Earth science was recognized with the 2017 Provincial and Territorial Geologists Medal.

Table 1. British Columbia's regional geologists.

Regional Geologist	Office	Region
Vacant	Smithers	Northwest
John De Grace	Prince George	Northeast and North Central
Vacant	Kamloops	South Central
Fiona Katay	Cranbrook	Southeast
Bruce Northcote	Vancouver	Southwest



Fig. 14. JoAnne Nelson at her poster at Cordilleran Roundup in 1990 (top) and Joanne Nelson near Johnny Mountain, 2014 (bottom).

JoAnne remains active and will continue to contribute the Cordilleran Geology as an Emeritus Geoscientist with the Survey.

Acknowledgment

We thank George Owsiacski of Total Earth Science Services (Victoria) for the desktop publishing of this volume.

References cited

- Aeroquest Airborne, 2012. Report on a helicopter-borne magnetic survey (Aeroquest Job #11-046) for Geoscience BC. Geoscience BC Report 2012-2, 11 p.
- Angen, J.J., Nelson, J.L., Rahimi, M., and Hart, C., 2017. Mapping in the Tatsi and Zymo ridge areas of west-central British Columbia: Implications for the origin and history of the Skeena arch. In Geological Fieldwork 2016, British Columbia Ministry of Energy and Mines, British Columbia Geological Survey Paper 2017-1, pp. 35-48.
- Arnold, H., Ferbey, T., and Hickin, A.S., 2016. Ice-flow indicator compilation, British Columbia and Yukon. British Columbia Ministry of Energy and Mines, British Columbia Geological Survey Open File 2016-4, Geological Survey of Canada, Open File 8083, scale 1:1,750,000.
- British Columbia Geological Survey, 2018. British Columbia Coal Industry Overview 2017. British Columbia Ministry of Energy, Mines and Petroleum Resources, British Columbia Geological Survey Information Circular 2018-2, 13 p.
- Britten, R., 2017. Regional metallogeny and genesis of a new deposit type-Disseminated awaruite (Ni₃Fe) mineralization hosted in the Cache Creek terrane. *Economic Geology*, 112, 517-550.
- Bustard, A.L., and Ferbey, T., 2016. An index of base and precious metal regional- to property-scale subglacial till geochemical and mineralogical surveys in British Columbia. British Columbia Ministry of Energy and Mines, British Columbia Geological Survey Open File 2016-2, scale 1:2,250,000.
- Bustard, A.L., Han, T., and Ferbey, T., 2017. Compiled till geochemical data for British Columbia. British Columbia Ministry of Energy and Mines, British Columbia Geological Survey GeoFile 2017-9, 7 p.
- Clarke, G., Northcote, B., Katay, F., and DeGrace, J.R., 2018. Exploration and Mining in British Columbia, 2017: A summary. In: Provincial Overview of Exploration and Mining in British Columbia, 2017. British Columbia Ministry of Energy, Mines and Petroleum Resources, British Columbia Geological Survey Information Circular 2018-1, in press.
- Cui, Y., Fortin, G., Meredith-Jones, S., Zhao, S., and Jones, L., 2017a. MapPlace 2 (beta) workshop. British Columbia Ministry of Energy and Mines, British Columbia Geological Survey Information Circular 2017-3, 89 p.
- Cui, Y., Miller, D., Schiarizza, P., and Diakow, L.J., 2017b. British Columbia digital geology. British Columbia Ministry of Energy, Mines and Petroleum Resources, British Columbia Geological Survey Open File 2017-8, 9 p.
- Cui, Y., Zhao, S., Fortin, G., Meredith-Jones, S., and Jones, L.D., 2018. Development of MapPlace 2 geospatial web service to disseminate geoscience in British Columbia. In: Geological Fieldwork 2017, British Columbia Ministry of Energy, Mines and Petroleum Resources, British Columbia Geological Survey Paper 2018-1, pp. 183-195.
- Ferbey, T., Plouffe, A., and Hickin, A.S., (Eds.), 2017. Indicator minerals in till and stream sediments of the Canadian Cordillera. Geological Association of Canada, Special Paper, Volume 50,

- Mineralogical Association of Canada, Topics in Mineral Sciences, Volume 47, 250 p.
- Han, T., and Rukhlov, A.S., 2017. Regional Geochemical Survey (RGS) data update and release using the newly developed RGS database. British Columbia Ministry of Energy and Mines, British Columbia Geological Survey GeoFile 2017-11, 7 p.
- Han, T., Rukhlov, A.S., Naziri, M., and Moy, A., 2016. New British Columbia lithogeochemical database: Development and preliminary data release. British Columbia Ministry of Energy and Mines, British Columbia Geological Survey GeoFile 2016-4, 6 p.
- Levson, V.M., 2001. Regional till geochemical surveys in the Canadian Cordillera: sample media, methods and anomaly evaluation. In: McClenaghan, M.B., Bobrowsky, P.T., Hall, G.E.M., and Cook, S.J., (Eds.), *Drift Exploration in Glaciated Terrain*, Geological Society London Special Publication 185, pp. 45-68.
- Love, D.A., Clark, A.H., Hodgson, C.J., Mortensen, J.K., Archibald, D.A., and Farrar, E., 1998. The timing of adularia-sericite-type mineralization and alunite-kaolinite-type alteration, Mount Skukum epithermal gold deposit, Yukon Territory, Canada; ⁴⁰Ar-³⁹Ar and U-Pb geochronology. *Economic Geology*, 93, 437-462.
- Mao, M., Rukhlov, A.S., Rowins, S.M., Spence, J., and Coogan, L.A., 2016. Apatite Trace Element Compositions: A Robust New Tool for Mineral Exploration. *Economic Geology*, 111, 1187-1222.
- Mihalynuk, M.G., Diakow, L.J., Friedman, R.M., and Logan, J.M., 2016. Chronology of southern Nicola arc stratigraphy and deformation. In: *Geological Fieldwork 2015*, British Columbia Ministry of Energy and Mines, British Columbia Geological Survey Paper 2016-1, pp. 31-63.
- Mihalynuk, M.G., Zagorevski, A., English, J.M., Orchard, M.J., Bidgood, A.K., Joyce, N., and Friedman, R.M., 2017. Geology of the Sinwa Creek area (104K/14). In: *Geological Fieldwork 2016*, British Columbia Ministry of Energy and Mines, British Columbia Geological Survey Paper 2017-1, pp. 153-178.
- Millonig, L.J., and Groat, L.A., 2013. Carbonatites in western North America-occurrences and metallogeny. In: Colpron, M., Bissig, T., Rusk, B.G., and Thompson, F.H., (Eds.), *Tectonics, Metallogeny, and Discovery: The North American Cordillera and Similar Accretionary Settings*: Society of Economic Geologists, Special Publication 17, pp. 245-264.
- Millonig, L.J., Beinlich, A., Raudsepp, M., Devine, F., Archibald, D.A., Linnen, R.L., and Groat, L.A., 2017. The Engineer mine, British Columbia: An example of epithermal Au-Ag mineralization with mixed alkaline and subalkaline characteristics. *Ore Geology Reviews*, 83, 235-257.
- Nixon, G.T., Scheel, J.E., Friedman, R.M., Wall, C.J., Gabites, J., Miller, D., and Scoates, J.S., 2017. Geology and geochronology of the Turnagain ultramafic-mafic intrusion, British Columbia. British Columbia Ministry of Energy, Mines, and Petroleum Resources, British Columbia Geological Survey Geoscience Map 2017-1, scale 1:10,000.
- Nelson, J.L., Barresi, T., Knight, E., and Boudreau, N., 2006. Geology of the Usk map area (93I/09). British Columbia Ministry of Energy, Mines and Petroleum Resources, British Columbia Geological Survey Open File 2006-3, scale 1:50,000.
- Nelson, J.L., Kennedy, R., Angen, J., and Newman, S., 2007. Geology of Terrace Area (NTS 103I/9, 10, 15, 16). British Columbia Ministry of Energy, Mines and Petroleum Resources, British Columbia Geological Survey Open File 2007-4, scale 1:70,000.
- Nelson, J.L., Kyba, J., McKeown, M., and Angen, J., 2008. Geology of the Chist Creek map area (NTS 103I/08). British Columbia Ministry of Energy, Mines and Petroleum Resources, British Columbia Geological Survey Open File 2008-3, scale 1:50,000.
- Ootes, L., Elliott, J.M., and Rowins, S.M., 2017. Testing the relationship between the Llewellyn fault, gold mineralization, and Eocene volcanism in northwest British Columbia: A preliminary report. In: *Geological Fieldwork 2016*, British Columbia Ministry of Energy and Mines, British Columbia Geological Survey Paper 2017-1, pp. 49-59.
- Pell, J., 1994. Carbonatites, nepheline syenites, kimberlites and related rocks in B.C. British Columbia Ministry of Energy, Mines and Petroleum Resources, British Columbia Geological Survey Bulletin 88, 136 p.
- Preto, V.A., 1979. Geology of the Nicola Group between Merritt and Princeton. British Columbia Ministry of Energy, Mines and Petroleum Resources, British Columbia Geological Survey Bulletin 69, 90 p.
- Riddell, J., and Han, T., 2017. Ash chemistry database for British Columbia Rocky Mountain bituminous coals. Ministry of Energy and Mines, British Columbia Geological Survey GeoFile 2017-10, 15 p.
- Rukhlov, A.S., and Bell, K., 2010. Geochronology of carbonatites from the Canadian and Baltic Shields, and the Canadian Cordillera: clues to mantle evolution. *Mineralogy and Petrology*, 98, 11-54.
- Schiarizza, P., 2016. Towards a regional stratigraphic framework for the Nicola Group: Preliminary results from the Bridge Lake-Quesnel River area. In: *Geological Fieldwork 2015*. British Columbia Ministry of Energy and Mines, British Columbia Geological Survey Paper 2016-1, pp. 13-30.
- Schiarizza, P., 2017. Ongoing stratigraphic studies in the Nicola Group: Stump Lake-Salmon River areas, south-central British Columbia. In: *Geological Fieldwork 2016*. British Columbia Ministry of Energy and Mines, British Columbia Geological Survey Paper 2017-1, pp. 17-33.
- Shilts, W.W., 1993. Geological Survey of Canada's contribution to understanding the composition of glaciated sediments. *Canadian Journal of Earth Sciences*, 30, 333-353.

Revised stratigraphy of the Hazelton Group in the Iskut River region, northwestern British Columbia



JoAnne Nelson^{1, a}, John Waldron², Bram van Straaten¹, Alex Zagorevski³,
and Chris Rees⁴

¹British Columbia Geological Survey, Ministry of Energy, Mines and Petroleum Resources, Victoria, BC, V8W 9N3

²Department of Earth and Atmospheric Sciences, University of Alberta, Edmonton, AB, T6G 2E3

³Geological Survey of Canada, Ottawa, ON, K1A 0E8

⁴Imperial Metals Corporation, Vancouver, BC, V6C 3B6

^acorresponding author: JoAnne.Nelson@gov.bc.ca

Recommended citation: Nelson, J., Waldron, J., van Straaten, B., Zagorevski, A., and Rees, C., 2018. Revised stratigraphy of the Hazelton Group in the Iskut River region, northwestern British Columbia. In: Geological Fieldwork 2017, British Columbia Ministry of Energy, Mines and Petroleum Resources, British Columbia Geological Survey Paper 2018-1, pp. 15-38.

Abstract

The Iskut River region hosts many significant porphyry, precious-metal vein and volcanogenic massive sulphide deposits. Most of these deposits are related to the Hazelton Group (latest Triassic to Middle Jurassic) and affiliated intrusions. Current knowledge of the Hazelton Group is the outcome of piecemeal, local mapping contributions over many years by different workers at different scales, resulting in inconsistencies and errors in stratigraphic nomenclature. Given that exploration interest in the region remains high, and that considerable work has recently been done in the region, a reappraisal of this nomenclature, applying provisions in the North American Stratigraphic Code is required. In our new stratigraphic framework, newly recognized units are given local geographic names; others are correlated with previously established units. Two newly defined lowermost Hazelton units, the Klastline formation (new informal name) and the Snippaker unit, are latest Triassic, showing that earliest Hazelton volcanism and sedimentation were coeval with formation of the Red Chris porphyry deposit. These, along with siliciclastic rocks of the Jack Formation (Lower Jurassic) and mainly andesite successions such as the Betty Creek Formation, comprise the lower Hazelton Group. The upper Hazelton Group includes the Iskut River Formation (mainly Aalenian-Bajocian) comprising the bimodal volcanic-sedimentary succession within the Eskay rift that hosts the Eskay volcanogenic massive sulphide deposit; mainly sedimentary units such as the Spatsizi Formation and Quock Formation that occur throughout central Stikinia; the Mount Dilworth Formation, a stratified Middle Jurassic felsic volcanic unit that occurs outside but near the Eskay rift; and the Eddontenajon formation (new informal name), an unusual Pleinsbachian-Toarcian bimodal volcanic-sedimentary sequence that outcrops near the hamlet of Iskut.

Keywords: Iskut, Stewart, Golden Triangle, Hazelton Group, Iskut River Formation, Betty Creek Formation, Snippaker unit, Klastline formation, Eddontenajon formation, Unuk River andesite unit, Brucejack Lake felsic unit, Johnny Mountain dacite unit, Willow Ridge mafic unit, Bruce Glacier felsic unit, Mount Madge sedimentary unit, Downpour Creek siliciclastic unit, Palmiere dacite-mudstone unit, Mount Dilworth Formation, Spatsizi Formation, Quock Formation, Triassic, Jurassic, Stikinia

1. Introduction

The Iskut River region, between Stewart and Iskut (Fig. 1), hosts many significant porphyry, precious-metal vein and volcanogenic massive sulphide (VMS) deposits. Mining commenced at the Red Chris porphyry Cu-Au deposit in 2015, and at the Brucejack (Valley of the Kings) gold deposit in 2017. Deposits comparable to the past-producing Eskay Creek precious-metal VMS orebody remain targets of exploration interest. Past-producing gold mines at Premier, Snip, and Johnny Mountain are currently being reassessed for additional resources (Fig. 2). Significant developed prospects include the Kerr-Sulphurets-Mitchell-Iron Cap (KSM) porphyry Cu-Au, the GJ porphyry, and porphyry and precious metal targets in the Snippaker Mountain-Johnny Mountain area (Fig. 2).

Most deposits in the Iskut region are related to the Hazelton Group (latest Triassic-Middle Jurassic) and affiliated intrusions. The Hazelton Group represents the final arc construction

phase in Stikinia before and during the onset of collision with Laurentia (Nelson et al., 2013). It is distributed throughout the region (Figs. 1, 3; Ash et al., 1997a; Lewis 2001, 2013; Alldrick et al., 2006); coeval and cogenetic intrusions of the Texas Creek plutonic suite (ca. 195-186 Ma; Anderson, 1993) are also widely distributed. The Hazelton Group includes all volcanic and sedimentary strata that lie above the Stuhini Group (Upper Triassic) and below Upper Jurassic to Lower Cretaceous synorogenic siliciclastic rocks of the Bowser Lake Group. Tipper and Richards (1976) defined the Hazelton Group from work near Smithers, and subdivided it into formations based on the relative abundance of volcanic and non-volcanic rocks, and subaerial and submarine facies. Since then, significant advances in our understanding of the Hazelton Group have been made through detailed mapping, geochronology, and biochronology. For example, Tipper and Richards (1976) considered that the Hazelton Group is entirely Early Jurassic,

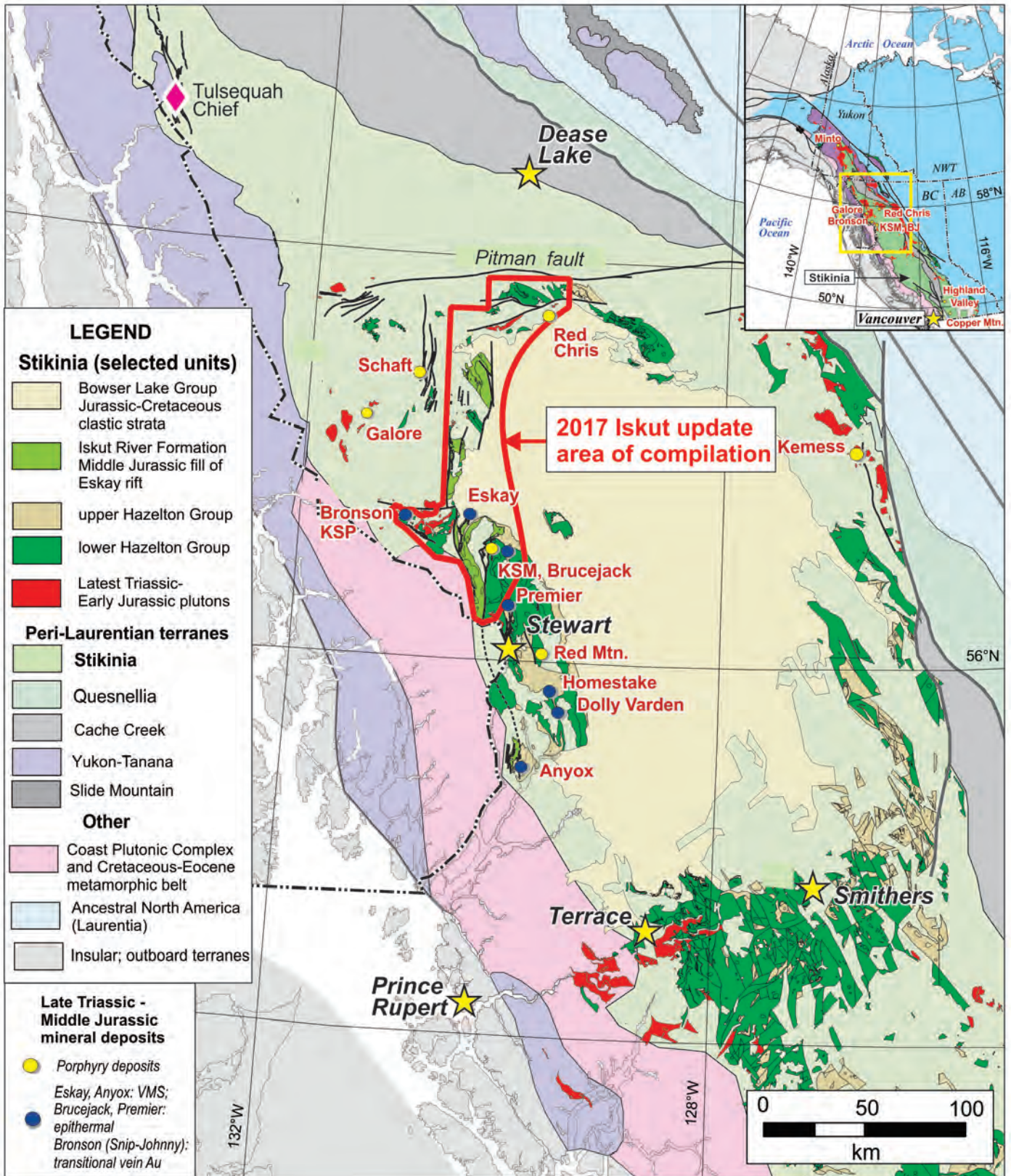


Fig. 1. Regional setting of the Iskut River study area.

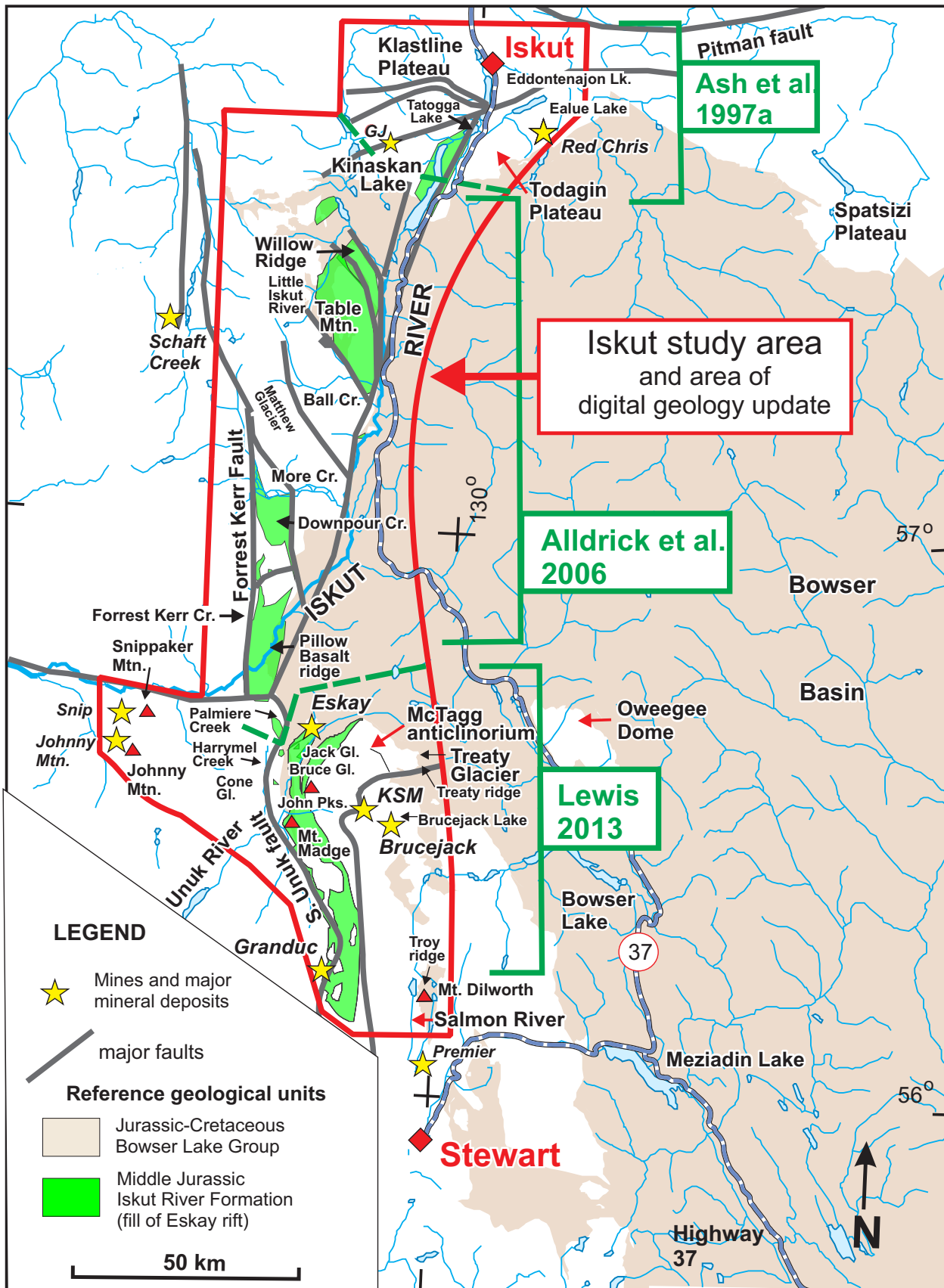


Fig. 2. Geography of the Iskut River region, showing mines, major projects, and key geological features. Areas covered by principal existing geological sources (Lewis, 2013; Alldrick et al., 2006; Ash et al., 1997a, b) are shown for reference.

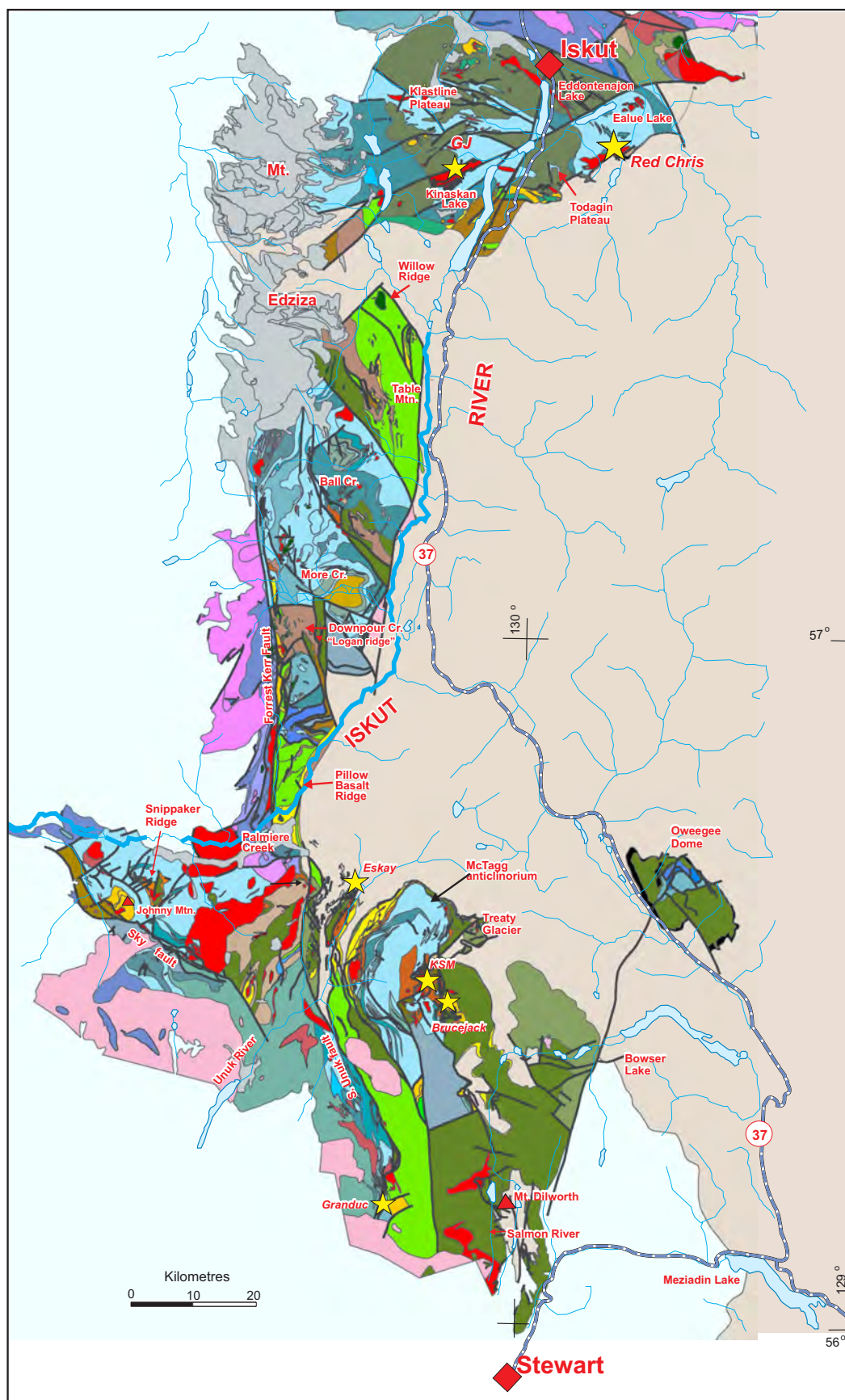


Fig. 3. a) Preliminary compiled geology for the Iskut River region, b) legend.

LEGEND

STRATIFIED ROCKS

TERTIARY-QUATERNARY

Tertiary and Quaternary basalt, minor alkalic felsic volcanic strata

EOCENE

UPPER JURASSIC-LOWER CRETACEOUS Bowser Lake Group

UPPERMOST TRIASSIC-MIDDLE JURASSIC Hazelton Group

Upper Hazelton Group

BAJOCIAN AND YOUNGER Quock Formation

AALENIAN-BAJOCIAN

Iskut River Formation

- ESKAY RHYOLITE MEMBER: rhyolite, rhyolite breccia in footwall of Eskay orebody
- BRUCE GLACIER FELSIC UNIT: rhyolite and dacite volcanics, coherent bodies, domes, cryptodomes
- WILLOW RIDGE MAFIC UNIT: basalt, pillow basalt; basalt and diabase dikes
- MT. MADGE SEDIMENTARY UNIT: siliceous argillite, felsic tuff, chert, carbonaceous mudstone
- KINASKAN CONGLOMERATE UNIT: coarse to medium conglomerate, sedimentary breccia, sandstone
- DOWNPOUR CREEK SILICICLASTIC UNIT: sandstone, siltstone, mudstone, conglomerate

LOWER TO MIDDLE JURASSIC (PLEINSBACHIAN-AALENIAN) Spatsizi Formation

- Sandstone, siltstone, mudstone, tuff
- Limestone, lime-matrix sandstone and conglomerate; fossiliferous

LOWER JURASSIC (PLEINSBACHIAN-TOARCIAN)

Eddontenajon formation

- Felsic units: rhyolite, dacite volcanoclastic strata and minor coherent bodies (mainly Todagin Plateau)
- Basalt: flows, pillowed flows (mainly Todagin Plateau)

lower Hazelton Group

LOWER JURASSIC (SINEMURIAN-PLEINSBACHIAN) Betty Creek Formation

- Undifferentiated Betty Creek Formation, mainly andesite volcanoclastics, also felsic, sedimentary units.
- Unnamed felsic units within Betty Creek Formation (rhyolite near Ball Creek, Downpour Creek)
- UNUK RIVER ANDESITE UNIT* andesite volcanoclastics (mainly coarse breccias) and flows
- BRUCEJACK LAKE FELSIC UNIT (PLEINSBACHIAN): dacite flows, lapilli tuff, welded tuff
- JOHNNY MTN. DACITE (SINEMURIAN): dacite welded tuff, breccia

UPPERMOST TRIASSIC-LOWERMOST JURASSIC (RHAETIAN-LOWER SINEMURIAN) Jack Formation

- JACK FORMATION on periphery of McTagg anticlinorium: basal granitoid-clast conglomerate, conglomerate, quartz-bearing arkose, siltstone, mudstone
- Volcanoclastic units within Jack Formation: andesite volcanic breccia, conglomerate, felsic tuff
- SNIPPAKER UNIT (RHAETIAN), Snippaker Mountain: granitoid clast bearing polyolithic conglomerate, quartz-bearing arkose, siltstone, mudstone, fossiliferous limestone

UPPERMOST TRIASSIC-LOWER JURASSIC

- Conglomerate in Sky fault zone south of Johnny Mountain; coarse, matrix-supported monomict so somewhat polymict conglomerate with volcanic and limestone clasts.

SINEMURIAN

- Bimodal volcanic - siliceous argillite - tuff unit at southern end of McTagg anticlinorium; contains Sinemurian radiolaria but physically resembles Iskut River Formation.

UPPERMOST TRIASSIC (RHAETIAN), POSSIBLY LOWER JURASSIC Klastline formation

- KLASTLINE FORMATION: volcanic rocks. Andesite breccias with plagioclase ± hornblende, ± augite phenocrysts; pyroclastic and epiclastic deposits; minor limestone olistoliths.
- KLASTLINE FORMATION: sedimentary rocks. Mudstone, siltstone, volcanic sandstone.
- KLASTLINE FORMATION: limestone. Continuous fossiliferous limestone north of Ealue Lk.; small bioherms and olistoliths on Klastline Plateau. Locally contain Rhaetian macrofaunas.

LOWER JURASSIC

Hazelton Group, undifferentiated

- Undifferentiated Hazelton Group; mainly Betty Creek Formation, but may include some upper Hazelton units (Spatsizi, Iskut River, Quock formations)

MIDDLE TO UPPER TRIASSIC Stuhini Group

- Undifferentiated Stuhini Group
- UPPER TRIASSIC (CARNIAN-NORIAN)
- Sandstone, mudstone, conglomerate, limestone, argillite, chert
- Andesite-clast conglomerate
- Epiclastic conglomerate, sandstone, mudstone, cpx-plag-phyric volcanic breccia
- Limestone
- Undifferentiated mafic and intermediate volcanic rocks
- Andesitic volcanoclastic strata, flows
- Basalt, augite-phyric basalt flows, breccias
- Sedimentary and lesser volcanic strata, undifferentiated
- Dacite north of More Creek
- Granduc mine series; semi-massive sulphide hosted in argillite, chert and magnetite iron formation; minor limestone, mafic volcanic rocks
- Sedimentary and lesser volcanic strata, undifferentiated

MIDDLE TRIASSIC

- Thin-bedded carbonaceous and pyritic silty shale, sandstone, chert-pebble conglomerate

UPPER PALEOZOIC (DEVONIAN-PERMIAN)

Stikine assemblage

- Phyllite, siltstone, graphitic argillite, siliceous tuff, sandstone
- Limestone, marble
- Basalt, andesite, rhyolite, variably foliated
- Felsic tuff, breccia, minor flows
- undivided volcanic and sedimentary strata

INTRUSIVE ROCKS

EARLY TERTIARY

- Granite, granodiorite, rhyolite dikes

JURASSIC? TERTIARY?

- Granite, feldspar porphyry

MIDDLE JURASSIC

- Diorite, diabase: intrusions coeval and cogenetic with Iskut River Formation mafic units.

EARLY OR MIDDLE JURASSIC

- Nickel Mountain gabbro-pyroxenite intrusion.

Intrusions coeval and cogenetic with lower Hazelton Group volcanism

EARLY JURASSIC

- BRUCEJACK LAKE SUITE (ca. 197-193 Ma): K-feldspar-plagioclase-hornblende porphyry subvolcanic equivalents of Brucejack Lake felsic unit.
- TEXAS CREEK SUITE (ca. 198-188 Ma): diorite, monzonite, syenite, commonly porphyritic subvolcanic equivalents of Betty Creek volcanic units. Includes Premier, Sulphurets, Mitchell, Lehto sub-suites.

LATEST TRIASSIC

- TATOGGA SUITE (ca. 207-198 Ma): hornblende quartz diorite, monzodiorite, monzonite, typically crowded plagioclase-hornblende porphyry. Host Red Chris, GJ. Subvolcanic equivalents of Klastline andesites.

Intrusions coeval and cogenetic with Stuhini Group volcanism

LATE TRIASSIC

Stikine Plutonic Suite (ca 216-226 Ma)

- GRANDUC SUITE: diorite
- Railway pluton, other intrusions: monzodiorite, diorite, quartz diorite, granodiorite.

Intrusions coeval and cogenetic with Paleozoic volcanism

LATE DEVONIAN - MISSISSIPPIAN

- Forrest Kerr and More Creek plutons: granodiorite, diorite, variably foliated.

Fig. 3. b) Legend.

but recent work by Barresi et al. (2015) showed that basal volcanic rocks near Terrace are ca. 205 Ma, within the Rhaetian stage (Gradstein et al., 2012; Cohen et al., 2013) of the Upper Triassic. In the 1990s, detailed studies of the Hazelton Group stratigraphy, spurred by the discovery and development of the Eskay Creek deposit, identified a heterogeneous succession of Middle Jurassic bimodal volcanic and sedimentary strata in the upper Hazelton Group that differ in age and character from older, predominantly andesitic units in the lower Hazelton Group (Anderson and Thorkelsen, 1990, Lewis et al., 2001a). Recently, Gagnon et al. (2012) developed a stratigraphic schema for the Hazelton Group throughout Stikinia, based on detailed studies by Gagnon (2010) and Barresi (2015). They proposed that it consists of two divisions. The lower Hazelton Group includes basal siliciclastic units (where present) and andesitic to variable volcanic successions. The upper Hazelton Group includes the Iskut River Formation, a distinctive unit of bimodal volcanic and interbedded sedimentary rocks that occupies a fault-bounded belt in western Stikinia (Fig. 1), and mainly sedimentary strata that immediately underlie the Bowser Lake Group throughout central and northern Stikinia. We follow their system of nomenclature in this paper.

As is commonly the case when different areas within a region are studied by different workers at different scales over many years, errors and inconsistencies, which constitute conceptual barriers, have been introduced into the stratigraphic nomenclature of the Hazelton Group. Because exploration interest in this mineral-rich area is high, and because new published and unpublished data are currently being integrated into the province-wide geology database (see Cui et al., 2017), a regionally consistent and stable stratigraphic scheme is required. In this paper we review key aspects of Hazelton Group lithostratigraphy, evaluate stratigraphic terms in the light of recent work and current understanding, and introduce a new stratigraphic framework for the Iskut River region. Our scheme retains some long-standing terms, abandons some obsolete or ill-conceived terms, and introduces new terms following procedures outlined in the North American Stratigraphic Code (North American Commission on Stratigraphic Nomenclature, 2005). Because the Hazelton Group displays significant longitudinal variation in the region, we present our analysis along a south-to-north transect, providing details from three areas: 1) Stewart-McTagg anticlinorium-Snippaker Mountain; 2) Forrest Kerr-Ball Creek-Table Mountain, and 3) Kinaskan Plateau-Klastline Plateau-Todagin Plateau.

2. Stewart-McTagg anticlinorium-Snippaker Mountain area

This area extends north from the Stewart mineral camp and includes the Unuk River drainage, Treaty Glacier, Snippaker Mountain, and Johnny Mountain (Fig. 2). It centres on the McTagg anticlinorium (Fig. 3), a regional structural culmination cored by Stuhini Group strata and flanked by Hazelton Group rocks. Eskay rift rocks form extensive exposures in the Unuk River valley, bounded on the west by the South Unuk fault.

Below we track the evolution of Hazelton nomenclature in the area (Fig. 4). For the most part, we follow stratigraphic assignments in Lewis et al. (2001a) and Lewis (2013) but with revisions as described below (Figs. 4, 5).

2.1. Basal Hazelton Group: Jack Formation; introduction of Snippaker unit

Along the margins of the McTagg anticlinorium, the Stuhini Group-Hazelton Group contact is an angular unconformity that is overlain by a basal conglomeratic unit (Lewis et al., 2001a, Lewis, 2013; Nelson and Kyba, 2014; Kyba and Nelson, 2015). This basal siliciclastic unit is named the Jack Formation after exposures near the Jack Glacier (Fig. 3; Henderson et al., 1992; Lewis et al., 2001a). It was originally defined as a wholly siliciclastic unit, identified primarily by cobble to boulder granitoid-clast conglomerate (Fig. 6a). Quartz-bearing arkosic sandstone, granulestone, and thinly bedded siltstones and mudstones are also present (Fig. 6b; Nelson and Kyba, 2014). Jack Formation sections at Bruce Glacier and Treaty Glacier contain andesitic volcanoclastic rocks that are in gradational contact with identical siliciclastic strata above and below (Fig. 6c; Nelson and Kyba, 2014). Near Treaty Glacier, ammonite collections from above the andesitic volcanoclastic layer are Late Hettangian to Early Sinemurian (Nadaraju and Lewis, 2001). Although Lewis et al. (2001a) assigned these andesitic volcanoclastic rocks to the overlying Unuk River unit, evidence of interfingering or continuity between the two is lacking, and we consider them part of the Jack Formation. Febbo et al. (2015) and Febbo (2016) identified similar andesitic pyroclastic units in the Jack Formation in the KSM deposit area.

The base of the Jack Formation is broadly latest Triassic to Early Jurassic. In the Atkins Glacier area (north of Treaty Glacier), a fossil collection from near the Stuhini Group-Jack Formation contact is considered Late Norian (Crickmayi zone; collection 93-ATP-7, Lewis, 2013) based on the ammonite *Choristoceras*(?). However, this ammonite is presently considered as Rhaetian (Ogg, 2012). Further work is needed to establish a more precise age and to determine if the unit sampled is part of the Stuhini Group rather than the Hazelton Group. A tuffaceous sandstone from the Jack Formation 2 km northwest of Brucejack Lake yielded ca. 197 Ma detrital zircons, and a volcanic conglomerate in the overlying Betty Creek Formation contains a ca. 196 Ma leucodiorite clast (Figs. 4, 5; J. Nelson, unpublished, 2017). These ages suggest that the top of the Jack Formation is mid-Sinemurian, at least locally (Fig. 5). Other samples of the Jack Formation contain mainly 220-226 Ma and minor Paleozoic detrital zircon populations (J. Nelson, unpublished, 2017). Together with the abundance of coarse-grained plutonic clasts, these distinctly older populations indicate that Jack Formation deposition represents a significant break from Stuhini Group volcanic and volcanoclastic accumulation, recording deep erosion into the Paleozoic section and Triassic Stikine suite plutons.

On Snippaker Mountain, the uppermost layer of the Stuhini

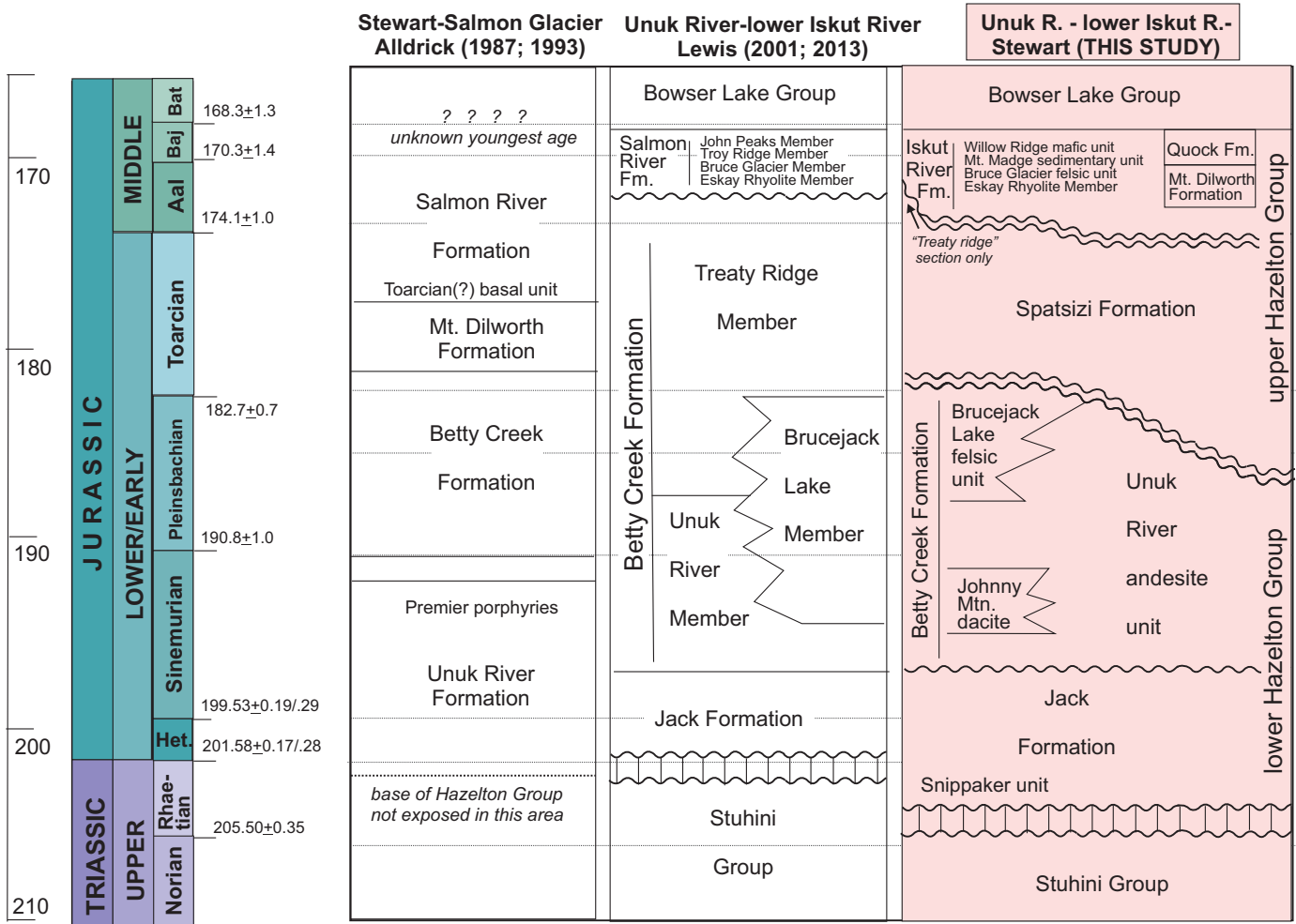


Fig. 4. Evolution of Hazelton Group stratigraphic nomenclature in the Stewart-McTagg-Snip area, southern Iskut River region.

Group consists of dull green greywacke in which pebbles of hypabyssal diorite increase in abundance up-section (Kyba and Nelson, 2015). This layer is unconformably overlain by a succession of orange-weathering sandstone, polymictic conglomerate, siltstone, and mudstone (Figs. 6d, e). Clasts in the conglomerate are well rounded and include granitoid rocks, chert, and volcanic rocks. Because the unit contains Late Triassic faunal assemblages (Nadaraju, 1993) it was previously included in the Stuhini Group (unit TrSs8, Lewis, 2013). However, because it unconformably overlies the Stuhini Group, physically resembles Jack Formation conglomerates (Kyba and Nelson, 2015), and contains detrital zircon populations identical to those in the Jack Formation (see below), we recommend that these siliciclastic rocks be included as an informal unit in the Jack Formation, and call it the Snippaker unit.

Small (tens of metres) rafts of highly fossiliferous limestone and clasts of individual fossils occur within the conglomerate (Fig. 6f). Fossil collections from these contain *Nevadathalamia* sp., *Placites* sp., *Rhacophyllites* sp., *Cladiscites* sp.; *Myophoria* sp., *Pinna* sp., *Weyla* sp., *Trigonia* sp., *Gryphae* sp., *Thamnastrea* sp., and *Thecosmilia* sp. (Nadaraju, 1993),

which were originally assigned to the Amoenum-Crickmayi zone, considered to be Upper Norian (Tozer, 1979). However, these faunal zones are now considered to be Rhaetian (Orchard and Tozer 1997; Grădinaru and Sobolev, 2010). An additional maximum age constraint for the Snippaker unit comes from the main population of detrital zircons in the underlying uppermost Stuhini pebble greywacke at ca. 203 Ma (J. Nelson, unpub. data). Main detrital zircon populations from the Snippaker unit at ca. 220-226 Ma are similar to main peaks in the Jack Formation (J. Nelson, unpub. data, 2017). It also contains late Paleozoic grains, and a ca. 212 Ma population. As with the main part of the Jack Formation, the appearance of distinctly older zircons is evidence of regional exhumation.

2.2. Betty Creek Formation: Replacement of Unuk River ‘Member’ by Unuk River andesite unit; replacement of Brucejack Lake ‘Member’ by Brucejack Lake felsic unit; introduction of Johnny Mountain dacite unit; and abandonment of Treaty Ridge ‘Member’

We follow Lewis et al. (2001a) in assigning most lower Hazelton volcanogenic strata to the Betty Creek Formation.

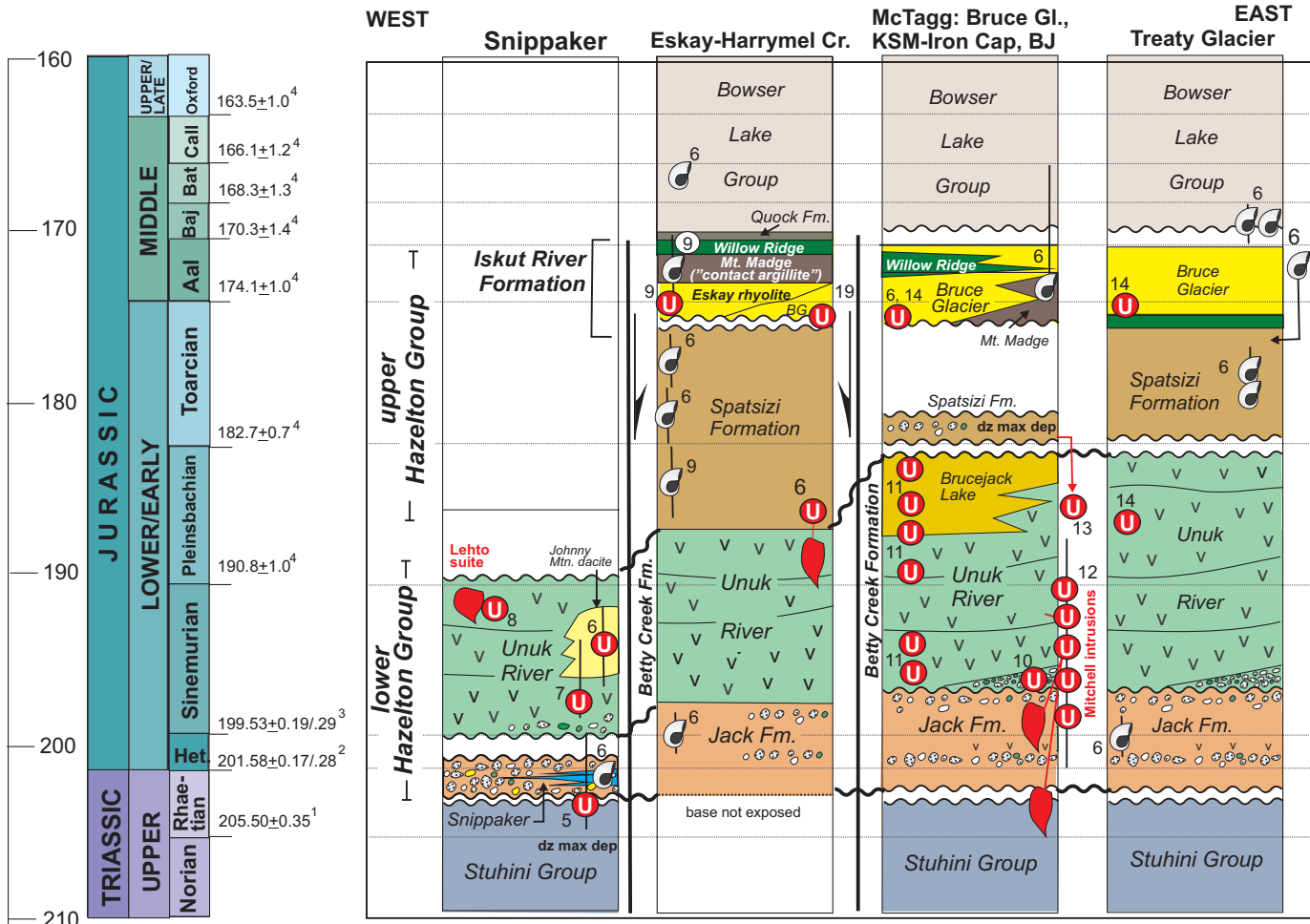


Fig. 5. Stratigraphic columns representing the Hazelton Group in the Stewart-McTagg-Snip area, southern Iskut River region. Numbers reference sources for fossil and radiometric ages. **1.** Norian-Rhaetian boundary (Wotzlav et al., 2014); **2.** Rhaetian-Hettangian boundary (Schaltegger et al., 2008); **3.** Hettangian-Sinemurian boundary (Schaltegger et al., 2008); **4.** Cohen et al. (2013); **5.** ca. 203.4 Ma youngest detrital population (J. Nelson, unpublished data, 2017); **6.** biochronologic and geochronologic compilations of Lewis et al. (2013) based on Nadaraju (1993); Nadaraju and Lewis (2001); Lewis et al. (2001b); **7.** ca. 198 Ma youngest detrital population (J. Nelson, unpublished data); **8.** ca. 192 Ma U-Pb zr (J. Nelson, unpublished data, 2017); **9.** Childe, 1996; **10.** ca. 197 Ma, U-Pb zr (J. Nelson, unpublished data, 2017); **11.** Greig (2013); MacDonald (1993); **12.** 198-189 Ma U-Pb zr (Febbo, 2016); **13.** ca. 186 Ma youngest detrital zircon population (J. Nelson, unpublished data, 2017); **14.** Cutts et al. (2015).

Alldrick (1987, 1993) referred to the lowest exposed Hazelton Group unit near the Salmon River, consisting of interbedded green andesitic volcanoclastic and sedimentary strata, as the Unuk River Formation. The name Unuk River was derived from earlier assignment of volcanic rocks in the Unuk River valley farther north and west by Grove (1971, 1986). Overlying maroon and green, mostly epiclastic andesitic units were assigned to the Betty Creek Formation (Alldrick, 1987, 1993). Noting that the distinction between these two units was mainly based on colour and not regionally significant, Lewis et al. (2001a) reassigned andesitic rocks of the Unuk River 'Formation' to the Betty Creek Formation, giving it a 'Member' status (Fig. 4). Other proposed members of the Betty Creek Formation were the felsic Brucejack Lake Member and sedimentary Treaty Ridge Member.

We consider subdivision of the Betty Creek Formation into

formal members (Lewis et al., 2001a; Lewis, 2013) to be problematic. In formal stratigraphic nomenclature (see North American Commission on Stratigraphic Nomenclature, 2005) a member is defined as a single unit with a defined bottom and top. In the Betty Creek Formation, volcanic lithotypes do not form discrete unrepeatable layers but multiple bodies at different stratigraphic levels. Thus we abandon the formal term 'Member' for subdivisions of the Betty Creek Formation in this area and instead propose that it be divided into three informal subdivisions (Fig. 4): the Unuk River andesite unit, the Johnny Mountain dacite unit (ca. 194 Ma, Lewis et al., 2001b), and the Brucejack Lake felsic unit (ca. 185-178 Ma; Lewis et al., 2001b). As described further below (see section 2.3) Lewis et al. (2001a) considered the succession of mainly sedimentary rocks above these volcanogenic units as part of the Betty Creek Formation and referred to them as the Treaty Ridge Member

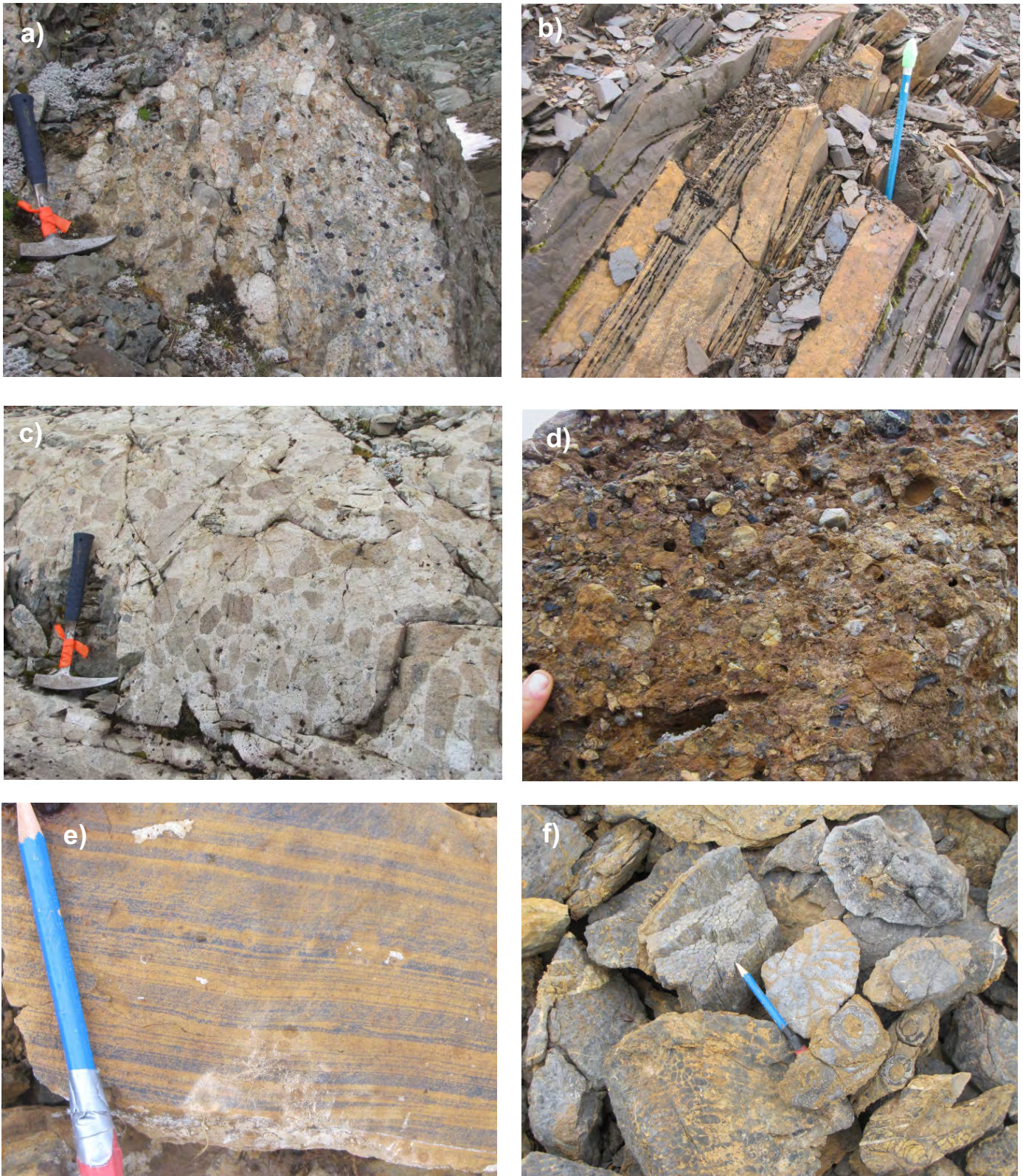


Fig. 6. Representative photos of the Jack Formation and Snippaker clastic unit. **a)** Basal polymictic conglomerate, Jack Formation near Jack Glacier (413850 E, 6269040 N). **b)** Thinly bedded calcareous siltstone, fine-grained sandstone, and carbonaceous mudstone; Jack Formation mudstone±sandstone and siltstone facies, near Jack Glacier (413557 E, 627708 N). **c)** Andesite block breccia; Jack Formation middle volcanoclastic facies (413278 E, 6270599 N). **d)** Snippaker unit polymictic conglomerate. Light clasts are felsic to intermediate high-level intrusive rocks and silicified rocks; dark clasts are chert. Weathered-out clasts are limestone (377358 E, 6281369 N). **e)** Snippaker unit, thinly bedded sandstone and mudstone (376848 E, 6281354 N). **f)** Corals from partly dismembered boundstone raft, Snippaker unit (379725 E, 6279752 N).

(Fig. 4). However, this succession displays the same lithological characteristics, age and stratigraphic position as the Spatsizi Formation in the upper Hazelton Group elsewhere (Gagnon et al., 2012), and Treaty ridge is an informal topographic term. Thus we reassign the succession to the Spatsizi Formation and propose that the term ‘Treaty Ridge Member’ be abandoned (Figs. 4, 5).

2.2.1. Unuk River andesite unit

We agree with the decision of Lewis et al. (2001a) to include all lower Hazelton Group andesites previously referred to as the Unuk River Formation (Alldrick, 1987) in the Betty Creek Formation. They include both pyroclastic (Fig. 7a) and epiclastic (Fig. 7b) deposits. In general, subaerial and epiclastic deposits increase up-section in the andesitic unit, but a simple transition is not traceable throughout the region (cf. Alldrick, 1987, 1993). For example, in the section 2 km northwest of Brucejack Lake, maroon and green volcanic clast-bearing conglomerate is at the base of the Betty Creek Formation, lying directly on the Jack Formation (Fig. 7c; Nelson and Kyba, 2014). Facies distinctions can be usefully documented locally, for example on the Brucejack property where increasing oxidation upwards may have exerted chemical control on mineralization (W. Board, pers. comm., 2013; S. Flasha, pers. comm., 2017), but cannot be used regionally.

The base of the Unuk River andesite unit above the Jack Formation is sharp and ranges from paraconformable to unconformable. It represents an abrupt transition from siliciclastic sedimentation to mixed, predominantly andesitic pyroclastic and epiclastic accumulation. Near the Iron Cap deposit, a volcanic breccia lies at the base of the unit. It contains irregular, angular dark green andesite and lesser pinkish felsic clasts, overlain in part by a pillowed mafic flow (Nelson and Kyba, 2014). North of Treaty Glacier, the basal bed is a coarse, matrix-supported, polymictic volcanic-hypabyssal clast conglomerate, overlain by monomictic andesite pyroclastic breccia (Nelson and Kyba, 2014). Northwest of Brucejack Lake, the polymictic basal volcanic conglomerate contains a ca. 196 Ma porphyritic diorite block (J. Nelson unpublished, 2017) along with mostly andesite cobbles. On Snippaker Mountain, the base of the Unuk River andesite unit cuts down through the Snippaker unit into the underlying Stuhini Group (Kyba and Nelson, 2015). A matrix-supported basal conglomerate includes both volcanic blocks derived from the underlying Stuhini Group and intraformational sedimentary clasts. A detrital zircon sample of this conglomerate contains a youngest population at ca. 198 Ma, along with older Late Triassic populations derived from the Stuhini Group and comagmatic intrusions (J. Nelson unpublished, 2017). In summary, U-Pb ages place the base of the Unuk River andesite unit in the mid-Sinemurian (ca. 197 Ma), slightly younger than the Jack Formation, indicating abrupt onset of voluminous andesitic volcanism. Youngest U-Pb ages, obtained from minor felsic rocks in the Unuk River andesite unit, are ca. 187 Ma (Cutts et al., 2015). U-Pb ages of Texas Creek suite

intermediate porphyritic intrusions, notably the Mitchell suite at KSM (Febbo et al., 2015; Febbo, 2016) and the Lehto suite in the Snippaker area (Kyba and Nelson, 2015), overlap those of the Unuk River andesite unit (Fig. 5). We consider them intrusive and extrusive equivalents.

2.2.2. Johnny Mountain dacite unit

Johnny Mountain (Fig. 2) is underlain by a succession of bedded dacite lapilli tuff and breccia (Fig. 7d) that unconformably overlies the Stuhini Group (Kyba and Nelson, 2015). It was previously assigned to the Brucejack Lake Member (Lewis et al., 2001a), and mapped in error, as felsic and mafic Salmon River Formation (Lewis, 2013). A U-Pb age from this unit is ca. 194 Ma (Lewis et al., 2001b; Lewis, 2013). Given that the unit is markedly older than the rocks at the Brucejack Lake type locality (ca. 183-188 Ma; Lewis et al., 2001b; Lewis, 2013; Greig, 2013) and given its geographic distance from Brucejack Lake, we suggest that the succession forms a distinct unit and propose the name Johnny Mountain dacite unit. It is coeval with nearby porphyry bodies such as at Red Bluff and Inel (Kyba and Nelson, 2015) and probably represents an extrusive equivalent.

2.2.3. Brucejack Lake felsic unit

Near Brucejack Lake, the Unuk River andesite unit is overlain by a felsic unit including potassium feldspar-, plagioclase- and hornblende-phyric flows, breccias, and bedded welded to non-welded felsic tuffs (Fig. 7e) that are intruded by a flow-banded coherent plagioclase-phyric body, which grades upwards into flows (MacDonald, 1993). MacDonald (1993) interpreted this unit, which we refer to as the Brucejack Lake felsic unit (cf. ‘Member’ of Lewis, et al., 2001a; Lewis, 2013, Fig. 4) as a flow-dome complex, representing the extrusive and high-level intrusive products of a local magmatic centre. The intrusive and extrusive rocks of the unit have yielded ca. 183-188 Ma U-Pb ages (Lewis et al., 2001b; Lewis, 2013; Greig, 2013). Polymictic conglomerates with well-rounded cobbles to boulders at the base of the unit 2 km northwest of Brucejack Lake (Fig. 7f) suggest that the lower contact of the unit is an unconformity. Felsic rocks of similar age also occur in the Unuk River drainage and are included in the unit.

2.3. Spatsizi Formation and abandonment of ‘Treaty Ridge Member’ for basal rocks in the upper Hazelton Group

Examining stratigraphic relationships across Stikinia, Gagnon et al. (2012) recognized that the Hazelton Group consists of two parts, separated by a diachronous contact. In the Iskut River region, the lower part includes the Rhaetian to Sinemurian basal sedimentary units (Jack Formation) and overlying voluminous volcanogenic strata (Betty Creek Formation) described above. Regionally, the basal unit of the upper Hazelton Group is the Spatsizi Formation, defined on the Spatsizi Plateau of north-central Stikinia (Fig. 2) as a Pleinsbachian through Aalenian siliciclastic sequence with minor volcanic components (Figs. 8, 9; Spatsizi Group of

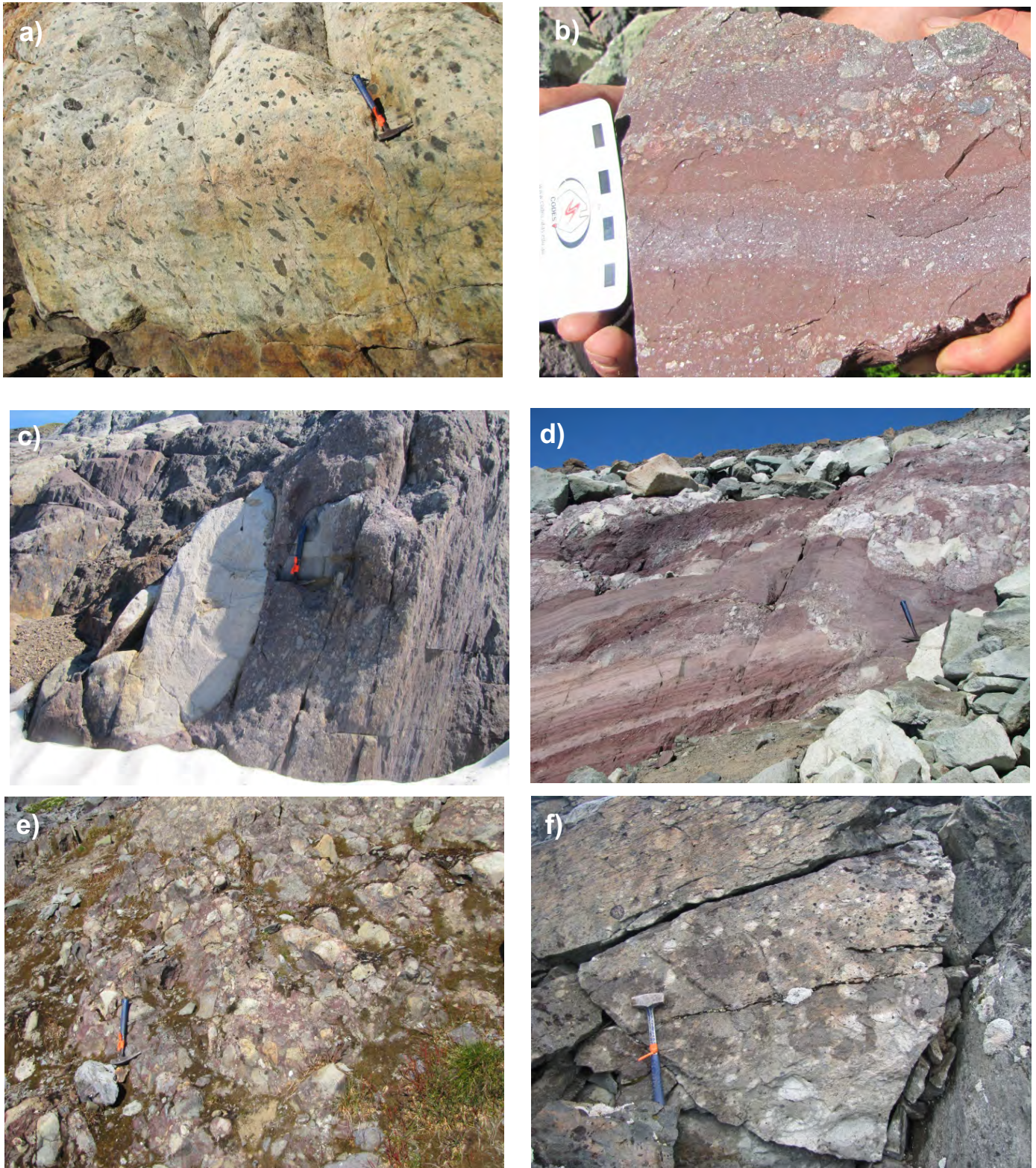


Fig. 7. Representative photos of the Betty Creek Formation. **a)** Sparse clasts in andesite lapilli tuff, Unuk River andesite unit 2 km northwest of Brucejack Lake (426273 E, 6260107 N). **b)** Interbedded pebble conglomerate with volcanic clasts and tuff; Unuk River andesite unit, Treaty Glacier (427578 E, 6272959 N). **c)** Tabular crowded plagioclase-phyric boulder (light-toned left foreground) in basal Unuk River andesite unit (425715 E, 6260099 N); U-Pb zircon age ca. 197 Ma (J. Nelson, unpub. data). **d)** Felsic-clast breccia, Johnny Mountain dacite unit (374608 E, 6276356 N). **e)** Welded tuff and pyroclastic breccia, Brucejack Lake felsic unit (426343 E, 6261610 N). **f)** Local conglomerate at the base of the Brucejack Lake felsic unit (426101 E, 6260852 N).

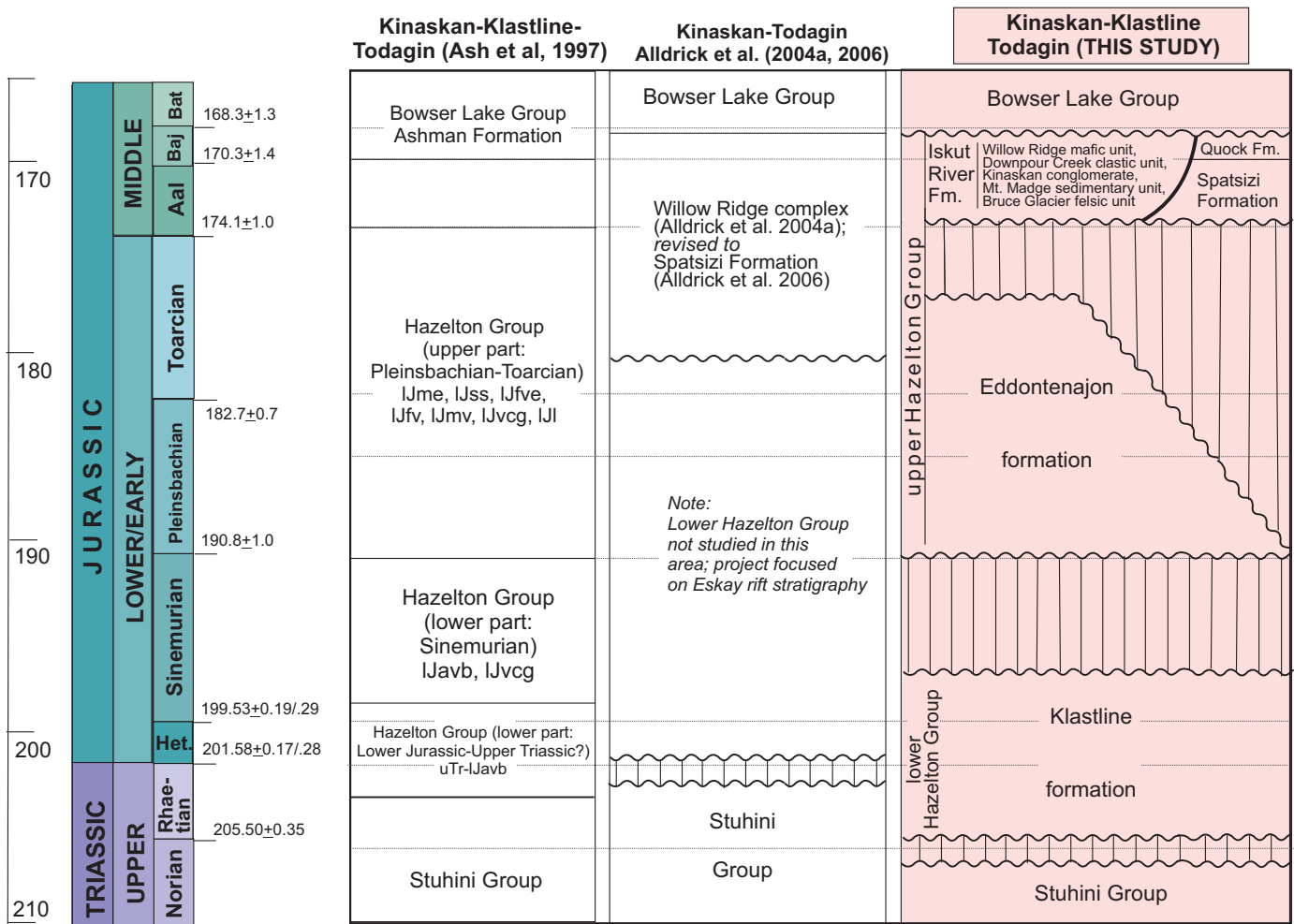


Fig. 8. Evolution of Hazelton Group stratigraphic nomenclature in the Kinaskan-Klastline-Todagin area, northern of Iskut River region.

Thomson et al., 1986; revised to Spatsizi Formation within the Hazelton Group by Evenchick and Thorkelson (2005) and Gagnon et al., 2012). In its type area, the Spatsizi Formation is divided into four members based on proportions of sandstone vs. shale and siltstone, interpreted as the result of cycles of transgression and regression (Fig. 9; Thomson et al., 1986). In the Iskut region, we use the first appearance of similar rocks above the Unuk River andesite unit to define the base of the upper Hazelton Group.

Near Treaty Glacier, the sedimentary succession consists of volcanic sandstone, conglomerate, and local bioclastic sandy limestone, mudstone-siltstone rhythmites, and limestone. It overlies the Unuk River andesite unit, which includes a ca. 187 Ma U-Pb felsic unit (Cutts et al., 2015). Two ammonite collections from a single locality near the top of the sedimentary section are Late Aalenian (PDL-886 and GJ-099; Nadaraju 1993; Lewis, 2013). Similar sedimentary rocks are also exposed within the Eskay anticline, near John Peaks-Bruce Glacier, and in the Cone Glacier-Julian Creek area west of the Unuk River. These sedimentary sections contain abundant Upper Pleinsbachian to Upper Toarcian macrofossils

(Nadaraju, 1993).

Although Lewis et al. (2001a) and Lewis (2013) referred to this succession as Treaty Ridge Member of the Betty Creek Formation, the lithologic character, fossil age, and stratigraphic position of the unit are similar to those of the Spatsizi Formation in its type area (Figs. 5, 9). We recommend that these strata be included in the upper Hazelton Group and be referred to as the Spatsizi Formation. Because Treaty ridge is an informal and poorly described location, we further recommend that the term ‘Treaty Ridge Member’ be abandoned.

2.4. The Eskay rift, the Iskut River Formation, and abandonment of ‘Salmon River Formation’

A several kilometre-thick succession of interlayered basalt, rhyolite, and sedimentary rocks in the upper Hazelton Group occupies a narrow, elongate north-trending belt, extending from Kinaskan Lake in the north to Anyox in the south (Figs. 1-3; Anderson, 1993; Lewis, 2001, 2013; Lewis et al., 2001a; Alldrick et al., 2005b; Gagnon et al., 2012; Barresi, 2015). This narrow, fault-bounded zone has been referred to as the Eskay rift (e.g., Evenchick and McNicoll, 2002;

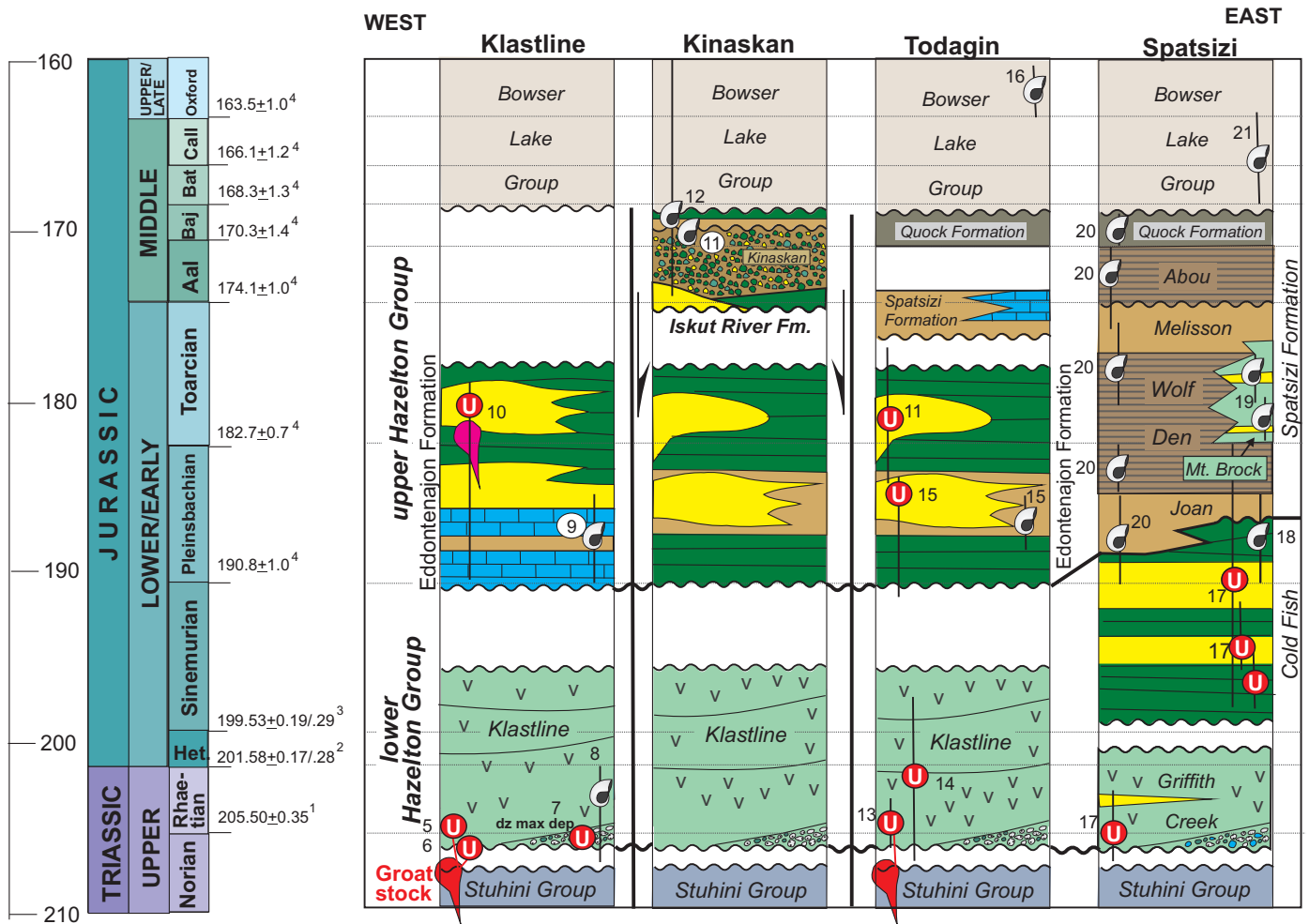


Fig. 9. Stratigraphic columns representing the Hazelton Group in the Kinaskan-Klastline-Todagin area, northern Iskut River region. Numbers reference sources for fossil and radiometric ages. **1.** Norian-Rhaetian boundary (Wotzlaw et al., 2014); **2.** Rhaetian-Hettangian boundary (Schaltegger et al., 2008); **3.** Hettangian-Sinemurian boundary (Schaltegger et al., 2008); **4.** Cohen et al. (2013); **5.** Groat stock 205-207 Ma (Peatfield et al., 2016); **6.** Groat stock 205.1 ± 0.8 (Ash et al., 1997b); **7.** A. Zagorevski, unpub. Dz 10ZE-176. Main population 205.7 ± 0.8 Ma; **8.** Upper Triassic, Suessi zone (Late Norian-Rhaetian, collections 32781, 32767, 40482; Souther, 1972); **9.** Early Jurassic (collection 32786; Souther, 1972); contains pectinid similar to *P. bodenbenderi* behr similar to *Weyla* in Joan Member (Early Pleinsbachian; see Gagnon et al., 2012); **10.** Felsite intrusions 182-186 Ma (Ash et al., 1997a); **11.** D. Alldrick and J. Nelson, unpub. data, 2017; **12.** Possibly middle-Upper Jurassic macrofossils (collection 32834, Souther, 1972); **13.** Red stock 203.8 ± 1.3 Ma (Ash et al., 1997b); **14.** Trachyte north of Ealue Lk, 202.1 ± 4.2 Ma (Ash et al., 1997b); **15.** $185.6 \pm 6.1-0.6$ Ma, Freboidi zone (Lower Pleinsbachian; Palfy et al., 2000); **16.** Early Oxfordian (collection 32778, Souther, 1972); **17.** Thorkelson et al. (1995); **18.** Early Pleinsbachian fossils in Cold Fish volcanics (Evenchick, 1986); **19.** Toarcian fossils in Mt. Brock volcanics (Read and Psutka, 1990); **20.** Thomson et al. (1986); **21.** Bathonian-Callovian fossils in Bowser Lake Group (Evenchick, 1986).

Alldrick et al., 2005b). Gagnon et al. (2012) proposed the name Iskut River Formation for this succession in the Iskut River region and elsewhere in western Stikinia. Previously, Lewis et al. (2001a) and Lewis (2013) used the term ‘Salmon River Formation’ for these rocks. However, as originally defined on Mount Dilworth by Grove (1971, 1986) and Alldrick (1987), the ‘Salmon River Formation’ is not a bimodal-volcanic rock and sedimentary succession but rather comprises a <10 m thick basal layer of Toarcian(?) calcareous grit overlain by 50-100 m of thinly bedded siltstone, shale, tuff and radiolarian chert, and then more than 1000 m of siliciclastic strata (Alldrick 1993). Furthermore, Gagnon and Waldron (2011) recognized that the siliciclastic rocks on Mount Dilworth are part of the Bowser

Lake Group, which unconformably overlies the Hazelton Group (Fig. 4). Thus, because the term ‘Salmon River Formation’ was appropriated for an entirely different succession of rocks (in contradiction to the North American Stratigraphic Code), and because, as originally defined, the Salmon River Formation, was miscorrelated, Gagnon et al. (2012) proposed that the term ‘Salmon River Formation’ be abandoned, a recommendation that we follow.

The Iskut River Formation is laterally equivalent to the upper parts of the Hazelton Group elsewhere, but it is much thicker than correlative units, displays distinct volcanic-rich, locally variable facies, and occupies a unique tectonic setting. It has yielded uppermost Toarcian, Aalenian to Early Bajocian fossils

and ca. 179-173 Ma U-Pb zircon ages (Childe, 1996; Cutts et al., 2015; J. Nelson and D. Alldrick, unpublished, 2017). The base of the unit in the Treaty Glacier area is constrained by Late Aalenian fossils at the top of the underlying Spatsizi Formation (Nadaraju, 1993).

The Iskut River Formation is a highly variable succession in which mafic and felsic volcanic and sedimentary units occur in differing stratigraphic sequences, with multiple stratigraphic repetitions in some areas. Similar to subdivisions of the Betty Creek Formation, most of these units do not lend themselves to formal member status. In the following we: abandon the John Peaks Member (Lewis et al., 2001a; Lewis, 2013) and replace it with Willow Ridge mafic unit; downgrade the Bruce Glacier Member (Lewis et al., 2001a; Lewis, 2013) to an informal unit; retain the 'Eskay Rhyolite Member' (Lewis et al., 2001a; Lewis 2013); and introduce the Mount Madge sedimentary unit for the Troy Ridge Member, which we abandon (Fig. 4).

2.4.1. Willow Ridge mafic unit

Basalt is the most voluminous rock type in the Iskut River Formation throughout its extent. It is abundant in the Unuk River valley (Lewis, 2013; Fig. 3), where it was called the John Peaks Member (Lewis et al., 2001a). However, the John Peaks massif is underlain by an Early Jurassic pluton, which Lewis (2013) named the John Peaks pluton. Because John Peaks do not expose the basalts and because the same name is used for two different rock bodies, we propose that the term 'John Peaks Member' be abandoned. Alldrick et al. (2004b) proposed Willow Ridge as a type section of basalt typical of the Iskut River Formation. This locality, between Table Mountain and Kinaskan Lake (Figs. 2, 3), displays typical variations within the unit and is road accessible. We recommend the term Willow Ridge mafic unit for these rocks.

2.4.2. Bruce Glacier felsic unit

Non-welded to welded lapilli tuff (Fig. 10), felsic volcanic breccia and coherent flows, and volcanic conglomerates occur extensively around the periphery of the McTagg anticlinorium, where they form the local basal unit of the Iskut River Formation (Fig. 3). This unit also occurs in the Eskay anticline, in the footwall of the Eskay deposit, and overlying Betty Creek strata west of Harymel Creek (Lewis, 2013). In the Bruce Glacier area, it unconformably overlies the Jack, Betty Creek and Spatsizi formations. Similar felsic rocks also occur at higher stratigraphic levels, such as at the top of the Iskut River Formation on Treaty ridge and above pillow basalts of the Willow Ridge mafic unit on Pillow Basalt ridge and Table Mountain (see below). Because of this repetition, we refer to these felsic rocks as the Bruce Glacier felsic unit, rather than retaining the formal 'Member' status used by Lewis et al. (2001a). Six SHRIMP U-Pb zircon ages from the unit range from 178.5 ± 1.8 to 173.3 ± 1.8 Ma (Cutts et al., 2015). These ages agree well with the multigrain TIMS ages presented in Lewis (2013), and support the Middle Jurassic age of the Iskut River Formation.



Fig. 10. Bruce Glacier felsic unit, welded lapilli tuff (412848 E, 6270707 N).

2.4.3. Eskay Rhyolite Member

The Eskay Rhyolite Member (Lewis et al., 2001a) forms the immediate footwall of the Eskay deposit at the northern end of the Eskay anticline (Fig. 5) where it was rigorously defined by mapping and core logging as a single, linear flow-dome complex of coherent to brecciated flows that show peperitic contacts with the overlying argillite, which is the host for massive sulphide mineralization (Bartsch, 2001; Barrett and Sherlock, 1996; Childe, 1996). Childe (1996) obtained a U-Pb zircon age of 175 ± 2 Ma from the Eskay rhyolite, identical within error to ages in the Bruce Glacier felsic unit. Geochemistry of the rhyolite ($Al/Ti > 100$) also distinguishes it from other felsic bodies in the area, although this does not constitute a lithostratigraphic criterion.

2.4.4. Mount Madge sedimentary unit

The Eskay Rhyolite Member is overlain by thinly bedded black argillaceous mudstone and felsic tuff. This unit hosts most of the mineralization at Eskay Creek where it is referred to as the Contact argillite (Barrett and Sherlock, 1996). Elsewhere in the Iskut River Formation, tuff-argillite units occur as thin, discontinuous lenses enclosed within volcanic rocks. They were included in the Troy Ridge Member as defined by Lewis et al. (2001a) because of their similarity to siliceous strata at the type locality on Troy ridge. However, the rocks on Troy ridge are now assigned to the regionally extensive Quock Formation (see section 2.6. below). We suggest that Mount Madge (Fig. 2) be the type locality for isolated occurrences in the Iskut River Formation, because Lewis (2001, 2013) has documented two prominent layers on its higher slopes. Other examples occur north of the McTagg anticlinorium, at the head of Treaty Glacier, and near Granduc (Lewis, 2001, 2013).

2.5. Mount Dilworth Formation

Dacite and rhyolite form laterally continuous exposures on Mount Dilworth and Troy ridge in the Salmon River

area, above the Betty Creek Formation and below the Quock Formation (see below). They constitute the Mount Dilworth Formation as originally defined by Alldrick (1987). A U-Pb zircon SHRIMP age of 173.6 ± 1.7 Ma from the northern ridge of Mount Dilworth (Cutts et al., 2015) shows that these rocks are coeval with the Bruce Glacier felsic unit of the Iskut River Formation. We suggest that the Mount Dilworth Formation be retained as part of the upper Hazelton Group, distinguished from felsic units in the Iskut River Formation by its tabular geometry, regional extent, and lack of interfingering with mafic units. It indicates widespread Aalenian felsic activity proximal to, but outside of, the Eskay rift.

2.6. Quock Formation

The highest unit of the Hazelton Group regionally is the Quock Formation, which ranges from Bajocian in the Spatsizi Plateau area (Fig. 9) to Callovian near Terrace (Gagnon et al., 2012). It comprises 50-100 m of thinly bedded, dark grey siliceous argillite with pale felsic tuff laminae, and radiolarian chert. The dark and light striping led to the unit being informally but unforgettably termed 'pyjama beds' by Howard Tipper of the Geological Survey of Canada. It is at least in part a facies equivalent of the Iskut River Formation.

The Quock Formation forms a thin but regionally continuous layer on Mount Dilworth and Troy ridge, above the Mount Dilworth Formation and below the Bowser Lake Group. It was previously called the Troy ridge facies of the Salmon River Formation (Anderson and Thorkelson 1990), and later the Troy Ridge Member of the Salmon River Formation (Lewis et al., 2001a; Lewis, 2013). Because Troy ridge is an informal locality, we favour the usage of Gagnon et al. (2012) and propose that these rocks be included in the Quock Formation, which forms a thin but areally extensive layer at the top of the Hazelton Group throughout Stikinia, outside of the Eskay rift.

3. Ball Creek-Forrest Kerr Creek-Table Mountain (central) area

This area extends north from the confluence of Forrest Kerr Creek and the Iskut River and includes the Downpour Creek, More Creek, and Ball Creek drainages, Table Mountain, and Willow Ridge (Fig. 2). Rocks of the Iskut River Formation are exposed in northerly, fault-bounded graben in contact with older units of the Stuhini Group and Paleozoic stratified and intrusive bodies.

Souther (1972) mapped the area at a 1:250,000 scale, providing a broad bedrock framework and important age constraints from macrofossil collections (Fig. 11). Subsequent 1:50,000-scale mapping was supported by macrofossil and microfossil collections and sparse U-Pb geochronology (Read et al., 1989; Logan et al., 2000). Alldrick et al. (2004a, b; 2005, a, b; 2006) mapped from Forrest Kerr Creek to Kinaskan Lake (Fig. 2), identifying a series of geographically named sub-basins in the Eskay rift, each with a distinct stratigraphy, and used unique codes for each lithotype in each sub-basin (see list of sub-basin names on Fig. 11, which correspond to major

legend subdivisions in Alldrick et al., 2006). In the following, we apply Hazelton Group terminology developed above for the Stewart-McTagg anticlinorium-Snippaker Mountain area to previously unnamed units. We also propose new informal names for rocks in the Iskut River Formation that do not occur farther south: Kinaskan conglomerate unit, Downpour Creek siliciclastic unit, and Palmiere dacite-mudstone unit.

3.1. Units in the lower Hazelton Group

3.1.1. Jack Formation(?)

At two localities along a southern tributary to Ball Creek, east of the Matthew Glacier (Figs. 2, 12), a siliciclastic sedimentary-volcanic succession (unit 13 of Souther, 1972) yielded Hettangian ammonites (*Psiloceras canadense* Frebold). These rocks overlie the Stuhini Group in the hinge zone of a syncline (Souther, 1972). Although lacking the characteristic conglomerates, these rocks are coeval with the Jack Formation elsewhere and, like Jack Formation equivalents, form the basal unit of the Hazelton Group in this area.

3.1.2. Betty Creek Formation

Isolated occurrences of Lower Jurassic andesites between Downpour Creek and the Little Iskut River are herein assigned to the Unuk River andesite unit. Felsic units near Downpour Creek (Logan et al., 2000; Alldrick et al., 2005b) and Ball Creek (Alldrick et al., 2004a, b) are designated as unnamed rhyolites in the Betty Creek Formation (Fig. 12). The unit near Downpour Creek is Sinemurian based on a conodont collection in overlying strata (Logan et al., 2000). The rhyolites near Ball Creek occur in a succession containing Pleinsbachian ammonites (Souther, 1972).

3.2. Units in the upper Hazelton Group

The Iskut River Formation was first defined based on stratigraphic sections in this area (Gagnon et al., 2012). Below we assign previously unnamed basaltic sequences to the Willow Ridge mafic unit, rhyolites to the Bruce Glacier felsic unit, and fine-grained siliceous sequences to the Mount Madge sedimentary unit, as described from the southern area. The area also contains units not seen in the southern sub-area (Fig. 12). Sections many hundreds of metres thick of mainly medium-grained siliciclastic beds near Downpour Creek and on Table Mountain are assigned to the Downpour Creek siliciclastic unit (new name). Conglomerates south of Downpour Creek and on western Table Mountain are assigned to the Kinaskan conglomerate (new name). Also not recognized in the south, the Palmiere unit (new name) is a unique felsic volcanoclastic-mudstone succession that occurs on both sides of the Iskut River near Palmiere Creek (Fig. 2).

3.2.1. Willow Ridge mafic unit

As is the case elsewhere in the region, basalt and pillow basalt are the most widespread and thickest Iskut River Formation rock types. They form particularly thick, km-scale sections on the eponymous Pillow Basalt ridge (Fig. 13a), and on Table

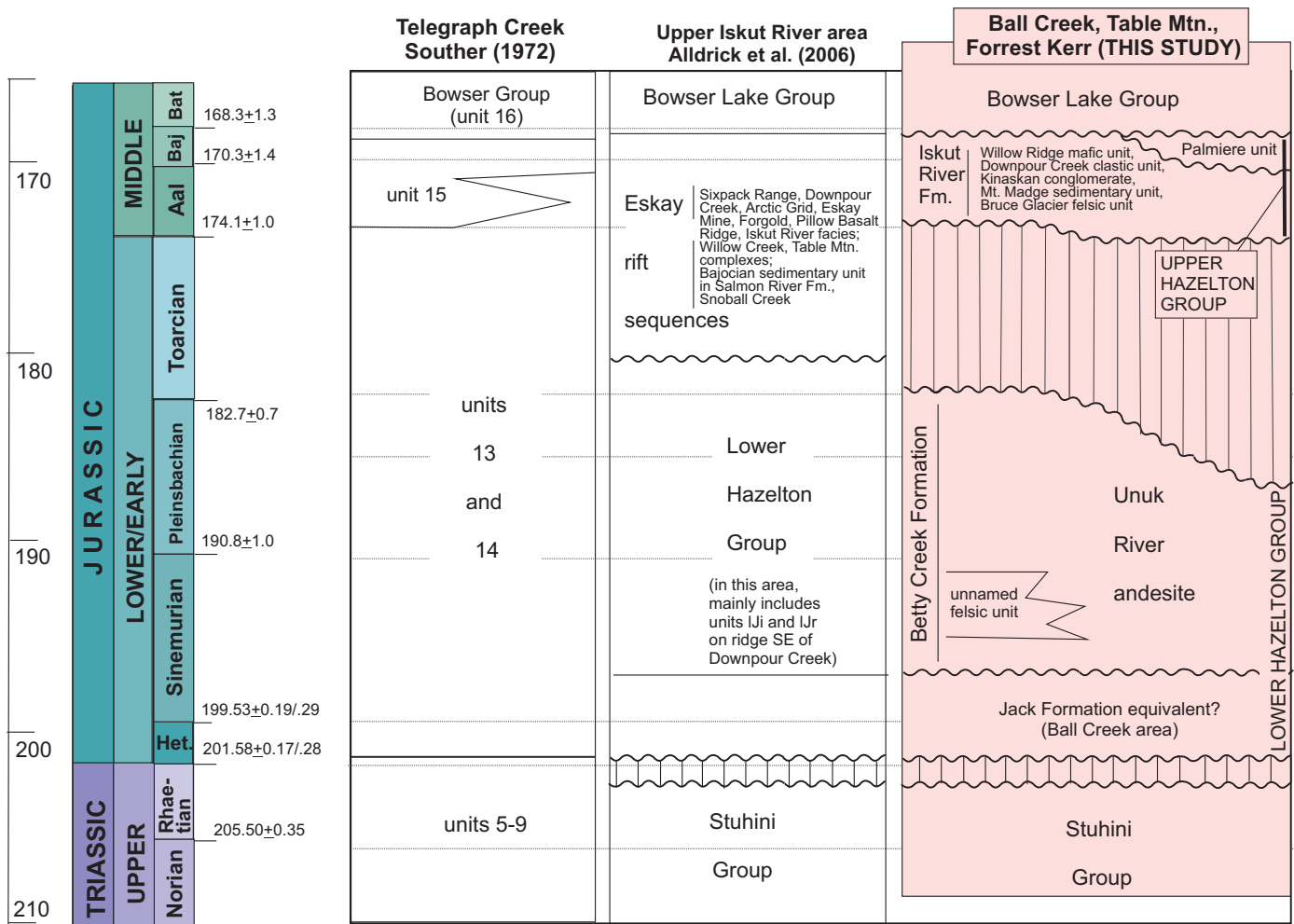


Fig. 11. Evolution of Hazelton Group stratigraphic nomenclature in the Forrest Kerr-Ball Creek-Table Mountain area, central Iskut River region.

Mountain and adjacent Willow Ridge south of Kinaskan Lake. On Pillow Basalt ridge, a small rhyolite in a sedimentary inlier yielded a U-Pb TIMS age of ca. 174 Ma (J. Nelson and D. Alldrick, unpublished data, 2017). Voluminous feeder dikes and sills form part of the unit. Basalts are of non-arc, tholeiitic character, variably contaminated by incorporation of older arc crust (Barresi et al., 2015b).

3.2.2. Bruce Glacier felsic unit

Small domes and cryptodomes with peperitic margins occur on Pillow Basalt ridge, near Forrest Kerr Creek (Figs. 2, 13b), on Table Mountain, and on Willow Ridge, most commonly surrounded by sedimentary facies, but also enclosed within basalts (Alldrick et al., 2004b, 2005b). Felsic volcanoclastic and coherent bodies also occur near Kinaskan Lake.

3.2.3. Mount Madge sedimentary unit

Two discontinuous intervals of thinly bedded to laminated, fine-grained, siliceous argillite and felsic tuff occur on Pillow Basalt ridge (Fig. 13c). One of these encloses a small rhyolite dome or cryptodome that has yielded a U-Pb age

of 174.07 ±0.2 Ma (J. Nelson and D. Alldrick, unpublished, 2017), coeval within error with the Eskay Rhyolite and the Bruce Glacier felsic unit (Childe, 1996; Cutts et al., 2015).

3.2.4. Kinaskan conglomerate unit (new name)

Conglomeratic deposits interfinger with Willow Ridge basalts along the southern shores of Kinaskan Lake, on Table Mountain, and between Downpour Creek and Pillow Basalt ridge. Clasts are both intraformational basalts and rhyolites and extrabasinal, derived from adjacent older Hazelton, Stuhini, and Paleozoic stratified units and intrusive bodies (Figs. 13d, e). They transition across short distances from monomictic breccias to polymictic conglomerates; clast roundness increases with clast diversity. On western Table Mountain, the base of the unit consists of breccias that are interpreted to be paleotalus derived from underlying fault-brecciated lower Hazelton volcanic rocks (Alldrick et al., 2004b). They grade upward into polymictic conglomerates with a sandstone matrix that contain rounded rhyolite and basalt clasts derived from the Iskut River Formation. A suite of monomictic sedimentary breccias north of Pillow Basalt ridge consists of individual deposits derived

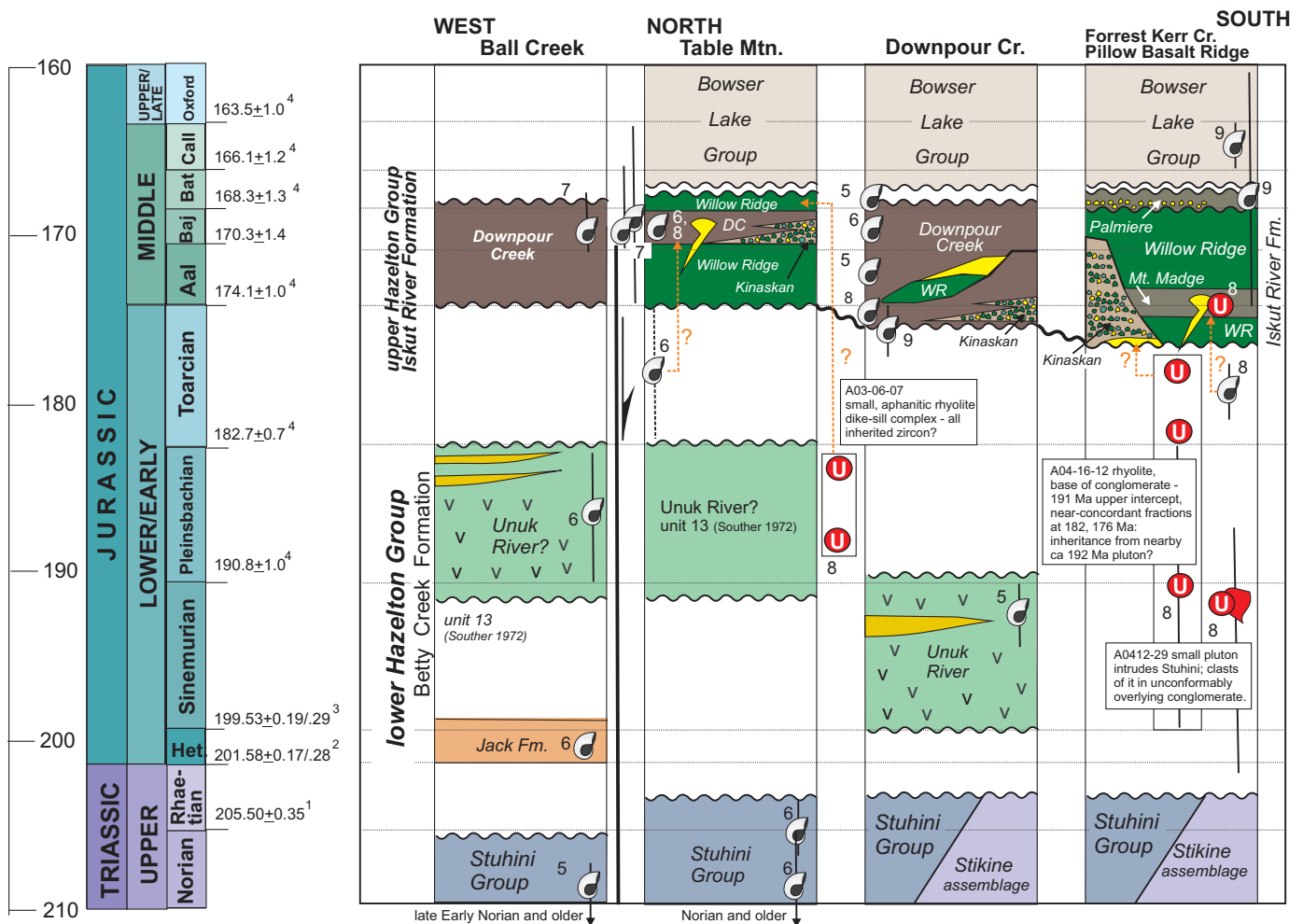


Fig. 12. Stratigraphic columns representing the Hazelton Group in the Forrest Kerr-Ball Creek-Table Mountain area, central Iskut region. Numbers reference sources for fossil and radiometric ages. **1.** Norian-Rhaetian boundary (Wotzlaw et al., 2014); **2.** Rhaetian-Hettangian boundary (Schaltegger et al., 2008); **3.** Hettangian-Sinemurian boundary (Schaltegger et al., 2008); **4.** Cohen et al. (2013); **5.** Logan et al. (2000); **6.** Souther (1972); **7.** Evenchick et al. (2001); **8.** D. Alldrick and J. Nelson, unpub. data (2017); **9.** Read et al. (1989).

from diverse volcanic and intrusive sources that interfinger on a scale of less than a hundred metres (Alldrick et al., 2005b). These units are localized next to probable syn-sedimentary faults, some of which were later remobilized as thrust faults (Alldrick et al., 2004b, 2005b).

3.2.5. Downpour Creek siliciclastic unit (new name)

The Kinaskan conglomerate unit grades upsection and laterally into a succession of sandstone, siltstone and mudstone that we refer to as the Downpour Creek siliciclastic unit, after exposures near Downpour Creek (Fig. 2). The Downpour Creek siliciclastic unit yielded Late Toarcian to Bajocian and perhaps Bathonian macrofossils (Souther, 1972; Logan et al., 2000). A key collection from a small outlier in a synclinal keel overlying lower Hazelton Group rocks yielded abundant, diverse latest Toarcian shelly fauna (J. Nelson and D. Alldrick, unpublished, 2017), which best constrains the age of the base of the Iskut River Formation in this area.

Table Mountain is underlain by two basaltic units separated by interbedded sandstone, siltstone and mudstone assigned to the Downpour Creek siliciclastic unit (Fig. 13f). Small bodies of rhyolite and basalt occur within it. Rare beds of fine-grained siliceous argillite resemble the Mount Madge sedimentary unit, but they are not separated in regional mapping. The unit grades laterally into a narrow zone near the western bounding fault of coarse clastic deposits (Alldrick et al., 2004b) that we assign to the Kinaskan conglomerate unit. This sequence has yielded Late Toarcian, Early Bajocian, and Middle Bajocian macrofossil assemblages (Souther, 1972; J. Nelson and D. Alldrick, unpublished data, 2017).

3.2.6. Palmiere dacite-mudstone unit (new name)

The southern end and southeastern slopes of Pillow Basalt ridge are underlain by a distinctive unit of dacite-clast volcanic breccia, dacite-clast conglomerate, arkosic sandstone, and dark grey to black silty argillite and mudstone (Alldrick et al.,

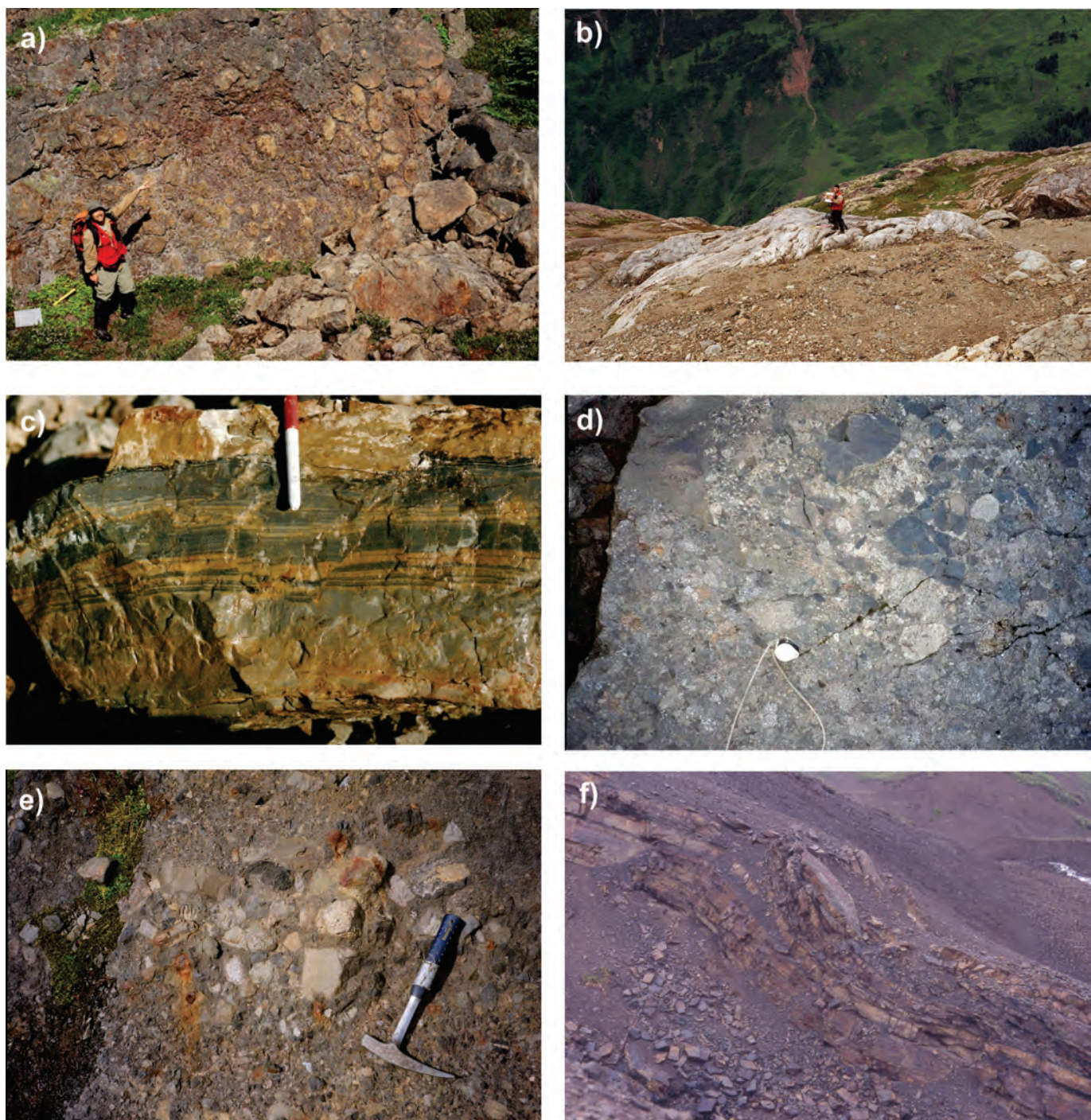


Fig. 13. Representative photographs of the Iskut River Formation. **a)** Willow Ridge mafic unit, pillow basalt, Pillow Basalt ridge (401436 E, 6298614 N). **b)** Bruce Glacier felsic unit, small rhyolite dome-cryptodome complex, ‘Four Corners’ area (401000 E, 6307500 N). **c)** Mt. Madge sedimentary unit, laminated siliceous argillite and pale felsic tuff offset by small syndimentary (?) faults, Pillow Basalt ridge (403000 E, 6301000 N). **d)** Kinaskan conglomerate unit, breccia, Sixpack ridge (405608 E, 630318 N). **e)** Kinaskan conglomerate unit, polymictic conglomerate, Sixpack ridge (405424 E, 6303410 N). **f)** Downpour Creek clastic unit interbedded sandstone and siltstone, Table Mountain (415000 E, 6360000 N). Monocline typical of mild deformation seen in these strata.

2005a, b). Correlative felsic breccia and argillite occur on the ridge northeast of Palmiere Creek, south of the Iskut River. Relationships on Pillow Basalt ridge suggest that the Palmiere unit overlies all older Iskut River units as well as thrust faults

that imbricate them (Alldrick et al., 2005a, 2006). The Palmiere dacite-mudstone unit is overlain by the Bowser Lake Group. On the southern end of Pillow Basalt ridge, dacite breccias show incipient fragmentation textures. Large olistoliths of

limestone are scattered within it. One has yielded Early Permian conodonts (F129, Read et al., 1989). A macrofossil collection from the unit is Middle or possibly early Late Jurassic (F141, Read et al., 1989).

The Palmiere unit appears to be the youngest unit in the Iskut River Formation. Its suggested unconformable relationship to other Iskut River units and structures should be further investigated, and more precise ages obtained. The Palmiere unit could provide constraints on episodes of transtension and transpression, or transfer from releasing to restraining bends, within the overall Eskay rift (Alldrick et al., 2005b).

4. Kinaskan Plateau-Klastline Plateau-Todagin Plateau area

This area was initially mapped at 1:250,000 scale by Souther (1972). The Klastline and Todagin plateau areas were subsequently mapped at 1:50,000 scale (Ash et al., 1996, 1997a, b). In their study of the Stuhini, Hazelton, and Bowser Lake groups in the Spatsizi Plateau area, Evenchick and Thorkelson (2005) overlapped the eastern limit of the present study near Ealue Lake and included a partial re-interpretation of mapping by Ash et al. (1997a) on the Todagin Plateau (Evenchick and Green, 2004). To constrain the northern termination of the Eskay rift, Alldrick et al. (2004a, 2006) extended mapping to Kinaskan Lake and southern Todagin Plateau.

In the following, we replace the codes that were used for two new Hazelton map units recognized in the area by Ash et al. (1997a) with informal stratigraphic names, and substitute units within the Iskut River Formation for unit codes used in Alldrick et al. (2004a, 2006; Figs. 8, 9). Uppermost Triassic (to lowermost Jurassic?) andesites in the lower Hazelton Group are included in the Klastline formation and Lower Jurassic (partly or wholly Pleinsbachian to Toarcian) bimodal volcanic and sedimentary strata in the upper Hazelton Group are included in the Eddontenajon formation. Also, we correlate a siliciclastic-limestone unit in the upper Hazelton Group with the redefined Spatsizi Formation of Gagnon et al. (2012), and an overlying thinly bedded siliceous unit with the Quock Formation. Conglomerates and sedimentary breccias, basalt and felsic volcanic rocks near Kinaskan Lake are considered part of the Iskut River Formation, and named accordingly.

4.1. The lower Hazelton Group

4.1.1. Klastline formation (new name)

Ash et al. (1996, 1997a, b) recognized extensive andesitic volcanoclastic deposits and lesser flows unconformably above the Stuhini Group on the Klastline and Todagin plateaus (Fig. 14a) and referred to them using informal map code designations (units TrJavb and IJavb in Ash et al., 1997a). Pending detailed study, we propose the informal name Klastline formation for these rocks.

The andesites contain plagioclase phenocrysts accompanied by either pyroxene or hornblende. They unconformably overlie steeply dipping greywacke-argillite and pyroxene-phyric basalt of the Stuhini Group (Ash et al., 1996, 1997a; C. Rees,

unpublished, 2017). Mapping of the Todagin Plateau near the Red Chris mine (Rees et al., 2015; C. Rees, unpublished, 2017) confirmed the existence of the lower Hazelton volcanic unit, and at one locale documented a conglomerate at its base above the Stuhini Group. The basal conglomerate contains intrusive and chert clasts (Fig. 14b). Its matrix, quartz-bearing arkose with orange-weathering carbonate cement, physically resembles the Snippaker unit. Detrital zircon peaks at 225 and 330-355 Ma indicate regional exhumation of the Stuhini Group and its Paleozoic basement (J. Nelson and B. van Straaten unpublished 2017). A detrital zircon sample from basal volcanogenic sandstone on the Klastline Plateau displays a major peak of ca. 205.4 Ma (A. Zagorevski, unpublished, 2017). This maximum depositional age likely approximates the actual age of the sandstone because the preservation of microlites suggests a proximal volcanic source. Klastline andesites have been interpreted as the volcanic equivalents of the ca. 206 Ma Red and Groat stocks (Friedman and Ash, 1997; Hollis, 2011), which intrude the underlying Stuhini Group. We suggest that this be named the Tatogga intrusive suite, after Tatogga Lake. The Klastline formation is intruded by numerous smaller undated bodies of the same suite.

North of Ealue Lake, a trachyte from the Klastline formation yielded a ca. 202 Ma U-Pb zircon age (Ash et al., 1997b). Farther north and at higher elevation on the tableland, a linear body of fossiliferous limestone and limestone breccia is intercalated with the plagioclase-phyric volcanic breccias. The limestone contains Late Triassic conodonts (Ash et al., 1997b). Because of its age, the limestone was previously considered to be a small inlier of the Stuhini Group below the volcanic pile (Ash et al., 1997a). However, limestone breccia contains volcanic matrix, and volcanic clasts occur within limestone (Fig. 14c; J. Nelson, unpublished, 2014), suggesting that this limestone represents small bank deposits on the Klastline volcanic edifice.

On Klastline Plateau, small bodies of limestone and fossiliferous hash with a volcanoclastic matrix occur within the andesitic succession. They were described by Ash et al. (1997a, b) as olistoliths. One of these occurrences is an andesite breccia containing small colonial corals, brachiopods, and gastropods, which appear to have been incorporated as individuals in a volcanic mass flow deposit (Fig. 14d; J. Nelson, unpublished, 2014). Fossils from three collections include *Paleocardita*, *Myophoria*, *Pinna*, and *Plicatula perimbricata* Gabb; assigned a Late Norian (Suessi zone) age (E.T. Tozer in Souther, 1972). Some of these genera are also recognized in the Rhaetian of Europe (Hallam and Wignall, 1997). The base of the Rhaetian is now placed between ca. 205.5 Ma and its top at ca. 201.58 Ma (Ogg, 2012). Given its current age constraints, the Klastline formation is latest Triassic (Rhaetian), with possible range into earliest Jurassic. It is coeval with the Griffith Creek volcanics in the Spatsizi area (Fig. 9; Thorkelsen et al., 1995) and with the Snippaker unit to the south (Fig. 5). It is physically isolated from, and older than, the Betty Creek Formation, and represents a separate, earlier episode of Hazelton andesitic volcanism.

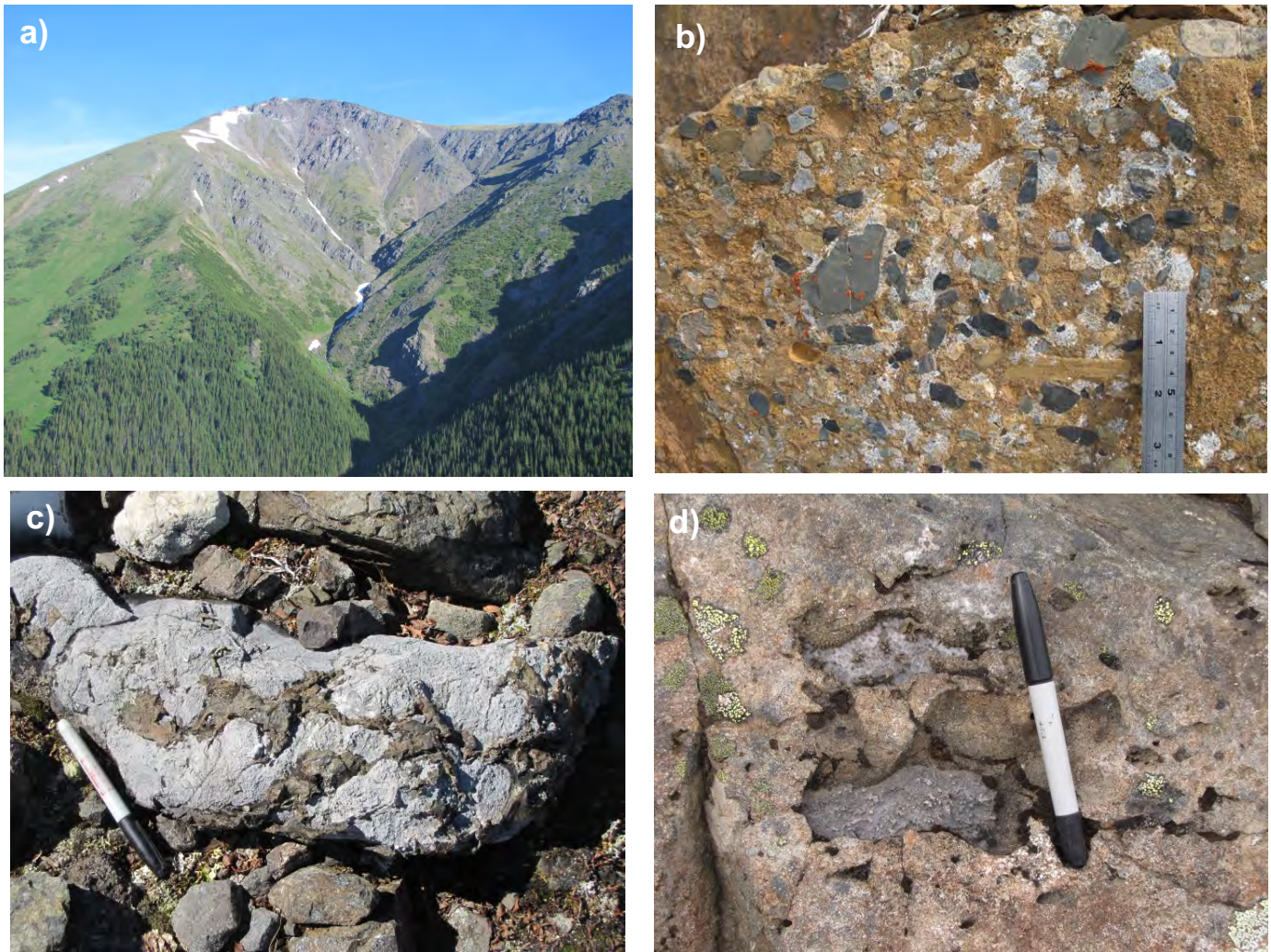


Fig. 14. Representative photographs of Klastline formation. **a)** Andesite breccia forms mountains west of Tatogga Lake. **b)** Basal conglomerate west of Red Chris (446000 E, 6394000 N). **c)** Limestone with andesitic tuff inclusions displaying embayed and flame-like boundaries, north of Ealue Lake (448290 E, 6406500 N). **d)** Coral clasts in andesite breccia, Klastline Plateau (429680 E, 6402520 N).

4.2. Units in the upper Hazelton Group

4.2.1. Eddontenajon formation (new name)

Pleinsbachian to Toarcian basalt, pillow basalt, rhyolite and interbedded limestone, calcareous sandstone and shale occur on southern Todagin Plateau and as scattered outliers on Klastline Plateau, unconformably overlying Klastline formation andesites (Figs. 3, 9). These rocks were designated as IJmv (mafic volcanic rocks), IJfv (felsic volcanic rocks) and IJl (limestone) by Ash et al. (1997a). Ash et al. (1997b) reported a ca. 180 Ma age from a rhyolite on Todagin Plateau. At the Todagin section, a rhyolite (U-Pb zircon, 185.6 +6.1-0.6 Ma) is interbedded with sandstone from which a late Early Pleinsbachian ammonite fauna was collected (Palfy et al., 2000). Another rhyolite in this area yielded a 181 ±4 Ma U-Pb zircon age (J. Nelson and D. Alldrick, unpublished, 2017). Souther (1972) reported Early Jurassic fossils from one locality on Klastline Plateau.

The sedimentary components of this unit resemble the Spatsizi Formation in age and character. However the bimodal

volcanic rocks physically resemble those of the Iskut River Formation. A local name for this unit is appropriate, leaving potential correlations and interpretations for future work. We consider it part of the upper Hazelton Group because of its age and unconformable relationship to the Klastline formation.

4.2.2. Spatsizi Formation

A thin equivalent of the Spatsizi Formation outcrops along the southern edge of the Todagin Plateau, unconformably overlying the Stuhini Group and Klastline formation (Rees et al., 2015; C. Rees, unpublished mapping, 2017) and probably the Eddontenajon formation farther west. It includes bioclastic calcarenite that grades into fine-grained limestone, and feldspathic-lithic sandstone.

4.2.3. Quock Formation

Chert and siliceous argillite with pale felsic tuff laminae occur on the southern Todagin Plateau as a thin, continuous unit above the Spatsizi Formation and immediately below the

basal beds of the Bowser Lake Group (Rees et al., 2015; Fig. 9).

4.2.4. Iskut River Formation

The northernmost outcrops of possible Iskut River Formation lie west and east of southern Kinaskan Lake (Fig. 3). They include immature, poorly bedded conglomerates and sedimentary breccias of the Kinaskan conglomerate unit (see above; Alldrick et al., 2004b), interfingering with basalt and felsic volcanic rocks. The conglomerate contains macrofossils considered Bajocian and younger (Souther, 1972; D. Alldrick and J. Nelson, unpublished). This succession abuts the Eddontenajon formation at the western edge of Todagin Plateau. Although different in age (Middle Jurassic vs. Pleinsbachian-Toarcian), the two units have similar characteristics, i.e., basalt and rhyolite with interlayered siliciclastic beds. The contact between them is mostly covered and interpreted to be structural. Further mapping and geochronological work in this area is required to establish their relationship.

5. Discussion

Integration of mapping studies conducted in the Iskut region of western Stikinia has brought new understanding of the Hazelton Group, and provides a stratigraphic framework for related intrusions and mineral deposits. Newly defined uppermost Triassic (to lowermost Jurassic?) basal Hazelton units include the Klastline formation near the hamlet of Iskut and the Snippaker unit in the lower Iskut River area. Detrital zircon and fossil ages in these units indicate deposition in the Rhaetian (ca. 206-203 Ma) coeval with the emplacement of the Tatogga intrusive suite and porphyry mineralization at Red Chris and GJ. Close association of the Klastline formation and Tatogga intrusive suite suggests a temporal and probably causative link between the local onset of Hazelton volcanism and porphyry intrusion and mineralization. The abrupt appearance of older detrital zircon populations in basal Hazelton conglomerates attests to tectonically-induced denudation immediately preceding the onset of Hazelton deposition.

The Hazelton magmatic axis apparently shifted southwards by nearly a hundred kilometres between latest Triassic and Early Jurassic time, to the lower Iskut-McTagg region. Early Betty Creek volcanism coincided with emplacement of Texas Creek plutons. Of these, the Mitchell suite gave rise to the Kerr, Sulphurets, Mitchell and Iron Cap porphyry systems, and plutons of the Lehto suite caused porphyry and related gold mineralization in the Snip-Johnny Mountain-Inel-KSP camp. Epithermal gold mineralization at Valley of the Kings was formed during the waning stages of the magmatic episode, overlapping ages of felsic volcanic and intrusive rocks of the Brucejack Lake felsic unit.

All Middle Jurassic upper Hazelton Group units that fill the Eskay rift are included in the Iskut River Formation, as recommended by Gagnon et al. (2012). This supersedes the abandoned term Salmon River Formation. The Iskut River Formation is divided into seven informal, lithostratigraphic units: the Willow Ridge mafic unit, Bruce Glacier felsic unit,

Mount Madge sedimentary unit, Kinaskan conglomerate, Downpour Creek siliciclastic unit, and Palmiere unit; and one formal member, the Eskay Rhyolite Member. The informal terms are applicable throughout the northern part of the Eskay rift, and probably beyond.

The Eskay rift opened as a post-arc extensional to mildly transtensional, terrane-scale feature in response to the collision of Stikinia with adjacent terranes (Nelson et al., 2013). Mainly andesite volcanism in the lower Hazelton Group was succeeded by bimodal basalt-rhyolite volcanism in the rift, which provided the setting for volcanogenic massive sulphide deposits such as Eskay Creek and Anyox. In detail, the Eskay deposit lies in an interval of fine-grained sedimentary strata immediately above footwall rhyolite (Childe, 1996). The association of thin Mount Madge siliceous sedimentary units with rhyolite is thus an important exploration criterion in the Iskut River Formation. This critical association has been observed on Pillow Basalt ridge and to the north in the “Four Corners” area (Alldrick et al., 2005b). Dark siliceous mudstone beds in the middle sedimentary unit on Table Mountain (Downpour Creek unit) host laminated syngenetic pyrite (Alldrick et al., 2004b).

Work with the existing set of geological maps and supporting data has identified a number of knowledge gaps in the area that will benefit from future studies. First, the newly defined Klastline formation needs detailed documentation through mapping and construction of reference sections. Its absolute age is currently based on a few unpublished U-Pb ages. Its internal and external unit relationships require re-examination, in particular its unconformable contacts with the Stuhini Group. Comparison of ages and geochemistry with the many small plutons of the Tatogga intrusive suite will test the degree of consanguinity between intrusive and extrusive magmatism. Porphyry mineralization of the Castle occurrence (BC MINFILE 104G 076) and newly discovered epithermal veins in the Saddle zone have yet to be studied in this context.

Second, the Eddontenajon formation also requires further study. Structural and stratigraphic relationships between the Eddontenajon formation (Lower Jurassic) and Iskut River Formation (Middle Jurassic) on the western margin of the Todagin Plateau need clarification. This will result in greater understanding of the apparent northern termination of the Eskay rift. Was it simply a propagating rift tip? Or did the north-trending rift terminate against nearly orthogonal faults of the Pitman system (Fig. 1)? Did bimodal Eddontenajon volcanism evolve into that of the Iskut River Formation? How do their trace-element chemistries compare?

Third, an age from the Bruce Glacier unit on the east limb of the Eskay anticline (174.10 ± 0.68/-0.72 Ma; Childe, 1996), is currently the sole radiometric age used to establish the absolute age of the Aalenian in the 2012 Geological Time Scale (Schmitz, 2012). Near the sample locality, it is overlain by sedimentary strata that contain Late Aalenian fauna (Nadaraju and Lewis, 2001). The Treaty ridge section offers an excellent opportunity to improve understanding of Aalenian stage boundaries via combined fossil zonation and absolute ages.

This section contains Late Aalenian fossils at the top of the Spatsizi Formation (formerly Treaty Ridge Member; Nadaraju, 1993; Lewis, 2013), overlain by basalt and rhyolite of the Iskut River Formation. The rhyolite has yielded a concordant, U-Pb age of 174.7 ± 1.4 Ma (Cutts et al., 2015). The current age pick for the base of the Aalenian, 174.1 ± 1.0 Ma (Ogg and Hinnov, 2012), thus probably requires downward revision. The fossiliferous strata contain thin felsic tuff beds (P. Lewis, personal communication, 2017), offering an opportunity for establishing additional absolute age constraints in this important section.

6. Conclusions

A revised stratigraphic framework for the Hazelton Group in the Iskut River region sets it in the context of Stikinia-wide recommendations (Gagnon et al., 2012), highlights the importance of basal units within the uppermost Triassic, and offers a technically correct terminological scheme that meets the requirements of the North American Stratigraphic Code.

- The Hazelton Group is divided into upper and lower parts. The lower Hazelton Group comprises basal siliciclastic units (Jack Formation, Snippaker unit), and andesite and minor felsic volcanogenic accumulations (Klastline formation, Betty Creek Formation). The upper Hazelton Group comprises the Spatsizi, Mount Dilworth and Quock formations regionally, the Eddontenajon formation locally and, within the Eskay rift, the Iskut River Formation.
- The Klastline formation and Snippaker unit are of Rhaetian, latest Triassic age, coeval with the Griffith Creek volcanics in the Spatsizi Plateau (Thorkelsen et al., 1995) and the lower Telkwa Formation near Terrace (Barresi et al., 2015a).
- Lithostratigraphic subdivisions of the Betty Creek and Iskut River formations are recast as informal units, with the exception of the Eskay Rhyolite Member.

Stratigraphic names recommended here will be applied to map units in the upcoming revision of Iskut geology in the digital geological map of British Columbia, to be released this year.

Acknowledgments

We acknowledge the contributions of the original mappers, notably first authors Peter Lewis, Dani Alldrick, and Chris Ash. Their detailed work will continue to provide guidance to future students of the Iskut region. This work builds on theses by J.-F. Gagnon and Tony Barresi; we appreciate their analysis of Hazelton Group stratigraphic relationships. A conversation with Peter Lewis in 2017 gave important corrections and guidance. Tony Barresi reviewed the manuscript and offered helpful suggestions for improvement.

References cited

Alldrick, D.J., 1987. Geology and mineral occurrences of the Salmon River valley, Stewart area (NTS 104A, B). British Columbia Ministry of Energy and Mines, British Columbia Geological

- Survey Open File 1987-22, scale 1:50,000.
- Alldrick, D.J., 1993. Geology and metallogeny of the Stewart mining camp, northwestern British Columbia (104B, 103O). BC. Ministry of Energy and Mines, British Columbia Geological Survey Bulletin 85, 105 p.
- Alldrick, D.J., Stewart, M.L., Nelson, J.L., and Simpson, K.A., 2004a. Geology and mineral deposits of the More Creek-Kinaskan Lake area, northwestern BC. British Columbia Ministry of Energy and Mines, British Columbia Geological Survey Open File 2004-2, scale 1:50,000.
- Alldrick, D.J., Stewart, M.L., Nelson, J.L., and Simpson, K.A., 2004b. Tracking the Eskay rift through northern British Columbia—Geology and mineral occurrences of the upper Iskut area. In: Geological Fieldwork 2003, British Columbia Ministry of Energy and Mines, British Columbia Geological Survey Paper 2004-1, pp. 1-18.
- Alldrick, D.J., Nelson, J.L., and Barresi, T., 2005a. Geology of the Volcano Creek-More Creek area. British Columbia British Columbia Ministry of Energy and Mines, British Columbia Geological Survey Open File 2005-5, scale 1:50,000.
- Alldrick, D.J., Nelson, J.L., and Barresi, T., 2005b. Geology and mineral occurrences of the Upper Iskut River Area: Tracking the Eskay rift through northern British Columbia (Telegraph Creek NTS 104G/1, 2; Iskut River NTS 104B/9, 10, 15, 16). In: Geological Fieldwork 2004. British Columbia Ministry of Energy, Mines and Petroleum Resources, British Columbia Geological Survey Paper 2005-1, pp. 1-30.
- Alldrick, D.J., Nelson, J.L., Barresi, T., Stewart, M.L., and Simpson, K.A., 2006. Geology of the upper Iskut River area, British Columbia British Columbia Ministry of Energy and Mines, British Columbia Geological Survey Open File 2006-2, scale 1:100,000.
- Anderson, R.G., 1993. A Mesozoic stratigraphic and plutonic framework for northwestern Stikinia (Iskut River area), northwestern British Columbia. In: Dunne, G.C. and McDougall, K.A., (Eds.), Mesozoic paleogeography of the western United States, II. Society of Economic Paleontologists and Mineralogists, Pacific Section, Los Angeles, California, pp. 477-494.
- Anderson, R.G., and Thorkelson, D.J., 1990. Mesozoic stratigraphy and setting for some mineral deposits in Iskut River map area, northwestern British Columbia. In: Current Research 1989, Geological Survey of Canada Paper 90-1E, pp. 131-139.
- Ash, C.H., Stinson, P.K., and MacDonald, R.W.J., 1996. Geology of the Todagin Plateau and Kinaskan Lake area, northwestern British Columbia (104H/12, 104G/9). In: Geological Fieldwork 1995, British Columbia Ministry of Energy and Mines, British Columbia Geological Survey Paper 1996-1, pp. 155-174.
- Ash, C.H., MacDonald, R.J.W., Stinson, P.K., Fraser, T.M., Read, P.R., Psutka, J.F., Nelson, K.J., Arden, K.M., Friedman, R.M., and Lefebvre, D.V., 1997a. Geology and mineral occurrences of the Tatogga Lake area, NTS 104G/9NE, 16SE and 104H/12NW, 13SW. British Columbia Ministry of Energy, Mines and Petroleum Resources, British Columbia Geological Survey Open File 1997-3, scale 1:50,000.
- Ash, C.H., MacDonald, R.W.J., and Friedman, R., 1997b. Stratigraphy of the Tatogga Lake area, northwestern British Columbia (104H/12&13, 104G/9&16). In: Geological Fieldwork 1996, British Columbia Ministry of Energy and Mines, British Columbia Geological Survey Paper 1997-1, pp. 283-290.
- Barresi, T., 2015. Tectono-magmatic and metallogenetic evolution of the Late Triassic to Middle Jurassic Hazelton Group in northwest British Columbia. Ph.D. thesis, Dalhousie University, 333 p.
- Barresi, T., Nelson, J.L., and Friedman, R., 2015a. Evolution of the Hazelton arc near Terrace, British Columbia: Stratigraphic, geochronological and geochemical constraints on a Late Triassic-Early Jurassic arc and Cu-Au porphyry belt. Canadian Journal of Earth Sciences 52, 466-494.
- Barresi, T., Nelson, J.L., and Dostal, J., 2015b. Geochemical

- constraints on magmatic and metallogenic processes: Iskut River Formation, volcanogenic massive sulfide-hosting basalts, NW British Columbia, Canada. *Canadian Journal of Earth Sciences*, 52, 1-20.
- Barrett, T.J., and Sherlock, R.L., 1996. Geology, litho geochemistry and volcanic setting of the Eskay Creek Au-Ag-Cu-Zn deposit, northwestern British Columbia. *Exploration and Mining Geology*, 5, 339-368.
- Bartsch, R.D., 2001. Lithology, petrology and geochemistry of the Proutt Plateau, Chapter 3. In: Lewis, P.D., Toma, A., Tosdal, R.M., (Eds.), *Metallogenesis of the Iskut River Area, Northwestern British Columbia*, Mineral Deposit Research Unit, Special Publication Number 1, pp. 31-46.
- Cohen, K.M., Finney, S., and Gibbard, P.L., 2013. International Chronostratigraphic Chart v2013/01. International Commission on Stratigraphy, IUGS.
- Childe, F., 1996. U-Pb geochronology and Nd and Pb isotope characteristics of the Au-Ag-rich Eskay Creek volcanogenic massive sulphide deposit, British Columbia. *Economic Geology* 91, 1209-1224.
- Cui, Y., Miller, D., Schiarizza, P., and Diakow, L.J., 2017. British Columbia digital geology. British Columbia Ministry of Energy, Mines and Petroleum Resources, British Columbia Geological Survey Open File 2017-8, 9 p.
- Cutts, J.A., McNicoll, V.J., Zagorevski, A., Anderson, R.G., and Martin, K., 2015. U-Pb geochronology of the Hazelton Group in the McTagg anticlinorium, Iskut River area, northwestern British Columbia. In: *Geological Fieldwork 2014, British Columbia Ministry of Energy and Mines*, British Columbia Geological Survey Paper 2015-1, pp. 87-102.
- Evenchick, C.A., 1986. Structural style of the northeast margin of the Bowser Basin, Spatsizi map area, north-central British Columbia. In: *Current Research, Part B, Geological Survey of Canada, Paper 86-1B*, pp. 733-739.
- Evenchick, C.A., and Green, G.M., 2004. Geology, Kluea Lake, British Columbia. Geological Survey of Canada, Map 2028A, scale 1:50,000.
- Evenchick, C.A., and McNicoll, V.J., 2002. Stratigraphy, structure, and geochronology of the Anyox pendant, northwest British Columbia, and implications for mineral exploration. *Canadian Journal of Earth Sciences*, 39, 1313-1332.
- Evenchick, C.A., and Thorkelson, D., 2005. Geology of the Spatsizi River map area, north-central British Columbia. *Geological Survey of Canada Bulletin 577*, 276 p.
- Evenchick, C.A., Poulton, T.P., Tipper, H.W., and Braidek, I., 2001. Fossils and facies of the northern two-thirds of the Bowser Basin, British Columbia; Geological Survey of Canada, Open File 3956, 103 p., (map scale 1:250,000), doi:10.4095/212067.
- Febbo, G.E., 2016. Structural evolution of the Mitchell Au-Cu-Ag-Mo porphyry deposit, northwestern British Columbia. M.Sc. thesis, University of British Columbia, 340 p.
- Febbo, G.E., Kennedy, L.A., Savell, M., Creaser, R.A., and Friedman, R.M., 2015. Geology of the Mitchell Au-Cu-Ag-Mo porphyry deposit, northwestern British Columbia, Canada. In: *Geological Fieldwork 2014, British Columbia Ministry of Energy and Mines*, British Columbia Geological Survey Paper 2015-1, pp. 59-86.
- Friedman, R.M., and Ash, C.H., 1997. U-Pb age of intrusions related to porphyry Cu-Au mineralization in the Tatogga Lake area, northwestern British Columbia (104H/12NW, 104G/9NE). In: *Geological Fieldwork 1996, British Columbia Ministry of Energy and Mines*, British Columbia Geological Survey Paper 1997-1, pp. 291-297.
- Gagnon, J.-F., 2010. Stratigraphic and tectonic evolution of the Jurassic Hazelton trough-Bowser basin, northwest British Columbia. Unpublished Ph.D. thesis, University of Alberta, 207 p.
- Gagnon, J.-F., and Waldron, J.W.F., 2011. Sedimentation styles and depositional processes in a Middle to Late Jurassic slope environment, Bowser basin, northwestern British Columbia. *Marine and Petroleum Geology* 28, 698-715.
- Gagnon, J.F., Barresi, T., Waldron, J.W.F., Nelson, J.L., Poulton, T.P., and Cordey, F., 2012. Stratigraphy of the upper Hazelton Group and Jurassic evolution of the Stikine terrane, British Columbia. *Canadian Journal of Earth Sciences*, 49, 1027-1052.
- Gradstein, F.M., Ogg, J.G., Schmitz, M., and Ogg, G., 2012. *The Geologic Time Scale*. Elsevier, 1176 p.
- Grădinaru, E., and Sobolev, E.S., 2010. First record of Rhabdoceras suessi (Ammonoidea, Late Triassic) from the Transylvanian Triassic Series of the Eastern Carpathians (Romania) and a review of its biochronology, paleobiogeography and paleoecology. *Central European Geology* 53, 261-309.
- Greig, C., 2013. Brucejack property geology. Pretium Resources Inc. Map, scale 1:6000, http://s1.q4cdn.com/222336918/files/doc_downloads/geology/2013.03.19%20Property%20Geology.pdf Last accessed December 2017.
- Grove, E.W., 1971. Geology and mineral resources of the Stewart area, British Columbia. *British Columbia Ministry of Energy, Mines and Petroleum Resources Bulletin* 58, 229 p.
- Grove, E.W., 1986. Geology and mineral resources of the Unuk River-Salmon River-Anyox area. *British Columbia Ministry of Energy, Mines and Petroleum Resources Bulletin* 63, 152 p.
- Hallam, A., and Wignall, P.B., 1997. *Mass Extinctions and their Aftermath*. Oxford University Press, 328 p.
- Henderson, J.R., Kirkham, R.V., Henderson, M.N., Payne, J.G., Wright, T.O., and Wright, R.L., 1992. Stratigraphy and structure of the Sulphurets area, British Columbia. In: *Current Research, Part A: Geological Survey of Canada Paper 92-1A*, pp. 323-332.
- Hollis, L., 2011. Assessment Report on the 2010 geological mapping, core re-logging, spectral and geophysical program at the GJ/Kinaskan property, BC, Canada. BC Ministry of Energy and Mines, Assessment Report 32303, 208 p., map scale 1:6000.
- Kyba, J., and Nelson, J., 2015. Stratigraphic and tectonic framework of the Khyber-Sericite-Pins mineralized trend, lower Iskut River, northwest British Columbia. In: *Geological Fieldwork 2014, British Columbia Ministry of Energy and Mines*, British Columbia Geological Survey Paper 2015-1, pp. 41-58.
- Lewis, P.D., 2001. Geological maps of the Iskut River area. In: Lewis, P.D., Toma, A., and Tosdal, R.M., (Eds.), *Metallogenesis of the Iskut River Area, Northwestern British Columbia*. Mineral Deposit Research Unit, Special Publication Number 1. NTS 104B/8, 104B/9, 104B/10, 1:50,000-scale maps.
- Lewis, P.D., 2013. Iskut River Area Geology, Northwest British Columbia (104B/08, 09, 10 & part of 104B/01, 07, 11). Geoscience BC Report 2013-05; 3 1:50,000-scale maps, legend and notes; .shp files.
- Lewis, P.D., Macdonald, A.J., and Bartsch, R.D., 2001a. Hazelton Group/Bowser Lake Group stratigraphy in the Iskut River area-progress and problems, Chapter 2. In: Lewis, P.D., Toma, A., and Tosdal, R.M., (Eds.), *Metallogenesis of the Iskut River Area, Northwestern British Columbia*. Mineral Deposit Research Unit, Special Publication Number 1, pp. 9-30.
- Lewis, P.D., Mortensen, J.K., Childe, F., Friedman, R.M., Gabites, J.M., Ghosh, D., and Bevier, M.L., 2001b. Geochronology data set. In: Lewis, P.D., Toma, A., and Tosdal, R.M., (Eds.), *Metallogenesis of the Iskut River Area, Northwestern British Columbia*. Mineral Deposit Research Unit, Special Publication Number 1, pp.89-96.
- Logan, J.M., Drobe, J.R., and McClelland, W.C., 2000. Geology of the Forrest Kerr-Mess Creek area, northwestern British Columbia, B.C. Ministry of Energy and Mines, *British Columbia Geological Survey Bulletin* 104, 164 p., map scale 1:100,000.
- MacDonald, A.J., 1993. Lithostratigraphy and geochronometry, Brucejack Lake, northwestern British Columbia (104B/08E). In: *Geological Fieldwork 1992, British Columbia Ministry of Energy*

- and Mines, British Columbia Geological Survey Paper 1993-1, pp. 315-323.
- Nadaraju, G. 1993. Triassic-Jurassic biochronology of the eastern Iskut River map area, northwestern British Columbia. Unpublished M.Sc. thesis, The University of British Columbia, 258 p.
- Nadaraju, G., and Lewis, P.D., 2001. Biochronology data set, Chapter 8. In: Lewis, P.D., Toma, A., and Tosdal, R.M., (Eds.), *Metallogenesis of the Iskut River Area, Northwestern British Columbia*. Mineral Deposit Research Unit, Special Publication Number 1, pp. 9-30.
- Nelson, J.L., and Kyba, J. 2014. Structural and stratigraphic control if porphyry and related mineralization in the Treaty Glacier-KSM-Brucejack-Stewart trend of northwestern Stikinia. In: *Geological Fieldwork 2013*, British Columbia Ministry of Energy and Mines, British Columbia Geological Survey Paper 2014-1, pp. 111-140.
- Nelson, J.L., Colpron, M., and Israel, S., 2013. The Cordillera of British Columbia, Yukon and Alaska: Tectonics and metallogeny. In: Colpron, M., Bissig, T., Rusk, B.G. and Thompson, J.F., (Eds.), *Tectonics, Metallogeny and Discovery: The North American Cordillera and Similar Accretionary Settings*. Society of Economic Geologists Special Publication 17, Chapter 3, pp. 53-103.
- North American Commission on Stratigraphic Nomenclature 2005. *North American Stratigraphic Code*. American Association of Petroleum Geologists Bulletin 89, 1547-1591.
- Ogg, J.G., 2012. Triassic, Chapter 25. In: Gradstein, F.M., Ogg, J.G., Schmitz, M. and Ogg, G. *The Geologic Time Scale*. Elsevier, pp. 681-730.
- Ogg, J.G., and Hinnov, L.A. 2012. Jurassic, Chapter 26. . In: Gradstein, F.M., Ogg, J.G., Schmitz, M. and Ogg, G. *The Geologic Time Scale*. Elsevier, pp. 731-791.
- Orchard, M.J., and Tozer, E.T. 1997. Triassic conodont biochronology, its calibration with the ammonoid standard, and a biostratigraphic summary for the Western Canada Sedimentary Basin. In: Moslow, T. and Wittenberg, J., (Eds.), *Triassic of Western Canada Basin*, Canadian Society of Petroleum Geologists Bulletin 45, 675-692.
- Palfy, J., Mortensen, J.K., Smith, P.L., Friedman, R.M., McNicoll, V., and Villeneuve, M., 2000. New U-Pb zircon ages integrated with ammonite biochronology from the Jurassic of the Canadian Cordillera. *Canadian Journal of Earth Sciences* 37, 549-567.
- Peatfield, G.R., Giroux, G.H., and Cathro, M.S., 2016. Revised technical report on the Donnelly-GJ deposit area, GJ Property, Liard Mining Division, British Columbia, Canada. Skeena Resources Limited, 113 p. <https://www.skeenaresources.com/assets/docs/reports/gj-revised-report-160418-20160513113737.pdf> Last accessed December 2017.
- Read, P.B., and Psutka, J.F., 1990. Geology, Ealue Lake east half (104H/13E) and Cullivan Creek (104H/14) map areas. Geological Survey of Canada Open File 2241, scale 1:50,000.
- Read, P.B., Brown, R.L., Psutka, J.F., Moore, J.M., Journeay, M., Lane, L.S., and Orchard, M.J., 1989. Geology, More and Forest Kerr creeks (parts of 104B/10,15,16 & 104G/1, 2), northwestern British Columbia; Geological Survey of Canada, Open File 2094, scale 1:50,000.
- Rees, C., Riedell, K.B., Profett, J.M., Macpherson, J., and Robertson, S., 2015. The Red Chris porphyry copper-gold deposit, northern British Columbia, Canada: Igneous phases, alteration and controls of mineralization. *Economic Geology* 110, 857-888.
- Schaltegger, U., Guex, J., Bartolini, A., Schoene, B., and Ovtcharova, M., 2008. Precise U-Pb age constraints for end-Triassic mass extinction, its correlation to volcanism and Hettangian post-extinction recovery. *Earth Planetary Science Letters* 267, 266-275.
- Schmitz, M.D., 2012. Radiometric ages used in GTS2012, Appendix 2. . In: Gradstein, F.M., Ogg, J.G., Schmitz, M. and Ogg, G. *The Geologic Time Scale*. Elsevier, pp. 1045-1082.
- Souther, J.G., 1972. Telegraph Creek map-area, 104G, British Columbia. Geological Survey of Canada Paper 71-44, 38 p., 1:250,000 map.
- Thomson, R.C., Smith, P.L., and Tipper, H.W., 1986. Lower to Middle Jurassic (Pleinsbachian to Bajocian) stratigraphy of the northern Spatsizi area, north-central British Columbia. *Canadian Journal of Earth Sciences* 23, 1963-1973.
- Thorkelson, D.J., Mortensen, J.K., Marsden, H., and Taylor, R.P., 1995. Age and tectonic setting of Early Jurassic episodic volcanism along the northeastern margin of the Hazelton trough, northern British Columbia. In: Miller, D.M. and Busby, C., (Eds.), *Jurassic Magmatism and Tectonics of the North American Cordillera*, Geological Society of America Special Paper 299, pp. 83-94.
- Tipper, H.W., and Richards, T.A., 1976. Jurassic stratigraphy and history of north-central British Columbia; Geological Survey of Canada, Bulletin 270, 73 p.
- Tozer, E.T. 1979. Latest Triassic ammonoid faunas and biochronology, western Canada. In: *Current Research, Part B*, Geological Survey of Canada Paper 79-1B, pp. 127-135.
- Wotzlaw, J-F., Goex, J., Bartolini, A., Galley, Y., Krystyn, L., McRoberts, C.A., Taylor, D., Schoene, B., and Schaltegger, U., 2014. Towards accurate numerical calibration of the Late Triassic: High-precision U-Pb geochronology constraints on the duration of the Rhaetian. *Geology* 42, 571-574.

Late Early to Middle Jurassic Hazelton Group volcanism and its tectonic setting, McBride River area, northwest British Columbia



Bram I. van Straaten^{1, a} and Sebastian Bichlmaier¹

¹ British Columbia Geological Survey, Ministry of Energy, Mines and Petroleum Resources, Victoria, BC, V8W 9N3

^a corresponding author: Bram.vanStraaten@gov.bc.ca

Recommended citation: van Straaten, B.I., and Bichlmaier, S., 2018. Late Early to Middle Jurassic Hazelton Group volcanism and its tectonic setting, McBride River area, northwest British Columbia. In: Geological Fieldwork 2017, British Columbia Ministry of Energy, Mines and Petroleum Resources, British Columbia Geological Survey Paper 2018-1, pp. 39-66.

Abstract

Continued mapping and geochronologic studies on the northeast margin of Stikinia east of Dease Lake indicate that Late Triassic plutonic rocks of the Cake Hill pluton are unconformably overlain by late Early to Middle Jurassic rocks in the upper part of the Hazelton Group. The unconformity, which has been traced laterally for 50 km, spans at least 30 m.y. and represents one of the few examples of unroofed Stuhini arc in northern Stikinia. The unconformity is overlain by sedimentary rocks of the Spatsizi Formation (up to 0.2 km thick, Toarcian) and volcanic rocks of the Horn Mountain Formation (at least 3.5 km thick, Aalenian-Bajocian). The recently-defined Horn Mountain Formation is unusual because it postdates typical Late Triassic to Early Jurassic arc volcanism in northern Stikinia, and was deposited during accretion of the Stikine and Cache Creek terranes. In the lower part of the Horn Mountain Formation, partly or wholly subaqueous, massive green augite-plagioclase-phyric volcanic breccia pass upward to a subaerial volcanic edifice composed of interlayered maroon augite-plagioclase-phyric flows, volcanic breccia and tuff. Felsic volcanic rocks cap the succession. The Horn Mountain Formation is cut by the Three Sisters pluton (ca. 173-169 Ma, Aalenian-Bajocian) and McBride River pluton. The McBride River granodiorite has hitherto been interpreted as Early Jurassic (ca. 184 Ma), but based on crosscutting relationships we suggest a Middle Jurassic or younger age to be more plausible. The Bowser Lake Group (Bajocian) conformably overlies the Horn Mountain Formation; it records initiation of erosion from the Stikinia-Cache Creek tectonic welt. Chert and limestone clast-bearing pebble to cobble conglomerate (>330 m thick) is interpreted to have formed close to range front faults along the building orogen. The coarse clastic facies transitions to interbedded subaerial siltstone, sandstone, chert clast-bearing conglomerate, and mafic flows (>430 m thick) farther south. In the northern part of the study area, the Horn Mountain Formation and Bowser Lake Group are structurally overlain by rocks of the Whitehorse trough, juxtaposed along the Kehlechoa thrust fault (south vergent). In the hanging wall, Sinwa Formation limestones (Upper Triassic) are unconformably overlain by Takwahoni Formation sedimentary rocks (Lower Jurassic). The Takwahoni Formation succession comprises a lithologically variable unit of fine-grained siliciclastic rocks, polymictic conglomerate and volcanic rocks (Sinemurian?) that appears to grade upward to a thick unit of interbedded sandstone and siltstone (Pliensbachian). In the northernmost part of the map area, rocks of the Whitehorse trough are structurally overlain by rocks of the Cache Creek terrane along the King Salmon thrust fault (south vergent).

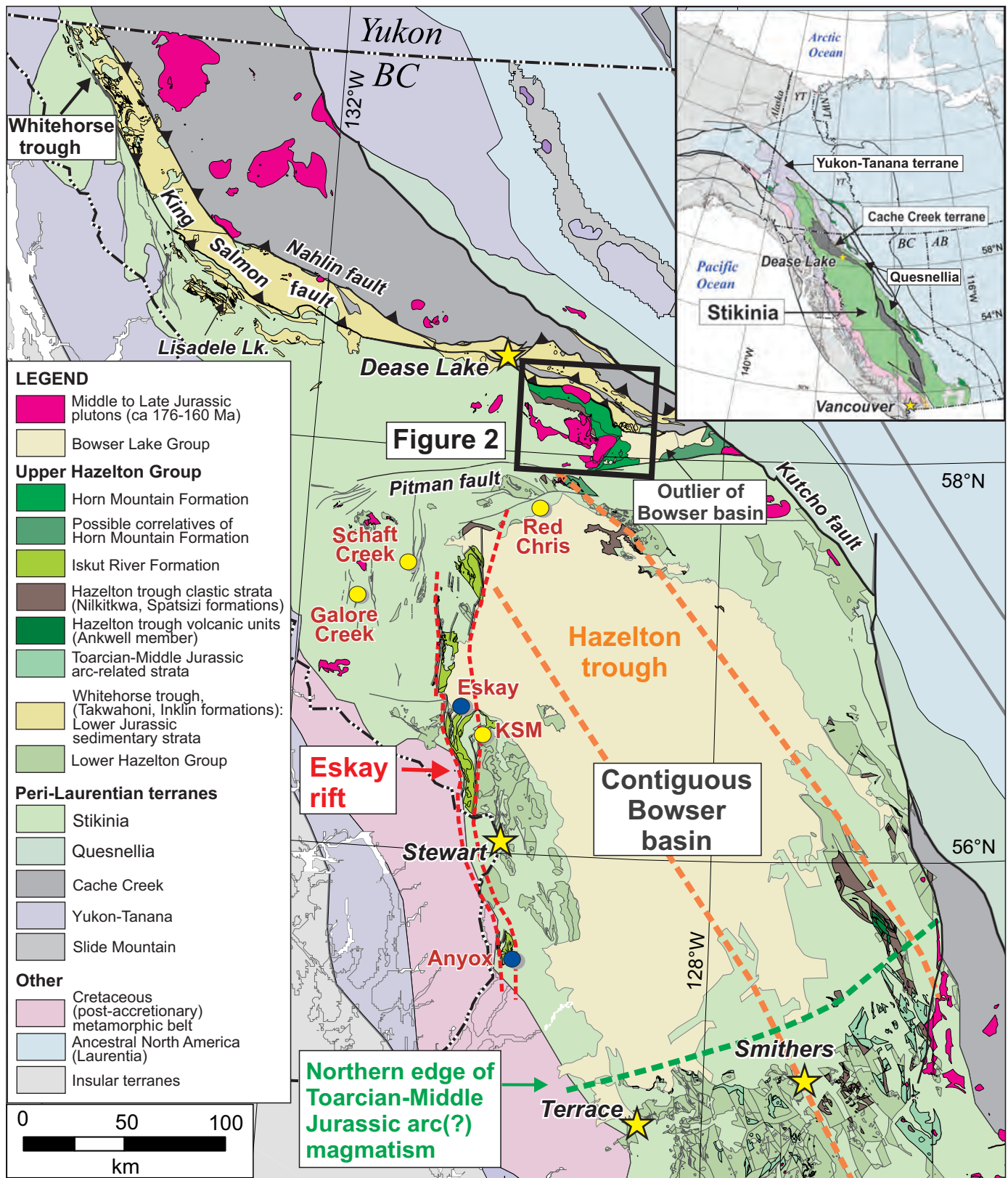
At Tanzilla and McBride, northwest of the study area, the Horn Mountain Formation hosts large advanced argillic alteration systems. However in the present area, evidence of alteration and mineralization is more modest. Four grab samples from two intrusion-related hydrothermal alteration zones west and southeast of the McBride River returned no anomalous metal values. Several Cu-Ag mineral occurrences with limited alteration footprints are hosted in the middle and upper part of the Horn Mountain Formation in the southeast part of the map area. Polymetallic veins near the Kehlechoa and King Salmon thrust faults locally contain significant gold and silver.

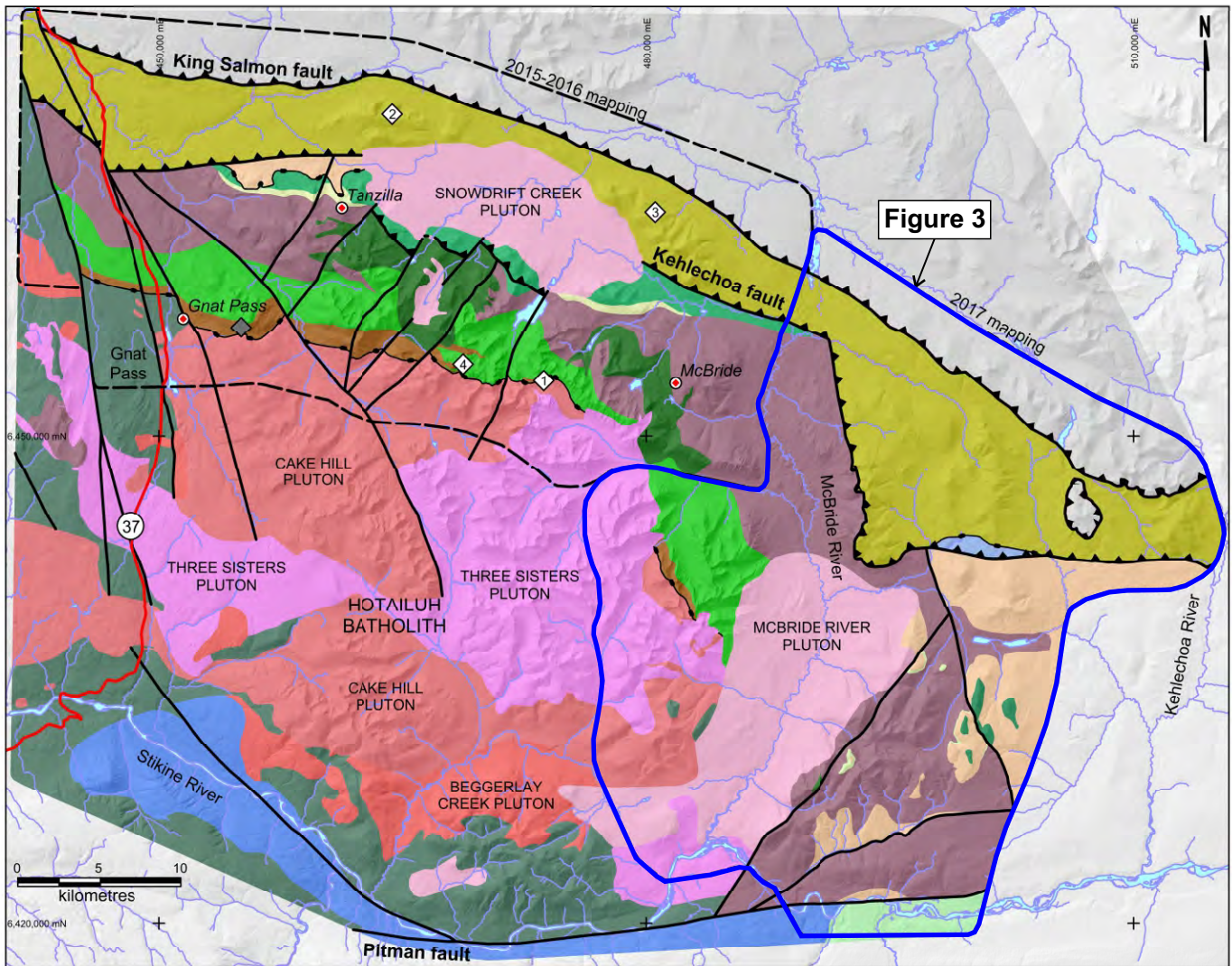
Keywords: Horn Mountain Formation, Spatsizi Formation, Hazelton Group, Bowser Lake Group, Stuhini Group, Cake Hill pluton, Three Sisters pluton, McBride River pluton, Hotailuh batholith, Takwahoni Formation, Sinwa Formation, Kehlechoa fault, Jurassic, McBride River, Tanzilla, Stikine terrane

1. Introduction

This paper presents the results of the third year of a mapping project focussed on an unusual volcano-sedimentary succession southeast of Dease Lake (northern Stikinia; Fig. 1). Before this project, the succession was poorly understood. Part of it was assigned to the Takwahoni Formation (Lower Jurassic), part to the Stuhini Group (Triassic), and part to Triassic-Jurassic volcanic rocks that could correlate with either the Stuhini Group or the Hazelton Group (Gabrielse, 1998). Detailed mapping by van Straaten and Nelson (2016) directed

at understanding the host rocks of large hydrothermal alteration zones at Tanzilla (Fig. 2), identified a sedimentary succession (up to 1 km thick) overlain by a volcanic succession (ca. 5.4 km thick). They found the units to be late Early to Middle Jurassic, and defined the volcanic unit as the Horn Mountain Formation (part of the upper Hazelton Group). Mapping in 2016 extended the along-strike length of this succession from Gnat Pass to the McBride River (Fig. 2; van Straaten and Gibson, 2017; van Straaten et al., 2017). The Horn Mountain Formation is unusual because it postdates typical Late Triassic to Early Jurassic





Legend

Overlap

Cretaceous

Sustut Group

Middle(?) - Late Jurassic

Snowdrift Cr., McBride R. pluton
granodiorite, diorite

Cache Creek

Paleozoic - Jurassic

Cache Creek terrane

King Salmon fault

Whitehorse trough

Early Jurassic

Takwahoni Formation

Late Triassic

unconformity

Sinwa limestone

Kehlechoa fault

Stikinia

Middle Jurassic

Three Sisters pluton
quartz diorite, quartz monzonite, granite

Bowser Lake Group

Mafic volcanic rocks

Sedimentary rocks

Horn Mountain Formation

Upper mafic volcanic rocks

Upper felsic volcanic rocks

Early-Middle Jurassic

Horn Mountain Formation

Subvolcanic mafic intrusive

Middle maroon volcanic rocks

Lower(most) mafic volcanic rocks

Spatsizi Formation

Sedimentary rocks

unconformity

Stikinia (cont.)

Late Triassic

Cake Hill pluton
quartz monzodiorite, granite

Gnat Lakes, Beggerlay Cr. pluton
gabbro, ultramafite

Triassic

Stuhini Group

Paleozoic

Stikine assemblage

Mineral occurrence

Geochronology sample
This study; Iverson et al., 2012

Highway

UTM Zone 9 NAD83
Parts of NTS 104H, 104I

Fig. 2. Regional geology. Modified after Read and Psutka (1990), Gabrielse (1998), van Straaten et al. (2012, 2017). See Figure 1 for location.

volcanic arc successions in northern Stikinia, formed during accretion of the Stikine and Cache Creek terranes, and occupies a position adjacent to their suture (van Straaten and Nelson, 2016). Between the Tanzilla gossan and the McBride River, the Horn Mountain Formation hosts several porphyry- and epithermal-style mineral occurrences attributed to a Middle Jurassic magmatic-hydrothermal event. The syncollisional Middle Jurassic magmatic event represents a potential new metallogenic epoch for the Canadian Cordillera and is prospective for porphyry- and epithermal-style mineralization (van Straaten and Nelson, 2016).

Herein we present the results of two months of 1:20,000-scale mapping carried out by two field teams along the McBride River, representing an eastward continuation of work carried out in 2015 and 2016 (Fig. 3). We demonstrate continuity of the Spatsizi and Horn Mountain formations to a strike length of at least 80 km. We show the Horn Mountain volcanic rocks to be conformably overlain by largely subaerial synorogenic siliciclastic strata of the Bowser Lake Group. This contact records the interaction between Middle Jurassic (Bajocian) volcanism and initial debris shed from the Stikinia-Cache Creek tectonic welt, and provides further evidence for the syncollisional nature of the volcanic rocks.

2. Geological setting

The study area is in the Intermontane belt of the Canadian Cordillera, near the northeastern margin of the Stikine terrane (Stikinia; Fig. 1). Stikinia represents a multi-episodic volcanic island arc complex that accreted to ancestral North America during the Middle Jurassic (Nelson and Mihalynuk, 1993; Mihalynuk et al., 1994; Evenchick et al., 2007; Nelson et al., 2013). Volcanic and sedimentary rocks of the Stikine assemblage (Devonian to Permian), basement to Stikinia, are overlain by volcanic and related sedimentary rocks of the Stuhini Group (Triassic) and the Hazelton Group (Early to Middle Jurassic; Tipper and Richards, 1976; Marsden and Thorkelson, 1992). Also in the Intermontane belt, the Quesnel terrane (Quesnellia), is a volcanic island arc with a similar Devonian to Early Jurassic history. The two volcanic arcs are separated by the Cache Creek terrane, an accretionary complex of oceanic crustal rocks, primitive arc ophiolites, pelagic rocks, carbonate rocks, and blueschists (Fig. 1). The northeastern margin of Stikinia and adjacent Cache Creek terrane are covered by Lower Jurassic siliciclastic rocks of the Whitehorse trough (Fig. 1; Colpron et al., 2015). Accretion of Stikinia to the Cache Creek terrane, Quesnellia, and ancestral North America is recorded by deposition of Bowser Lake Group siliciclastic rocks (Middle Jurassic) in a foreland basin atop Stikinia (Evenchick et al., 2007). Combined, Stikinia and Quesnellia host most of the porphyry copper deposits in the Canadian Cordillera (Logan and Mihalynuk, 2014).

In the present study area (Figs. 2, 3), we recognize two successions in the upper part of the Hazelton Group that extend southeast from areas mapped by van Straaten and Nelson (2016) and van Straaten and Gibson (2017); the

Spatsizi Formation, a predominantly sedimentary unit and the Horn Mountain Formation, a predominantly volcanic unit conformably above the Spatsizi Formation. These units form a westerly trending belt, about 80 km long and 10 km wide, north and east of the Hotailuh batholith, along the northeastern edge of Stikinia (Figs. 1, 2). Both units unconformably overlie Late Triassic rocks of the Cake Hill pluton. Prior to this project, the sedimentary rocks were mapped as the Takwahoni Formation (Lower Jurassic), structurally overlain by volcanic rocks of the Stuhini Group (Triassic) and an undivided Triassic-Jurassic unit above an inferred thrust (Hotailuh fault; Anderson, 1983; Gabrielse, 1998). The area east of the McBride River was previously interpreted as undivided Triassic-Jurassic and Lower Jurassic volcanic rocks (Gabrielse, 1998); the latter based on a four-point Rb-Sr whole rock isochron age of 191 ± 9 Ma from rocks near Mount Sister Mary (Erdman, 1978). However, rocks previously mapped as part of the Takwahoni Formation contain an Early to Middle Jurassic detrital zircon population (ca. 176 Ma peak; Iverson et al., 2012) and the contact between the Spatsizi Formation and the overlying volcanic rocks is conformable, not structural (van Straaten et al., 2012; van Straaten and Nelson, 2016), thus removing the need for the putative Hotailuh thrust (Fig. 2). These Hazelton Group units are bounded to the north by the Kehlechoa thrust fault, which separates it from rocks of the Whitehorse trough (Takwahoni Formation), to the west by the Gnat Pass fault, and to the east by overlying siliciclastic strata of the Bowser Lake Group. Farther north, Cache Creek terrane rocks in the hanging wall of the south-verging King Salmon thrust structurally overlie the Takwahoni Formation (Fig. 2).

3. Lithostratigraphic units

Rocks in the study area lie within three tectonostratigraphic domains that are separated by two north-dipping thrust faults; the Kehlechoa fault in the south and the King Salmon fault in the north. Stratigraphic units in the footwall of the Kehlechoa fault are part of Stikinia; those in between the Kehlechoa and King Salmon faults are part of the Whitehorse trough; those in the hanging wall of the King Salmon fault are part of the Cache Creek terrane (Figs. 3, 4; Table 1). In the following descriptions we use classifications for sedimentary rocks from Hallsworth and Knox, (1999) and for igneous rocks from Gillespie and Styles (1999).

3.1. Stikinia

3.1.1. Stikine assemblage (Paleozoic)

Dark green phyllitic greenstone and light green phyllite assigned to the Stikine assemblage are exposed south of the Pitman fault (Fig. 3; Read and Psutka, 1990).

3.1.2. Stuhini Group (Triassic)

A 0.5 km block or roof pendant of dark green augite-plagioclase porphyry and mafic volcanic breccia is enclosed within the Cake Hill pluton in the southwest part of the map area (Fig. 3; van Straaten et al., 2012). A body of mafic volcanic

Table 1. Summary of volcano-sedimentary units on Stikinia and within the Whitehorse trough, excluding overlap assemblages. Mineral abbreviations after Kretz (1983).

Age	Unit	Description	Position
Early Jurassic	Laberge Group	<p>Greywacke (JLTgw): Alternating medium to thick beds of fine- to medium-grained feldspathic wacke to feldspathic arenite (70-100%) and thin to medium beds of internally massive to locally laminated siltstone (0-30%). Sandstone contains 20-70% subangular to euhedral Pl, 5-10% round to subround Qtz, and occasional argillite rip-up clasts. Moderately resistant, grey to orange weathering. Contains early Pliensbachian, late Pliensbachian fossils (Gabrielse, 1998), late Sinemurian-early Pliensbachian and possibly early Pliensbachian fossils (T. Poulton, pers. comm., 2017).</p> <p>Lower unit; ~3000 m thick. Contains 8 (late) Sinemurian, 1 late Pliensbachian, 1 late Pliensbachian-early Toarcian and 5 Toarcian fossil collections (Gabrielse, 1998).</p> <p>Argillite, siltstone and sandstone facies (JLTs): Laminated to thin-bedded argillite, siltstone and very fine- to fine-grained sandstone. Rare medium-grained feldspathic arenite. Very recessive, mostly observed as dark grey weathering angular scree.</p> <p>Volcaniclastic sandstone facies (JLTsv): Interbedded fine- to medium-grained volcaniclastic sandstone, very fine- to medium-grained sandstone and siltstone. Volcaniclastic sandstone is moderately sorted and contains very fine-, fine- and medium-grained sand-sized subangular to euhedral Pl (80%), black mafic grains (15%), Qtz (5%) and locally minor microphenocrystic volcanic clasts. Lesser crystal tuff, lapilli-tuff and lapillistone with subangular volcanic clasts containing 40-60% equant Pl (0.5-3 mm) and 20% equant and elongate black mafic crystals (0.5-2 mm). Rare pebble conglomerate with limestone, volcanic and/or Qtz clasts. Rare coarse- to very coarse-grained sandstone. Locally common mud- to siltstone rip-up clasts. Recessive to locally moderately resistant, dark grey weathering.</p> <p>Mafic volcanic facies (JLTv): Massive lapillistone, lapilli-tuff and tuff breccia with subangular volcanic clasts containing 30-50% euhedral equant Pl (3-5 mm) and 20% equant to elongate black mafic crystals (Aug and possibly Hbl; 1-3 mm). Interbedded with siltstone, very fine- to fine-grained sandstone and fine- to medium-grained volcaniclastic sandstone. Latter contains predominantly subangular to euhedral Pl, minor mafic grains and rare Qtz. Rare polymictic conglomerate with volcanic and limestone clasts. Resistant, orange-grey weathering.</p> <p>Conglomerate facies (JLTcg): Polymictic pebble to cobble to rare boulder conglomerate with light grey limestone clasts (locally up to 1 m), (sub)volcanic clasts (35-40%, 2-20 mm, euhedral equant Pl; 15%, 1-3 mm equant to elongate mafic crystals), plutonic clasts (equigranular, 1-4 mm, leucocratic tonalite (?); equigranular, 1-2 mm, Hbl diorite; Qtz-porphyratic, 3-4 mm, Hbl Qtz diorite) and white to light grey Qtz clasts. Lesser poorly sorted sandstone, granule conglomerate and monomictic (limestone) pebble to boulder conglomerate. Interbedded with argillite, siltstone and very fine- to fine-grained sandstone. Minor lapilli-tuff, lapillistone and tuff breccia (similar to JTLv). Conglomerate weathers in positive relief relative to enclosing fine-grained rocks. Mostly resistant, orange grey to dark grey to light grey weathering.</p> <p>Limestone (uTrSs); ≥400 m thick. Massive recrystallized limestone; where less recrystallized the protolith is a wackestone to packstone with abundant fossil fragments (0.1-2 cm) in a lime mud matrix. Resistant, light grey weathering. Contains upper Norian conodonts (Gabrielse, 1998).</p>	Whitehorse trough
Late Triassic	Sinwa Fm.	<p>Undivided sedimentary unit (mJBLs).</p> <p>Sedimentary facies 1; >430 m thick. Interbedded 1) recessive, maroon to greenish-grey laminated to thin-bedded siltstone to fine-grained sandstone, 2) recessive to moderately resistant, thin- to thick-bedded, internally massive to cross-bedded, maroon, light greenish grey to dark grey, medium- to very coarse-grained lithic arenite with abundant chert grains, 3) resistant, green-grey to orange-brown very thick-bedded chert pebble (to cobble) conglomerate with predominantly subrounded to rounded grey, white, reddish, greenish, brown, black radiolarian chert clasts and lesser (0-5%) medium grey limestone clasts in a medium-grained sand- to granule-sized matrix. Rare <1 m-thick maroon lapilli-tuff beds. Intercalated mafic flows (mJBLv) and lustrous black organic detritus (up to 1-4 cm) suggests subaerial deposition. Brown-grey very thinly laminated limestone bed (5-40 cm thick) near the base of the facies in the southwest.</p> <p>Sedimentary facies 2. "interbedded marine shale and greenish breccia, siltstone, and tuffaceous shale" (Gabrielse, 1998). Contains early Bajocian ammonites (Gabrielse, 1998).</p> <p>Conglomerate facies; >330 m thick. Medium to very thick, internally massive to locally fining upward beds of pebble (to cobble) conglomerate, interbedded with minor very thin to thin beds of medium-grained sandstone to granule conglomerate. Contains 50-95% rounded to subrounded light to dark grey, green and red radiolarian chert pebbles and 5-50% subrounded to rounded light grey limestone pebbles to cobbles. Contains woody fragments (Gabrielse, 1998). Resistant, orange-grey knobly weathering.</p>	Stikinia
Middle Jurassic	Bowser Lake Group		

Table 1. Continued.

Age	Unit	Description	Position
Middle Jurassic	Bowser Lake Group	<p>Mafic volcanic rocks (mJBLv); ≤60 m thick. Coherent rocks with 10-15% commonly brownish or reddish altered Aug (0.1-1 mm) and 30-50% Pl (0.1-0.2 mm). Generally found as 10-30 m thick stratiform units, commonly with narrow (20-30 cm thick) brecciated bottoms and tops, indicating they are flows. Locally, the base has moderately well-developed columnar joints (0.5-0.75 m wide). Laminated, well-sorted tuff to lapillistone (clast-supported; with up to 3-4 mm volcanic clasts, generally with a matrix-deficient open framework) commonly underlies flows. In one location a flow is directly underlain and overlain by siltstone and sandstone (mJBLs). Minor lapilli-tuff and lapillistone with grey, green and reddish Aug-Pl-phyric clasts and chert granules to pebbles. Resistant; orangey-brown weathering (flows) to recessive, brownish-grey weathering (tuff, lapilli-tuff, lapillistone).</p> <p>Upper felsic volcanic rocks (mJHMUv); 0-100 m thick. Crudely to well-stratified felsic tuff, lapilli-tuff, lapillistone, tuff breccia and breccia. Contains maroon, creamy orange, light grey, white, creamy green and brick red Pl-phyric and lesser aphyric clasts; common flow-banded and rare spherulitic clasts. Stratiform maroon to cream, flow banded, Pl-phyric coherent intervals (~5-50 m thick) are generally directly underlain and overlain by lapillistone, tuff breccia and breccia with clasts that have identical textures, suggesting these coherent intervals represent felsic flows. Rare welded lapilli-tuff. Clasts and coherent rocks contain 10-25% equant to rectangular Pl (0.5-2 mm). Rarely contains minor grey limestone clasts. Moderately resistant; weathers light grey, maroon, pale green.</p> <p>Middle maroon volcanic rocks (lmJHMMv); >1500 m thick. Interlayered flows, volcanic breccia, tuff breccia, lapillistone, lapilli-tuff and tuff. Aug-Pl-phyric flows (maroon to maroonish-grey to greyish-green, 5-20 m thick) transition to monomictic autoclastic breccia. Flows are locally amygdaloidal; their texture and composition ranges from 1) fine-crystalline with 25-30% lath-shaped Pl (0.5 x 2 mm) and 5-15% equant Aug (0.5 mm), to 2) medium-crystalline with 20-35% stubby Pl (1-2 mm x 2-4 mm), 5-10 % equant to rare elongate Aug (?; 1 mm), and up to 7% microdiorite xenoliths, to 3) rare coarse-crystalline with 40% Pl (1-2 mm) and 30% Aug (2-10 mm). Crudely stratified maroon to brick red tuff, crystal tuff, lapilli-tuff. Maroon lapillistone, tuff breccia, breccia contains varicoloured (maroon, green, grey, brick red) subangular Aug-Pl-phyric clasts and lesser aphyric clasts in a matrix with abundant angular to euhedral Pl. Minor well-stratified volcaniclastic siltstone to very fine- to coarse-grained volcaniclastic sandstone (with common angular to euhedral Pl) interbedded with tuff and lapilli-tuff. Minor felsic tuff, lapilli-tuff, lapillistone, volcanic breccia and a felsic flow. Rare welded lapilli-tuff. Resistant, dark grey, maroonish grey to brick red weathering.</p>	Stikinia
Early-Middle Jurassic	Upper part of Hazelton Group	<p>Lower mafic volcanic rocks (lmJHMLv); ≥2000 m thick. Massive, monomictic volcanic breccia to tuff breccia; predominantly clast supported. Subangular grey, greyish green and green clasts (0.5-100 cm) contain 15-25% Aug (0.5-7 mm) and 20-60% equant to lath-shaped Pl (0.2-2.5 mm). Rare tuff, crystal tuff, and volcaniclastic sandstone beds. Locally, the base of the unit contains Aug-Pl-phyric coherent rocks, commonly with <5 mm wide very fine-grained dark grey irregular to wispy bands and minor in-situ brecciated domains grading into volcanic breccia; these may represent local flows and flow-margin autobreccias. Very resistant and cliff-forming; greenish grey weathering.</p> <p>Lower volcaniclastic sandstone (lmJHMLvs); 0-60 m thick. Thin- to medium-bedded (commonly wavy) volcaniclastic sandstone (locally calcite-cemented), laminated siltstone, and crystal tuff. Sandstone contains abundant angular to subangular Pl grains. Fairly recessive, tannish grey weathering.</p> <p>Lower felsic volcanic rocks (lmJHMLvf); 0-20 m thick. Felsic lapillistone, lapilli-tuff and lesser tuff, tuff breccia and breccia. Contains predominantly angular to subangular white, cream to greenish-grey aphanitic to Pl-phyric felsic clasts, locally subordinate mafic volcanic clasts, and rare Qtz-phyric or flow-banded felsic clasts. Resistant, yellowish grey weathering.</p>	Horn Mountain Formation
	Spatzi Formation	<p>Argillite, siltstone and sandstone (lmJSPs); ~0.2 km thick. Interbedded laminated siltstone and thin- to medium-bedded fine- to medium-grained sandstone. Fining upward, internally massive to locally laminated sandstone beds with scoured bases generally grade upward into parallel laminated sandstone. Generally silicified. Local small-scale syn-sedimentary faults. Thick- to very thick-bedded, medium- to coarse-grained feldspathic arenite with abundant Pl, 10-20% Qtz and ~5% mafic grains; locally contains minor white felsic (?) clasts. Rare mafic tuff and tuff breccia with Aug-Pl-phyric volcanic clasts. Recessive to moderately resistant, rusty brown weathering. Contains Toarcian fossils (Gabrielse, 1998).</p> <p>Basal sandstone and conglomerate (lmJSPcg); 20-50 m thick. Thin- to medium-bedded, medium- to very coarse-grained feldspathic arenite (locally calcite-cemented) with 20-40% Qtz grains; Qtz-rich granule conglomerate with granitic pebbles. Moderately resistant, light grey weathering.</p>	

rocks 2 km to the southeast is interpreted as Stuhini Group (after Gabrielse, 1998), but could also be part of the Horn Mountain Formation.

3.1.3. Hazelton Group (Lower to Middle Jurassic)

Volcano-sedimentary rocks in the upper part of the Hazelton Group are exposed on both sides of the McBride River (Fig. 3). We divide them into a lower sedimentary succession (Spatsizi Formation; up to 0.2 km thick), and a conformably overlying, mainly volcanic succession (Horn Mountain Formation; at least 3.5 km thick; Fig. 4). On the west flank of Peak 2102 m, the Spatsizi Formation unconformably overlies the Cake Hill pluton (Late Triassic); southeast of the peak, the Horn Mountain Formation unconformably overlies the Cake Hill pluton. Elsewhere in the western part of the map area, the stratigraphic level occupied by the unconformity, Spatsizi Formation and lower part of the Horn Mountain Formation is cut by the Three Sisters pluton (Middle Jurassic). In the eastern part of the map area, the middle and upper part of the Horn Mountain Formation is conformably overlain by the Bowser Lake Group

3.1.3.1. Spatsizi Formation

The Spatsizi Formation (defined by Thomson et al., 1986 and modified by Evenchick and Thorkelson, 2005 and Gagnon et al., 2012) is exposed in a 0.6 by 5 km area centered on Peak 2102 m in the western part of the map area (Fig. 3). It unconformably overlies the quartz-rich phase of the Cake Hill pluton (Late Triassic; Section 4.1.), and is conformably overlain by volcanic rocks of the Horn Mountain Formation. In the present map area, we recognize a basal sandstone and conglomerate unit (20–50 m thick), and an overlying argillite, siltstone, and sandstone unit (~0.2 km thick; Table 1), similar to subdivisions along strike to the northwest in the adjoining map area (van Straaten and Gibson, 2017).

The unconformity above hornblende granodiorite of the Cake Hill pluton is defined on the west flank of Peak 2102 m. After a covered interval of 1.5 m, coarse- to very coarse-grained quartz-rich feldspathic arenite and granule conglomerate with granitic pebbles (Fig. 5a) appear. Calcic exoskarn is commonly observed in calcareous sandstone near the contact, and locally adjacent to felsic dikes that cut the Spatsizi argillite, siltstone and sandstone unit. The skarn consists of brown garnet and green diopside bands alternating with cream-coloured bands containing minor epidote. Late Early to Middle Jurassic felsic intrusions (unit EMJf or MJTSgr, see Sections 4.2., 4.3.) were likely responsible for skarn development and we speculate that the flow of metasomatic fluids may have focussed along the anisotropy provided by the unconformity. Geochronological results from the hornblende granodiorite (216.2 ± 1.2 Ma, van Straaten et al., 2012), and ammonite collections from the Spatsizi Formation in the map area (Toarcian, Gabrielse, 1998) and fossils along strike to the west-northwest (late Pliensbachian to Toarcian, van Straaten et al., 2017) indicate a significant hiatus across the unconformity. Consistent with the

interpretation of an unconformity, grain size in the granodiorite does not decrease towards the contact, granodiorite dikes are lacking in the Spatsizi Formation, and the contact lacks evidence of a fault.

Crudely bedded medium- to very coarse-grained quartz-rich feldspathic arenite and granule conglomerate with granitic pebbles in the basal unit (Fig. 5a) grade upward to a unit of argillite, siltstone, and sandstone (Fig. 5b). Abundant incomplete Bouma-like sequences include fining upward, internally massive to locally laminated sandstone beds with scoured bases that generally grade upward into parallel laminated siltstone. These sandstone-siltstone couplets are interpreted as subaqueous mass flow deposits. Interbedded argillite, siltstone and very fine- to medium-grained sandstone are generally strongly silicified and contain 5–10% disseminated pyrite (Section 7.1.). The unit also includes thick to very thick feldspathic arenite beds, and rare mafic volcanic rocks.

The base of the Spatsizi Formation marks the change from latest Triassic - Early Jurassic uplift and erosion of northern Stikinia to late Early Jurassic subsidence and sedimentation. The basal unconformity represents one of the few well-documented examples of the pre-late Early Jurassic unroofing of a Triassic pluton in northern Stikinia. The associated hiatus spans at least 30 m.y. (Fig. 4), a period of time that saw widespread lower Hazelton Group volcanism and the latest Triassic and Early Jurassic porphyry copper metallogenic epochs farther south (e.g., Galore Creek, Red Chris, KSM; Logan and Mihalynuk, 2014). The unconformity in the Dease Lake area contrasts with the latest Triassic sub-Hazelton Group unconformity in the south, which spans <5 m.y. (Nelson et al., 2018). Regionally, the Spatsizi Formation is correlated with the predominantly siliciclastic Nilkitkwa Formation east and northeast of Smithers (Marsden and Thorkelson, 1992). The north-northwest trend of the Spatsizi and Nilkitkwa formations records Pliensbachian to Toarcian marine sedimentation in a back-arc or intra-arc depression (Hazelton trough, Fig. 1; Tipper and Richards, 1976; Marsden and Thorkelson, 1992; Gagnon et al., 2012).

3.1.3.2. Horn Mountain Formation

Herein, we significantly expand the known along-strike extent of the Horn Mountain Formation (defined by van Straaten and Nelson, 2016) to 80 km. This predominantly volcanic succession displays relatively consistent stratigraphy and lithological characteristics along its strike length. In the McBride River study area, we recognize three subdivisions that are similar to those in the adjoining map area to the northwest (van Straaten and Gibson, 2017); the lower mafic volcanic unit, the middle maroon volcanic unit and the upper felsic volcanic unit (Fig. 4, Table 1). The lowermost volcanic units and the upper mafic volcanic unit of van Straaten and Gibson (2017) were not observed in the study area.

West of the McBride River, moderately northeast-dipping volcanic rocks of the Horn Mountain Formation conformably overlie the Spatsizi Formation. Here, the Horn Mountain lower mafic volcanic unit is overlain by the middle maroon volcanic

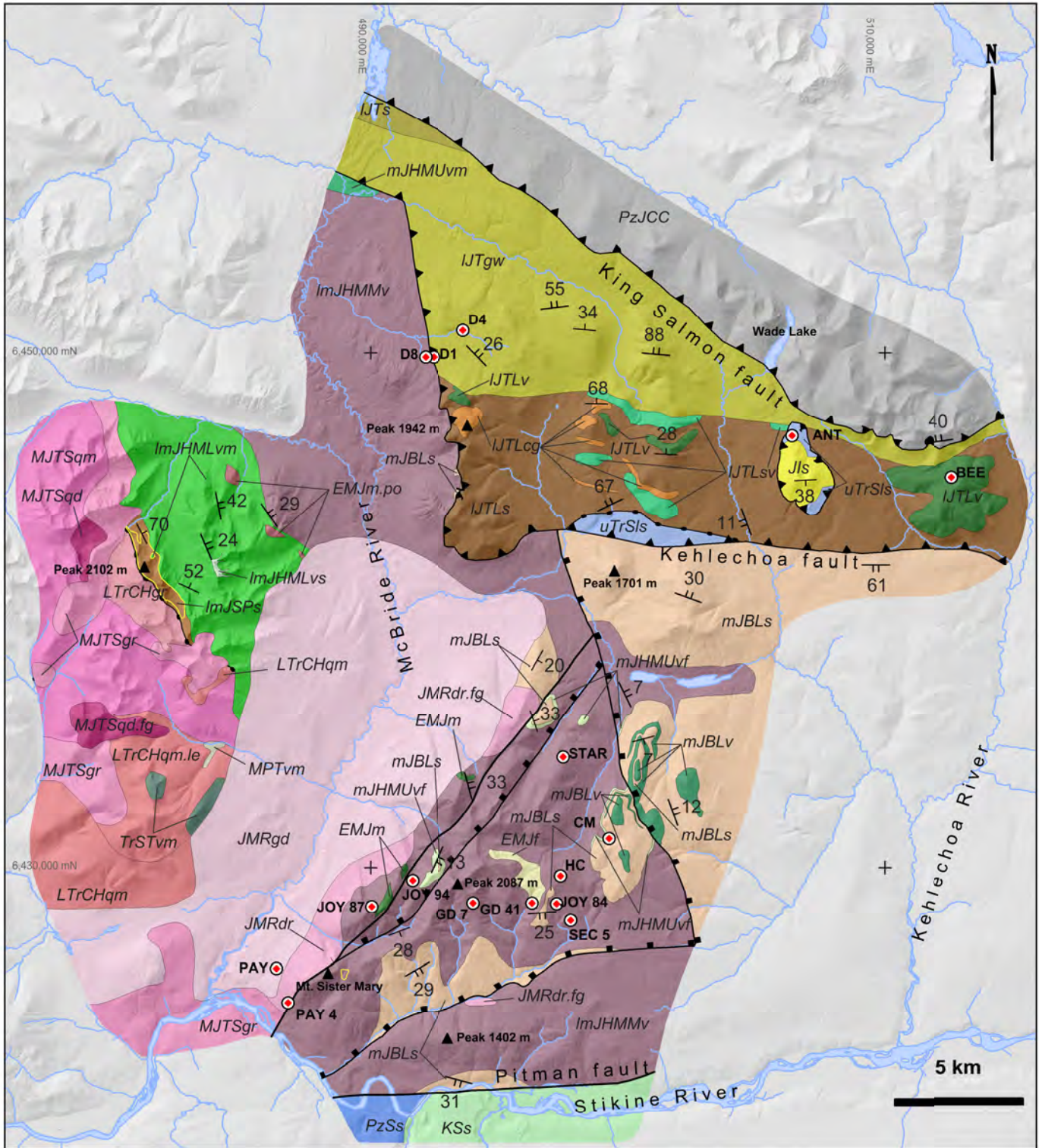


Fig. 3. Geologic map of field area. See Figure 2 for location.

unit with an apparent conformable contact. Along the McBride River, the Horn Mountain Formation is cut by the McBride River pluton (Middle Jurassic or younger, Section 4.4.). East of the McBride River, the Horn Mountain Formation is moderately to gently southeast-, east- and northeast-dipping to subhorizontal, and cut by north-northeast to north-northwest

trrending faults (Section 5.1.). Here, the formation comprises the middle maroon volcanic unit, which is generally overlain by the upper felsic volcanic unit; both are conformably overlain by sedimentary rocks of the Bowser Lake Group in the north, east and south (Fig. 3).

Stratified rocks

Overlap assemblages

Miocene-Pleistocene, Tuya Formation

MPTvm Olivine basalt

Cretaceous, Sustut Group

KSs Undivided

Stikinia

Middle Jurassic, Bowser Lake Group

mJBLs Sandstone, conglomerate and shale

mJBLv Mafic volcanic rocks

Lower to Middle Jurassic, upper Hazelton Group

Middle Jurassic, Horn Mountain Formation

mJHMUvm Upper mafic volcanic rocks

mJHMUvf Upper felsic volcanic rocks

Lower to Middle Jurassic, Horn Mountain Formation

ImJHMMv Middle maroon volcanic rocks

ImJHMLvm Lower mafic volcanic rocks

ImJHMLvs Lower volcanoclastic sandstone

Lower to Middle Jurassic, Spatsizi Formation

ImJSPs Argillite, siltstone and sandstone

Triassic, Stuhini Group

TrSTvm Mafic volcanic rocks

Paleozoic, Stikine assemblage

PzSs Undivided

Whitehorse Trough

Lower Jurassic, Laberge Group

Lower Jurassic, Takwahoni Formation

IJTs Siltstone

IJTgw Greywacke

Lower unit

IJTLsv Volcanoclastic sandstone

IJTLv Mafic volcanic rocks

IJTLs Argillite and siltstone

IJTLcg Conglomerate

Cache Creek

Paleozoic to Jurassic

PzJCC Undivided

Jurassic, Inklin Formation

JIs Sandstone and siltstone

Upper Triassic, Sinwa Formation

uTrSls Limestone

Intrusive rocks

Jurassic, McBride River pluton

JMRgd Hornblende-biotite granodiorite

JMRdr Hornblende-clinopyroxene(?) diorite

Middle Jurassic, Three Sisters pluton

MJTSgr Biotite monzogranite

MJTSqm Biotite quartz monzonite

MJTSqd Hornblende quartz diorite

Early to Middle Jurassic, Horn Mountain intrusions

EMJf Felsic intrusive

EMJm.po Platy plagioclase porphyry

EMJm Mafic intrusive

Late Triassic, Cake Hill pluton

LTrCHgr Hornblende monzogranite

LTrCHqm Hornblende quartz monzodiorite

 Bedding, tops known, right-way up

 Bedding, tops unknown

 Contact

 Unconformity

 Fault

 Reverse fault

 Normal fault

 Altered or gossanous rocks

 Peak

 MINFILE/mineral occurrence

UTM Zone 9 NAD83
Parts of NTS 104H/14, 15;
104I/02, 03, 06, 07

Fig. 3. Continued.

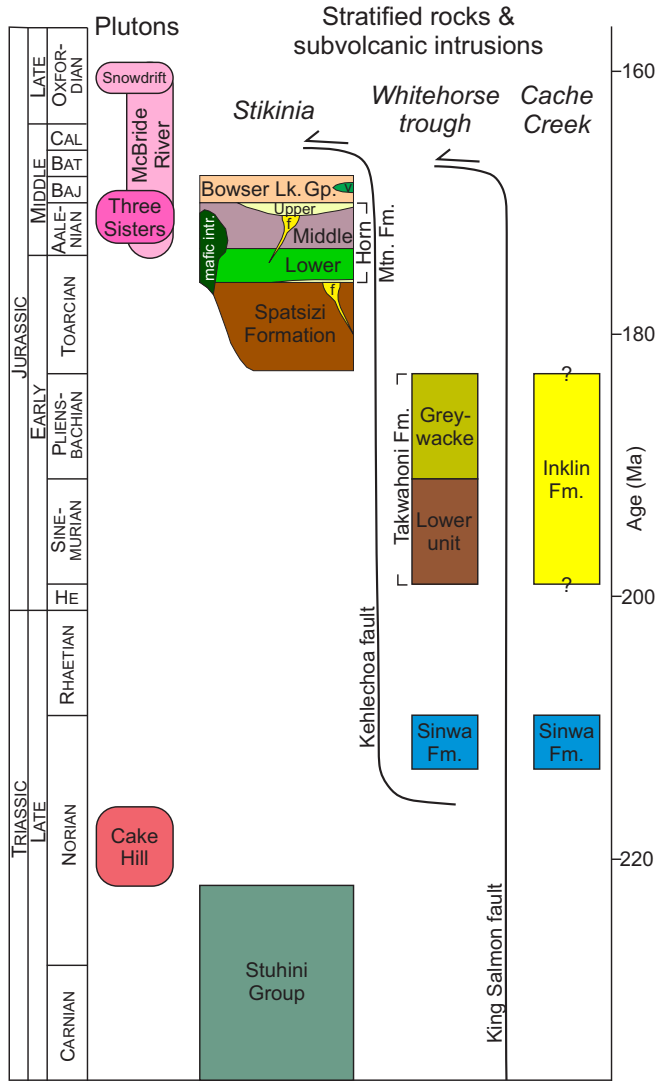


Fig. 4. Schematic stratigraphic, plutonic, and structural relationships for Triassic to Jurassic rocks in the map area. Abbreviations: felsic intrusive (f), Bowser Lake mafic volcanic rocks (v), Hettangian (He), Bajocian (Baj), Bathonian (Bat), Callovian (Cal). Chronostratigraphic ages from Cohen et al. (2013, updated February 2017).

The lower mafic volcanic unit is at least 2 km thick and consists predominantly of massive greenish-grey monomictic volcanic breccia to tuff breccia with augite-plagioclase-phyric clasts (Fig. 6a; Table 1). In most locations, the base of the unit is marked by a felsic volcanic subunit (up to 20 m thick; Fig. 6b). The lower contact of the unit is conformable, displaying gradational to locally sharp relationships with rocks in the upper part of the Spatsizi Formation. On the northwest ridge of Peak 2102 m, a ~5 m-thick gradational contact shows interfingering siltstone, sandstone and felsic volcanic rocks. In the valley east of Peak 2102 m, stratified sedimentary rocks (locally with m-scale intraclasts) were observed immediately below and above the felsic volcanic subunit. We consider that the unit was deposited subaqueously because similar lower Horn Mountain Formation units along strike to the northwest locally contain

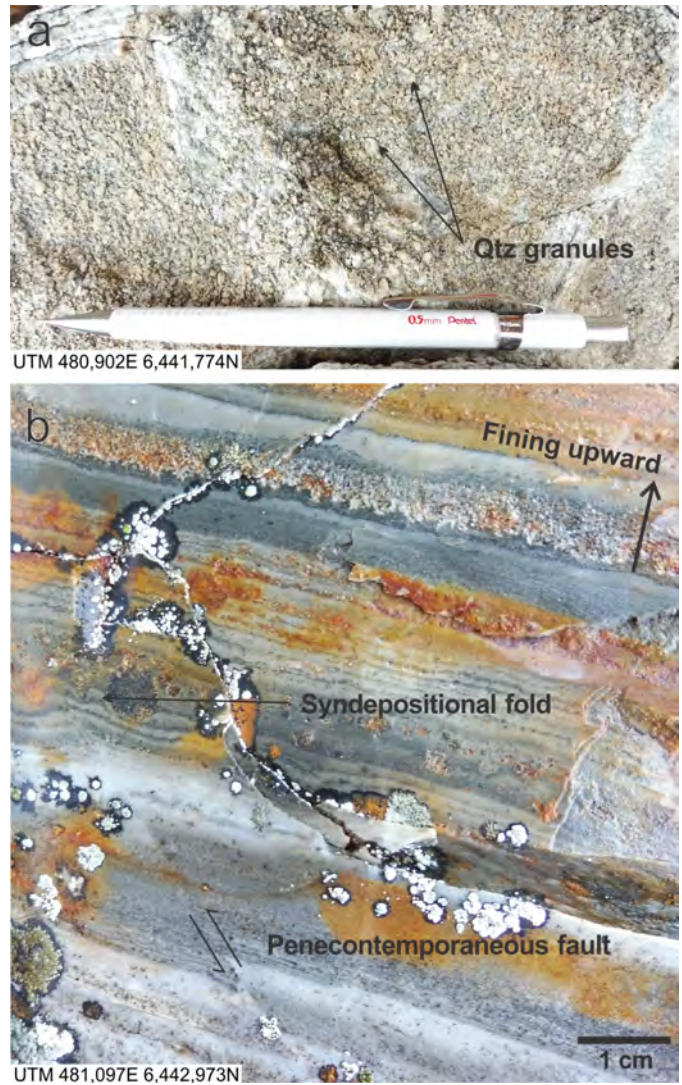


Fig. 5. Spatsizi Formation. **a)** Basal conglomerate unit (1mJSPcg). Granule conglomerate with quartz fragments in a very coarse sandstone matrix. **b)** Argillite, siltstone and sandstone unit (1mJSPs). Strongly silicified thinly laminated to thinly bedded siltstone and fine-grained sandstone.

pillows and interfinger with sedimentary rocks interpreted as submarine (van Straaten and Gibson, 2017). A mafic volcanic breccia with minor granitic clasts outcrops 5.3 km southeast of Peak 2102 m, ~400 m from the Cake Hill pluton. The contact was not observed, but it is likely unconformable. In the adjoining map area to the northwest, similar Horn Mountain granitic clast-bearing mafic volcanic breccias rest directly on the Cake Hill pluton (van Straaten and Gibson, 2017). Within the lower mafic unit, a volcanoclastic sandstone subunit (up to 60 m thick) was mapped 2.8 km east of Peak 2102 m; it is inferred to pinch out along a short distance.

The middle maroon volcanic unit contains interlayered mafic to intermediate lapilli-tuff, tuff, flows, lapillistone, tuff breccia and breccia (Fig. 7, Table 1). Clasts are augite-plagioclase-phyric, plagioclase-phyric and aphyric. The



Fig. 6. Horn Mountain Formation. **a)** Lower mafic volcanic unit (lmJHMLvm). Massive monomictic augite-plagioclase-phyric volcanic breccia to tuff breccia cut by a metre-scale subvolcanic mafic dike (EMJm). **b)** Lower felsic volcanic subunit (lmJHMLvf). Tuff breccia with felsic flow-banded clasts.

thickness of the unit is difficult to estimate due to a lack of marker units, truncation by the McBride River pluton, and poorly constrained offset along faults. It is at least 1.5 km thick, but may be significantly thicker. We interpret the bedding-parallel coherent intervals as flows because they 1) overlie and underlie breccias interpreted as flow-marginal autobreccias; 2) overlie red baked tuffs; and 3) gradationally overlie spatter deposits with rare cow-pat-shaped vesicular clasts. Delicate pumiceous clasts and welded lapilli-tuff suggest subaerial deposition. The unit contains minor 0.1-20 m-thick felsic volcanic intervals composed of tuff, lapilli-tuff, lapillistone and volcanic breccia. A 70 m-thick interval of felsic volcanic rocks, including a spherulitic to flow-banded felsic coherent rock interpreted as a flow, are 1.7 km north-northeast of Peak 2087 m. In one location near the base of the northwest ridge of Peak 2087 m we observed abundant limestone clasts in brick red tuff and lapilli-tuff. The broad ridge incorporating Peak 1402 m north of the Stikine River exposes a succession of rusty brown to maroon augite-plagioclase-phyric coherent rocks, brown weathering lapilli-tuff to lapillistone with plagioclase-phyric lapilli and local intervals (probable intrusions) of coarse platy plagioclase porphyry. We include this unit, designated as mJgv and mJvp by Read and Psutka (1990), within the middle

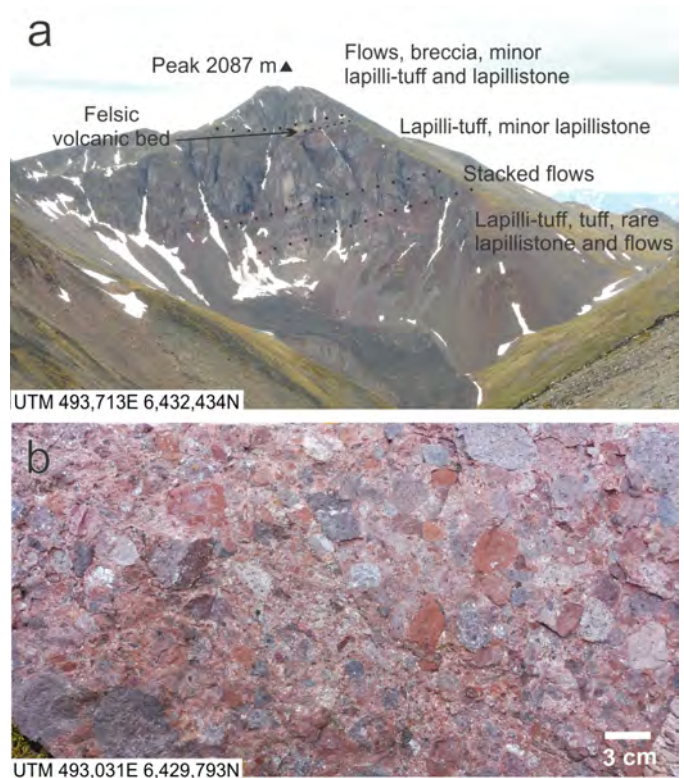


Fig. 7. Horn Mountain Formation, middle maroon volcanic unit (lmJHMMv). **a)** View of interlayered lapilli-tuff, tuff, flows, lapillistone, tuff breccia, breccia and rare felsic volcanic rocks on the north face of Peak 2087 m. **b)** Massive, clast-supported maroon lapillistone.

maroon volcanic unit. The lower contact of the middle maroon volcanic unit was not observed, but the presence of maroon lapilli-tuff to crystal tuff in the top of the lower mafic volcanic unit suggests that the contact is gradational.

The upper felsic volcanic unit is up to 100 m thick, and contains felsic tuff, lapillistone, tuff breccia, breccia and flows. Clasts are plagioclase-phyric to aphyric and commonly flow banded (Fig. 8). The unit thins to 2-4 m in the southwest, and is either absent or thin and recessive in the south and southeast. The lower contact is gradational based on the following



Fig. 8. Horn Mountain Formation, upper felsic volcanic unit (mJHMUvf). Tuff breccia with angular flow-banded felsic clasts.

observations. 1) On a ridge 2.9 km north-northeast of Peak 2087 m, maroon augite-plagioclase-phyric flows (middle maroon volcanic unit) are conformably overlain by felsic lapillistone with flattened pumices grading up to purple and white felsic tuff breccia with flow-banded clasts (upper felsic volcanic unit). 2) Two kilometres north-northeast of the CM prospect, maroon crystal tuff and tuff (middle maroon volcanic unit) are overlain by felsic tuff breccia and a flow-banded felsic flow (upper felsic volcanic unit). 3) At the CM prospect, maroon to brick red crystal tuff and lapilli-tuff (middle maroon volcanic unit) are overlain by a 50 m-thick flow-banded purple and white felsic coherent rock (upper felsic volcanic unit).

3.1.4. Bowser Lake Group (Middle Jurassic)

Bowser Lake Group sedimentary rocks conformably overlie the Horn Mountain Formation east of the McBride River. We distinguish two sedimentary, one conglomerate and one volcanic facies (Table 1).

Sedimentary facies 1 (Table 1) is the most common in the map area, and comprises maroon to greenish-grey siltstone and sandstone (Fig. 9) with lesser chert clast-bearing conglomerate.



Fig. 9. Bowser Lake Group (mJBLs), sedimentary facies 1. Maroon laminated to thinly-bedded siltstone and fine-grained sandstone with local cross bedding.

Organic detritus and interbedded volcanic flows (see below) attest to subaerial deposition.

Minor volcanic rocks (mJBLv, Table 1) are found within sedimentary facies 1. They include augite-plagioclase-phyric coherent rocks (Fig. 10a) and subordinate mafic tuff, lapilli-tuff and lapillistone. In many instances the coherent rocks show brecciated lower and upper contacts, suggesting they are extrusive (Fig. 10b). These coherent rocks can be distinguished from mafic feeder dikes of the Horn Mountain Formation (EMJm, Table 2) by their smaller grain size and orangey-brown weathering colour. Laminated, very well-sorted tuff to lapillistone commonly underlie the flows and likely represent airfall deposits that preceded the effusive stage. In one location, we observed possible adhesion warts (Fig. 10c), which form by wind drifting sand across a damp surface (e.g., Olsen et al., 1989).

Gabrielse (1998) described “interbedded marine shale and greenish breccia, siltstone, and tuffaceous shale” containing early Bajocian ammonites on Peak 1701 m. Based on the predominantly fine-grained siliciclastic nature and submarine depositional environment, we assign these rocks to sedimentary facies 2 (Table 1). The facies likely includes poorly exposed fine-grained siliciclastic rocks in the northeast part of the map area near the Kehlechoa fault.

The conglomerate facies (Table 1) is exposed 3.5 km southeast of Peak 1701 m. It comprises a succession, at least 330 m thick, of chert ± limestone clast-bearing conglomerate with minor sandstone interbeds.

Light brown weathering chert clast-bearing pebble conglomerate and recessive, dark grey-to cream-weathering, laminated to very thinly bedded siltstone and very fine-grained sandstone is exposed along the north bank of the Stikine River. It is tentatively assigned to the Bowser Lake Group, but could also be part of the Sustut Group mapped by Read and Psutka (1990) across the Pitman fault to the south.

The lower contact of the Bowser Lake Group is conformable based on observations at six locations. 1) Three-and-a-half kilometres southwest of Peak 2087 m, the top of the Horn Mountain middle maroon volcanic unit contains maroon tuff to lapilli-tuff with rare chert clasts, indicating interfingering with Bowser Lake Group chert clast-bearing conglomerates. It is overlain by a light green felsic lapillistone bed (2-4 m thick) with rare limestone clasts (Horn Mountain upper felsic volcanic unit) and maroon to greenish-grey laminated to thinly-bedded siltstone to fine-grained sandstone with rare 5-40 cm-thick internally laminated limestone beds and very thick chert clast-bearing pebble conglomerate beds (Bowser Lake Group). 2) One kilometre northwest of Peak 2087 m, felsic lapillistone grades into stratified crystal tuff (Horn Mountain upper felsic volcanic unit) and is conformably overlain by an internally laminated limestone bed and maroon to sea-green siltstone to fine-grained sandstone (Bowser Lake Group). 3) Six-and-a-half kilometres south-southwest of Peak 1701 m, maroon lapilli-tuff with flow-banded felsic clasts fines upward into very thickly-bedded maroon crystal tuff (Horn Mountain upper

Table 2. Summary of intrusive units. Mineral abbreviations after Kretz (1983).

Age	Phase	Description	Relationships to adjacent units	Geochronology
Jurassic	McBride River pluton	<p>Hbl-Bt granodiorite (JMrgd). Massive, equigranular (2-5 mm). Contains 15-30% mafic minerals; euhedral Bt books (2-6 mm) and euhedral, prismatic Hbl (<1 cm long) in approximately equal proportions. Common dark grey dioritic xenoliths. Recessive, medium grey weathering.</p> <p>Hbl-Cpx(?) diorite to Qtz diorite (JMrd). Equigranular (1-3 mm) to Pl porphyritic (2-4 mm). Includes Hbl diorite (JTSd)². Moderately recessive, medium to dark grey weathering.</p> <p>Fine-grained mafic-rich microdiorite (JMrd-fg). Massive, equigranular (0.1-0.5 mm) microdiorite with 50-70% lath-shaped to anhedral Pl and 30-40% vaguely elongate to anhedral black mafic minerals. Moderately recessive, blocky, medium grey weathering. Includes green-grey meta diabase (mId)⁵.</p> <p>Hbl-Cpx-Pl porphyry dikes (Jdr). Hbl-Pl, Cpx-Pl and Hbl-Cpx-Pl porphyritic dikes. Aphyric to microdioritic groundmass, locally contains acicular Hbl.</p>	<p>Cuts Horn Mountain lower mafic volcanic unit and mafic intrusive unit.</p> <p>Cuts Horn Mountain middle maroon volcanic unit and felsic intrusive unit.</p> <p>Cuts Bowser Lake Group sedimentary rocks, which also display features of contact metamorphism.</p> <p>Cuts Takwahoni lower unit, Horn Mountain middle maroon volcanic unit, Bowser Lake Group. Follows north-trending Kehlechoa fault.</p>	<p>U-Pb zircon: 184±8 Ma⁴ (see Section 4.4.)</p>
		<p>Potassic phase (MJTSgr). Bt and lesser Hbl-Bt monzogranite to rare Qtz syenite. Massive, equigranular (1-3 mm). Rare Qtz eyes (4-5 mm). Moderately recessive, orange-pinkish weathering. Includes Hbl-Bt granite (JTSg)⁵.</p>	<p>Cuts Cake Hill Qtz-rich phase, Three Sisters mafic and central felsic phase. Cuts and includes pendants of platy Pl porphyry.</p>	<p>U-Pb zircon: 171±1 Ma⁴, 169.1±0.8 Ma³, 168.57±0.54 Ma²</p>
Middle Jurassic	Three Sisters pluton	<p>Central felsic phase (MJTSqm). Bt Qtz monzonite. Massive, equigranular (1-4 mm) to locally Pl and Kfs porphyritic. Contains cm- to dm-scale, sub-angular, equigranular (0.1-2 mm) dioritic xenoliths. Resistant, medium grey weathering.</p> <p>Mafic phase (MJTSqd). Hbl-rich (minor Bt-Cpx Hbl-rich) Qtz diorite³. Includes a Hbl-Cpx diorite body with platy Pl (1-3 x 5-20 mm) and euhedral Cpx and Hbl (1-3 mm) set in an equigranular (0.1 mm) groundmass with lath-shaped to anhedral Pl (40-70%) and equant black mafic minerals (<30%). Locally contains platy Pl porphyritic melanocratic xenoliths. Resistant, brownish dark grey to black weathering.</p> <p>Fine-grained mafic-intermediate phase (MJTSqd,fg)³. Hbl-Bt Qtz diorite. Equigranular (1-1.5 mm) to sparsely Pl porphyritic (1.5-3 mm).</p>	<p>Intrudes, brecciates, and includes xenoliths of Three Sisters mafic phase.</p>	<p>U-Pb zircon: 177.13±0.59 Ma², 172.75±0.87 Ma², 169.0±1.3 Ma³</p> <p>Ar-Ar Hbl: 171.9±1.7 Ma³</p>
				<p>Ar-Ar Hbl: 173.2±Ma³</p>

Table 2. Continued.

Age	Phase	Description	Relationships to adjacent units	Geochronology
Late Early-Middle Jurassic	Horn Mountain-related subvolcanic intrusions	Felsic intrusive (EMJf). Creamy white, green-grey, pale yellow to maroon dikes, sills and other intrusive bodies. Generally flow banded, locally spherulitic. Generally contains 5-20% white to orange stubby to lath-shaped Pl (1-3 mm) and very rare minor Qtz (<0.5 mm). Resistant, yellowish weathering. Platy Pl porphyry (EMJm.po). Platy Pl-phyric dikes, sills and other intrusive bodies. Contains 30-50% platy Pl (0.5-3 cm) and locally <5% Aug (5 mm) in a dark grey aphanitic to microdioritic groundmass. Mafic intrusive (EMJm). Aug-Pl-phyric dikes, sills and other intrusive bodies. Contains 15-40% Pl laths (0.1-1 mm) and 10-15% dark green/black equant Aug (0.5-1 cm). Resistant, dark greenish grey weathering.	Cuts Spatsizi Formation, Horn Mountain middle maroon volcanic rocks and base of Bowser Lake Group. Cuts Spatsizi Formation; Horn Mountain lower mafic volcanic unit and middle maroon volcanic unit. Cuts Cake Hill quartz-rich phase; Horn Mountain lower mafic volcanic unit, lower volcaniclastic sandstone unit, middle maroon volcanic unit and upper felsic volcanic unit.	
Late Triassic	Cake Hill pluton	Cake Hill Qtz-rich phase (LTrCHgr). Hbl granodiorite to monzogranite. Massive, equigranular (2-4 mm) with minor ubiquitous Qtz eyes (5-7 mm). Contains tabular Hbl and lacks xenoliths. Moderately resistant, light-medium grey weathering. Cake Hill pluton (LTrCHqm) ³ . Equigranular (3-4 mm) Hbl to lesser Bt-Hbl Qtz monzodiorite and Qtz monzonite. Tabular Hbl bearing, trace Ttn usually ubiquitous; trace Mag in places. Moderately resistant, light-medium grey weathering. Leucocratic phase (LTrCHqm.le) ³ . Equigranular (1-3 mm), light-coloured and Ep altered Hbl Qtz monzodiorite, granodiorite, Qtz diorite, tonalite(?)	Unconformably overlain by Spatsizi basal sandstone and conglomerate unit. Interpreted to be unconformably overlain by Horn Mountain lower mafic volcanic unit.	U-Pb zircon: 217.91±0.24 Ma, 216.2±1.2 Ma ³ U-Pb zircon: 221±3 Ma ⁴ , 218.2±1.3 Ma ³

Note: ¹ van Straaten and Nelson (2016); ² Takaichi (2013a; b); ³ van Straaten et al. (2012); ⁴ Anderson and Bevier (1992); ⁵ Read and Psutka (1990).

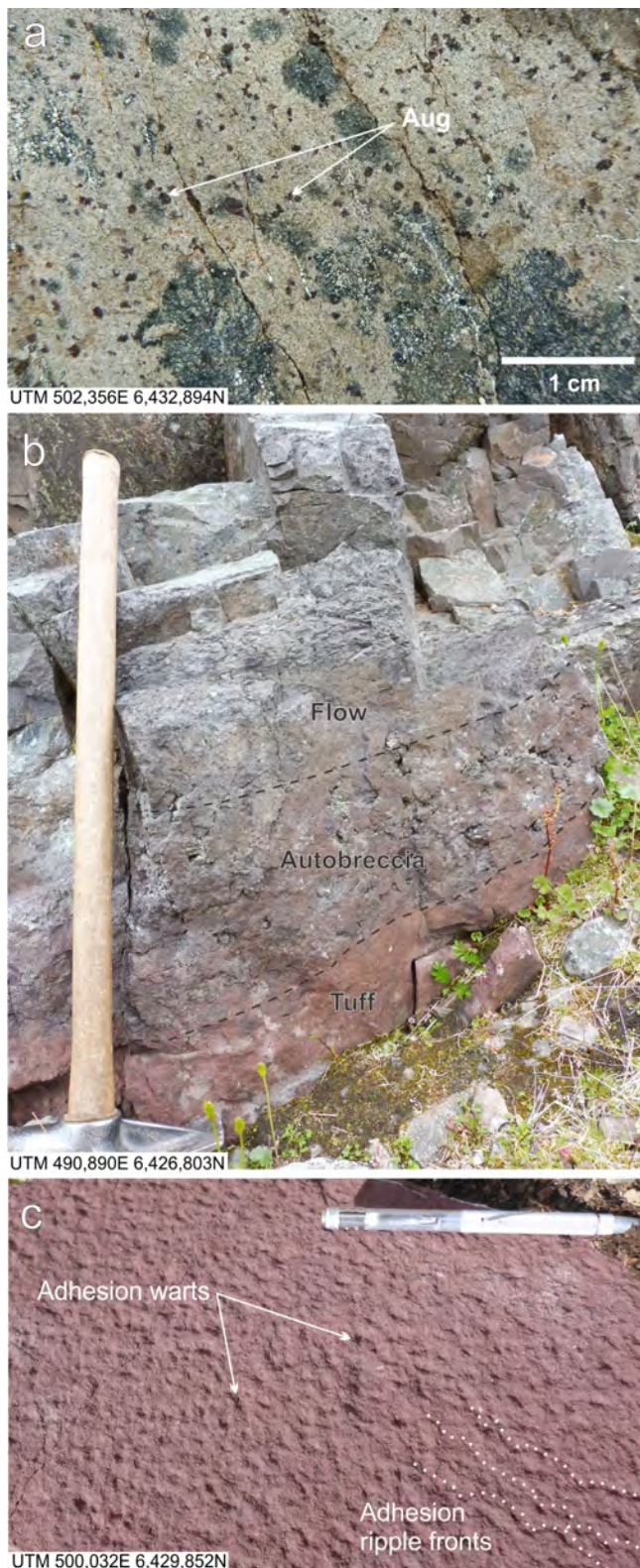


Fig. 10. Bowser Lake Group, mafic volcanic rocks (mJBLv). **a)** Close up of fine-grained augite-plagioclase-phyric coherent rock with characteristic reddish altered augite. **b)** Red tuff overlain by brecciated lower contact of fine-grained augite-plagioclase-phyric flow. **c)** Possible adhesion warts in crudely laminated crystal tuff. Weak alignment and asymmetry may indicate incipient adhesion ripples.

felsic volcanic unit) and grades into laminated to thinly-bedded siltstone to fine-grained sandstone (Bowser Lake Group). 4) Two kilometres north-northeast of the CM prospect, a 15-m-thick flow-banded felsic flow is overlain by cream-coloured tuff breccia with flow-banded clasts that grades upward into maroon crystal tuff and tuff (Horn Mountain upper felsic volcanic unit) and laminated maroon siltstone (Bowser Lake Group). 5) Half a kilometre west of the CM prospect, the top of the Horn Mountain middle maroon volcanic unit contains green chert-grain bearing lapillistone indicating interfingering with Bowser Lake Group. It is overlain by a 50 m-thick purple and white flow-banded felsic coherent rock (Horn Mountain upper felsic volcanic unit), maroon and green-grey sandstone and chert clast-bearing pebble conglomerate (Bowser Lake Group). 6) The immediate footwall of the north-trending Kehlechoa fault exposes a narrow strip of chert clast-bearing pebble to granule conglomerate and sandstone that interfingers with, and ultimately overlies, the Horn Mountain middle maroon volcanic unit (Fig. 19; van Straaten and Nelson, 2016).

Regionally, deposition of Cache Creek-derived chert clast-bearing conglomerate of the Bowser Lake Group records the onset of erosion from the Stikinia - Cache Creek tectonic welt (Evenchick et al., 2007). Bowser Lake Group strata in the map area are on the western margin of a northern outlier of the Bowser basin (Fig. 1) and contain early Bajocian ammonites on Peak 1701 m (Fig. 3; Tipper, 1978; Gabrielse, 1998). The biostratigraphic age is similar to a preliminary detrital zircon maximum depositional age (ca. 170 Ma) for Bowser Lake strata overlying Horn Mountain volcanic rocks in the Tanzilla area (van Straaten and Gibson, 2017). Together with early Bajocian fossils from chert-clast bearing granule conglomerate overlying a Whitehorse trough succession in the Lisadele Lake area (Fig. 1; Mihalynuk et al., 1999; Sirmohammad et al., 2011), these occurrences represent the oldest documented rocks in the Bowser Lake Group. Rocks at the base of the Bowser Lake Group get progressively younger towards the south. Basal strata in the northern part of the contiguous Bowser basin (Fig. 1) are Bathonian; in the centre and south they are Callovian to Oxfordian (Evenchick et al., 2010). Within the contiguous Bowser basin, the Bowser Lake Group (Middle Jurassic to Cretaceous) comprises a shallowing-upward succession deposited in submarine fan, submarine slope, shallow-marine shelf to deltaic environments (Evenchick and Thorkelson, 2005). The oldest (Bathonian) strata in the northern and northeastern part of the contiguous Bowser basin were deposited in submarine fan to submarine slope environments, followed by deposition in shallow-marine shelf and deltaic environments by the early Oxfordian (Evenchick and Thorkelson, 2005; Evenchick et al., 2010).

In the present map area, the conglomerate facies likely formed in alluvial fans or braided river systems close to range front faults along the building orogen, with limestone cobbles to boulders derived from Sinwa Formation rocks in the hanging wall of thrust ramps. Interbedded fine-grained siliciclastic rocks and lesser chert clast-bearing conglomerate beds (sedimentary

facies 1), and minor mafic volcanic flows (volcanic facies) were likely deposited in a more distal subaerial setting. We correlate the sedimentary facies 2 in the map area with coeval strata in the Tanzilla area (Fig. 2) where Bowser Lake conglomerate, sandstone and siltstone unconformably overlie the Horn Mountain Formation; clasts are locally-derived and the succession contains marine fossils (van Straaten and Nelson, 2016). The sedimentary rocks may have formed an elongate marine basin on the northern margin (present coordinates) of waning Horn Mountain volcanic centres.

3.2. Whitehorse trough

Strata of the Whitehorse trough are exposed in a west-northwest to east-southeast trending fault panel bounded by the Kehlechoa and King Salmon thrust faults; the belt abruptly narrows from ~13 km in the north central part of the map area to ~3-5 km in the west (Figs. 2, 3). Limestones of the Sinwa Formation are exposed in the immediate hanging wall of the Kehlechoa fault, and are overlain by siliciclastic rocks, polymictic conglomerates, and volcanic rocks of the Takwahoni Formation (Lagerbe Group; Table 1).

3.2.1. Sinwa Formation (Upper Triassic)

Light to medium grey Sinwa Formation limestones (Table 1; Late Norian, Gabrielse, 1998) form the basement to the Whitehorse trough succession. The Sinwa Formation-Takwahoni contact is hidden by a 35 m-long covered interval. The lowest Takwahoni Formation rocks exposed are fine- to medium-grained sandstones (this study), which yielded Sinemurian fossils along strike (Gabrielse, 1998). Based on the apparent time gap, the contact is likely an unconformity.

3.2.2. Takwahoni Formation (Lower Jurassic)

3.2.2.1. Lower unit

The southern portion of the Kehlechoa-King Salmon fault panel exposes a right-way-up, moderately north-dipping and lithologically-variable sequence. Within this sequence we distinguish four facies: argillite, siltstone and sandstone (Fig. 11); volcanoclastic sandstone; volcanic (Fig. 12); and conglomerate (Fig. 13, Table 1). The conglomerate and volcanic facies are exposed mainly on ridges, and detailed mapping suggests they form laterally discontinuous 100 m- to 3 km-scale bodies in argillite, siltstone and very fine- to fine-grained sandstone (Fig. 3). This map pattern is mimicked on a smaller scale, where we found several 0.1-50 m bulbous conglomerate bodies enveloped by fine-grained siliciclastic rocks (Fig. 13a). The conglomerate is predominantly polymictic and contains limestone, (sub)volcanic and lesser plutonic clasts (Fig. 13b). The (sub)volcanic clasts in the conglomerate facies and volcanic clasts in the volcanic facies are compositionally and texturally similar, except for the greater size range and larger average size of plagioclase phenocrysts in clasts in the conglomerate (Table 1). Several ~10-15 m limestone olistoliths are present within the conglomerate and volcanoclastic sandstone facies.

The lower unit has yielded fossil collections with Sinemurian



Fig. 11. Takwahoni Formation lower unit, argillite, siltstone and sandstone facies (IJTLs). Interbedded laminated to medium-bedded siltstone and medium-grained sandstone.

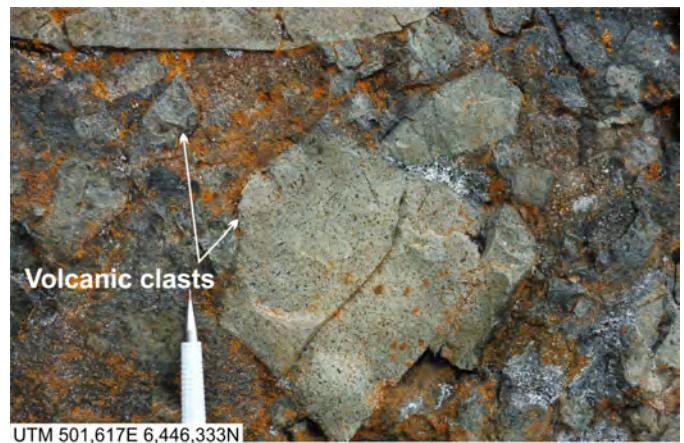


Fig. 12. Takwahoni Formation lower unit, mafic volcanic facies (IJTLv). Massive, clast-supported volcanic breccia.

and Toarcian ages (Gabrielse, 1998; Table 1). This has led Gabrielse (1998) and van Straaten and Nelson (2016) to infer several thrust faults separating Sinemurian and Toarcian rocks. During our mapping we observed identical lithologies within areas previously interpreted as Sinemurian and Toarcian, and found no evidence for major thrust faults. Based on these observations, and an apparent conformable contact with the overlying greywacke unit (Pliensbachian; see below), we suggest the lower unit may be an internally conformable succession and largely Sinemurian.

Rocks beneath a klippe of Sinwa limestone and Inklin Formation south of Wade Lake are very poorly exposed. They have been tentatively interpreted as Takwahoni lower argillite, siltstone and sandstone facies (south) and Takwahoni greywacke unit (north). The main outcrops on the rounded peak west of the Kehlechoa River and north of the Kehlechoa

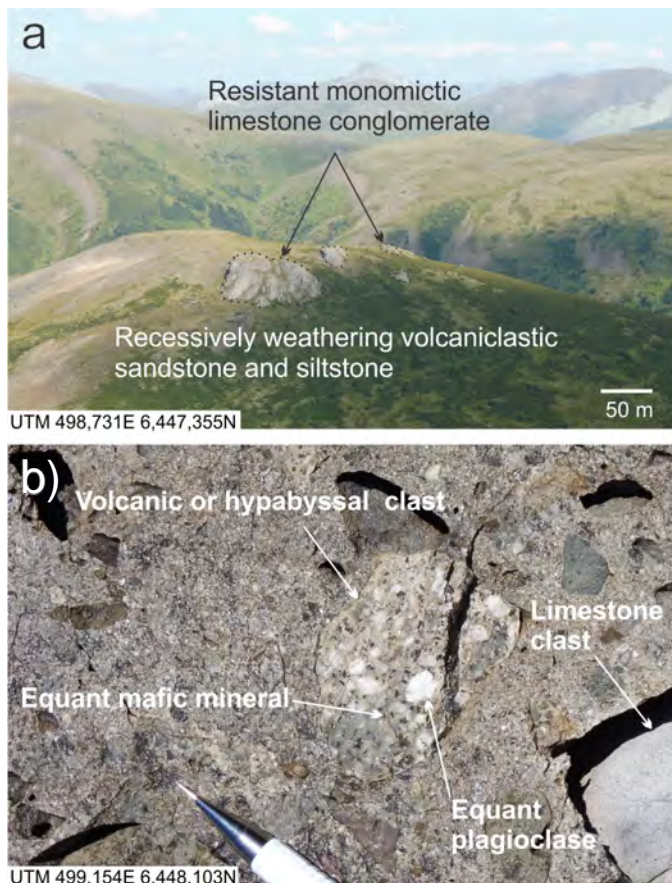


Fig. 13. Takwahoni Formation lower unit. **a)** Resistant bulbous bodies of monomictic limestone clast-bearing conglomerate within recessively weathering siltstone and volcaniclastic sandstone (IJTLsv). View northeast. **b)** Close up of polymictic conglomerate (IJTLcg) with limestone and (sub)volcanic clasts. Volcanic or hypabyssal clasts contain distinct coarse plagioclase and equant mafic minerals.

fault were not visited. They were previously grouped with an undivided unit of maroon-weathering plagioclase-phyric flows, volcanic conglomerate, volcanic breccia, and tuff (Upper Triassic to Lower Jurassic; unit TrJv of Gabrielse, 1998). This undivided volcanic unit included rocks north of the Cake Hill pluton that are now re-interpreted as the Horn Mountain maroon volcanic unit (Fig. 2; van Straaten and Nelson, 2016; van Straaten and Gibson, 2017). Along its ~100 km strike length, the Kehlechoa fault carries only Sinwa limestone (Upper Triassic) and Takwahoni Formation (Lower Jurassic) in its hanging wall. We consider it unlikely that the volcanic rocks in the hanging wall of the Kehlechoa fault are part of the Horn Mountain Formation, and tentatively re-interpret the exposures as a laterally discontinuous, several square kilometre-sized body of Takwahoni volcanic rocks (IJTLv; Fig. 3).

3.2.2.2. Greywacke unit

The northern half of the Kehlechoa-King Salmon fault panel exposes a right-way-up, moderately north-dipping

succession of interbedded feldspathic wacke, feldspathic arenite and siltstone. Medium- to coarse-grained feldspathic wacke with volcanic clasts (top of the Takwahoni lower unit) grade into interbedded fine- to medium-grained sandstone and siltstone (base of the Takwahoni greywacke unit) across a distance of ~100 m. The lack of evidence for large-scale faulting and the subtle change in rock type suggest the contact is gradational. Ammonites collected near the base of the unit returned late Sinemurian-early Pliensbachian and possible early Pliensbachian ages (T. Poulton, pers. comm., 2017), in accordance with several early and late Pliensbachian fossil collections reported by Gabrielse (1998).

3.3. Cache Creek terrane

3.3.1. Sinwa Formation (Upper Triassic)

Distinctly light grey weathering Sinwa Formation limestone is commonly exposed in the immediate hanging wall of the King Salmon fault. It is massive to rarely medium- to thickly-bedded, generally recrystallized and fractured. Following Gabrielse (1998), limestone exposures on the north and south side of a rounded knob 4.5 km south of Wade Lake are interpreted as a klippe of Cache Creek terrane (Fig. 3).

Within the Cache Creek terrane east-northeast of the study area, Sinwa limestone overlies the Kutcho assemblage, a Late Permian to Middle Triassic primitive intra-oceanic volcanic arc succession (Schiarrizza, 2012) accreted to Stikinia in the Late Triassic (Logan and Mihalynuk, 2014). The Sinwa Formation therefore represents a common unit between the Whitehorse through and parts of the Cache Creek terrane.

3.3.2. Inklin Formation (Jurassic)

Recessively weathering thinly-bedded feldspathic wacke, laminated siltstone and phyllite appear to overlie Sinwa limestone on a rounded knob 4.5 km south of Wade Lake. Fine- to medium-grained and minor coarse-grained sandstone contains rare quartz grains and fine-grained sandstone rip-up clasts. Following Gabrielse (1998) it is interpreted as Inklin Formation above the inferred King Salmon thrust fault. The age of the Inklin Formation is poorly constrained within the Dease Lake area. However, a detailed study in the Atlin Lake area suggests it is early Sinemurian to late Pliensbachian (Johansson et al., 1997).

3.4. Overlap units

3.4.1. Sustut Group (Cretaceous)

Sandstone, siltstone, and mudstone (locally muscovite-bearing) with chert-clast bearing conglomerate interbeds are found south of the Pitman fault (Read and Psutka, 1990), and are assigned to the Tango Creek Formation (Sustut Group).

3.4.2. Tuya Formation (Miocene to Pleistocene)

A small basaltic volcanic centre was mapped by Gabrielse (1998) in the southwestern part of the study area.

4. Intrusive units

4.1. Late Triassic: Cake Hill pluton

The map area includes the eastern part of the Hotailuh batholith, a composite body that extends for 2275 km² (Fig. 2). Hornblende quartz monzodiorite to quartz monzonite of the Cake Hill pluton (Late Triassic; Table 2) represents one of the oldest phases of the batholith, and is exposed in the southwestern part of the map area (Fig. 3; van Straaten et al., 2012). A minor leucocratic phase was recognized by van Straaten et al. (2012).

The quartz-rich phase of the Cake Hill pluton forms a 6 km² body in the western part of the map area. The hornblende granodiorite to monzogranite (Fig. 14) is unconformably overlain by Spatsizi Formation sedimentary rocks (Section 3.1.3.1.). A U-Pb zircon sample from this phase returned a 216.2 ± 1.2 Ma age (van Straaten et al., 2012), slightly younger than 217.91 ± 0.24 Ma from a hornblende monzogranite body in the adjacent map area to the northwest (Fig. 2; Section 6.1.). This unit represents the youngest and most evolved phase of the Cake Hill pluton.

4.2. Early to Middle Jurassic subvolcanic intrusions

Augite-plagioclase-phyric mafic intrusions (EMJm, Table 2) form 1 m- to 1 km-scale dikes and intrusive bodies (Fig. 6a). Several north-northeast-trending bodies cut the Horn Mountain middle maroon volcanic unit east of the McBride River (Fig. 3). The intrusions are texturally and mineralogically similar to volcanic clasts within the Horn Mountain lower mafic and middle maroon volcanic units; they likely represent feeder dikes.

Decimetre- to 1 km-scale dikes, sills and other intrusive bodies of coarse platy plagioclase porphyry (EMJm.po, Table 2) cut the Spatsizi Formation and the Horn Mountain lower mafic volcanic unit and middle maroon volcanic unit. Rare coarse platy plagioclase-phyric clasts within the Horn Mountain middle maroon volcanic unit indicate that the intrusions are subvolcanic feeders.

We distinguish at least two felsic intrusive episodes (EMJf,



Fig. 14. Cake Hill pluton, quartz-rich phase (LTrCHgr). Massive, equigranular, hornblende granodiorite (LTrCHgr) cut by pink dikelets (Three Sisters potassic phase, MJTSgr).

Table 2). West of the McBride River near Peak 2102 m, the Spatsizi Formation is commonly cut by felsic dikes and other intrusive bodies; intrusive felsic breccias are exposed at two locations (van Straaten et al., 2012; this study). Felsic intrusions are notably absent in the Horn Mountain Formation west of the McBride River, suggesting they represent feeders to the Horn Mountain lower felsic volcanic subunit (Section 3.1.3.2.). East of the McBride River, the Horn Mountain middle maroon volcanic unit is commonly cut by m-scale flow-banded felsic dikes and intrusive bodies up to 1.5 km² in size (Fig. 15). One flow-banded felsic dike cuts basal Bowser Lake sedimentary rocks 3.5 km southwest of Peak 2087 m. The distribution, dimension, and stratigraphic level of these intrusions suggest that they are the roots of felsic volcanic centres that fed the Horn Mountain upper felsic volcanic unit.

4.3. Middle Jurassic: Three Sisters pluton

The Three Sisters pluton (Middle Jurassic) represents the youngest documented phase of the Hotailuh batholith. Extensive exposures of the pluton are limited to the southwestern part of the map area (Fig. 3). The pluton has been divided into four phases: mafic; fine-grained mafic-intermediate; central felsic; and marginal potassic (Anderson, 1983; van Straaten et al., 2012; Table 2).

The mafic phase forms several relatively small (<1-2 km²) medium-grained hornblende quartz diorite bodies (van Straaten et al., 2012). A 1.5 km² mafic intrusive body 2 km west of Peak 2102 m contains similar coarse platy plagioclase (Fig. 16) as the platy plagioclase porphyry (EMJm.po, Table 2). However, we assign it to the mafic phase because it is fine to medium grained and mafic rich. It may indicate a common magma source for the mafic phase of the Three Sisters pluton and Horn Mountain (sub)volcanic rocks. A fine-grained hornblende-biotite quartz diorite body in the southwest part of the map area is the type locality for the fine-grained mafic-intermediate phase (van Straaten et al., 2012).

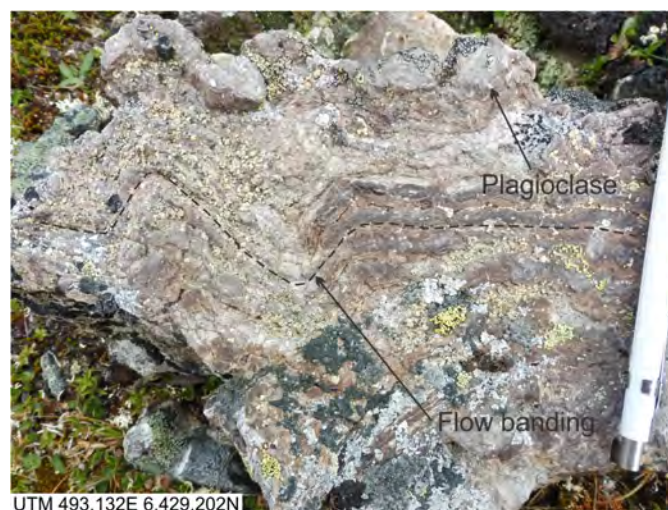


Fig. 15. Felsic intrusive, (EMJf). Folded flow banding in plagioclase-phyric felsic intrusive body.

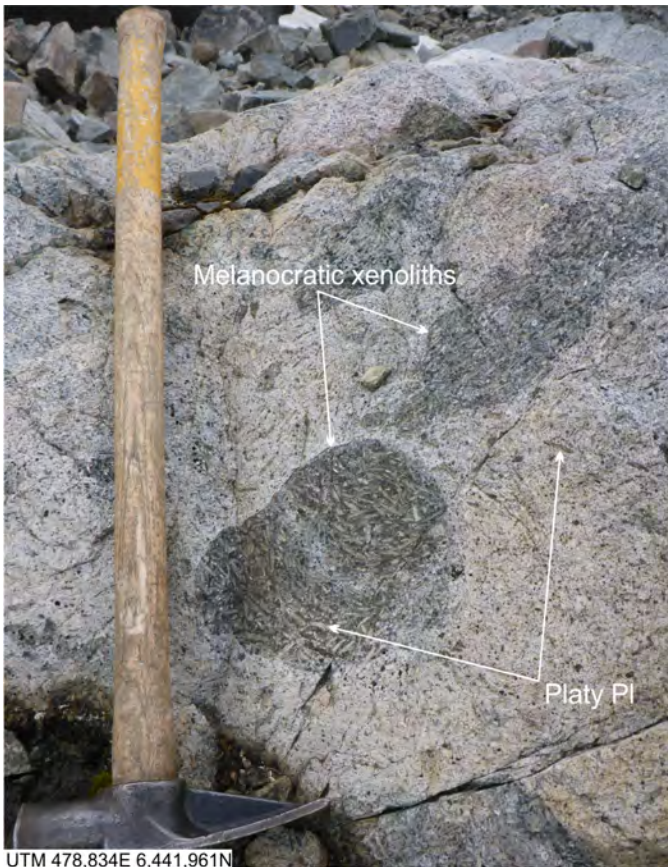


Fig. 16. Three Sisters pluton, mafic phase (MJTSqd). Hornblende-clinopyroxene diorite with melanocratic xenoliths; both contain coarse platy plagioclase.

The central felsic phase is the most extensive unit of the Three Sisters pluton. It is typically resistant and forms numerous ridges and peaks in the western part of the map area (Fig. 3). It consists primarily of biotite quartz monzonite, and contains common fine-grained dioritic xenoliths (Fig. 17). The central felsic phase cuts and includes xenoliths of the mafic phase.

The marginal potassic phase is the youngest unit of the Three Sisters pluton. It varies from fine to medium grained, and ranges in composition from biotite to hornblende-biotite monzogranite to quartz syenite (Table 2). Dikes of the potassic phase cut the Cake Hill quartz-rich phase (Fig. 14), the platy plagioclase porphyry (EMJm.po), and the Three Sisters mafic and central felsic phases.

4.4. Middle Jurassic (or younger): McBride River pluton

The McBride River pluton forms a 150 km² body in the southern half of the map area where it is interpreted to underlie the lower McBride River valley and adjacent forested slopes. Where exposed at or above treeline it consists mainly of medium-grained hornblende-biotite granodiorite (Fig. 18a). Along its western margin, the pluton cuts the Horn Mountain lower mafic volcanic unit. At the interface of the two units, granodiorite dikes and dikelets cut medium-grey weathering augite-plagioclase-phyric volcanic breccia (Fig. 18b). Along its



Fig. 17. Three Sisters pluton, central felsic phase (MJTSqm). Massive, equigranular quartz monzodiorite containing a fine-grained dioritic xenolith.



Fig. 18. McBride River pluton (JMRgd). **a)** Massive, equigranular hornblende-biotite granodiorite containing a dioritic xenolith. **b)** Massive, equigranular, hornblende-biotite granodiorite dike intruding massive volcanic breccia with augite-plagioclase-phyric volcanic clasts (Horn Mountain lower mafic volcanic unit, lmJHMLvm).

eastern margin the pluton cuts a mafic intrusive body (EMJm, Fig. 3) which, based on nearby mafic dikes, appears to cut the Horn Mountain middle maroon volcanic unit.

The McBride River pluton was previously assigned an Early Jurassic age, based on a 184 ± 8 Ma weighted $^{207}\text{Pb}/^{206}\text{Pb}$ age for three multigrain abraded zircon fractions interpreted to have undergone Pb loss (Anderson and Bevier, 1992) and a 186 ± 13 Ma K-Ar hornblende age (Stevens et al., 1982). An earlier analysis of this sample yielded a 166 ± 8 Ma upper concordia intercept based on a line forced through the origin and three nearly concordant zircon fractions (Anderson et al., 1982). The earlier U-Pb zircon results were dismissed by Anderson and Bevier (1992) based on systematic errors resulting from the inaccurate estimation of the common Pb composition. However, the ca. 184 Ma age is difficult to reconcile with crosscutting relationships and new age determinations. The pluton unequivocally crosscuts the Horn Mountain Formation lower mafic volcanic unit and mafic intrusions, and likely crosscuts the Horn Mountain middle maroon volcanic unit. Underlying the Horn Mountain Formation, the Spatsizi Formation contains Toarcian fossils (Henderson and Perry, 1981; Gabrielse, 1998) and a ca. 176 Ma detrital zircon population (Iverson et al., 2012). Rocks at the top of the Horn Mountain Formation are ca. 173-170 Ma (van Straaten and Gibson, 2017). Given that coarse-grained phaneritic rocks such as the McBride River pluton require emplacement depths of a few kilometres, it seems unlikely that the pluton is significantly older than ca. 173-170 Ma. The McBride River pluton shares some characteristics with the central felsic phase of the Three Sisters pluton (Middle Jurassic) in that it contains biotite and common fine-grained xenoliths. However, the pluton is most similar to the Snowdrift Creek pluton, a mostly recessive-weathering Late Jurassic biotite-hornblende granodiorite with common mafic xenoliths exposed in the adjacent map area to the northwest (Fig. 2; van Straaten and Gibson, 2007). Awaiting results from a sample submitted for U-Pb zircon analysis, we tentatively suggest that the ca. 184 age of Anderson and Bevier (1992) is incorrect and that the McBride River pluton is Middle Jurassic or younger.

Three dioritic intrusions outcrop east of the McBride River pluton (Fig. 3). Medium-grained hornblende diorite to quartz diorite (unit JMRdr, Table 2) is exposed for approximately 9 km² southeast of the McBride River pluton, but contacts with the pluton were not observed. Dikes and dikelets of the diorite cut the Horn Mountain middle maroon volcanic unit and the felsic intrusive unit. Our observations corroborate mapping by Read and Psutka (1990), who recognized a hornblende diorite and gabbro unit (their unit JTSdi) in the same area. A 3 km² body of fine-grained diorite (unit JMRdr.fg, Table 2) outcrops along a ridge northeast of the McBride River pluton (Fig. 3); again, contacts with the pluton were not exposed. To the north, and across a fault to the east, the fine-grained diorite cuts laminated to thin-bedded siltstone and sandstone of the Bowser Lake Group. At both locations, the sedimentary rocks are silicified, likely from contact metamorphism. A small meta-diorite body (unit mJd of Read and Psutka, 1990) is tentatively assigned to the same unit. The dioritic intrusions resemble the Three Sisters mafic phase and fine-grained mafic-intermediate

phase (see above; Table 2). However, the Three Sisters mafic phase and fine-grained mafic-intermediate phase (ca. 172-173 Ma cooling ages, Table 2) are slightly older than and have never before been observed cutting the Bowser Lake Group (ca. 170 Ma; Table 1, van Straaten and Gibson, 2017).

Common clinopyroxene-hornblende-plagioclase porphyry dikes cut and follow the Kehlechoa fault 3.5 km south of Peak 1942 m (unit Jdr, Table 2). Their crosscutting relationship suggests a Late Jurassic age, similar to the Snowdrift Creek pluton and related diorite dikes observed in the adjacent map area to the northwest (van Straaten and Nelson, 2016).

5. Structure

We divide the map area into three tectonostratigraphic domains, separated by the Kehlechoa and King Salmon thrust faults (Fig. 2). The southern domain comprises Spatsizi sedimentary rocks overlain by Horn Mountain volcanic rocks and Bowser Lake sedimentary rocks of Stikinia. The central domain includes mostly sedimentary strata of the Whitehorse trough between the Kehlechoa and King Salmon faults. The northern domain includes rocks assigned to the Cache Creek terrane in the hanging wall of the King Salmon fault.

On Stikinia, Hazelton Group stratified rocks northwest and north of the McBride River pluton form a homoclinal, right-way-up, northeast-dipping sequence; bedding attitudes flatten towards the northeast (Fig. 3). An outlier of the Horn Mountain lower mafic volcanic unit is on the northeast ridge of Peak 2102 m (Fig. 3); the outcrop pattern is caused by an approximately 150 m-wide s-fold with moderately to steeply northeast-dipping long limbs and a gently southwest-dipping short limb. In the southeastern part of the map area, a sequence of Horn Mountain Formation and Bowser Lake Group is right-way-up and defines an approximate dome shape. In the centre, Horn Mountain middle maroon volcanic rocks predominate, with Horn Mountain upper felsic volcanic rocks exposed on some ridge tops. Bowser Lake Group sedimentary rocks overlie the succession along the margins of the dome in the south, east and north (Fig. 3).

The central structural domain comprises Sinwa limestone (Upper Triassic) unconformably overlain by a right-way-up, moderately north-dipping predominantly sedimentary sequence of the Takwahoni Formation (Lower Jurassic). Local variations in bedding attitudes in the Takwahoni Formation may be related to syn-sedimentary deformation and/or minor folds and faults. One 10 m-scale chevron fold with a north-dipping axial plane was observed in the footwall of the King Salmon thrust fault. In contrast to the Takwahoni Formation in the adjacent map area to the west (van Straaten and Gibson, 2017; van Straaten et al., 2017), we did not find any evidence for large-scale folding.

5.1. Major faults

We mapped two sets of faults and lineaments in the study area. The older set includes southwest- and north-northwest-striking normal/strike-slip faults that cut the Bowser Lake

Group and older units of Stikinia. Younger, generally west- to northwest-striking thrust faults (including the King Salmon and Kehlechoa faults) juxtapose the Cache Creek terrane to the north with Whitehorse trough strata and, in turn, Stikinia. They also appear to truncate faults of the older set (Fig. 3).

5.1.1. Early normal/strike-slip faults

Several southwest-trending normal/strike-slip faults are in the southeast part of the map area. East of the McBride River, the more westerly of two subparallel south-southwest-trending faults forms a well-defined topographic and aeromagnetic lineament. In two saddles, we found highly altered and veined subcrop with common slickensides. The movement on this fault is equivocal. In the north, the base of northeast-dipping Bowser Lake Group rocks is at higher topographic elevations east of the fault, suggesting west-side down or sinistral movement. However, in the centre, the fault juxtaposes Horn Mountain middle maroon volcanic rocks (west) against Horn Mountain upper felsic volcanic rocks (east), suggesting east-side down movement. Some of the stratigraphic differences across the fault may also be caused by relatively abrupt lateral facies changes. The eastern fault forms a well-defined topographic and moderately defined aeromagnetic lineament. Stratigraphic differences across the fault suggest west-side-down or sinistral movement. Farther south, the location of the two faults is poorly constrained. Similarly south-southwest trending topographic and aeromagnetic lineaments cut the McBride River pluton (Aeroquest Airborne, 2012; van Straaten et al., 2012), but no significant offset is apparent. A south-southwest-striking fault with an approximately 10 m west-side-down movement was observed at the CM prospect. A west-southwest-striking fault is inferred north of the Stikine River. Offset of the south-

dipping Horn Mountain Formation-Bowser Lake Group contact (Sections 3.1.3.2., 3.1.4.) suggests a north-side-down movement. The latest movement along these faults is Middle Jurassic or younger.

Two north-northwest-striking normal faults are east of the McBride River. One of these faults is interpreted to cut subhorizontal strata east of the CM prospect, and is inferred to cut the south-southwest-trending faults south of Peak 1701 m (Fig. 3). West of the fault, Horn Mountain volcanic rocks are present from the valley bottom to 1610 m elevation, and are overlain by the Bowser Lake Group. To the east, rocks from valley bottom to the ridge top are all part of the Bowser Lake Group. An approximately 300 m east-side-down movement is inferred, but some of the apparent offset could be due to rapid lateral facies changes. Two outcrops west of the fault trace (1.4 km northeast of the CM prospect) show unusual, moderately to steeply southwest-dipping bedding attitudes that may reflect minor reactivation with a top-to-the-southwest reverse sense, similar to the north-northwest-trending segment of the Kehlechoa fault (see below). The immediate footwall of the north-northwest-striking segment of the Kehlechoa fault (see below) exposes an approximately 80 m-wide strip of Bowser Lake chert clast-bearing conglomerates south of Peak 1942 m (Figs. 3, 19; van Straaten and Nelson, 2016). These rocks are in fault contact with the Horn Mountain Formation along north-trending and subvertical to steeply east-dipping recessive zones interpreted as east-side-down normal faults (Fig. 19).

5.1.2. Late thrust faults

The Kehlechoa and King Salmon thrust faults (Fig. 2; Gabrielse, 1998) formed as south-vergent structures in a regime

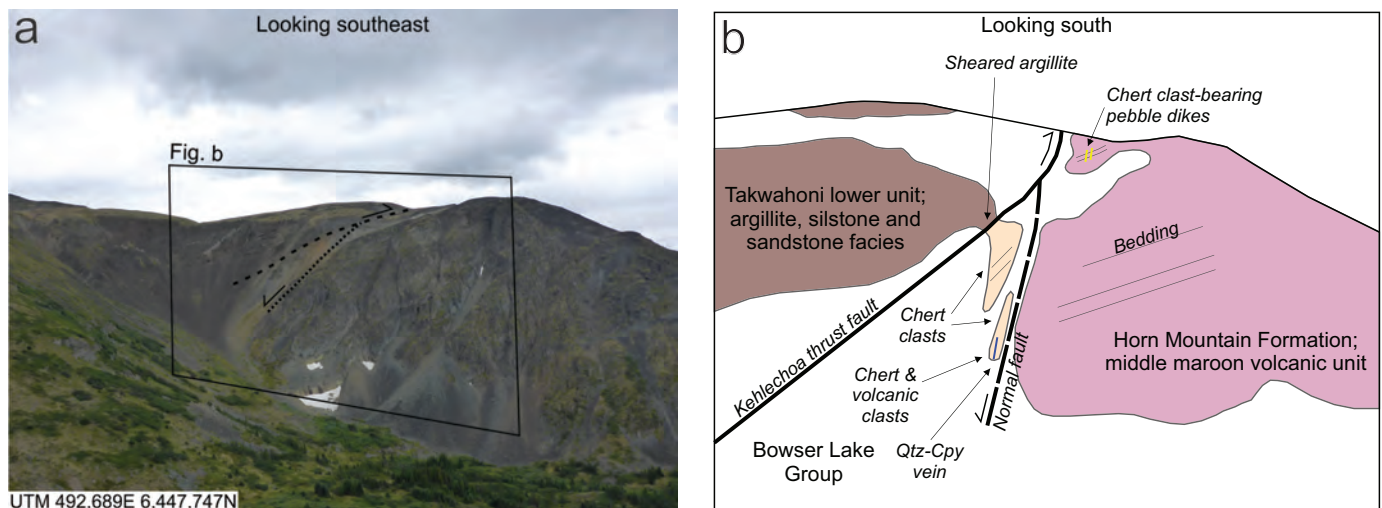


Fig. 19. North-northeast-trending Kehlechoa thrust fault, 750 m southwest of Peak 1942 m. **a)** Oblique view to the southeast. **b)** Diagram looking south. Fine-grained siliciclastic rocks of the Takwahoni lower unit (IJTLs) in the hanging wall of the Kehlechoa fault. The footwall comprises Horn Mountain middle maroon volcanic unit rocks (ImJHMMv) cut by chert-bearing pebble dikes (Fig. 9 in van Straaten and Nelson, 2016), and down-dropped Bowser Lake Group (mJBLs) conglomerates in which volcanic and chert clasts at the base (Fig. 10 in van Straaten and Nelson, 2016) grade to chert clasts at the top. The bottom of the down-dropped Bowser Lake succession is cut by a 10-20 cm-wide vertical quartz-chalcocopyrite vein that returned >1% Cu and 0.391 g/t Au (sample 15BvS-25-11, Table 3).

of north-south to north-northeast to south-southwest shortening during accretion of the Quesnel, Cache Creek and Stikine terranes (Mihalynuk et al., 2004). Auriferous polymetallic quartz veins may have formed as extensional veins related to these thrusts (Section 7.3.).

The Kehlechoa thrust fault separates the Sinwa and Takwahoni formations to the north from the Horn Mountain Formation and Bowser Lake Group to the south. The west-trending segment of the fault is not exposed. It places older rocks (Late Triassic to Early Jurassic) above younger rocks (late Early Jurassic to Middle Jurassic), suggesting south-directed reverse movement similar to that on the King Salmon fault. Along its north-northwest-trending segment, the location and nature of the Kehlechoa fault is better constrained. Outcrop patterns suggest that it is subvertical to moderately east-dipping. At one exposure, sheared argillaceous rocks separate a hanging wall containing fine-grained siliciclastic rocks of the Takwahoni lower unit (IJTLs) from a footwall of Horn Mountain middle maroon volcanic rocks and a narrow down-dropped block of Bowser Lake Group (Fig. 19; van Straaten and Nelson, 2016). We interpret this zone as an east-side-down normal fault in the underlying Stikinia panel, reactivated as a dextral-reverse lateral ramp or tear fault. Movement on the Kehlechoa fault is bracketed by fossils in Bowser Lake sedimentary rocks in the footwall (early Bajocian, ca. 170 Ma using the Cohen et al., 2013 scale), and the stitching Snowdrift Creek pluton in the adjacent map area to the northwest (160.43 ± 0.16 Ma, van Straaten and Gibson, 2017).

The King Salmon thrust fault separates sedimentary rocks of the Takwahoni Formation (footwall) from fine-grained siliciclastic, carbonate, and ultramafic rocks of the Cache Creek terrane (hanging wall). It is interpreted as a north-dipping, south-verging thrust with Sinwa limestone commonly in the immediate hanging wall of the fault (Gabrielse, 1998). A rounded knob 4.5 km south of Wade Lake is interpreted as a klippe, carrying Sinwa Formation limestone (Upper Triassic) and Inklin Formation (Jurassic).

5.1.3. Other faults

The Pitman fault is a poorly exposed east-trending regional structure with a strike length of at least 200 km. The south side of the fault exposes Stikine assemblage unconformably overlain by Sustut Group (Fig. 3; Read and Psutka, 1990). Significant differences in stratigraphy across the fault suggest a long-lived history. To the east, the fault is interpreted to cause 3 km of sinistral offset of the Kutcho and Thudaka terrane-bounding faults (Gabrielse, 1985; Evenchick and Thorkelson, 2005).

6. Geochronology

Below we report the preliminary results from four U-Pb zircon samples collected during the 2016 field season in the adjacent Tanzilla - McBride field area to the northwest (Fig. 2); detailed methods and final results will be reported elsewhere. U-Pb zircon analyses were carried out at the Pacific Centre for Isotopic and Geochemical Research (University of British

Columbia). Preliminary maximum depositional ages are calculated for laser ablation inductively coupled plasma mass spectrometry (LA-ICP-MS) detrital zircon analyses using the weighted mean age of the youngest zircon population (excluding discordant grains and outliers). Future work will use zircon trace element data and methods of Ludwig (2012) and Dickinson and Gehrels (2009) to further constrain maximum depositional ages.

6.1. Cake Hill pluton, quartz-rich phase

A sample of equigranular hornblende monzogranite from the quartz-rich phase of the Cake Hill pluton (Sample 1, Fig. 2) returned a preliminary age of 217.91 ± 0.24 Ma (Fig. 20). The sample was processed using a chemical abrasion thermal ionization mass spectrometry (CA-TIMS) technique, which is assumed to fully mitigate Pb loss in grains. The youngest concordant grouping is represented by the youngest grain (Fig. 20); we interpret the slightly older grains as autocrystic zircon crystallization in the cooling magma (e.g., Samperton et al., 2015). The age is somewhat older than a 216.2 ± 1.2 Ma LA-ICP-MS age for the quartz-rich phase of the Cake Hill pluton in the map area (van Straaten et al., 2012).

6.2. Horn Mountain Formation

A sample of a felsic lapilli-tuff bed with abundant aphyric to plagioclase-phyric clasts from the Horn Mountain lowermost mafic volcanic unit (sample 16BvS-15-111a; sample 4, Fig. 2) returned a unimodal zircon peak at 215.0 ± 1.4 Ma (Fig. 21a). A fine felsic tuff bed from the same location (16BvS-15-111b; van Straaten et al., 2017) was not analyzed further. The age overlaps with a maximum depositional age of 214.8 ± 1.5 Ma for a Spatsizi basal conglomerate (van Straaten and Gibson,

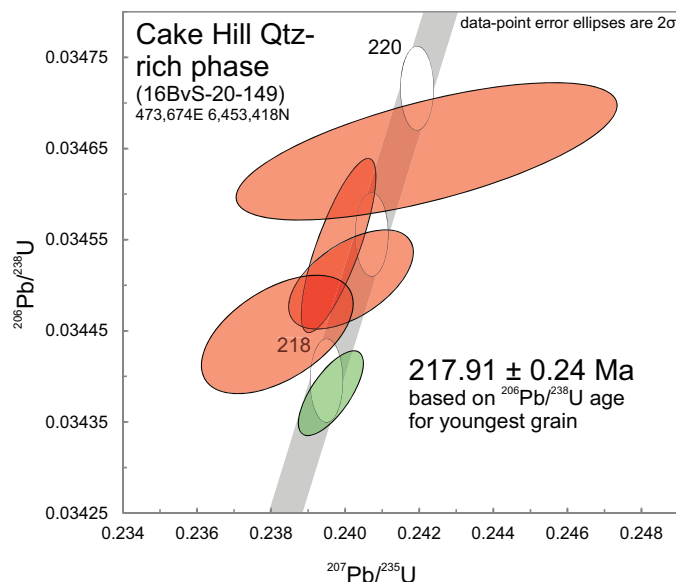


Fig. 20. Uranium-lead zircon concordia diagram showing chemical abrasion thermal ionization mass spectrometry results from the Cake Hill pluton quartz-rich phase (LTrCHgr).

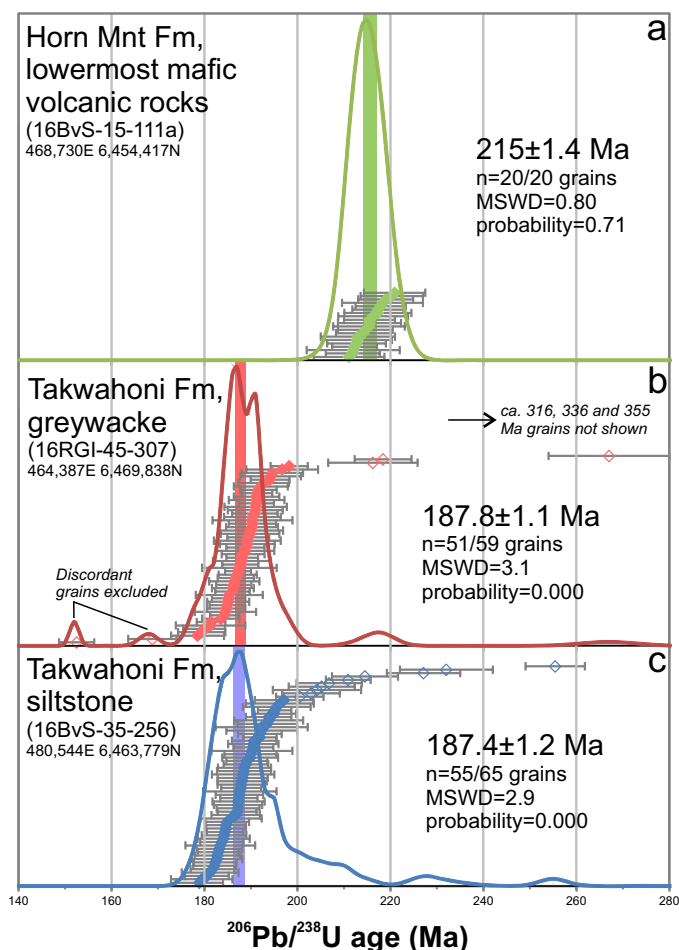


Fig. 21. Detrital zircon $^{206}\text{Pb}/^{238}\text{U}$ age distribution plots, probability curves, and preliminary maximum depositional ages. **a)** Felsic lapillituff bed in Horn Mountain Formation lowermost mafic volcanic unit (1mJHMLMvm). **b)** Takwahoni Formation greywacke unit (IJTgw). **c)** Takwahoni Formation siltstone unit (IJTs). Ages are marked with coloured diamonds (open symbols are discordant grains and outliers excluded from age calculation) with two standard deviation analytical error represented by grey bars. The probability distribution is plotted with bold coloured lines and the preliminary maximum depositional age listed on the plots is represented by a coloured vertical line.

2017) and the quartz-rich phase of the Cake Hill pluton (see above). Based on the presence of Early Jurassic fossils and zircon populations along strike (Gabrielse, 1998; Iverson et al., 2012) we interpret these zircons as having been derived from erosion of the underlying Cake Hill pluton (Late Triassic). The lack of penecontemporaneous zircons within the Spatsizi and lower Horn Mountain formations (this study; van Straaten and Gibson, 2017) suggests the source magmas to the alkaline mafic and felsic volcanic products did not crystallize zircon.

6.3. Takwahoni Formation

A coarse-grained, moderately-sorted feldspathic arenite from the Takwahoni greywacke unit (IJTgw; sample 16RGI-45-307; Sample 2, Fig. 2) yielded predominantly Early Jurassic zircons (Fig. 21b). The preliminary maximum depositional age

has a larger Mean Square Weighted Deviation (MSWD=3.1) than expected for such a population (target MSWD=1.4). This indicates that the scatter is greater than expected based on the precision of individual measurements, suggesting that: 1) all grains are not of the same true age, or 2) uncertainty is underestimated. We tentatively attribute the spread in ages due to the presence of overlapping Early Jurassic zircon populations. In addition to Early Jurassic zircons, the sample contains two Late Triassic and four Paleozoic grains.

Two thick beds of medium-grained, moderately-sorted feldspathic arenite in a section of predominantly siltstone (Takwahoni siltstone unit, IJTs; sample 16BvS-35-256; sample 3, Fig. 2) returned predominantly Early Jurassic zircons (Fig. 21c). Similar to the sample above, the preliminary maximum depositional age has a larger MSWD (2.9) than expected for such a population, likely resulting from overlapping Early Jurassic zircon populations. This sample also contains seven latest Triassic to earliest Jurassic, one Late Triassic, two early Late Triassic, and one Late Permian grain.

The preliminary maximum depositional age from both samples agree with Pliensbachian biostratigraphic constraints in Gabrielse (1998). The samples returned only three grains (ca. 215–218 Ma) that overlap with the Stikine plutonic suite (ca. 216–222 Ma, Table 2), suggesting that Whitehorse trough rocks in the study area were not sourced from the Cake Hill and related plutons. Possible sources for the Pliensbachian zircons include distal felsic ash fall or erosional products from lower Hazelton volcanic centres in the Stewart - Iskut area (e.g., Brucejack Lake felsic unit; Nelson et al., 2018), Nordenskiöld volcanic centres in the Whitehorse trough in southern Yukon (Colpron et al., 2015), and extrusive equivalents and/or erosion of the Aishihik and Long Lake plutonic suites along the BC-Yukon border (ca. 192–178 Ma, Mihalyuk, 1999; Colpron et al., 2016).

7. Mineral occurrences

We divide mineral occurrences in the map area (Fig. 3) according to mineralization characteristics, alteration style, alteration footprint, and host rock. Two sizeable intrusion-related gossans are west and southeast of the McBride River. Several volcanic rock-hosted Cu-Ag mineral occurrences, generally with limited alteration footprints, are hosted by the Horn Mountain Formation in the southeast part of the map area. A number of (locally auriferous) polymetallic veins are near the Kehlechoa and King Salmon thrust faults.

Preliminary assay data from eight altered and/or mineralized rock samples collected in 2015 and 2017 are presented in Table 3. Samples were jaw crushed and pulverized at the British Columbia Geological Survey, and analyzed at Bureau Veritas in Vancouver. The samples were dissolved using an aqua regia digestion before being analyzed by inductively coupled plasma-emission spectroscopy/mass spectrometry (ICP-ES/MS). Results of external standards and duplicates were monitored to ensure analytical reproducibility and accuracy. Detailed methods and complete results will be reported elsewhere.

Table 3. Assay results and coordinates of mineralized and altered rock samples.

Sample	Location	Easting	Northing	unit DL	Mo	Cu	Pb	Zn	Ag	Ni	Co	Mn	Fe	As	Au	Cd	Sb	Bi	W	S
					ppm	ppm	ppm	ppm	ppm	ppm	ppm	ppm	ppm	ppm	ppm	ppm	ppm	ppm	ppm	ppm
15BvS-25-11	3 km S D1	493040	6447048		8.0	>1%	10.2	46	22.0	3.8	4.8	161	5.07	11.2	391.4	1.1	0.6	2.6	0.1	0.33
17BvS-12-90	0.6 km E MSM	488954	6425909		4.5	43.2	9.4	11	0.1	2.1	2.2	26	1.53	1.5	<0.5	<0.1	0.2	0.9	<0.1	0.86
17BvS-2-11	Pk2102	481116	6441759		4.7	350.5	2.3	13	0.2	13.5	5.6	87	1.74	7.2	1.3	<0.1	0.3	0.3	0.3	0.91
17BvS-16-134	Pk2102	481595	6442112		4.4	35.1	5.6	52	<0.1	11.1	15.9	202	4.65	36.9	<0.5	0.2	0.3	0.3	0.1	2.55
17BvS-17-139	Pk2102	482194	6440885		0.3	155.7	7.4	19	0.3	5.0	61.5	165	11.96	5.3	5.1	<0.1	<0.1	1.6	0.1	6.59
17BvS-28-270	1 km NW Star	496771	6435397		0.1	>1%	13.0	41	22.7	2.4	3.7	339	1.22	5.4	60.5	1.1	1.2	0.9	<0.1	<0.05
17SBI-37-300	CM	499170	6431066		0.4	>1%	3.4	21	23.5	0.9	1.3	358	1.02	6.7	2.8	0.5	7.6	<0.1	0.3	<0.05
17SBI-41-361	5 km SE Pk2102	484610	6437844		0.2	10.3	21.3	26	<0.1	1.5	0.9	205	0.45	7.5	<0.5	0.1	0.1	<0.1	0.2	<0.05
<i>External standards and duplicates</i>																				
17SBI-41-361dup					0.3	42.5	21.3	31	<0.1	1.6	0.8	220	0.45	5.8	<0.5	<0.1	0.1	<0.1	0.3	<0.05
BCGS Till 2013 STD					0.7	170.1	225.9	399	1.8	212.2	50.0	1644	7.63	64.3	22.9	1.1	6.4	0.3	<0.1	<0.05
Expected*					0.8	170.0	240.0	410	2.2	250.0	60.0	1780	8.94	70.0	31.0	1.0	16.4	0.2	2.3	<0.01

Coordinates in NAD83, Zone 9 north
 Aqua regia digestion followed by ICP-ES/MS analysis
 Abbreviations: DL-detection limit, MSM=Mount Sister Mary, Pk2102=Peak 2102 m, N-north, E-east, S-south, W-west
 * BCGS Till 2013 expected values from A. Rukhlov, pers. comm. (2016)

7.1. Intrusion-related gossans

Two sizeable gossans are west and southeast of the McBride River. They likely formed by magmatic-hydrothermal activity related to Jurassic intrusions. Rusty red-brown weathering gossanous rocks are exposed in a zone (~0.5 by 4 km) centred on Peak 2102 m. The alteration is strongly controlled by lithology (Fig. 3). The Spatsizi Formation basal sandstone and conglomerate unit generally lacks sulphides, and instead displays common calcic skarn mineral assemblages. The strongest alteration is in interbedded argillite, siltstone, and fine-grained sandstone of the Spatsizi argillite, siltstone and sandstone unit, where strong silicification is accompanied by 5-10% (locally up to 20%) disseminated pyrite. Iron-oxide coated fracture sets likely represent oxidized pyrite veinlets, with vein densities up to one percent (Fig. 22). Thickly to very thickly bedded sandstone packages and rare mafic volcanic rocks within the Spatsizi argillite, siltstone and sandstone unit are generally less altered. Alteration in the overlying Horn Mountain lower mafic volcanic unit is limited to the lower contact, which contains oxidized pyrite and rare oxidized quartz-pyrite veinlets. The gossan is cut by relatively abundant altered felsic dikes (unit EMJf, Table 2); they likely represent feeders to the Horn Mountain lower felsic volcanic subunit (Section 4.2.). The Three Sisters pluton (Middle Jurassic) is exposed less than 1.5 km to west. It is likely that one of these felsic intrusive phases is responsible for the formation of this gossan. Grab samples returned no anomalous metal values (17BvS-2-11, 17BvS-16-134 and 17BvS-17-139, Table 3). A felsic dike near the Cake Hill pluton - Horn Mountain lower mafic volcanic unit contact (5.1 km southeast of Peak 2102 m) contains 2% disseminated pyrite; a grab sample yielded no anomalous metal values (17SBI-41-361, Table 3).

A prominent gossan (approximately 0.4 by 0.3 km) is exposed on a subalpine saddle 0.6 km east of Mount Sister Mary (Fig. 3); the southern portion is within the Stikine River



Fig. 22. Strongly silicified Spatsizi Formation sedimentary rocks (1mJSPs) with 5-10% disseminated pyrite and common iron oxide-coated fracture sets, likely representing sheeted pyrite veinlets.

Provincial Park. Within the gossan, strong silicification and bleaching are accompanied by 5-10% disseminated pyrite. The protolith is a uniformly-textured plagioclase-phyric rock, similar to flows in the Horn Mountain middle maroon volcanic unit. A grab sample returned no anomalous metal values (17BvS-12-90, Table 3). The altered and gossanous rocks are cut by late- to post-mineral chalky white-altered fine-grained diorite intrusions (JMRdr.fg, Table 2) that lack sulphides. Two showings within the Stikine River Provincial Park (Pay, MINFILE 104H 007; Pay 4, MINFILE 104H 027) are approximately 2.5 km west of the gossan.

Three additional mineral occurrences are hosted in the Hotailuh batholith in the southwestern part of the map area, and are described in van Straaten et al. (2012).

7.2. Volcanic rock-hosted Cu-Ag mineral occurrences

Several Cu-Ag mineral occurrences are hosted in Horn Mountain volcanic rocks, subvolcanic felsic intrusions, and faults in the southeastern part of the map area. Mineralization generally comprises chalcocite, chalcopyrite, bornite and/or native copper; obvious widespread hydrothermal alteration footprints are lacking. The occurrences have been variably classified as epigenetic veins and volcanic redbed copper in the MINFILE database (British Columbia Geological Survey, 2017). However, their presence in or close to felsic (sub) volcanic rocks may suggest a relatively low-temperature epithermal origin. Trenching and drilling at the CM prospect (MINFILE 104I 016, Fig. 3) intersected fine disseminations and stringers of chalcocite, bornite, and copper oxides accompanied by pervasive kaolinization, K-feldspar alteration, and local quartz-carbonate stringers in a vertical northeast-striking fault; a 6.1 m drill interval assayed 0.39% Cu and 8.57 g/t Ag (Chisholm, 1971). Chip samples across the zone averaged 1.94% Cu and 35.7 g/t Ag over 10 m (Yeager and Ikona, 1984). The trench exposes chalcocite and copper oxide stringers and local massive to vuggy quartz-calcite-chalcocite-copper oxide veinlets (Fig. 23). The mineralization is hosted in a cream to purple-grey, flow-banded plagioclase porphyry (likely a flow) of the Horn Mountain upper felsic volcanic unit, where it is cut by a south-southwest-striking fault with an approximately 10 metre west-side-down movement. A grab sample returned >1% Cu and 23.5 g/t Ag (17SBI-37-300, Table 3).

A light grey, bleached and silicified flow-banded plagioclase porphyry contains common copper oxides and locally abundant quartz-sulphide-copper oxide veinlets 1.3 km northwest of the Star showing (MINFILE 104I 027). The host rock is a felsic intrusion, and a grab sample returned >1% Cu, 22.7 g/t Ag and trace Au (17BvS-28-270, Table 3). At the nearby Star showing, local chalcocite and malachite are in north-trending subvertical brittle fault zones that cut gently dipping to subhorizontal strata of the Horn Mountain middle maroon volcanic unit. A historic grab sample returned 4.5% Cu (Mann and Reynolds, 1969).

We noted two gossanous outcrops with ~2% percent disseminated pyrite hosted in felsic intrusions and adjacent Horn Mountain middle maroon volcanic rocks in the valley

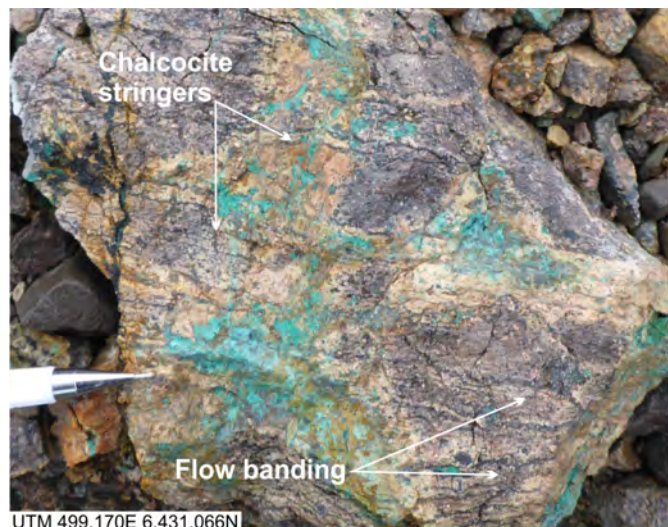


Fig. 23. Chalcocite and copper oxide stringers parallel to flow banding in felsic coherent rock (Horn Mountain upper felsic volcanic unit, mJHMUvf).

below the Joy 94 showing (MINFILE 104I 021). A nearby cirque to the southwest hosts the Joy 87 showing (MINFILE 104H 009). Gifford (1969) reported several chalcopyrite and malachite fractures that returned assay results up to 2.01% Cu, 6.9 g/t Ag, 1.37 g/t Au (Joy 87) and 5.7% Cu, 17 g/t Ag, trace Au (Joy 94).

Five additional copper and copper-silver mineral occurrences are east of Peak 2087 m (MINFILES 104H 010, 028, 029, 030 and 104I 015); descriptions refer to chalcocite, bornite and/or native copper as disseminations, in fractures or fault zones. Historic samples returned 0.21% Cu from a trench at Joy 84 (MINFILE 104H 010; Gifford, 1969) and 0.2% Cu and trace Ag from a 30 cm-long drill interval at HC (MINFILE 104I 015; Chisholm, 1971).

7.3. Polymetallic veins

Several polymetallic and locally auriferous quartz±carbonate veins are near the Kehlechoa and King Salmon thrust faults. A grab sample of quartz-chalcopyrite-malachite vein 2.8 km south of the D8 showing returned >1% Cu, 0.39 g/t Au and 22 g/t Ag (15BvS-25-11, Table 3). The vertical vein strikes 020 degrees and is 10-20 cm wide. The quartz vein cuts chert and volcanic clast-bearing conglomerate of the Bowser Lake Group, and is in the footwall of the Kehlechoa thrust fault (Fig. 19). Quartz and quartz-carbonate veins with chalcopyrite, bornite, galena, sphalerite and/or arsenopyrite locally contain high gold, silver, copper, lead and zinc values at the nearby D1, D4 and D8 showings (MINFILES 104I 093, 100, 101). A subvertical northwest-striking quartz-calcite vein at the D1 showing returned 116 g/t Au and 590 g/t Ag over 25 cm (Yeager and Ikona, 1982; 1985).

Quartz-calcite-chalcopyrite veins are in an east-northeast trending probable shear zone that cuts Sinwa Formation limestone at the ANT showing (MINFILE 104I 009; Hampton,

1962a). Chalcopyrite in quartz stringers and fracture fillings have been noted at the BEE showing (MINFILE 104I 010; Hampton, 1962b); the sulphides are hosted in Takwahoni Formation volcanic rocks.

8. Discussion: Regional extent and significance of the Horn Mountain Formation

Work on this project has identified the Horn Mountain Formation as a distinct late Early to Middle Jurassic volcanic unit. It extends along the northeastern edge of Stikinia for at least 80 km; evaluation of the regional literature indicates that it likely continues for at least 120 km (Fig. 1; van Straaten and Nelson, 2016). The Horn Mountain Formation represents an unusual volcanic sequence in the upper part of the Hazelton Group. It is coeval with accretion of the Stikine and Cache Creek terranes, as indicated by conformable contacts with rocks of the Bowser Lake Group, and so far similar volcanic successions have not been documented elsewhere in northern Stikinia. The Horn Mountain Formation postdates widespread arc volcanism recorded in the lower part of the Hazelton Group. In northern Stikinia, the upper part of the Hazelton Group consists mainly of Pliensbachian and younger sedimentary rocks assigned to the Spatsizi Formation in the north and the Nilkitkwa and Smithers formations in the south; both are succeeded by mudstone and minor tuff of the Quock Formation (Gagnon et al., 2012). Volcanic rocks are mainly in a narrow, north-south oriented belt of tholeiitic pillow basalts, sedimentary rocks, and minor rhyolites assigned to the Iskut River Formation (Gagnon et al., 2012; Barresi et al., 2015). This Middle Jurassic (Aalenian to Bajocian) succession is interpreted to have formed in a series of sub-basins that define the Eskay rift (Barresi et al., 2015; Fig. 1). The Iskut River Formation contrasts markedly with the Horn Mountain Formation in lithology, depositional style, structural setting, and litho-geochemistry (van Straaten and Nelson, 2016). As discussed elsewhere (van Straaten and Nelson, 2016), timing relationships with respect to subduction-related volcanic deposits elsewhere in the Hazelton Group and timing of Stikinia - Cache Creek collision suggest that the Horn Mountain Formation does not record normal subduction-related arc magmatism. Instead we speculate that volcanism was generated by re-melting of subduction-modified lithosphere during collision between the Stikine and Quesnel terranes, well after cessation of subduction in the Late Triassic.

9. Conclusions

This paper presents the results of the third year of a mapping project focussed on the Horn Mountain Formation (late Early to Middle Jurassic), a predominantly volcanic unit in the upper part of the Hazelton Group that regionally hosts advanced argillic alteration zones with potential for porphyry-style systems at depth. The Horn Mountain Formation is unusual because it is younger than any known volcanic succession of arc affinity in northern Stikinia.

The oldest rocks in the field area are part of the Cake Hill pluton. New U-Pb zircon data for the youngest hornblende

granodiorite to monzogranite phase yield a preliminary age of 217.91 ± 0.24 Ma, slightly older than a previous determination of 216.2 ± 1.2 Ma reported by van Straaten et al. (2012). The pluton is cut by an unconformity that extends laterally for at least 50 km and represents one of the few well-documented examples of unroofed Stuhini arc in northern Stikinia. The unconformity marks an hiatus of ~30 m.y. Detrital zircons in the overlying volcano-sedimentary succession are mostly derived from the Cake Hill pluton, and suggest that Late Triassic igneous activity in the area continued until ca. 215 Ma.

The unconformity is overlain by rocks in the upper part of the Hazelton Group in which the Spatsizi Formation (a sedimentary sequence up to 0.2 km thick) is conformably overlain by the Horn Mountain Formation (a volcanic succession at least 3.5 km thick). The volcanic rocks are unusual within northern Stikinia as they postdate widespread arc volcanism of the lower part of the Hazelton Group, are coeval with deposition of predominantly sedimentary rocks in the upper part of the Hazelton Group, and are concurrent with accretion of the Stikine and Cache Creek terranes. Sedimentary rocks of the Spatsizi Formation (Toarcian) grade into mafic volcanic breccia of the lower part of the Horn Mountain Formation. They were, at least in part, deposited in a subaqueous environment. Increasingly higher volume volcanism led to the formation of a subaerial volcanic edifice and deposition of interlayered flows, volcanic breccia and tuff of the middle maroon volcanic unit. Lower and middle units are cut by cogenetic mafic feeder dikes and intrusions. An upper felsic volcanic unit caps the succession.

The Horn Mountain Formation is cut by the Three Sisters pluton (ca. 173-169 Ma) and the McBride River pluton. The McBride River granodiorite has hitherto been interpreted as Early Jurassic (ca. 184 Ma), but this age is difficult to reconcile with the unequivocal crosscutting relationships observed in the field and we suggest that a Middle Jurassic or younger age is more plausible.

The Bowser Lake Group (Bajocian) conformably overlies the Horn Mountain Formation, and records the onset of erosion from the Stikinia - Cache Creek tectonic welt. Chert and limestone clast-bearing pebble to cobble conglomerate (>330 m thick) is interpreted to have formed close to range front faults along the building orogen. The coarse clastic facies transitions to interbedded subaerial siltstone, sandstone, chert clast-bearing conglomerate and mafic flows (>430 m thick) farther south.

The Kehlechoa thrust fault places rocks of the Whitehorse trough above the Horn Mountain Formation and Bowser Lake Group. The hanging wall panel contains Sinwa Formation limestone (Upper Triassic) unconformably overlain by Takwahoni Formation sedimentary rocks (Early Jurassic). The Takwahoni Formation comprises a lithologically variable package of fine-grained siliciclastic rocks, polymictic conglomerate, and volcanic rocks (Sinemurian?) that appears to grade upward into a thick unit of interbedded sandstone and siltstone (Pliensbachian). Two detrital zircon samples from the upper unit returned a largely unimodal ca. 187-188 Ma

(Pliensbachian) population; significant Late Triassic zircons are lacking. The detrital zircon data are compatible with derivation from local Stikinia sources or axial transport from sources within or adjacent to the Whitehorse trough in southern Yukon, and suggest that the Cake Hill and related plutons were not significant sources.

Two intrusion-related hydrothermal alteration zones are west and southeast of the McBride River; limited sampling returned no anomalous metal values. Several Cu-Ag mineral occurrences with restricted alteration footprints are hosted in the middle and upper part of the Horn Mountain Formation in the southeast part of the map area. Polymetallic veins are near the Kehlechoa and King Salmon thrust faults; some have returned significant gold and silver values.

The Horn Mountain Formation represents a rare example of syncollisional volcanism that is coeval with accretion of the Stikine and Quesnel island arcs. Continuing study of its nature and relationships to adjacent terranes will aid in the understanding of collisional tectonics of the northern Canadian Cordillera.

Acknowledgments

We thank Marc Beaton and Rachel Gavin for their capable and enthusiastic assistance during the field season, and Tundra Helicopters for safe flying. Thanks to JoAnne Nelson for constructive commentary that significantly improved the manuscript. We also thank Terry Poulton (Geological Survey of Canada, Calgary) for providing preliminary macrofossil age determinations and Richard Friedman (University of British Columbia, Vancouver) for providing preliminary U-Pb zircon geochronology results.

References cited

- Aeroquest Airborne, 2012. Report on a helicopter-borne magnetic survey (Aeroquest Job #11-046) for Geoscience BC. Geoscience BC Report 2012-2, 11 p.
- Anderson, R.G., 1983. Geology of the Hotailuh batholith and surrounding volcanic and sedimentary rocks, north-central British Columbia. Unpublished Ph.D. thesis, Carleton University, Ottawa, Ontario, Canada, 669 p.
- Anderson, R.G., and Bevier, M.L., 1992. New late Triassic and early Jurassic U-Pb zircon ages from the Hotailuh Batholith, Cry Lake map area, North - Central British Columbia. In: Radiogenic age and isotopic studies: Report 6, Geological Survey of Canada Paper 92-02, pp. 145-152.
- Anderson, R.G., Loveridge, W.D., and Sullivan, R.W., 1982. U-Pb isotopic ages of zircon from the Jurassic plutonic suite, Hotailuh Batholith, north-central British Columbia. Current Research, Part C, Rb-Sr and U-Pb isotopic age studies, Report 5 Paper 82-1C, Geological Survey of Canada.
- Barresi, T., Nelson, J.L., and Dostal, J., 2015. Geochemical constraints on magmatic and metallogenic processes: Iskut River Formation, volcanogenic massive sulfide-hosting basalts, NW British Columbia, Canada. *Canadian Journal of Earth Sciences*, 52, 1-20.
- British Columbia Geological Survey, 2017. MINFILE-British Columbia mineral inventory database. Available from <http://minfile.gov.bc.ca/>.
- Chisholm, E., 1971. Progress Report - McBride River Project. British Columbia Ministry of Energy and Mines, Assessment Report 3237, 32 p.
- Cohen, K.M., Finney, S.C., Gibbard, P.L., and Fan, J.-X., 2013. The ICS International Chronostratigraphic Chart. *Episodes*, 36, 199-204. Updated version (February, 2017) available from <http://www.stratigraphy.org/>.
- Colpron, M., Crowley, J.L., Gehrels, G., Long, D.G.F., Murphy, D.C., Beranek, L., and Bickerton, L., 2015. Birth of the northern Cordilleran orogen, as recorded by detrital zircons in Jurassic synorogenic strata and regional exhumation in Yukon. *Lithosphere*, 7, 541-562.
- Colpron, M., Israel, S., and Friend, M., 2016. Yukon plutonic suites. Yukon Geological Survey, Open File 2016-37, 1:750,000 scale.
- Dickinson, W.R., and Gehrels, G.E., 2009. Use of U-Pb ages of detrital zircons to infer maximum depositional ages of strata: A test against a Colorado Plateau Mesozoic database. *Earth and Planetary Science Letters*, 288, 115-125.
- Erdman, L.R., 1978. Petrology, geochronology and geochemistry of Jurassic volcanic and granitic rocks of the Cry Lake and Spatsizi map sheets, north-central British Columbia. Unpublished B.Sc. thesis, The University of British Columbia, Vancouver, B.C., Canada, 63 p.
- Evenchick, C.A., and Thorkelson, D.J., 2005. Geology of the Spatsizi River map area, north-central British Columbia. Geological Survey of Canada Bulletin 577, 276 p.
- Evenchick, C.A., McMechan, M.E., McNicoll, V.J., and Carr, S.D., 2007. A synthesis of the Jurassic-Cretaceous tectonic evolution of the central and southeastern Canadian Cordillera: Exploring links across the orogen. *Geological Society of America Special Papers*, 433, 117-145.
- Evenchick, C.A., Poulton, T.P., and McNicoll, V.J., 2010. Nature and significance of the diachronous contact between the Hazelton and Bowser Lake groups (Jurassic), north-central British Columbia. *Bulletin of Canadian Petroleum Geology*, 58, 235-267.
- Gabrielse, H., 1985. Major dextral transcurrent displacements along the Northern Rocky Mountain Trench and related lineaments in north-central British Columbia. *Geological Society of America Bulletin*, 96, 1-14.
- Gabrielse, H., 1998. Geology of Cry Lake and Dease Lake map areas, North-Central British Columbia. Geological Survey of Canada Bulletin 504, 147 p.
- Gagnon, J.-F., Barresi, T., Waldron, J.W.F., Nelson, J.L., Poulton, T.P., and Cordey, F., 2012. Stratigraphy of the upper Hazelton Group and the Jurassic evolution of the Stikine terrane, British Columbia. *Canadian Journal of Earth Sciences*, 49, 1027-1052.
- Gifford, R., 1969. Bowser Resources Ltd., McBride River Project, British Columbia. British Columbia Ministry of Energy and Mines, Property Files 019716, 019720, 019721 and 019723.
- Gillespie, M.R., and Styles, M.T., 1999. BGS rock classification scheme. Volume 1. Classification of igneous rocks. British Geological Survey Research Report RR99-06, 52 p.
- Hallsworth, C.R., and Knox, R.W.O., 1999. BGS rock classification scheme. Volume 3. Classification of sediments and sedimentary rocks. British Geological Survey Research Report RR99-03, 44 p.
- Hampton, M., 1962a. Geological Report on the ANT Mineral Claim Group. British Columbia Ministry of Energy and Mines, Assessment Report 437, 9 p.
- Hampton, M., 1962b. Geological Report on the BEE Mineral Claim Group. British Columbia Ministry of Energy and Mines, Assessment Report 438, 10 p.
- Henderson, C.M., and Perry, D.G., 1981. A Lower Jurassic heteropodid bryozoan and associated biota, Turnagain Lake, British Columbia. *Canadian Journal of Earth Sciences*, 18, 457-468.
- Iverson, O., Mahoney, J.B., and Logan, J.M., 2012. Dease Lake geoscience project, part IV: Tsaybahe group: Lithological and geochemical characterization of Middle Triassic volcanism in

- the Stikine arch, north-central British Columbia. In: Geological Fieldwork 2011, British Columbia Ministry of Energy, Mines and Natural Gas, British Columbia Geological Survey Paper 2012-1, pp. 17-22.
- Johannson, G.G., Smith, P.L., and Gordey, S.P., 1997. Early Jurassic evolution of the northern Stikinian arc: evidence from the Laberge Group, northwestern British Columbia. *Canadian Journal of Earth Sciences*, 34, 1030-1057.
- Kretz, R., 1983. Symbols for rock-forming minerals. *American Mineralogist*, 68, 227-279.
- Logan, J.M., and Mihalynuk, M.G., 2014. Tectonic controls on Early Mesozoic paired alkaline porphyry deposit belts (Cu-Au \pm -Ag-Pt-Mo) within the Canadian Cordillera. *Economic Geology*, 109, 827-858.
- Ludwig, K.R., 2012. Isoplot 3.75. A Geochronological Toolkit for Microsoft Excel. Special Publication No. 5, Berkley Geochronology Center.
- Mann, D., and Reynolds, N.W., 1969. Geological report on the STAR claims. British Columbia Ministry of Energy and Mines, Assessment Report 2154, 15 p.
- Marsden, H., and Thorkelson, D.J., 1992. Geology of the Hazelton Volcanic Belt in British Columbia: Implications for the Early to Middle Jurassic evolution of Stikinia. *Tectonics*, 11, pp. 1266-1287.
- Mihalynuk, M.G., 1999. Geology and Mineral Resources of the Tagish Lake Area, (NTS 104M/8,9,10E, 15 and 104N/12W), Northwestern British Columbia. British Columbia Ministry of Energy and Mines, British Columbia Geological Survey Bulletin 105, 202 p.
- Mihalynuk, M.G., Erdmer, P., Ghent, E.D., Archibald, D.A., Friedman, R.M., Cordey, F., Johannson, G.G., and Beanish, J., 1999. Age constraints for emplacement of the northern Cache Creek terrane and implications of blueschist metamorphism. In: Geological Fieldwork 1998, British Columbia Ministry of Energy and Mines, British Columbia Geological Survey Paper 1999-1, pp. 127-141.
- Mihalynuk, M.G., Erdmer, P., Ghent, E.D., Cordey, F., Archibald, D.A., Friedman, R.M., and Johannson, G.G., 2004. Coherent French Range blueschist: Subduction to exhumation in <2.5 m.y.? *Geological Society of America Bulletin*, 116, 910.
- Mihalynuk, M.G., Nelson, J., and Diakow, L.J., 1994. Cache Creek terrane entrapment: Oroclinal paradox within the Canadian Cordillera. *Tectonics*, 13, 575-595.
- Nelson, J., and Mihalynuk, M., 1993. Cache Creek ocean: Closure or enclosure? *Geology*, 21, 173-176.
- Nelson, J., Colpron, M., and Israel, S., 2013. The Cordillera of British Columbia, Yukon and Alaska: tectonics and metallogeny. In: Colpron, M., Bissig, T., Rusk, B., and Thompson, J.F.H., (Eds.), *Tectonics, metallogeny and discovery: the North American cordillera and similar accretionary settings*. Society of Economic Geologists, Special Publication 17, pp. 53-109.
- Nelson, J.L., Waldron, J., van Straaten, B.I., Zagorevski, A., and Rees, C., 2018. Revised stratigraphy and regional digital map representation of the Hazelton Group in the Iskut River region, northwestern British Columbia. In: Geological Fieldwork 2018, British Columbia Ministry of Energy, Mines and Petroleum Resources, British Columbia Geological Survey Paper 2018-1, pp. 15-38.
- Olsen, H., Due, P.H., and Clemmensen, L.B., 1989. Morphology and genesis of asymmetric adhesion warts - a new adhesion surface structure. *Sedimentary Geology*, 61, 277-285.
- Read, P.B., and Psutka, J.F., 1990. Geology of Ealue Lake East-half (104H/13E) and Cullivan Creek (104H/14) map areas, British Columbia. Geological Survey of Canada Open File 2241, Geological Survey of Canada.
- Samperton, K.M., Schoene, B., Cottle, J.M., Brenhin Keller, C., Crowley, J.L., and Schmitz, M.D., 2015. Magma emplacement, differentiation and cooling in the middle crust: Integrated zircon geochronological-geochemical constraints from the Bergell Intrusion, Central Alps. *Chemical Geology*, 417, 322-340.
- Schiarizza, P., 2012. Geology of the Kutcho assemblage between the Kehlechoa and Tucho Rivers, northern British Columbia (NTS 104I/01, 02). In: Geological Fieldwork 2011, British Columbia Ministry of Energy and Mines, British Columbia Geological Survey Paper 2012-1, pp. 75-98.
- Shirmohammad, F., Smith, P.L., Anderson, R.G., and McNicoll, V.J., 2011. The Jurassic succession at Lisadele Lake (Tulsequah map area, British Columbia, Canada) and its bearing on the tectonic evolution of the Stikine terrane. *Volumina Jurassica*, 9, 43-60.
- Stevens, R.D., DeLabio, R.N., and Lachance, G.R., 1982. Age determinations and geological studies. In: K-Ar isotopic ages, report 16, Geological Survey of Canada Paper 82-2, pp. 5-11.
- van Straaten, B.I., and Gibson, R., 2017. Late Early to Middle Jurassic Hazelton Group volcanism and mineral occurrences in the McBride-Tanzilla area, northwest British Columbia. In: Geological Fieldwork 2016, British Columbia Ministry of Energy and Mines, British Columbia Geological Survey Paper 2017-1, pp. 83-115.
- van Straaten, B.I., and Nelson, J.L., 2016. Syncollisional late Early to early Late Jurassic volcanism, plutonism, and porphyry-style alteration on the northeastern margin of Stikinia. In: Geological Fieldwork 2015, British Columbia Ministry of Energy and Mines, British Columbia Geological Survey Paper 2016-1, pp. 113-143.
- van Straaten, B.I., Gibson, R., and Nelson, J.L., 2017. Preliminary bedrock geology of the Tanzilla and McBride area (NTS 104I/03, 04, 05, 06). British Columbia Ministry of Energy and Mines, British Columbia Geological Survey Open File 2017-9, 1:50,000 scale.
- van Straaten, B.I., Logan, J.M., and Diakow, L.J., 2012. Mesozoic magmatism and metallogeny of the Hotailuh Batholith, northwestern British Columbia. British Columbia Ministry of Energy, Mines and Natural Gas, British Columbia Geological Survey Open File 2012-6, 58 p.
- Takaichi, M., 2013a. Assessment Report on the 2012 Geological, Geochemical, Program at the McBride Property, BC, Canada. British Columbia Ministry of Energy and Mines, Assessment Report 34265, 17 p.
- Takaichi, M., 2013b. Assessment Report on the 2012 Geological, Geochemical, and Geophysical Program at the Eagle Property, BC, Canada. British Columbia Ministry of Energy and Mines, Assessment Report 34266, 22 p.
- Thomson, R.C., Smith, P.L., and Tipper, H.W., 1986. Lower to Middle Jurassic (Pliensbachian to Bajocian) stratigraphy of the northern Spatsizi area, north-central British Columbia. *Canadian Journal of Earth Sciences*, 23, 1963-1973.
- Tipper, H.W., 1978. Jurassic biostratigraphy, Cry Lake map-area, British Columbia. In: Current Research, Part A, Geological Survey of Canada Paper 78-1A, pp. 25-27.
- Tipper, H.W., and Richards, T.A., 1976. Jurassic stratigraphy and history of north-central British Columbia. *Geological Survey of Canada Bulletin 270*, Geological Survey of Canada, 82 p.
- Yeager, D.A., and Ikona, C.K., 1982. Report on the D1 Mineral Claim. British Columbia Ministry of Energy and Mines, Assessment Report 10699, 30 p.
- Yeager, D.A., and Ikona, C.K., 1984. Geochemical and geological report on the Mt. Sister Mary Property. British Columbia Ministry of Energy and Mines, Assessment Report 12292, 40 p.
- Yeager, D.A., and Ikona, C.K., 1985. Report on the D1, D3, D4, D6, D8, and D9 Mineral Claims. British Columbia Ministry of Energy and Mines, Assessment Report 14004, 27 p.

Testing the relationship between the Llewellyn fault, Tally-Ho shear zone, and gold mineralization in northwest British Columbia



Luke Ootes^{1, a}, Sébastien Castonguay², Richard Friedman³, Fionnuala Devine⁴, and Reid Simmonds⁵

¹ British Columbia Geological Survey, Ministry of Energy, Mines and Petroleum Resources, Victoria, BC, V8W 9N3

² Geological Survey of Canada, Natural Resources Canada, Quebec City, QC, G1K 9A9

³ Pacific Centre for Geochemical and Isotopic Research, University of British Columbia, Vancouver, BC, V6T 1Z4

⁴ Merlin Geosciences Inc., Atlin, BC, V0W 1A0

⁵ School of Earth and Ocean Sciences, University of Victoria, Victoria, BC, V8P 5C2

^a corresponding author: Luke.Ootes@gov.bc.ca

Recommended citation: Ootes, L., Castonguay, S., Friedman, R., Devine, F., and Simmonds, R., 2018. Testing the relationship between the Llewellyn fault, Tally-Ho shear zone, and gold mineralization in northwest British Columbia. In: Geological Fieldwork 2017, British Columbia Ministry of Energy, Mines and Petroleum Resources, British Columbia Geological Survey Paper 2018-1, pp. 67-81.

Abstract

The Llewellyn fault represents a significant geological feature in northwest British Columbia. The fault is a southeast-striking, steeply dipping brittle dextral strike-slip structure that overprints 'early' ductile deformation, which is preserved as foliations, lineations, and folds in the host rocks. The Tally-Ho shear zone, Yukon, shares similar early ductile deformation and is overprinted by the Llewellyn fault. In general, the deformation corridor demarcates the eastern limit of metamorphic suites (Triassic and older rocks of the Nisling terrane and Boundary Ranges metamorphic suite) and the western limit of the younger Stuhini (Triassic) and Laberge (Jurassic) groups. Previous work and this study demonstrate that brittle strike-slip deformation along the Llewellyn fault occurred between ca. 56 and 50 Ma. New field observations indicate the early ductile deformation is represented by one foliation (S_{main}) along the Llewellyn fault and Tally-Ho shear zone corridor. Two granodiorite intrusions crosscut the early deformation features, and new U-Pb zircon chemical abrasion ID-TIMS results indicate they crystallized at ca. 75 Ma. In the Tally-Ho shear zone, the S_{main} is parallel to a foliation in an adjacent granodiorite, mapped as part of the Whitehorse plutonic complex (ca. 120 Ma). In British Columbia, a deformed rhyolite along the Llewellyn fault yielded a preliminary ca. 120 Ma age. Based on these results, we infer that the early ductile fabrics formed before ca. 75 Ma and, potentially, after ca. 120 Ma.

A goal of this study was to establish if the early ductile and late brittle structures represent a crustal-scale, ductile-brittle deformation continuum. If so, could various gold mineralization styles (epithermal, mesothermal, intrusion-related) along the structural corridor be related in time and be part of an orogenic gold mineralizing system? This study demonstrates that, although the early ductile and late brittle deformation share the same space, they developed at least ca. 20 Ma apart and are not part of a structural continuum. This result indicates the various styles of gold mineralization developed during temporally distinct tectonic events.

Keywords: Llewellyn fault, Tally-Ho shear zone, U-Pb geochronology, gold

1. Introduction

This study was designed to document the geologic setting and controls of gold mineralization spatially associated with selected major fault zones of the Canadian Cordillera. The chosen field laboratory extends from the Tagish Lake area of northwest British Columbia northward to the Wheaton River area in southern Yukon (Fig. 1). This area is the locus of a series of vein-hosted gold prospects and deposits, including past-producing mines (e.g., Engineer, Mount Skukum) that are spatially related to the Llewellyn fault and Tally-Ho shear zone (e.g., Hart and Radloff, 1990; Mihalynuk et al., 1999; Tizzard et al., 2009; Ootes et al., 2017). The area also encompasses multiple lithotectonic suites that are affected by the faults (Fig. 2). The timing of deformation along the fault zones and the temporal and genetic relationships with intrusion-related,

mesothermal, and epithermal-style gold systems remain to be clearly established.

Herein we present new field observations about the relationship between the Llewellyn fault and the Tally-Ho shear zone (Hart and Radloff, 1990; Tizzard et al., 2009) and five new chemical abrasion ID-TIMS U-Pb zircon ages. These data constrain the timing of ductile and the late brittle strain and associated gold mineralization that characterizes this deformation corridor.

2. Background and geology

The Llewellyn fault extends along strike northwest from British Columbia to the Tally-Ho shear zone in Yukon (Figs. 1, 2). In general, this deformation zone marks the boundary between the Nisling terrane to the west and Stikine

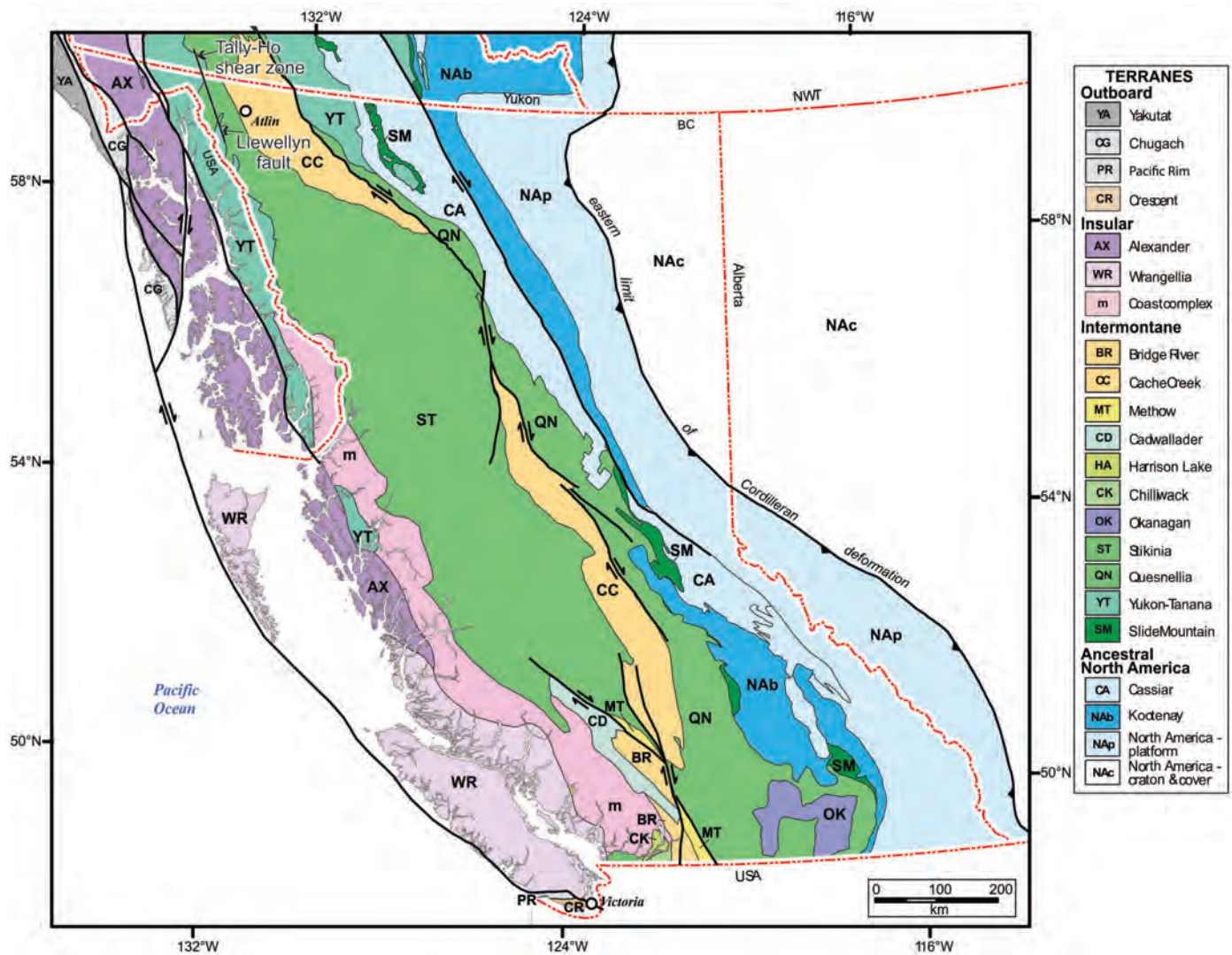


Fig. 1. Terrane map of British Columbia and neighbouring jurisdictions. Modified after Nelson et al. (2013).

terrane to the east (Fig. 2; Hart and Radloff, 1990; Mihalynuk et al., 1999) and is spatially associated with a variety of gold prospects and minor past producers (Fig. 2). This gold mineralization has characteristics that range from mesothermal (Montana Mountain mines; Fig. 2; Roots, 1981; Walton, 1986; Hart and Pelletier, 1989), to epithermal (Mount Skukum and Engineer mines; Love, 1990, Love et al., 1998; Millinog et al., 2017), to intrusion-related (Bennett plateau and Middle ridge prospects, Golden Eagle project; Mihalynuk et al., 2003; Wark, 2012).

Reconnaissance fieldwork, data compilation, and preliminary reports (Castonguay et al., 2017; Ootes et al., 2017) have underlined that the epithermal gold mineralization at the Engineer and Mount Skukum deposits coincide both spatially and temporally with Eocene magmatism (also see Love et al., 1998; Millinog et al., 2017). These first-order observations led to the suggestion of a relationship between large-scale deformation zones, gold mineralization, and Eocene magmatism in southwest Yukon and northwest British Columbia.

2.1. Tally-Ho shear zone

2.1.1. Overview

North of the BC-Yukon border, the Tally-Ho shear zone is defined by a corridor of strongly deformed amphibolite, marble, and schist, assigned to the Povoas Formation of the Lewes River Group (Upper Triassic; equivalent to Stuhini Group in British Columbia). This corridor is bounded on either side by younger intrusions (Fig. 2; Doherty and Hart, 1988; Hart and Radloff, 1990; Tizzard et al., 2009). The shear zone can be traced for ~40 km along strike and is best exposed between Tally-Ho Mountain and Mount Hodnett (Hart and Radloff, 1990; Tizzard et al., 2009). The shear zone comprises marbles and amphibolites that have a southwest-dipping penetrative foliation to mylonitic fabric, and a shallow southeast- or northwest-plunging mineral lineation (Fig. 3; Hart and Radloff, 1990). Bedding is locally preserved in marble layers, but is strongly transposed into the foliation as the mylonite zones are approached (Hart and Radloff, 1990; Tizzard et al., 2009).

Hart and Radloff (1990) interpreted that the Tally-Ho shear

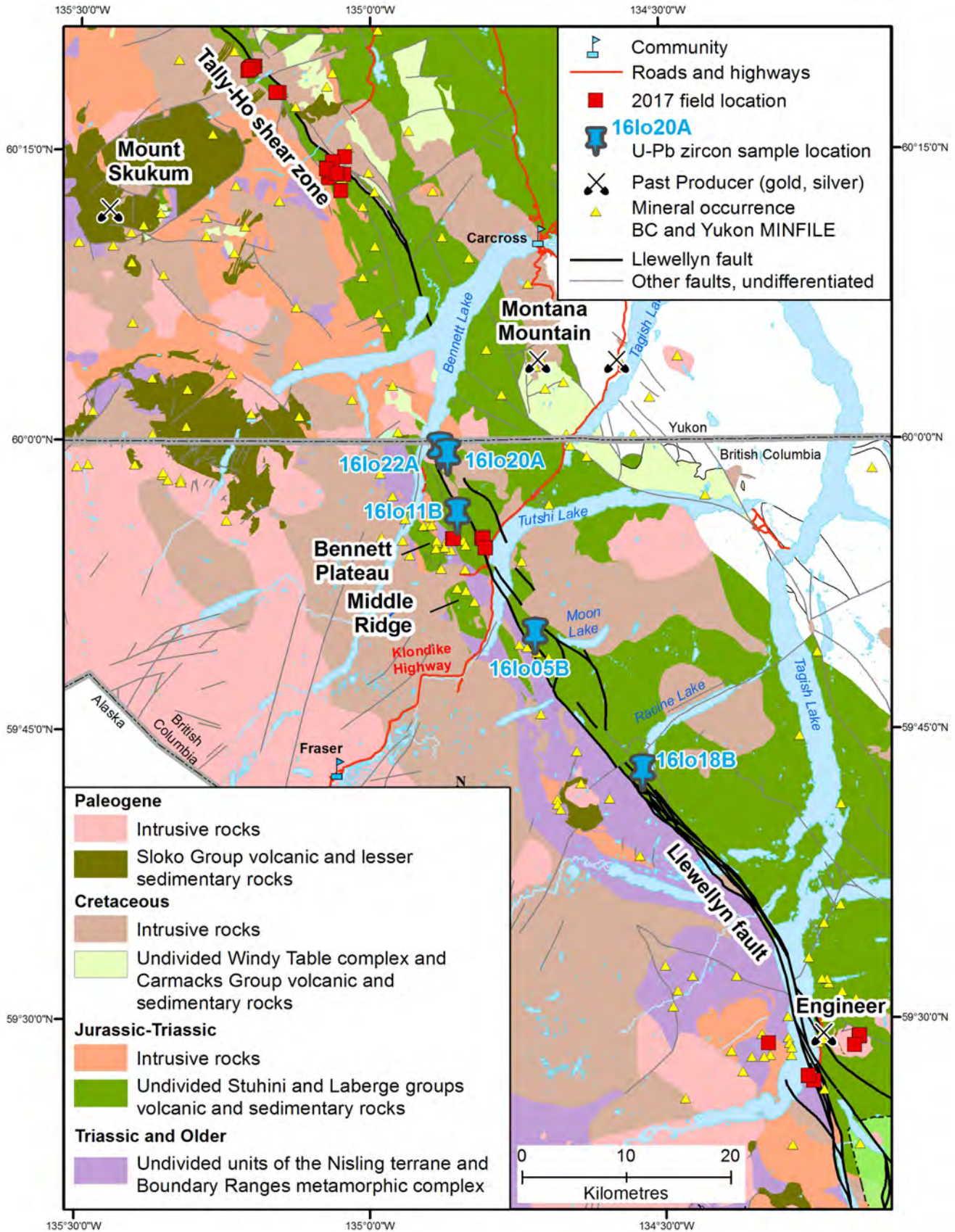


Fig. 2. Simplified geology near the Llewellyn fault and Tally-Ho shear zone. Geology is after Doherty and Hart (1988), Hart and Pelletier (1989), Hart and Radloff (1990), and Mihalyuk et al. (1999). Rocks of the Cache Creek assemblage (upper right) are unfilled.

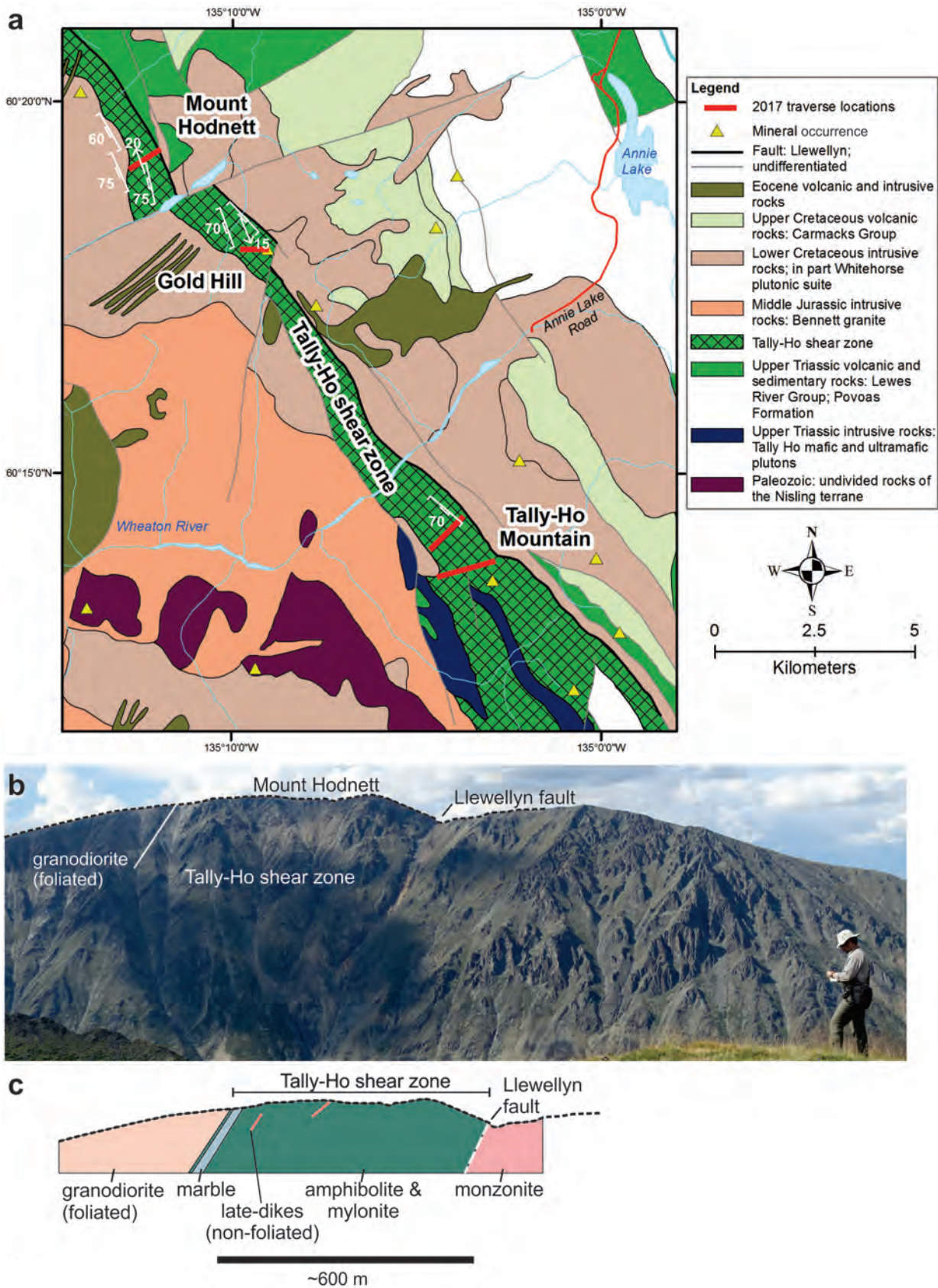


Fig. 3. a) Simplified geology of the Tally-Ho shear zone, southern Yukon (modified after Hart and Radloff, 1990). Generalized foliations (line with pendants) and lineations (arrows) are from this study and Hart and Radloff (1990). **b)** View of Mount Hodnett and Tally-Ho shear zone from Gold Hill. View is north. **c)** Geological sketch of Mount Hodnett, in upper left of photo; in part modified after Tizzard et al. (2009).

zone records predominantly sinistral deformation between 230 and 220 Ma, and speculated on its potential importance as a terrane-bounding thrust fault. Revising this interpretation, Tizzard et al. (2009) considered that the shear zone represents a top-to-the-east crustal thrust fault that was later folded during Nisling-Stikine collision. Accordingly, foliated gabbro and pyroxenite (hangingwall) were thrust over Povoas Formation (shear zone and footwall) and subsequently affected by upright folds (Tizzard et al., 2009). Uranium-lead zircon ages of ca. 208 Ma for leucogabbro in the hangingwall and ca. 173 Ma for undeformed K-feldspar porphyritic granite west of the shear zone bracket the timing of thrusting and subsequent folding (Tizzard et al., 2009).

Brittle deformation features are parallel to and overprint the Tally-Ho shear zone ductile fabrics. These include faults with dextral offset and fractures (Hart and Radloff (1990). Hart and Radloff (1990) mapped one particular brittle fault zone along the east side of the Tally-Ho shear zone, which they correlated to the Llewellyn fault (Figs. 2, 3).

2.1.2. Field observations

Traverses across the Tally-Ho shear zone were conducted in the Tally-Ho Mountain, Gold Hill, and Mount Hodnett areas of Yukon (Figs. 2, 3). The best exposed and accessible section appears to be at Mount Hodnett (Fig. 3). Exposed units include (from west to east): weakly to moderately foliated granodiorite in sheared contact with steeply west-dipping amphibolite and marble; strongly sheared mafic volcanoclastic rocks (mylonite); and foliated metabasalt (Figs. 3 and 4). Bedding (S_0) is preserved and folded in the marble. Folds have shallow northwest, or southeast plunging axes and axial planes are parallel to the main foliation (S_{main} ; Fig. 4a). The S_{main} occurs in all rocks but is best developed in mylonitic volcanoclastic beds, where the composite layering may be a result of S_{main} being parallel to S_0 (Fig. 4b). East of this, the shear zone is mostly strongly foliated (S_{main}) amphibolite/metabasalt (Fig. 4c). Kinematic indicators, albeit rare, include shear bands, sigmoidal porphyroclasts, and quartz vein boudins, suggest apparent northeast-directed motion. However, the shallowly plunging stretching and/or mineral lineation on S_{main} indicates strike-slip movement. Locally, the older ductile fabrics are offset and kinked along discrete brittle faults. Along the eastern side of the shear zone the foliated amphibolite/metabasalt is structurally interlayered with moderately foliated monzonite (Fig. 3c). This juxtaposition is the result of sub-vertical brittle high strain zones marked by cataclasite that overprints the foliation in the metabasalt (Figs. 3, 4d). This brittle fault zone is <10 m wide and consists of cataclasite and carbonate alteration. Drill collars attest that the zones have been tested by exploration drilling. All units are intruded by unfoliated feldspar-porphyritic intermediate dikes (Fig. 4d).

The granodiorite west of the shear zone (Fig. 3a) was assigned to the Whitehorse plutonic suite (ca. 120 Ma; Hart and Radloff, 1990). This granodiorite contains a foliation, defined by biotite and hornblende that are now partially altered to chlorite. This

foliation strikes south-southeast and dips west ($165^\circ/70^\circ\text{W}$) and is parallel to the S_{main} in the deformation zone (ca. $170^\circ/75^\circ\text{W}$; Figs. 3, 4). Because only one foliation has been identified in the shear zone (Fig. 4), it is best interpreted as having been derived from the same deformation (also see Hart and Radloff, 1990).

2.2. Llewellyn fault

2.2.1. Overview

The Llewellyn fault is a southeast-striking, steeply dipping brittle dextral strike-slip structure that overprints early ductile fabrics. The structure continues for >100 km, from the Tulsequah area in the south to beyond the BC-Yukon border in the north (Mihalynuk et al., 1994, 1999). The Llewellyn fault represents a domain boundary (Fig. 2), with the Boundary Ranges metamorphic suite to the west (pre-Triassic; part of Stikine or Nisling terrane?) and Stuhini and Laberge group volcano-sedimentary rocks to the east (Triassic-Jurassic; part of the Stikine Terrane; Fig. 2; Mihalynuk et al., 1999). Along the Llewellyn structure, the rocks contain penetrative fabrics (folds, foliations, and lineations) that trend south-southeast, and have been interpreted to indicate sinistral shear (Mihalynuk et al., 1999). The ductile deformation post-dates deposition of the Laberge Group (Jurassic). Older deformation fabrics may occur in pre-Triassic rocks (e.g., Boundary Ranges metamorphic complex), but the subparallel nature of the fabrics along the Llewellyn fault precludes subdivision (e.g., Mihalynuk et al., 1999). Upper Cretaceous and Eocene plutons crosscut the ductile fabrics, providing a minimum age for the ductile deformation (Mihalynuk et al., 1999).

Brittle deformation along the Llewellyn fault is temporally constrained by vein-hosted gold mineralization at Engineer Mine. There, vanadian illite, produced by fluid-rock interaction during epithermal vein formation, has been dated by ^{40}Ar - ^{39}Ar at ca. 50 Ma (Millonig et al., 2017). As the epithermal veins at Engineer are related to brittle deformation along the Llewellyn fault, this age approximates the timing of brittle strike-slip movement (e.g., Ootes et al., 2016; Millonig et al., 2017). This timing coincides with Cordillera-wide dextral strike-slip faulting (e.g., Gabrielse et al., 2006).

2.2.2. Field observations

Some locations along the Llewellyn fault, previously investigated by Ootes et al. (2017), were revisited in 2017. In the Bennett plateau and Tagish Lake areas, British Columbia, traverses were conducted across the Llewellyn fault zone (Figs. 2, 3). At Bennett plateau, the 'Skarn zone' (Fig. 2) is known to host gold and base-metal mineralization that developed with a series of hydrothermal quartz-actinolite veins hosted in metasedimentary rocks of the Stuhini Group (Fig. 5; Mihalynuk et al., 1999; Wark, 2012). These veins are boudinaged and folded (z-shaped; Figs. 5a, b). Where identifiable, bedding and foliation strike northwest and dip steeply to moderately east (ca. $345^\circ/50^\circ\text{E}$). A 2 m-wide porphyry intrusion with a fine-grained siliceous matrix and quartz-feldspar-biotite phenocrysts (granodiorite) intruded

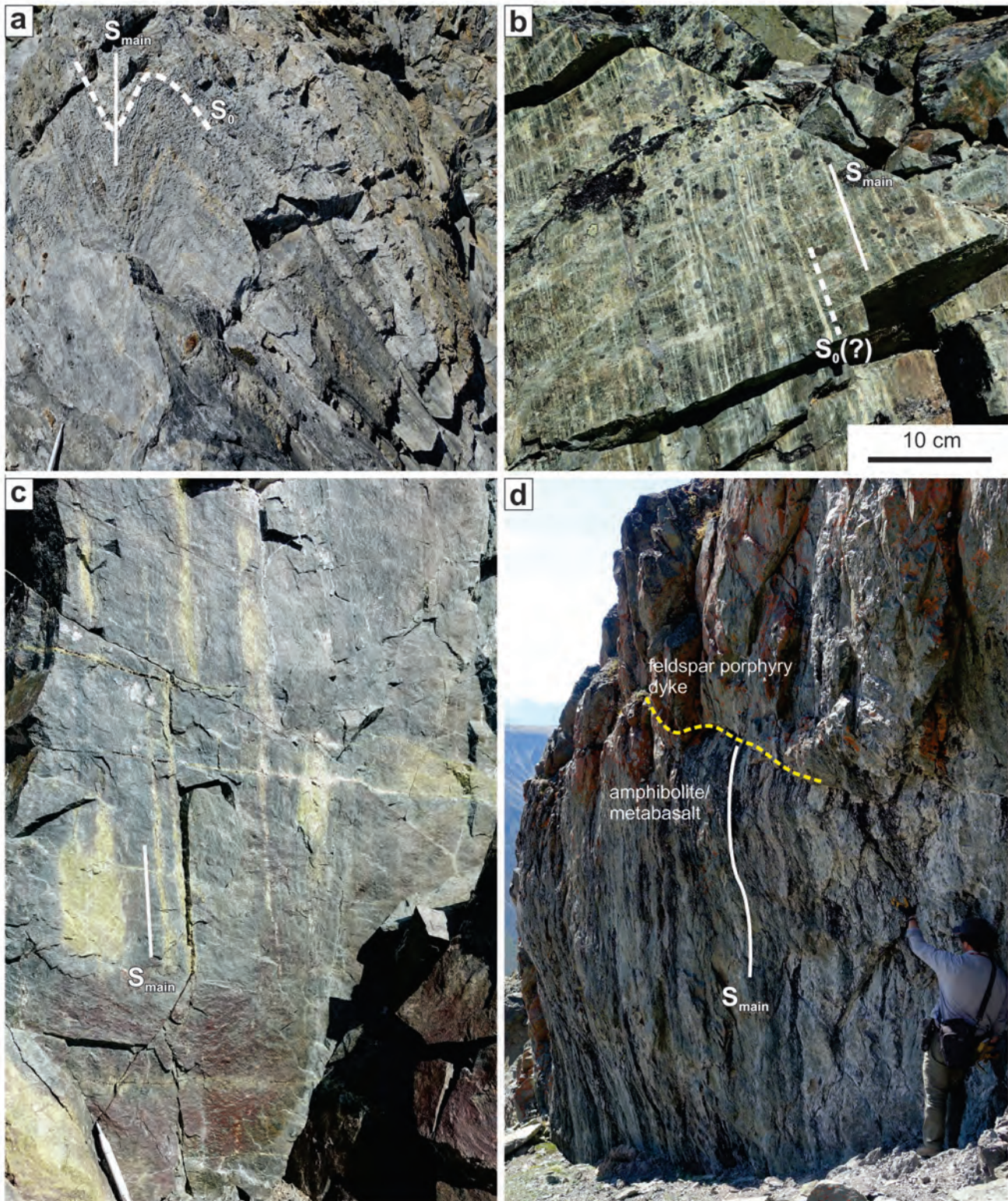


Fig. 4. Tally-Ho shear zone, Mount Hodnett. **a)** Povoas Formation marble, with folded bedding (S_0) and subvertical axial trace (S_{main}). View is to the north and folds plunge gently northward, and parallel locally developed mineral lineations. Scribe for scale (bottom left) is 13 cm long. **b)** Volcaniclastic unit 5 m east of the marble. S_0 and S_{main} form a composite layering. This unit has been interpreted as a mylonite (Hart and Radloff, 1990; Tizzard et al., 2009). View is north. **c)** Typical amphibolite unit in the shear zone, with S_{main} defined by aligned alteration pods defined by epidote. Scribe for scale (bottom left). View is south. **d)** Recessive-weathering cataclasite zone where brittle fault intersects the foliated amphibolite. The rock face represents the intersection of the amphibolite and the fault plane and person is standing on the cataclasite zone. The top half of the outcrop is a massive, intermediate feldspar-porphyry dike that intruded after ductile deformation but is caught in the brittle fault. View is southwest.

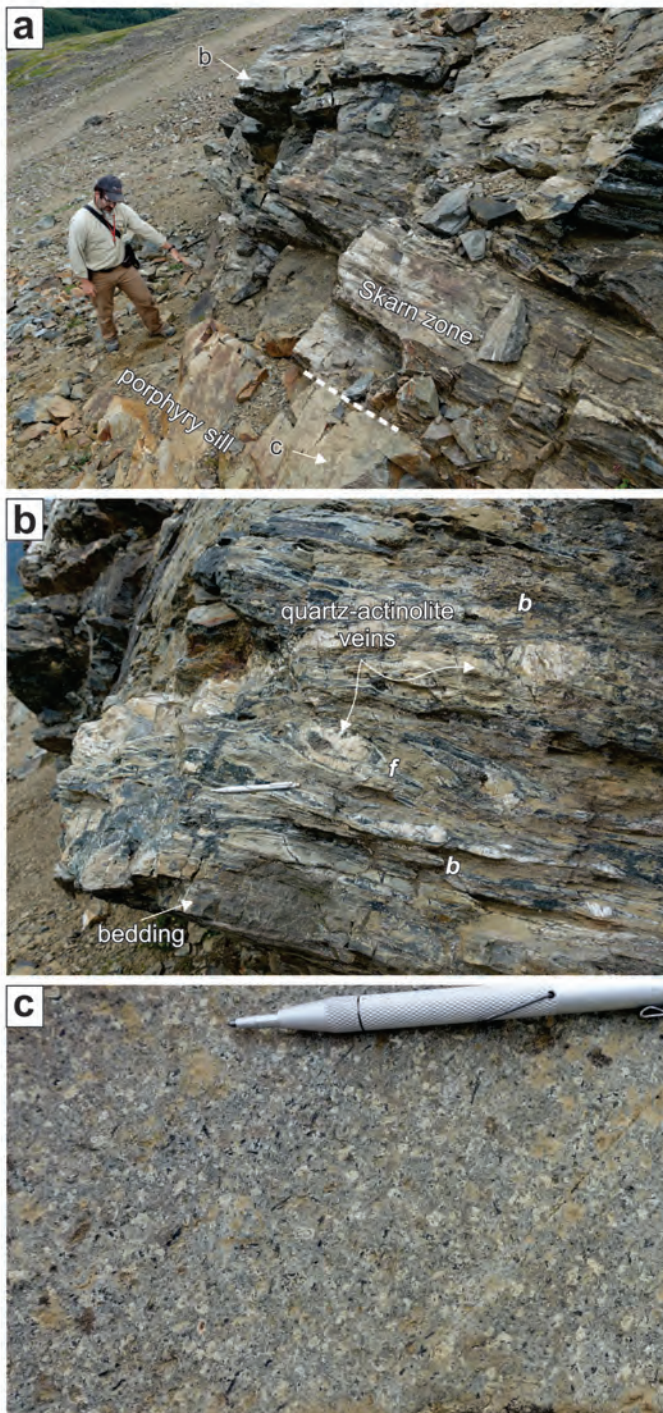


Fig. 5. **a)** Typical exposure of the Skarn zone near Bennett plateau, where a porphyry sill intruded previously deformed metasedimentary rocks of the Stuhini Group that host hydrothermal quartz-actinolite veins. View is northeast. **b)** Example of folded (*f*) and boudinaged (*b*) quartz-actinolite veins in metasedimentary rocks in the Skarn zone. Scribe for scale (bottom left) is 13 cm long. View is east. **c)** Weathered surface of post-deformation granodiorite porphyry sill. A sample of this sill was collected for U-Pb zircon geochronology (sample 16lo11B) and yielded an age of 76.30 ± 0.05 Ma.

the Skarn zone (Figs. 5a, c). The granodiorite post-dates deformation but the intrusive contact is parallel to the fabrics in the host-rock (Fig. 5a).

A composite gneiss, assigned to the Boundary Ranges metamorphic suite, outcrops immediately west of the Llewellyn fault near the Wann River at the south end of Tagish Lake (Figs. 6a, b; Mihalyuk et al., 1999). The gneiss is a mixed unit of diorite to granite, with local garnet-amphibolite representing boudinaged mafic dikes, or enclaves (Fig. 6b). Intrusive relationships are complicated by the strong structural overprint, defined by a foliation in massive rock types (e.g., granite) and gneissic layering (Fig. 6b). Veins, ca. 5 cm wide, are defined by quartz crystals with long axes perpendicular to vein margins (Fig. 6b). These veins belong to a spectrum of syn- to post- S_{main} shear and extensional structures.

Between 100 and 500 m southeast and directly along strike of these quartz veins are the vein-hosted showings Lum/Wann (Au-Ag-Cu-Pb-Zn; MINFILE 104M 109) and Brown (Ag-Au-Cu-Pb-Zn-Mo; MINFILE 104M 026). Approximately 750 m to the south, within dense bush cover, is float with tetrahedrite-bearing quartz veins (presumed to be the Brownie showing; Fig. 6c). This float is derived from weathering of an adjacent cliff face, but the remainder of the veins are in subcrop. Based on preliminary observations, these veins appear to be parallel to layering, presumably S_{main} in the host rocks.

3. U-Pb zircon geochronology

To further test the timing of deformation along the Llewellyn fault, in 2016 we collected samples for U-Pb geochronology from five separate sites along the strike of the fault where contact relationships are well exposed (Fig. 2). Additional samples, collected in 2017, are being processed.

3.1. CA-ID-TIMS analytical techniques

The U-Pb zircon chemical abrasion isotope dilution thermal ionization mass spectrometry (CA-ID-TIMS) procedures described here are modified from Mundil et al. (2004), Mattinson (2005), and Scoates and Friedman (2008). After rock samples underwent standard mineral separation procedures, the zircons were handpicked in alcohol. The clearest, crack- and inclusion-free grains are selected, photographed, and then annealed in quartz glass crucibles at 900°C for 60 hours. Annealed grains were transferred into 3.5 mL PFA screwtop beakers, ultrapure HF (up to 50% strength, 500 mL) and HNO_3 (up to 14 N, 50 mL) were added, and caps closed finger tight. The beakers were placed in 125 mL PTFE liners (up to four per liner) and about 2 mL HF and 0.2 mL HNO_3 of the same strength as acid in the beakers containing the samples were added to the liners. The liners were then slid into stainless steel ParrTM high-pressure dissolution devices, sealed, and heated to a maximum of 200°C for 8-16 hours (typically 190°C for 12 hours). Beakers were removed from the liners and the zircon separated from leachate. Zircons were rinsed with >18 M Ω .cm water and subboiled acetone. Then, 2 mL of subboiled 6N HCl was added and the beakers set on a hotplate at 80° - 130°C .

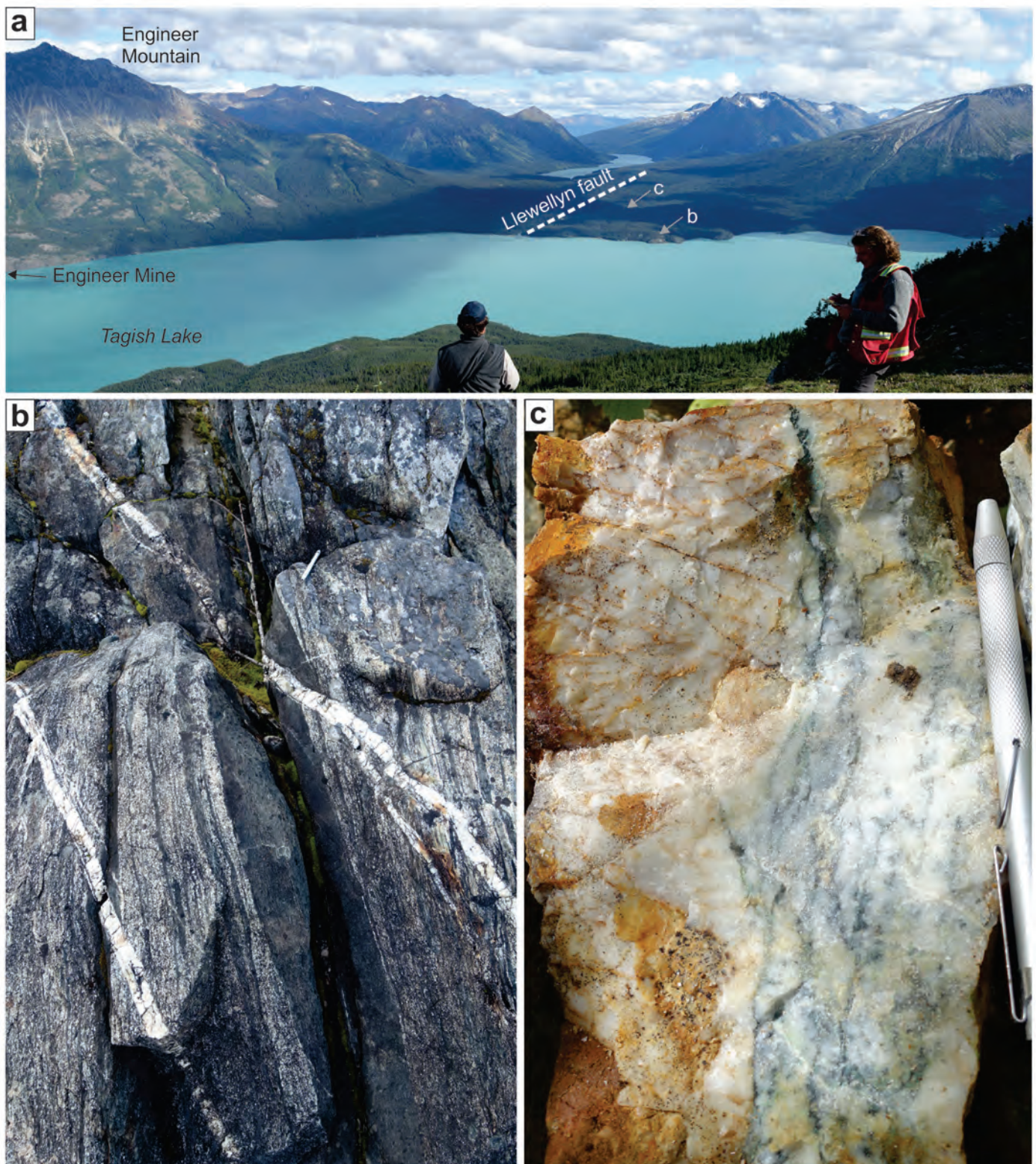


Fig. 6. a) Panoramic view of the trace of the Llewellyn fault at the south end of Tagish Lake. Mount Engineer is an Eocene volcanic complex. Locations of photographs in b) and c) are indicated. View is southeast. **b)** Mixed gneiss of the Boundary Ranges metamorphic suite, immediately west of the Llewellyn fault at the south end of Tagish Lake. The gneiss has felsic and mafic protoliths. Quartz veins, with quartz with long axes normal to vein margins, appear to post-date the main foliation, but are part of a spectrum of syn- to post-deformation. **c)** Hydrothermal quartz-carbonate vein with laminated metallic mineralization (tetrahedrite) at the Brownie prospect. The sample is in float and it likely eroded from adjacent till-blanketed escarpment. Preliminary results (n=5) indicate the veins carry a range of precious and base-metals: Au (200 to 8300 ppb); Ag (140 to 360 ppm); Cu (1100 to 8200 ppm); Pb (2650 to >5000 ppm); Zn (1800 to 4950 ppm); and Hg (2800 to 9600 ppm). Location is ~750 m south of Tagish Lake.

for 30 minutes and, again, rinsed with water and acetone. Masses were estimated from the dimensions (volumes) of grains. Single zircon grains were transferred into clean 300 mL PFA microcapsules (crucibles), and 50 mL 50% HF and 5 mL 14 N HNO₃ was added. Each was then spiked with a ²³³⁻²³⁵U-²⁰⁵Pb tracer solution (EARTHTIME ET535), capped, and again placed in a Parr liner (8-15 microcapsules per liner). HF and nitric acids in a 10:1 ratio, respectively, were added to the liner, which was then placed in a Parr high-pressure device and dissolution achieved at 220°C for 40 hours. The resulting solutions were dried on a hotplate at 130°C, and 50 mL 6N HCl was added to microcapsules and fluorides dissolved in high-pressure Parr devices for 12 hours at 180°C. HCl solutions were transferred into clean 7 mL PFA beakers and dried with 2 mL of 0.5 N H₃PO₄. Samples were loaded onto degassed, zone-refined Re filaments in 2 mL of silicic acid emitter (Gerstenberger and Haase, 1997).

Isotopic ratios were measured with a single collector VG Sector 54 thermal ionization mass spectrometer equipped with analogue Daly photomultiplier. Analytical blanks are 0.1 pg for U and up to 1.1 pg for Pb. U fractionation was determined directly on individual runs using the EARTHTIME ET535 mixed ²³³⁻²³⁵U-²⁰⁵Pb isotopic tracer and Pb isotopic ratios were corrected for fractionation of 0.25 ± 0.04%/amu, based on replicate analyses of NBS-982 reference material and the values recommended by Thirlwall (2000). Data reduction employed the Excel-based program of Schmitz and Schoene (2007). Standard concordia diagrams were constructed and regression intercepts and weighted averages calculated with Isoplot (Ludwig, 2003). Unless otherwise noted, all errors are quoted at 2σ (95% level of confidence). Isotopic ages are calculated with the decay constants $\lambda_{238} = 1.55125E-10$ and $\lambda_{235} = 9.8485E-10$ (Jaffey et al., 1971) and a ²³⁸U/²³⁵U ratio of 137.88. EARTHTIME U-Pb synthetic solutions were analyzed on an on-going basis to monitor the accuracy of results.

3.2. Results

3.2.1. K-feldspar porphyritic granite (sample #16lo20A)

A sample was collected from a medium-grained granite with k-feldspar phenocrysts from east of the Llewellyn fault and south of the BC-Yukon border (Fig. 2). The granite pluton intruded foliated Laberge Group metasedimentary rocks and was mapped as middle Cretaceous to Tertiary (unit LKqm in Mihalynuk et al., 1999). The granite does not contain a foliation or display evidence of brittle faulting. Five prismatic grains selected from the zircon separates yield three overlapping concordant results and two slightly older, marginally concordant to slightly discordant results (Fig. 7a; Table 1). A ²⁰⁶Pb/²³⁸U weighted mean of the three youngest overlapping concordant results yield an age of 56.58 ± 0.07 Ma, interpreted as the crystallization age of the granite. Two results that are marginally concordant to slightly discordant have ²⁰⁶Pb/²³⁸U ages only 100 Ka (±2σ) older than the weighted mean and are interpreted as antecrysts (Fig. 7a; Table 1).

3.2.2. Equigranular granite (sample #16lo22A)

Equigranular biotite-hornblende granite was collected from east of Bennett Lake and south of the British Columbia-Yukon border (Fig. 2). The granite was mapped as a middle Cretaceous to Tertiary pluton and interpreted to crosscut both ductile and brittle Llewellyn structures (unit LKgl in Mihalynuk et al., 1999; Pennington pluton discussed in Hart and Radloff, 1990). The granite lacks a ductile fabric, but contains closely spaced (<30 cm) brittle fractures, striking 360° and dipping 65°E, directly along strike of the Llewellyn fault (Fig. 2) and probably related to the fault. The sample yielded prismatic igneous zircon and five single grains were selected for analysis by CA-ID-TIMS. The results overlap on concordia and a ²⁰⁶Pb/²³⁸U weighted mean of four of the five results yields a crystallization age of 56.46 ± 0.06 Ma. One result is slightly older (56.75 Ma) and interpreted as an antecryst (Fig. 7b; Table 1).

3.2.3. Granodiorite porphyry (16lo11B)

A 2 m-wide quartz-, feldspar-, and biotite-phyric intrusion with a fine-grained siliceous matrix (granodiorite porphyry) intrudes metasedimentary rocks of the Stuhini Group at Bennett plateau (Figs. 2 and 5). The metasedimentary rocks contain hydrothermal quartz-actinolite veins that were folded and boudinaged, and the area that contains these veins has been termed the Skarn zone. The granodiorite intrusion parallels the host rock fabrics, but post-dates the ductile deformation (Fig. 5). A sample of the granodiorite porphyry yielded good-quality igneous zircons. Four zircons were selected for analysis and yield overlapping, concordant results. A ²⁰⁶Pb/²³⁸U weighted mean age of 76.30 ± 0.05 Ma is interpreted as the crystallization of the intrusion (Fig. 7c; Table 1).

3.2.4. Granodiorite (sample #16lo05B)

West of Moon Lake, within the trace of the Llewellyn fault, a fine- to medium-grained, weakly porphyritic (~0.5 cm-wide feldspar) granodiorite (unit Mgd in Mihalynuk et al., 1999), with moderate carbonate alteration and partially chloritized biotite and hornblende, cuts across the contact between the Stuhini Group and the Boundary Ranges metamorphic suite. The eastern contact of the granodiorite is parallel to bedding and foliation in Stuhini Group argillite; the granodiorite lacks a foliation and post-dates the ductile deformation preserved in the host argillite. The granodiorite is crosscut by a southeast-striking brittle fault, identifiable in the outcrop as a 2 m-wide zone of fault gouge with intense fracturing and carbonate alteration (see Figure 4a in Ootes et al., 2017). We collected a sample of least-altered granodiorite from near the contact with the host argillite.

The sample yielded good-quality igneous zircon and five single grains were selected for analysis. The results are concordant to slightly discordant and have a range of ²⁰⁶Pb/²³⁸U ages, from ca. 92 Ma to 74 Ma (Fig. 7d; Table 1). The youngest zircon, at ca. 74 Ma, gives the best estimate for the time of crystallization of the granodiorite sample. Older zircons with marginally concordant to discordant results and ²⁰⁶Pb/²³⁸U dates

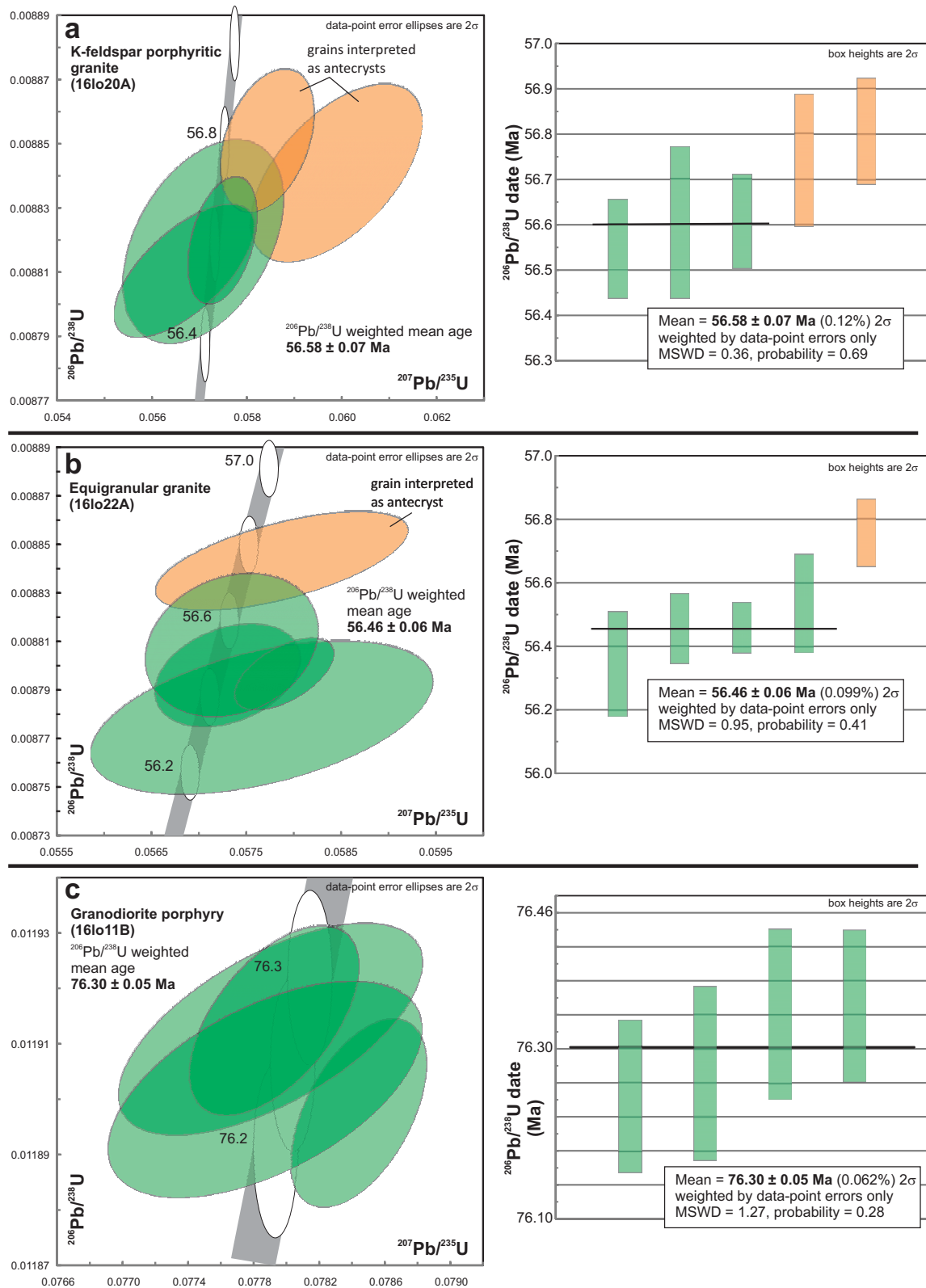


Fig. 7. Results of chemical abrasion ID-TIMS U-Pb zircon geochronology. **a-b)** K-feldspar phenocrystic granite and equigranular granite (Bennett granite) from east of Bennett Lake and south of the BC-Yukon border. **c)** Granodiorite porphyry from the Skarn zone, Bennett plateau. In figures a-c) Concordia plot is on the left and corresponding weighted mean diagram is on the right. Green ellipses and bars indicate results used in age determinations; orange ellipses and bars indicate results not used in age determinations. MSWD=mean square of weighted deviates. Sample locations are in Figure 2, analytical results are in Table 1.

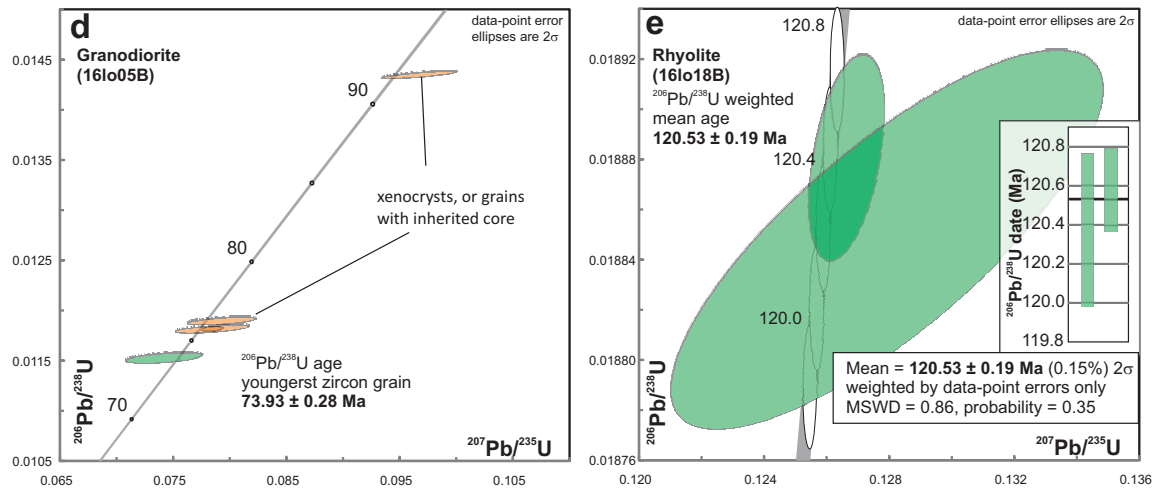


Fig. 7 continued. Results of chemical abrasion ID-TIMS U-Pb zircon geochronology. **d)** Granodiorite samples from west of Moon Lake. **e)** Rhyolite from west of Racine Lake; inset is the weighted mean of the two zircons analyzed. Green ellipses and bars indicate results used in age determinations; orange ellipses and bars indicate results not used in age determinations. MSWD=mean square of weighted deviates. Sample locations are in Figure 2, analytical results are in Table 1.

of ca. 76 Ma ($n=3$) and ca. 90 Ma are interpreted as xenocrysts, or as composite grains with older inherited cores and younger rims (Fig. 7d).

3.2.5. Rhyolite (161o18B)

Southwest of Racine Lake and directly east of Teepee Peak is a zone of imbricated Stuhini Group and minor Laberge Group rocks (Mihalynuk et al., 1999). The best exposures are on a hummock-like ridge that is transected by the brittle Llewellyn fault and related splays. The western-most splay separates Stuhini and Laberge group from Boundary Ranges metamorphic suite rocks (Mihalynuk et al., 1999). Outcrops along the ridge contain a ridge-parallel foliation ($\sim 135^\circ/80^\circ\text{SW}$) that is locally affected by steeply plunging minor folds (s-shaped). The rock types in the west are predominantly argillite and in the east black shale (slate) and marble. An intermediary unit of 'rhyolite' and associated rocks was identified by Mihalynuk et al. (1999) and during this study. The rhyolite unit weathers chalky white and contains plagioclase and quartz phenocrysts and is commonly moderately to strongly foliated, consistent with the other units on the outcrop. The rhyolite is also carbonate altered, potentially related to brittle faulting along this zone. A sample of massive rhyolite with carbonate alteration was selected for geochronology. Only two of six zircons survived the journey from separation to mass spectrometry but yield overlapping and concordant U/Pb ages. A $^{206}\text{Pb}/^{238}\text{U}$ weighted mean of the analyses indicate a crystallization age of ca. 121 Ma (Fig. 7e; Table 1).

4. Discussion

4.1. Timing of deformation

The new U-Pb geochronology allows the timing of deformation along the Llewellyn fault to be bracketed. The crystallization age for the granodiorite pluton west of Moon Lake

(161o05b) is ca. 74 Ma; the age for the granodiorite porphyry sill on Bennett plateau (161o11b) is 76 Ma (Figs. 7d, e). Both of these intrusions post-date ductile deformation in the Stuhini and Laberge groups and Boundary Ranges metamorphic suite. Therefore ductile deformation pre-dates 76-74 Ma. The granodiorite west of Moon Lake is crosscut by the brittle Llewellyn fault, constraining the brittle deformation to younger than ca. 74 Ma.

Near the BC-Yukon border, two granitic plutons sampled for this study (161o20a, 161o22a; Fig. 2) yield indistinguishable ages of ca. 56.5 and 56.6 Ma (Figs. 7a, b). Both intrusive phases post-date ductile deformation. The slightly older K-feldspar porphyritic granite lacks evidence of brittle deformation. However, the slightly younger equigranular granite pluton (161o20a) contains fractures that are along strike, and parallel to, the brittle fault trace, although these fractures contain neither carbonate alteration nor fault gouge such as along the Llewellyn fault to the south (e.g., see Figure 4 in Ootes et al., 2017). Thus, either brittle deformation was protracted and the granite records the latest in a long movement history or, given that the pluton is relatively homogenous, it acted as a rigid body during brittle movement and was only fractured. We favour the latter interpretation because the fractures in the granite ($360/65^\circ\text{E}$) are directly in line with the fault trace. Brittle deformation continued after the granite intruded, as indicated by $^{40}\text{Ar}/^{39}\text{Ar}$ dating of vanadinite from Engineer Mine (~ 70 km to the southeast, Fig. 2), which indicates brittle movement and associated epithermal veining along the fault at ca. 50 Ma (Millonig et al., 2017). In addition, epithermal quartz veins at Mount Skukum (~ 40 km to the northwest) are related to regional strike-slip brittle faults, and these veins and associated alteration have been dated at ca. 54 Ma (Love et al., 1998). This timing (Fig. 8) is coeval with Cordilleran-scale brittle dextral strike-slip faulting (e.g., Gabrielse et al., 2006). It does remain

Table 1. Results of chemical abrasion ID-TIMS U-Pb zircon geochronology.

Sample (a)	Compositional Parameters										Radiogenic Isotope Ratios						Isotopic Ages						
	Wt. mg	U ppm	Pb ppm	Th U	$^{206}\text{Pb}^*$ $\times 10^{-13}$ mol	mol % $^{206}\text{Pb}^*$	Pb* Pb _c	^{206}Pb ^{204}Pb	^{208}Pb ^{206}Pb	^{207}Pb ^{206}Pb	% err	^{238}U ^{206}Pb	^{207}Pb ^{206}Pb	corr. coef.	^{207}Pb ^{206}Pb	^{235}U ^{238}U	^{207}Pb ^{206}Pb	^{235}U ^{238}U	^{207}Pb ^{206}Pb	^{235}U ^{238}U			
16lo20A - K-feldspar porphyritic granite (*507641m E, 6647497m N)																							
A	0.004	292	2.7	0.385	0.4415	98.64%	21	0.50	1365	0.124	0.04912	2.331	0.05988	2.467	0.00884	0.257	0.568	154	55	59.0	1.4	56.74	0.15
B	0.005	229	2.1	0.353	0.4213	98.45%	18	0.55	1194	0.113	0.04694	2.301	0.05708	2.408	0.00882	0.295	0.417	46	55	56.4	1.3	56.61	0.17
C	0.005	327	3.0	0.365	0.5791	98.93%	27	0.51	1739	0.117	0.04788	1.308	0.05843	1.372	0.00885	0.206	0.377	93	31	57.66	0.77	56.81	0.12
D	0.004	244	2.3	0.339	0.3319	97.91%	14	0.58	888	0.109	0.04666	1.997	0.05668	2.119	0.00881	0.193	0.661	32	48	56.0	1.2	56.55	0.11
E	0.006	484	4.4	0.370	0.9796	99.00%	29	0.82	1847	0.119	0.04727	0.969	0.05749	1.026	0.00882	0.184	0.392	63	23	56.8	0.6	56.61	0.10
16lo22B - equigranular granite (*507270m E, 6649185m N)																							
A	0.0112	266	2.4	0.382	1.0967	99.32%	43	0.61	2739	0.122	0.04725	1.040	0.05731	1.087	0.00880	0.197	0.324	62	25	56.58	0.60	56.46	0.11
B	0.0046	333	3.1	0.377	0.5599	98.71%	22	0.60	1430	0.121	0.04764	2.431	0.05767	2.555	0.00878	0.294	0.469	82	58	56.9	1.4	56.35	0.17
C	0.0066	152	1.4	0.418	0.3701	98.40%	18	0.49	1160	0.134	0.04747	1.769	0.05788	1.878	0.00884	0.188	0.613	73	42	57.1	1.0	56.76	0.11
D	0.0055	461	4.2	0.422	0.9323	99.36%	46	0.50	2877	0.135	0.04774	0.669	0.05790	0.738	0.00880	0.139	0.570	86	16	57.15	0.41	56.46	0.08
E	0.0096	219	2.0	0.384	0.7763	99.16%	35	0.54	2210	0.123	0.04722	1.267	0.05735	1.294	0.00881	0.275	0.205	60	30	56.62	0.71	56.54	0.16
16lo11B - granodiorite porphyry (*507977m E, 6642004m N)																							
A	0.0082	320	4.0	0.499	1.3073	99.34%	46	0.71	2803	0.160	0.04782	0.383	0.07844	0.430	0.01190	0.117	0.516	90.2	9.1	76.68	0.32	76.24	0.09
B	0.0029	384	4.9	0.495	0.5606	99.05%	32	0.44	1950	0.159	0.04743	0.895	0.07790	0.971	0.01191	0.131	0.625	71	21	76.17	0.71	76.34	0.10
C	0.0040	362	4.5	0.460	0.7124	99.19%	37	0.48	2279	0.147	0.04744	0.485	0.07793	0.542	0.01191	0.117	0.567	71	12	76.19	0.40	76.35	0.09
E	0.0036	201	2.6	0.469	0.3576	98.59%	21	0.42	1311	0.150	0.04745	0.937	0.07787	1.004	0.01190	0.135	0.552	72	22	76.14	0.74	76.27	0.10
16lo05B - granodiorite (*515870m E, 6630703m N)																							
A	0.0079	103	1.3	0.519	0.3933	97.85%	14	0.71	861	0.166	0.04669	3.536	0.07425	3.718	0.01153	0.379	0.519	33	85	72.7	2.6	73.93	0.28
B	0.0220	31	0.5	0.396	0.4148	98.47%	19	0.53	1210	0.127	0.04890	2.618	0.09677	2.792	0.01435	0.223	0.796	143	61	93.8	2.5	91.86	0.20
C	0.0055	94	1.3	0.654	0.2581	98.19%	17	0.39	1019	0.210	0.04836	2.888	0.07937	3.051	0.01190	0.291	0.592	117	68	77.6	2.3	76.28	0.22
D	0.0153	97	1.2	0.542	0.7300	99.39%	50	0.37	3012	0.174	0.04817	0.896	0.07854	0.961	0.01183	0.184	0.436	108	21	76.77	0.71	75.78	0.14
E	0.0091	113	1.5	0.534	0.5046	97.59%	12	1.03	767	0.171	0.04816	3.169	0.07850	3.356	0.01182	0.316	0.621	107	75	76.7	2.5	75.76	0.24
16lo18B - deformed and altered rhyolite (*526116m E, 6617833m N)																							
B	0.0172	113	2.3	0.532	1.5266	99.20%	38	1.01	2317	0.170	0.04864	0.715	0.12663	0.773	0.01888	0.178	0.431	131	17	121.07	0.88	120.58	0.21
C	0.0014	120	3.2	0.607	0.1303	90.72%	3	1.10	199	0.194	0.04922	4.142	0.12792	4.397	0.01885	0.328	0.791	158	97	122.2	5.1	120.37	0.39

(a) A, B etc. are labels for fractions composed of single zircon grains or fragments; all fractions annealed and chemically abraded after Mattinson (2005) and Scoates and Friedman (2008).

(b) Nominal fraction weights estimated from photomicrographic grain dimensions, adjusted for partial dissolution and chemical abrasion.

(c) Nominal U and total Pb concentrations subject to uncertainty in photomicrographic estimation of weight and partial dissolution during chemical abrasion.

(d) Model Th/U ratio calculated from radiogenic $^{208}\text{Pb}/^{206}\text{Pb}$ ratio and $^{207}\text{Pb}/^{235}\text{U}$ age.

(e) Pb* and Pb_c represent radiogenic and common Pb, respectively; mol % $^{206}\text{Pb}^*$ with respect to radiogenic, blank and initial common Pb.

(f) Measured ratio corrected for spike and fractionation only. Mass discrimination of $0.25 \pm 0.04\%$ amu based on analysis of NBS-982; all Daly analyses.

(g) Corrected for fractionation, spike and all common Pb assumed to be procedural blank: $^{206}\text{Pb}/^{204}\text{Pb} = 18.50 \pm 1.0\%$; $^{207}\text{Pb}/^{204}\text{Pb} = 15.50 \pm 1.0\%$; $^{208}\text{Pb}/^{204}\text{Pb} = 38.40 \pm 1.0\%$ (all uncertainties 1-sigma).

(h) Errors are 2-sigma, propagated using the algorithms of Schmitz and Schoene (2007) and Crowley et al. (2007).

(i) Calculations are based on the decay constants of Jaffey et al. (1971). $^{238}\text{U}/^{235}\text{U} = 137.88$. $^{206}\text{Pb}/^{238}\text{U}$ and $^{207}\text{Pb}/^{206}\text{Pb}$ ages corrected for initial disequilibrium in $^{230}\text{Th}/^{238}\text{U}$ using Th/U [magma] = 3.

*UTM Zone 8, NAD 83

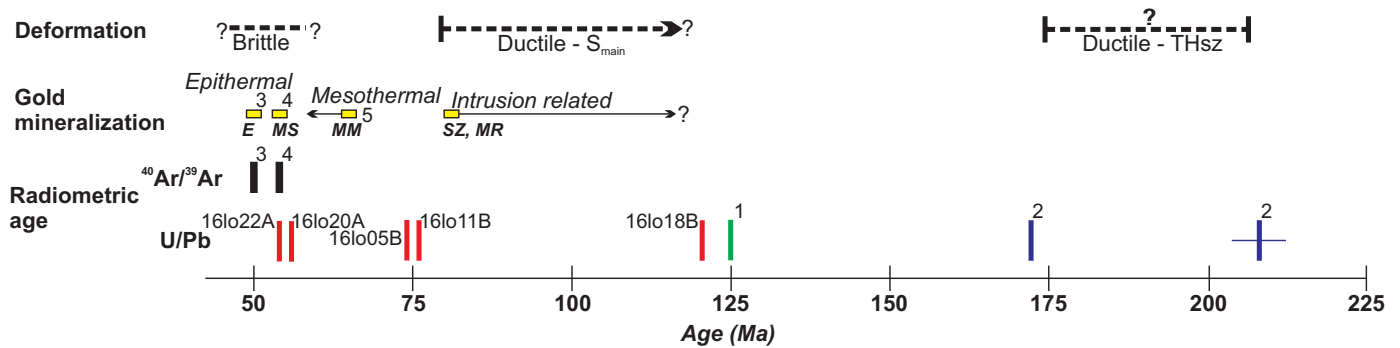


Fig. 8. Timeline summary of deformation and gold mineralization near the Llewellyn fault and Tally-Ho shear zone. Uranium-lead age constraints are from: this study (labelled by sample number); 1) Mihalynuk et al. (2003); 2) Tizzard et al. (2009). ⁴⁰Ar/³⁹Ar mica results are from: 3) Millonig et al. (2017) and 4) Love et al. (1998), and constrain the time of epithermal gold mineralization at Engineer Mine (E) and Mount Skukum Mine (MS). The suggested timing: of mesothermal gold mineralization at Mountana Mountain mines (MM) is from Hart and Pelletier (1989); of intrusion-related mineralization at the Skarn zone (SZ) is from this study; and of Middle ridge (MR) is from Mihalynuk et al. (2003). ?=uncertainty; S_{main}=main foliation along Llewellyn and Tally-Ho deformation corridor; THsz=Tally-Ho shear zone. See text for discussion.

possible that brittle movement began prior to ca. 56 Ma and the plutons overlap the initiation of brittle deformation along the Llewellyn fault.

Ductile deformation fabrics (foliations, folds, lineations) along the Llewellyn fault pre-date ca. 75 Ma. During this study, only one penetrative foliation (S_{main}) has been observed along the entire Llewellyn fault and Tally-Ho shear zone corridor. Although S_{main} is locally folded, no crenulation cleavage has been observed. The rhyolite southwest of Racine Lake, with an age of ca. 121 Ma (see above), pre-dates the development of S_{main}. However, two items need to be considered regarding the age of this rhyolite and the minimum timing of S_{main}. First, only two U-Pb zircon results are presented. Although two results would typically be considered insufficient, they may still be valid because both zircons are concordant and their ²⁰⁶Pb/²³⁸U ages overlap (Fig. 7e; Table 1). Also, the ca. 121 Ma age is not unique in the region. South of Bennett plateau, volcanic rocks underlying a mountain known as 'Middle ridge', yielded a U-Pb zircon age of ca. 125 Ma (Mihalynuk et al., 2003) for a unit originally mapped as Jurassic volcanic rocks (Fig. 2; unit ImJv on Mihalynuk et al., 1999). Furthermore, the Whitehorse plutonic complex is also ca. 120 Ma, although mostly preserved in Yukon (e.g., Hart and Radloff, 1990). Second, outcrops along the ridge are covered in grey lichen, making high-quality field observations difficult. The ridge is extensively overprinted by brittle faults, which are splays off the main Llewellyn fault. Although the rhyolite appears to share the same foliation as the surrounding rock units, it remains conceivable, but unlikely, that it post-dates ductile deformation and was imbricated with the foliated units during brittle faulting.

To further bracket the maximum age of S_{main}, the best location may be along the Tally-Ho shear zone, particularly at Mount Hodnett where S_{main} in the shear zone is parallel and probably formed at the same time as the foliation in the neighbouring granodiorite pluton (again mapped as Whitehorse plutonic complex; Hart and Radloff, 1990). Tizzard et al. (2009) preferred the explanation that the foliation is distinct and

related to a fault that juxtaposes the granodiorite and Tally-Ho shear zone. We collected a sample of this granodiorite in 2017 for U-Pb zircon dating. Should it yield a Jurassic or Triassic age, then development of S_{main} between 208 and 173 Ma may still hold (Tizzard et al., 2009). If the granodiorite is part of the Whitehorse plutonic suite, then the best interpretation is that S_{main} post-dates ca. 120 Ma. Based on the information at hand, we speculated that S_{main}, the only foliation preserved along the Llewellyn-Tally-Ho corridor, developed before ca. 75 Ma and potentially after ca. 120 Ma (Fig. 8).

4.2. Gold mineralization and deformation

A goal of this study was to test the apparent relationship between the various styles of gold mineralization that are related to both the ductile and brittle structures, as well as magmatism, along the Llewellyn fault (Fig. 2). The gold mineralization styles range from epithermal to mesothermal to intrusion-related (see Section 2). The orogenic gold deposit model typically relates a crustal continuum of gold deposits to first-order crustal breaks and synchronous magmatism (e.g., Goldfarb et al., 2005; Dubé and Gosselin, 2007). Therefore, the question arises as to whether the gold mineralization styles along the Llewellyn deformation corridor are interrelated, and if so are they part of an orogenic-style mineralizing system? In this model, the ductile and brittle deformation need to be contemporaneous, and gold mineralization is forming synchronously at various depths in the crust (e.g., Goldfarb et al., 2005).

The hypothesis fails because the field relationships and U-Pb zircon geochronology demonstrate a time gap of at least ca. 20 Ma between ductile and brittle deformation (Fig. 8). The older ductile deformation is defined by a regional foliation (S_{main}) in the Stikine terrane rocks (Stuhini, Lewes River, and Laberge groups) and possibly the Boundary Ranges metamorphic complex. The S_{main} is older than ca. 75 Ma (Figs. 7 and 8). Therefore intrusion-related gold mineralization that formed before or during the early-ductile phase of deformation, such

as in the Skarn zone at Bennett plateau and perhaps Middle ridge (Mihalynuk et al., 2003), predates ca. 75 Ma. According to our new U-Pb zircon age from a rhyolite west of Racine Lake, and speculations regarding fabric development along the Tally-Ho shear zone (Section 2.1.2.), some of the ductile deformation may post-date ca. 120 Ma. If intrusion-related gold mineralization, such as that at Bennett plateau and possibly Middle ridge developed during the time period 120 to 75 Ma, then this mineralization falls within the time-frame and style typical of the Tintina gold belt in Yukon and Alaska (e.g., Hart, 2007).

The epithermal-style gold mineralization, such as at Engineer Mine and Mount Skukum, have been dated at ca. 55 to 50 Ma and are clearly related to brittle deformation (Fig. 8; Love, 1990; Love et al., 1998; Millonig et al., 2017; Ootes et al., 2017). This time frame of brittle deformation corresponds to similar Cordillera-scale faults (e.g., Gabrielse et al., 2006). What remains unresolved is the absolute timing of mineralization at Montana Mountain (Yukon), which is considered mesothermal, post-dates Upper Cretaceous volcanic rocks, and has been suggested to be younger than Paleocene (Fig. 8; Roots, 1981; Walton, 1986; Hart and Pelletier, 1989). An attempt to date mineralization using the Re-Os arsenopyrite method was unsuccessful due to insufficient Re in the arsenopyrite (P. Mercier-Langevin, personal communication, 2017).

5. Conclusions

The Llewellyn fault overprints early ductile fabrics in British Columbia and the Tally-Ho shear zone, Yukon. Epithermal gold mineralization at the past-producing Mount Skukum and Engineer mines are related to this brittle deformation, and field and radiometric ages indicate that deformation and gold mineralization was between ca. 56 and 50 Ma (e.g., Love, 1990; Love et al., 1998; Millonig et al., 2017; Ootes et al., 2017). The brittle faults overprint an older ductile deformation history along the Llewellyn fault and Tally-Ho shear zone corridor. Previous work suggested the Tally-Ho shear zone developed between 208 and 173 Ma (Tizzard et al., 2009). Observations from this study indicate that the Tally-Ho shear zone contains only one fabric (S_{main}), and that this fabric is also in a neighbouring granodiorite pluton, previously considered part of the Whitehorse plutonic complex (ca. 120 Ma; Hart and Radloff, 1990). A rhyolite along the Llewellyn fault contains S_{main} . Based on our field and geochronologic data, we tentatively conclude that S_{main} developed after 120 Ma. Two granodiorite intrusions post-date the ductile deformation and yield U-Pb zircon crystallization ages of ca. 76 and 74 Ma. These new results indicate that the ductile deformation occurred before ca. 75 Ma. Intrusion-related gold mineralization, for example at the Skarn zone and possibly at Middle ridge (Mihalynuk et al., 2003; Wark, 2012), are deformed and pre-date 75 Ma. If these intrusion-related gold mineralizing systems developed between 120 and 75 Ma, then they may share characteristics with the Tintina gold belt in Yukon and Alaska.

This study further indicates that the Llewellyn fault extends into Yukon and crosscuts the Tally-Ho shear zone, and that this corridor shares the same early ductile deformation history (Hart and Radloff, 1990; Mihalynuk et al., 1999). A ca. 20 Ma time-gap between early and late deformation (Fig. 8) shows that gold mineralization associated with the ductile fabrics and with the brittle structures formed at different times, and therefore are related to distinct tectonic events.

Acknowledgments

This study complements, and is integrated with, a Geological Survey of Canada Targeted Geoscience Initiative research project, in collaboration with the Yukon Geological Survey. We thank BC Gold Corp. (Engineer Mine now owned by Blind Creek Resources), Troymet Exploration Corp., and Terralogic Exploration Inc. for access to properties and data. The study benefited from field assistant J. Elliott (2016, University of Victoria) and field visits and discussions with S. Casselman (Yukon Geological Survey) and S. Rowins and A. Hickin (British Columbia Geological Survey). Helicopter support was provided by Capital Helicopters, (Whitehorse, YT) and Discovery Helicopters (Atlin, BC). The U-Pb zircon work was at the University of British Columbia; H. Lin conducted mineral separation and assisted with mass spectrometry and T. Ockerman performed activities in the clean lab. Constructive and thoughtful reviews by N. Pinet and L. Aspler improved the clarity of the paper. This is NRCan Contribution number 20170305.

References cited

- Castonguay, S., Ootes, L., Mercier-Langevin, P., Rowins, S., and Devine, F., 2017. Orogenic gold along Cordilleran faults; key characteristics and analogies between Phanerozoic and Archean settings. In: Rogers, R., (Ed.), Targeted Geoscience Initiative-2016 Report of Activities, Geological Survey of Canada, Open File 8199, pp. 35-37.
- Crowley, J.L., Schoene, B. and Bowring, S.A., 2007. U-Pb dating of zircon in the Bishop Tuff at the millennial scale. *Geology*, 35, 1123-1126.
- Doherty, R.A. and Hart, C.J.R., 1988. Preliminary geology of Fenwick Creek (105D/3) and Alligator Lake (105D/6) map areas. Yukon Geological Survey, Open File 1988-2, 2 maps, 1:50,000 scale.
- Dubé, B., and Gosselin, P. 2007. Greenstone-hosted quartz-carbonate vein deposits. In: Goodfellow, W.D., (Ed.), Mineral Deposits of Canada: A Synthesis of Major Deposit-Types, District Metallogeny, the Evolution of Geological Provinces, and Exploration Methods. Geological Association of Canada, Mineral Deposits Division, Special Publication No. 5, pp. 49-73.
- Gabrielse, H., Murphy, D.C., and Mortensen, J.K., 2006. Cretaceous and Cenozoic dextral orogen-parallel displacements, magmatism, and paleogeography, north-central Canadian Cordillera. In: Haggart, J.W., Enkin, R.J. and Monger, J.W.H., (Eds.), Paleogeography of the North American Cordillera: Evidence For and Against Large-Scale Displacements. Geological Association of Canada, Special Paper 46, pp. 255-276.
- Gerstenberger, H., and Haase, G., 1997. A highly effective emitter substance for mass spectrometric Pb isotopic ratio determinations. *Chemical Geology*, 136, 309-312.
- Goldfarb, R.J., Baker, T., Dubé, B., Groves, D.I., Hart, C.J.R., and

- Gosselin, P., 2005. Distribution, character, and genesis of gold deposits in metamorphic terranes. In: J.W. Hedenquist, J.W., Thompson, J.F.H., Goldfarb, R.J., and Richards, J.P., (Eds.), *Economic Geology 100th Anniversary Volume*, pp. 407-450.
- Hart, C.J.R., 2007. Reduced intrusion-related gold-systems. In: Goodfellow, W.D., (Ed.), *Mineral Deposits of Canada: A Synthesis of Major Deposit-Types, District Metallogeny, the Evolution of Geological Provinces, and Exploration Methods*. Geological Association of Canada, Mineral Deposits Division, Special Publication No. 5, pp. 95-112.
- Hart, C.J.R., and Pelletier, K.S., 1989. Geology of Carcross (105D/2) and Part of Robinson (105D/7) Map Areas. Indian and Northern Affairs Canada, Yukon Geological Survey, Open File 1989-1, 84 p.
- Hart, C.J.R., and Radloff, J.K., 1990. Geology of Whitehorse, Alligator Lake, Fenwick Creek Carcross and part of Robinson map areas (105D/11, 6, 3, 2 & 7). Yukon Geological Survey, Open File 1990-4.
- Jaffey, A.H., Flynn, K.F., Glendenin, L.E., Bentley, W.C., and Essling, A.M., 1971. Precision measurement of half-lives and specific activities of ²³⁵U and ²³⁸U. *Physical Review C*, 4, 1889-1906.
- Love, D.A., 1990. Structural controls on veins of the Mount Skukum gold deposit, southwestern Yukon. Geological Survey of Canada, Paper 90-1E, pp. 337-346.
- Love, D.A., Clark, A.H., Hodgson, C.J., Mortensen, J.K., Archibald, D.A., and Farrar, E., 1998. The timing of adularia-sericite-type mineralization and alunite-kaolinite-type alteration, Mount Skukum epithermal gold deposit, Yukon Territory, Canada; ⁴⁰Ar - ³⁹Ar and U-Pb geochronology. *Economic Geology*, 93, 437-462.
- Ludwig, K.R., Isoplot 3.00, A Geochronological Toolkit for Microsoft Excel. University of California at Berkeley, kludwig@bgc.org.
- Mattinson, J.M., 2005. Zircon U-Pb chemical abrasion ("CA-TIMS") method: Combined annealing and multi-step partial dissolution analysis for improved precision and accuracy of zircon ages. *Chemical Geology*, 220, 47-66.
- Mihalynuk, M.G., Devine, F., and Friedman, R.M., 2003. Marksmen partnership: potential for shallow submarine VMS (Eskay-style) and intrusive-related gold mineralization, Tutshi Lake area. Ministry of Energy and Mines, British Columbia Geological Survey, GeoFile 2003-9, 1 poster.
- Mihalynuk, M.G., Smith, M., Hancock, K.D., Dudka, S.F., and Payne, J., 1994. Geology of the Tulsequah River and Glacier Creek Area (NTS 104K/12, 13). Ministry of Energy, Mines and Petroleum Resources, British Columbia Geological Survey Open File 1994-3, 3 sheets, 1:50,000 scale.
- Mihalynuk, M.G., Mountjoy, K.J., Currie, L.D., Smith, M.T., and Rouse, J.N., 1999. Geology and mineral resources of the Tagish Lake area (NTS 104M/8, 9, 10E, 15 and 104N/12W) northwestern British Columbia. Ministry of Employment and Investment, British Columbia Geological Survey Bulletin 105, 190 p.
- Millonig, L.J., Beinlich, A., Raudsepp, M., Devine, F., Archibald, D.A., Linnen, R.L., and Groat, L.A., 2017. The Engineer Mine, British Columbia: An example of epithermal Au-Ag mineralization with mixed alkaline and subalkaline characteristics. *Ore Geology Reviews*, 83, 235-257.
- Mundil, R., Ludwig, K. R., Metcalfe, I., and Renne, P. R., 2004. Age and timing of the Permian mass extinctions: U/Pb dating of closed-system zircons. *Science*, 305, 1760-1763.
- Nelson, J.L., Colpron, M., and Israel, S., 2013. The Cordillera of British Columbia, Yukon, and Alaska: Tectonics and metallogeny. In: Colpron, M., Bissing, T., Rusk, B.G., and Thompson, J.F.H., (Eds.), *Tectonics, Metallogeny, and Discovery: The North American Cordillera and similar accretionary settings*. Society of Economic Geologists, Special Publication 17, pp. 53-109.
- Ootes, L., Elliott, J.M., and Rowins, S.M., 2017. Testing the relationship between the Llewellyn fault, gold mineralization, and Eocene volcanism in northwest British Columbia: A preliminary report. In: *Geological Fieldwork 2016*, British Columbia Ministry of Energy and Mines, British Columbia Geological Survey Paper 2017-1, pp. 49-59.
- Roots, C.F., 1981. Geological setting of gold-silver veins on Montana Mountain. In: *Yukon Geology and Exploration 1979-80*, Indian and Northern Affairs Canada/Department of Indian and Northern Development: Exploration and Geological Services Division, pp. 116-122.
- Scoates, J.S., and Friedman, R.M., 2008. Precise age of the platinumiferous Merensky Reef, Bushveld Complex, South Africa, by the U-Pb ID-TIMS chemical abrasion technique. *Economic Geology*, 103, 465-471.
- Schmitz, M.D., and Schoene, B., 2007. Derivation of isotope ratios, errors, and error correlations for U-Pb geochronology using ²⁰⁵Pb-²³⁵U-(²³³U)-spiked isotope dilution thermal ionization mass spectrometric data. *Geochemistry, Geophysics, Geosystems*, 8, Q08006, doi:10.1029/2006GC001492.
- Stacey, J.S., and Kramers, J.D., 1975. Approximation of terrestrial lead isotopic evolution by a two-stage model. *Earth and Planetary Science Letters*, 26, 207-221.
- Thirlwall, M.F., 2000. Inter-laboratory and other errors in Pb isotope analyses investigated using a ²⁰⁷Pb-²⁰⁴Pb double spike. *Chemical Geology*, 163, 299-322.
- Tizzard, A.M., Johnston, S.T., and Heaman, L.M., 2009. Arc imbrication during thick-skinned collision within the northern Cordilleran accretionary orogen, Yukon, Canada. *Geological Society, London, Special Publications*, 318, 309-327.
- Walton, L., 1986. Textural characteristics of the Venus vein and implications for ore shoot distribution. In: *Yukon Geology Volume 1*, Exploration and Geological Services Division, Indian and Northern Affairs Canada, pp. 67-71.
- Wark, J.M., 2012. Technical Report, Golden Eagle Property. 43-101 Technical Report for Troymet Exploration Ltd., July 2012, 471 p. <https://www.troymet.com/projects/golden-eagle>.

Geologic and geochronologic update of the Turtle Lake area, NTS 104M/16, northwest British Columbia



Mitchell G. Mihalynuk^{1, a}, Alexandre Zagorevski², Dejan Milidragovic¹,
Maria Tsekhmistrenko³, Richard M. Friedman⁴, Nancy Joyce², Alfredo Camacho⁵,
and Martyn Golding⁶

¹ British Columbia Geological Survey, Ministry of Energy, Mines and Petroleum Resources, Victoria, BC, V8W 9N3

² Geological Survey of Canada, Ottawa, ON, K1A 0E8

³ Department of Earth Sciences, University of Oxford, Oxford, OX1 3AN, UK

⁴ Pacific Centre for Isotopic and Geochemical Research, The University of British Columbia, Vancouver, BC, V6T 1Z4

⁵ Department of Mechanical Engineering, University of Victoria, Victoria, BC, V8P 5C2

⁶ Geological Survey of Canada, Vancouver, BC, V6B 5J3

^a corresponding author: Mitch.Mihalynuk@gov.bc.ca

Recommended citation: Mihalynuk, M.G., Zagorevski, A., Milidragovic, D., Tsekhmistrenko, M., Friedman, R.M., Joyce, N., Camacho, A., and Golding, M., 2018. Geologic and geochronologic update of the Turtle Lake area, NTS 104M/16, northwest British Columbia. In: Geological Fieldwork 2017, British Columbia Ministry of Energy, Mines and Petroleum Resources, British Columbia Geological Survey Paper 2018-1, pp. 83-128.

Abstract

The Turtle Lake map area straddles the boundary between exotic, oceanic crustal and mantle rocks of the Cache Creek terrane, and Laberge Group (Early Jurassic) Whitehorse trough forearc strata atop the Stikine terrane. Exposed in the Turtle Lake area are extensive platformal carbonate rocks of the Horsefeed Formation, a regional hallmark of the Cache Creek terrane, that were deposited over at least 25 m.y. Juxtaposition of Stikine and Cache Creek terranes was accommodated by collapse of the Whitehorse trough in mid-Middle Jurassic (starting ~174 Ma) and creation of a fold and thrust fault belt. This belt was cut by the Fourth of July batholith (~172 Ma) and lamprophyre dikes, emplaced and cooled by ~162 Ma, and followed by a magmatic lull between ~165-130 Ma. In the Turtle Lake area, we find a single granitic dike that crystallized in this time interval, at ~145 Ma. By 125 Ma, the Coast Belt arc had ignited, as recorded by voluminous volcanic and intrusive rocks in the west, and persisted until ~50 Ma. In the Turtle Lake area, volcanism accompanied uplift by ~110 Ma, as indicated by a unimodal detrital zircon population in karst deposits. The youngest known representative intrusions are ~56 Ma quartz diorite stocks. One of these stocks cuts the faulted contact between Whitehorse trough strata and harzburgite mantle tectonite. An analogous geological setting hosts epithermal gold-silver vein mineralization at the Engineer Mine, ~30 km to the south-southwest. The youngest rocks affected by crustal scale faulting and linked, mainly south-side-down, extensional faults are the ~80 Ma Windy-Table suite volcanic strata. We have yet to properly document the extensional faulting episode, but future work aimed at doing so will have important implications for regional tectonic reconstruction, and evaluation of mineral potential.

Keywords: Cache Creek terrane, Stikine terrane, Laberge Group, Horsefeed Formation, Kedahda Formation, Windy-Table suite, mantle tectonite, Turtle Lake, Tagish Lake, Atlin, regional mapping, conodont, geochronology, geochemistry

1. Introduction

The Turtle Lake map area of northern-most western British Columbia overlaps the boundary between Stikine and Cache Creek terranes on existing terrane assemblage maps (Fig. 1a; Wheeler et al., 1988; Colpron and Nelson, 2011). The Stikine terrane is characterized by Late Devonian to Early Permian and Middle Triassic to Lower Early Jurassic volcanic arc magmatic rocks. In the Turtle Lake area (Figs. 1b, 2), immature volcanic wacke to fine siliciclastic rocks of the Laberge Group (Lower to Middle Jurassic) are presumed to overlap and completely blanket the Stikine terrane. Farther west, Stikinia is represented by Late Triassic (and older?) arc rocks of the Stuhini Group (Souther, 1971; Mihalynuk et al., 1999; Lewes River Group in Yukon, Wheeler, 1961). To the east (Fig. 1b), platformal limestone, pelagic sedimentary, and ophiolitic rocks were

historically included in the Cache Creek terrane (Carboniferous to Lower Jurassic). However, parts of Cache Creek terrane may be related to Stikinia (English et al., 2010; Zagorevski et al., 2016; McGoldrick et al., 2017).

Systematic regional mapping in the Turtle Lake map area (Fig. 2) was conducted as part of the provincial-federal Geomapping for Energy and Minerals (GEM2) program. A major objective of the mapping was to resolve the age, kinematics, and magnitude of displacement along the Stikine-Cache Creek terrane boundary. Addressing these problems is critical to deciphering what happens to the northern extent of the mineralized Late Triassic-Early Jurassic porphyry belt, which is well-developed 200 km to the south but appears to be cut out by faults near the British Columbia-Yukon border. A re-evaluation of geological relationships along previously known faults led

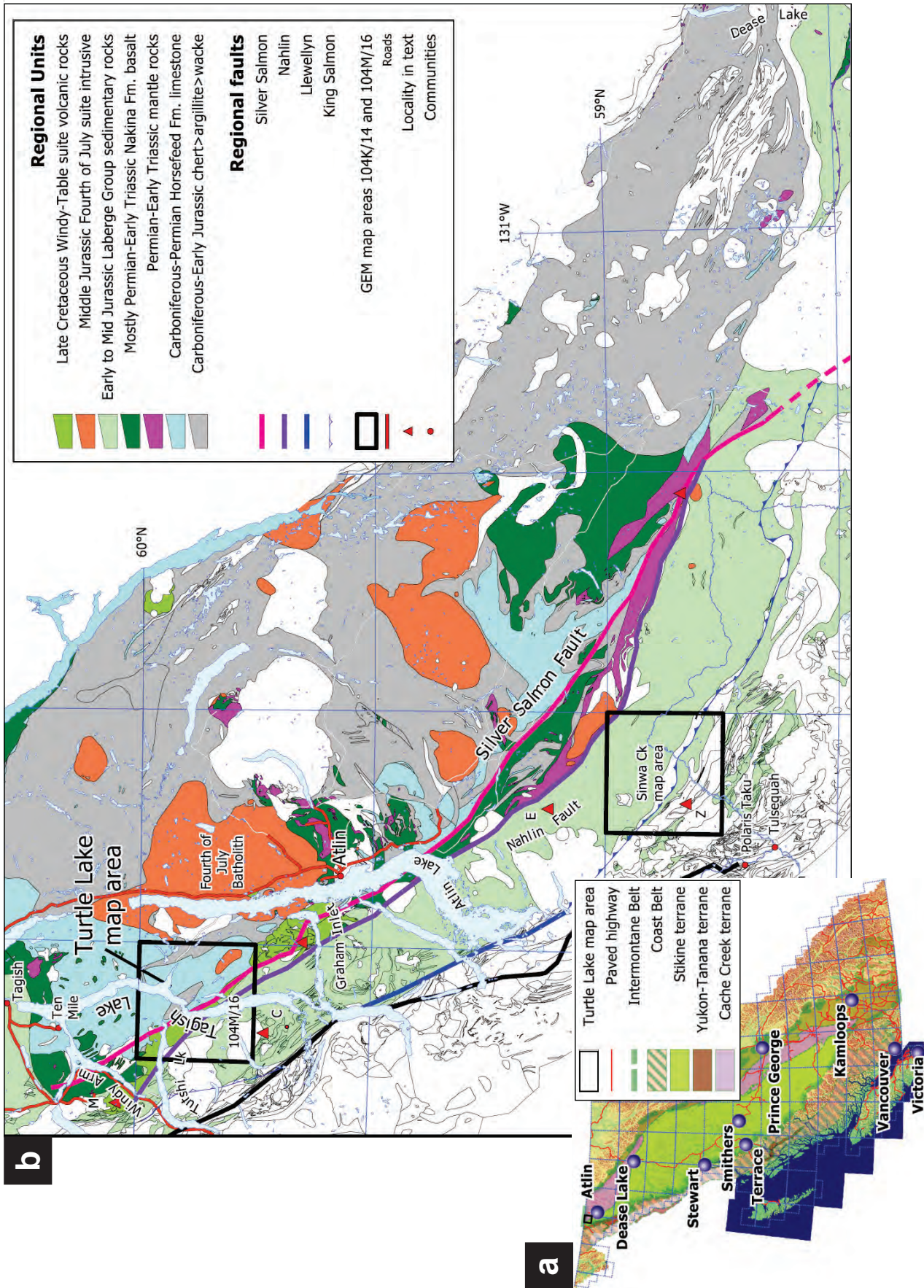


Fig. 1. a) Tectonic setting and location of the Turtle Lake map area in northwestern British Columbia. **b)** Regional geological setting showing the location of the quadrangles mapped as part of the Geomapping for Energy and Minerals initiative. Localities mentioned in the text are shown as labelled triangles: C – Mount Clive, E – Eclogite Ridge, M – Montana Mountain, Z – site of ~242 Ma detrital zircons in Mihalynuk et al. (2017).

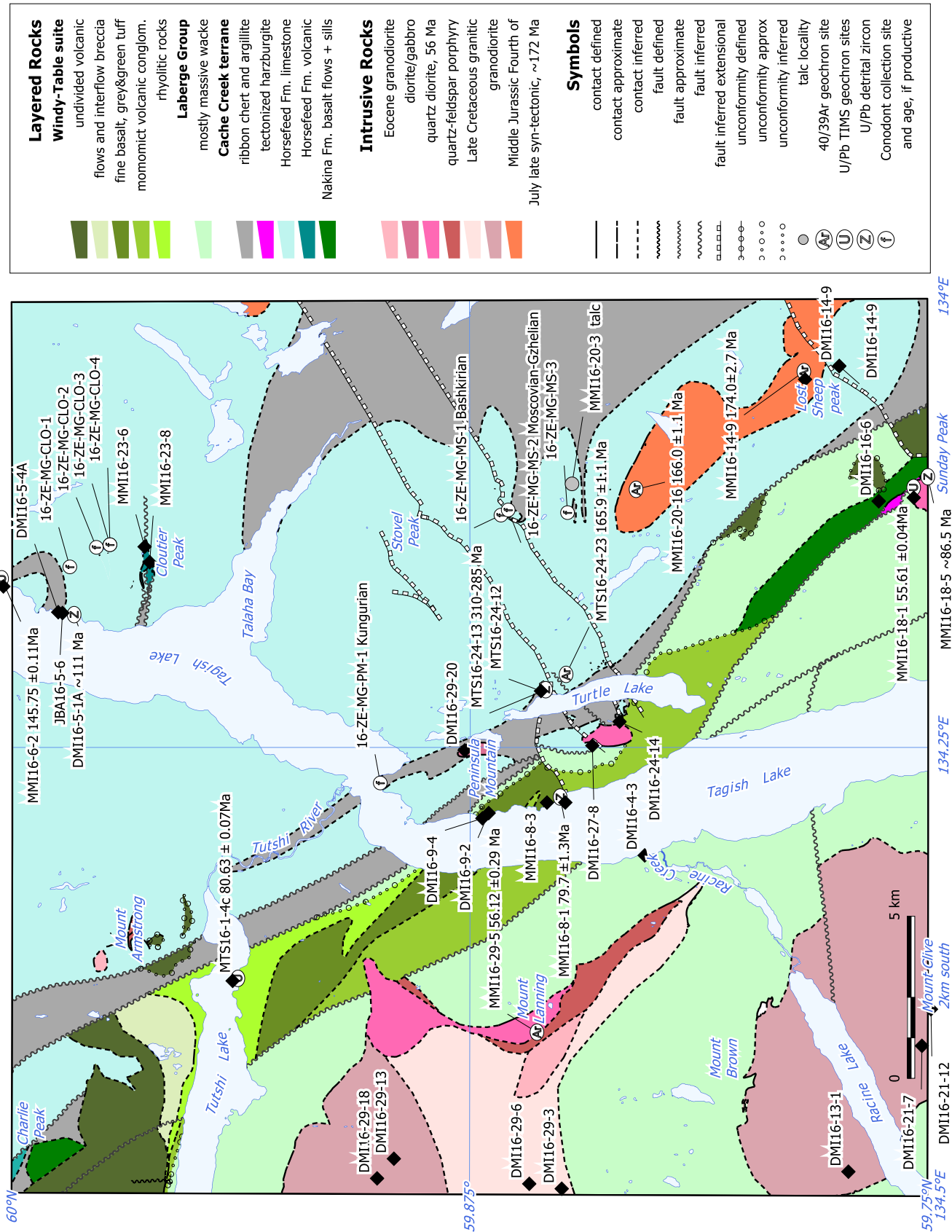


Fig. 2. Simplified geological map of the Turtle Lake map area updated from Mihalynuk et al. (1996, 1999) with location of samples for which geochronology and geochemistry results are reported herein.

to extension of the Silver Salmon fault from the Nakina area to northern British Columbia and southern Yukon, where it marks the present Stikine-Cache Creek boundary (Turtle Lake fault of Zagorevski et al., 2017). Herein we present results of systematic mapping, geochronology, geochemistry, and paleontology in the Turtle Lake area. Our data indicate that motion on the Silver Salmon fault affects rocks as young as Late Cretaceous and that fault zone fabrics are cut by an Early Eocene diorite stock. More regional work will be needed to evaluate offsets and make meaningful predictions about the apparent northward disappearance of the Late Triassic porphyry belt.

2. Physiography and previous work

The Turtle Lake map area is bisected by the main branch of Tagish Lake, which extends ~70 km southward from the northern border of the map area, adjacent Yukon (Fig. 1b). The lake provides excellent boat access; with boat launches at the community of Tagish or at Ten Mile, 22 km north of the British Columbia-Yukon border. The northwestern part of the map area can also be accessed by boat using Tutshi Lake, which is accessed from the Klondike Highway, ~17 km west of the map area. Tutshi Lake trends east across the northwest part of the Turtle Lake map area and drains into Tagish Lake via Tutshi River. Racine Lake, extends east-northeast across the southwestern corner of the map area, draining into Tagish Lake via cataract-laden Racine River. It is accessible via aircraft.

Whereas most of the area can be accessed by multi-day foot traverses, the most efficient mode of travel is by helicopter from a base in Atlin, 45 km southeast of the its central part. Extensive tree cover and brushy swamps in the northeastern part of the map area render large regions without helicopter landing sites, so the only option is foot traverse.

East of the high Coast Mountains, the Turtle Lake area is part of an orographic dry belt that receives only moderate winter snow and lacks glaciers. The highest points are Stovel Peak (1825 m) and Sunday Peak (1920 m) east of Tagish Lake and Mount Lanning (1902 m) and Mount Brown (2010 m) west of Tagish Lake, which all rise from the Tagish Highland plateau. Less than 20% of the area is above tree line, but the forests are relatively open, and usually easily navigated. Most of the eastern part of the map area is underlain by carbonate rocks with subterranean drainage and, by late summer, running surface water above treeline is almost non-existent.

Early systematic surveys of the area were conducted by Gwillim (1901), and Cairnes (1913). Quadrangle mapping covered the area at 1:250,000 scale as part of the Bennett sheet (104M) by Christie (1957). Bultman (1979) mapped the boundaries of the Whitehorse Trough through the region as part of an unpublished Ph.D. thesis, having a footprint that extended well beyond the Turtle Lake area. More detailed surveys at 1:50,000 scale almost surround the Turtle Lake map area (Mihalynuk and Rouse, 1988; Bloodgood et al., 1989; Mihalynuk and Mountjoy, 1990; Mihalynuk and Mountjoy, 1990; Mihalynuk et al., 1991; Mihalynuk and Smith, 1992a). Only the area north of the Turtle Lake mapsheet lacks systematic

quadrangle mapping at scales greater than 1:250,000 (Wheeler, 1961), although Monger (1975) covered much of the area at a 1:63,360 scale.

3. Regional geology and nomenclature

The eastern ~2/3 of the map area is underlain by extensive carbonate and lesser chert and argillaceous strata of the Cache Creek terrane (Fig. 2). Most abundant are limestones of the Horsefeed Formation (Carboniferous to Permian). They are the oldest known rocks in the Turtle Lake area (Late Carboniferous) as established by fusilinids (see Monger, 1975) and to a lesser extent, by conodonts (Golding and Orchard, 2017; see below). The western ~1/3 of the map area is underlain by coarse siliciclastic marine strata of the Laberge Group, the age of which is well-established, predominantly by ammonites (e.g., Mihalynuk et al., 1999; Johannson et al., 1997). Along most of their mapped extent, these two major rock packages are separated by the Nahlin fault zone, which trends northwest. However, Late Cretaceous volcanic strata of the Windy-Table suite and Peninsula Mountain suite (that we show here to largely belong to the former), and slivers of oceanic crustal rocks and mantle, are caught in between. Large (several tens of km²) homogeneous plutons at the western edge of the map area are outliers of the Coast Plutonic complex (~55 to 120 Ma).

Monger (1975) and Mihalynuk et al. (1999) reviewed the history of Cache Creek terrane nomenclature, which is not repeated here. However, we reiterate concerns raised by Zagorevski et al. (2016), that the present extent of Cache Creek terrane must include a major suture. Accordingly, it is a composite terrane in need of redefinition.

Mafic and minor intermediate volcanic rocks in sharp fault contact with Cache Creek limestones along eastern Tagish Lake were interpreted as the older of two volcanic packages. These rocks were mapped as Pennsylvanian to Triassic by Christie (1957), Upper Paleozoic by Monger (1975), and Middle to Late Triassic by Bultman (1979). Along strike in adjacent map sheets, they were mapped as Middle to Late Triassic (Mihalynuk et al., 1991, 1999; Mihalynuk and Smith, 1992a, b; Zagorevski et al., 2017). The younger package is mafic to felsic in composition and gently dipping where best exposed north of Tutshi Lake. It was included with “volcanic rocks of uncertain age” by Christie (1957), Late Cretaceous and/or Early Tertiary Sloko Group by Monger (1975), Middle to possibly Late Cretaceous Hutshi Formation by Bultman (1979) and, in adjacent areas, as either Lower to Middle Jurassic volcanic suite, or Late Cretaceous Windy-Table suite by Mihalynuk et al. (1999) and Zagorevski et al. (2017). Based on new geochronological data reported here, we suggest that most, if not all, of these rocks should be assigned to the Windy-Table suite.

3.1.1. Cache Creek terrane

In the Turtle Lake map area, Cache Creek terrane comprises the Horsefeed Formation limestone, Kedahda Formation chert (Watson and Mathews, 1944), and minor Nakina Formation mafic volcanic rocks (Monger, 1975). Although major

problems with this stratigraphic nomenclature exist (Monger, 1975; Mihalynuk et al., 1999; Zagorevski et al., 2016), we follow it for regional consistency until a thorough redefinition of the Cache Creek terrane is undertaken.

3.1.2. Horsefeed Formation limestone

The Horsefeed Formation is the most extensive unit in the Turtle Lake map area. These rocks have been described in detail by Monger (1975) who estimated their original thickness to be 1.5 km and obtained fossil ages ranging from Late Carboniferous (Middle Pennsylvanian) to Late Permian. The Horsefeed Formation is a mostly massive, variably recrystallized limestone, generally cream-coloured, but ranges to yellow and grey with local zones of red or black (Fig. 3). Layering that is apparent at a distance is commonly not discernable up close. Bioclasts, especially crinoids, can be locally found. However, well-preserved fossils are rare due to recrystallization, which is especially intense south of Stovel Peak where radiating talc splays are abundant in hydrothermally altered limestones in the contact metamorphic aureole of a Middle Jurassic pluton (Fig. 4a). Local variants of the Horsefeed Formation include well-bedded limestone (Figs. 3a, b), limestone interbedded with chert (Figs. 3b, c, d), limestone breccia (Figs. 3e, f), fusulinid packstone (Fig. 3g) and tuffaceous limestone (Fig. 3h).

Well-bedded limestone, with layers 0.05 to 2 m thick, tend to be darker grey (Fig. 3b) where bedding is thinnest, perhaps due to greater organic content. At two localities, thin (0.1-0.4 m) beds of packstone (Fig. 3a) contain fusulinids up to 1 cm in diameter (Fig. 3g). Fusulinids range from well preserved (where individual living chambers can be discerned with an unaided eye) to strongly deformed (Fig. 3g). Monger (1975) reported a late Early Permian fossil age from one of these localities. Limestone locally contains chert nodules, lenses and discontinuous layers up to 0.5 m thick that are grey to black (Figs. 3b, c). Chert layers are locally boudinaged within the recrystallized carbonate. Sparse younging indicators suggest a general increase in chert upsection towards the Kedahda Formation, consistent with the observations of Monger (1975).

Limestone breccias are common and likely have more than one origin. Conformable breccia beds have thicknesses in excess of 10 m. Most are clast supported, and whereas some layers appear uniform, with mm to cm-scale angular clasts set in a carbonate cement (Fig. 3e), they can contain outsized blocks up to several m in diameter. Other layers contain cm-dm clasts (Fig. 3f). Still others locally form semi-concordant sill and dike-like bodies in ribbon cherts (Fig. 5a; see below), some with blocks of deformed chert metres across floating in carbonate breccia. Other discordant breccia bodies, generally cemented by carbonate, are along brittle fault zones. All are likely produced by mass flow. Monger (1975) attributed isoclinally folded blocks of chert and interlayered limestone west of Mt. Cloutier to similar syn-sedimentary gravity sliding. In the Tagish area, fossils in breccia blocks tend to be of the same age as the fossils in the contiguous main mass of limestone (Monger, 1975). Immediately east of Turtle Lake, a

several metre-thick bed containing angular clasts of limestone, minor chert, and sparse rhyolite was sampled for detrital zircon age determination. Zircons recovered from this bed range from Middle Pennsylvanian through Early Permian (see below).

Exposed on a low ridge south of Stovel Peak, and at two sites along the east shore of Tagish Lake (Fig. 2), are limestone breccias with a calcarenite matrix containing a maroon hematitic cement that stands out against a backdrop of mainly white-weathering Horsefeed Formation (Figs. 4b, c). South of Stovel Peak, the calcarenite matrix is well laminated (Fig. 4c) and consists of spherical and round grains. The laminae drape and are folded around breccia clasts. Lamination in the matrix material indicates post-brecciation sedimentary infill, suggestive of a paleokarst origin, which is supported by Early Cretaceous detrital zircons from one sample of the laminated matrix (see below).

Green and maroon tuffaceous beds that are centimeters to a few metres thick form inconspicuous low outcrops on the northwest flank of Mt. Cloutier (Fig. 3h) and along eastern Tagish Lake, across from the mouth of the Tutshi River. These contain angular lapilli and ash-sized, aphanitic to finely plagioclase-phyric clasts in a carbonate matrix. Fine calcite-filled amygdales are common. Fine tuff layers are typically foliated, and the foliation is locally crenulated. Tuffaceous strata on Cloutier Peak are roughly along strike with Early Permian limestone (Monger, 1975). However, our samples of limestone interbedded with tuff did not yield conodonts (see below). Tuffaceous limestone breccia east of Turtle Lake contains detrital zircons that cluster at ~285 Ma, which we interpret as the best estimate of the maximum depositional age (see below), consistent with Early Permian deposition.

3.1.3. Kedahda Formation chert

The Kedahda Formation is best exposed on the east shore of Tagish Lake (northwest of Cloutier Peak, Figs. 5a, b), on the low ridges south of Stovel Peak, and north and east of Turtle Lake (Fig. 2). In these areas, well-bedded Kedahda Formation comprises 2-15 cm thick layers of black chert and 0.5-2 cm thick layers of argillite. The chert, locally varies from black to tan or nearly white. Radiolaria have been generally destroyed by recrystallization. Chert is generally more abundant than argillite. However, this may be due to recessive weathering of argillite such that it is only exposed in creek bottoms or low-profile outcrops along lake shores. Syn-sedimentary deformation structures include clastic dikes (Fig. 5a) and gravity slides.

Direct age determinations from chert in the Turtle Lake area are lacking. An early Early Permian fossil age (Monger, 1975) was determined for a breccia block contained in the chert unit north of Turtle Lake (where exposed on Tagish Lake), indicating that chert at that locality is early Permian or younger. Along strike, ~20 km southeast of the Turtle Lake map area (north of Graham Inlet), chert interbedded with wacke yielded Middle to Late Triassic radiolaria (Mihalynuk et al., 1999). Regionally, chert ranges from Paleozoic to Late Triassic, with abundant

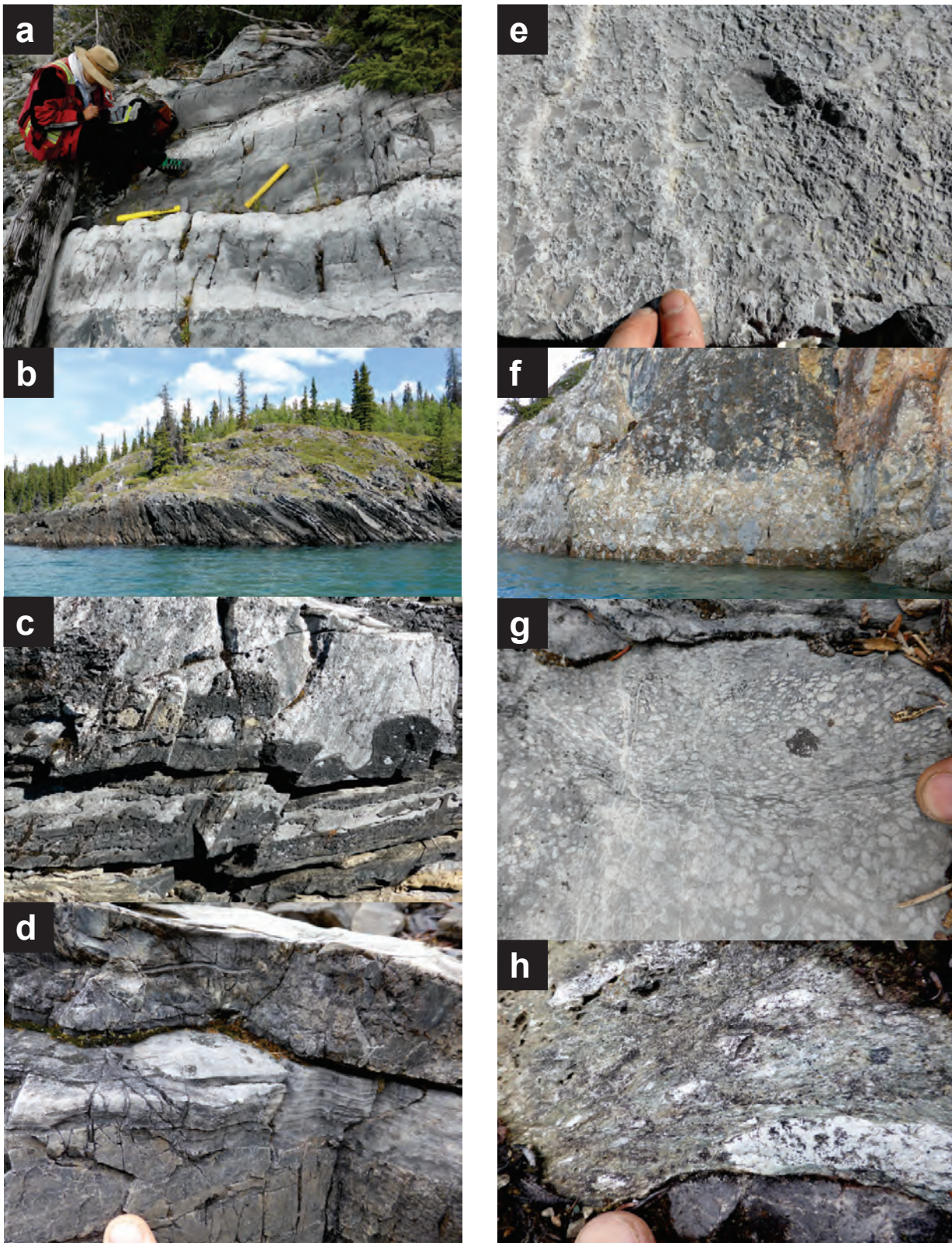


Fig. 3. Examples of Horsefeeed Formation limestones, which are generally massive, that display structures. **a)** Thick bedded, fusulinid-rich bioclastic limestone. **b)** Massive chert grading to medium- to thin-bedded, grey cherty limestone upsection, to the right of photo (south). **c)** Straight and irregular zones of chert and limestone. **d)** Laminae from limestone continues into chert lens (above finger) indicating diagenetic replacement of limestone. **e)** Fine, homogeneous monomictic limestone-clast breccia. **f)** Coarse, mainly monomictic limestone-clast breccia. **g)** Fusulinid packstone; finger on high-strain zone. **h)** Foliation in green tuffaceous limestone wraps around flattened, white lapilli; in sharp contact with a grey limestone bed at bottom of photo.

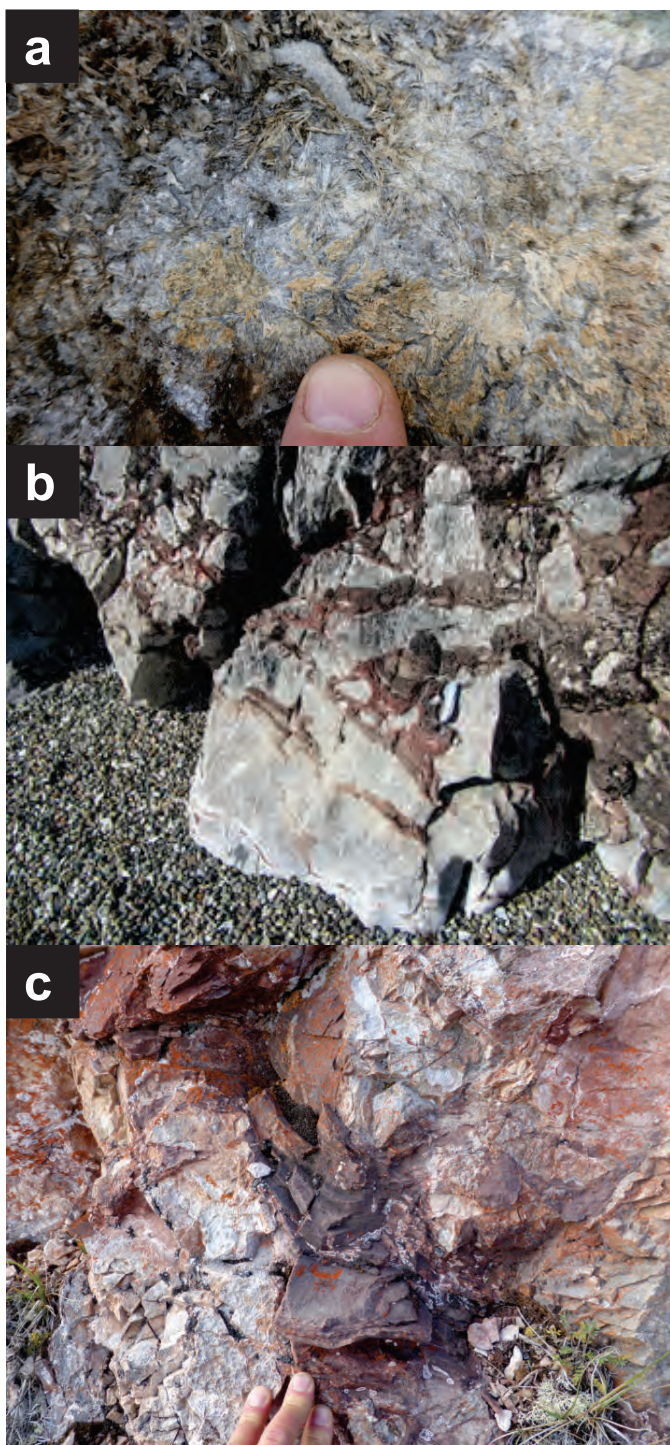


Fig. 4. a) Radiating talc crystals grow in thermally metamorphosed Horsefeed Formation. **b), c)** Bioclastic framework-intact limestone breccia with laminated, hematitic calcarenite matrix. Detrital zircons extracted from the matrix yielded an Early Cretaceous population, supporting the interpretation of the breccia as a paleokarst deposit (see below).

Middle Triassic chert in the Nakina Lake area (Mihalynuk et al., 1999, 2003), and voluminous Late Triassic chert in the Teslin area (Cordey et al., 1991). Probably the most common

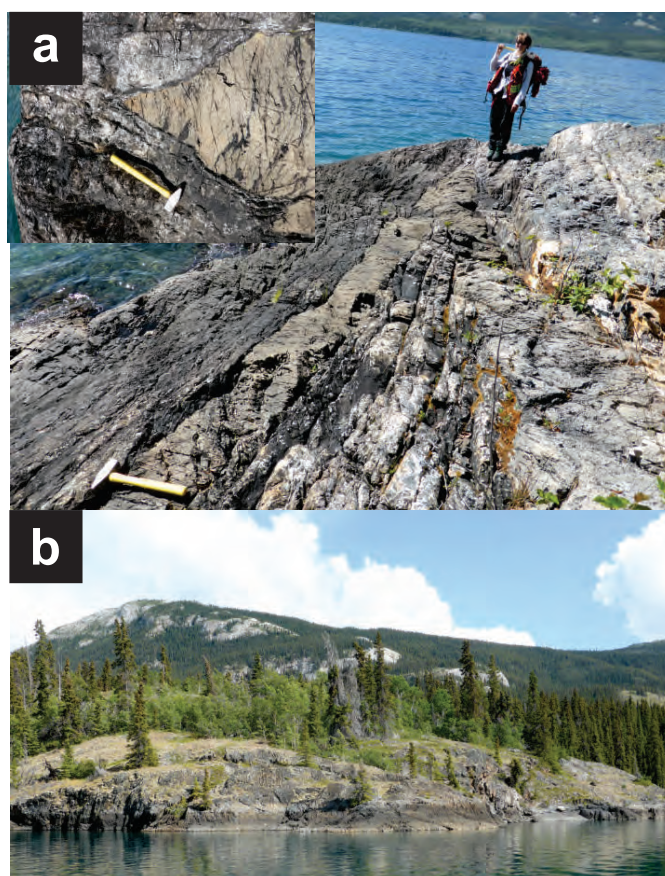


Fig. 5. a) Tan-weathering clastic carbonate intrusions cut well-bedded Kedahda Formation chert. Inset shows sill termination (in front of person). View to the northwest. **b)** Well-bedded Kedahda Formation ribbon chert along the eastern shore of Tagish Lake. View along strike to the southeast. On horizon is massive carbonate underlying the northern ridge of Mount Cloutier.

age of chert in the Tagish-Atlin region in British Columbia is Middle Triassic.

3.1.4. Nakina Formation basalt

Dark green to black, highly fractured to blocky weathering, aphanitic to finely feldspar- and pyroxene-phyric mafic rocks are well exposed on the east flank of Sunday Peak, extending in a belt toward Peninsula Mountain (Fig. 2). The Nakina Formation comprises rocks interpreted as basalt flows and tuff (Mihalynuk et al., 1999). Pillow basalt is locally exposed, but there is a substantial volume of hypabyssal diabase sills and dikes with very similar petrographic characteristics. Sparse geochemical data suggest that these mafic rocks have island arc to backarc tholeiite characteristics. These volcanic and shallow intrusive rocks are adjacent to a fault-bound sliver of mantle tectonite and both have previously been included in the Graham Creek suite (Mihalynuk et al., 1999). Elsewhere in the Cache Creek terrane, the association of island arc tholeiites and mantle tectonites has been interpreted to represent a structurally dismembered ophiolite (English et al., 2010; Zagorevski et al., 2016; McGoldrick et al., 2017). Graham Creek rocks were

previously considered probable correlatives of the Cache Creek ophiolitic rocks, but were separated because a gradational contact with overlying Laberge Group could be inferred (Mihalynuk et al., 1999), whereas, evidence for Cache Creek terrane basement was, at the time, more equivocal. Recent detrital zircon evidence from with wacke deposited on the Cache Creek terrane supports correlation with Laberge Group (Colpron et al., 2015), and a stratigraphic linkage of Cache Creek and Laberge Group by earliest Jurassic.

3.2. Laberge Group

Descriptions of the Laberge Group strata in areas immediately adjacent to the Turtle Lake mapsheet are detailed in Mihalynuk et al. (1999). The sedimentology, depositional setting, and paleontology of the Laberge Group have been addressed by many studies (e.g., Wheeler, 1961; Tempelman-Kluit, 1978; Tempelman-Kluit, 1984; Dickie and Hein, 1995; Hart et al., 1995; Hart, 1997; Johannson et al., 1997; Mihalynuk et al., 1999; Lowey, 2003; Lowey, 2004; Colpron et al., 2015). In the Turtle Lake area, the Laberge Group consists mainly of thick-bedded coarse wackestone, thin-bedded siltstone, and lesser rhythmically bedded sandstone and mudstone. The scale of interlayering is too fine to resolve at the 1:50,000 scale of our mapping.

3.2.1. Rhythmic sandstone-mudstone couplets (Richthofen formation)

Distinctive, rhythmically bedded, tan and black, sandstone-mudstone couplets (Fig. 6a) comprise what is possibly the lowest exposed unit of the Laberge Group in the Turtle Lake map area. Thin parallel beds are typically 2-5 cm thick, normally graded, and display bioturbation. Syndepositional folds and faults as well as intraformational angular unconformities are common. Outcrops are commonly well-cleaved.

This unit is a characteristic component of the informal Richthofen formation, which is recognized as forming the Early Jurassic base of the Laberge Group in the type area of Yukon (Hettangian to Pliensbachian; Tempelman-Kluit, 1984), consistent with observations in the Turtle Lake area. However, this unit is also observed at localities that are well above the base of the Laberge Group, in agreement with the suggestion of Lowey (2004), that it ranges to Toarcian (upper Lower Jurassic).

3.2.2. Thick-bedded coarse greywacke

Orange to brown or grey, blocky weathering greywacke is the most common Laberge Group rock type in the map area. Beds are generally 0.3-2 m thick, but are locally >10 m thick. Coarse feldspar and lithic grains predominate, although quartz grains can comprise up to ~15% of the rock. Rare beds of arkosic or lithic sandstone contain only minor muddy matrix. Sparse pebbles and cobbles of arc-like magmatic and sedimentary rocks are common. Northwest of Sunday Peak, greywacke contains conspicuous black volcanic clasts with blocky feldspar phenocrysts (Fig. 6b). These resemble volcanic clasts that are

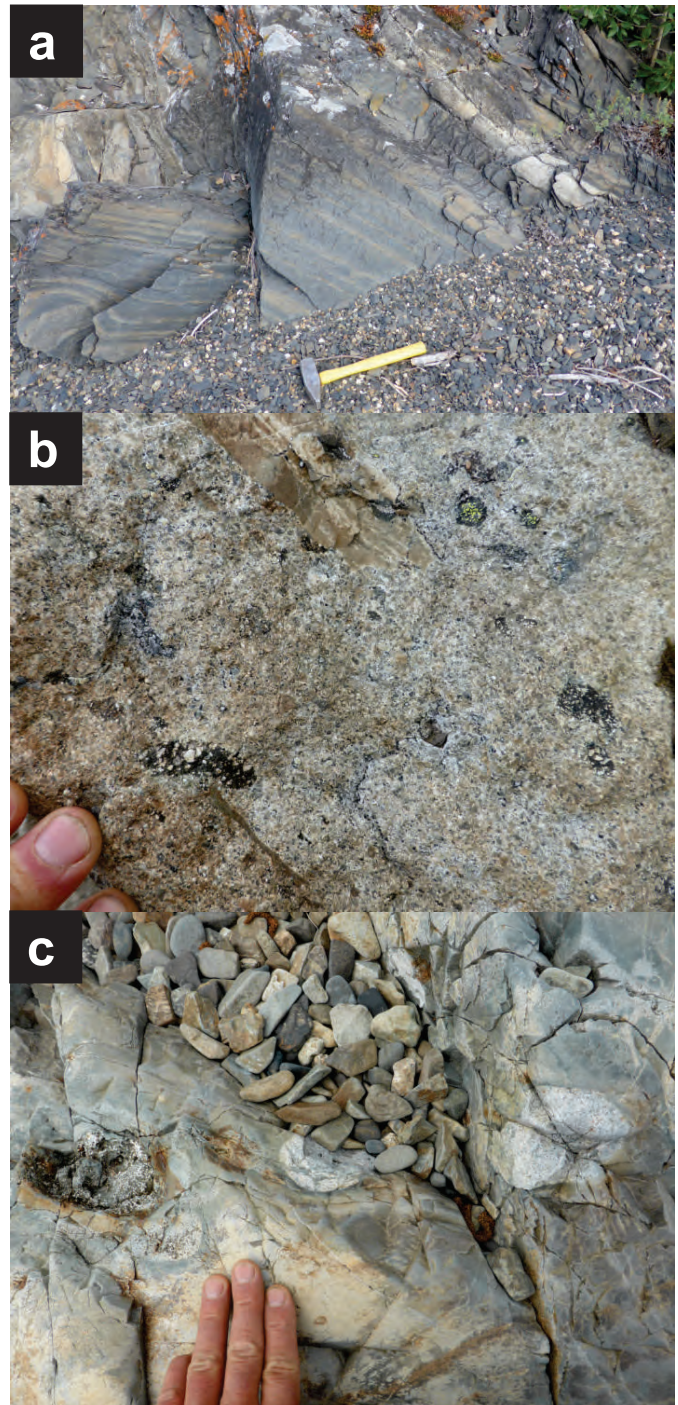


Fig. 6. Variation of Laberge Group lithologies. **a)** Rhythmically bedded tan wackestone and black argillaceous siltstone is typically bioturbated and strongly cleaved. **b)** Very coarse wacke to granule conglomerate with sparse oversized boulders. Distinctive, flattened black clasts with blocky feldspars are interpreted as collapsed pumaceous blocks. **c)** Polymictic matrix-supported conglomerate. Clasts range from diorite to granite and (outside of view) conglomerate to limestone.

common in the Eclogite Ridge section of the Laberge Group, about 100 km to the south (Canil et al., 2005). In other places, cobbles of arc provenance can comprise over 10% of the unit (Fig. 6c).

3.2.3. Thin-bedded siltstone

Rusty-weathering, indurated, well-bedded siltstone erodes to form slopes of fine angular talus. This unit consists of siltstone and argillaceous siltstone in beds that are typically less than 10 cm thick and may locally be cross stratified.

3.3. Windy-Table suite

The Windy-Table suite (Late Cretaceous; Mihalynuk et al., 1999) was first defined in the Windy Arm (western branch of Tagish Lake in Yukon) and Table Mountain areas (Fig. 1b). In the Turtle Lake area, the Windy-Table suite is exposed in a belt extending northwest from Sunday Peak. The base of the Windy-Table suite is seen at Sunday Peak and eastern Tutshi Lake (Fig. 7), where basal reworked rhyolite breccia (Figs. 7a, b) unconformably overlies Laberge Group and harzburgite tectonite. Three units predominate the suite near Tutshi Lake: a basal rhyolite to trachyte (Fig. 8a), overlying andesitic flows and interflow breccia and tuff (Fig. 8b), and heterolithic lapilli tuff and breccia (Fig. 8c). Near Peninsula Mountain, monomict volcanic conglomerate is predominant. Thinner units of fine-grained basalt and grey and green tuff are not divisible at the scale of Figure 2, where they are shown combined.

3.3.1. Rhyolitic rocks

Two types of rhyolitic rocks crop out in the Turtle Lake area: breccia at Sunday Peak (Fig. 7b), and rhyolite tuff at Tutshi Lake (Fig. 8a). New geochronologic and stratigraphic evidence that we report (see also Zagorevski et al., 2017) suggest that the units belong to the lower and middle parts of the Windy-Table suite.

On the eastern side of Sunday Peak (Fig. 7a), rhyolite breccia (Fig. 7b) marks the contact between mantle rocks (Figs. 7a, c) of the Cache Creek terrane and Whitehorse trough strata. Rhyolite breccia displaying finely embayed clasts (Fig. 7b) is in fault contact with strongly foliated serpentinized harzburgite to the east (Fig. 7c). Near its western limit of exposure, the rhyolite breccia is in contact with Laberge Group strata. At this locality, subangular fragments of the Laberge Group appear mixed with the rhyolite and may be conglomeratic, indicating an unconformable relationship, but thermal alteration caused by the nearby Sunday Peak stock (Fig. 7d) obscures relationships. A pebble dike or surface fissure infill contains a mix of rhyolite breccia and clasts of harzburgite within harzburgite (Fig. 7a inset). A sample of the main breccia layer yielded new U-Pb data that suggest an age of ~86.5 Ma (see below).

Along the shores of eastern Tutshi Lake, white and orange, rubbly-weathering rhyolite tuff (Fig. 8a) and trachytic flows occupy the structurally lowest exposed parts of the suite. Rhyolite tuff is composed of aphanitic cream and tan lapilli and blocks in layers up to tens of metres thick. Locally the unit contains a few percent of medium-grained, pinkish orthoclase crystals and rare medium-grained quartz eyes. Wispy chlorite layers are likely relicts of flattened pumice lapilli.

Near the base of the precipitous south face of Charlie Peak, along the western edge of the map area, a discontinuous section

is exposed. Starting at lake level, poorly bedded Laberge Group wacke becomes red and oxidized up section, until it is overlain by well-bedded, shallowly north-dipping, maroon and green volcanic sandstone containing granules of underlying Laberge Group and rhyolite and green felsic tuffaceous interbeds that have a waxy luster. Above is the main mass of Windy-Table volcanic strata with rhyolite at its base. The contact is interpreted as an angular unconformity even though definitive bedding could not be found in immediately underlying Laberge Group strata, which are extensively folded in most other localities. Below we report a new U-Pb zircon age from the thickest mapped part of the rhyolite unit.

3.3.2. Coarse volcanic wacke

Coarse-grained volcanic wacke to feldspar-phyric granule conglomerate displays poorly developed layering. This unit may be a fine-grained equivalent of the conglomerate along the southwest side of the Peninsula Mountain where it is separated from Kedahda Formation chert by covered intervals. However, volcanic wacke and Middle to Late Triassic chert are interbedded near Graham Inlet to the southeast (Mihalynuk et al., 1999; Zagorevski et al., 2017), demonstrating the difficulty in correlating this unit regionally.

3.3.3. Fine-grained to aphanitic basalt

Dark grey to black, tan weathering, fine-grained to aphanitic amygdaloidal basalt is typically grey to mint green on fresh surfaces and brecciated, forming massive intervals tens of metres across. In some localities, probable flows display vague pillow forms (Fig. 9a), but these are obscured by autoclastic and subsequent fracturing. The basalts contain fine phenocrysts of augite, and very fine-grained needles of plagioclase, indicating that clinopyroxene preceded plagioclase on the basalt liquidus. Most of these rocks have island arc tholeiite affinity, serving to distinguish them from E-MORB basalts of the Horsefeed Formation, but they are difficult to distinguish lithologically and geochemically from Nakina Formation, and may be partly correlative (see below).

3.3.4. Grey and green tuff

Angular block to lapilli tuff is dark green to black-weathering, and where wave-washed or fresh, displays a lighter grey (Fig. 9b) or green ash-rich matrix. Clasts tend to be sparsely pyroxene-phyric, some with fine feldspar, or aphanitic. Matrix-deficient samples have a basaltic composition. In a few localities, sparse, irregular black clasts of indurated rock may be siltstone. Some clasts display white rims. Rarely this unit contains aphanitic clasts that are entirely white and may be of felsic composition (Fig. 9c). At one locality, light-coloured clasts predominate the rock (Fig. 9d), but here they contain coarse prismatic crystals that are probably hornblende, and ghosts of green to white crystals, probably feldspars that were chloritized and then further altered and bleached. Below we report an age from this unit of 79.7 Ma.

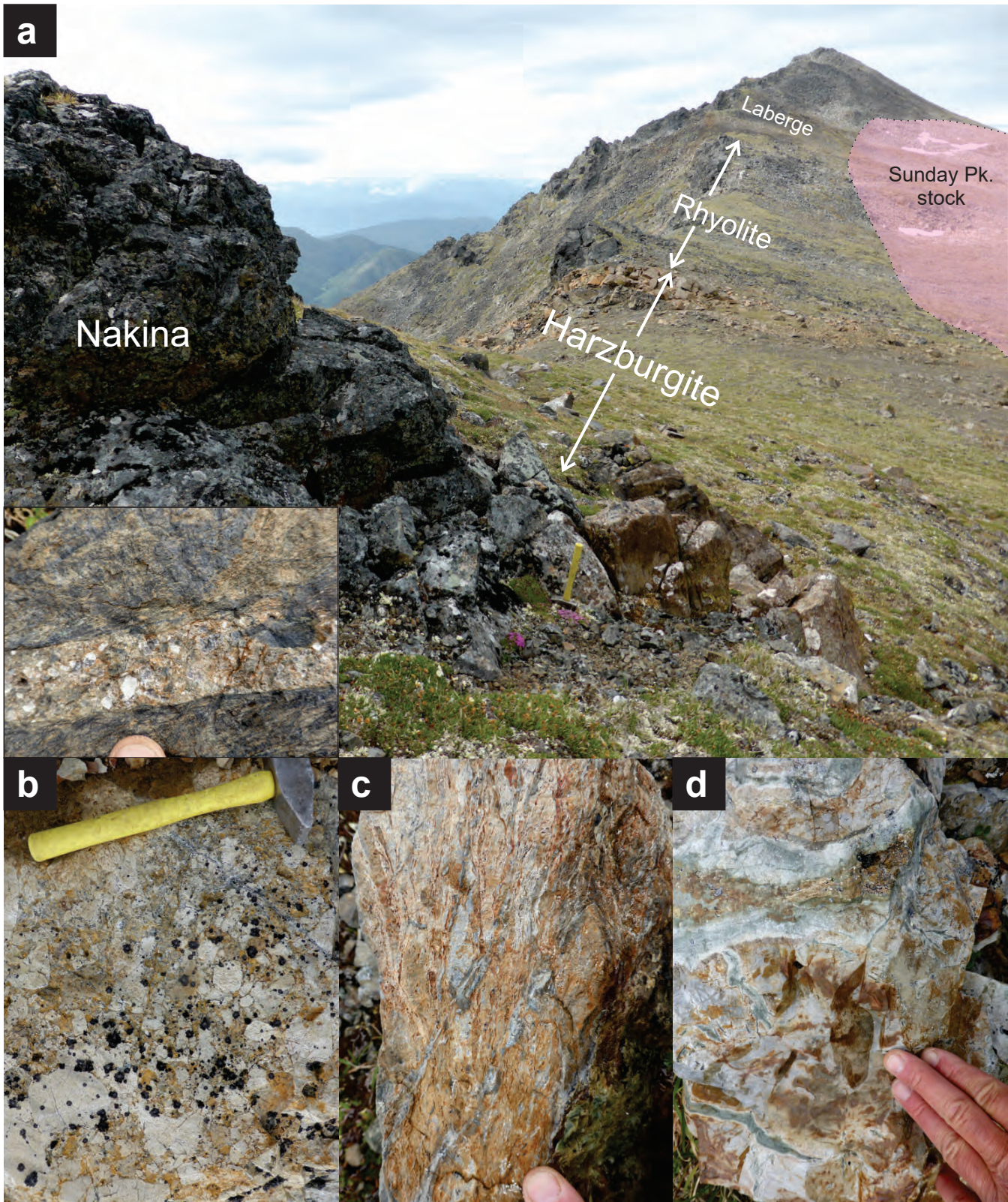


Fig. 7. Contact relationships in the saddle east of Sunday Peak. **a)** View to the southwest parallel to the steep face of the peak shows dun-weathering harzburgite extending from near foreground to just beyond the low point of the saddle. Immediately beyond the far harzburgite outcrop is a resistant knob of rhyolite breccia (close up view in **b**), which is foliated and in direct contact with serpentinite (exact contact beneath finger in **c**). Light weathering-resistant breccia gives way to rusty weathering, rounded ridge underlain by Laberge Group. clastic rocks. Light weathering rocks along the far right side of the photo (**a**) are thermally altered (as in **d**) by the Sunday Peak stock that partly underlies the far snow patch (approximate distribution is shown).

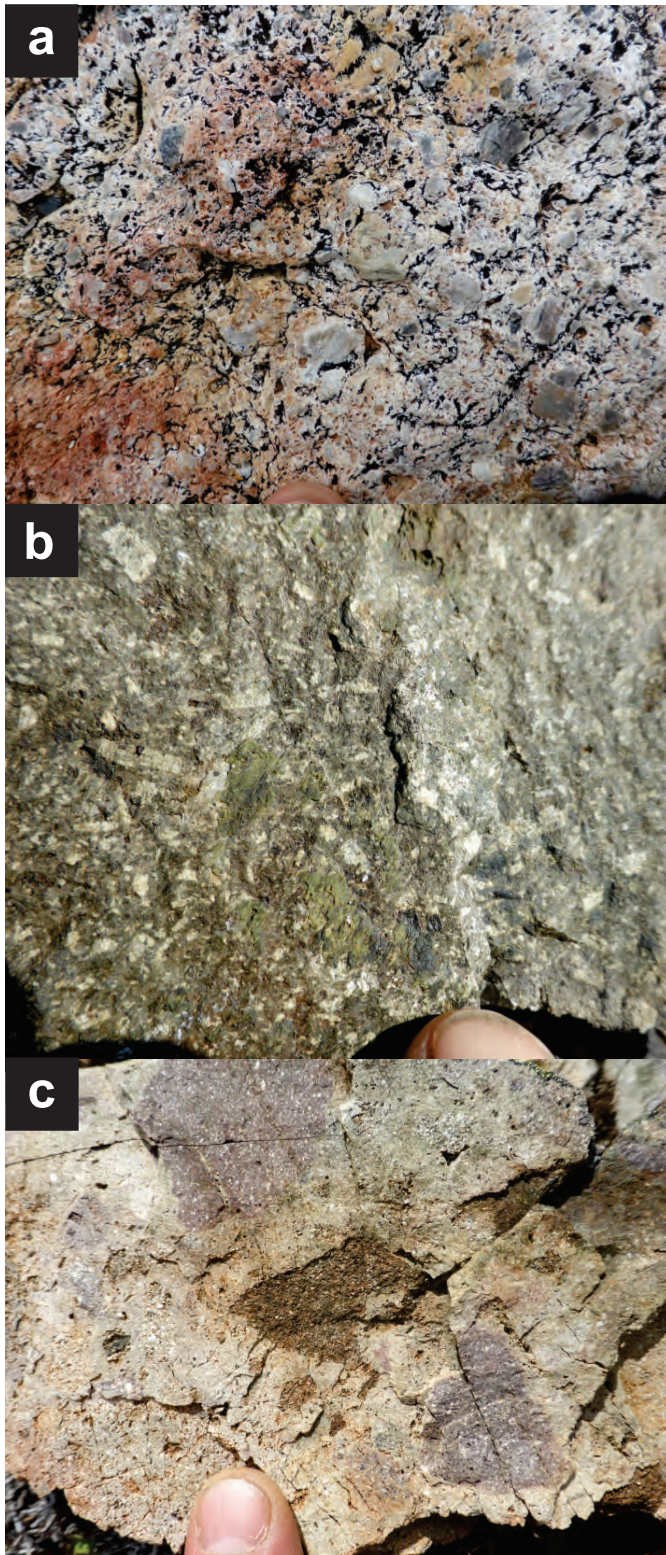


Fig. 8. Characteristic Windy-Table suite rock types near eastern Tutshi Lake. **a)** Rhyolite at the base of the section, south shore, eastern Tutshi Lake. **b)** Tabular feldspar porphyry of autoclastic flows above the rhyolite, north of eastern Tutshi Lake. **c)** Variegated fine- to medium-grained, tabular plagioclase porphyry tuff near Sunday Peak is similar to units north and south of eastern Tutshi Lake, and if reworked, the conglomerate facies near Peninsula Mountain (Figs. 9 e, f).

3.3.5. Monomictic volcanic conglomerate

Rounded blocks up to 1 m in diameter of orange or green-weathering, (Figs. 9e, f) brown to green pyroxene-feldspar porphyry typically float in a matrix of medium-grained grey volcanic wacke to angular granulestone. Pyroxene crystals are medium- to coarse-grained, black, chloritized and comprise up to ~5% of the volcanic clasts. Feldspar is mainly fine- to medium-grained and comprises up to ~30% of the clasts. Clasts vary in colour, grain size, and angularity, but have a uniform mineralogy and are presumably derived from a single volcanic source.

3.3.6. Feldspar-phyric flows and interflow breccia

Coarse, white tabular feldspar crystals up to ~1 cm in length comprise ~20% of the rock. An olive brown matrix contains ~1% fine black blocky relicts of mafic crystals, probably pyroxene or hornblende, altered to chlorite. Epidote alteration and veins are common (Fig. 8b). Flows range from a few m to probably more than 10 m thick. Although the rubbly nature of most outcrops makes definition of upper and lower flow surfaces uncertain, the relatively resistant flows form subhorizontal topographic benches. Recessive interflow breccia is the same composition as the flows and is generally massive with internal bedding and reworking of clasts to form conglomerate observed in a few localities.

3.3.7. Heterolithic tuff

Rocks of the Windy-Table suite, which are not mapped as parts of the foregoing units, are predominantly fine- to medium-grained feldspar-phyric block and lapilli ash tuff (Fig. 8c, included on Figure 2 with 'undivided volcanic') of probable intermediate composition, and containing varying proportions of felsic volcanic clasts. Other distinctive lithologies, which are too isolated to map at 1:50,000 scale, are also included. Some examples are: discontinuous rhyolitic tuff layers (locally containing coarse biotite); and andesitic flows (in one case displaying indistinct pillows).

4. Intrusive rocks

Elliptical to irregularly-shaped stocks of quartz diorite to granite composition are less than one to several km² in size where they cut the eastern margin of the Cache Creek terrane between Sunday Peak (Fig. 10a) and Mount Lanning. Larger bodies, tens of km² in size and mainly of granodioritic composition, cut rocks of the Whitehorse trough farther west and closer to the main mass of the Coast Plutonic complex. Based on geological relationships and K-Ar cooling ages of other bodies in the suite, the ages of stocks and plutons in the Turtle Lake map area were assumed to be Late Cretaceous to Early Tertiary (Mihalynuk et al., 1996), but based on our new isotopic age determinations, are now known to extend from Middle Jurassic to Eocene.

Most stocks and plutons are heterogeneous. For example, the Middle Jurassic (174 ± 2.7 Ma) elongate pluton extending from Lost Sheep peak ~10 km northwest, is compositionally and

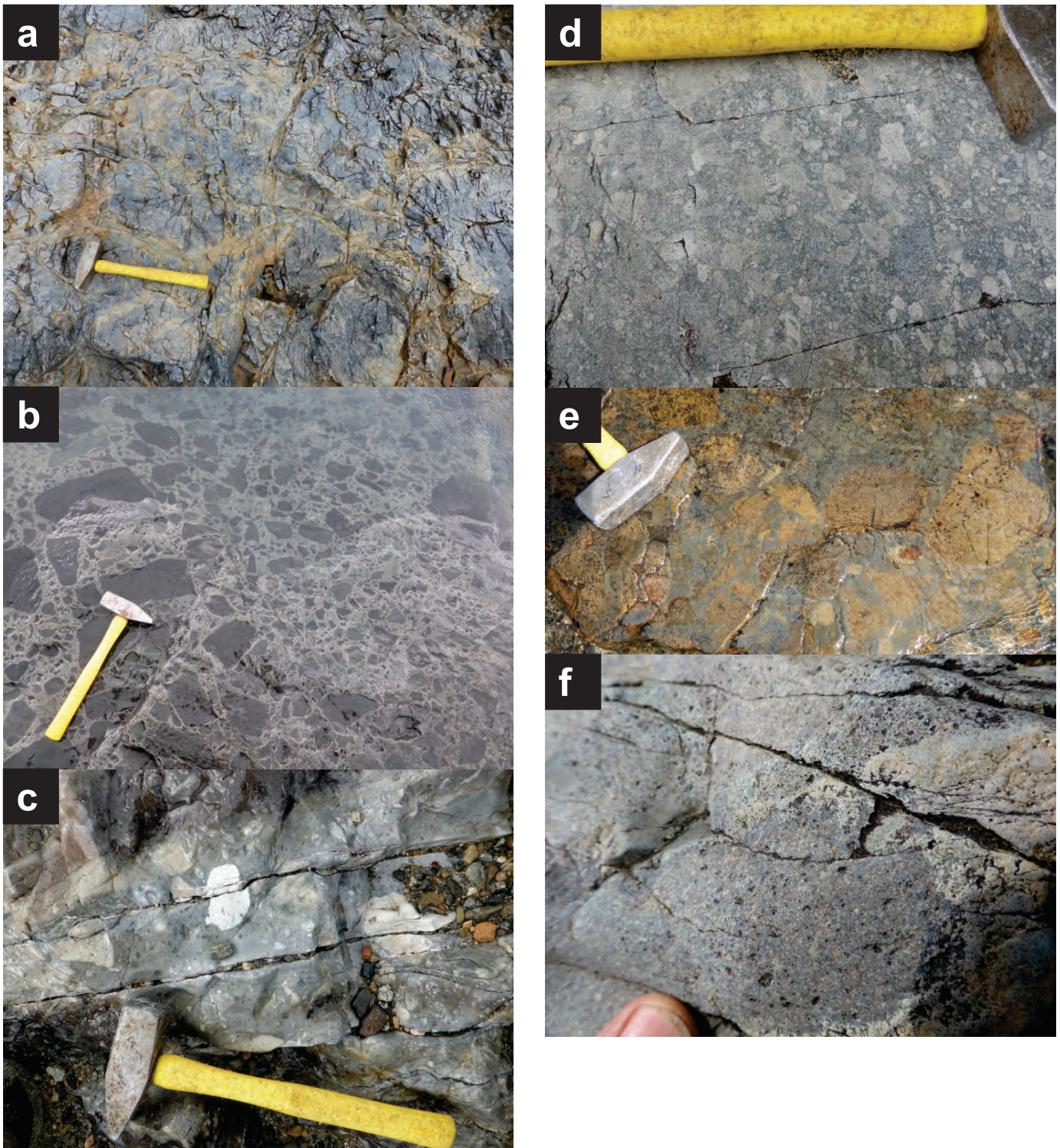


Fig. 9. Variations in the Windy-Table suite at Peninsula Mountain. **a)** Aphanitic brecciated basalt with vague pillow forms. **b)** Angular breccia blocks floating in an ash tuff matrix. **c)** Heterolithic tuffaceous conglomerate with light and dark clasts. Clasts are light coloured due to alteration, but also due to more felsic compositions. **d)** Felsic tuffite is composed largely of angular fragments. **e)** Monomictic volcanic conglomerate. Despite colour and grain size variation, the phenocryst assemblage is consistent. **f)** Close-up of conglomerate showing homogeneous pyroxene-feldspar-phyrlic clasts and greywacke to granulestone matrix.

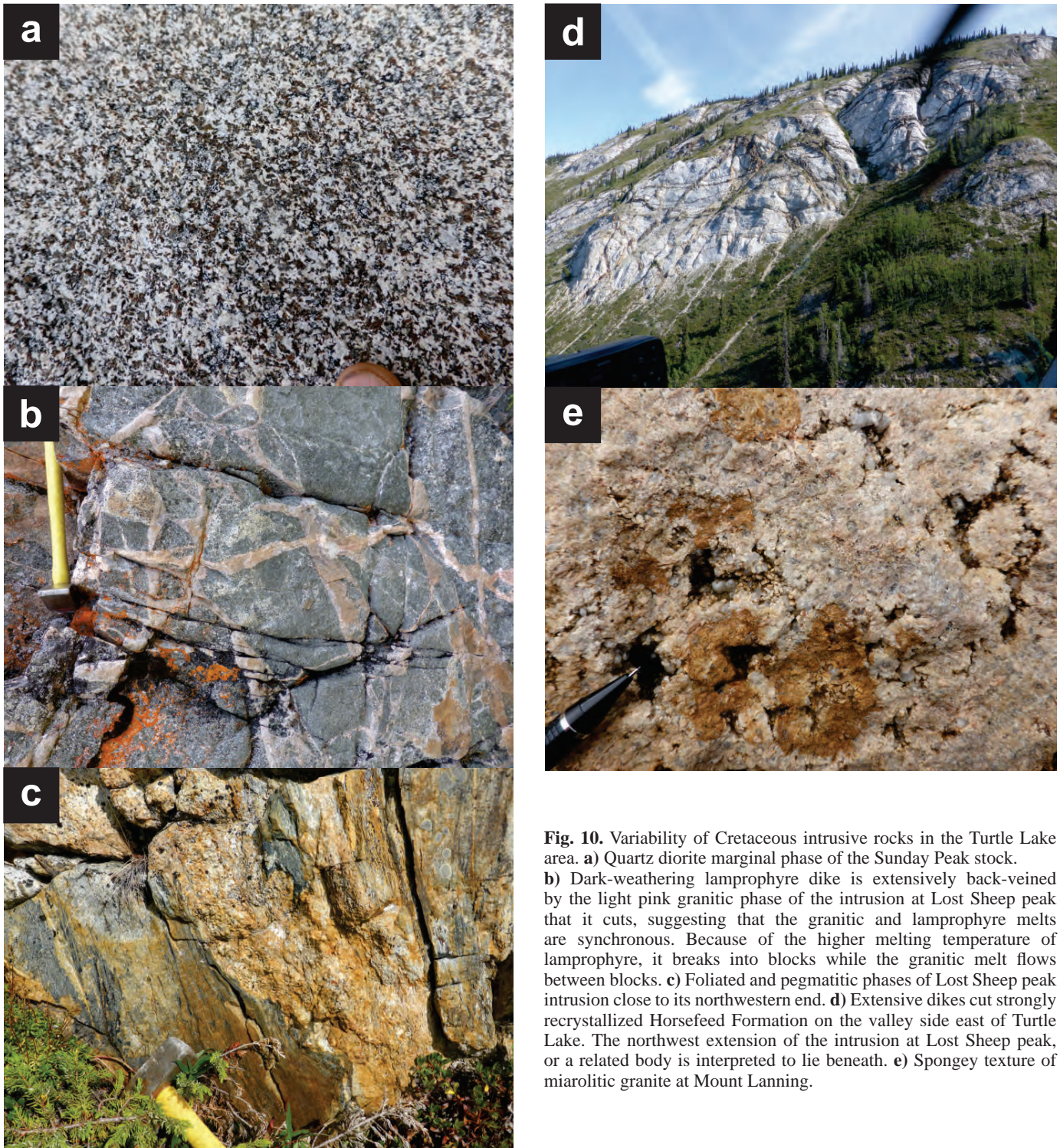


Fig. 10. Variability of Cretaceous intrusive rocks in the Turtle Lake area. **a)** Quartz diorite marginal phase of the Sunday Peak stock. **b)** Dark-weathering lamprophyre dike is extensively back-veined by the light pink granitic phase of the intrusion at Lost Sheep peak that it cuts, suggesting that the granitic and lamprophyre melts are synchronous. Because of the higher melting temperature of lamprophyre, it breaks into blocks while the granitic melt flows between blocks. **c)** Foliated and pegmatitic phases of Lost Sheep peak intrusion close to its northwestern end. **d)** Extensive dikes cut strongly recrystallized Horsefeed Formation on the valley side east of Turtle Lake. The northwest extension of the intrusion at Lost Sheep peak, or a related body is interpreted to lie beneath. **e)** Spongy texture of miarolitic granite at Mount Lanning.

texturally variable with multiple cross-cutting phases ranging from aplite to lamprophyre (Fig. 10b). Near its northern limit, medium-grained granodioritic phases can be strongly foliated and cut by non-foliated quartz diorite to granite or pegmatite (Fig. 10c) with hornblende and biotite cooling ages of ~166-162 Ma (see below). Continuation of this elongate body in the subsurface is indicated by a zone of strong recrystallization and

extensive dike emplacement in Horsefeed Formation limestone east of Turtle Lake (Fig. 10d), and by its aeromagnetic response, which extends the belt across an area with little outcrop.

Underlying northern Sunday Peak is a semi-circular granodioritic stock with a quartz-dioritic border phase (Fig. 10a). Crystallization of its northern border is now precisely dated at 56.01 ± 0.04 Ma (see below).

Large plutons west of Tagish Lake tend to be more isotropic and granodioritic in composition (ranging from quartz diorite to granite), although separate composite zones can be mapped. For example, between Mount Lanning and Racine River, northwest-trending porphyritic and quartz-dioritic belts can be mapped (Fig. 2). East of Mount Lanning a zone of spectacularly miarolitic granite crops out over at least 2 km² (Fig. 10e). From a late quartz dioritic phase we obtained a new cooling age of 56.12 ± 0.29 Ma (see below).

Most plutons have a high magnetic susceptibility relative to the rocks that they intrude and are well defined by a recent regional aeromagnetic survey (Boulanger and Kiss, 2017). However, the elongate, composite body that extends from Racine River, across Mount Lanning to the ridges south of Tutshi Lake, shows only a muted magnetic response. Approximately 3 km² of the plateau between Mount Lanning and Mount Brown is covered with granitic boulders, commonly more than a metre in diameter. The total lack of a regional aeromagnetic response is consistent with the interpretation that these boulders are coarse moraine overlying Laberge Group sedimentary rocks rather than of local derivation from a nearby intrusion in the subsurface. Currently unexplained is an aeromagnetic high in the northeast corner of the Turtle Lake sheet that was not mapped during the course of our survey. We suspect that this belongs to an apophysis of the Fourth of July batholith, the contact of which is currently mapped 5 km to the east.

4.1. Lamprophyre dikes

Dark green biotite-rich lamprophyre dikes extensively cut rocks in the Turtle Lake map area and are especially conspicuous where they cut granitoid bodies or Horsefeed Formation limestone. They range from centimetres to about 15 m in thickness and commonly display chilled margins and parallel internal zones with varying contents and compositions of xenoliths or amygdales. Differences in relative resistance to weathering of the xenoliths and amygdales give the weathered dikes a knobby appearance. At one locality on northeast Lost Sheep peak, chrome diopside xenocrysts were tentatively identified in outcrop, but could not be confirmed petrographically. A southeast-trending set of these dikes cut a granitic phase of the intrusion at Lost Sheep peak and are back-veined by that phase (Fig. 10b), suggesting that the two are penecontemporaneous. Cooling ages of ~168-174 Ma from biotite and hornblende separates of two dikes are presented below.

5. Structure

A lack of distinctive marker horizons challenges structural interpretation of the Turtle Lake area. Nevertheless, outcrop-scale structure can be observed and, in some cases, can be reasonably linked to map-scale structures.

5.1. Folds

Massive Horsefeed limestone of the Cache Creek terrane does not reveal mountain-scale folds; whereas, in the well-stratified

Laberge Group, west-verging folds and thrust faults are clearly displayed (Fig. 11a). However, argillaceous or chert-rich layers outline km-scale folds along Tagish Lake, and spectacular refolded folds are displayed at outcrop scales where Horsefeed Formation limestone has been strongly recrystallized in the thermal aureole of intrusions (Fig. 11b). At one locality, we interpret chaotic infolding of limestone breccia and chert as due to soft sediment deformation, but that tightening of such folds has resulted in refolding with an axial cleavage (Fig. 11c).

Outcrop-scale folds in fault zones are common in the Cache Creek terrane. Such folds are readily apparent in bedded chert-argillite of the Kedahda Formation and near the contact between Kedahda and Horsefeed formations (Fig. 11d). Steep easterly plunges of folds in fault zones are common.

5.2. Faults

Fault styles in the Cache Creek terrane and Whitehorse trough contrast strongly. Late Middle Jurassic collapse of the Whitehorse Trough (Thorstad and Gabrielse, 1986; Mihalynuk et al., 2004) produced a fold and thrust belt characterized by transport of the interior parts of the trough over its southwest margin (Mihalynuk et al., 1999; English, 2004). Bedding-parallel thrusts can be identified by close examination of outcrops, or are clear at mountainside scale where hangingwall or footwall cutoffs are displayed (Fig. 11a). Such fold and thrust belt style of deformation is not apparent in the Cache Creek terrane of the Turtle Lake area, although, along strike to the northwest, Monger (1975) mapped a thrust belt along Windy Arm where structural repetition of stratigraphy is confirmed by fossil age determinations.

High-angle faults that cut Cache Creek terrane rocks at the outcrop scale are common, but identification of marker horizons and quantifiable offset by faults that can be mapped at 1:50,000 scale, are lacking. Zones of disruption m to 10s of m across that juxtapose disparate rock packages are also common, with implied large (hundreds of metres to many kilometres), but unquantified offsets. Faults with outcrop-scale offset include zones of brittle and ductile shear, which are especially well displayed by Horsefeed Formation carbonates. At one locality, a fusulinid packstone has been subjected to ductile deformation recorded by elongation of originally ovoid fusulinids (Fig. 3g). Major faults within the Horsefeed Formation show admixture of other lithologies such as angular aphanitic felsic or deformed shale and chert fragments (Fig. 12a). Within other Horsefeed Formation faults, carbonate blocks are milled and rounded with only sparse extraformational fragments (Fig. 12b).

Faults in the Kedahda Formation are extensively developed across strike widths of 10s to 100s of m. Chaotic folds (Fig. 12c), small-scale duplexing, and disaggregation of layers and milling of fragmented bed segments (Fig. 12d), are common. Such widespread disruption of the Kedahda Formation suggests that either strain is preferentially partitioned into this unit, or that the unit is comprised of, and originally accumulated as, a series of fault slivers, such as in an accretionary complex.

Within the volcanic rocks at Peninsula Mountain, one major

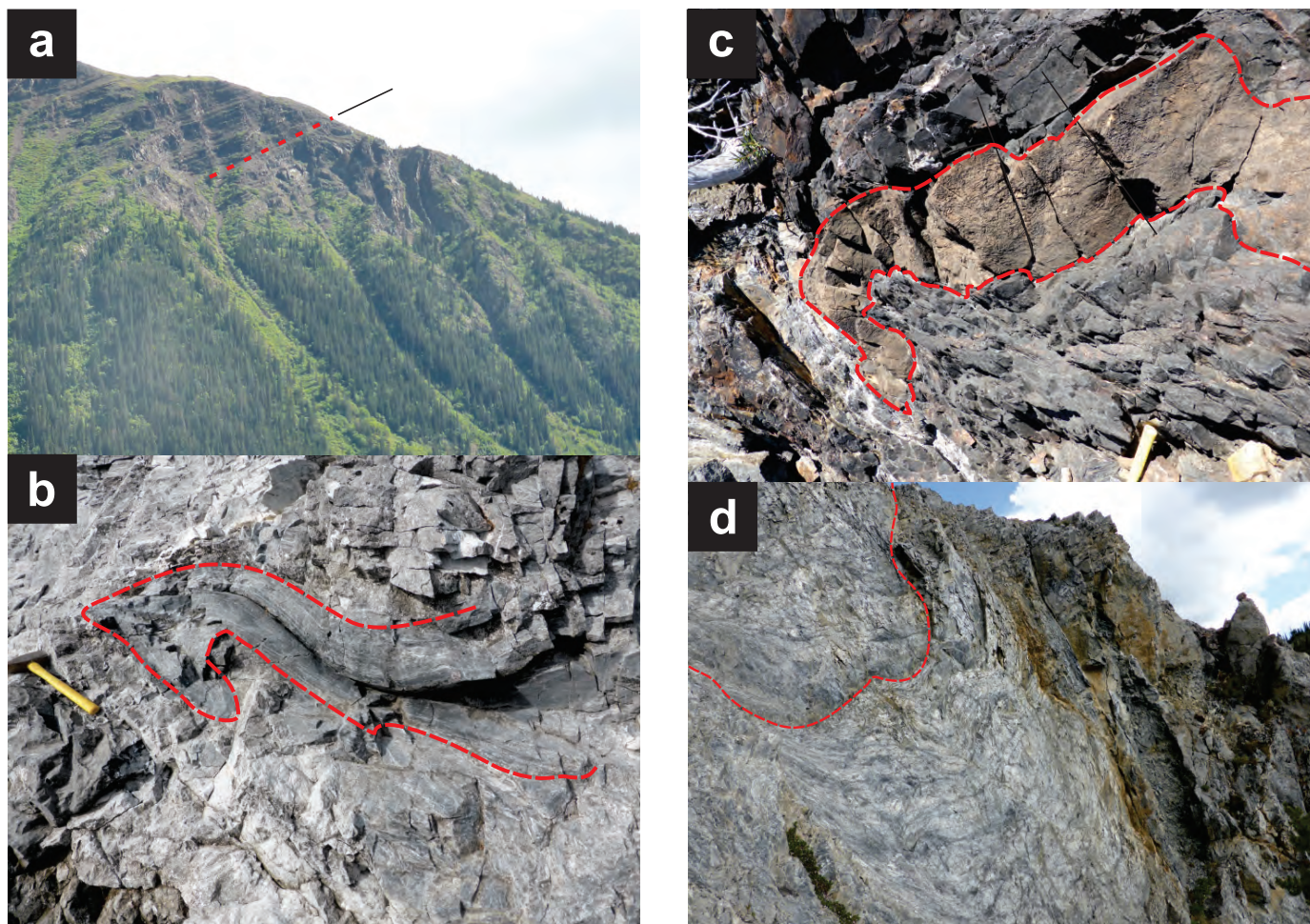


Fig. 11. Folds in the Turtle Lake map area. **a)** Southerly view of well-bedded Laberge Group strata extensively folded in the mid-right part of the photo (between the treeline and skyline, below projection of line) in the footwall of thrust with hangingwall of consistently east-dipping planar strata. **b)** Multiply-folded Horsefeed Formation limestone where thermally metamorphosed along western shore of Tagish Lake. **c)** tan carbonate layer and infolded grey bedded chert are refolded and cleaved. **d)** Steeply plunging fold in the Horsefeed Formation near the contact with the Kedahda Formation south of Stovel Peak.

fault has been mapped. It is a ~40 m wide zone displaying an anastomosing scaly fabric (Fig. 12e) around blocks of volcanic and extraformational fragments such as dioritic intrusive, serpentinized ultramafite (Fig. 12e inset) and carbonate. Dikes extensively intrude the fault zone, subparallel with the fabric. One dike has been deformed within the fabric and cut by a subsequent dike with an average strike of ~245° and dip of ~75°. At least during dike emplacement, the fault was probably extensional towards the southeast (~155°).

In outcrops across Tagish Lake, along its west shore, quasi-ductile extensional fabrics are also developed where dikes extensively cut and thermally metamorphose Laberge Group strata (Fig. 12f). A locally pervasive fabric (striking 160°, dipping ~65° WSW) cuts folded bedding (striking ~340° and dipping moderately to steeply overturned), and layers developed within that fabric are extended and rotated sinistrally. A top to the south-southeast sense of motion is indicated.

Faults between major lithologic packages can also be discrete. For example, along the eastern shore of Tagish Lake,

north of Tutshi Island, orange-weathering volcanoclastic rocks that we map as Windy-Table suite (Fig. 2), are abruptly juxtaposed across a decimetre-thick breccia zone with massive Horsefeed Fm. carbonate (Fig. 12g). There is little evidence of shearing during or after juxtaposition of these lithologies. One possibility is that the contact is part of an unconformity surface that has been repeated to the west by faulting. In contrast, near Sunday Peak, juxtaposition of Windy-Table rhyolite breccia with harzburgite is accompanied by a locally strong ductile fabric (Fig. 7c) that suggests significant syn- or post-juxtaposition movement. Rhyolite breccia west of the harzburgite is separated from the nearest main mass of Windy-Table volcanic rocks to the southeast by the nearly 500 m vertical elevation of the cliffs of southeastern Sunday Peak. A down-to-the-southeast fault separation is suggested, consistent with other indications of extensional faulting.

Limestone underlying Stovel Peak and the two unnamed mountains to the south is tentatively interpreted to be roughly equivalent and repeated by extensional faulting. However,

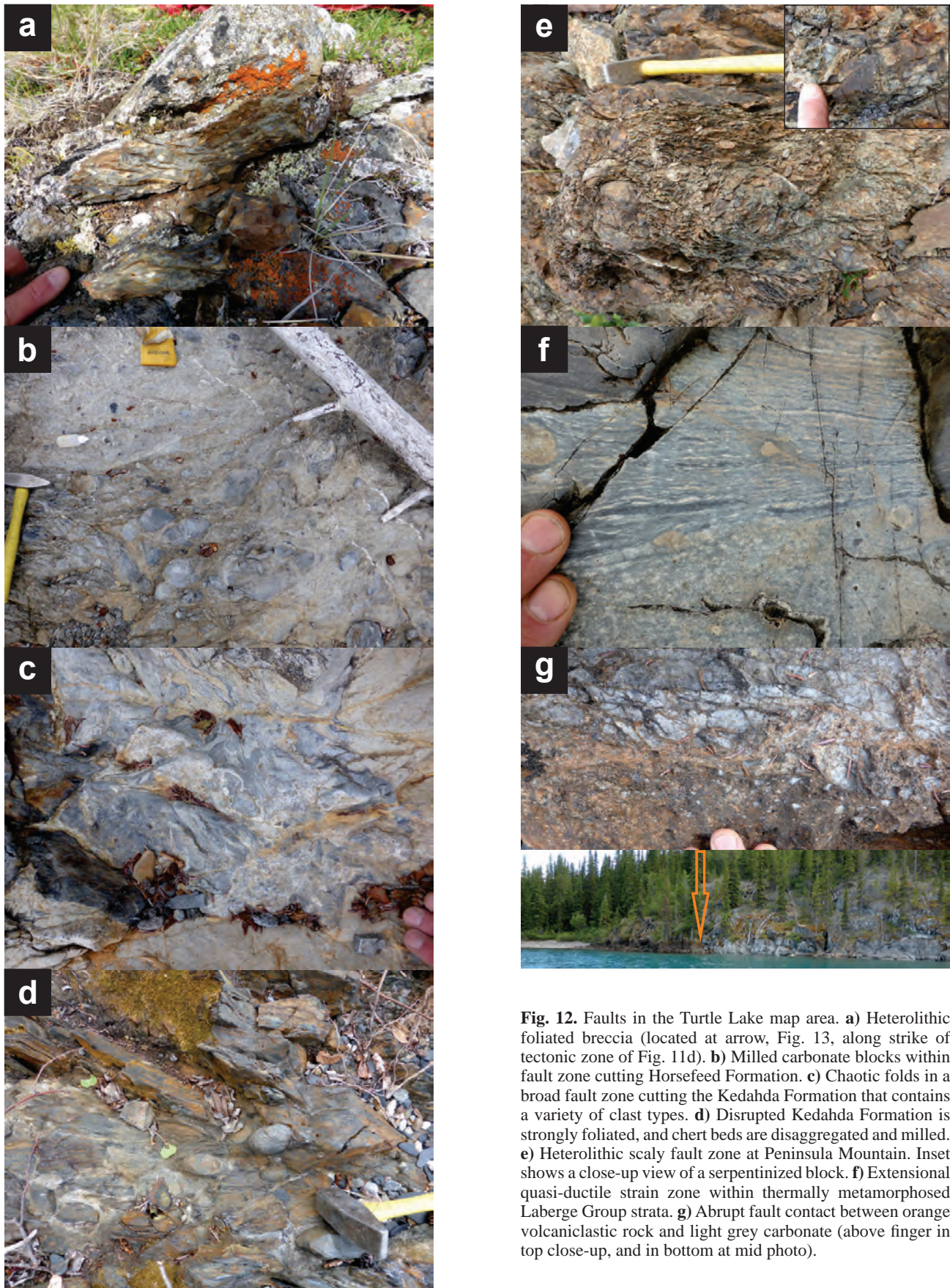


Fig. 12. Faults in the Turtle Lake map area. **a)** Heterolithic foliated breccia (located at arrow, Fig. 13, along strike of tectonic zone of Fig. 11d). **b)** Milled carbonate blocks within fault zone cutting Horsefeed Formation. **c)** Chaotic folds in a broad fault zone cutting the Kedadha Formation that contains a variety of clast types. **d)** Disrupted Kedadha Formation is strongly foliated, and chert beds are disaggregated and milled. **e)** Heterolithic scaly fault zone at Peninsula Mountain. Inset shows a close-up view of a serpentinized block. **f)** Extensional quasi-ductile strain zone within thermally metamorphosed Laberge Group strata. **g)** Abrupt fault contact between orange volcaniclastic rock and light grey carbonate (above finger in top close-up, and in bottom at mid photo).

support for this interpretation is currently limited to: aerial reconnaissance (Fig. 13); identification of a dip slope fault zone that crops out along one of the inferred fault traces (Fig. 12a); and extrapolation of the fault zones to faults previously mapped in areas adjacent to the Turtle Lake map sheet (Figs. 1b, 2). Testing this idea is important because extensional faults with nearby syn-kinematic magmatic rocks is a setting in which gold-silver deposits are known to form, for example, in the Republic graben, southern BC, and northeast Washington State (e.g., Boleneus et al., 2001).

6. Geochronology

Accurate age determination is especially useful in outcrop impoverished areas like the Turtle Lake map sheet, where geological relationships that could be used to establish relative age progression are not exposed. Here we report on biochronological (conodont) and isotopic age determinations.

6.1. Conodonts

Eight samples were collected from Horsefeed Formation limestone where bioclastic grains were evident. All conodont samples were processed at the Geological Survey of Canada in Vancouver, using standard techniques as outlined in Stone (1987) and (Jeppsson et al., 1999) with results summarized in Table 1. Of these samples, three yielded conodonts (a 37.5% success rate). These conodonts date from the early (Bashkirian)

and middle-upper (Moscovian-Gzhelian) parts of the Late Carboniferous (Pennsylvanian), and the last stage of the Early Permian (Kungurian).

These new conodont age determinations extend the ages of fossils at Stovel Peak, formerly known to contain late Early Permian fusulinids (Monger, 1975), to Late Carboniferous (Bashkirian). Also extended is the range of ages of fossils at Peninsula Mountain, formerly ranging from middle to upper Late Carboniferous (Monger, 1975), and now ranging to Early Permian, confirming an early Early Permian age previously obtained from a clast (Monger, 1975). Such revisions from a limited number of samples demonstrates that the sections are more age-extensive and/or interleaved at both localities and that our understanding of the Horsefeed Formation remains rudimentary.

6.2. Isotopic analyses

We used multiple isotopic systems and dating techniques for which laboratory procedures are well established. To date zircons extracted from igneous rocks, we used chemical abrasion-thermal ionization mass spectroscopy (CA-TIMS) at the Pacific Centre for Isotopic and Geochemical Research (PCIGR) at The University of British Columbia. Sample preparation and analytical procedures are reported in Friedman et al. (2016; abridged in Mihalynuk et al., 2016). For detrital zircons, high-quality portions of single zircon grains were analyzed by laser

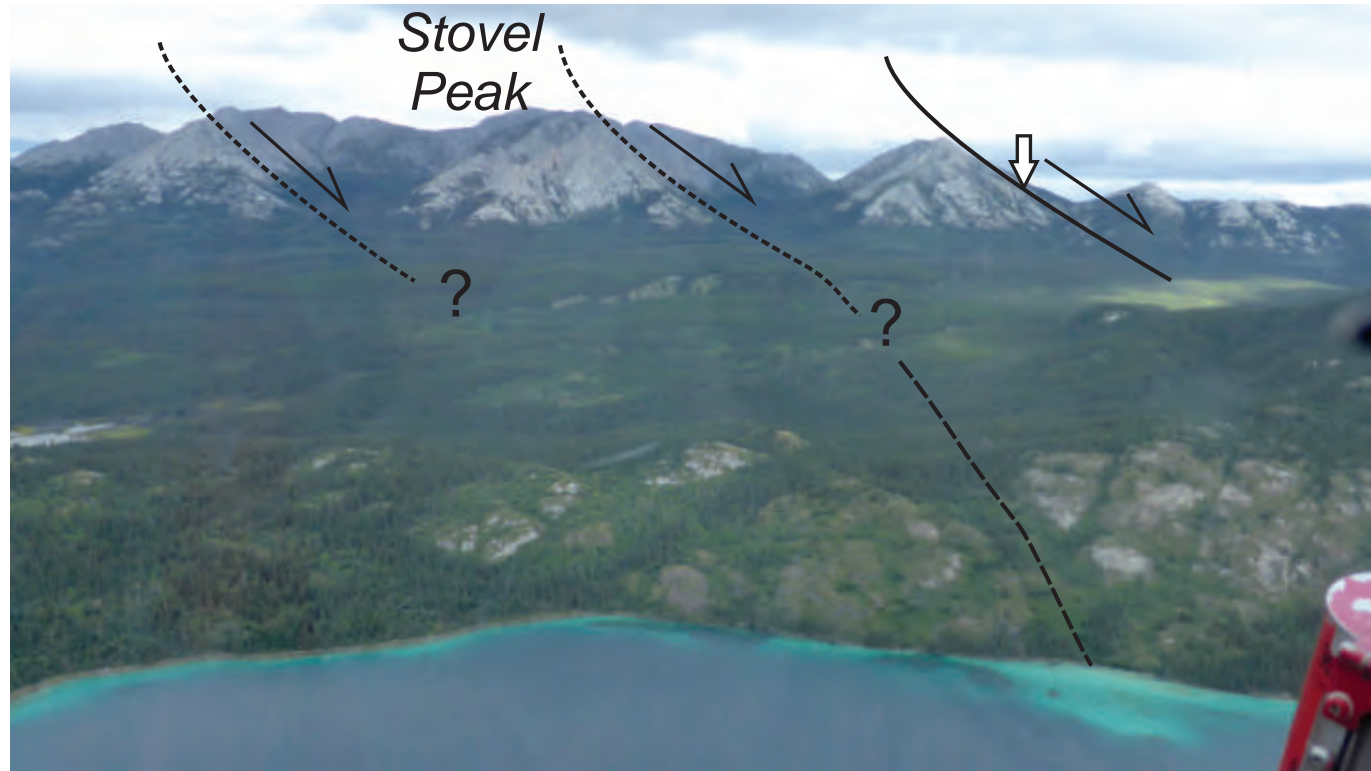


Fig. 13. A view from above northern Turtle Lake toward the northeast, of Stovel Peak and ridges to the south. Inferred south-side-down extensional faults repeat thick Horsefeed Formation limestone. During our mapping, traverses crossed only the southern inferred structure, but there we observed a dip-slope fault (approximate location indicated by white arrow, see also Figs. 11d and 12a). One of the faults is interpreted to track westward to offset limestone near Turtle Lake (see Fig. 2).

Table 1. Results from samples collected for conodont extraction and identification (see Fig. 2 for locations).

Curation Number	Field Number	UTM E	UTM N	Microfossil Content	Locality	Formation	Conodont Fauna	New Age
V-003694	16-ZE-MG-MS-1	549273	6636880	conodont	Mount Stovel	Horsefeed Fm.	<i>Idiognathoides</i> cf. <i>corrugata</i> (Harris and Hollingsworth, 1933); <i>Idiognathoides</i> sp.; <i>Neognathodus</i> cf. <i>symmetricus</i> (Lane, 1967)	Bashkirian
V-003695	16-ZE-MG-MS-2	549438	6636661	conodont	Mount Stovel	Horsefeed Fm.	<i>Gondolella</i> sp.	Moscovian-Gzhelian
V-003696	16-ZE-MG-MS-3	549375	6634857	barren	Mount Stovel	Horsefeed Fm.	None	Indeterminate
V-003716	16-ZE-MG-CLO-1	547505	6649965	barren	Mount Cloutier	Horsefeed Fm.	None	Indeterminate
V-003717	16-ZE-MG-CLO-2	548126	6649166	barren	Mount Cloutier	Horsefeed Fm.	None	Indeterminate
V-003718	16-ZE-MG-CLO-3	548213	6648754	barren	Mount Cloutier	Horsefeed Fm.	None	Indeterminate
V-003719	16-ZE-MG-CLO-4	548213	6648754	barren	Mount Cloutier	Nakina Fm.	None	Indeterminate
V-003720	16-ZE-MG-PM-1	540846	6640452	conodont	Peninsula Mtn.	Horsefeed Fm.	<i>Mesogondolella idahoensis</i> (Youngquist et al., 1951); <i>Streptognathodus</i> sp.	Kungurian

ablation-inductively coupled plasma mass spectrometry (LA-ICPMS) for U-Th-Pb isotope contents (see Friedman et al., 2016 for techniques). Two samples were analyzed by Sensitive High Resolution Ion MicroProbe (SHRIMP) at the Geological Survey of Canada in Ottawa, Ontario, and the procedures used were those reported in Mihalynuk et al. (2017; with analytical and calibration details in Stern, 1997; Stern and Amelin, 2003). $^{40}\text{Ar}/^{39}\text{Ar}$ age determinations were carried out at the University of Manitoba Geochronology Laboratory in Winnipeg, Manitoba; methods are described below.

6.2.1. $^{40}\text{Ar}/^{39}\text{Ar}$ methods

Samples containing the freshest hornblende and biotite were broken in to pea-sized pieces using a hydraulic splitter and the pieces were pulverized in a hardened steel piston and sleeve apparatus. Single crystals were handpicked before irradiation. Standards and unknowns were placed in 2 mm deep wells in 18 mm diameter aluminium disks for irradiation in the cadmium-lined, in-core CLICIT facility of the Oregon State University TRIGA reactor. Standards were placed strategically so that the lateral neutron flux gradients across the disk could be evaluated. Irradiation duration was 10 hours. Standards used were Fish Canyon sanidine (28.2 Ma; Kuiper et al., 2008) and GA1550 biotite (98.5 Ma; Spell and McDougall, 2003). Planar

regressions were fit to the standard data, and the $^{40}\text{Ar}/^{39}\text{Ar}$ neutron fluence parameter, J, interpolated for the unknowns. Uncertainties in J are estimated at 0.1-0.2% (1s), based on Monte Carlo error analysis of the planar regressions (Best et al., 1995).

All $^{40}\text{Ar}/^{39}\text{Ar}$ analytical work was performed using a Thermo Fisher Scientific ARGUSVI multi-collector mass spectrometer, linked to a stainless steel Thermo Fisher Scientific extraction/purification line and Photon Machines (55 W) Fusions 10.6 CO₂ laser. Argon isotopes (from mass 40 to 37) were measured using Faraday detectors with low noise $1 \times 10^{12} \Omega$ resistors and mass 36 was measured using a compact discrete dynode (CDD) detector. Irradiated samples were placed in a Cu sample tray, with a K-Br cover slip, in the extraction line under high vacuum and baked with an infrared lamp for 24 hours. Biotite analyses were performed on single crystals whereas hornblende analyses were performed on aliquots consisting of 3 crystals that were either fused or step-heated using the laser, and reactive gases were removed, after ~3 minutes, by three NP-10 SAES getters (two at room temperature and one at 450°C) before being admitted to an ARGUSVI mass spectrometer by expansion. Five argon isotopes were measured simultaneously during a period of 6 minutes. Measured isotope abundances were corrected for extraction-line blanks, which were determined

before every sample analysis. Line blanks averaged ~ 3.05 fA for mass 40 and ~ 0.01 fA for mass 36. The sensitivity for argon measurements is $\sim 6.312 \times 10^{17}$ moles/fA as determined from measured aliquots of Fish Canyon Sanidine (Dazé et al., 2003; Kuiper et al., 2008).

Mass discrimination was monitored by online analysis of air pipettes and gave a mean of $D=1.0035 \pm 0.0014$ per amu, based on 39 aliquots interspersed with the unknowns. A value of 295.5 was used for the atmospheric $^{40}\text{Ar}/^{36}\text{Ar}$ ratio (Steiger and Jäger, 1977) for the purposes of routine measurement of mass spectrometer discrimination using air aliquots, and correction for atmospheric argon in the $^{40}\text{Ar}/^{39}\text{Ar}$ age calculation. Corrections were made for neutron-induced ^{40}Ar from potassium, ^{39}Ar and ^{36}Ar from calcium, and ^{36}Ar from chlorine (Roddick, 1983; Renne et al., 1998; Renne and Norman, 2001). Data collection was performed using Pylon (Ross, 2017) and data reduction, error propagation, age calculation and plotting were performed using MassSpec software (version 8.091). The decay constants used were those recommended by Steiger and Jäger (1977).

6.3. Isotope geochronology results

Below we summarize the results of our geochronologic studies. A comprehensive set of isotopic data tables and photomicrographs is presented elsewhere (Mihalynuk et al., 2018).

6.3.1. CA-TIMS

The three samples analyzed by the CA-TIMS method were collected from: 1) a granitic dike that cuts the deformed chert-argillite section along the eastern shore of Tagish Lake; 2) a rhyolite tuff along the southern shore of Tutshi Lake; and 3) a weakly altered quartz diorite that underlies Sunday Peak. Locations are plotted on Figure 2 and UTM coordinates are provided along with isotope data in Table 2.

6.3.1.1. Granitic dike, Tagish Lake; MMI16-6-2

On the east shore of Tagish Lake, at a latitude of 60.003°N , a northwest-trending, orange-weathering, felsic, altered, medium- to coarse-grained feldspar porphyritic, ~ 40 cm thick dike cuts a strongly folded, cleaved and faulted section of chert and graphitic argillaceous strata (Fig. 14a) to form rounded phacoids within a strongly sheared argillaceous matrix. Only brittle fractures with millimetres of offset affect the dike, which was collected to constrain the minimum age of deformation, as well as the crystallization age of the unusual dike lithology.

Analyses from four grains (Table 2) overlap concordia at 145.75 ± 0.11 Ma (Fig. 14c), and this precise date is considered the crystallization age of the dike.

6.3.1.2. Windy Table suite, rhyolite tuff, Tutshi Lake; MTS16-1-4c

A white and rust-weathering rhyolite lapilli tuff (Fig. 8a) on the south shore of eastern Tutshi Lake is interpreted as the lowest volcanic unit of the Windy Table suite exposed in that

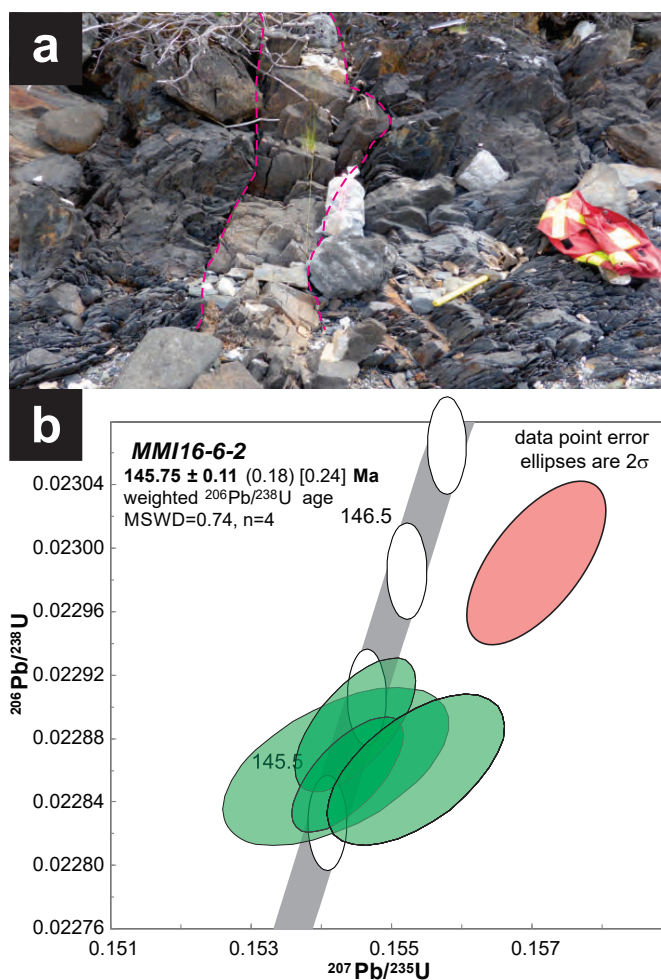


Fig. 14. a) Dike cuts almost orthogonal to strong cleavage and foliation in chert-argillite section (dike contacts are approximately outlined by fuchsia dashed lines). b) Concordia diagram showing cluster of 4 concordant grains at 145.75 ± 0.11 Ma.

part of the map area (Fig. 2). We collected about 40 kg of fresh material from which zircons were separated. Five zircons were analyzed (Table 2). Analytical results from the grains fall into two populations, with concordant U-Pb isotopic ratios and mutually overlapping error 2s ellipses. Two grains are between 80.8 and 81 Ma, and three grains are at 80.63 ± 0.07 Ma (Fig. 15), which we interpret as the crystallization age of the unit. The older population likely represents precursor magmatic products cannibalized during migration and eruption of the rhyolite magma.

6.3.1.3. Sunday Peak stock quartz diorite; MMI16-18-1

The Sunday Peak pluton is one of a suite of zoned granodioritic to dioritic intrusions that cut the Whitehorse trough. On the basis of lithologic similarity and sparse K-Ar geochronology (e.g., Bultman, 1979, recalculated in Breitsprecher and Mortensen, 2004), these intrusions have formerly been considered mainly Late Cretaceous (Mihalynuk et al., 1996, 1999). At Sunday Peak, a ~ 0.6 km² stock cuts and thermally metamorphoses

Table 2. U-Pb zircon TIMS analytical results and computed ages for samples MMI16-6-2 (UTM 546011E, 6649818N), MTS16-1-4c (UTM 534680E, 6644710N), and MMI16-18-1 (UTM 550280E, 6624344N).

Sample (a)	Compositional Parameters											Radiogenic Isotope Ratios						Isotopic Ages										
	Wt.	U	Pb	Th	$^{206}\text{Pb}^*$	mol %	Pb^*	Pb_c	$\frac{^{206}\text{Pb}}{^{204}\text{Pb}}$	$\frac{^{208}\text{Pb}}{^{206}\text{Pb}}$	$\frac{^{207}\text{Pb}}{^{206}\text{Pb}}$	$\frac{^{207}\text{Pb}}{^{235}\text{U}}$	$\frac{^{206}\text{Pb}}{^{238}\text{U}}$	corr.	$\frac{^{207}\text{Pb}}{^{206}\text{Pb}}$	$\frac{^{207}\text{Pb}}{^{235}\text{U}}$	$\frac{^{206}\text{Pb}}{^{238}\text{U}}$	$\frac{^{207}\text{Pb}}{^{235}\text{U}}$	$\frac{^{206}\text{Pb}}{^{238}\text{U}}$									
	mg	ppm	ppm	U	$\times 10^{-13}$	mol	$^{206}\text{Pb}^*$	Pb_c	(pg)	Pb_c	(e)	(e)	(g)	% err	(h)	(g)	% err	(h)	(g)	% err	(h)	(i)	(h)	(i)	(h)	(i)	(h)	(i)
MMI-16-6-2																												
A	0.0021	388	9.0	0.260	0.7608	98.87%	25	0.71	1639	0.083	0.048912	0.770	0.154486	0.852	0.022863	0.178	0.546	143.60	18.05	145.60	116	145.72	0.26					
B	0.004	682	15.6	0.250	0.9320	99.12%	32	0.68	2093	0.080	0.048946	0.373	0.154472	0.454	0.022889	0.151	0.654	145.23	8.76	145.85	0.62	145.89	0.22					
C	0.0028	369	8.4	0.237	0.9689	99.27%	38	0.59	2528	0.076	0.048978	0.345	0.154362	0.449	0.022858	0.129	0.680	146.80	8.08	145.76	0.57	145.69	0.19					
D	0.008	587	13.6	0.224	0.9862	98.58%	19	1.17	1300	0.072	0.049279	0.580	0.155332	0.662	0.022861	0.171	0.581	161.14	13.56	146.61	0.90	145.71	0.25					
E	0.0012	537	12.4	0.224	0.6232	98.86%	24	0.59	1629	0.072	0.049542	0.426	0.157050	0.517	0.022991	0.185	0.627	173.56	9.93	148.12	0.71	146.53	0.27					
MMI-16-1-4c																												
A	0.0021	504	7.2	0.455	0.5428	96.86%	9	1.45	589	0.147	0.048005	2.186	0.083223	2.332	0.012573	0.191	0.781	99.53	51.69	81.17	182	80.55	0.15					
B	0.0066	260	3.4	0.319	0.8981	98.29%	17	1.29	1080	0.103	0.047942	0.719	0.083615	0.795	0.012649	0.135	0.620	96.39	17.01	81.54	0.62	81.03	0.11					
C	0.0073	563	7.2	0.274	2.1440	98.98%	28	1.82	1811	0.088	0.047508	0.412	0.082416	0.488	0.012582	0.144	0.638	74.85	9.78	80.41	0.38	80.60	0.12					
D	0.0028	104	14.1	0.285	1.5949	99.03%	29	1.28	1914	0.091	0.047607	0.374	0.082671	0.449	0.012595	0.134	0.667	79.77	8.87	80.65	0.35	80.68	0.11					
E	0.0044	228	3.2	0.398	0.5298	97.60%	12	1.07	770	0.128	0.047829	0.931	0.083522	10.16	0.012665	0.140	0.646	90.84	22.05	81.45	0.79	81.13	0.11					
MMI-16-18-1																												
A	0.0064	480	4.4	0.470	1.1113	99.04%	31	0.89	1923	0.151	0.04781	0.415	0.056325	0.494	0.008658	0.152	0.627	58.38	9.90	55.64	0.27	55.57	0.08					
B	0.0048	602	5.5	0.486	1.0480	99.18%	37	0.71	2256	0.156	0.04708	0.358	0.056322	0.432	0.008671	0.131	0.670	54.72	8.53	55.64	0.23	55.66	0.07					
D	0.0104	173	17	0.358	0.6485	97.02%	9	1.64	620	0.115	0.04719	1.177	0.056331	1.274	0.008667	0.166	0.629	56.28	28.05	55.64	0.69	55.63	0.09					
E	0.0041	704	6.4	0.388	1.0481	98.64%	21	1.19	1363	0.124	0.046837	0.756	0.055892	0.834	0.008655	0.161	0.562	40.91	18.07	55.22	0.45	55.55	0.09					

(a) A, B etc. are labels for fractions composed of single zircon grains or fragments; all fractions annealed and chemically abraded after Mattinson (2005) and Scoates and Friedman (2008).

(b) Nominal fraction weights estimated from photomicrographic grain dimensions, adjusted for partial dissolution during chemical abrasion.

(c) Nominal U and total Pb concentrations subject to uncertainty in photomicrographic estimation of weight and partial dissolution during chemical abrasion.

(d) Model Th/U ratio calculated from radiogenic $^{206}\text{Pb}/^{206}\text{Pb}$ ratio and $^{207}\text{Pb}/^{235}\text{U}$ age.

(e) Pb^* and Pbc represent radiogenic and common Pb, respectively; mol % $^{206}\text{Pb}^*$ with respect to radiogenic, blank and initial common Pb.

(f) Measured ratio corrected for spike and fractionation only. Mass discrimination of $0.30 \pm 0.05\%$ amu based on analysis of NBS-982; all Daly analyses.

(g) Corrected for fractionation, spike, and all common Pb was assumed to be procedural blank. $^{206}\text{Pb}/^{204}\text{Pb} = 18.50 \pm 1.0\%$; $^{207}\text{Pb}/^{204}\text{Pb} = 15.50 \pm 1.0\%$; $^{208}\text{Pb}/^{204}\text{Pb} = 38.40 \pm 1.0\%$ (all uncertainties 1σ).

(h) Errors are 2σ , propagated using the algorithms of Schmitz and Schoene (2007) and Crowley et al. (2007).

(i) Calculations are based on the decay constants of Jaffey et al. (1971). $^{206}\text{Pb}/^{238}\text{U}$ and $^{207}\text{Pb}/^{235}\text{U}$ ages corrected for initial disequilibrium in $^{230}\text{Th}/^{238}\text{U}$ using Th/U [magma] = 3.

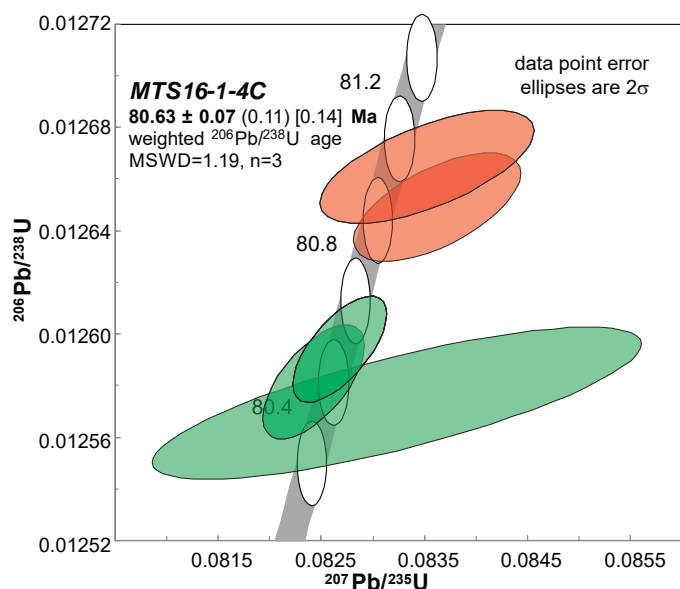


Fig. 15. Concordia plot showing cluster of three grains overlapping concordia at 80.63 ± 0.07 Ma.

rocks on both sides of a terrane-bounding fault: harzburgite of the Cache Creek terrane and wacke of Whitehorse trough (as well as overlapping Windy-Table suite felsic volcanic conglomerate). Thus, an age determination from the stock constrains the latest phase of major fault motion as well as the age of the conglomerate. Four zircons were analyzed (Table 2). All have concordant U-Pb isotopic ratios with mutually overlapping error 2s ellipses (Fig. 16), producing a precise age of 55.61 ± 0.04 Ma.

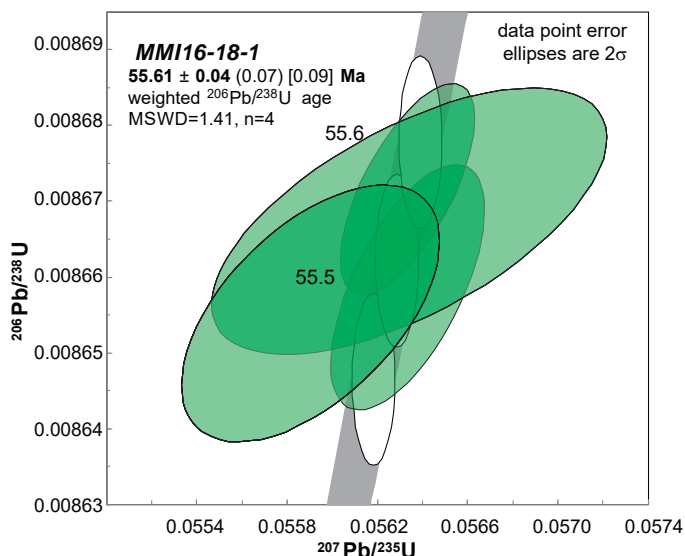


Fig. 16. Concordia diagram for sample MMI16-18-1 of Sunday peak quartz diorite (rock sampled is shown in Fig. 10a). Analyses plot as a 4-grain cluster that overlaps concordia at 55.61 ± 0.04 Ma.

6.3.2. Detrital zircon SHRIMP

Two samples were collected for analysis by the SHRIMP method: one from a volcanic conglomerate on Sunday Peak, and the other from the maroon sandstone matrix of a breccia consisting of Horsefeed Formation limestone blocks. Locations are plotted on Figure 2 and UTM coordinates are provided along with the data for age determinations in Table 3.

6.3.2.1. Horsefeed Formation hematitic breccia matrix; sample DMI16-5-1A

We collected samples of the laminated hematitic calcarenite matrix to breccias in the Horsefeed Formation from exposures along the eastern shoreline of Tagish Lake and from a low ridge south of Stovel Peak. Petrographic work showed that the ridge sample contains only rare quartz grains, so the lakeshore sample, with more abundant quartz grains, was analyzed with the expectation that detrital zircon contents would be proportional to the abundance of quartz grains.

Of the zircon grains recovered from the lakeshore sample, 124 grains were selected and mounted for analysis. Most of these grains are clear and pale brown, and are euhedral well-faceted equant, stubby, and elongate prisms. About 10% of the grains have rounded grain boundaries. Clear bubble- and rod-shaped inclusions, and brown bubble-shaped inclusions are relatively common. In SEM-cathodoluminescence (CL) images, most grains exhibit distinct oscillatory zoning, and lesser sector zoning (Fig. 17a). CL response from the grains varies from very dark (relatively high U content) to bright (relatively low U content). Cores are visible in ~10% of the grains. Of the zircon grains analyzed, the youngest population is 111 Ma (Table 3; $n=19$, MSWD=1.3, POF=0.17, and the youngest grain 107 Ma (Fig. 17b). This age is nearly 150 m.y. younger than the youngest known age limit of the Horsefeed Formation, based on Late Permian fossils south of the mouth of Talaha Bay (Monger, 1975). We interpret the hematitic breccia as Cretaceous karst infill representing a period exposure.

6.3.2.2. Windy-Table suite, felsic volcanic conglomerate and breccia at Sunday Peak; sample MMI16-16-9

Conglomeratic, reworked felsic volcanic breccia (Fig. 18a) occurs east of Sunday Peak between Laberge Group sedimentary rocks to the west and harzburgite mantle tectonite to the east (Fig. 2). An unconformable contact with the harzburgite was established on the basis of serpentinite clasts in the conglomerate and dikelets of volcanic breccia in the harzburgite (Fig. 7a inset). However, contact relations between the volcanic conglomerate and breccia and the adjacent rocks of the Laberge Group are masked by deformation and subsequent thermal alteration by the Sunday Peak intrusion (Fig. 7d). Consequently, it was unclear if the volcanic conglomerate was an intraclast-bearing layer within the Laberge Group that had lapped against harzburgite exposed in the Early to Middle Jurassic. If part of the Laberge Group, then stratigraphic and structural continuity since Middle Jurassic could be established (with strong post-deformational shearing along

Table 3. U-Pb zircon SHRIMP analytical results and computed ages for samples MMI16-18-5 (UTM 550621E, 6623917N) and DMI16-5-1 (UTM 546012E, 6649818N).

Spot name	U (ppm)	Th (ppm)	Th/U	²⁰⁶ Pb* (ppm)	²⁰⁴ Pb/ ²⁰⁶ Pb	f(206) ²⁰⁴ % ±	²⁰⁸ Pb/ ²⁰⁶ Pb	²³⁸ U/ ²⁰⁶ Pb % ±	²⁰⁷ Pb/ ²⁰⁶ Pb % ±	²⁰⁷ Pb/ ²³⁵ U % ±	²⁰⁶ Pb/ ²³⁸ U % ±	Corr Coeff	²⁰⁷ Pb/ ²⁰⁶ Pb % ±	²⁰⁶ Pb/ ²³⁸ U % ±	²⁰⁶ Pb ± ²³⁸ U							
DMI16-5-1A; Lab#11838; Turtle Lake Sandstone; UTM 546012E, 6649818N																						
11838-119.1	265	68	0.27	3.8	1.3E-3	41	2.22	0.039	63.3	59.1	1.5	0.0542	5.4	0.080	24.4	0.0166	1.8	0.072	0.0351	24.3	107	2
11838-096.1	552	350	0.65	8.0	6.8E-4	41	1.18	0.197	9.7	58.7	1.7	0.0562	3.9	0.107	10.3	0.0168	1.8	0.174	0.0462	10.2	108	2
11838-094.1	224	139	0.64	3.3	5.1E-4	71	0.88	0.192	14.3	58.3	2.5	0.0566	6.4	0.115	13.4	0.0170	2.5	0.189	0.0492	13.1	109	3
11838-103.1	258	120	0.48	3.8	2.4E-4	100	0.41	0.158	15.1	58.3	2.1	0.0541	5.8	0.119	9.5	0.0171	2.1	0.221	0.0507	9.2	109	2
11838-089.1	585	393	0.69	8.6	2.3E-4	71	0.41	0.194	18.4	58.2	1.6	0.0516	4.2	0.114	7.0	0.0171	1.7	0.238	0.0482	6.8	109	2
11838-079.1	356	263	0.76	5.1	7.6E-4	50	1.32	0.198	12.8	58.6	1.8	0.0453	9.6	0.079	21.5	0.0168	1.9	0.091	0.0339	21.4	109	2
11838-124.1	1061	927	0.90	15.5	4.6E-4	35	0.80	0.276	5.2	58.3	1.5	0.0479	7.5	0.097	10.7	0.0170	1.6	0.147	0.0411	10.6	110	2
11838-121.1	311	243	0.81	4.5	1.1E-3	41	1.94	0.263	11.3	57.8	2.3	0.0528	5.1	0.084	20.8	0.0170	2.5	0.118	0.0361	20.7	110	3
11838-123.1	279	298	1.10	4.2	-3.9E-4	71	-0.68	0.370	7.8	57.6	1.8	0.0494	5.5	0.133	9.0	0.0175	1.9	0.211	0.0551	8.8	111	2
11838-110.1	196	168	0.89	2.9	8.4E-4	58	1.45	0.272	13.2	57.2	2.3	0.0527	6.3	0.096	20.0	0.0172	2.5	0.123	0.0403	19.8	111	3
11838-076.1	513	209	0.42	7.7	5.6E-4	50	0.97	0.126	14.3	57.0	1.5	0.0481	9.5	0.095	15.7	0.0174	1.5	0.098	0.0398	15.6	112	2
11838-107.1	674	394	0.60	10.1	3.1E-4	50	0.54	0.173	8.0	56.8	1.6	0.0480	3.4	0.105	6.7	0.0175	1.6	0.242	0.0434	6.5	112	2
11838-112.1	300	244	0.84	4.5	1.8E-4	100	0.31	0.213	19.0	56.4	2.2	0.0535	5.0	0.124	7.7	0.0177	2.2	0.282	0.0508	7.4	113	2
11838-080.1	460	341	0.77	6.9	4.4E-4	58	0.76	0.236	9.2	56.5	2.2	0.0529	4.6	0.113	9.9	0.0176	2.3	0.228	0.0465	9.7	113	2
11838-097.1	144	93	0.67	2.2	1.2E-3	58	2.14	0.204	20.7	54.8	2.5	0.0605	11.9	0.104	30.9	0.0179	2.8	0.090	0.0423	30.8	115	3
11838-084.1	170	101	0.62	2.6	1.5E-3	58	2.52	0.174	27.2	54.2	3.2	0.0697	7.7	0.120	28.8	0.0180	3.5	0.122	0.0483	28.6	115	4
11838-074.1	347	277	0.82	5.3	8.1E-4	45	1.41	0.287	15.6	55.1	1.5	0.0547	8.1	0.105	16.7	0.0179	1.6	0.096	0.0427	16.6	115	2
11838-104.1	1604	1556	1.00	28.1	5.9E-5	71	0.10	0.314	3.3	49.0	1.8	0.0497	2.1	0.137	3.1	0.0204	1.8	0.594	0.0488	2.5	130	2
11838-120.1	155	74	0.49	3.6	1.6E-3	38	2.77	0.105	28.8	36.1	2.2	0.0518	5.7	0.103	35.4	0.0269	2.4	0.068	0.0278	35.3	176	4
11838-100.1	245	109	0.46	6.3	-1.7E-4	100	-0.30	0.123	13.3	33.7	1.9	0.0555	4.8	0.238	6.6	0.0297	1.9	0.285	0.0580	6.3	187	3
11838-116.1	468	249	0.55	11.9	4.0E-4	45	0.69	0.160	9.1	33.7	1.9	0.0510	3.7	0.183	7.4	0.0295	2.0	0.265	0.0452	7.2	188	4
11838-092.1	263	133	0.52	7.2	1.1E-4	100	0.19	0.167	9.2	31.1	1.5	0.0542	4.0	0.233	5.4	0.0321	1.5	0.280	0.0526	5.2	203	3
11838-122.1	171	79	0.48	4.7	-1.9E-4	100	-0.33	0.153	12.4	31.2	1.9	0.0504	5.3	0.235	7.4	0.0321	2.0	0.263	0.0531	7.2	203	4
11838-085.1	1254	651	0.54	35.3	1.3E-4	45	0.22	0.161	4.4	30.4	1.5	0.0511	1.9	0.223	3.0	0.0328	1.5	0.490	0.0492	2.6	208	3
11838-088.1	233	72	0.32	6.6	1.1E-3	33	1.98	0.057	33.2	29.7	1.5	0.0506	4.8	0.153	18.9	0.0330	1.7	0.089	0.0335	18.8	214	3
11838-114.1	291	92	0.33	8.6	1.9E-4	71	0.32	0.088	12.3	28.9	1.8	0.0536	3.6	0.241	5.7	0.0344	1.8	0.319	0.0508	5.4	218	4
11838-083.1	394	126	0.33	11.8	5.2E-4	41	0.90	0.093	13.9	28.5	3.7	0.0516	7.1	0.211	11.7	0.0348	3.8	0.322	0.0439	11.1	222	8

Mount IP832, K100a spot size (13x16µm), 2.5 minute raster, 6 mass scans. Primary beam intensity ~3.0 nA

Spot name follows the convention x-y.z; where x = lab number, y = grain number and z = spot number

Uncertainties reported at 1σ and are calculated by using SQUID 2.50.11.10.15, rev. 15 Oct 2011

F(206)²⁰⁴ refers to mole percent of total ²⁰⁶Pb that is due to common Pb, calculated using the ²⁰⁶Pb-method; common Pb composition used is the surface blank (4/6: 0.05770; 7/6: 0.89500; 8/6: 2.13840)

* refers to radiogenic Pb (corrected for common Pb)

Error in ²⁰⁶Pb/²³⁸U calibration 1.35% (included). Standard Error in Standard calibration was 0.38% (not included in above errors but required when comparing data from different mounts).

Apparent ages shown in bold font are those which were used in the weighted mean age calculations

For sample DMI16-5-1A, analyses not included in the age calculation were those which exceeded 3.0% common Pb, or were from older populations

For sample MMI16-16-9, many analyses contained high common Pb, but the 3 youngest analyses clearly represent a young generation of growth and are therefore not disregarded on the basis of high common Pb

below detection limit analyses and those with relatively high common Pb excluded. Only data for apparent ages less than 220 Ma are shown, see Mihalynuk et al., 2018 for full listing of analytical data

Table 3. Continued.

MMI16-16-9; Lab#11839; Sunday Peak Conglomerate; UTM 550621E, 6623917N																			
11839-075.1	1327	687	0.54	14.9	0.195	5.7	76.6	1.5	0.0484	2.9	0.087	3.3	0.0131	1.5	0.446	0.0484	2.9	83.5	1.2
11839-097.1	2513	1198	0.49	29.0	0.157	4.8	74.3	1.4	0.0497	2.2	0.091	2.8	0.0134	1.4	0.492	0.0492	2.4	85.9	1.2
11839-081.1	1770	699	0.41	20.5	0.129	7.4	73.9	1.5	0.0495	6.0	0.083	8.0	0.0135	1.5	0.193	0.0447	7.8	86.5	1.4
11839-077.1	151	56	0.39	3.9	0.097	30.0	32.5	2.3	0.0587	5.2	0.150	25.7	0.0300	2.5	0.097	0.0362	25.6	194	4
11839-013.1	90	24	0.28	2.5	0.186	19.1	32.1	3.0	0.0591	14.1	0.365	17.3	0.0320	3.3	0.189	0.0826	17.0	195	6
11839-098.1	128	38	0.30	3.4	0.099	22.1	32.1	1.7	0.0586	5.7	0.219	12.1	0.0309	1.8	0.147	0.0514	12.0	196	3
11839-039.1	91	31	0.35	2.4	0.063	66.1	31.6	3.1	0.0687	10.6	0.152	43.8	0.0304	3.5	0.079	0.0361	43.7	196	6
11839-033.1	101	32	0.33	2.7	0.133	25.2	31.9	4.0	0.0602	11.6	0.189	26.4	0.0308	4.2	0.157	0.0446	26.0	197	8
11839-032.1	146	39	0.28	3.8	0.043	65.7	31.9	1.9	0.0555	5.5	0.125	33.8	0.0304	2.2	0.065	0.0297	33.8	198	4
11839-073.1	451	147	0.34	12.0	0.095	12.6	32.0	1.5	0.0524	3.2	0.191	7.7	0.0310	1.5	0.194	0.0447	7.6	198	3
11839-109.1	130	44	0.35	3.5	0.162	15.1	32.2	1.6	0.0477	6.1	0.268	12.1	0.0316	1.8	0.149	0.0615	12.0	198	3
11839-070.1	196	60	0.32	5.3	0.084	22.0	31.6	2.0	0.0568	9.4	0.203	15.7	0.0312	2.1	0.133	0.0470	15.6	199	4
11839-115.1	146	47	0.34	4.0	0.133	17.9	31.6	1.6	0.0566	5.7	0.314	11.0	0.0322	1.8	0.166	0.0708	10.8	199	3
11839-100.1	279	159	0.59	7.5	0.169	9.4	32.0	1.5	0.0478	4.1	0.191	7.1	0.0312	1.5	0.212	0.0445	7.0	199	3
11839-108.1	182	61	0.35	4.9	0.087	15.6	31.6	2.4	0.0538	4.6	0.224	6.9	0.0316	2.4	0.345	0.0515	6.4	200	5
11839-009.1	224	93	0.43	6.1	0.118	14.5	31.4	1.9	0.0561	4.2	0.217	9.0	0.0316	2.0	0.216	0.0498	8.8	201	4
11839-012.1	288	129	0.46	7.8	0.114	15.6	31.2	1.5	0.0575	6.6	0.203	12.9	0.0317	1.6	0.124	0.0466	12.8	202	3
11839-037.1	199	61	0.32	5.5	0.084	20.6	30.9	2.2	0.0568	4.6	0.219	10.3	0.0321	2.2	0.213	0.0495	10.1	204	4
11839-094.1	277	108	0.40	7.5	0.084	19.8	31.3	1.5	0.0462	4.4	0.153	14.2	0.0316	1.6	0.112	0.0352	14.1	204	3
11839-019.1	239	58	0.25	6.6	0.083	17.5	30.8	1.8	0.0528	4.5	0.216	8.1	0.0323	1.8	0.223	0.0486	7.9	205	4
11839-067.1	321	121	0.39	8.9	0.122	13.5	30.5	1.5	0.0582	9.1	0.202	15.4	0.0323	1.6	0.102	0.0453	15.3	206	3
11839-040.1	111	42	0.39	3.0	0.044	91.8	30.0	2.4	0.0619	16.2	0.089	84.9	0.0318	2.9	0.034	0.0204	84.8	209	6
11839-106.1	150	53	0.37	4.3	0.165	13.6	30.1	1.8	0.0491	5.3	0.277	10.0	0.0336	1.9	0.194	0.0597	9.8	211	4
11839-036.1	167	42	0.26	4.7	0.078	27.9	29.8	1.6	0.0546	8.5	0.186	19.1	0.0330	1.7	0.091	0.0410	19.0	212	3
11839-040.2	135	43	0.33	3.9	0.092	25.5	29.7	2.8	0.0541	5.7	0.202	15.5	0.0333	2.9	0.188	0.0439	15.3	213	6
11839-014.1	401	163	0.42	11.6	0.147	9.2	29.4	1.5	0.0574	5.1	0.239	7.9	0.0338	1.5	0.191	0.0514	7.7	214	3
11839-021.1	214	66	0.32	6.2	0.091	17.3	29.2	1.5	0.0581	7.6	0.235	11.9	0.0339	1.6	0.133	0.0502	11.8	215	3
11839-076.1	369	163	0.46	10.8	0.160	8.6	29.3	1.5	0.0574	3.3	0.246	6.0	0.0340	1.5	0.247	0.0526	5.9	215	3
11839-015.1	130	29	0.23	3.7	0.032	80.6	29.2	2.1	0.0586	5.4	0.179	22.9	0.0334	2.3	0.102	0.0389	22.8	215	5
11839-034.1	272	93	0.35	7.9	0.100	15.3	29.3	1.5	0.0528	4.3	0.207	9.9	0.0338	1.6	0.157	0.0446	9.8	215	3
11839-103.1	298	212	0.73	8.7	0.237	7.8	29.4	1.5	0.0503	8.4	0.212	11.4	0.0338	1.5	0.135	0.0454	11.3	216	3
11839-035.1	374	103	0.28	10.9	0.059	21.0	29.2	1.5	0.0543	3.4	0.212	8.7	0.0339	1.5	0.174	0.0454	8.6	216	3
11839-082.1	1110	255	0.24	32.5	0.073	7.5	29.3	1.4	0.0517	1.9	0.230	3.2	0.0341	1.4	0.436	0.0491	2.9	216	3
11839-044.1	120	40	0.34	3.6	0.102	19.8	29.0	1.7	0.0581	13.0	0.258	15.5	0.0344	1.7	0.111	0.0545	15.4	217	4
11839-107.1	343	298	0.90	10.0	0.264	6.9	29.2	1.8	0.0499	6.6	0.201	10.8	0.0339	1.8	0.168	0.0430	10.6	217	4
11839-018.1	302	80	0.28	8.8	0.075	16.6	29.1	1.5	0.0520	6.6	0.217	10.0	0.0341	1.5	0.153	0.0462	9.9	217	3
11839-042.1	375	389	1.07	10.9	0.337	6.4	29.0	1.5	0.0522	3.7	0.175	13.3	0.0339	1.6	0.118	0.0375	13.2	218	3
11839-022.1	452	129	0.30	13.3	0.091	9.3	28.9	1.4	0.0482	3.2	0.223	4.0	0.0343	1.4	0.358	0.0473	3.8	218	3
11839-024.1	263	97	0.38	7.8	0.107	24.8	28.9	2.1	0.0526	4.0	0.234	6.6	0.0344	2.1	0.314	0.0493	6.3	218	4
11839-025.1	281	63	0.23	8.3	0.066	14.8	28.9	1.8	0.0523	7.2	0.242	8.2	0.0345	1.8	0.223	0.0508	8.0	219	4
11839-081.2	421	175	0.43	12.4	0.128	10.4	28.8	1.5	0.0561	3.0	0.221	8.0	0.0343	1.5	0.189	0.0466	7.8	219	3
11839-020.1	313	85	0.28	9.3	0.087	13.9	28.7	1.7	0.0554	6.9	0.238	9.6	0.0346	1.8	0.183	0.0500	9.4	219	4
11839-029.1	306	67	0.22	9.0	0.034	39.6	28.8	1.5	0.0542	3.6	0.195	11.6	0.0342	1.6	0.135	0.0414	11.5	219	3
11839-065.1	133	55	0.43	3.9	0.110	26.8	28.6	1.6	0.0582	8.8	0.177	26.9	0.0341	1.9	0.072	0.0376	26.8	219	4

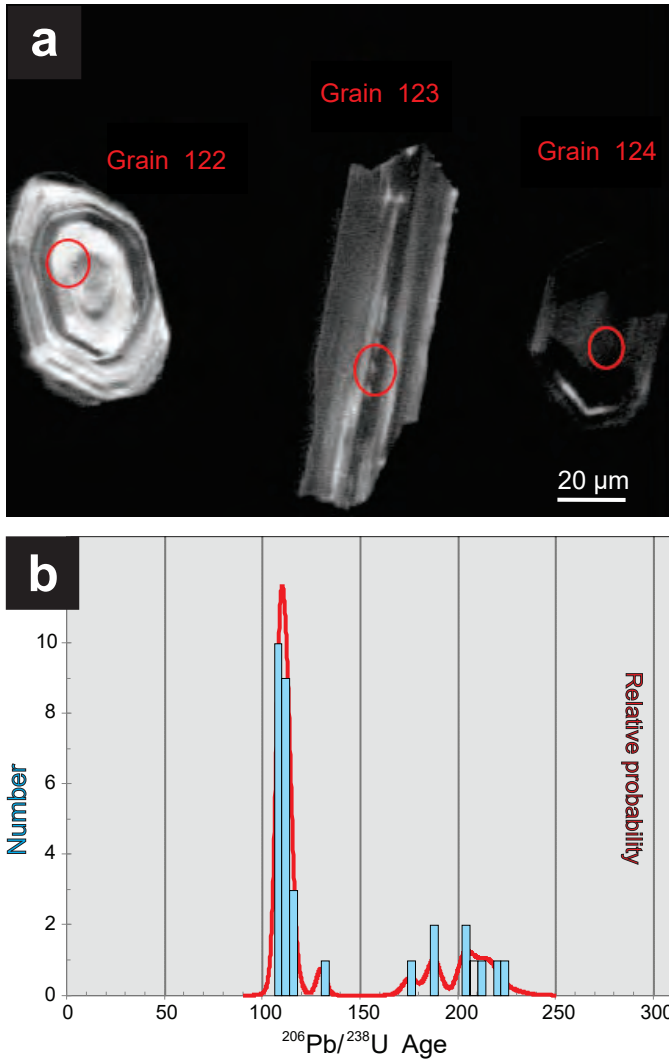


Fig. 17. Laminated maroon calcarenite between blocks of Horsefeed Formation limestone contain Early Cretaceous detrital zircons and are interpreted as karst collapse deposits. **a)** Cathodoluminescence images of representative zircons analyzed by SHRIMP. **b)** Zircon age distribution plot.

the Laberge wacke and Harzburgite-conglomerate contacts resulting in a relative offset that is less than the footprint of the felsic conglomerate unit). A sample ~25 cm in diameter of the stratigraphically lowest conglomerate containing almost entirely felsic volcanic clasts was collected for detrital zircon analysis.

Approximately 120 grains were mounted for analysis, representing a full range of zircon morphologies (a subset is shown in Table 3 and Fig. 18b). Most grains are clear and colourless, equant to stubby prisms with well-preserved facets and minor clear bubble-shaped inclusions. In SEM-CL images (Fig. 18b), most grains exhibit distinct oscillatory zoning. Sector zoning is present in one third of the crystals. Core-like regions are seen in ~10% of the grains. A maximum depositional age is given by three Late Cretaceous grains. The youngest of the three grains is 84 Ma, whereas their combined

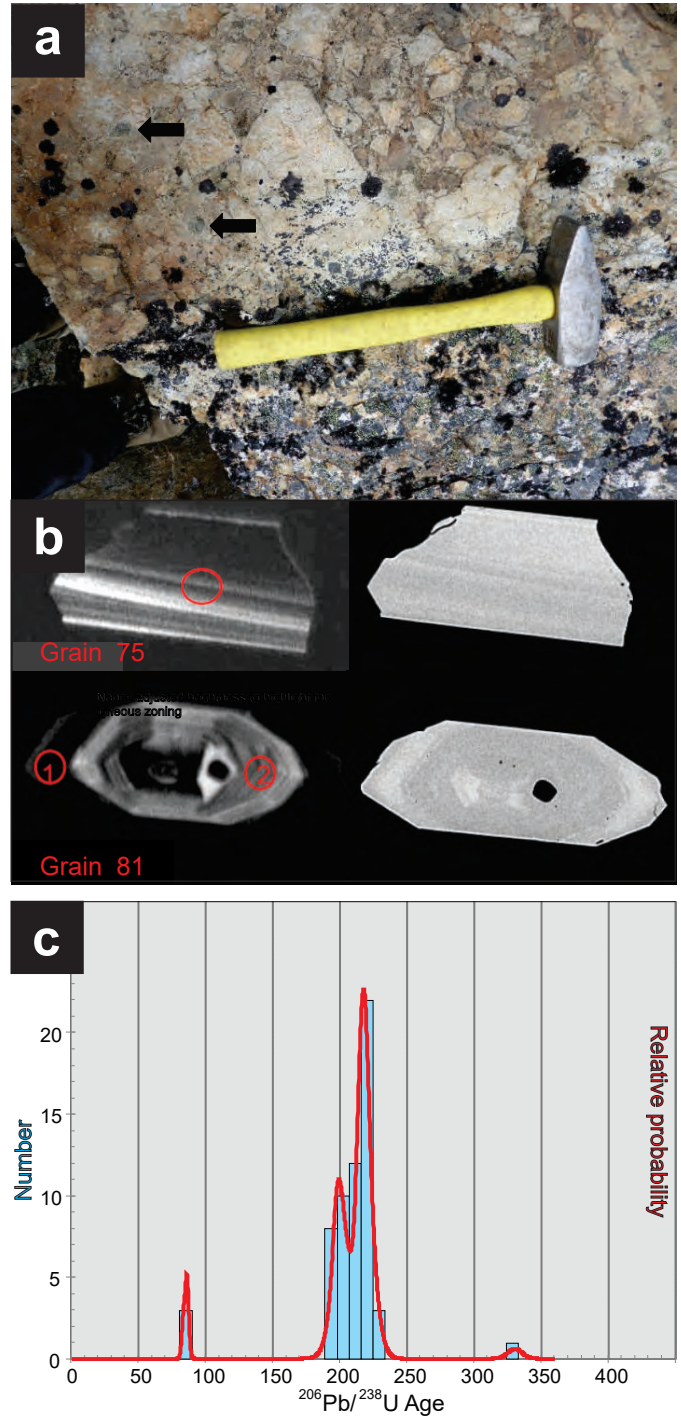


Fig. 18. a) Reworked felsic volcanic breccia at Sunday Peak sampled for age determination. Dark green clasts above the end of the hammer handle may be derived from the adjacent mantle tectonite. A dikelet containing fragments of felsic volcanic rock as well as serpentinized mantle peridotite cuts mantle tectonite is pictured in the inset of Fig. 7a. **b)** Cathodoluminescent and reflected light images of young zircons analyzed by SHRIMP. Grain 81 is especially informative, it has an 86.5 Ma rim (1) and a 216 Ma core (2). **c)** Zircon age distribution plot with a sub-population of 19 zircons that yields an age of 111 ± 1 Ma (see Mihalynuk et al., 2018).

weighted average age is 85 Ma, (Fig. 18c). Grain 81 (Fig. 18b) has a high-U 86.5 Ma rim and a 216 Ma core with lower U content. We interpret the youngest zircons to represent the age of syn-volcanic deposition and correlate the unit with strata of the same age (85.0 ± 1.8 Ma) near the base of the Windy-Table suite, as recently shown by Zagorevski et al. (2017).

6.3.3. Detrital zircon LA-ICPMS

The two samples analyzed by LA-ICPMS were collected from: a tuffaceous conglomerate containing chert and rhyolite fragments above the eastern shore of Turtle Lake (Fig. 2; Table 4), and an intermediate tuff along the eastern shore of Tagish Lake at the base of Peninsula Mountain (Table 5).

6.3.3.1. Horsefeed Formation, tuffaceous limestone breccia east of Turtle Lake; sample MTS16-24-13

Green and grey-weathering tuffaceous limestone breccia underlies the slopes east of northern Turtle Lake. Outcrop compositions range from predominantly volcanic to limestone clast-bearing. A sample was collected from a relatively volcanic-rich protolith that contained both aphanitic green and cream-coloured, lapilli-sized volcanic clasts as well as angular limestone and rare chert (Fig. 19a). Of the zircon grains separated, 39 were suitable for LA-ICPMS analysis (Table 4); all were angular fragments with strong growth-zoning (Figs. 19b, c). The zircon fragments returned an age distribution with a peak at ~ 295 Ma (37 grains, Fig. 19d), and a minor ill-defined sub population at ~ 310 Ma (2 grains). Nearly two of three grains (64%) display overlapping $^{206}\text{Pb}/^{238}\text{U}$ ($2\sigma < 5\%$) and $^{207}\text{Pb}/^{235}\text{U}$ ($2\sigma < 10\%$) ages, and $^{207}\text{Pb}/^{206}\text{Pb}$ ages that are geologically meaningful and concordant within error. Five of these grains cluster at ~ 285 Ma, which we interpret as the best estimate of the maximum depositional age.

6.3.3.2. Windy-Table suite volcanic rocks at Peninsula Mountain; sample MMI16-8-1

Volcaniclastic strata crop out on the west side of Peninsula Mountain and are well exposed along the shore of Tutshi Lake. Contacts with Laberge Group wacke and argillite to the south are not exposed, but to the north, a fault zone containing panels of chert and argillite juxtapose the unit with limestone of the Horsefeed Formation. Age relations are ambiguous, but most previous workers considered the Peninsula Mountain volcanic strata to be Triassic. Reasons to doubt the Triassic age assignment arose during the field program: tuffaceous and conglomeratic sections at Peninsula Mountain are lithologically similar to strata of probable Cretaceous age to the north and south in the Turtle Lake map area, and strata of presumed Triassic age a few km outside the southeast corner of the map area, were found to be Cretaceous and correlated with the Windy-Table suite (Zagorevski et al., 2017). To address the uncertainty about the affiliation of volcanic rocks at Peninsula Mountain, we collected a sample of grey-green feldspar-phyric breccia (Fig. 9b) for LA-ICPMS analysis.

Six usable zircons were recovered and analyzed (Table 5);

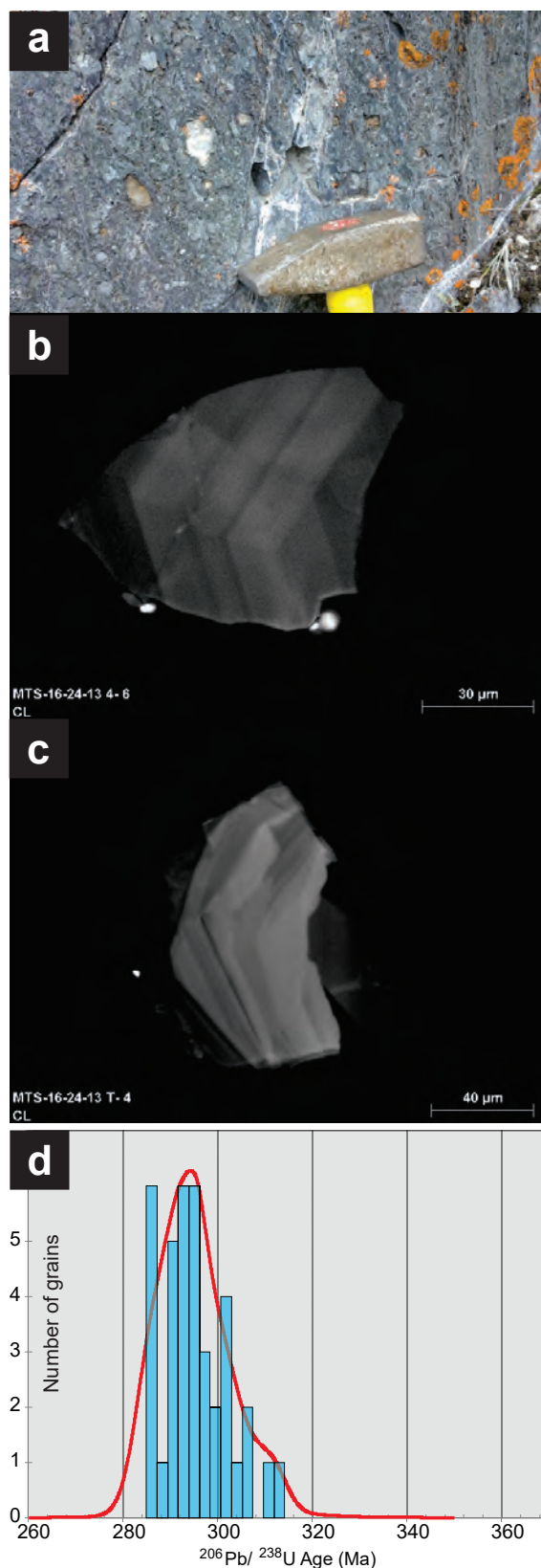


Fig. 19. a) Outcrop of tuffaceous sharpstone conglomerate sampled for age determination. b), c) Cathodoluminescence images of representative, strongly zoned, zircon crystal fragments typical of the unit. d) Zircon age distribution plot shows zircons dated range from Mid Pennsylvanian through Early Permian.

Table 4. U-Pb zircon LA-ICPMS analytical results and computed ages, sample MTS16-24-13 (UTM 543823E, 6635458N).

Sample no.	Isotopic Ratios					Isotopic Ages							
	²⁰⁷ Pb/ ²³⁵ U	2σ (abs)	²⁰⁶ Pb/ ²³⁸ U	2σ (abs)	ρ	²⁰⁷ Pb/ ²⁰⁶ Pb	2σ (abs)	²⁰⁷ Pb/ ²³⁵ U	2σ (Ma)	²⁰⁶ Pb/ ²³⁸ U	2σ (Ma)	²⁰⁷ Pb/ ²⁰⁶ Pb	2σ (Ma)
MTS_16_24_13_1	0.386	0.040	0.0467	0.0015	0.257	0.061	0.006	328	29	294.1	9.4	520	220
MTS_16_24_13_2	0.337	0.043	0.0460	0.0012	0.041	0.054	0.007	291	32	290.1	7.7	250	260
MTS_16_24_13_3	0.345	0.032	0.0465	0.0010	0.067	0.054	0.005	298	24	292.7	5.8	350	210
MTS_16_24_13_4	0.370	0.089	0.0465	0.0029	0.337	0.054	0.012	303	64	293	18	200	420
MTS_16_24_13_5	0.316	0.034	0.0454	0.0010	0.115	0.050	0.005	276	26	286.5	6.3	150	210
MTS_16_24_13_6	0.343	0.024	0.0466	0.0010	0.183	0.053	0.004	298	18	293.7	5.9	300	150
MTS_16_24_13_7	0.333	0.038	0.0462	0.0009	0.159	0.052	0.006	288	29	291.2	5.7	200	240
MTS_16_24_13_8	0.342	0.031	0.0479	0.0016	0.102	0.052	0.005	296	24	301.6	9.7	230	200
MTS_16_24_13_9	0.351	0.029	0.0460	0.0011	0.054	0.055	0.005	303	21	290.1	7	350	170
MTS_16_24_13_10	0.338	0.029	0.0454	0.0011	0.236	0.054	0.005	293	22	286.2	6.5	300	180
MTS_16_24_13_11	0.331	0.030	0.0471	0.0011	0.412	0.051	0.005	288	23	296.6	6.9	200	190
MTS_16_24_13_12	0.345	0.052	0.0484	0.0017	0.109	0.052	0.008	294	39	305	11	160	310
MTS_16_24_13_13	0.330	0.035	0.0479	0.0013	0.167	0.050	0.005	286	27	301.6	7.9	120	210
MTS_16_24_13_14	0.322	0.026	0.0464	0.0015	0.074	0.050	0.004	287	23	292.2	9.5	210	190
MTS_16_24_13_15	0.318	0.036	0.0467	0.0012	0.243	0.049	0.005	277	28	294.4	7.2	90	220
MTS_16_24_13_16	0.290	0.040	0.0479	0.0014	0.104	0.044	0.006	255	31	301.3	8.4	-120	270
MTS_16_24_13_17	0.314	0.018	0.0465	0.0012	0.106	0.048	0.003	276	14	292.9	7.4	100	140
MTS_16_24_13_18	0.333	0.028	0.0452	0.0012	0.327	0.053	0.005	290	21	285.2	7.1	260	190
MTS_16_24_13_19	0.320	0.038	0.0476	0.0012	0.059	0.049	0.006	278	29	300	7.6	120	250
MTS_16_24_13_20	0.331	0.033	0.0481	0.0011	0.025	0.050	0.005	288	25	302.8	6.6	150	210
MTS_16_24_13_21	0.317	0.032	0.0468	0.0014	0.020	0.050	0.005	277	25	295.1	8.7	130	210
MTS_16_24_13_23	0.306	0.031	0.0492	0.0010	0.446	0.046	0.004	268	25	309.5	6.1	-30	190
MTS_16_24_13_24	0.369	0.085	0.0489	0.0039	0.135	0.055	0.013	302	65	307	24	240	490
MTS_16_24_13_25	0.320	0.048	0.0474	0.0017	0.032	0.051	0.008	276	37	299	11	120	310
MTS_16_24_13_26	0.305	0.028	0.0452	0.0010	0.165	0.050	0.005	268	22	285.2	6.1	170	190
MTS_16_24_13_27	0.334	0.027	0.0468	0.0010	0.058	0.053	0.004	291	20	294.5	6	290	170
MTS_16_24_13_28	0.304	0.044	0.0454	0.0012	0.056	0.050	0.007	264	34	286	7.4	100	290
MTS_16_24_13_29	0.307	0.020	0.0460	0.0008	0.150	0.050	0.004	270	16	289.6	5.2	160	160
MTS_16_24_13_30	0.363	0.027	0.0497	0.0009	0.354	0.054	0.004	313	20	312.4	5.5	320	170
MTS_16_24_13_31	0.343	0.062	0.0479	0.0019	0.059	0.051	0.010	290	47	302	11	70	350
MTS_16_24_13_32	0.329	0.048	0.0462	0.0018	0.013	0.050	0.008	283	36	291	11	90	280
MTS_16_24_13_33	0.353	0.033	0.0453	0.0010	0.240	0.054	0.006	304	25	285.4	6.3	290	210
MTS_16_24_13_34	0.369	0.035	0.0473	0.0012	0.239	0.054	0.006	316	26	297.6	7.1	290	210
MTS_16_24_13_35	0.349	0.025	0.0473	0.0010	0.114	0.051	0.004	302	19	298.2	6.2	190	170
MTS_16_24_13_36	0.344	0.045	0.0457	0.0014	0.030	0.052	0.007	295	34	287.8	8.9	170	260
MTS_16_24_13_37	0.347	0.026	0.0470	0.0006	0.164	0.053	0.004	301	19	295.8	3.5	270	160
MTS_16_24_13_38	0.333	0.039	0.0468	0.0011	0.040	0.051	0.006	288	30	294.5	7	180	240
MTS_16_24_13_39	0.346	0.026	0.0463	0.0008	0.031	0.054	0.004	300	20	292	5	310	160

collectively they define an age of 79.7 ± 1.3 Ma (Fig. 20), consistent with Late Cretaceous, not Triassic deposition.

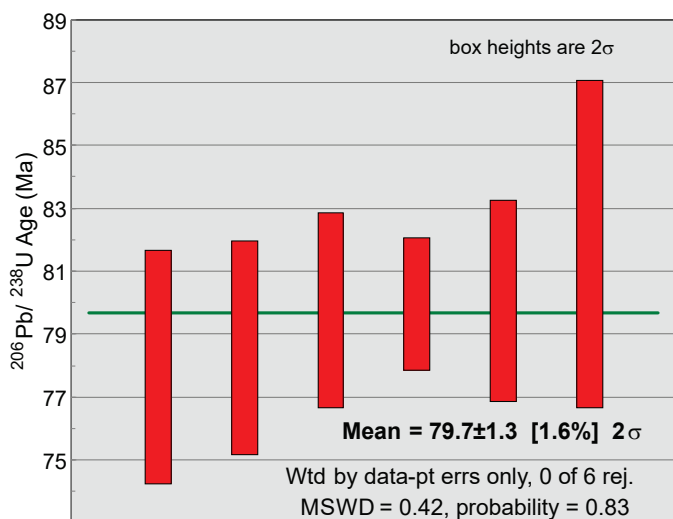


Fig. 20. $^{206}\text{Pb}/^{238}\text{U}$ age determined from regression of ages of six zircons, yields a mean of 79.6 ± 1.3 Ma.

6.3.4. $^{40}\text{Ar}/^{39}\text{Ar}$ results

We collected samples for $^{40}\text{Ar}/^{39}\text{Ar}$ analysis from a late synkinematic phase of the intrusion at Lost Sheep peak and a late quartz diorite phase at Mount Lanning (Fig. 2). We also collected samples from lamprophyre dikes cutting both the intrusion on the northeast flank of Lost Sheep peak, and limestone (part of the swarm above the east shore of Turtle Lake; Fig. 10d). Biotite was separated from all samples. Hornblende from two of these samples was also separated and analyzed to confirm biotite results. For additional quality assurance, duplicate aliquots were run for each mineral and the best behaved release spectrum was selected as the representative cooling age for that sample/mineral. Sample collection locations are plotted on Figure 2 and UTM coordinates are provided in Tables 6, 7 and 8).

6.3.4.1. Synkinematic Lost Sheep peak intrusion; sample MMI16-20-16

The Lost Sheep peak intrusion is a variably foliated, 2.5 km by >9 km, northwest elongated body in the southeast corner of the Turtle Lake map area. It probably averages granodiorite composition, but ranges from gabbro to granitic with mafic phases tending to be the most intensely foliated. Pegmatitic granitic phases are not foliated but comeingle with the variably sheared mafic to intermediate enclaves (Fig. 10c). Fine- to medium-grained hornblende and biotite can comprise more than 30% of the rock and tend to be intimately intergrown, together with titanite (<1% ~4%). We sampled the freshest part of an intermediate, foliated phase of the intrusion, ~400 m from the northeastern contact with the aim of obtaining a post-deformational cooling age.

Separates of both biotite and hornblende were hand-picked. Selected biotite grains yielded a plateau age of 161.61 ± 0.85 Ma,

which considers 100% of ^{39}Ar released (Table 6; Fig. 21). Hornblende separated from this sample returned an age of 166.0 ± 1.1 Ma from 81.7% of ^{39}Ar liberated (see Mihalynuk et al., 2018).

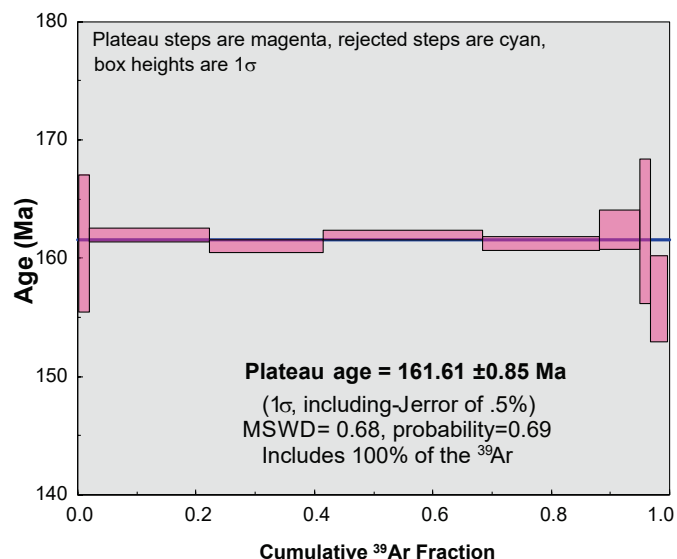


Fig. 21. Synkinematic Lost Sheep peak gabbroic to granitic intrusion biotite step heating spectrum yields a 161.61 ± 0.85 Ma age by considering 100% of ^{39}Ar released.

6.3.4.2. Biotite quartz diorite at Mount Lanning; sample MMI16-29-05

Fresh, unfoliated, medium- to fine-grained, leucocratic, biotite quartz diorite (Fig. 22a) appears to be one of the latest phases of the ~160 km² intrusion that underlies Mount Lanning. It cuts and thermally metamorphoses deformed Laberge Group strata. It is a northwest-trending pluton with an irregular outline, except in the south where it is a southward-tapering, steeply dipping tabular body that terminates near Racine Creek (Fig. 2). It is one of the largest intrusive domains lacking published isotopic age work. A clean separate of vitreous, elastic, black biotite was obtained.

Analysis of two biotite grains yielded statistically identical results of: 56.12 ± 0.29 Ma from 100% of the ^{39}Ar released (Fig. 22b) and 55.99 ± 0.29 Ma from 97.7% of ^{39}Ar released (see Mihalynuk et al., 2018). The fresh mineralogy and field relationships of the quartz diorite at Mount Lanning are consistent with the young, Eocene age.

6.3.4.3. Lamprophyre dikes; samples MMI16-14-9, MTS16-24-23

Lamprophyre dikes have a long-established association with gold mineralization (e.g., Young, 1948; Rock and Groves, 1988), although their role in gold deposit genesis is not without controversy (e.g., Kerrich and Wyman, 1994). In the Atlin gold camp, altered lamprophyre dikes are found with lode gold mineralization at the Yellowjacket deposit, and are intimately associated with precious metal-rich base metal sulphide veins

Table 5. U-Pb zircon LA-ICPMS analytical results and computed ages, sample MMI16-8-1 (UTM 540468N, 6634980N).

Sample no. Analysis ID	CL image	Isotopic Ratios					Isotopic Ages							
		$^{207}\text{Pb}/^{235}\text{U}$ (abs)	$^{206}\text{Pb}/^{238}\text{U}$ (abs)	ρ	$^{207}\text{Pb}/^{206}\text{Pb}$ (abs)	2σ (abs)	$^{207}\text{Pb}/^{235}\text{U}$ (Ma)	$^{206}\text{Pb}/^{238}\text{U}$ (Ma)	2σ (Ma)	$^{207}\text{Pb}/^{206}\text{Pb}$ (Ma)	2σ (Ma)			
MMI_16_8_1_1	MMI 16-8-1 T-3	0.083	0.016	0.0125	0.0005	0.126	0.0461	0.0096	79.0	15.0	80.1	3.2	-150	340
MMI_16_8_1_2	MMI 16-8-1 T-7	0.131	0.028	0.0128	0.0008	0.011	0.0710	0.0160	123.0	25.0	81.9	5.2	610	450
MMI_16_8_1_4	MMI 16-8-1 2-3	0.099	0.011	0.0125	0.0003	0.245	0.0528	0.0054	95.0	10.0	80.0	2.1	220	200
MMI_16_8_1_5	MMI 16-8-1 2-4	0.089	0.016	0.0122	0.0006	0.273	0.0469	0.0077	85.0	15.0	78.0	3.7	0	320
MMI_16_8_1_6	MMI 16-8-1 2-6	0.099	0.017	0.0123	0.0005	0.080	0.0560	0.0100	95.0	16.0	78.6	3.4	300	380
MMI_16_8_1_7	MMI 16-8-1 2-7	0.111	0.018	0.0125	0.0005	0.070	0.0630	0.0100	106.0	16.0	79.8	3.1	460	310

Table 6. $^{40}\text{Ar}/^{39}\text{Ar}$ data from biotite and hornblende of the late syn-kinematic phase of the Lost Sheep peak intrusion, sample MMI16-20-16 (UTM 550127E, 6632781N).

Sample no MMI16-20-16	J 2.702E-03	$\pm(1\sigma)$ 2.084E-06	Relative Isotopic abundances (fAmps)*																
			Ar40	Ar39	Ar38	Ar37	Ar36	Ca/K	Cl/K	$^{40}\text{Ar}^{39}/\text{Ar}(k)$	$^{40}\text{Ar}^{39}/\text{Ar}(k)$	Age	\pm						
Power (%)	Ar40	\pm	Ar39	\pm	Ar38	\pm	Ar37	\pm	Ar36	\pm	Ca/K	\pm	Cl/K	\pm	$^{40}\text{Ar}^{39}/\text{Ar}(k)$	\pm	Age (Ma)	\pm	
0.50	58.837	0.0644	1.6898	0.0615	0.0128	0.0301	0.0521	0.0266	0.0012	0.0007	0.365	0.188	0.014	0.052	34.611	1.286	99.46	161.3	5.7
1.00	647.407	0.1056	18.5084	0.0645	0.2770	0.0300	0.3151	0.0277	0.0126	0.0008	0.202	0.018	0.008	0.005	34.765	0.129	99.45	161.9	0.6
1.50	607.808	0.1107	17.4892	0.0575	0.2423	0.0295	0.1210	0.0271	0.0105	0.0010	0.082	0.018	0.004	0.005	34.557	0.122	99.50	161.0	0.5
2.00	857.842	0.1276	24.5236	0.0625	0.2730	0.0288	0.0871	0.0267	0.0155	0.0009	0.042	0.013	0.003	0.003	34.772	0.097	99.47	162.0	0.4
2.50	629.049	0.1177	18.0925	0.0664	0.2281	0.0301	0.0904	0.0291	0.0083	0.0008	0.059	0.019	0.001	0.005	34.613	0.134	99.62	161.3	0.6
3.00	214.164	0.0797	6.0986	0.0636	0.1586	0.0290	0.0385	0.0267	0.0048	0.0007	0.075	0.052	0.040	0.014	34.864	0.372	99.34	162.4	1.7
3.50	57.189	0.0696	1.6267	0.0631	0.0285	0.0296	0.0669	0.0271	0.0018	0.0007	0.490	0.201	0.015	0.053	34.840	1.379	99.15	162.3	6.1
5.00	91.482	0.0785	2.7001	0.0639	0.0076	0.0291	-0.0197	0.0258	0.0026	0.0007	0.087	0.114	0.044	0.032	33.566	0.811	99.14	156.6	3.6

Sample no MMI16-20-16	J 2.706E-03	$\pm(1\sigma)$ 2.030E-06	Relative Isotopic abundances (fAmps)*																
			Ar40	Ar39	Ar38	Ar37	Ar36	Ca/K	Cl/K	$^{40}\text{Ar}^{39}/\text{Ar}(k)$	$^{40}\text{Ar}^{39}/\text{Ar}(k)$	Age	\pm						
Power (%)	Ar40	\pm	Ar39	\pm	Ar38	\pm	Ar37	\pm	Ar36	\pm	Ca/K	\pm	Cl/K	\pm	$^{40}\text{Ar}^{39}/\text{Ar}(k)$	\pm	Age (Ma)	\pm	
2.00	242.824	0.0921	6.5098	0.0623	0.0778	0.0283	0.6559	0.0258	0.0617	0.0013	1.136	0.046	0.006	0.013	34.537	0.344	92.61	161.2	1.5
2.50	311.163	0.0870	8.4645	0.0630	0.1123	0.0323	3.0659	0.0279	0.0473	0.0014	4.092	0.051	0.000	0.011	35.300	0.275	95.95	164.6	1.2
2.80	284.920	0.0942	7.6289	0.0617	0.1101	0.0304	3.0739	0.0292	0.0387	0.0013	4.556	0.060	0.004	0.012	36.065	0.304	96.47	168.0	1.4
3.00	182.195	0.0857	4.7633	0.0628	0.1316	0.0310	2.0801	0.0295	0.0497	0.0015	4.945	0.098	0.039	0.019	35.404	0.486	92.46	165.0	2.2
3.50	180.015	0.0776	4.9943	0.0614	0.0139	0.0315	2.1422	0.0261	0.0081	0.0010	4.860	0.087	0.028	0.018	35.798	0.452	99.21	166.8	2.0
4.00	94.758	0.0739	2.6890	0.0636	0.0388	0.0302	1.1819	0.0249	0.0019	0.0009	4.984	0.160	0.006	0.033	35.265	0.853	99.96	164.4	3.8
5.00	21.328	0.0665	0.5934	0.0614	0.0377	0.0328	0.3732	0.0243	0.0001	0.0009	7.142	0.884	0.150	0.163	36.238	3.832	100.63	168.7	17.0

* Corrected for blank mass discrimination, and radioactive decay
Sensitivity 6.312E-17 ± 1.047E-18 (mol/fAmp)

Table 7. ⁴⁰Ar/³⁹Ar data from biotite and hornblende of the quartz diorite at Mount Lanning, sample MMI16-29-05 (UTM 533100E, 6635600N).

Sample no MMI16-29-05	Biotite	J 2.712E-03 ± (1σ) 2.309E-06		Relative Isotopic abundances (fAmps)*												Age (Ma)	± (1σ)		
		Ar40 (1σ)	Ar39 (1σ)	Ar38 (1σ)	Ar37 (1σ)	Ar36 (1σ)	Ca/K (1σ)	Cl/K (1σ)	⁴⁰ Ar*/ ³⁹ Ar(k)	± (1σ)	⁴⁰ Ar* (%)								
Grain 1																			
Power (%)	Ar40 (1σ)	Ar39 (1σ)	Ar38 (1σ)	Ar37 (1σ)	Ar36 (1σ)	Ca/K (1σ)	Cl/K (1σ)	⁴⁰ Ar*/ ³⁹ Ar(k)	± (1σ)	⁴⁰ Ar* (%)	Age (Ma)	± (1σ)							
0.10	117.586	0.0734	3.8713	0.0676	0.1206	0.0299	0.0431	0.0257	0.2620	0.0031	0.123	0.074	0.018	0.022	10.372	0.342	34.17	50.0	1.6
0.60	0.786	0.0624	0.0200	0.0626	0.0737	0.0331	0.0081	0.0294	0.0040	0.0008	4.465	21.496	10.746	34.047	98.406	308.940	250.72	426.8	1193.1
0.90	17.702	0.0664	1.2764	0.0599	0.0627	0.0290	0.0069	0.0264	0.0147	0.0011	0.059	0.230	0.101	0.066	10.454	0.557	75.43	50.4	2.7
1.10	55.914	0.0684	4.0737	0.0661	0.0838	0.0324	0.0635	0.0279	0.0253	0.0012	0.173	0.076	0.021	0.023	11.887	0.214	86.66	57.2	1.0
1.30	119.251	0.0727	9.8662	0.0615	0.1739	0.0295	0.0416	0.0297	0.0162	0.0011	0.046	0.034	0.015	0.009	11.595	0.083	95.99	55.9	0.4
1.50	133.052	0.0786	11.3168	0.0657	0.2333	0.0311	0.0210	0.0263	0.0073	0.0009	0.020	0.026	0.024	0.008	11.559	0.075	98.38	55.7	0.4
2.00	283.948	0.0903	24.0875	0.0639	0.4295	0.0294	0.0724	0.0258	0.0119	0.0010	0.033	0.012	0.016	0.004	11.636	0.039	98.78	56.1	0.2
5.00	2026.80	0.1717	170.6799	0.0840	2.8817	0.0315	1.4313	0.0276	0.1429	0.0019	0.093	0.002	0.013	0.001	11.624	0.022	97.95	56.0	0.1
Grain 2																			
0.50	15.691	0.0626	0.3288	0.0645	0.0058	0.0306	0.0317	0.0263	0.0421	0.0013	1.077	0.920	-0.054	0.272	9.858	2.314	20.68	47.6	11.0
1.00	74.380	0.0739	3.3074	0.0684	0.0511	0.0288	0.0234	0.0290	0.1219	0.0018	0.079	0.098	-0.011	0.025	11.594	0.308	51.59	55.9	1.5
1.30	113.368	0.0748	8.4412	0.0663	0.1535	0.0321	0.0310	0.0287	0.0503	0.0013	0.042	0.038	0.014	0.011	11.660	0.108	86.88	56.2	0.5
1.60	177.728	0.0827	14.8549	0.0627	0.2689	0.0299	0.0283	0.0272	0.0220	0.0010	0.021	0.021	0.016	0.006	11.520	0.058	96.35	55.5	0.3
2.00	229.961	0.0908	19.1745	0.0711	0.3934	0.0319	0.0184	0.0285	0.0236	0.0010	0.010	0.017	0.023	0.005	11.622	0.051	96.97	56.0	0.2
2.50	542.108	0.1076	45.3618	0.0652	0.7643	0.0334	0.0867	0.0270	0.0456	0.0015	0.021	0.007	0.013	0.002	11.647	0.030	97.52	56.1	0.1
3.00	759.736	0.1274	63.8520	0.0762	1.1845	0.0321	0.4518	0.0298	0.0494	0.0016	0.079	0.005	0.018	0.001	11.666	0.027	98.11	56.2	0.1
4.00	650.328	0.1175	54.9349	0.0639	0.9228	0.0291	1.0015	0.0279	0.0302	0.0011	0.204	0.006	0.013	0.002	11.677	0.027	98.70	56.2	0.1
5.00	59.126	0.0716	4.8951	0.0645	0.0860	0.0314	0.2529	0.0257	0.0077	0.0008	0.580	0.060	0.015	0.019	11.630	0.165	96.33	56.0	0.8

* Corrected for blank, mass discrimination, and radioactive decay
Sensitivity 6.312E-17 ± 1.047E-18 (mol/fAmp)

Table 8. $^{40}\text{Ar}/^{39}\text{Ar}$ data from biotite and hornblende of lamprophyre dikes at 'Lost Sheep Peak' (MIMI16-14-9, UTM zone 8, 553871E, 6627723N) and at Turtle Lake (MTS16-24-23, UTM 542755E, 6633812N).

Sample no <i>MMI16-14-9</i>	Biotite	J 2.710E-03 ±(1σ) 2.053E-06		Relative Isotopic abundances (fAmps)*										$^{40}\text{Ar}^*/\text{Ar}(\text{K})$	±(1σ)	$^{40}\text{Ar}^*$ (%)	Age (Ma)	±(1σ)																
		Ar40	±(1σ)	Ar39	±(1σ)	Ar38	±(1σ)	Ar37	±(1σ)	Ar36	±(1σ)	Ca/K	±(1σ)						Cl/K	±(1σ)														
0.20	226.469	0.0839	±(1σ)	6.4042	±(1σ)	0.0561	±(1σ)	0.0748	±(1σ)	0.0299	±(1σ)	0.2457	±(1σ)	0.0261	±(1σ)	0.0319	±(1σ)	0.0011	±(1σ)	0.443	±(1σ)	0.004	±(1σ)	0.014	±(1σ)	33.890	±(1σ)	0.309	±(1σ)	95.88	±(1σ)	158.5	±(1σ)	1.4
1.00	53.595	0.0726	±(1σ)	1.4581	±(1σ)	0.0598	±(1σ)	0.0471	±(1σ)	0.0280	±(1σ)	0.0606	±(1σ)	0.0300	±(1σ)	0.0001	±(1σ)	0.0007	±(1σ)	0.481	±(1σ)	0.058	±(1σ)	0.240	±(1σ)	36.774	±(1σ)	1.534	±(1σ)	100.09	±(1σ)	171.4	±(1σ)	6.8
1.50	435.049	0.0997	±(1σ)	12.0060	±(1σ)	0.0642	±(1σ)	0.1281	±(1σ)	0.0287	±(1σ)	0.0259	±(1σ)	0.0279	±(1σ)	0.0028	±(1σ)	0.0007	±(1σ)	0.025	±(1σ)	0.005	±(1σ)	0.027	±(1σ)	36.144	±(1σ)	0.201	±(1σ)	99.81	±(1σ)	168.6	±(1σ)	0.9
2.00	491.540	0.1182	±(1σ)	13.6562	±(1σ)	0.0688	±(1σ)	0.2003	±(1σ)	0.0317	±(1σ)	0.0876	±(1σ)	0.0261	±(1σ)	0.0026	±(1σ)	0.0007	±(1σ)	0.074	±(1σ)	0.007	±(1σ)	0.022	±(1σ)	35.917	±(1σ)	0.189	±(1σ)	99.85	±(1σ)	167.6	±(1σ)	0.8
2.50	278.945	0.0861	±(1σ)	7.6261	±(1σ)	0.0639	±(1σ)	0.1331	±(1σ)	0.0298	±(1σ)	0.0617	±(1σ)	0.0276	±(1σ)	0.0080	±(1σ)	0.0007	±(1σ)	0.093	±(1σ)	0.015	±(1σ)	0.042	±(1σ)	36.249	±(1σ)	0.312	±(1σ)	99.16	±(1σ)	169.1	±(1σ)	1.4
3.00	89.137	0.0725	±(1σ)	2.4709	±(1σ)	0.0695	±(1σ)	-0.0024	±(1σ)	0.0292	±(1σ)	0.0734	±(1σ)	0.0273	±(1σ)	0.0029	±(1σ)	0.0007	±(1σ)	0.345	±(1σ)	0.039	±(1σ)	0.129	±(1σ)	35.726	±(1σ)	1.023	±(1σ)	99.09	±(1σ)	166.7	±(1σ)	4.6
3.50	121.342	0.0736	±(1σ)	3.3700	±(1σ)	0.0638	±(1σ)	0.0729	±(1σ)	0.0310	±(1σ)	0.1367	±(1σ)	0.0278	±(1σ)	0.0020	±(1σ)	0.0007	±(1σ)	0.471	±(1σ)	0.027	±(1σ)	0.097	±(1σ)	35.829	±(1σ)	0.691	±(1σ)	99.56	±(1σ)	167.2	±(1σ)	3.1
5.00	227.299	0.0806	±(1σ)	6.5465	±(1σ)	0.0653	±(1σ)	0.1063	±(1σ)	0.0288	±(1σ)	0.1632	±(1σ)	0.0281	±(1σ)	0.0041	±(1σ)	0.0008	±(1σ)	0.290	±(1σ)	0.011	±(1σ)	0.050	±(1σ)	34.529	±(1σ)	0.353	±(1σ)	99.50	±(1σ)	161.4	±(1σ)	1.6

Sample no <i>MTS16-24-23</i>	Biotite	J 2.711E-03 ±(1σ) 1.854E-06		Relative Isotopic abundances (fAmps)*										$^{40}\text{Ar}^*/\text{Ar}(\text{K})$	±(1σ)	$^{40}\text{Ar}^*$ (%)	Age (Ma)	±(1σ)																
		Ar40	±(1σ)	Ar39	±(1σ)	Ar38	±(1σ)	Ar37	±(1σ)	Ar36	±(1σ)	Ca/K	±(1σ)						Cl/K	±(1σ)														
0.20	1084.096	0.1400	±(1σ)	28.5600	±(1σ)	0.0658	±(1σ)	0.3758	±(1σ)	0.0285	±(1σ)	0.4881	±(1σ)	0.0262	±(1σ)	0.3019	±(1σ)	0.0026	±(1σ)	0.194	±(1σ)	0.010	±(1σ)	0.010	±(1σ)	34.823	±(1σ)	0.103	±(1σ)	91.79	±(1σ)	162.8	±(1σ)	0.5
0.50	7.285	0.0592	±(1σ)	0.1880	±(1σ)	0.0687	±(1σ)	-0.0058	±(1σ)	0.0298	±(1σ)	0.0012	±(1σ)	0.0270	±(1σ)	0.0007	±(1σ)	0.0006	±(1σ)	0.070	±(1σ)	1.638	±(1σ)	1.638	±(1σ)	37.626	±(1σ)	13.951	±(1σ)	97.14	±(1σ)	175.2	±(1σ)	61.9
1.00	104.978	0.0636	±(1σ)	2.9123	±(1σ)	0.0622	±(1σ)	0.0308	±(1σ)	0.0291	±(1σ)	0.0302	±(1σ)	0.0272	±(1σ)	0.0060	±(1σ)	0.0008	±(1σ)	0.117	±(1σ)	0.107	±(1σ)	0.006	±(1σ)	35.418	±(1σ)	0.771	±(1σ)	98.32	±(1σ)	165.4	±(1σ)	3.4
1.50	233.016	0.0836	±(1σ)	6.4290	±(1σ)	0.0619	±(1σ)	0.0356	±(1σ)	0.0309	±(1σ)	0.0889	±(1σ)	0.0275	±(1σ)	0.0112	±(1σ)	0.0008	±(1σ)	0.157	±(1σ)	0.049	±(1σ)	0.020	±(1σ)	35.712	±(1σ)	0.353	±(1σ)	98.59	±(1σ)	166.7	±(1σ)	1.6
2.00	263.217	0.0891	±(1σ)	7.2392	±(1σ)	0.0642	±(1σ)	0.0055	±(1σ)	0.0306	±(1σ)	0.0910	±(1σ)	0.0284	±(1σ)	0.0129	±(1σ)	0.0009	±(1σ)	0.143	±(1σ)	0.045	±(1σ)	0.034	±(1σ)	35.818	±(1σ)	0.327	±(1σ)	98.57	±(1σ)	167.2	±(1σ)	1.5
2.50	203.942	0.0787	±(1σ)	5.7801	±(1σ)	0.0643	±(1σ)	0.0393	±(1σ)	0.0305	±(1σ)	0.1011	±(1σ)	0.0279	±(1σ)	0.0101	±(1σ)	0.0008	±(1σ)	0.199	±(1σ)	0.055	±(1σ)	0.017	±(1σ)	34.754	±(1σ)	0.396	±(1σ)	98.56	±(1σ)	162.4	±(1σ)	1.8
3.00	190.516	0.0851	±(1σ)	5.2739	±(1σ)	0.0577	±(1σ)	0.0954	±(1σ)	0.0303	±(1σ)	0.0537	±(1σ)	0.0272	±(1σ)	0.0089	±(1σ)	0.0007	±(1σ)	0.116	±(1σ)	0.059	±(1σ)	0.016	±(1σ)	35.608	±(1σ)	0.399	±(1σ)	98.63	±(1σ)	166.3	±(1σ)	1.8
3.50	63.252	0.0719	±(1σ)	1.7484	±(1σ)	0.0625	±(1σ)	-0.0165	±(1σ)	0.0309	±(1σ)	0.0228	±(1σ)	0.0265	±(1σ)	0.0025	±(1σ)	0.0007	±(1σ)	0.148	±(1σ)	0.174	±(1σ)	0.063	±(1σ)	35.731	±(1σ)	1.299	±(1σ)	98.83	±(1σ)	166.8	±(1σ)	5.8
5.00	22.944	0.0615	±(1σ)	0.6231	±(1σ)	0.0593	±(1σ)	-0.0471	±(1σ)	0.0288	±(1σ)	0.0010	±(1σ)	0.0250	±(1σ)	0.0008	±(1σ)	0.0007	±(1σ)	0.020	±(1σ)	0.460	±(1σ)	0.255	±(1σ)	36.417	±(1σ)	3.522	±(1σ)	98.96	±(1σ)	169.9	±(1σ)	15.7

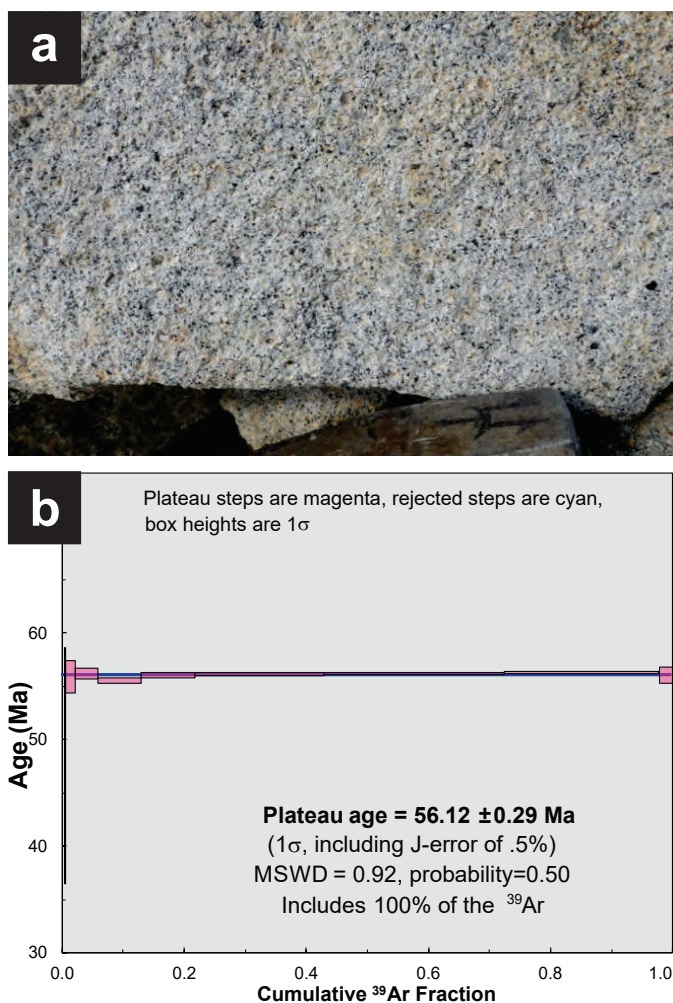


Fig. 22. a) Mount Lanning quartz diorite with fresh biotite collected for a cooling age determination. b) Biotite step heating spectrum yields a 56.12 ± 0.29 Ma age by considering 100% of ^{39}Ar released.

at the Atlin Ruffner mine (past producing), where they cut weakly deformed granodiorite of the Fourth of July batholith. Considering such precious metal affiliation, we selected two sites for geochronological investigation: conspicuous southwest-trending lamprophyre dikes that cut the intrusion at Lost Sheep peak (MMI16-14-9), and limestone near Turtle Lake (MTS16-24-23).

On steep faces of Lost Sheep peak lamprophyre dikes are well exposed in fresh landslide scars, but otherwise tend to be weathered slots floored with biotite-rich gruss in the host granodiorite. We sampled the thickest (~15 m) and freshest of the well-exposed biotite-rich dikes (possibly a composite of superimposed dikes) on the northeast flank of Lost Sheep peak. The dike is dark green to black, medium- to coarse-grained and has a knobby weathered appearance due to an abundance of xenoliths, xenocrysts, xenocryst aggregates (Fig. 23a), and calcite filled amygdales or ocelli. We picked the freshest and highest purity hornblende and biotite grains to obtain clean separates for $^{40}\text{Ar}/^{39}\text{Ar}$ age determination, but microscopic

intergrowths of the two minerals and pyroxene (Figs. 23b, c) likely escaped detection.

Step heating of the best quality biotite grain produced an age of 168.2 ± 1.0 Ma from 75.8% of ^{39}Ar released. Hornblende analyses returned an age of 174.0 ± 2.7 Ma from 74.5% of ^{39}Ar released (Fig. 23d). the preferred interpreted age for this sample. Results from a second hornblende aliquot were rejected, but integrating all ^{39}Ar from both aliquots yields an age of 171 ± 10 Ma (for hornblende spectra see Mihalynuk et al., 2018).

Extensively diked limestone on the steep slope above eastern Turtle Lake includes fine to medium-grained lamprophyre. Intimate mineral intergrowths precluded isolation of pure mineral separates, but about 10 grains of visually pure biotite were obtained. Even then, the coarsest biotite grains are rutilated (see triangular mesh of dark needles, Fig. 23e). A separate of intergrown hornblende and biotite was also obtained for total fusion analysis, but was not used. The best quality biotite grain yielded a release spectrum from which consideration of 100% of the gas gives an $^{40}\text{Ar}/^{39}\text{Ar}$ age of 163.6 ± 2.2 Ma (Fig. 23f). Removal of the first three steps yields an age of 162.80 ± 0.93 Ma from 53.9% of ^{39}Ar released. Rejection of the first step yields an age of 165.9 ± 1.1 Ma, and is probably closest to the actual crystallization age of the dike.

7. Geochemistry

We analyzed mafic to felsic volcanic and ultramafic mantle units from the Turtle Lake map area in an attempt to elucidate the tectonic and physio-chemical settings in which they formed.

7.1. Methods for major and trace element geochemistry

Samples from the Turtle Lake map sheet were crushed and processed using lithium metaborate/tetraborate fusion and nitric acid dissolution and analyzed for major and trace elements at Activation Laboratories (Ancaster, Ontario) using inductively coupled plasma-optical emission spectrometry (ICP-OES) and inductively coupled plasma-mass spectrometry (ICP-MS; 4Lithores analytical package; Table 9). At a 95% confidence level, the uncertainty in measurement of major elements significantly exceeding their quantification limit (3.33 times the detection limit), is $\leq 4\%$ relative. The uncertainty in P_2O_5 , which is present in low abundances (< 0.75 wt.%), is significantly larger, ranging between 5 and 70% relative at a 95% confidence level.

Most lithophile trace elements in the majority of samples from the Turtle lake map area have concentrations that exceed their quantification limits. The uncertainty in individual measurements, at a 95% confidence level, for transitional metals (e.g., Ni, Cr, V) is $\leq 30\%$. The relative uncertainty in measurement of rare earth elements (REE) at the 95% confidence interval is typically $< 15\%$ for most samples presented in Table 9. The relative uncertainty in measurement of high field strength elements (HFSE) at a 95% confidence interval is generally $< 30\%$.

The results of instrumental neutron activation analysis

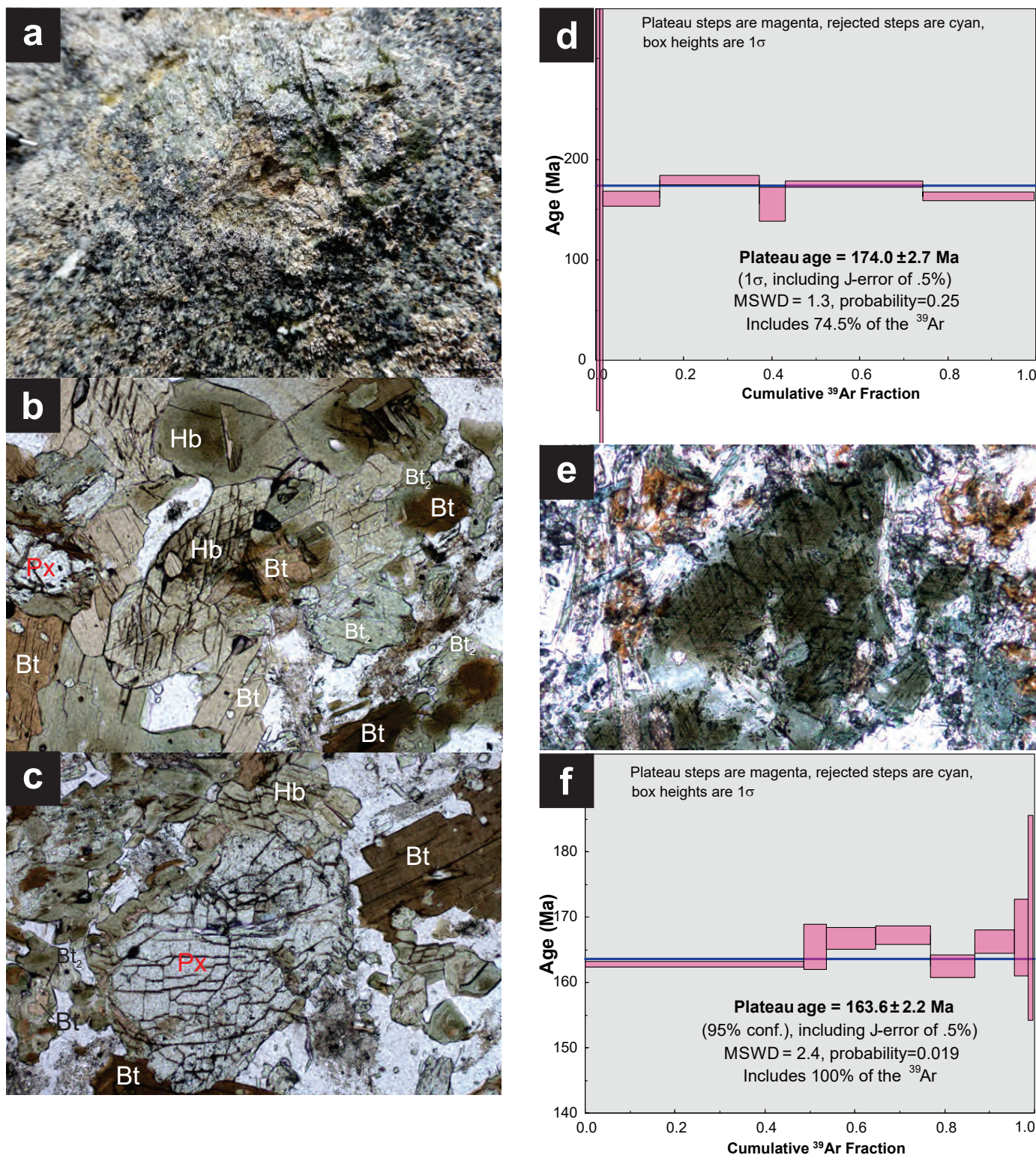


Fig. 23. **a)** Medium-grained lamprophyre from near middle of ~15 m thick dike at northeast flank of Lost Sheep peak contains aggregates up to ~4 cm across of bright green crystals, probably chrome diopside. **b)** Pleochroic green clinopyroxene (diopsidic? augite, Px) is mantled by pleochroic green to brown hornblende (Hb) with fine domains of dark brown to orange-brown biotite (phlogopitic?, Bt) and green pleochroic biotite (Bt₂). Hornblende and biotite have partly altered to chlorite (Chl). **c)** Pleochroic green-brown hornblende (Hb) mantles pyroxene (Px) and is in textural equilibrium with pleochroic brown to orange-tan biotite (Bt) and replaced by pleochroic green biotite (Bt₂). **d)** ³⁹Ar step heating spectrum from a select hornblende grain yielded an age of 174.0 ± 2.7 Ma from 74.5% of ³⁹Ar released. **e)** Photomicrograph showing rutilated, pleochroic green biotite in a lamprophyre dike east of Turtle Lake. **f)** ³⁹Ar step heating spectrum from a select biotite grain yielded an age of 163.6 ± 2.2 Ma from 100% of ³⁹Ar released.

Table 9. Major and trace element composition of samples from the Turtle Lake map sheet (NTS 104M/16).

Sample Suite	MMI16-8-3 IAT	DMI16-9-2A IAT	DMI16-9-2B IAT	DMI16-9-4A IAT	DMI16-16-4A IAT	DMI16-16-6A IAT	MMI16-8-1 Windy-Table
Lithology	basalt	basalt	basalt	basalt	basalt	basalt	lapilli tuff
Easting	540290	539942	539942	549775	549362	549834	540468
Northing	6635377	6637146	6637146	6637335	6625441	6625399	6634980
Major elements (wt.%)							
SiO ₂	48.98	49.48	47.93	50.49	49.27	48.33	53.95
Al ₂ O ₃	15.08	13.28	13.01	14.39	13.8	14.81	20.18
Fe ₂ O ₃ (T)	10.93	10.07	11.11	10.17	10.98	8.67	7.15
MnO	0.12	0.135	0.173	0.172	0.184	0.172	0.16
MgO	5.89	7.88	7.54	7.99	8.68	5.12	2.33
CaO	6.51	7.1	6.47	6.32	9.31	16.68	6.28
Na ₂ O	3.86	2.23	3.05	4.51	3.31	1.05	3.08
K ₂ O	0.17	0.18	0.15	0.05	0.21	0.08	2.80
TiO ₂	1.36	1.08	1.33	1.35	1.23	0.99	0.67
P ₂ O ₅	0.10	0.11	0.11	0.14	0.12	0.09	0.21
LOI	7.29	8.59	9.00	4.13	3.45	3.62	2.46
Total	100.30	100.10	99.88	99.72	100.50	99.61	99.28
Trace elements (ppm)							
Sc	39	34	40	37	40	33	11
Be	< 1	< 1	< 1	< 1	< 1	< 1	2
V	286	288	339	346	313	252	91
Cr	270	210	250	200	280	190	60
Co	38	32	38	36	40	30	10
Ni	90	70	90	70	140	70	< 20
Cu	70	60	70	70	40	50	10
Zn	70	80	80	90	70	60	120
Ga	16	15	15	16	14	20	22
Ge	1.4	1	1.5	0.9	1.1	2.3	1.5
As	7	< 5	< 5	< 5	< 5	< 5	< 5
Rb	7	4	4	< 1	3	1	99
Sr	192	121	160	59	132	32	558
Y	27.7	25	31	31.6	26	23.2	26.3
Zr	76	68	89	80	80	59	181
Nb	1.5	1	0.9	1.1	1.3	1.2	11.5
Mo	< 2	< 2	< 2	< 2	< 2	< 2	< 2
Ag	< 0.5	< 0.5	< 0.5	< 0.5	< 0.5	< 0.5	0.6
In	< 0.1	< 0.1	< 0.1	< 0.1	< 0.1	< 0.1	< 0.1
Sn	< 1	< 1	< 1	< 1	1	1	< 1
Sb	0.8	< 0.2	0.3	0.3	< 0.2	< 0.2	1.6
Cs	3.7	3.7	3.2	1.2	0.2	0.1	12.7
Ba	145	128	188	23	52	11	1715
La	3.55	2.38	2.61	3.22	3.00	2.55	27.4
Ce	10.5	7.4	8.61	9.81	8.93	7.71	50.2
Pr	1.7	1.29	1.49	1.65	1.44	1.23	5.55
Nd	8.86	6.85	7.94	8.95	7.62	6.63	21.3
Sm	3.12	2.68	3.18	3.11	2.67	2.34	4.4
Eu	1.16	0.968	1.13	1.04	1.06	0.842	1.37
Gd	4.20	3.50	4.49	4.49	3.75	3.32	4.13
Tb	0.77	0.66	0.82	0.83	0.68	0.60	0.67
Dy	4.89	4.45	5.39	5.31	4.51	3.82	4.04
Ho	1.02	0.92	1.13	1.09	0.96	0.83	0.81
Er	3.05	2.70	3.35	3.10	2.74	2.48	2.44
Tm	0.452	0.401	0.503	0.475	0.399	0.36	0.368
Yb	3.03	2.71	3.19	3.16	2.69	2.3	2.51
Lu	0.436	0.408	0.502	0.516	0.43	0.36	0.377
Hf	1.9	1.6	2.2	2.0	1.8	1.5	4
Ta	0.08	0.07	0.06	0.08	0.1	0.07	0.41
W	0.7	< 0.5	< 0.5	< 0.5	< 0.5	< 0.5	0.9
Tl	0.06	< 0.05	< 0.05	< 0.05	< 0.05	< 0.05	0.58
Pb	< 5	< 5	< 5	< 5	< 5	< 5	9
Bi	< 0.1	< 0.1	< 0.1	< 0.1	< 0.1	< 0.1	< 0.1
Th	0.24	0.21	0.15	0.21	0.31	0.23	8.59
U	0.12	0.21	0.08	0.26	0.10	0.11	6.98

Table 9. Continued.

Sample Suite	MMI16-23-6 Horsefeed	MMI16-23-8 Horsefeed	DMI16-5-4A Horsefeed	JBA16-5-6 Horsefeed	MMI16-14-9	MTS16-24-12	DMI16-4-3A
Lithology	E-MORB	E-MORB	E-MORB	E-MORB	lamprophyre	lamprophyre	CAB dike
Easting	548161	547679	546083	546059	553871	543783	538671
Northing	6647699	6647539	6650302	6650173	6627723	6635617	6632389
Major elements (wt.%)							
SiO ₂	45.84	38.34	47.26	48.76	51.52	41.52	50.96
Al ₂ O ₃	13.52	10.59	12.86	14.84	11.92	10.80	13.7
Fe ₂ O ₃ (T)	11.71	10.99	14.65	12.07	7.17	8.75	8.51
MnO	0.17	0.12	0.21	0.20	0.13	0.14	0.15
MgO	7.17	6.89	6.25	6.85	12.50	10.85	7.76
CaO	12.99	15.14	9.31	9.25	7.83	10.30	9.13
Na ₂ O	2.11	0.12	1.23	2.83	3.53	2.23	2.09
K ₂ O	0.55	2.05	0.18	0.16	2.45	2.76	3.44
TiO ₂	1.05	0.80	2.15	1.59	0.96	1.31	0.95
P ₂ O ₅	0.08	0.09	0.25	0.15	0.53	0.74	0.52
LOI	3.94	15.73	5.63	3.26	1.42	9.24	2.98
Total	99.12	100.90	99.97	99.94	99.95	98.65	100.2
Trace elements (ppm)							
Sc	43	24	47	43	18	25	26
Be	< 1	< 1	< 1	< 1	3	2	2
V	275	127	380	332	140	205	210
Cr	280	230	100	210	870	650	390
Co	58	44	47	45	40	43	31
Ni	130	160	70	90	330	260	100
Cu	20	80	210	140	20	80	40
Zn	90	70	90	90	90	80	80
Ga	16	10	20	18	16	15	15
Ge	2.1	1	1.9	2.1	1.2	1.1	1.3
As	7	< 5	< 5	< 5	< 5	< 5	< 5
Rb	7	28	4	3	97	115	79
Sr	468	176	171	215	891	690	769
Y	19.8	13.2	44	28.6	18.2	24.8	27.2
Zr	40	43	124	89	187	177	147
Nb	3.8	3.9	5.3	5.7	25.2	17.3	5.7
Mo	< 2	< 2	< 2	< 2	2	3	3
Ag	< 0.5	< 0.5	< 0.5	< 0.5	0.6	0.5	< 0.5
In	< 0.1	< 0.1	< 0.1	< 0.1	< 0.1	< 0.1	< 0.1
Sn	< 1	< 1	1	< 1	< 1	1	< 1
Sb	0.7	0.4	0.4	1.5	< 0.2	1.3	0.4
Cs	0.2	0.9	0.2	0.1	9.8	9.7	3
Ba	38	79	79	226	2591	2470	1611
La	3.36	2.62	9.22	7.11	73.8	52.7	28.7
Ce	8.66	6.23	23.6	17.7	130	106	59.4
Pr	1.3	0.92	3.47	2.47	13.9	12.8	7.36
Nd	6.5	4.28	16.9	11.8	50.9	51	31.5
Sm	2.21	1.49	5.36	3.53	8.72	10.1	7.4
Eu	0.953	0.362	1.91	1.27	2.36	2.79	2.11
Gd	3.01	2.01	6.88	4.53	6.11	7.93	7.05
Tb	0.54	0.36	1.21	0.82	0.77	1.03	1.03
Dy	3.72	2.32	7.82	5.29	3.83	5.26	5.27
Ho	0.76	0.5	1.55	1.05	0.64	0.9	0.99
Er	2.2	1.52	4.32	3	1.69	2.36	2.55
Tm	0.321	0.238	0.618	0.426	0.227	0.307	0.335
Yb	2.06	1.63	3.91	2.92	1.33	1.9	2.14
Lu	0.317	0.286	0.566	0.441	0.202	0.28	0.329
Hf	1.0	1.0	3.2	2.1	3.8	3.9	3.1
Ta	0.21	0.22	0.34	0.37	1.31	0.92	0.35
W	< 0.5	0.8	6	< 0.5	0.6	0.7	< 0.5
Tl	< 0.05	< 0.05	0.06	< 0.05	0.75	0.73	0.67
Pb	< 5	< 5	< 5	< 5	6	7	8
Bi	< 0.1	< 0.1	< 0.1	< 0.1	< 0.1	< 0.1	< 0.1
Th	0.28	0.21	0.63	0.52	23.9	9.03	5.2
U	0.45	0.64	0.3	0.16	6.87	3.09	2.97

Table 9. Continued.

Sample Suite	<u>DMI16-14-9A</u>	<u>DMI16-21-7A</u>	<u>MMI16-6-2</u>	<u>MMI16-18-1</u> Eocene	<u>DMI16-29-20A</u> Eocene intrusion	<u>DMI16-24-14A</u> Eocene intrusion	<u>DMI16-27-8A</u> Eocene Intrusion
Lithology	CAB dike	CAB dike	QFP dike	quartz diorite	diorite	diorite	quartz diorite
Easting	554057	532804	547085	549939	514894	542848	542089
Northing	6626649	6623895	6652002	6674246	6637897	6633199	6634018
Major elements (wt.%)							
SiO ₂	53.33	51.19	65.57	65.47	49.58	55.90	66.81
Al ₂ O ₃	13.46	16.27	17.04	15.93	19.41	18.80	15.08
Fe ₂ O ₃ (T)	7.23	7.22	1.61	4.46	10.59	8.09	4.11
MnO	0.13	0.12	0.03	0.10	0.14	0.18	0.08
MgO	10.8	6.38	0.86	1.36	3.92	2.69	1.36
CaO	7.5	6.07	3.88	3.05	10.56	6.89	3.01
Na ₂ O	3.26	4.02	3.67	3.57	2.99	4.00	4.07
K ₂ O	1.57	3.24	2.43	4.17	0.68	1.68	3.75
TiO ₂	0.80	1.19	0.21	0.63	1.37	1.20	0.51
P ₂ O ₅	0.20	0.43	0.05	0.15	0.33	0.43	0.20
LOI	1.97	3.72	4.69	1.48	0.70	0.71	1.00
Total	100.3	99.85	100.10	100.40	100.30	100.60	99.97
Trace elements (ppm)							
Sc	24	23	4	9	25	17	6
Be	1	1	< 1	2	< 1	1	2
V	159	179	27	64	328	155	49
Cr	630	220	50	110	< 20	< 20	30
Co	35	24	3	7	25	10	7
Ni	240	90	< 20	< 20	< 20	< 20	< 20
Cu	< 10	40	< 10	< 10	20	< 10	10
Zn	60	60	< 30	90	100	100	50
Ga	15	15	16	17	19	18	17
Ge	1.1	1.1	0.8	1.3	1.1	1.2	1.1
As	< 5	< 5	< 5	< 5	< 5	< 5	< 5
Rb	35	82	74	149	14	34	109
Sr	400	747	450	350	772	749	378
Y	17.4	16.8	4	26.1	16.2	27.6	20.2
Zr	118	113	65	193	42	141	232
Nb	7.9	14.5	1.7	10.3	3.1	8.3	12.9
Mo	< 2	< 2	< 2	< 2	< 2	2	3
Ag	< 0.5	< 0.5	< 0.5	0.6	< 0.5	< 0.5	0.7
In	< 0.1	< 0.1	< 0.1	< 0.1	< 0.1	< 0.1	< 0.1
Sn	1	< 1	< 1	3	< 1	1	1
Sb	< 0.2	0.6	0.2	0.5	0.5	0.5	0.5
Cs	3.4	2.2	4.3	7.3	0.4	1.4	1.6
Ba	1006	3175	4129	1647	640	1516	1962
La	16.9	21.1	8.89	38.1	12.5	23.5	37.3
Ce	34.8	42.5	15.4	69.6	26.3	48.4	68.5
Pr	4.25	5.2	1.65	7.71	3.35	6.07	7.3
Nd	17.5	21.8	6.01	28	14.2	25.5	25.9
Sm	3.79	4.6	1.08	5.63	3.62	5.92	4.99
Eu	1.13	1.5	0.474	1.04	1.31	1.73	1.1
Gd	3.56	4.14	0.93	4.89	3.54	5.44	4.03
Tb	0.57	0.56	0.14	0.79	0.54	0.83	0.6
Dy	3.26	3.03	0.74	4.44	3.2	4.95	3.38
Ho	0.62	0.57	0.14	0.88	0.61	0.98	0.68
Er	1.79	1.63	0.38	2.53	1.7	2.79	2.01
Tm	0.265	0.225	0.052	0.394	0.232	0.398	0.313
Yb	1.71	1.44	0.33	2.64	1.47	2.47	2.2
Lu	0.258	0.223	0.055	0.402	0.215	0.392	0.335
Hf	2.5	2.3	1.5	4.8	1.1	2.5	4.7
Ta	0.52	0.92	0.13	1.11	0.22	0.47	1.06
W	< 0.5	< 0.5	< 0.5	1.8	< 0.5	3.8	0.7
Tl	0.37	0.53	0.54	1.4	0.07	0.25	0.59
Pb	< 5	5	< 5	35	< 5	8	14
Bi	0.3	< 0.1	< 0.1	< 0.1	< 0.1	0.1	< 0.1
Th	3.65	4.47	2.15	22.1	2.03	3.99	13.1
U	1.14	1.56	1.31	6.96	0.67	1.03	4.31

Table 9. Continued.

Sample Suite	<u>DMI16-16-6B</u> Eocene Intrusion	<u>DMI16-13-1A</u> L. Cretaceous	<u>DMI16-21-12A</u> L. Cretaceous	<u>DMI16-29-13A</u> L. Cretaceous	<u>DMI16-29-18A</u> L. Cretaceous	<u>DMI16-29-3A</u> L. Cretaceous	<u>DMI16-29-6A</u> L. Cretaceous
Lithology	quartz diorite	quartz diorite	quartz diorite	granodiorite	granodiorite	granodiorite	granodiorite
Easting	549834	528839	540468	529087	528466	528206	528349
Northing	6625399	6626085	6634980	6639906	6640410	6634793	6635781
Major elements (wt.%)							
SiO ₂	63.88	66.34	66.04	73.93	74.26	71.65	71.29
Al ₂ O ₃	15.91	14.56	15.47	13.33	13.26	14.36	14.28
Fe ₂ O ₃ (T)	4.58	3.7	3.92	2.18	2.16	2.27	2.58
MnO	0.09	0.07	0.08	0.06	0.05	0.06	0.06
MgO	2.02	1.64	2.17	0.27	0.22	0.7	0.7
CaO	3.78	3.31	2.69	1.09	0.94	1.56	1.61
Na ₂ O	3.99	3.72	3.79	4.04	3.92	3.96	3.99
K ₂ O	4.07	3.97	3.98	4.23	4.18	4.24	4.31
TiO ₂	0.63	0.46	0.48	0.17	0.15	0.24	0.29
P ₂ O ₅	0.21	0.21	0.17	0.05	0.03	0.09	0.11
LOI	0.88	1.18	1.46	0.37	0.57	0.61	0.74
Total	100.00	99.16	100.30	99.74	99.74	99.75	99.96
Trace elements (ppm)							
Sc	9	7	6	2	2	3	4
Be	2	2	2	3	4	3	2
V	73	61	55	13	9	24	32
Cr	70	40	80	< 20	< 20	30	30
Co	10	8	8	1	1	3	4
Ni	40	< 20	50	< 20	< 20	< 20	< 20
Cu	< 10	20	< 10	< 10	< 10	< 10	< 10
Zn	60	60	50	40	40	< 30	< 30
Ga	15	16	16	17	17	14	15
Ge	1.1	1.2	1.1	1.5	1.5	1.3	1.3
As	< 5	< 5	< 5	< 5	< 5	< 5	< 5
Rb	149	138	139	129	140	138	133
Sr	480	397	409	127	111	246	325
Y	18	16.5	15.9	23.1	28.3	12.9	12.2
Zr	221	212	227	192	164	160	211
Nb	13.4	10.9	10.4	13	10.3	7.4	7.3
Mo	< 2	< 2	3	< 2	< 2	< 2	< 2
Ag	0.7	0.7	0.7	0.7	< 0.5	< 0.5	0.6
In	< 0.1	< 0.1	< 0.1	< 0.1	< 0.1	< 0.1	< 0.1
Sn	1	2	2	1	2	1	1
Sb	< 0.2	0.3	< 0.2	< 0.2	< 0.2	< 0.2	0.4
Cs	4.7	4.5	2.7	2.3	3.2	2.9	2.6
Ba	2057	1734	1660	843	673	1231	1498
La	38	40.7	30.3	36.8	32.2	29.4	29.6
Ce	66.6	71.5	54.2	67.2	61	48.9	49
Pr	7.06	7.36	5.89	6.95	6.65	5	4.89
Nd	24.4	25.2	21.1	23.5	23.5	17.1	16.3
Sm	4.44	4.54	3.86	4.42	5.1	3.11	2.95
Eu	1.21	1.07	0.935	0.371	0.351	0.581	0.639
Gd	3.77	3.55	3.28	3.63	4.41	2.29	2.23
Tb	0.56	0.5	0.51	0.6	0.77	0.36	0.37
Dy	3.26	2.8	2.68	3.61	4.72	2.11	2.22
Ho	0.61	0.56	0.52	0.75	0.94	0.42	0.41
Er	1.75	1.6	1.58	2.45	2.97	1.21	1.13
Tm	0.257	0.246	0.237	0.387	0.449	0.199	0.168
Yb	1.75	1.64	1.61	2.73	3.16	1.36	1.16
Lu	0.299	0.277	0.257	0.44	0.521	0.233	0.194
Hf	5.2	4.5	4.6	5.2	4.1	3.2	4.1
Ta	1.18	0.98	0.99	1.34	1.13	0.84	0.71
W	2.7	1	27.6	< 0.5	< 0.5	< 0.5	1.1
Tl	0.92	0.81	0.72	0.61	0.68	0.73	0.73
Pb	19	20	19	14	11	17	15
Bi	< 0.1	0.1	0.1	< 0.1	< 0.1	0.1	0.1
Th	18.6	19.1	16.7	20.1	21.2	13.3	11.8
U	3.64	6.91	7.20	6.57	6.59	5.18	4.39

(INAA) and sodium peroxide assays, also performed by Activation Laboratories, are presented in Table 9.

7.2. Geochemistry results

Thirty-one samples of igneous rocks typically encountered in the Turtle Lake map area were analyzed. Based on their petrographic and geochemical character they have been grouped into the following principal suites: island arc tholeiite (6), enriched mid-ocean ridge basalt (E-MORB; 4), calc-alkaline basaltic to andesitic rocks (4), lamprophyre (2), and intermediate to felsic rocks (15).

7.2.1. Basaltic to intermediate volcanic rocks

Six samples of pervasively altered augite and plagioclase-phyric basalt and basaltic fragmental rock assigned to the island arc tholeiite suite (Fig. 24) and collected from the eastern shore of Tagish Lake, south of Peninsula Mountain, and the southeastern corner of the study area near Sunday Peak (Fig. 2), have moderate to high LOI (3.5-9.0 wt.%), relatively uniform SiO_2 (51-55 wt.%; reported on anhydrous, LOI-free basis) and Al_2O_3 (14.4-16.4 wt.%), and variable MgO (5.4-9.0 wt.%) concentrations. On a Primitive Mantle (PM; Palme and O'Neill, 2003)-normalized extended trace element diagram (Fig. 25a), these samples have relatively unfractionated rare earth element (REE) profiles, with slight depletion in the most incompatible light REE (LREE). Notably, these samples have pronounced relative depletions in the high-field strength elements (HFSE) Nb and Ta, diagnostic of an island arc tholeiitic (IAT) magmatic affinity. Furthermore, the trace element compositions of the IAT suite overlap the compositions of IAT reported by English et al. (2010) from the Nakina area of the Cache Creek terrane (Figs. 25a and 26). A single sample of lapilli tuff with a basaltic

andesite composition (Fig. 24; $\text{SiO}_2=56$ wt.%) also collected for geochronology from the Windy-Table suite has a pronounced calc-alkaline trace element profile characterized by a strong enrichment in LREE relative to the more incompatible heavy REE (HREE).

In contrast to the IAT suite, the amygdaloidal aphanitic basaltic rocks in the Horsefeed Formation (LOI=3-16 wt.%) have lower abundances of SiO_2 (45-51 wt.%), Al_2O_3 (12.6-15.5 wt.%), while having similar MgO concentrations (6.7-8.2 wt.%). Furthermore, they display slight enrichment of LREE relative to HREE and lack the conspicuous depletion in Nb and Ta (Fig. 25b) displayed by the volcanic rocks of the IAT suite. The basaltic rocks of the Horsefeed formation plot in the mantle array of Pearce (2008), and have compositions that are intermediate between N-MORB and E-MORB (Fig. 26). Although the overlap is not complete (Fig. 26), the E-MORB reported here largely overlap the E-MORB of the Nakina area (English et al., 2010).

Three weakly altered dikes sampled from Mount Clive, Lost Sheep peak, and the western shore of Tagish Lake have basaltic compositions (LOI=2-4 wt.%; $\text{SiO}_2=53-55$ wt.%; $\text{Al}_2\text{O}_3=14.2-17.1$ wt.%, MgO=6.7-11.1 wt.%; Fig. 24), but display variable mineralogy ranging from augite+biotite-phyric to hornblende+plagioclase-phyric. Field relationships, and relatively fresh mineralogy suggest that these dikes are Late Cretaceous or younger. These dikes have similar trace element patterns, characterized by strong enrichment in LREE and depletion of HREE relative to N-MORB, and pronounced depletion in Nb, Ta and Ti (Fig. 25c).

7.2.2. Lamprophyre

Two lamprophyre samples have variable LOI (1-9 wt.%), but relatively uniform SiO_2 (46.9-52.7 wt.%), Al_2O_3 (12 wt.%), and MgO (12.3-12.8 wt.%) concentrations. The combined $\text{Na}_2\text{O}+\text{K}_2\text{O}$ concentration (>5.5 wt.%) is high, but consistent with the sample's biotite-rich alkaline affinity. The two samples have sub-parallel trace element profiles (Fig. 25c), characterized by strongly fractionated, LREE-enriched patterns, and marked Nb-Ta-Ti negative anomalies, which are typical of calc-alkaline lamprophyres (Rock, 1991). The lamprophyres also display strong enrichments in LILE (80-500 x PM, matching the LILE contents of the intermediate-felsic rocks analyzed as part of this study.

7.2.3. Intermediate and felsic samples

Fifteen samples of intermediate- SiO_2 to felsic compositions were analyzed. All samples display pronounced, PM-normalized enrichments of LREE relative to HREE, and strong relative depletions in Nb, Ta, and Ti. In addition, most intermediate to felsic samples show enrichments in Zr-Hf relative to the similarly incompatible REE. Although most samples display significant overlap, some systematic differences between suites may be diagnostic. First, rocks assigned to the Fourth of July suite are the most alkaline, and thereby have the highest abundances of Hf, Zr, and LREE and lowest abundances of

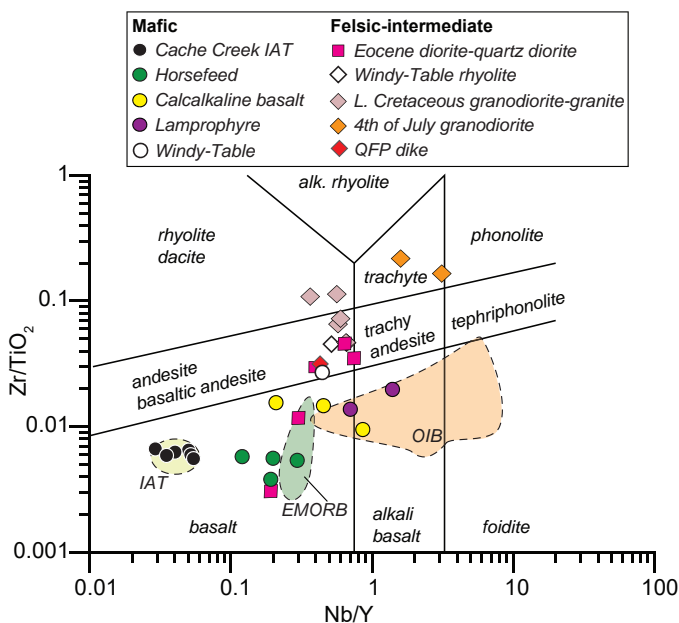


Fig. 24. Rock analyses presented in this report plotted on the modified Zr/TiO_2 vs. Nb/Y classification diagram (Pearce, 1996).

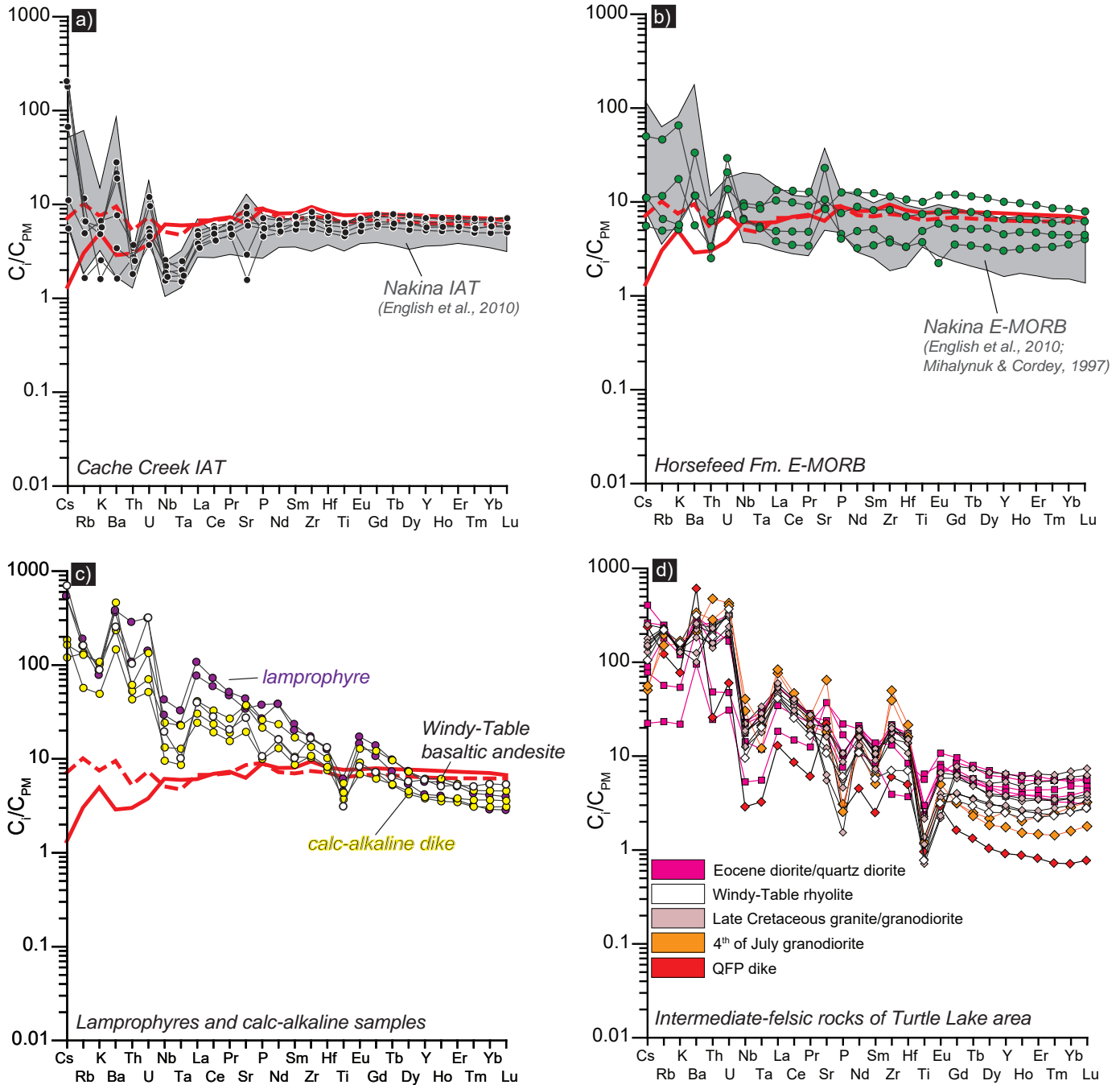


Fig. 25. Primitive mantle-normalized (Palme and O’Neill, 2003) trace element profiles for mafic (a-c) and intermediate to felsic d) rocks of the Turtle Lake map area. Average compositions (Gale et al., 2013) of normal-MORB (N-MORB) and back-arc basin basalt (BABB) are shown for reference.

HREE. In addition, samples of the Fourth of July suite display U-shaped HREE profiles. Second, Late Cretaceous plutonic rocks ($\text{SiO}_2=67-75$ wt.% and $\text{Al}_2\text{O}_3=13.4-15.7$ wt.%) are typically quartz dioritic to granodioritic in composition and are distinguished from the dioritic to quartz dioritic Eocene plutonic rocks ($\text{SiO}_2=50-68$ wt.% and $\text{Al}_2\text{O}_3=15.3-19.7$ wt.%) by higher SiO_2 and lower Al_2O_3 concentrations.

8. Discussion

Based on macrofossil evidence, the extensive Horsefeed Formation carbonate was deposited in the Late Carboniferous to Early Permian in a tectonic setting that was stable throughout the time span (Monger, 1975). Volcanic rocks interbedded with the Horsefeed Formation are uncommon, but where present, they display within-plate geochemical characteristics and are probably the relicts of ocean islands or plateaux, the

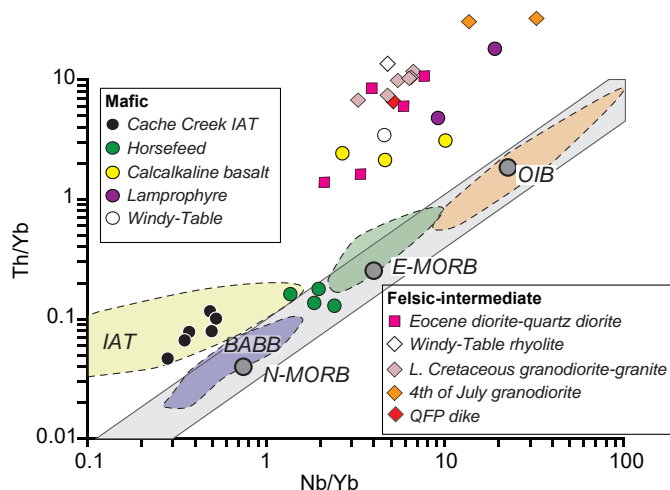


Fig. 26. Th/Yb vs. Nb/Yb diagram (after Pearce, 2008) showing the compositions of the rocks analyzed as part of this study and compared to the composition of oceanic basalts, which plot in the MORB-OIB array (grey band). Fields of IAT, BABB, E-MORB, and OIB are based on the classification of Cache Creek basalts of English et al. (2010).

massive bases of which were subducted (English et al., 2010; Zagorevski et al., 2016). Tuffaceous layers in the Horsefeed Formation point to explosive volcanism during deposition of the carbonate platform. Near Mount Cloutier these tuffs are of EMORB composition. We attempted to date one of the tuff layers using conodonts, but were unsuccessful. However, the polymictic sharpstone conglomerate that we sampled at Turtle Lake contained detrital zircons spanning Middle Pennsylvanian through Early Permian (~25 m.y.). This is the same time span as the most widespread fossil ages obtained from the Horsefeed Formation of the Turtle Lake area (Monger, 1975), and suggests that these fossil-bearing carbonate environments were dependant on volcanic substrates. But is plateau magmatism over a 25 m.y. time span reasonable? Was Horsefeed Formation deposited instead atop an age-progressive chain of islands like Hawaii?

Isolated within-plate volcanic islands, or even those forming seamount chains over hotspots such as the Hawaii-Emperor chain, are prone to submergence at rates faster than carbonate deposition (Detrick and Crough, 1978; Moore and Fornari, 1984) and are unlikely to provide a regionally extensive substrate with sufficient longevity to explain the Horsefeed Formation. Plateaus, such as the Ontong-Java and Kurguelen, the largest plateaus on earth, are tens of thousands of km² in extent, and are long-lived. For example, Ontong-Java plateau formed during at least two separate magmatic pulses, ~121 Ma and ~90 Ma (Tejada et al., 1996), separated by a 30 m.y. magmatic hiatus. Kurguelen formed semicontinuously since ~119 Ma (Duncan, 2002) with present day volcanic activity in the central plateau region. Plateaus such as these could provide a stable long-lasting substrate for thick, regional limestone deposition over 25 m.y. with synchronous within-plate magmatic additions during the carbonate bank deposition.

However, Kurguelen is at least partly underlain by rifted continental crust (we see no evidence in detrital zircons of continental crust) and Ontong-Java is currently too deep to form a substrate for carbonate banks. Part of the difficulty in identifying an analogue for Horsefeed Formation substrate is that thick sections of plateau crust are lacking in northwest British Columbia, and are inferred to have been subducted. Based on existing evidence, the Horsefeed Formation was deposited in an environment isolated from arc volcanic rocks and it was adjacent to basins where chert accumulated.

Ophiolitic magmatic and mantle rocks of the Cache Creek terrane have supra-subduction zone geochemical affinities (English et al., 2010; Zagorevski et al., 2016; McGoldrick et al., 2017), and mostly Late Permian to Early Triassic isotopic ages (Gordey et al., 1998; Mihalynuk et al., 2003; Zagorevski, 2016). Thus, Horsefeed Formation limestone and intercalated within-plate basalts are both geochemically and temporally unrelated to the ophiolitic sections. Although the Kedahda Formation in the Turtle Lake area lacks fossil ages, most stratigraphic evidence points to Kedahda chert as synchronous with, and overlying, the Horsefeed Formation limestones. Deposition of limestone breccia atop soft sediment-deformed chert, and injection of breccia dikes into ribbon chert (Fig. 5b) suggests that the two depositional environments coexisted in close proximity, perhaps where limestone debris flowed into an adjacent pelagic basin.

Jurassic fold and thrust deformation is regionally recognized in areas adjacent to the Turtle Lake mapsheet (e.g., Mihalynuk et al., 1999), farther southeast (see Mihalynuk et al., 2004; English, 2004; Mihalynuk et al., 2017) and in Yukon (e.g., Monger, 1975 and Colpron et al., 2015 and references therein). This deformation is not readily recognizable in the massive Horsefeed Formation limestone of the Turtle Lake area, where marker beds outlining folds and thrusts are lacking, and such structures are not shown on existing maps (Monger, 1975, p. 27). Alternatively, these limestones may have developed a thick(er)-skinned thrust belt where strain was localized into very few thrusts. This appears to be the case to the northwest, in the Windy Arm area (Monger, 1975), where large homoclinal areas are preserved in the limestones; whereas on-strike cherts are intensely folded and imbricated (Gordey, 1991).

Fold and thrust deformation is regionally constrained to have finished by ca. 172 Ma, the age of the Fourth of July plutonic suite, which cuts across and thermally metamorphosed deformed strata. Cooling ages from Fourth of July batholith and related intrusions record the combined effects of conductive and convective cooling of the batholith and satellite intrusions, and tectonic and erosional exhumation. Lamprophyre dikes cutting the undeformed margin of the Lost Sheep peak intrusion yield biotite ages of 168.2 ± 1.0 Ma and a hornblende cooling age of 174.0 ± 2.7 Ma from 74.5% of ³⁹Ar released. Integration of all ³⁹Ar released yields an age of 171 ± 10 Ma. These cooling ages are consistent with those from the Fourth of July batholith nearby (Mihalynuk et al., 2004 and references therein), and the intrusion is probably a satellite of the main batholith. Other

plutons of the Fourth of July suite (part of the regional Three Sisters suite, Woodsworth et al., 1992) cut the outboard edge of the Cache Creek terrane, and yield crystallization ages of ~174-172 Ma (summarized in Mihalynuk et al., 2004). Lamprophyre dikes that cut the Fourth of July batholith have been considered a late stage intrusive phase of the batholith emplacement (Aitken, 1959; Mihalynuk et al., 1999; Ash, 1994). Back-veining of the 174.0 ± 2.7 Ma lamprophyre dike that cuts Lost Sheep Peak intrusion provides consistent textural and geochronologic evidence of this late-stage magmatic relationship.

Hornblende and biotite cooling ages from the synkinematic Lost Sheep peak intrusion record a difference of between 3 and 6 m.y. (inside and outside limits of error). If the age data are reliable, they may be interpreted as recording the rate of cooling from hornblende 166.0 ± 1.1 Ma to biotite 161.61 ± 0.85 Ma closure temperatures (~600 to ~310°C, Harrison and Fitzgerald, 1986; Harrison et al., 1985; or differing by ~300°C, Dodson, 1973; Baxter, 2010) of ~70° to 30°C/m.y., at the limits of error.

Lamprophyre cooling ages that we report are consistent with dikes east and west of Atlin Lake dated by Harris et al. (2003) as 165.3 ± 1.6 Ma and 161.8 ± 1.6 Ma (biotite, each a combination of 2 aliquots). Regionally, these dikes have been mapped from east of Atlin Lake to the east shore of Tagish Lake. On the west shore of Tagish Lake, only a single lamprophyre dike has been mapped by us, and none have been noted farther west. It appears that the zone of diking dies out across Tagish Lake, or the zone was cut off by faulting. It is also possible that our observations are incomplete. For example, a lamprophyre dike was reported at Mt. Clive by Cairnes (1913); although, that dike is presumably part of different suite, of Cretaceous or younger, as Cretaceous granodiorite underlies Mt. Clive. Dike orientation is a field criterion that may help to distinguishing different lamprophyre suites; however, it is not without ambiguity. Dated Middle Jurassic lamprophyre dikes trend northwest-southeast, but south and northeast trends are also recorded.

From east of Atlin Lake to Turtle Lake, the Fourth of July batholith, its outliers, and related lamprophyre dikes, provide constraints on post ~170 Ma crustal displacements implying that lateral transport within the zone of intrusions, if present, has been insufficient to totally truncate lamprophyre dikes. Further investigation of the lamprophyre dikes is warranted because they are a rare example of a potential east-west tie line in the Cordillera, plus they contain abundant crustal xenoliths and are therefore good probes into the crustal composition at their time of emplacement (a record that we did not exploit).

Trans-crustal faulting has resulted in juxtaposition of Cache Creek terrane mantle and upper crustal rocks as well as supracrustal Laberge Group and Windy-Table suite strata. Middle Triassic chert is interbedded with wacke (north of Graham Inlet) and is juxtaposed with pillow basalt, slivers of gabbro, and serpentinized mantle tectonite. Similarly, panels of volcanic rocks at Peninsula Mountain are separated from the Horsefeed Formation by thin domains (less than ~200 m thick) of structurally-disrupted ribbon chert, in places

admixed with blocks of many different lithologies, including serpentinite (Fig. 12e). No relicts of blueschist or other high P/T metamorphic facies have been discovered along this boundary thus far. It is interpreted as demarking the outboard margin of the Cache Creek terrane.

Detrital zircons separated from reworked rhyolite breccia at Sunday Peak are as young as 85 Ma and are correlated with the Windy-Table suite. Some of the zircons have Late Triassic (216 Ma) cores (Figs. 18b, c). Late Triassic was a common magmatic age during construction of the Stikine arc (Stuhini or Lewes River groups), and may indicate that by Late Cretaceous the basement through which the source volcanic rocks erupted, was predominantly Stuhini Group. Alternatively, the Laberge Group, which contains abundant Late Triassic zircons (e.g., Colpron et al., 2015) and immediately underlies parts of the rhyolite breccia, may have been sampled by the Windy-Table suite magmas.

Prior to the new ~80 Ma U-Pb age determination reported here, volcanic rocks at Peninsula Mountain were correlated with volcanic strata that grade into Triassic Kedahda Formation ribbon chert and Laberge-like wacke near Graham Creek, ~20 km south-southeast of Sunday Peak. Such observations were consistent with interpretations of earlier workers (e.g., Bultman, 1979) who considered the Peninsula Mountain suite as basement of the Whitehorse Trough, mainly based on regional southwest dips that project beneath the Laberge Group. Reassignment of 'Middle to Late(?) Triassic Peninsula Mountain volcanic suite' rocks (Mihalynuk and Smith, 1992b) to Windy-Table suite, was required for rocks 7 km east-southeast of Sunday Peak, to explain a new ~85 Ma U-Pb age on rhyolite layers (Zagorevski et al., 2017) originally thought to be deposited with Kedahda Formation chert. The same inconsistency arises from our new ~80 Ma date from 'Peninsula Mountain suite' volcanic rocks in the Turtle Lake area, suggesting that the correlation error is pervasive, and as a consequence, we reassign all 'Peninsula Mountain suite' rocks to Windy-Table suite (largely consistent with original mapping by Monger, 1975). It is possible that not all of the volcanic rocks at Peninsula Mountain belong to the Windy-Table suite as indicated, for example, by island arc tholeiite compositions that are indistinguishable from the most widespread basalts of the Cache Creek terrane, but more detailed mapping and sampling for age determinations will be required to determine if this is so. In support of our reassignment is the absence of notable Middle Jurassic (see above) lamprophyre dikes within the volcanic rocks at Peninsula Mountain, in stark contrast to the eastern side of Turtle Lake where the dike swarm is well developed.

Evidence for Cretaceous extension is accumulating in the Turtle Lake area. Extensional fabrics that have top-to-the-southeast sense of offset are consistent with the orientation of syn-deformational dike swarms in the thermal metamorphic halo of the Racine pluton (Fig. 12f). An extensional fault is inferred to approximately trace the southeast flank of Sunday Peak, explaining at least 500 m of down-to-the-southeast

vertical offset of Windy-Table volcanic strata from near the peak (Fig. 2), to near the valley floor to the south. An extensional fault crossing Turtle Lake may explain along-strike termination of limestone bodies on either side of the lake (Figs. 2, 13). Projection of this inferred fault to the northeast links the steep face of the southwest carbonate ridge of Stovel Peak, at least partly paralleled by an exposed dip slope fault (Fig. 12a). Verification of these inferred faults will require more detailed, focused mapping but such verification is important because it carries broad tectonic significance. For example, the interpretation of paleomagnetic data by Harris et al. (2003) is predicated on the absence of such faults. These authors used geobarometry to show that the northern Fourth of July batholith has been exhumed by nearly 12 km, while the southern part has been exhumed by ~6 to 8 km. They then ascribed the differential uplift to regional tilting and used that tilt to 'correct' paleomagnetic inclination measurements by ~9°. However, such exhumation is also consistent with the south-side-down extensional faulting that we tentatively propose, which would result in northward tilting of block faults and a paleo-inclination 'correction' of the opposite sense (Fig. 27).

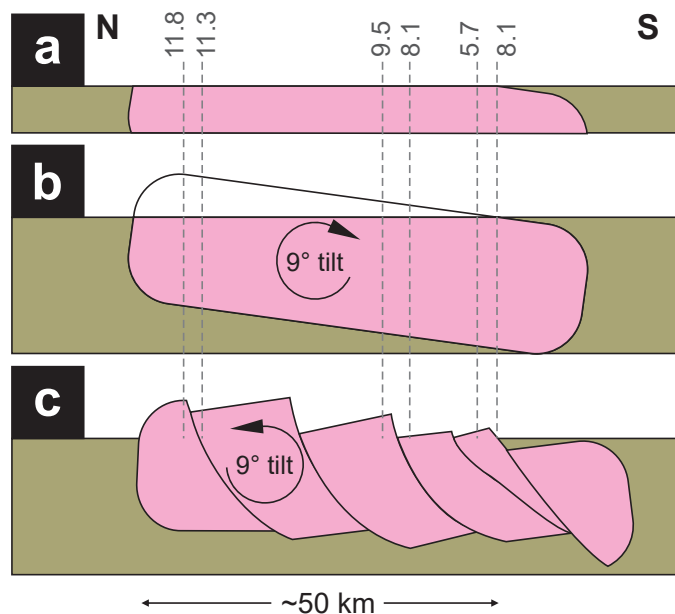


Fig. 27. A cross-section cartoon showing two mechanisms that explain Al in hornblende geobarometric results for the present-day Fourth of July batholith. Values are estimates of intrusion depth in kilometres (Harris et al., 2003). **a)** Distribution of sites in Fourth of July batholith where geobarometric values were obtained. **b)** Bulk 9° southward crustal tilting preferred by Harris et al. to explain geobarometric data, and **c)** Northward rotation of blocks between south-side-down extensional faults that are indicated, but not yet fully demonstrated, by our mapping. Note the opposite effects of (b) versus (c) on a hypothetical paleomagnetic inclination correction.

8.1. Updated geologic history and regional implications

Our work in the Turtle Lake map area helps to further define the Cache Creek and Stikine terranes, refine their geological histories, and interactions between them. Thick accumulations

of Horsefeed Formation limestone (1.5 km) indicate deposition across thousands of km² from Carboniferous to Permian (Monger, 1975). A stable, long-lived plateau substrate is probable, based on a transitional N-MORB to E-MORB geochemical signature of associated basaltic rocks in the Turtle Lake area and elsewhere (English et al., 2010), and isotopic evidence for magmatic additions to this plateau over 25 m.y., approximately coextensive with regionally developed platform limestone deposition in the Turtle Lake area. In contrast, ultramafic and oceanic crustal rocks of northern Cache Creek terrane are everywhere dated as Middle Permian (e.g., Mihalynuk et al., 2003, 2004; Zagorevski et al., 2016) to Early Triassic (Gordey et al., 1998). Ophiolitic rocks at Turtle Lake are correlated with undated mantle-gabbro-basalt along strike to the southeast, at Graham Creek. There the pillow basalt section is overlain by Middle to Late Triassic chert and wacke grading upwards into probable Laberge Group (Mihalynuk et al., 1999). Wacke overlapping both arc ophiolitic and Horsefeed carbonate rocks may provide a loose link between these domains, which formed in disparate tectonic environments. Wacke that we map as part of the Laberge Group in the Turtle Lake area, links the Graham Creek suite, now more firmly affiliated with Cache Creek ophiolites on the basis of similar geochemistry, but is the wacke succession on Cache Creek substrate really part of the Laberge Group? Recent detrital zircon evidence from the Whitehorse trough (west of Cache Creek terrane) and from strata overlying the Cache Creek terrane shows equivalent age distributions, strongly supporting a link by latest Triassic (Colpron et al., 2015). If so, what happened to the basement atop which the Horsefeed Formation was deposited? Only outcrop-sized relicts of it remain, and we infer, as others have (e.g., English et al., 2010), that this crust has been lost to subduction. Timing of this subduction is between the age of the youngest Horsefeed Formation, latest Early Permian, and the age of overlap demonstrated by detrital zircons, latest Triassic. Amalgamation of the Cache Creek terrane was probably multi-staged, as has been suggested by other workers (e.g., Logan and Mihalynuk, 2014), and consumption of the ocean plate carrying the Cache Creek ocean arc and the Horsefeed Formation, delivered the buoyant arc/plateau crust to the Stikine-Quesnel arc around 210 Ma, resulting in collision, angular unconformity, subduction termination, arc disruption, and a pulse of alkalic magmatism including rich Cu-Au-Ag porphyry deposit formation (Mihalynuk et al., 1994; Logan and Mihalynuk, 2014; Mihalynuk et al., 2016). Pre- and post-collisional subduction is recorded by blueschist and eclogite cooling ages ~221 and 224 Ma in the Stuart Lake area (Ghent et al., 1993) and by the youngest blueschists, ~174 Ma in the Dease Lake area (Mihalynuk et al., 2004).

Partial subduction of thick Horsefeed Formation carbonate rocks may have led to efficient transfer of Cu and other chalcophile elements from the mantle wedge (e.g., Canil and Fellows, 2017). In northernmost British Columbia, where the Horsefeed Formation is extensive, Late Triassic copper porphyry deposits are not known. However, until we can

establish the amount of transcurrent motion on the Nahlin, Silver Salmon and related faults, we cannot fully evaluate this apparent spatial relationship.

Final subduction termination is recorded by emplacement and cooling of the youngest blueschists, with the resultant fold and thrust belt cut by ~172 Ma late syn- and post-kinematic Fourth of July batholith and subsequent lamprophyre dikes, which had mostly cooled to biotite closure temperatures by ~162 Ma, at a rate of between 30°-70°C/m.y.

Between ~165-125 Ma, only rare magmatism is recorded; we have found only a single 145 Ma granitic dike in the Turtle Lake area. This North American-wide magmatic lull has been recognized for decades (e.g., Armstrong, 1974, 1988, 155-125 Ma) and has recently been correlated with relict subducted lithosphere at mid-mantle depths, which accumulated in massive high velocity slabs. Location and geometry of these slabs support subduction of oceanic crust attached to the leading edge of North America, westward beneath the intra-oceanic Insular Superterrane (Sigloch and Mihalynuk, 2013; Sigloch and Mihalynuk, 2017).

By 125 Ma, oceanic lithosphere was again forced to subduct beneath the western North American margin (newly defined by addition of the Insular Superterrane). Arc magmatism may have resumed west of the Turtle Lake area, as recorded by a volcanic succession north of Tutshi Lake (Mihalynuk et al., 2003; Zagorevski et al., 2017), and at ~110 Ma, magmatic contributions are recorded in clastic matrix of karst deposits in the Horsefeed Formation. However, it was not until ~85 Ma that widespread volcanism in the Turtle Lake area outpaced erosion, with deposition and preservation of the Windy-Table suite and correlatives extending in an orogen-parallel belt for hundreds of kilometres (Zagorevski et al., 2017).

Cutting the ~85 Ma basal volcanic conglomerate of the Windy-Table suite is a high-angle transcurrent fault marking the leading edge of the Cache Creek terrane. Known as the Silver Salmon fault (Mihalynuk et al., 2017), the amount of offset across it has yet to be constrained. An array of mainly south-side-down extensional faults, some with individual offsets of more than 500 m, also cut the Windy-Table suite, and may be kinematically linked to the Silver Salmon fault. These extensional faults have yet to be evaluated for their potential to focus hydrothermal fluids and mineralization.

By Early Eocene (~56 Ma) the final magmatic epoch recorded in the Turtle Lake area commenced. Sloko Group volcanism recorded south of the Turtle Lake area is represented in the uplifted study area by small zoned plutons and stocks. Sunday Peak intrusion is one such example. It cut and thermally metamorphosed the crustal-scale Silver Salmon fault. These Eocene magmatic centres can be economically important, as demonstrated by rich epithermal gold mineralization at the Engineer Mine, which is genetically and temporally related to Eocene magmatic rocks and is hosted by Laberge Group strata, structurally prepared adjacent to the crustal-scale Llewellyn fault (Mihalynuk et al., 1999; Millonig et al., 2017; Ootes et al., 2017, 2018). Our new dating of intrusions at Sunday Peak

and Mount Lanning, both formerly considered Cretaceous, both hosted by Laberge Group, and both adjacent crustal-scale faults, reveals the same combination of key geologic elements as at the Engineer Mine, ~30 km to the south. To our knowledge, however, neither the Sunday Peak nor the Mount Lanning area have received modern mineral exploration attention.

9. Summary

Our regional geological mapping, geochronologic and geochemical results help to further refine the geological evolution of the Turtle Lake area. Key new observations and data sets include the following.

- New conodont ages of early (Bashkirian) and middle-upper (Moscovian-Gzhelian) parts of the Late Carboniferous (Pennsylvanian), and the last stage of the Early Permian (Kungurian) are consistent with previous fossil age determinations from the >1.5 km thick limestones of the Horsefeed Formation.
- A new detrital zircon age from Horsefeed Formation tuffaceous limestone breccia echoes the ~25 m.y. biochronological age range, suggesting continuous additions to the volcanic substrate, possibly an oceanic plateau, as is also suggested by their transitional N-MORB to E-MORB composition.
- Soft sediment intermingling of carbonate breccia and pelagic strata suggest proximity of, and connections between, the two depositional environments.
- New geochemical data support correlation of arc tholeiite basalt and harzburgite at Sunday Peak with ophiolitic rocks of the Cache Creek terrane.
- Thick sections of Laberge Group wacke mapped either side of the ophiolitic belt extending both north and south of Sunday Peak suggest an unconformable relationship, later modified by high-angle faulting.
- Regional folds and thrusts affecting Cache Creek terrane and Laberge Group are cut by the Lost Sheep peak intrusion, formerly considered Cretaceous, but now constrained by a crosscutting lamprophyre dikes to Middle Jurassic, part of the regional Three Sisters plutonic suite.
- Lamprophyre dikes that cut granitic phases of the Lost Sheep Peak intrusion are locally back-veined by the granite indicating a comagmatic, but not necessarily co-genetic relationship.
- Calc-alkalic lamprophyre dikes cut the Lost Sheep peak intrusion and surrounding Horsefeed Formation and have cooling ages of 168.2 ± 1.0 to 174.0 ± 2.7 Ma.
- Strong fabric development in early phases of the Lost Sheep peak intrusion indicate that it was late syn- to post-kinematic.
- Cooling of the Lost Sheep peak intrusion through the argon diffusion in hornblende and biotite closure temperature occurred between ~166-162 Ma; a cooling rate of ~70° to 30°C/m.y. is implied.

- In the Turtle Lake area, dated magmatic rocks that fall within the Late Jurassic to Early Cretaceous North American magmatic lull are limited to a single 145.75 ± 0.11 Ma granitic dike.
- Cretaceous magmatism may have resumed by ~ 125 Ma in the Boundary Ranges to the west, but earliest records in the Turtle Lake area are a unimodal population of ~ 110 Ma detrital zircons from a karst deposit in Horsefeed limestone.
- A belt of Late Cretaceous volcanic rocks correlated with the Windy-Table suite is now dated at three sites as ~ 86.5 Ma, 80.63 ± 0.07 Ma and 79.7 ± 1.3 Ma.
- The crustal-scale, high-angle, Silver Salmon fault affects rocks at the base of the Windy-Table suite, constraining youngest motion to less than ~ 86.5 Ma.
- Motion on the Silver Salmon fault may be kinematically linked with an as yet inadequately mapped set of east- to northeast-trending extensional faults displaying mainly south-side-down offsets, locally at least 500 m.
- The Silver Salmon fault is cut by the youngest recognized magmatic unit in the map area, a suite of quartz diorite stocks dated as 56.01 ± 0.04 Ma and 56.12 ± 0.29 Ma, coeval with magmatic rocks at the Engineer mine.

Acknowledgments

James Balchin, Siobhan McGoldrick, and Chris Lawley provided key assistance in field data collection. Norm Graham and Paula Vera of Discovery Helicopters safely and efficiently conveyed crews and gear. This report was reviewed and improved by Jim Monger.

References cited

- Aitken, J.D., 1959. Atlin map-area, British Columbia. Geological Survey of Canada, Memoir 307, 89 p.
- Armstrong, R.L., 1974. Magmatism, orogenic timing, and orogenic diachronism in the Cordillera from Mexico to Canada. *Nature*, 247, 348-351.
- Armstrong, R.L., 1988. Mesozoic and early Cenozoic magmatic evolution of the Canadian Cordillera. *Geological Society of America Special Papers*, 218, pp. 55-92.
- Ash, C.H., 1994. Origin and tectonic setting of ophiolitic ultramafic and related rocks in the Atlin area, northwestern British Columbia. British Columbia Ministry of Energy, Mines and Petroleum Resources, British Columbia Geological Survey, Bulletin 94, 140 p.
- Baxter, E.F., 2010. Diffusion of Noble Gases in Minerals. *Reviews in Mineralogy and Geochemistry*, 72, 509-557.
- Best, M.G., Christiansen, E.H., Deino, A.L., Grommé, C.S., Tingey, D.G., 1995. Correlation and emplacement of a large, zoned, discontinuously exposed ash flow sheet; the $^{40}\text{Ar}/^{39}\text{Ar}$ chronology, paleomagnetism, and petrology of the Pahrnagat Formation, Nevada. *Journal of Geophysical Research*, 100, 24593-24609.
- Bloodgood, A., Rees, C.J., and Lefebvre, D.V., 1989. Geology of the Atlin area (NTS 104N/11W, 12E). British Columbia Ministry of Energy, Mines and Petroleum Resources, British Columbia Geological Survey, Open File 1989-15.
- Boleneus, D.E., Raines, G.L., Causey, J.D., Bookstrom, A.A., Frost, T.P., and Hyndman, P.C., 2001. Assessment method for epithermal gold deposits in northeast Washington State using weights-of-evidence GIS modeling. US Geological Survey, Open File 01-501, 52 p.
- Boulanger, O., and Kiss, F., 2017. Aeromagnetic survey of the Llewellyn area, NTS 104-M/9,10,15,16 and parts of 104-M/11,14, British Columbia. British Columbia Ministry of Energy and Mines, British Columbia Geological Survey, Geoscience Map 2017-4.
- Breitsprecher, K., and Mortensen, J.K., 2004. BCAGE 2004A-1-a database of isotopic age determinations for rock units from British Columbia. British Columbia Ministry of Energy and Mines, British Columbia Geological Survey, Open File 2004-03 (Release 2.0), 7766 records, 9.3 Mb.
- Bullman, R.B., 1979. Geology and tectonic history of the Whitehorse Trough west of Atlin, British Columbia. Unpublished Ph.D. thesis, Yale University, 284 p.
- Cairnes, D.D., 1913. Portions of Atlin District, British Columbia: with special reference to lode mining. Geological Survey of Canada Memoir 37, 129 p.
- Canil, D., and Fellows, S.A., 2017. Sulphide-sulphate stability and melting in subducted sediment and its role in arc mantle redox and chalcophile cycling in space and time. *Earth and Planetary Science Letters*, 470, 73-86.
- Canil, D., Mihalynuk, M., MacKenzie, J.M., Johnston, S.T. and Grant, B., 2005. Diamond in the Atlin Nakina region, British Columbia: insights from heavy minerals in stream sediments. *Canadian Journal of Earth Sciences*, 42, 2161-2171.
- Christie, R.L., 1957. Bennett, British Columbia. Geological Survey of Canada, Map 19-1957.
- Colpron, M., Crowley, J.L., Gehrels, G., Long, D.G., Murphy, D.C., Beranek, L., and Bickerton, L., 2015. Birth of the northern Cordilleran orogen, as recorded by detrital zircons in Jurassic synorogenic strata and regional exhumation in Yukon. *Lithosphere*, 7, 541-562.
- Colpron, M., and Nelson, J.L., 2011. A digital atlas of terranes for the Northern Cordillera. British Columbia Ministry of Energy and Mines, British Columbia Geological Survey, GeoFile 2011-11.
- Cordey, F., Gordey, S.P., and Orchard, M.J., 1991. New biostratigraphic data for the northern Cache Creek Terrane, Teslin map area, southern Yukon. In: *Current Research; Part E*, Geological Survey of Canada Paper 1991-1, pp. 67-76.
- Crowley, J.L., Schoene, B., and Bowering, S.A., 2007. U-Pb dating of zircon in the Bishop Tuff at the millennial scale. *Geology*, 35, 1123-1126.
- Dazé, A., Lee, J.K., and Villeneuve, M., 2003. An intercalibration study of the Fish Canyon sanidine and biotite $^{40}\text{Ar}/^{39}\text{Ar}$ standards and some comments on the age of the Fish Canyon Tuff. *Chemical Geology*, 199, 111-127.
- Detrick, R.S., and Crough, S.T., 1978. Island subsidence, hot spots, and lithospheric thinning. *Journal of Geophysical Research: Solid Earth*, 83, 1236-1244.
- Dickie, J.R., and Hein, F.J., 1995. Conglomeratic fan deltas and submarine fans of the Jurassic Laberge Group, Whitehorse Trough, Yukon Territory, Canada; fore-arc sedimentation and unroofing of a volcanic island arc complex. In: Chough, S.K., and Orton, G.J., (Eds.), *Fan deltas: Depositional styles and controls*. Special Volume, *Sedimentary Geology*, 98, 263-292.
- Dodson, M.H., 1973. Closure temperature in cooling geochronological and petrological systems. *Contributions to Mineralogy and Petrology*, 40, 259-274.
- Duncan, R.A., 2002. A time frame for construction of the Kerguelen Plateau and Broken Ridge. *Journal of Petrology*, 43, 1109-1119.
- English, J.M., 2004. Convergent margin tectonics in the North American Cordillera: implications for continental growth and orogeny. Unpublished Ph.D. thesis, University of Victoria, Victoria, 191 p. Available from <http://dspace.library.uvic.ca/handle/1828/391> accessed November, 2015.
- English, J.M., Mihalynuk, M.G., and Johnston, S.T., 2010.

- Geochemistry of the northern Cache Creek terrane and implications for accretionary processes in the Canadian Cordillera. *Canadian Journal of Earth Sciences*, 47, 13-34.
- Friedman, R.M., Mihalynuk, M.G., Diakow, L.J., and Gabites, J.E., 2016. Southern Nicola Arc Project 2015: Geochronologic data constraining Nicola arc history along a transect near 50°N. British Columbia Ministry of Energy and Mines, British Columbia Geological Survey GeoFile 2016-3.
- Gale, A., Dalton, C.A., Langmuir, C.H., Su, Y., and Schilling, J.-G., 2003. The mean composition of ocean ridge basalts. *Geochemistry, Geophysics, Geosystems*, 14, 489-518.
- Ghent, E.D., Stout, M.Z., and Erdmer, P., 1993. Pressure-temperature evolution of lawsonite-bearing eclogites, Pinchi Lake, British Columbia. *Journal of Metamorphic Geology*, 11, 279-290.
- Golding, M.L., and Orchard, M.J., 2017. Magnigondolella, a new conodont genus from the Triassic of North America. *Journal of Paleontology*, 1-14. NO Volume, on-line only at present Published online: 23 November 2017 <https://doi.org/10.1017/jpa.2017.123>.
- Gordey, S.P., 1991. Teslin map area, a new geological mapping project in southern Yukon. In: *Current Research, Part A*, Geological Survey of Canada Paper 91-1A, pp. 171-178.
- Gordey, S.P., McNicoll, V.J., and Mortensen, J.K., 1998. New U-Pb ages from the Teslin area, southern Yukon, and their bearing on terrane evolution in the northern Cordillera. In: *Geological Survey of Canada, Current Research-Radiogenic age and isotopic studies, Report 11*, pp. 129-148.
- Gwillim, J.C., 1901. Atlin mining district. *Geological Survey of Canada Annual Report 1899, Volume 12*, 48 p.
- Harris, M.J., Symons, D.T., Blackburn, W.H., Hart, C.J., and Villeneuve, M., 2003. Travels of the Cache Creek Terrane: a paleomagnetic, geobarometric and $^{40}\text{Ar}/^{39}\text{Ar}$ study of the Jurassic Fourth of July Batholith, Canadian Cordillera. *Tectonophysics*, 362, 137-159.
- Harris, R.W., and Hollingsworth, R.V., 1933. New Pennsylvanian conodonts from Oklahoma. *American Journal of Science*, 25, 193-204.
- Harrison, T.M., and Fitzgerald, J.D., 1986. Exsolution in hornblende and its consequences for $^{40}\text{Ar}/^{39}\text{Ar}$ age spectra and closure temperature. *Geochimica et Cosmochimica Acta*, 50, 247-253.
- Harrison, T.M., Duncan, I., and McDougall, I., 1985. Diffusion of ^{40}Ar in biotite: temperature, pressure and compositional effects. *Geochimica et Cosmochimica Acta*, 49, 2461-2468.
- Hart, C.J.R., 1997. A transect across northern Stikinia: Geology of the northern Whitehorse map area, southern Yukon Territory (105D/13-16). *Exploration and Geological Services Division, Yukon Region, Indian and Northern Affairs Canada, Bulletin*, 8, 112 p.
- Hart, C.J.R., Dickie, J.R., Ghosh, D.K., and Armstrong, R.L., 1995. Provenance constraints for Whitehorse Trough conglomerate; U-Pb zircon dates and initial Sr ratios of granitic clasts in Jurassic Laberge Group, Yukon Territory. In: *Jurassic magmatism and tectonics of the North American Cordillera*. Geological Society of America, Special Paper 299, pp. 47-63.
- Jaffey, A.H., Flynn, K.F., Glendenin, L.E., Bentley, W.C., and Essling, A.M., 1971. Precision measurement of half-lives and specific activities of ^{235}U and ^{238}U . *Physics Review*, C4, 1889-1906.
- Jeppsson, L., Anehus, R., and Fredholm, D., 1999. The optimal acetate buffered acetic acid technique for extracting phosphatic fossils. *Journal of Paleontology*, 73, 964-972.
- Johannson, G.G., Smith, P.L., and Gordey, S.P., 1997. Early Jurassic evolution of the northern Stikinian arc; evidence from the Laberge Group, northwestern British Columbia. *Canadian Journal of Earth Sciences*, 34, 1030-1057.
- Kerrick, R., and Wyman, D.A., 1994. The mesothermal gold-lamprophyre association: significance for an accretionary geodynamic setting, supercontinent cycles, and metallogenic processes. *Mineralogy and Petrology*, 51, 147-172.
- Kuiper, K.F., Deino, A., Hilgen, F.J., Krijgsman, W., Renne, P.R., and Wijbrans, J.R., 2008. Synchronizing rock clocks of Earth history. *Science*, 320, 500-504.
- Lane, H.R., 1967. Uppermost Mississippian and Lower Pennsylvanian conodonts from the type Morrowan region, Arkansas. *Journal of Paleontology*, 41, 920-942.
- Logan, J.M., and Mihalynuk, M.G., 2014. Tectonic controls on early Mesozoic paired alkaline porphyry deposit belts (Cu-Au \pm Ag-Pt-Pd-Mo) within the Canadian Cordillera. *Economic Geology*, 109, 827-858.
- Lowe, G.W., 2003. Preliminary lithostratigraphy of the Laberge Group (Jurassic), south-central Yukon: Implications concerning the petroleum potential of the Whitehorse Trough. *Yukon Exploration and Geology*, 129-142.
- Lowe, G.W., 2004. Sedimentology, stratigraphy and source rock potential of the Richthofen formation (Jurassic), northern Whitehorse Trough, Yukon. In: *Yukon Exploration and Geology, Yukon Geological Survey*, 177-191.
- Mattinson, J.M., 2005. Zircon U-Pb chemical abrasion (CA-TIMS) method: combined annealing and multi-step partial dissolution analysis for improved precision and accuracy of zircon ages. *Chemical Geology*, 220, 47-66.
- McGoldrick, S., Zagorevski, A., and Canil, D., 2017. Geochemistry of volcanic and plutonic rocks from the Nahlin ophiolite with implications for a Permo-Triassic arc in the Cache Creek terrane, northwestern British Columbia. *Canadian Journal of Earth Sciences*, 1-14. doi: 10.1139/cjes-2017-0069.
- Mihalynuk, M.G., and Cordey, F., 1997. Potential for Kutcho Creek volcanogenic massive sulphide mineralization in the northern Cache Creek terrane: a progress report. In: *Geological Fieldwork 1996*, British Columbia Ministry of Energy, Mines and Petroleum Resources, British Columbia Geological Survey Paper 1997-1, pp.157-170.
- Mihalynuk, M.G., and Mountjoy, K.J., 1990. Geology of the Tagish Lake area (104M/ 8, 9E). In: *Geological Fieldwork, 1989*, British Columbia Ministry of Energy, Mines and Petroleum Resources British Columbia Geological Survey Paper 1991-1, pp. 181-196.
- Mihalynuk, M.G., and Rouse, J.N., 1988. Preliminary geology of the Tutshi Lake area, northwestern British Columbia (104M/15). In: *Geological Fieldwork 1987*, British Columbia Ministry of Energy and Mines, British Columbia Geological Survey, Paper 1988-1, pp. 217-231.
- Mihalynuk, M.G., and Smith, M.T., 1992a. Geology and geochemistry of the Atlin (west) map area (104N/12W). *British Columbia Ministry of Energy, Mines and Petroleum Resources, British Columbia Geological Survey, Open File 1992-08*.
- Mihalynuk, M.G., and Smith, M.T., 1992b. Highlights of 1991 mapping in the Atlin-West Map area (104N/ 12). In: *Geological Fieldwork 1991*, British Columbia Ministry of Energy, Mines and Petroleum Resources, British Columbia Geological Survey, Paper 1992-1, pp. 221-227.
- Mihalynuk, M.G., Bellefontaine, K.A., Brown, D.A., Logan, J.M., Nelson, J.L., Legun, A.S., and Diakow, L.J., 1996. Geological compilation, northwest British Columbia (NTS 94E, L, M; 104F, G, H, I, J, K, L, M, N, O, P; 114J, O, P). *British Columbia Ministry of Energy and Mines, British Columbia Geological Survey Open File 1996-11*.
- Mihalynuk, M.G., Diakow, L.J., Friedman, R.M., and Logan, J.M., 2016. Chronology of southern Nicola arc stratigraphy and deformation. In: *Geological Fieldwork 2015*, British Columbia Ministry of Energy and Mines, British Columbia Geological Survey Paper 2016-1, pp. 31-64.
- Mihalynuk, M.G., P. Erdmer, Ghent, E.D., Cordey, F., Archibald, D.A., Friedman, R.M., and Johannson, G.G., 2004. Coherent French Range blueschist: Subduction to exhumation in < 2.5 m.y.? *Geological Society of America Bulletin*, 116, 910-922.
- Mihalynuk, M.G., Friedman, R.M., Joyce, N., Camacho, A.,

- and Zagorevski, A., 2018. Geochronologic data from samples collected in the Turtle Lake area, NTS 104M/16, northwest British Columbia. British Columbia Ministry of Energy, Mines and Petroleum Resources, British Columbia Geological Survey GeoFile in press.
- Mihalynuk, M.G., Johnston, S.T., English, J.M., Cordey, F., Villeneuve, M.J., Rui, L., and Orchard, M.J., 2003. Atlin TGI Part II: Regional geology and mineralization of the Nakina area (NTS 104N/2W and 3). In: Geological Fieldwork, British Columbia Ministry of Energy and Mines, British Columbia Geological Survey Paper 2003-1, pp. 9-37.
- Mihalynuk, M.G., Mountjoy, K.J., McMillan, W.J., Ash, C.H., and Hammack, J.L., 1991. Highlights of 1990 fieldwork in the Atlin area. In: Geological Fieldwork 1990, British Columbia Ministry of Energy, Mines and Petroleum Resources, British Columbia Geological Survey, Paper 1991-1, pp. 145-152.
- Mihalynuk, M.G., Mountjoy, K.J., Smith, M.T., Currie, L.D., Gabites, J.E., Tipper, H.W., Orchard, M.J., Poulton, T.P., and Cordey, F., 1999. Geology and mineral resources of the Tagish Lake area (NTS 104M/ 8,9,10E, 15 and 104N/ 12W), northwestern British Columbia. British Columbia Ministry of Energy and Mines, British Columbia Geological Survey, Bulletin 105, 202 p.
- Mihalynuk, M.G., Nelson, J., and Diakow, L.J., 1994. Cache Creek Terrane entrapment: oroclinal paradox within the Canadian Cordillera. *Tectonics*, 13, 575-595.
- Mihalynuk, M.G., Zagorevski, A., English, J.M., Orchard, M.J., Bidgood, A., K., Joyce, N., and Friedman, R.M., 2017. Geology of the Sinwa Creek area, northwest BC (104K/14). In: Geological Fieldwork 2016, British Columbia Ministry of Energy and Mines, British Columbia Geological Survey Paper 2017-1, pp. 153-178.
- Millonig, L.J., Beinlich, A., Raudsepp, M., Devine, F., Archibald, D.A., Linnen, R.L., and Groat, L.A., 2017. The Engineer Mine, British Columbia: An example of epithermal Au-Ag mineralization with mixed alkaline and subalkaline characteristics. *Ore Geology Reviews*, 83, 235-257.
- Monger, J., 1975. Upper Paleozoic rocks of the Atlin Terrane, northwestern British Columbia and south-central Yukon. Geological Survey of Canada, Paper 74-47, 63 p.
- Moore, J., and Fornari, D., 1984. Drowned reefs as indicators of the rate of subsidence of the Island of Hawaii. *Journal of Geology*, 92, 752-759.
- Ootes, L., Elliott, J.M., and Rowins, S.M., 2017. Testing the relationship between the Llewellyn fault, gold mineralization, and Eocene volcanism in northwest British Columbia: A preliminary report. In: Geological Fieldwork 2016, British Columbia Ministry of Energy and Mines, British Columbia Geological Survey Paper 2017-1, pp. 49-59.
- Ootes, L., Castonguay, S., Friedman, R., Devine, F., and Simmonds, R., 2018. Testing the relationship between the Llewellyn fault, Tally-Ho shear zone, and gold mineralization in northwest British Columbia. In: Geological Fieldwork 2017, British Columbia Ministry of Energy, Mines and Petroleum Resources, British Columbia Geological Survey Paper 2018-1, pp. 67-81.
- Palme, H., and O'Neill, H.St.C., 2003. Cosmochemical estimates of mantle composition. In: Holland, H.D., Turekian, K.K., Davis, A.M., (Eds.), *Treatise on Geochemistry*, vol. 2. Elsevier, Amsterdam, The Netherlands, pp. 1-38.
- Pearce, J.A., 1996. A users guide to basalt discrimination diagrams. In: Wyman D.A., (Ed.), *Trace element geochemistry of volcanic rocks: Applications for Massive Sulphide Exploration*. Geological Association of Canada, Short Course Notes, 12, pp. 79-113.
- Pearce, J.A., 2008. Geochemical fingerprinting of oceanic basalts with applications to ophiolite classification and the search for Archean oceanic crust. *Lithos*, 100, 14-48.
- Renne, P.R., and Norman, E.B., 2001. Determination of the half-life of ^{40}Ar by mass spectrometry. *Physical Review C*, 63, 047302.
- Renne, P.R., Cassata, W.S., and Morgan, L.E., 2009. The isotopic composition of atmospheric argon and $^{40}\text{Ar}/^{39}\text{Ar}$ geochronology: time for a change?. *Quaternary Geochronology*, 4, 288-298.
- Renne P.R., Swisher C.C., Deino A.L., Karner D.B., Owens T.L., and DePaolo D.J., 1998. Intercalibration of standards, absolute ages and uncertainties in $^{40}\text{Ar}/^{39}\text{Ar}$ dating. *Chemical Geology*, 145, 117-152.
- Rock, N.M.S., 1991. *Lamprophyres*, Springer, Boston, 285 p.
- Rock, N.M., and Groves, D.I., 1988. Do lamprophyres carry gold as well as diamonds? *Nature*, 332, 253-255.
- Roddick, J.C., 1983. High precision intercalibration of ^{40}Ar - ^{39}Ar standards. *Geochimica Cosmochimica Acta*, 47, 887-898.
- Ross, J., 2017. Pychron documentation. New Mexico Institute of Mining and Technology, 115 p. <<https://media.readthedocs.org/pdf/pychron/latest/pychron.pdf>> Last accessed January 11, 2018.
- Schmitz, M.D., and Schoene, B., 2007. Derivation of isotope ratios, errors, and error correlations for U-Pb geochronology using ^{205}Pb - ^{235}U (^{233}U)-spiked isotope dilution thermal ionization mass spectrometric data. *Geochemistry, Geophysics, Geosystems*, 8, Q08006 doi:10.1029/2006GC001492.
- Scoates, J.S., and Friedman, R.M., 2008. Precise age of the plantiferous Merensky Reef, Bushveld Complex, South Africa, by the U-Pb ID-TIMS chemical abrasion technique. *Economic Geology*, 103, 465-471.
- Sigloch, K., and Mihalynuk, M.G., 2013. Intra-oceanic subduction shaped the assembly of Cordilleran North America. *Nature*, 496, 50-56.
- Sigloch, K., and Mihalynuk, M.G., 2017. Mantle and geological evidence for a Late Jurassic-Cretaceous suture spanning North America. *Geological Society of America Bulletin*, 129, 1489-1520.
- Souther, J.G., 1971. Geology and mineral deposits of Tulsequah map-area, British Columbia. Geological Survey of Canada, Memoir 362, 84 p.
- Spell, T.L., and McDougall, I., 2003. Characterization and calibration of $^{40}\text{Ar}/^{39}\text{Ar}$ dating standards. *Chemical Geology*, 198, 189-211.
- Steiger R.H., and Jäger E., 1977. Subcommission on geochronology: convention on the use of decay constants in geo- and cosmochronology. *Earth and Planetary Science Letters*, 36, 359-362.
- Stern, R., 1997. The GSC Sensitive High Resolution Ion Microprobe (SHRIMP): Analytical techniques of zircon U-Th-Pb age determinations and performance evaluation. In: *Radiogenic Age and Isotopic Studies*, Report 10, Geological Survey of Canada, Current Research 1997-F, pp. 1-31.
- Stern, R.A., and Amelin, Y., 2003. Assessment of errors in SIMS zircon U-Pb geochronology using a natural zircon standard and NIST SRM 610 glass. *Chemical Geology*, 197, 111-142.
- Stone, J., 1987. Review of investigative techniques used in the study of conodonts. In: *Conodonts: Investigative Techniques and Applications*, British Micropalaeontological Society Series, pp. 17-34.
- Tejada, M.L.G., Mahoney, J.J., Duncan, R.A., and Hawkins, M.P., 1996. Age and geochemistry of basement and alkalic rocks of Malaita and Santa Isabel, Solomon Islands, southern margin of Ontong Java Plateau. *Journal of Petrology*, 37, 361-394.
- Tempelman-Kluit, D.J., 1978. Reconnaissance geology, Laberge map-area, Yukon. In: *Current Research, Part A*, Geological Survey of Canada, Paper 78-1A, pp. 61-66.
- Tempelman-Kluit, D.J., 1984. Geology, Laberge (105E) Carmacks (115I), Geological Survey of Canada, Open File 1101.
- Thorstad, L.E., and Gabrielse, H., 1986. The Upper Triassic Kutcho Formation, Cassiar Mountains, north-central British Columbia. Geological Survey of Canada, Paper 86-16, 53 p.
- Watson, K.D., and Mathews, W.H., 1944. The Tuya-Teslin area, northern British Columbia. British Columbia Department of Mines, Bulletin 19, 52 p.
- Wheeler, J.O., 1961. Whitehorse map-area, Yukon Territory, 105D. Geological Survey of Canada, Memoir 312, 156 p.

- Wheeler, J.O., Brookfield, A.J., Gabrielse, H., Monger, J.W.H., Tipper, H.W., and Woodsworth, G.J., 1988. Terrane map of the Canadian Cordillera. Geological Survey of Canada, Map 1712A.
- Woodsworth, G.J., Anderson, R.G., Armstrong, R.L., Struik, L.C., and van der Heyden, P., 1992. Plutonic regimes. In: *Geology of the Cordilleran Orogen in Canada, Geology of North America, Volume G-2*, pp. 493-531.
- Young, J.W., 1948. The relationship between lamprophyre dykes and ore deposits with special reference to British Columbia. Unpublished M.A.Sc. thesis, The University of British Columbia, 184 p.
- Youngquist, W., Hawley, R.W., and Miller, A.K., 1951. Phosphoria conodonts from southeastern Idaho. *Journal of Paleontology*, 25, pp. 356-364.
- Zagorevski, A., Mihalynuk, M.G., Joyce, N., and Anderson, R.G., 2017. Late Cretaceous magmatism in the Atlin-Tagish area, northern British Columbia (104M, 104N). In: *Geological Fieldwork 2016*, British Columbia Ministry of Energy and Mines, British Columbia Geological Survey Paper 2017-1, pp. 133-152.
- Zagorevski, A., Mihalynuk, M.G., McGoldrick, S., Bedard, J.H., Golding, M., Joyce, N., Canil, D., Corriveau, A.-S., Bogatu, A., Lawley, C., and Tremblay, A., 2016. Geological framework of ancient oceanic crust in northwestern British Columbia and southwestern Yukon GEM 2 Cordillera, Geological Survey of Canada, Open File 8140, 15 p.

Geology of the Decar area north of Trembleur Lake, NTS 93K/14



Dejan Milidragovic^{1, a}, Ryan Grundy^{1, 2}, and Paul Schiarizza¹

¹British Columbia Geological Survey, Ministry of Energy, Mines and Petroleum Resources, Victoria, BC, V8W 9N3

²School of Earth and Ocean Sciences, University of Victoria, Victoria, BC, V8W 3P6

^acorresponding author: Dejan.Milidragovic@gov.bc.ca

Recommended citation: Milidragovic, D., Grundy, R., and Schiarizza, P., 2018. Geology of the Decar area north of Trembleur Lake, NTS 93K/14. In: Geological Fieldwork 2017, British Columbia Ministry of Energy, Mines and Petroleum Resources, British Columbia Geological Survey Paper 2018-1, pp. 129-142.

Abstract

Upper Paleozoic to Lower Jurassic deformed rocks of the Cache Creek terrane in the Decar area, central British Columbia, include partly to completely serpentinized or carbonate-altered mantle tectonite (Trembleur ultramafite), flanked on both sides by predominantly argillaceous and siliceous fine-grained sedimentary rocks and aphanitic mafic volcanic rocks of the Sowchea succession and Sitlika assemblage. The volcano-sedimentary units have been metamorphosed at greenschist-facies as evidenced by actinolite-chlorite-epidote mineral assemblages in the metabasalts. Minor wacke, marble, and conglomerate are interbedded with the fine-grained metasedimentary rocks. The highest metamorphic grade (amphibolite facies) in the area are in the Rubyrock igneous complex, a Late Permian predominantly gabbro-dioritic intrusive complex that may represent the crustal portion of a dismembered ophiolitic sequence, formed above the harzburgite and lesser dunite of the Trembleur ultramafite. The entire Decar area displays a strong, relatively uniform, steeply dipping, northwest-striking structural fabric that may reflect regional northeast-southwest directed shortening during the collision of the Cache Creek terrane with Stikinia.

Keywords: Cache Creek terrane, Decar, awaruite, Trembleur, ultramafite, ophiolite

1. Introduction

The Cache Creek terrane of the North American Cordillera (Fig. 1) is a belt of tectonically imbricated Paleozoic and Mesozoic oceanic rocks, including volcanic and volcanoclastic rocks, chert, argillite, carbonate, conglomerate, and wacke, and ultramafic mantle tectonite with associated mafic plutonic rocks (Monger, 1977; English and Johnston, 2005; Nelson et al., 2013). Recently, Britten (2017) reported coarse-grained (>200 μm) awaruite (Ni_3Fe) mineralization of potential economic significance in Cache Creek ultramafic rocks on the Decar property, approximately 90 km northwest of Fort St. James in central British Columbia. Finer grained awaruite mineralization is also associated with ultramafic rocks of the northern Cache Creek terrane (Britten, 2017). Awaruite is ubiquitous in serpentinized ultramafic rocks (e.g., Nickel, 1956; Chamberlain et al., 1965; Ahmed and Bevan, 1981; Beard and Hopkinson, 2000; Klein and Bach, 2009) and the physicochemical conditions that lead to its early development are relatively well known (Frost, 1985; Sleep et al., 2004; Frost and Beard, 2007; Foustoukos et al., 2015). However, coarse-grained (>200 μm) mineralization is relatively uncommon (e.g., Sciortino et al., 2015; Britten, 2017), and how economically viable, coarse-grained awaruite deposits form is poorly understood.

Rocks of the Cache Creek terrane are widely regarded as a tectonically juxtaposed mix of: 1) oceanic lithosphere from varied and disparate paleoenvironments; and 2) subduction-

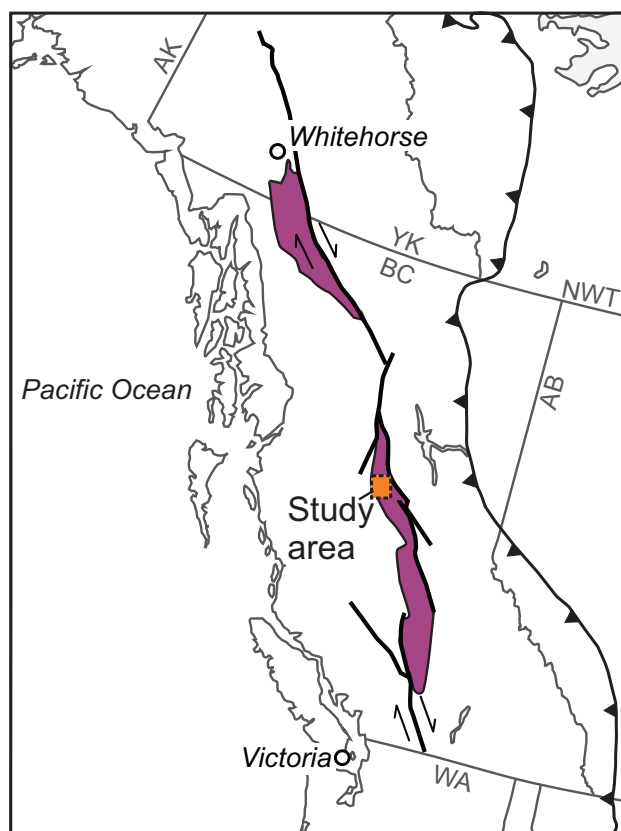


Fig. 1. Location of the study area and distribution of Cache Creek terrane (purple) in the Canadian Cordillera.

related volcanic and sedimentary rocks deposited in a forearc setting (Mihalynuk et al., 1994; Struik et al., 2001; English and Johnston, 2005; English et al., 2010). However recently, McGoldrick et al. (2017) suggested that original stratigraphic relationships in Cache Creek rocks of northwestern British Columbia are preserved, and argued for a genetic link between mantle tectonite and overlying arc basalts, placing them in a supra-subduction zone tectonic setting that is distinct from the intraoceanic setting indicated by ocean island basalt (OIB)-type volcanic rocks intercalated with thick carbonate successions. Accordingly, the Cache Creek terrane in northwestern British Columbia may consist of two fundamentally different and mappable domains: 1) intraoceanic carbonate and intraplate volcanic rocks and 2) an upper plate assemblage of arc mantle lithosphere, mafic and ultramafic cumulates, and related volcanic and sedimentary rocks (ophiolite).

At present, understanding of the stratigraphy and tectonic evolution of the Cache Creek terrane in central and southern British Columbia lags behind that of the Cache Creek terrane in northwestern British Columbia and Yukon. Thus, we undertook a 1:50,000 mapping and sampling project in the area of the Decar occurrence (part of Trembleur Lake, NTS 93K/14) to update existing geological maps, understand the petrological evolution of the mantle tectonite that hosts the prospective awaruite mineralization, and develop a chemostratigraphic framework for the Permo-Triassic volcanic and related intrusive rocks. Herein, we describe the preliminary results of this mapping and provide petrographic descriptions of the principal rock types.

2. Geological setting

The Cache Creek terrane is a ~1500 km-long belt of oceanic rocks exposed along the central axis of British Columbia (Fig. 1; Monger, 1977; Nelson et al., 2013). It records deposition of vast carbonate platforms, lesser ribbon chert, argillite, and coarse siliciclastic rocks, build-up of basaltic oceanic plateaus and seamounts, and emplacement of mafic to intermediate intrusive rocks (Monger, 1975; Mihalynuk et al., 1999; Struik et al., 2001; English et al., 2010). This activity is temporally bracketed by the Upper Mississippian foraminifera of the Kedahda Formation near Atlin (Monger, 1975) and the Middle Jurassic collision of the Cache Creek terrane with Stikinia (ca. 172 Ma), as defined by the oldest postkinematic intrusions in the Cache Creek terrane (Mihalynuk et al., 2004). Paleozoic to Middle Triassic macrofossils and microfossils with Tethyan affinities indicate that the Cache Creek terrane was in the Panthalassan Ocean, far from the North American continent, during most of its ≥ 160 m.y. existence (Monger and Ross, 1971; Orchard et al., 2001). A key feature of the Cache Creek terrane is the widespread occurrence of ultramafic rocks (Tardy et al., 2001; Lapierre et al., 2003; English et al., 2010; McGoldrick et al., 2016), interpreted to have originated as lithospheric mantle beneath the Cache Creek ocean that was emplaced as tectonic slivers.

The current tectonostratigraphic framework for Cache Creek

terrane in central British Columbia is based on 1:100,000-scale mapping by the Geological Survey of Canada and the British Columbia Geological Survey between 1995 and 2000 (MacIntyre and Schiarizza, 1999; Schiarizza and MacIntyre, 1999; Struik et al., 2001, 2007). The terrane includes three structurally disrupted components: 1) the Cache Creek complex 2) the Sitlika assemblage, which is typically found structurally beneath ophiolitic rocks of the Cache Creek complex in the western part of the terrane, and includes a Permo-Triassic intra-oceanic arc complex and an unconformably overlying Late Triassic-Early Jurassic siliciclastic succession; and 3) the Tezzeron succession, a Late Triassic-Early Jurassic siliciclastic unit along the eastern edge of the terrane, adjacent to the Quesnel arc terrane.

The Cache Creek complex, forming most of the Cache Creek terrane in central British Columbia, is subdivided into numerous subunits, commonly juxtaposed across Early to Middle Jurassic thrust faults and/or younger structures (Struik et al., 2001). The central and eastern parts of the complex consist mainly of rocks that probably accumulated as an accretionary complex (Struik et al., 2001). This part of the complex includes the Sowchea succession, consisting of Pennsylvanian-Early Jurassic fine-grained siliceous sedimentary rocks (cherty argillite and slate to muddy chert), with lesser limestone, greywacke, basalt, andesite, and conglomerate containing intraformational siltstone clasts. It also includes several carbonate rock-rich units, including: Pennsylvanian-Early Permian carbonate rocks with local thin basaltic breccia, volcanoclastic rocks, and ribbon chert (Pope succession); Middle-Late Permian micritic and bioclastic limestone (Copley succession); and Permian-Triassic limestone, limestone breccia, shale, and basaltic tuff (Kloch Lake succession). Other subunits of the Cache Creek Complex, found mainly to the west, are interpreted as components of a dismembered ophiolite (e.g., Boudier and Nicolas, 1985). These include: 1) harzburgite and lesser dunite, pyroxenite, and peridotite (Trembleur ultramafite), which display variable amounts of serpentinization, and calc-silicate alteration; 2) greenschist-facies mafic to ultramafic, altered and variably deformed intrusive and volcanic rocks assigned to the Rubyrock igneous complex; and 3) basalt and chert units, locally cut by mafic dikes and sills, that are spatially associated with the Trembleur ultramafite (North Arm succession of Schiarizza and MacIntyre, 1999, and MacIntyre and Schiarizza, 1999).

3. Geology of the Decar area

Our mapping in the Decar area (Fig. 2) reveals that the central part is underlain by ophiolitic rocks of the Cache Creek complex, including the Trembleur ultramafite and the Rubyrock igneous complex. To the southwest are siliciclastic rocks that belong to the upper part of the Sitlika assemblage (Upper Triassic-Lower Jurassic; MacIntyre and Schiarizza, 1999; Schiarizza and MacIntyre, 1999). Following Struik et al. (2001) we assign a basalt-chert unit, flanking the ultramafic rocks to the northeast, to the Sowchea succession. This unit was included in the North Arm succession (of suspected ophiolite affinity) by Schiarizza

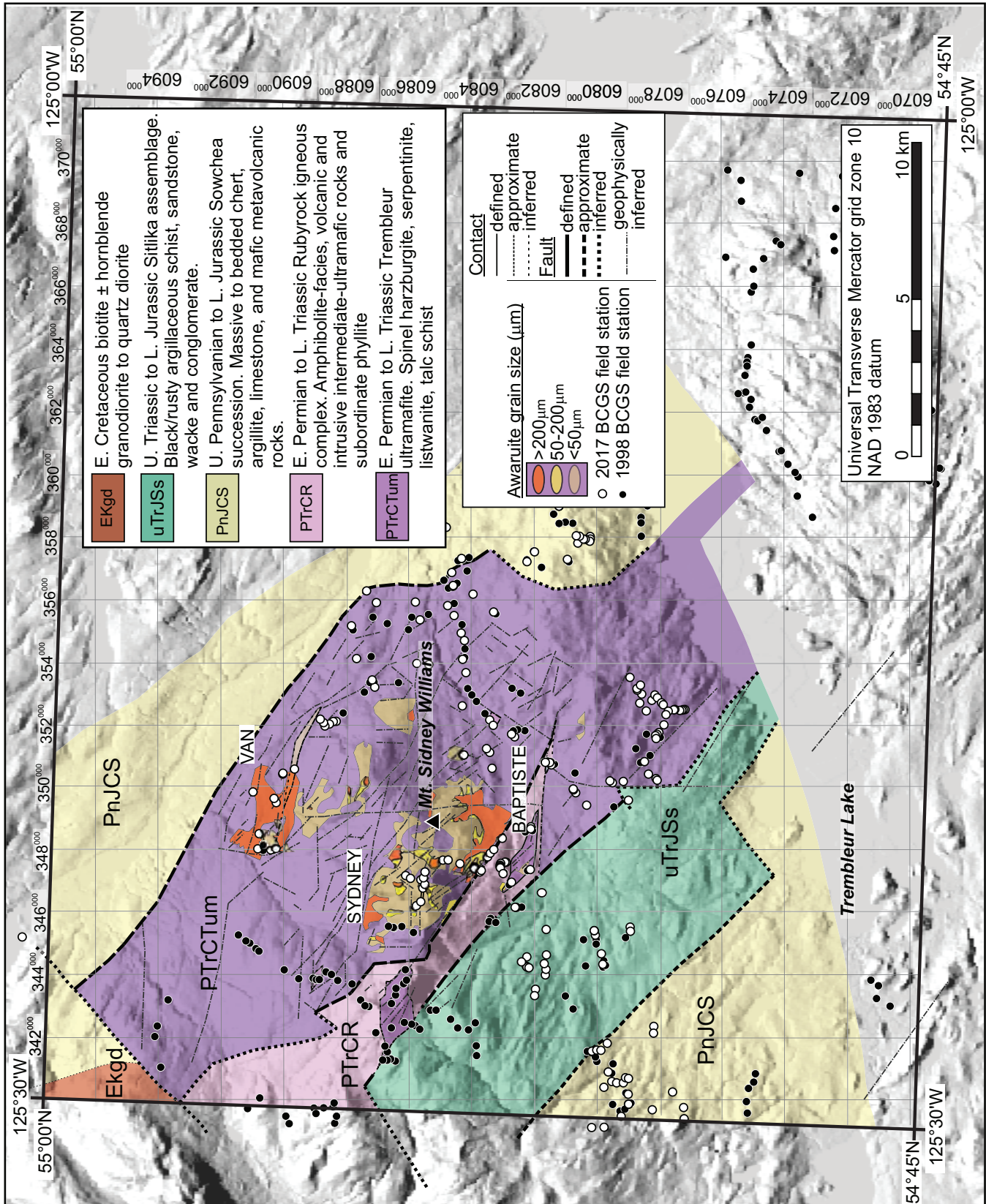


Fig. 2. Preliminary geology of the Decar area north of Trembleur Lake (93K/14).

and MacIntyre (1999) and MacIntyre and Schiarizza (1999). We also mapped a sedimentary-volcanic succession adjacent to the Sitlika assemblage in the southwestern part of the study as Sowchea succession because it is very similar to rocks exposed to the northeast. Previously, these rocks, specifically a unit of mafic sills and dikes with abundant screens of basalt and chert that was interpreted as transitional between the predominantly intrusive Rubyrock complex and the predominantly supracrustal North Arm succession (Schiarizza and MacIntyre, 1999; MacIntyre and Schiarizza, 1999), were included in the Rubyrock igneous complex. Although the contact between the Sitlika assemblage and the Sowchea succession is not exposed, it is interpreted to be structural. The structural juxtaposition of the two units is supported by the increase in the relative intensity of deformation near the contact, and the sharp transition from rocks with relatively high magnetic signatures to the southwest to rocks with relatively low magnetic signatures to the northeast, which follows the regional structural fabric (Struik et al., 2007) and coincides with the inferred fault contact.

Peridotite of the Trembleur ultramafite is weakly to strongly altered to either serpentinite or listwanite (magnesite \pm serpentine \pm talca \pm quartz; Hansen et al., 2005). Locally, serpentinitized peridotite hosts significant coarse-grained (50-400 mm) awaruite (Ni_3Fe), which Britten (2017) attributed to relatively late, fracture- or shear zone-focused, high-temperature ($\geq 400^\circ\text{C}$) serpentinitization (antigorite-lizardite) accompanied by growth of metamorphic olivine after Cache Creek terrane accreted to North America.

The Rubyrock igneous complex is structurally interleaved with the western part of the Trembleur ultramafite and is widely regarded (Schiarizza and MacIntyre, 1999; Struik et al., 2001; Britten, 2017) as the crustal portion of the ophiolite. The only age from the complex is 257 ± 5 Ma, obtained from a tonalite lens (unpublished TIMS U-Pb zircon date; Struik et al., 2001; Struik et al., 2007).

4. Main rock types

4.1. Trembleur ultramafite

4.1.1. Peridotite

Weakly serpentinitized peridotite is exposed in moderately to sparsely vegetated, elevated regions on Mount Sydney Williams and the unnamed ridge to the northeast (Fig. 2). The peridotite weathers yellow-brown to grey (Figs. 3a-b), and is dark grey to black on fresh surface. The dark fresh surface and weak to moderate magnetic susceptibility of the peridotite reflect microscopic secondary magnetite formed during serpentinitization. Warty textured, medium- to coarse-grained massive harzburgite, containing trace amounts of clear clinopyroxene (~1%) and medium brown spinel ($\leq 2\%$), is the most common peridotite lithology. Individual olivine crystals are generally not discernible in hand sample, whereas orthopyroxene crystals exhibit strong cleavage and light grey alteration (bastite), which ranges from a thin surficial coating to nearly complete replacement in highly serpentinitized harzburgite. In thin section, olivine crystals are ≤ 3 mm across,

display kink banding and/or undulose extinction, and have curvilinear grain boundaries. Orthopyroxene porphyroclasts are typically coarser (≤ 5 mm) and more euhedral than olivine. Exsolution of clinopyroxene along orthopyroxene cleavage planes is common and some grains display deformation of the exsolution lamellae. Orthopyroxene grains that are nearly completely bastite-altered usually have rims of black secondary spinel that increase in width with increasing degrees of serpentinitization. Clinopyroxene is not discernible in hand sample, but is distinguished from orthopyroxene in thin section by smaller grain size and cleavage-parallel exsolution of ubiquitous, thin, closely-spaced (< 10 mm) laminae of secondary spinel (Figs. 3c-e). Primary spinel is characteristically irregular, with a vermicular, interstitial habit (Fig. 3f), and commonly displays holly-leaf texture within orthopyroxene porphyroclasts. Primary spinels in the least serpentinitized samples are medium brown to dark red and, with increasing degrees of serpentinitization become black along grain boundaries, likely from magnetite alteration. Sulphide occurs in trace quantities as very small (< 10 mm) subhedral crystals. Harzburgite typically has a massive appearance (protogranular according to the classification of Mercier and Nicolas, 1975), but locally displays layers of coarser or modally more abundant orthopyroxene. Smooth weathering pods and dikes of replacive dunite (Kelemen and Dick, 1995) are relatively uncommon and are typically in sharp contact with their harzburgite host (Fig. 3b). Rare, thin (< 5 cm) dikes of coarse-grained pyroxenite, which locally cut harzburgite, are discordant, and have variable orientation.

4.1.2. Serpentinite

Pervasively ($> 90\%$) serpentinitized peridotite is ubiquitous in the Trembleur ultramafite, forming large homogeneous outcrops, crosscutting less serpentinitized harzburgite, or forming knockers within bodies of listwanite (Figs. 4a-c; 5a). Serpentinite weathers grey-brown, through grey, to light green and typically displays a moderate to strong schistosity, although it may also appear massive. Earliest serpentinitization is marked by growth of lizardite, indicated by hour-glass and mesh textures (e.g., Evans et al., 2013) in the least serpentinitized peridotites, and magnetite. The hour-glass and mesh textures are not evident in more completely serpentinitized peridotites, which feature fibrous to tabular interlocking serpentine, interpreted to be antigorite. Growth of high-relief, fine-grained, metamorphic olivine along serpentine microveinlets is interpreted as the latest and highest temperature alteration of the Trembleur ultramafite. Sample DMI17-10-1 (Figs. 4d-f), collected from the Baptiste deposit (Fig. 2), displays a texture in which the convergence of chrysotile veinlets, lined with olivine, defines 'cores' of antigorite that are mantled by metamorphic olivine. In addition to texture, metamorphic olivine is distinguished from primary mantle olivine by its dark to cloudy appearance in plane-polarized light, and its fine grain size. Identification of metamorphic olivine in Trembleur serpentinite, confirms its previous recognition by Britten (2017). Although awaruite

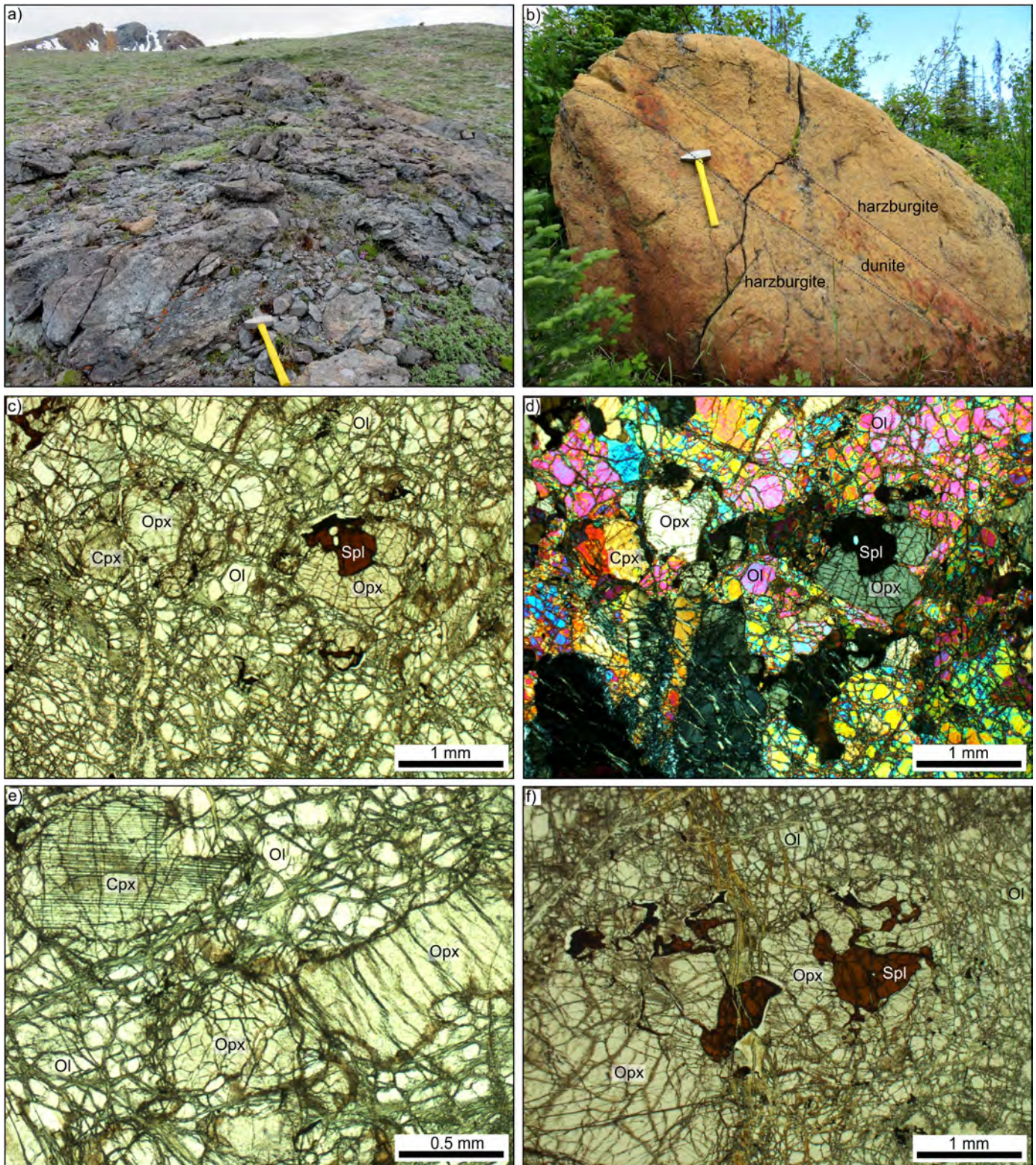


Fig. 3. **a)** An outcrop of harzburgite on the southeast-facing flank of Mount Sidney Williams. The heavily diked central peak is in the background. **b)** A large boulder of yellow-brown weathering harzburgite cut by a ~20 cm wide, smooth-weathering, tabular dunite dike. **c)** Plane-polarized light image of harzburgite 98PSC-33-5 collected from the westernmost peak of Mount Sidney Williams. **d)** Cross-polarized light image of harzburgite 98PSC-33-5. **e)** Plane-polarized light image of a clinopyroxene crystal with thin lamellae of oxide mineral(s) exsolved along cleavage planes. **f)** Plane-polarized light image of irregular, vermicular, spinel crystals intergrown with orthopyroxene. Abbreviations: Ol-olivine, Opx-orthopyroxene, Cpx-clinopyroxene, Spl-spinel.

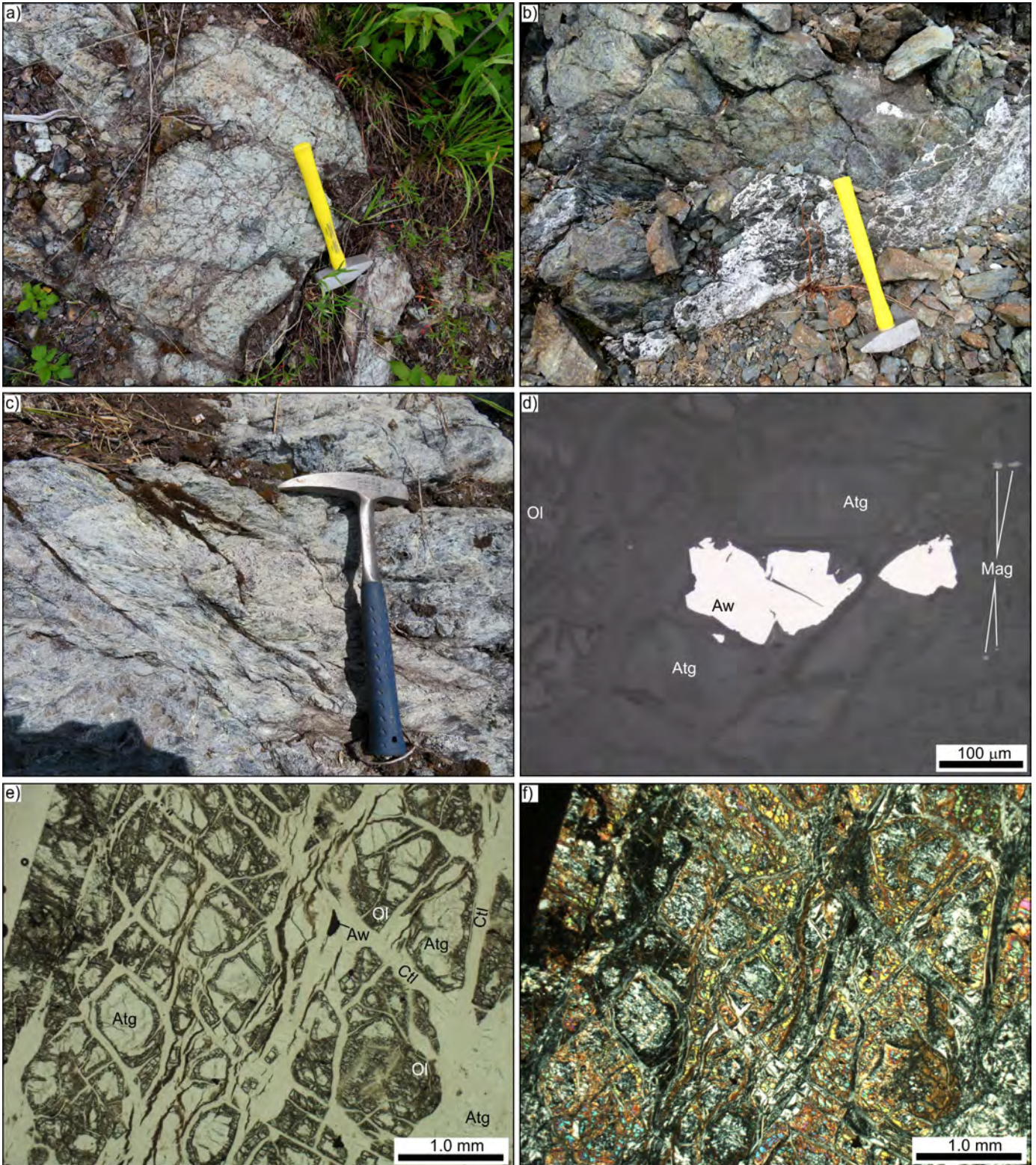


Fig. 4. a) An outcrop of light grey-weathering, homogeneous, serpentinite. b) Dark grey-green-weathering serpentinite cut by a white-weathering breccia. c) Strongly schistose, light grey- to green-weathering serpentinite. d) Reflected light image of anhedral awaruite (Aw) surrounded by antigorite. Higher relief grains on the left side of the image are olivine. e) Plane-polarized light image of sample DMI17-10-1 showing metamorphic olivine growing along microveinlets of serpentinite (antigorite and/or chrysotile) converging to form 'rims' around antigorite. f) Cross-polarized light image of the same sample DMI17-10-1 (same field of view as e). Abbreviations: Atg-antigorite, Mag-magnetite, Aw-awaruite, Ctl-chrysotile, Ol-olivine.

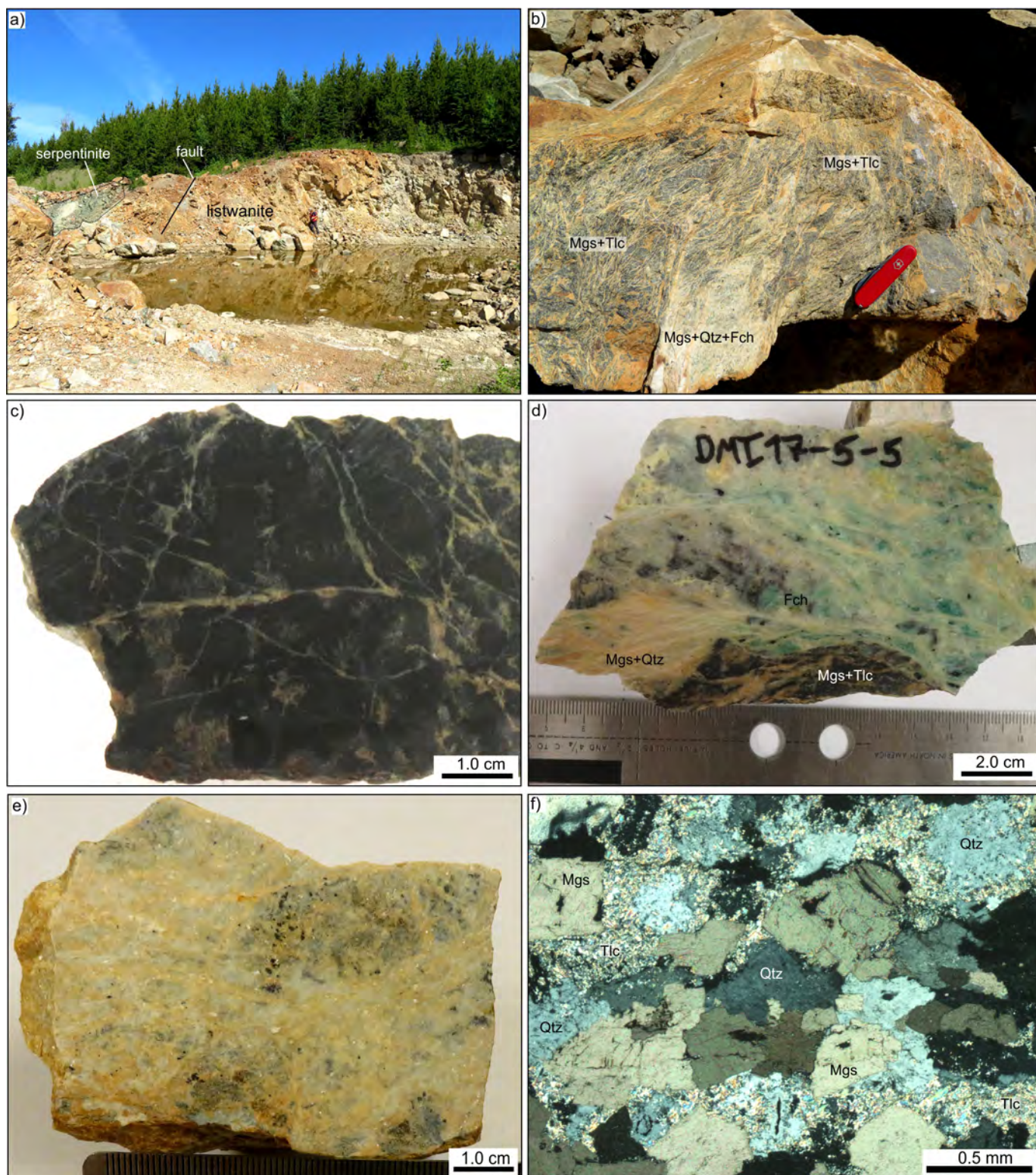


Fig. 5. a) Pit exposing mainly rusty-weathering listwanite; also m-scale knockers of green-weathering serpentinite. **b)** Heterogeneous listwanite comprising a dark heavily veined (Mgs+Tlc) domain and a more massive, lighter coloured (Mgs+Qtz+Fch) domain. Magnesite veins in the Mgs+Tlc domain show no preferred alignment. **c)** Hand sample of dark listwanite consisting of magnesite veins, serpentine and talc. **d)** Heterogeneous listwanite with dark domains of Mgs+Tlc and lighter domains of Mgs+Qtz. The conspicuous green colour is due to fine grained fuchsite. **e)** Heavily carbonitized listwanite largely composed of magnesite and quartz. Dark domains may contain relict talc. The dark, euhedral, fine-grained mineral is specular hematite. **f)** Cross-polarized light image of listwanite sample 98PSC-16-6 showing the incomplete carbonation of talc through reaction $Mg_3Si_4O_{10}(OH)_2 + 3CO_2 = 3MgCO_3 + 4SiO_2 + H_2O$ (Hansen et al., 2005). Abbreviations: Mgs-magnesite, Qtz-quartz, Tlc-talc, Fch-fuchsite.

likely formed from the onset of serpentinization (Frost and Beard, 2007; Klein and Bach, 2009), grains sufficiently large for field identification (>100-200 mm) only occur in samples containing antigorite +/-olivine.

4.1.3. Listwanite

Ultramafic rocks in the southeastern and eastern portion of the Trembleur ultramafite (Fig. 2) are extensively CO₂ altered. We apply the term 'listwanite' to all such rocks, following the definition of Hansen et al. (2005). Listwanite is characterized by ubiquitous magnesite, relatively low magnetic susceptibility, and rusty orange-weathering (Fig. 5a). The rusty orange-weathering likely reflects the presence of an ankeritic component in the magnesite, as suggested by Schiarizza and MacIntyre (1999). Significant variations in colour, texture, and hardness occur on hand-sample scale (Figs. 5b-c), reflecting different mineral assemblages including: serpentine-magnesite, talc-magnesite, and quartz-magnesite end members (Figs. 5b-f). High-standing knobs and ridges in the southeastern part of the Trembleur ultramafite are predominantly composed of magnesite and quartz-rich listwanite, hardened by extensive carbonation of serpentine, brucite, and talc. Listwanite also contains minor relict magnetite and may also contain fine-grained, disseminated, emerald green fuchsite, found exclusively with quartz±pyrite±specular hematite.

4.2. Intrusive rocks

Mafic to intermediate intrusive rocks form a major component of the Rubyrock igneous complex, southwest of the Trembleur ultramafite, and occur as small plugs and dikes which intrude and crosscut the ophiolitic and volcano-sedimentary units in the study area. The metaintrusive rocks of the Rubyrock igneous complex (Figs. 6a and b) are interleaved with probable metavolcanic and minor metasedimentary rocks (see section 4.3.2.) and separated from pervasively serpentinized, coarse awaruite-bearing (Baptiste deposit) rocks of the Trembleur ultramafite by a northwest-striking fault. The fault is also marked by a sharp contrast in total field magnetic response between the highly magnetic rocks of the Trembleur ultramafite, and the less magnetic rocks of the Rubyrock igneous complex (Verley, 2011).

Before amphibolite-facies metamorphism, the intrusive rocks of the Rubyrock intrusive suite were predominantly gabbro and diorite, with lesser clinopyroxenite±hornblendite. On the west side of Mount Sidney Williams (Fig. 2), they typically display a strong fabric (Fig. 6a), defined by aligned amphibole and cm- to dm-scale plagioclase-rich and amphibole-poor layers and lenses (Fig. 6b). Accessory titanite and clinozoisite are important metamorphic phases of the Rubyrock intrusive suite.

Homogeneous mafic to felsic intrusive rocks that have not undergone significant metamorphism outcrop throughout the study area and include fine-grained diabase dikes, isolated gabbroic plugs (Fig. 6c), and small felsic bodies with abundant rusty ankerite patches. The relationship between these bodies is uncertain, but they crosscut the ultramafic and volcano-

sedimentary units. An Early Cretaceous granodiorite pluton outcrops in the northwest corner of the study area (Struik et al., 2007), but was not sampled.

4.3. Layered rocks

4.3.1. Metavolcanic rocks

Volcanic rocks, of predominantly basaltic composition are prominent components of the Sowchea succession in both the eastern and western parts of the study area, and of the Rubyrock igneous complex (Fig. 2). They occur as both aphanitic volcanic flows and breccias, locally interbedded with lenses of metasedimentary rock. Primary mineralogy of the volcanic rocks has been extensively obliterated by greenschist facies metamorphism, resulting in light grey to green, weakly to strongly schistose, locally pyritiferous, actinolite-chlorite-epidote rocks (Figs. 7a and b). Amygdules and irregular veinlets, occupied by carbonate, chlorite and/or epidote, are typically the only macroscopic features of the aphanitic rocks (Fig. 7c). Rarely, aphanitic basalts contain plagioclase phenocrysts (Fig. 7d); clinopyroxene phenocrysts have not been observed. Fragmental volcanic rocks are common in both units (Figs. 7e and f).

Volcanic rocks observed in the study area do not display significant petrographic and textural differences. However, English et al. (2010) and McGoldrick et al. (2017) have demonstrated that the geochemical variability of volcanic rocks of the northern Cache Creek terrane may be used for petrological classification, and gaining new insights into the tectono-magmatic evolution of the Cache Creek terrane. These studies identified calcalkaline basalts and island arc tholeiites (IAT), in addition to basalts that span the MORB-OIB (mid-ocean ridge basalt-ocean island basalt) array (Pearce, 2008), adding new complexity to the geodynamic interpretations of the Cache Creek terrane. The relatively few geochemical analyses from the Cache Creek terrane in central British Columbia (Tardy et al., 2001; Lapierre et al., 2003), display a similar degree of variability (McGoldrick et al., 2017), suggesting that, despite the metamorphic overprint and similarities in field appearance, geochemical discrimination is an effective tool for assigning metavolcanic rocks in the study area to lithostratigraphic units. Geochemical analyses of 17 volcanic samples from the study area are ongoing.

4.3.2. Metasedimentary rocks

Metasedimentary rocks occur in the Sowchea succession and the Sitlika assemblage. Both units comprise predominantly fine-grained sedimentary rocks with moderately to well-developed cleavage. The field criteria used to distinguish the two units are the higher relative chert content of the Sowchea metasedimentary rocks versus the more argillaceous nature of the Sitlika assemblage metasedimentary rocks, and the high relative abundance of mafic metavolcanic rocks in the Sowchea succession. In addition, phyllite, chert, and highly fissile siltstone (Fig. 8f) are interlayered as possible rafts/enclaves with mafic metavolcanic and/or metaintrusive rocks

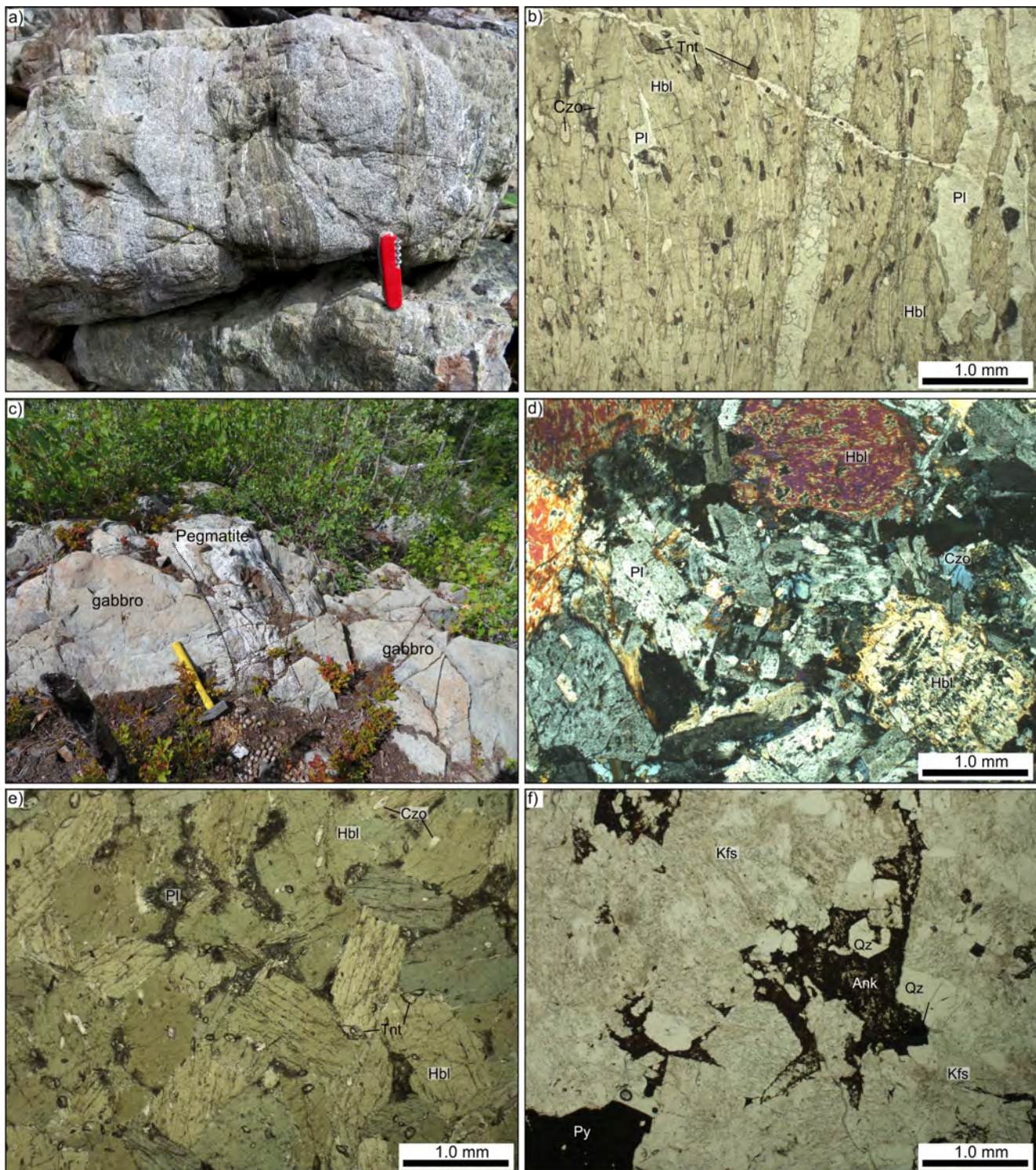


Fig. 6. **a)** Strong fabric in amphibolite-facies metamorphosed intrusive rocks of the Rubyrock igneous complex. Discontinuous lenses of amphibolite are hosted by predominantly plagioclase-rich metagabbro and metadiorite. **b)** Plane-polarized light image of sample 98PSC-14-10-1 collected from a). Strong metamorphic fabric is defined by aligned hornblende crystals and segregations of hornblende and plagioclase. Titanite and clinozoisite are important accessory phases. **c)** Massive gabbro cutting the Sowchea succession, east of Trembleur ultramafite cut by pegmatite. **d)** Cross-polarized light image of a sample DMI17-15-7, from gabbro in c). Clinopyroxene has been pervasively replaced by hornblende, plagioclase is partly saussuritized, and metamorphic clinozoisite is ubiquitous. **e)** Plane-polarized light image of isotropic amphibolite 98PSC-33-91 of the Rubyrock igneous complex, containing interstitial saussuritized plagioclase and accessory clinozoisite and titanite. **f)** Plane-polarized light image of massive quartz syenite DMI17-15-3, which intrudes the Trembleur ultramafite near its eastern contact with the Sowchea succession. The rock is rich (~20%) in rusty weathering carbonate (ankerite) and contains ~3 mm crystals of euhedral pyrite. Abbreviations: Hbl-hornblende, Pl-plagioclase, Czo-clinozoisite, Tnt-titanite, Kfs-K-feldspar, Ank-ankerite.

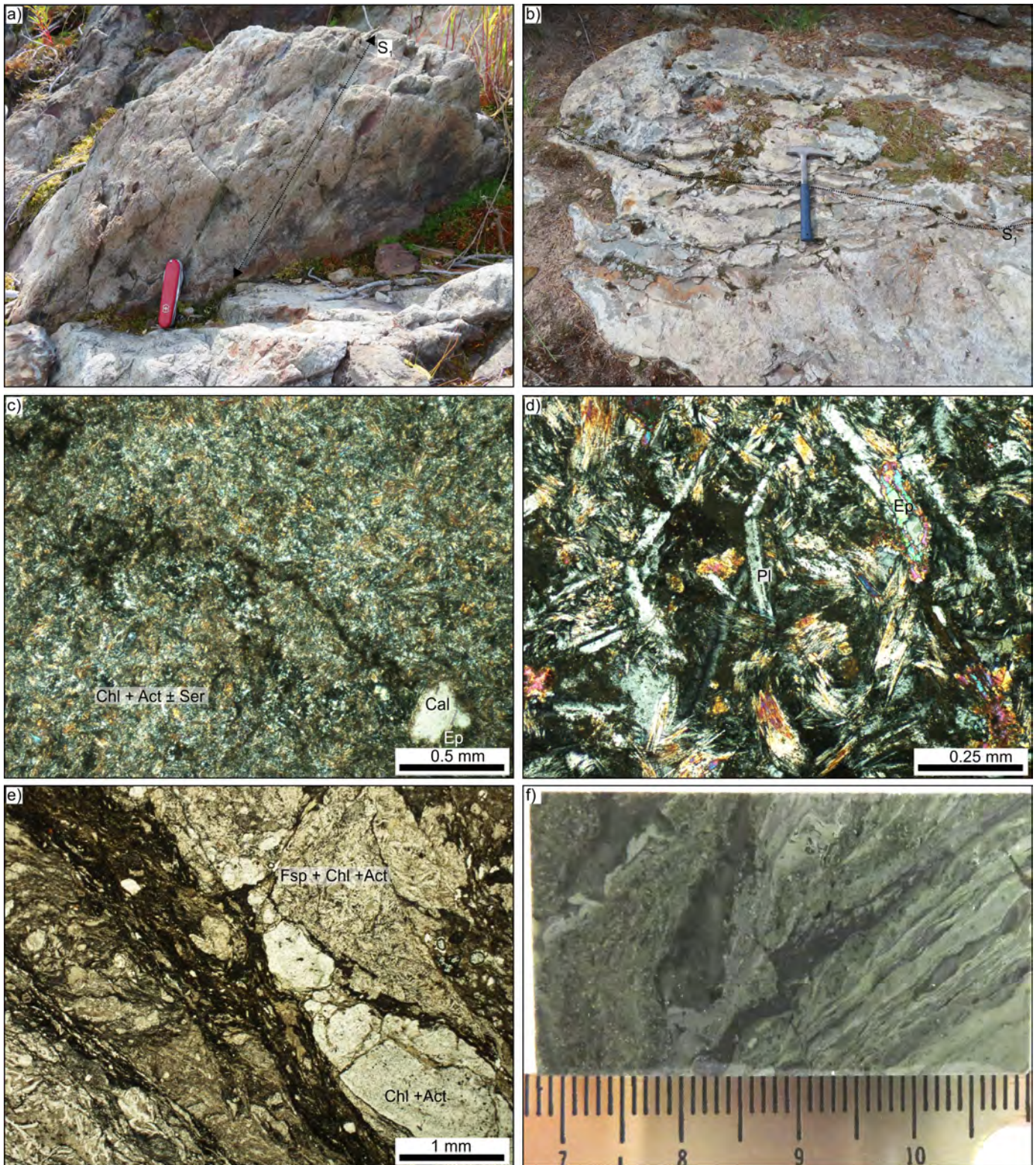


Fig. 7. **a)** Cream-weathering, moderately schistose (S.), chloritic metabasalt. **b)** Pink-cream-weathering, schistose (S.) aphanitic metabasalt. **c)** Cross-polarized light image of amygduloidal (calcite+epidote), aphanitic metabasalt (DMI17-1-2). Primary mineralogy has been largely replaced with fine intergrowths of actinolite, chlorite±sericite. **d)** Cross-polarized light image of plagioclase-phyric, aphanitic metabasalt (DMI17-2-15). Groundmass has largely been replaced by actinolite and dark sub-microscopic material. **e)** Plane-polarized light image of volcanic breccia (DMI17-8-5), showing possible flow foliation in the laminae of dark sub-microscopic material. Volcanic clasts are aphanitic to plagioclase porphyritic and composed of chlorite+actinolite±plagioclase. **f)** Polished slab of volcanic breccia (DMI17-1-10), showing well-developed laminae within a breccia fragment, interpreted as relict flow foliation.



Fig. 8. **a)** Dark, schistose meta-argillite of the Sitlika assemblage, interbedded with light-weathering, weakly-schistose, fine-grained sandstone. Local, discontinuous lamination is evident in the sandstone. Schistosity and bedding are parallel. **b)** Finely bedded meta-argillite of the Sitlika assemblage. Bedding and cleavage have steep, but opposing senses of dip. **c)** Monomictic limestone-cobble conglomerate of the Sitlika assemblage, with a medium- to coarse-grained, lithic-rich, sandstone matrix. Limestone clasts are rounded and typically oblate, and locally contain echinoderm macrofossils. Cleavage is well developed and steeply dipping. **d)** Argillaceous chert of the Sowchea succession with well-developed, bedding-parallel, steeply dipping cleavage. Bedding thickness decreases and argillaceous content increases to the left side of the photograph. **e)** Phyllitic schist of the Sowchea succession with steeply dipping cleavage. **f)** Interbedded dark-grey chert and highly-fissile pyritiferous phyllite of the Rubyrock igneous complex west of the Baptiste deposit.

of the Rubyrock igneous complex, west of the Trembleur ultramafite near the Baptiste deposit (Fig. 2). The local presence of chert suggests a possible Sowchea succession affinity of these relatively rare metasedimentary rocks. However, this correlation is speculative and masked by complexity induced by voluminous intrusion of mafic magma and the resulting relatively high metamorphic grade (amphibolite-facies).

4.3.2.1. Sitlika assemblage

The Sitlika unit consists of black to rusty-weathering, predominantly argillaceous schists, with lesser lithic-rich wacke, and local conglomerate (Figs. 8a-c). The schists contain thin alternating thin layers of siltstone and mudstone and bear a well-developed cleavage that is subparallel, or at low angle, to bedding (Fig. 8b). Less commonly, argillite is interbedded with fine-grained sandstone, which is itself locally laminated (Fig. 8a). Rusty-weathering conglomerate (Fig. 8c) contains rounded, oblate to discoidal pebbles and cobbles of fossiliferous limestone set in a medium- to coarse-grained lithic sandstone matrix.

4.3.2.2. Sowchea succession

Metasedimentary rocks are a significant component of two belts of rocks we assign to the Sowchea succession (Fig. 2) of Struik et al. (2001; 2007). The metasedimentary rocks are typically siliceous, and range in composition from massive chert, through banded ribbon chert, to finely-bedded cherty argillite (Figs. 8d-e). In the northeastern part of the study area, chert is massive and locally pyritiferous. In the southwestern belt, the fine-grained rocks are predominantly cherty, but are locally argillaceous. Our mapping indicates that, in the eastern part of the study area, metasedimentary rocks of the Sowchea succession may be less extensive than previously considered (cf., Struik et al., 2007) and may be subordinate to mafic metavolcanic rocks. Because rocks in the two belts are similar we reassign the rocks in the southwest that were previously included in the Rubyrock igneous complex (unit PTrCRgs of Struik et al., 2007) to the Sowchea succession.

4.3.2.3. Metasedimentary rocks in the Rubyrock igneous complex

Rusty weathering, grey-green, weakly magnetic phyllite outcrops on the southeast side of a northwest-trending brittle fault that juxtaposes it against highly magnetic, strongly serpentized, coarse awaruite-bearing metaperidotite of the Baptiste deposit (Fig. 2). Less than 1 km farther west, thin beds of dark grey chert, pyritiferous phyllite, and argillaceous schist are interlayered with light grey- to green-weathering, veined, chaotic amphibolite-facies metaintrusive and/or metavolcanic rocks, characteristic of the Rubyrock intrusive suite.

5. Structure

Previous mapping in the study area (MacIntyre and Schiarizza, 1999; Schiarizza and MacIntyre 1999; Britten, 2017) recognized a predominant subvertical northwest-

southeast trending fabric; our mapping confirms these observations (Figs. 9a and b). Bedding in both the Sowchea succession and the Sitlika assemblage is generally steep (Fig. 9a), dipping either northeast or southwest. A penetrative cleavage, either paralleling the steeply dipping beds or cutting them at a low angle, is best developed in meta-argillite of the Sitlika assemblage (Fig. 8b). Although less well developed, the orientation of cleavage in cherty metasedimentary rocks of the Sowchea succession is indistinguishable from that in the Sitlika assemblage. Moreover, the cleavage in metavolcanic rocks from both the Sowchea succession and Rubyrock igneous complex is identical in orientation to the cleavage in metasedimentary rocks. Minor folds typically plunge gently to the northwest; less commonly fold axes are steep or plunge to the southeast (Fig. 9b). Late deformation is locally manifested by a second, gently-dipping cleavage. Bedding and cleavage systematics of the metasedimentary rocks in the study area are consistent with NE-SW directed shortening.

A steeply dipping, northwest-striking brittle fabric, including spaced cleavage, thin zones (<30 cm) of fragmented carbonate-altered peridotite in a light grey, very fine-grained matrix (Fig. 9c), and zones of shear containing dm- to m-scale knockers of serpentinite in fine-grained foliated, talc±carbonate-rich matrix (Fig. 9d), is variably developed in the Trembleur ultramafic unit. Moreover, the Baptiste deposit, the largest and best studied prospect on the Decar property (Ronacher et al., 2013; Britten, 2017), is located along a major northwest-trending magnetic discontinuity (Verley, 2011) that juxtaposes coarse awaruite-bearing, fissile serpentinite against phyllitic sedimentary rocks, which are tentatively assigned to the sedimentary facies of the Rubyrock igneous complex. These structures are parallel to the predominant northwest-southeast fabric of the flanking volcanic-sedimentary successions.

6. Summary

The Cache Creek terrane in the Decar area of central British Columbia comprises variably serpentized and carbonate-altered mantle tectonite (Trembleur ultramafite), greenschist to amphibolite-facies mafic intrusive rocks and minor fine-grained sedimentary rocks (Rubyrock igneous complex), interlayered aphanitic volcanic flows, volcanic breccias, and cherty sedimentary rocks (Sowchea succession), and predominantly fine-grained siliciclastic sedimentary rocks (Sitlika assemblage). Volcano-sedimentary units are broadly subdivided into the predominantly volcanic, chert-rich Sowchea succession and the argillaceous, volcanic-free (Sitlika assemblage). This subdivision, however, must ultimately be confirmed by the geochemical affinity of volcanic units. A pervasive northwest-southeast trending fabric reflects significant northeast-southwest directed shortening, possibly during the collision between the Cache Creek terrane with Stikinia (Struik et al., 2001; English and Johnston, 2005).

Acknowledgments

We thank FPX Nickel Corp. for discussion and access to

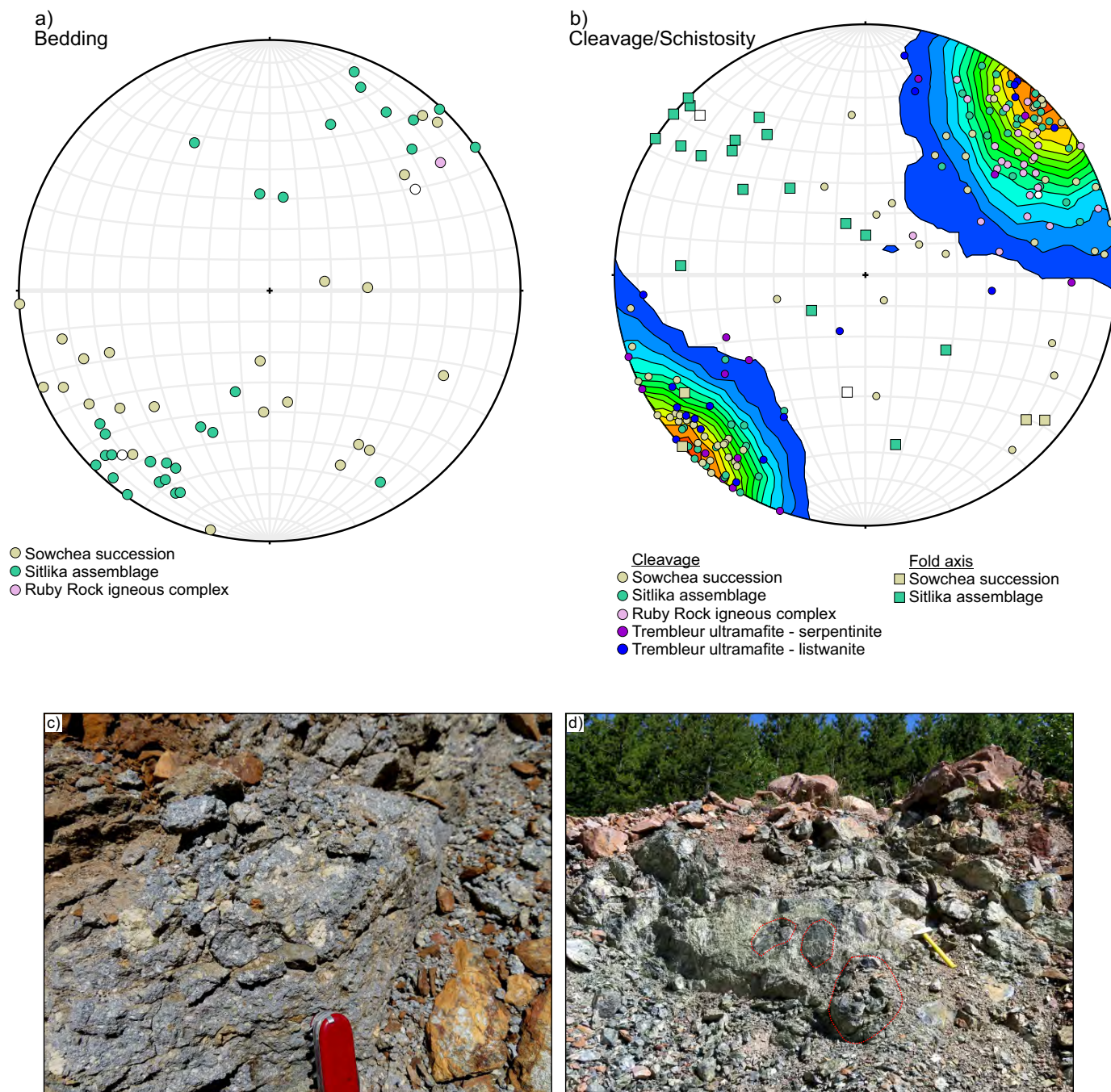


Fig. 9. Equal-area stereonet plots of poles to **a)** bedding and **b)** cleavage (with contours) and minor fold axes. Only the predominant cleavage sets are plotted. Plots and contours were produced using Stereonet 9.5. (Allmendinger et al., 2011; Cardozo and Allmendinger, 2013). **c)** Late, brittle fault in listwanite composed of angular, white weathering carbonate clasts (listwanite) in a very fine-grained, light grey matrix (possible pseudotachylite). **d)** A large (~10 m) block of heterogeneous serpentinite hosted within a zone of strong listwanite alteration. Within the serpentinite, large sub-rounded knockers of massive dark green serpentinite are surrounded by softer, light green, talc-rich matrix.

data. Tl'azt'en Nation and Bev John are thanked for hospitality. Reviews by L. Diakow and L. Aspöler improved the clarity and quality of this paper.

References cited

Ahmed Z., and Bevan J.C., 1981. Awaruite, iridian awaruite, and a new Ru-Os-Ir-Ni-Fe alloy from the Sakhakot-Qila complex, Malakand Agency, Pakistan. *Mineralogical Magazine*, 44, 225-230.

Allmendinger R.W., Cardozo N., and Fisher, D., 2011. *Structural geology algorithms: vectors and tensors*, 1st ed. Cambridge University Press, 302 p.

Beard, J.S., and Hopkinson, L., 2000. A fossil, serpentization-related hydrothermal vent, Ocean Drilling Program Leg 173, Site 1068 (Iberia Abyssal Plain): Some aspects of mineral and fluid chemistry. *Journal of Geophysical Research*, 105, 16,527-16,539.

Boudier, F., and Nicolas, A., 1985. Harzburgite and lherzolite subtypes in ophiolitic and oceanic environments. *Earth and Planetary Science Letters*, 76, 84-92.

- Britten, R., 2017. Regional metallogeny and genesis of a new deposit type-disseminated awaruite (Ni₃Fe) mineralization hosted in the Cache Creek terrane. *Economic Geology*, 112, 517-550.
- Cardozo, N., and Allmendinger, R.W., 2013. Spherical projections with OSX Stereonet. *Computers and Geosciences*, 51, 193-205.
- Chamberlain, J.A., McLeod, C.R., Traill, R.J., and Lachance, G.R., 1965. Native metals in the Muskox Intrusion. *Canadian Journal of Earth Sciences*, 2, 188-215.
- English, J.M., and Johnston, S.T., 2005. Collisional orogenesis in the northern Canadian Cordillera: Implications for Cordilleran crustal structure, ophiolite emplacement, continental growth, and the terrane hypothesis. *Earth and Planetary Science Letters*, 232, 333-344.
- English, J.M., Mihalynuk, M.G., and Johnston, S.T., 2010. Geochemistry of the northern Cache Creek terrane and implications for accretionary processes in the Canadian Cordillera. *Canadian Journal of Earth Sciences*, 47, 13-34.
- Evans, B.W., Hattori, K., and Baronnet, A., 2013. Serpentinite: What, why, where? *Elements*, 9, 99-106.
- Foustoukos, D.I., Bizimis, M., Frisby, C., and Shirey, S.B., 2015. Redox controls on Ni-Fe-PGE mineralization and Re/Os fractionation during serpentinization of abyssal peridotite. *Geochimica et Cosmochimica Acta*, 150, 11-25.
- Frost, B.R., 1985. On the stability of sulfides, oxides, and native metals in serpentinite. *Journal of Petrology*, 26, 31-63.
- Frost, R.B., and Beard, J.S., 2007. On silica activity and serpentinization. *Journal of Petrology*, 48, 1351-1368.
- Hansen, L.D., Dipple, G.M., Gordon, T.M., and Kellett, D.A., 2005. Carbonated serpentinite (Listwanite) at Atlin, British Columbia: a geological analogue to carbon dioxide sequestration. *Canadian Mineralogist*, 43, 225-239.
- Kelemen, P.B., and Dick, H.J.B., 1995. Focused melt flow and localized deformation in the upper mantle: juxtaposition of replacive dunite and ductile shear zones in the Josephine peridotite, SW Oregon. *Journal of Geophysical Research*, 100, 423-438.
- Klein, F., and Bach, W., 2009. Fe-Ni-Co-O-S phase relations in peridotite-seawater interactions. *Journal of Petrology*, 50, 37-59.
- Lapierre, H., Bosch, D., Tardy, M., and Struik, L.C., 2003. Late Paleozoic and Triassic plume-derived magmas in the Canadian Cordillera played a key role in continental crust growth. *Chemical Geology*, 201, 55-89.
- MacIntyre, D.M., and Schiarizza, P., 1999. Bedrock geology, Cunningham Lake (93K/11, 12, 13, 14). British Columbia Ministry of Energy and Mines, British Columbia Geological Survey Open File 1999-11; scale 1:100,000.
- McGoldrick, S., Zagorevski, A., Canil D., Corriveau, A.-S., Bichlmaier, S., and Carroll, S., 2016. Geology of the Cache Creek Terrane in the Peridotite Peak-Menatatlina Range Area, Northwestern British Columbia (Parts of NTS 104K/15, 16). In: *Geoscience BC Summary of Activities 2015, Report 2016-1*, pp. 149-162.
- McGoldrick, S., Zagorevski, A., and Canil, D., 2017. Geochemistry of volcanic and plutonic rocks from the Nahlin ophiolite with implications for a Permo-Triassic arc in the Cache Creek terrane, northwestern British Columbia. *Canadian Journal of Earth Sciences*, 54, 1214-1227.
- Mercier, J.C.C., and Nicolas, A., 1975. Textures and fabrics of upper-mantle peridotites as illustrated by xenoliths from basalts. *Journal of Petrology*, 16, 454-487.
- Mihalynuk, M.G., Erdmer, P., Ghent, E.D., Cordey, F., Archibald, D.A., Friedman, R.M., and Johannson, G.G., 2004. Coherent French Range blueschist: Subduction to exhumation in less than 2.5 m.y.? *Geological Society of America Bulletin*, 116, 910-922.
- Mihalynuk, M.G., Mountjoy, K.J., Smith M.T., Currie, L.D., Gabites, J.E., Tipper, H.W., Orchard, M.J., Poulton, T.P., and Cordey, F., 1999. Geology and mineral resources of the Tagish Lake area (NTS 104M/ 8, 9, 10E, 15 and 104N/12W), northwestern British Columbia. British Columbia Ministry of Energy and Mines, British Columbia Geological Survey Bulletin 105, 217 p.
- Mihalynuk, M.G., Nelson, J.L., and Diakow, L.J., 1994. Cache Creek terrane entrapment: Oroclinal paradox within the Canadian Cordillera. *Tectonics*, 13, 575-595.
- Monger, J.W.H., 1975. Upper Paleozoic rocks of the Atlin terrane, northwestern British Columbia and south-central Yukon. *Geological Survey of Canada, Paper 74-47*, 63 p.
- Monger, J.W.H., 1977. Upper Paleozoic rocks of the western Canadian Cordillera and their bearing on Cordilleran evolution. *Canadian Journal of Earth Sciences*, 14, 1832-1859.
- Monger, J.W.H., and Ross, C.A., 1971. Distribution of fusulinaceans in the western Canadian Cordillera. *Canadian Journal of Earth Sciences*, 8, 259-278.
- Nelson, J.L., Colpron, M., and Israel, S., 2013. The Cordillera of British Columbia, Yukon, and Alaska: Tectonics and metallogeny. In: Colpron, M., Bissing, T., Rusk, B.G., and Thompson, J.F.H., (Eds.), *Tectonics, Metallogeny, and Discovery: The North American Cordillera and similar accretionary settings*. Society of Economic Geologists, Special Publication 17, pp. 53-109.
- Nickel, E.H., 1956. The occurrence of native nickel-iron in the serpentine rock of the Eastern Townships of the Quebec Province. *Canadian Journal of Earth Sciences*, 6, 307-319.
- Orchard, M.J., Cordey, F., Rui, L., Bamber, E.W., Mamet, B., Struik, L.C., Sano, H., and Taylor, H.J., 2001. Biostratigraphic and biogeographic constraints on the Carboniferous to Jurassic Cache Creek terrane in central British Columbia. *Canadian Journal of Earth Sciences*, 38, 551-578.
- Pearce, J.A., 2008. Geochemical fingerprinting of oceanic basalts with applications to ophiolite classification and the search for Archean oceanic crust. *Lithos*, 100, 14-48.
- Ronacher, E., Baker, J., Palich, J., Broad, P., and Thesen, C., 2013. Resource update-Decar nickel property. Independent technical report, 159 p.
- Schiarizza, P., and MacIntyre, D.G., 1999. Geology of the Babine Lake-Takla Lake area, central British Columbia (93K/11, 12, 13, 14; 93N/3, 4, 5, 6). In: *Geological Fieldwork 1998*, British Columbia Ministry of Energy and Mines, British Columbia Geological Survey Paper 1999-1, pp. 33-68.
- Sciortino, M., Mungall, J.E., and Muinonen, J., 2015. Generation of high-Ni sulfide and alloy phases during serpentinization of dunite in the Dumont sill, Quebec. *Economic Geology*, 110, 733-761.
- Sleep, N.H., Meibom, A., Fridriksson Th., Coleman, R.G., and Bird, D.K., 2004. H₂-rich fluids from serpentinization: Geochemical and biotic implications. *Proceedings of the National Academy of Sciences*, 101, 12,818-12,823.
- Struik, L., Schiarizza, P., Orchard, M., Cordey, F., Sano, H., MacIntyre, D.G., Lapierre, H., and Tardy, M., 2001. Imbricate architecture of the upper Paleozoic to Jurassic oceanic Cache Creek terrane, central British Columbia. *Canadian Journal of Earth Sciences*, 38, 495-514.
- Struik, L.C., MacIntyre, D.G., and Williams, S.P., 2007. Nechako NATMAP project: A digital suite of geoscience information for central British Columbia. *Geological Survey of Canada Open File 5623*.
- Tardy, M., Lapierre, H., Struik, L.C., Bosch, D., and Brunet, P., 2001. The influence of mantle plume in the genesis of the Cache Creek oceanic igneous rocks: implications for the geodynamic evolution of the inner accreted terranes of the Canadian Cordillera. *Canadian Journal of Earth Sciences*, 38, 515-534.
- Verley, C.G., 2011. Report on the Decar Nickel property. Assessment Report, 52 p. Downloaded from SEDAR, (<https://www.sedar.com/DisplayCompanyDocuments.do?lang=EN&issuerNo=00004553>).

Geology of the Spanish Lake area, south-central British Columbia



Paul Schiarizza^{1, a}

¹ British Columbia Geological Survey, Ministry of Energy, Mines and Petroleum Resources, 300-865 Hornby Street, Vancouver, BC, V6Z 2G3

^a corresponding author: Paul.Schiarizza@gov.bc.ca

Recommended citation: Schiarizza, P., 2018. Geology of the Spanish Lake area, south-central British Columbia. In: Geological Fieldwork 2017, British Columbia Ministry of Energy, Mines and Petroleum Resources, British Columbia Geological Survey Paper 2018-1, pp. 143-156.

Abstract

In 2015, the British Columbia Geological Survey initiated a multi-year program to establish a regional stratigraphic framework for the Nicola Group (Triassic), the principal volcano-sedimentary component the Quesnel arc terrane in central and southern British Columbia. Field studies in the Spanish Lake area in 2017 were part of this program, and focused on a predominantly fine-grained sedimentary unit in the eastern part of the Nicola belt. This unit (assemblage one of the Nicola Group) consists mainly of Middle Triassic siltstone and argillite, but also includes pillowed basalt that has geochemical characteristics of mid-ocean ridge basalt, and volcanic sandstone that becomes predominant upsection. Assemblage one forms a northwest-trending belt that dips steeply, youngs to the southwest, and is stratigraphically overlain by Late Triassic Nicola Group assemblages. It, and adjacent Nicola rocks, are on the partially preserved forelimb of a major southwest-verging fold that probably formed in the Middle Jurassic. To the northeast, assemblage one is juxtaposed against Middle Triassic rocks of the Slocan Group, across a fault that postdates the southwest-verging fold. Assemblage one is inferred to represent the remnants of a back-arc basin that formed east of the Nicola arc. The Middle Triassic age of the basin implies that the Nicola arc, although represented mainly by Late Triassic rocks, was initiated during, or before, the Middle Triassic.

Keywords: Nicola Group, Slocan Group, Quesnel terrane, Middle Triassic, Upper Triassic, volcanic arc, back-arc basin, slate, siltstone, volcanic sandstone, pyroxene-phyric basalt

1. Introduction

Quesnel terrane (Fig. 1) is an important metallogenic belt, best known for its prolific porphyry Cu±Au-Mo-Ag deposits. These deposits are part of a Mesozoic arc complex that includes Triassic to Jurassic volcanic and sedimentary rocks, and related calc-alkaline and alkalic intrusions. The Nicola Group (Triassic) is the principal volcano-sedimentary component of this Mesozoic arc complex in central and southern British Columbia. In 2015, the British Columbia Geological Survey initiated a multi-year field-based program to establish a regional stratigraphic framework for the Group. This framework, combined with space-time-composition patterns of associated plutons, will contribute to a better understanding of the architecture of the arc, and improve the geologic framework within which to interpret the settings and controls of mineral occurrences.

Initial investigations in 2015, covered the entire width of Quesnel terrane in the Bridge Lake-Quesnel River area (Fig. 1), and established a preliminary stratigraphic framework for the Triassic rocks that included four informal Nicola Group assemblages and a separate assemblage to the east assigned to the Slocan Group (Schiarizza, 2016). In 2016, the eastern part of the Nicola Group and the adjacent Slocan Group were studied in the Stump Lake-Salmon River area, south of Kamloops (Fig. 1; Schiarizza, 2017). Fieldwork in 2017, in the northeast corner of the large 2015 study area, near the town of

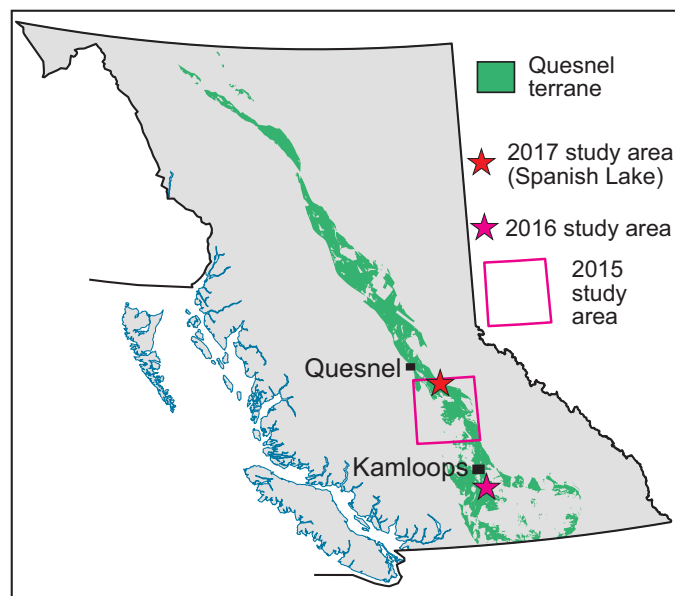


Fig. 1. Distribution of Quesnel terrane in British Columbia, with locations of the areas studied in 2015, 2016 and 2017 for the Nicola stratigraphic framework project.

Likely, is summarized herein. This work focuses on an eastern, fine-grained sedimentary component of the Nicola Group (assemblage one of Schiarizza, 2016), and its relationship to the main part of the Nicola arc to the west, and the Slocan Group to the east.

2. Setting

The Spanish Lake area is on the north side of eastern Quesnel Lake, east of the community of Likely. It is in the Quesnel Highland physiographic province (Holland, 1976), within the traditional territories of the Secwepemc, Esk'etemc, Tsilhqot'in, and Lhtako Dené First Nations. Networks of forestry and logging roads provide easy access to most parts of the area. These originate in Likely, which is connected to 150 Mile House, on Highway 97, by a paved road. Spanish Lake is in the northern part of the Quesnel Lake (93A) NTS map sheet; the geology was described by Campbell (1978), with revisions and updates by Struik (1983, 1988), Rees (1987), Bloodgood (1990), and Panteleyev et al. (1996).

The Nicola Group (Triassic), the predominant component of the Quesnel arc terrane, forms a northwest-trending belt that, in the Likely region, is 25 to 55 km wide (Fig. 2). This belt also includes abundant Late Triassic to Early Jurassic arc intrusions (only the very largest are shown on Fig. 2), and fault-bounded panels of Lower to Middle Jurassic arc-derived siliciclastic sedimentary rocks (Dragon Mountain succession of Logan and Moynihan, 2009). The Nicola Group is flanked to the east by a belt of Triassic sedimentary rocks, mainly black phyllite, siltstone, and quartz sandstone, which is assigned to the Slokan Group (Schiarizza, 2016). These rocks are underlain by a narrow, discontinuous belt of mafic schists (Crooked amphibolite) and, farther east, a wide belt of suspected Proterozoic and Paleozoic quartzites and pelitic schists (Snowshoe Group) that are locally cut by Devonian-Mississippian granitic rocks (Quesnel Lake gneiss). Cache Creek terrane, including late Paleozoic to early Mesozoic basalt, chert, limestone, siltstone, and ultramafic rocks, is west of the Nicola belt and is interpreted as an accretionary complex that formed during the subduction that generated the Quesnel magmatic arc. Younger rocks, in and adjacent to the Nicola belt, include Middle Jurassic and Early Cretaceous granitic intrusions, Eocene volcanic and sedimentary rocks, Oligocene-Pliocene conglomerate and sandstone (along the Fraser River), and flat-lying Neogene and Quaternary basalt (Fig. 2).

The Snowshoe Group is part of pericratonic Kootenay terrane, commonly interpreted as a deep-water facies deposited along the western margin of ancestral North America (Colpron and Price, 1995; Nelson et al., 2013). The Quesnel Lake gneiss (Ferri et al., 1999), and age-equivalent volcanic and plutonic rocks of the Eagle Bay assemblage to the south (Schiarizza and Preto, 1987; Paradis et al., 2006), reflect initiation of arc magmatism along the continental margin in the Devonian-Mississippian. The Crooked amphibolite, commonly included in Slide Mountain terrane, has been interpreted as oceanic crust that was thrust eastward above pericratonic rocks in the Early Jurassic (Rees, 1987) or Late Permian-Early Triassic (McMullin et al., 1990). The Slokan Group is part of a Triassic siliciclastic basin that was either carried eastward with the Crooked amphibolite on an Early Jurassic thrust (Rees, 1987), or was deposited unconformably above the Crooked amphibolite and the Snowshoe Group after emplacement of the

Crooked amphibolite on a Permo-Triassic thrust (McMullin et al., 1990).

The Nicola Group in the Likely region (Fig. 2) is subdivided into four informal assemblages following Schiarizza (2016). Most widespread are Carnian-early Norian volcanic sandstones, with local basalt flows and breccias, assigned to assemblage two. Younger rocks are exposed in the central part of the Nicola belt, reflecting a broadly synclinal architecture. These include a succession of basalt flows and related breccias (assemblage three), and an upper unit (assemblage four) characterized by polymictic conglomerate beds containing hypabyssal and plutonic rock fragments that are intercalated with sandstone, basalt and andesite. The oldest component of the Nicola Group (assemblage one, the focus of fieldwork in 2017) is a Middle Triassic siltstone-sandstone unit juxtaposed against the Slokan Group along the east edge of the Nicola belt (Fig. 2).

3. Geologic units in the Spanish Lake area

The Spanish Lake map area is underlain mainly by four parallel northwest trending units: the Slokan Group and assemblages one, two, and three of the Nicola Group (Figs. 3, 4). Structurally beneath the Slokan Group, in the northern part of the map area, are exposures of Crooked amphibolite, Snowshoe Group, and Quesnel Lake gneiss, which were examined in a cursory manner. Mafic to intermediate dike rocks are prominent locally, but do not form mappable units at the scale of Figure 3.

3.1. Snowshoe Group

The Snowshoe Group is exposed on the eastern edge of the study area (Fig. 3). These rocks are structurally overlain by the Crooked amphibolite to the north and northwest, but may be in direct contact with the Slokan Group across an unexposed contact that marks the south side of the belt (Fig. 3). The Snowshoe Group consists mainly of light grey, light brownish-grey weathered, fine- to medium-grained biotite-muscovite-quartz schist. Locally it includes biotite-muscovite quartzite, which commonly occurs as layers, 1-10 cm thick, separated by micaceous partings (Fig. 5). The Snowshoe Group is not dated here, or anywhere else in the region, but is inferred to be mid-Paleozoic and/or older, because it is cut by Devonian-Mississippian granite of the Quesnel Lake gneiss.

3.2. Quesnel Lake gneiss

Two separate bodies of foliated granitic rock crop out in the study area, one in the Snowshoe Group along the east edge of the area, and one structurally beneath the Crooked amphibolite in the northwest. Both units are included in the informal Quesnel Lake gneiss, but they are lithologically distinct. Rees (1987) referred to the eastern body as the 'eastern Quesnel Lake gneiss', and the other, together with other nearby bodies of similar composition (Fig. 2), as the 'western Quesnel Lake gneiss'. The eastern Quesnel Lake gneiss is a moderately to strongly foliated, medium-grained, equigranular rock comprising grey feldspar and quartz, with discontinuous foliae

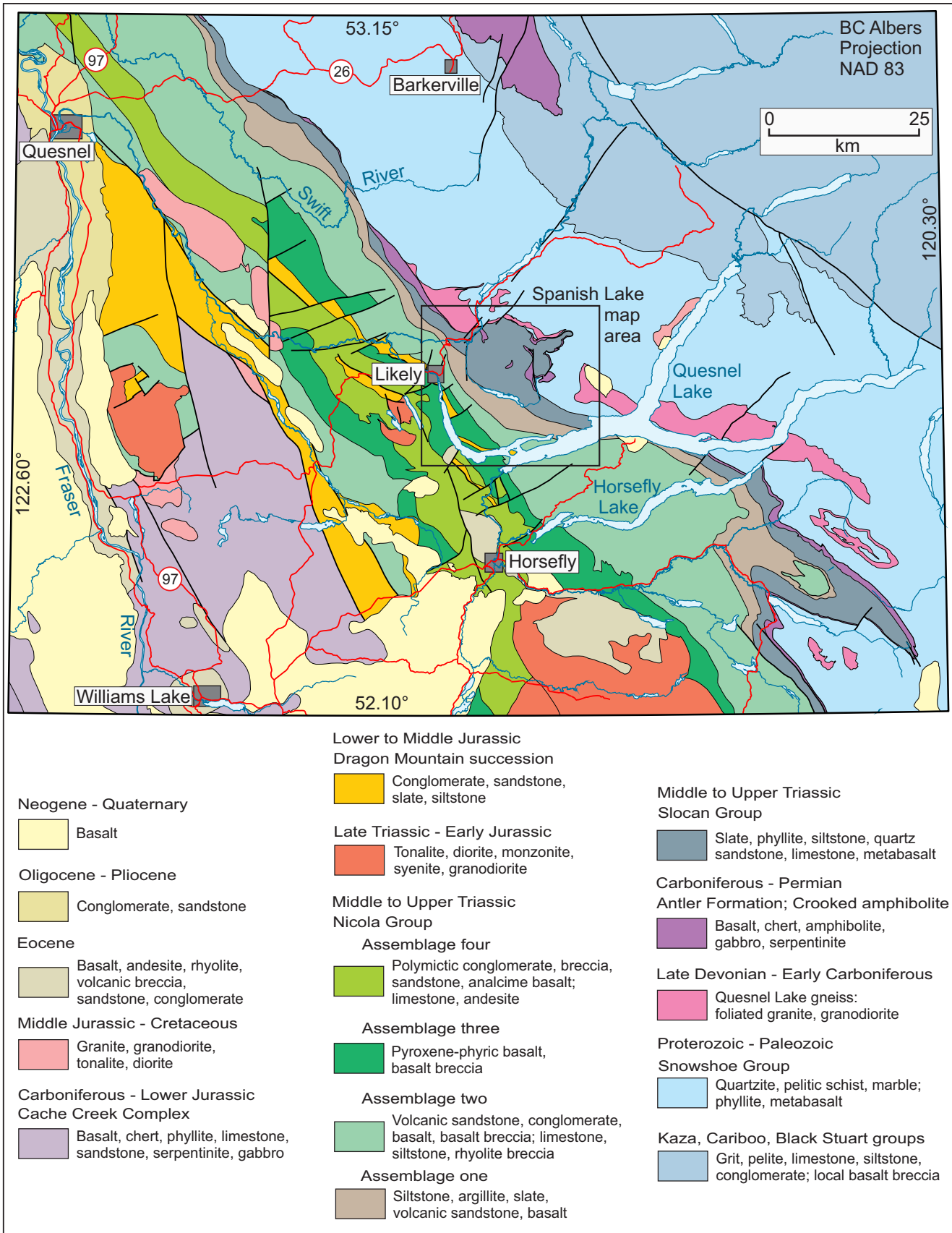


Fig. 2. Geological map of the Likely region, showing location of the Spanish Lake map area. Geology mainly from Logan et al. (2010) and Schiarizza (2016).

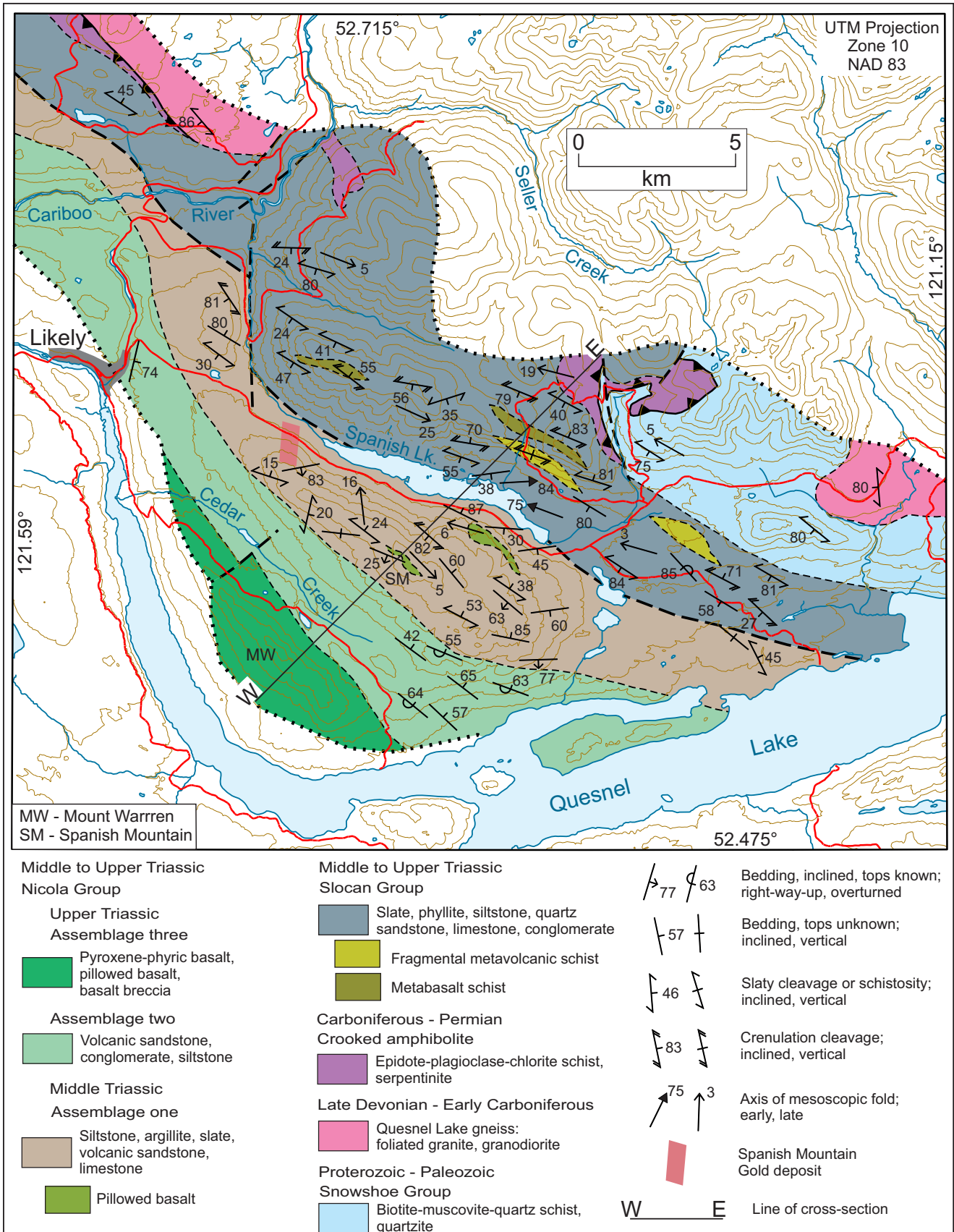


Fig. 3. Geology of the Spanish Lake map area. Geology based on 2015 and 2017 fieldwork, with some information from Rees (1987) and Bloodgood (1990).

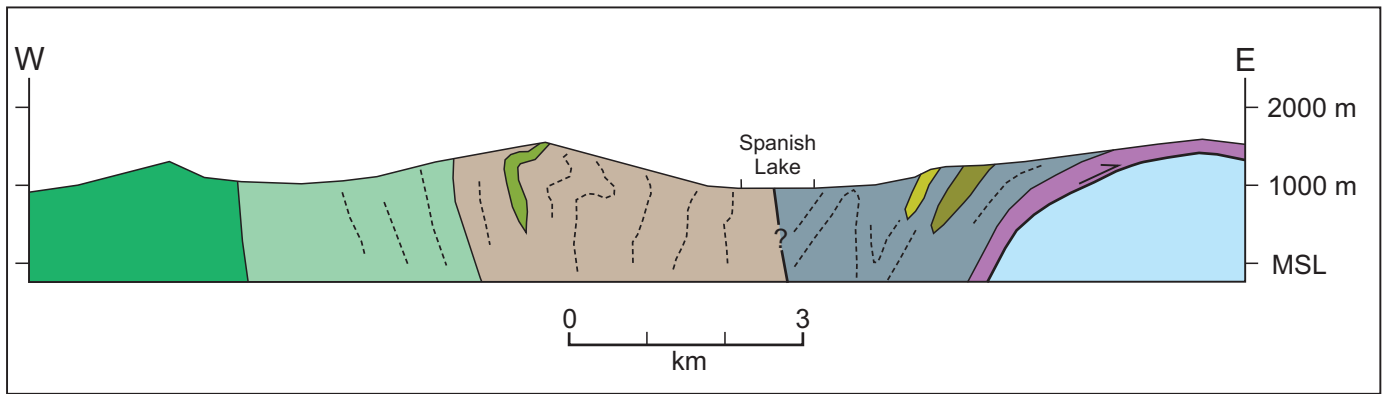


Fig. 4. Schematic vertical cross-section along line E-W shown on Figure 3.



Fig. 5. Platy quartzite, Snowshoe Group, 4.5 km northeast of Spanish Lake.



Fig. 6. Foliated granodiorite, eastern Quesnel Lake gneiss, 11.5 km east-northeast of Spanish Lake.

of biotite and epidote (Fig. 6). In contrast, the western Quesnel Lake gneiss contains large (several cm) augen of K-feldspar enclosed in a strongly foliated, coarse-grained matrix of quartz-feldspar-muscovite-biotite. Ferri et al. (1999) reported a U-Pb zircon crystallization age of 357.2 ± 1.0 Ma for a different body of western Quesnel Lake gneiss, just north of the study area.

3.3. Crooked amphibolite

The Crooked amphibolite crops out in several areas scattered across the northern part of the Spanish Lake area, where it forms a narrow unit structurally beneath the Slokan Group, and structurally above the Snowshoe Group and Quesnel Lake gneiss. It consists mainly of medium to dark green chlorite schist (Fig. 7), but locally includes isolated exposures of dark grey-green serpentinite. The predominant schists consist mainly of chlorite and plagioclase, accompanied by various combinations and proportions (trace to abundant) of epidote, biotite, actinolite, quartz, and ankerite. A strong schistosity, defined by oriented chlorite, may be parallel to a lenticular compositional layering (metamorphic segregation), defined



Fig. 7. Chlorite schist, Crooked amphibolite, 3.9 km northeast of Spanish Lake.

by dark chlorite-rich lenses alternating with lighter coloured plagioclase-rich lenses. This compositional layering occurs on a scale of 1 to 5 mm, and may be accentuated by parallel veins and lenses of quartz±epidote and/or ankerite.

The Crooked amphibolite is undated. The predominant chlorite schists have compositions that suggest a mafic volcanic protolith, and analyses presented by Rees (1987) show geochemical signatures that suggest derivation from ocean floor tholeiites. On this basis, and a similar structural relationship to underlying pericratonic rocks, the Crooked amphibolite is correlated with mafic volcanic units of the Antler Formation (Struik and Orchard, 1985) and Fennell Formation (Schiarizza and Preto, 1987) of Slide Mountain terrane, and inferred to be Upper Paleozoic (Rees, 1987).

3.4. Slocan Group

The Slocan Group forms a single continuous belt that extends from southeast to northwest across the Spanish Lake map area (Fig. 3). The Slocan designation follows Schiarizza (2016); the same rocks were mapped as unit uTrp by Struik (1983), the black phyllite unit by Rees (1987), and include unit Tra and part of unit Trb of Bloodgood (1990). The predominant rock types are phyllite, slate, and siltstone, but the group also includes quartz sandstone, limestone, and volcanic and volcanoclastic rocks. The base of the group was observed at one locality, about 3.5 km northeast of the east end of Spanish Lake, where it rests above the Crooked amphibolite across a contact that dips at a moderate angle to the southwest, more or less parallel to the well-developed schistosity in both units. The southwest contact of the group is an inferred fault that places it against assemblage one of the Nicola Group.

The Slocan Group consists mainly of dark grey to black slate and phyllite, commonly with laminae and thin beds of light grey-weathered siltstone (Fig. 8), and locally with thin- to medium-beds of dark grey slaty siltstone (Fig. 9) or dark grey silty to micritic limestone. Rare intraformational conglomerates



Fig. 8. Dark grey phyllite with light grey siltstone laminae, Slocan Group, north side of Spanish Lake.



Fig. 9. Dark grey slate with more massive bed of slaty siltstone, Slocan Group, 1 km northeast of the east end of Spanish Lake.

contain angular to subrounded fragments, as large as 12 cm, of siltstone and laminated siltstone in a dark grey phyllite matrix (Fig. 10). Locally the phyllite is medium greenish-grey and chloritic, pale grey-green and very siliceous, or pale silvery-green with large orange-weathered ankerite porphyroblasts.

Fine-grained, thin- to medium-bedded quartzose sandstone forms a section several tens of metres thick in the interior part of the Slocan belt, about 4.5 km east-southeast of Spanish Lake (see Fig. 4 of Schiarizza, 2016). A succession of coarser grained siliciclastic rocks occurs on the ridge north of the west end of Spanish Lake, and includes schistose sandstone, gritty sandstone, and small pebble conglomerate (Fig. 11). The clasts are predominantly polycrystalline quartz, plagioclase, and fine-grained sericite-quartz schist (similar in composition and texture to the schistose matrix). Calcareous sericite-quartz



Fig. 10. Framework-disrupted intraformational conglomerate containing laminated siltstone fragments in a dark grey phyllite matrix, Slocan Group, 500 m north of the east end of Spanish Lake.



Fig. 11. Gritty metasandstone, Slocan Group, 3 km north of the west end of Spanish Lake.

schist with relict grains and granules of monocrystalline and polycrystalline quartz also occurs in an isolated set of exposures just north of the east end of Spanish Lake. Locally these schists are conglomeratic (Fig. 12), with flattened angular fragments, up to 10 cm long, of mainly pale grey, fine-grained sericite-quartz schist with ovoid grains, ≤ 1 mm, of polycrystalline quartz, commonly rimmed with calcite. These ovoid grains may be relict amygdules, indicating a felsic volcanic origin for the clasts.

Mafic volcanic rocks map as two lenses within the Slocan Group, one about two km northeast of eastern Spanish Lake, the other on the ridge north of the west end of the lake (Fig. 3). These rocks are pale to medium green plagioclase-actinolite-biotite-chlorite (\pm epidote \pm calcite) schists that commonly contain 1-2 mm clots of actinolite-biotite-chlorite that may be altered mafic phenocrysts, and locally contain flattened



Fig. 12. Conglomeratic sericite-quartz schist, with possible felsic volcanic clasts, Slocan Group, 200 m northeast of the east end of Spanish Lake.

amygdules (1-5 mm) of quartz \pm biotite. Logan and Bath (2006) analyzed samples from the eastern lens (their Spanish Lake samples), and showed that they display geochemical characteristics of subduction-generated arc basalt, but are distinct from the arc basalts of the main part of the Nicola belt to the west. Additional samples, from both lenses, were collected in 2017; geochemical results are pending.

Volcaniclastic rocks are mapped in two places, one just south of the eastern volcanic lens, and the other about three kilometres to the east-southeast (Fig. 3). These rocks are mainly plagioclase-quartz-biotite-chlorite-sericite schists that contain coarse (up to 20 cm), flattened, poorly sorted metavolcanic fragments (Fig. 13). The fragments are commonly pale to medium grey-green, and most are similar in composition and texture to the mafic metavolcanic rocks of the two volcanic lenses.

The Slocan Group in the Spanish Lake area is mainly Middle Triassic, based on conodonts extracted from narrow limestone lenses that were sampled at three localities from a generally poorly exposed part of the group, 3 to 5 km east of Spanish Lake. Struik (1988) reported two collections from this area, one Ladinian and the other unrefined Middle Triassic, and Panteleyev et al. (1996) report a collection that is late Anisian-early Ladinian (sample 87MB-01-02). Struik (1988) also reported an unrefined Triassic age for a collection from Beehive Island, just offshore in Quesnel Lake, near the southwest margin of the unit.



Fig. 13. Schist with volcanic fragments, Slocan Group, 1.3 km north of the east end of Spanish Lake.

3.5. Nicola Group

Rocks underlying the southwest half of the Spanish Lake map area are included in the Nicola Group, and are assigned to three units following the nomenclature of Schiarizza (2016). These are, from northeast to southwest, assemblage one, assemblage two, and assemblage three.

3.5.1. Assemblage one

Assemblage one forms a northwest trending belt that is in fault contact with the Slokan Group to the northeast, and is overlain by assemblage two to the southwest, across a steeply dipping, locally overturned, stratigraphic contact. Assemblage one consists mainly of siltstone, but also includes argillite, slate, feldspathic sandstone, limestone, and basalt.

The predominant rock type is medium to dark grey siltstone that typically occurs as thin (1-10 cm) planar to lenticular beds separated by phyllosilicate partings and/or thin interbeds of dark grey slate (Fig. 14). Some intervals of dark grey slaty siltstone are not distinctly bedded, but may contain poorly defined laminae or thin beds. Dark grey argillite is also common, and occurs as thin (1-4 cm) lenticular beds separated by dark greenish-grey chloritic partings, or as thicker indistinctly bedded units with an imperfect slaty cleavage, and rusty porphyroblasts of ankerite and/or pyrite (Fig. 15). Medium to dark grey limestone

is rare, and forms layers or lenses, <1-2 m thick, intercalated with siltstone.

Green to grey, fine- to coarse-grained sandstone occurs locally in the northeastern part of assemblage one, and becomes more common at higher stratigraphic levels to the southwest. It occurs as thin- to thick-bedded intervals that are commonly intercalated with dark grey to green siltstone (Fig. 16). The sandstones are notably similar to those of assemblage two. They are feldspathic, but also include grey to green volcanic lithic grains and altered mafic minerals or lithic grains. Volcanic quartz forms a minor but conspicuous component of some sandstone beds on the low ridge east of Likely (Fig. 3).

Basalt forms two lenses within assemblage one, on Spanish Mountain and on the low slopes south of the east end of Spanish Lake (Fig. 3). The basalt is grey to green, massive to pillowed (Fig. 17), locally variolitic, and composed mainly of a low-grade metamorphic mineral assemblage that includes



Fig. 14. Thin-bedded siltstone, assemblage one of the Nicola Group, 2 km east-southeast of Spanish Mountain.



Fig. 16. Coarse-grained sandstone interbedded with siltstone, assemblage one of the Nicola Group, 1.5 km east of Spanish Mountain.



Fig. 15. Slaty argillite, assemblage one of the Nicola Group, 3 km northwest of Spanish Mountain.



Fig. 17. Pillowed basalt, assemblage one of the Nicola Group, Spanish Mountain.

calcite, plagioclase, epidote, chlorite, and actinolite. A sample analyzed by Logan and Bath (2006) from the lens south of eastern Spanish Lake (their Spanish Mountain sample) displays geochemical characteristics of normal mid-ocean ridge basalt, a result confirmed by a sample collected from the same unit in 2015. Additional samples from both lenses were collected in 2017; results are pending.

Assemblage one is mainly Middle Triassic, based on conodonts extracted from thin limestone lenses. Struik (1988) reported that a conodont collection from the northeast side of the assemblage on the shore of Quesnel Lake is early-middle Anisian (early Middle Triassic), and that another collection, also from the north shore of the lake but near the southwest contact of the assemblage, is late Ladinian to Carnian (Middle to Late Triassic). A third collection, from the central part of the assemblage, 2 km south of the east end of Spanish Lake, is early Anisian (Panteleyev et al., 1996; sample 87MB-16-02).

3.5.2. Assemblage two

Assemblage two forms a northwest-trending belt of sandstones, with local siltstone and conglomerate, southwest of assemblage one. Where best exposed, north of Quesnel Lake, the rocks in this belt young to the southwest, and appear to be conformable with adjacent siltstones and sandstones of assemblage one. However, the beds are commonly overturned, dipping steeply to the northeast (Fig. 3).

Assemblage two consists almost entirely of grey to green, fine- to coarse-grained, locally gritty, volcanogenic sandstone. Grains of feldspar are the predominant constituent, and are accompanied by feldspathic and mafic lithic grains, and variably altered mafic minerals (mainly pyroxene). The sandstone commonly forms distinct thin to thick beds that locally display normal grading. Thin beds of green to grey siltstone, or dark grey argillite, may be interbedded with the sandstones (Fig. 18), or form the tops of graded sandstone beds. Pebble conglomerate (Fig. 19) locally forms thin to



Fig. 18. Thin- to medium-bedded volcanic sandstone, with thin layers of siltstone and argillite, assemblage two of the Nicola Group, 5 km east of Mount Warren.



Fig. 19. Pebble conglomerate, assemblage two of the Nicola Group, 4.7 km southeast of Mount Warren.

very thick beds intercalated with sandstone. The subangular to subrounded clasts are mainly pyroxene±plagioclase-phyric and aphyric mafic volcanic rocks, but locally include feldspar porphyry, microdiorite, and siltstone.

Assemblage two has not been dated in the Spanish Lake map area, but assemblage one, directly beneath the contact on the north shore of Quesnel Lake, has yielded late Ladinian to Carnian (Middle to Late Triassic) conodonts (Struik, 1988). Rocks in the upper part of assemblage two, 20 km south of Spanish Lake, have yielded Late Carnian conodonts (Panteleyev et al., 1996; sample 88AP-10/3-C2), and correlative rocks elsewhere in the region are mainly Carnian to lower Norian (Schiarizza, 2016).

3.5.3. Assemblage three

Assemblage three is exposed in the southwest corner of the Spanish Lake map area, on and adjacent to the ridge system that includes Mount Warren (Fig. 3). It consists mainly of medium to dark green, brown-weathered, amygdaloidal pyroxene-phyric basalt that is typically massive, but locally pillowed (Fig. 20). Euhedral to subhedral pyroxene phenocrysts (commonly 1-10 mm) form 5-25% of the rock. Ovoid to amoeboid amygdules, filled with various combinations of quartz, epidote, calcite and chlorite, are typically <1-2 mm, but locally are as large as 2 cm. Small (1-2 mm) plagioclase phenocrysts are present in some exposures, and plagioclase laths may also be evident in the epidote-calcite-altered groundmass.

Basalt breccia, consisting of pyroxene porphyry fragments in a matrix of plagioclase, pyroxene and small lithic grains (Fig. 21), is associated with basalt flows near the Mount Warren summit. The breccias contain coarse (<1-20 cm) angular to subrounded fragments and vary from matrix to clast supported. The fragments are exclusively pyroxene porphyry, but show considerable textural variation (size and proportion of pyroxene phenocrysts, presence or absence of plagioclase phenocrysts and amygdules). Although some could be flow



Fig. 20. Pillowed pyroxene-phyric basalt, assemblage three of the Nicola Group, Mount Warren.



Fig. 21. Pyroxene porphyry breccia, assemblage three of the Nicola Group, 500 m northwest of Mount Warren.

breccias, it is suspected that they are mainly locally derived epiclastic deposits.

The contact between assemblage three and assemblage two is not exposed, nor particularly well constrained. It is inferred to be a steeply dipping, possibly overturned, stratigraphic contact (Fig. 4), based on regional relationships showing that assemblage three rests stratigraphically above assemblage two, and the structure in the westernmost exposures of assemblage two, where overturned beds dip steeply northeast (Fig. 3). Assemblage three is not well dated, but is inferred to be Norian based on its regional stratigraphic position (Schiarizza, 2016), between assemblage two (Carnian-Norian) and assemblage four (upper Norian-Rhaetian).

4. Dikes and sills

A suite of dioritic dikes and sills intrudes assemblage one of the Nicola Group on and around the Spanish Mountain ridge system. Most of these intrusions are fine-grained, equigranular hornblende diorite, but porphyritic varieties, with phenocryst of plagioclase, are common. More felsic dikes are present, but rare, and contain phenocrysts of plagioclase, hornblende, biotite and quartz. A characteristic feature of these intrusions is the presence of sparse to abundant mafic to ultramafic xenoliths, <1-3 cm across, including biotite hornblende and pyroxenite. Rhys et al. (2009) reported that, at the Spanish Mountain gold prospect, just west of Spanish Lake (Fig. 3), sills and dikes of this suite are affected by all phases of deformation, alteration and quartz veining that affect the host rocks of assemblage one. Four separate intrusive bodies yielded U-Pb zircon ages ranging from 185.6 ± 1.5 Ma to 187.3 ± 0.8 Ma (Rhys et al., 2009). These ages, the predominant dioritic composition, and the characteristic ultramafic xenoliths, suggest that the Spanish Mountain dikes and sills are related to a suite of ultramafic-mafic intrusions that cut Nicola and Slokan rocks in the Canim Lake area, 90 km SE of Spanish Lake. Diorite from one of these intrusions (Iron Lake complex) yielded a zircon U-Pb age of 190.4 ± 0.5 Ma, and diorite from another (Aqua Creek complex) yielded a zircon U-Pb age of 184.0 ± 0.4 Ma (Schiarizza et al., 2013).

Most other dikes and small intrusive bodies in the Spanish Lake area are suspected to be Triassic. These include pyroxene porphyry dikes, similar to the basalts of assemblage three, that locally cut siltstone and sandstone of assemblages one and two of the Nicola Group, and fine-grained, weakly foliated and chlorite-altered hornblende diorite that cuts the Slokan Group near the metabasalt lens north of the west end of Spanish Lake.

5. Structural geology

The Spanish Lake map area comprises two contrasting structural domains, separated by an inferred fault under Spanish Lake and adjacent low-lying areas. The eastern domain includes the Slokan Group and underlying Paleozoic rocks, and preserves northeast-verging folds cut by younger southwest-verging structures. The western domain encompasses the three Nicola Group assemblages, which define a southwest-younging, commonly overturned panel that forms part of the forelimb of a major southwest-verging fold. Mesoscopic structural fabrics are unevenly developed across the area, with a distinct break at the domain boundary. All units of the Slokan Group display a strong penetrative cleavage or schistosity, commonly cut by a younger well-developed crenulation cleavage. A penetrative cleavage is locally developed in fine-grained rocks of assemblage one, but is unevenly developed and generally not evident in the volcanic rocks or sandstones, and is absent from all Nicola rocks of assemblages two and three. The break in cleavage intensity coincides with a slight difference in metamorphic grade, as schists and phyllites of the Slokan Group commonly contain biotite, whereas slates of the Nicola Group (assemblage one) do not.

The structure of the Slocan Group is characterized by bedding that dips at moderate angles to the southwest, a penetrative phyllitic cleavage or schistosity (S1) that also dips to the southwest, more or less parallel to, or steeper than, the associated bedding, and a well-developed crenulation cleavage (S2) that dips at moderate to steep angles to the northeast. Mesoscopic folds (F1) associated with S1 schistosity are rare, but those observed plunge steeply to the northwest, southeast, or east. At least one medium-scale, northeast-verging F1 fold is documented by a panel of rocks, several hundred metres wide, that is subvertical and youngs to the east. Other variations in bedding and S1 orientations are due to folds related to the northeast-dipping S2 crenulation cleavage, with axes that plunge gently to the northwest or southeast (Fig. 22). Locally, fold axes of similar orientation are related to a crenulation cleavage that dips gently to the southwest. Relationships are unclear, but it is suspected that this crenulation cleavage is younger than the predominant northeast-dipping crenulation cleavage (S2).

Beds of assemblage one dip at moderate to steep angles and young to the southwest and contain a locally developed slaty cleavage that dips mainly to the northeast, at shallower angles than bedding (Fig. 23). The beds most commonly dip to the southwest, and are right-way-up, but locally dip northeast and are overturned. Local panels of gently dipping, right-way-up beds are inferred to form the short limbs of asymmetric folds (Fig. 4). Actual observations of mesoscopic folds that might be related to the slaty cleavage were rare, and these showed highly variable shapes and orientations, with axes plunging northwest, north, northeast, east and southeast. Younger folds, which deform the slaty cleavage, plunge gently northwest or southeast, and may display a weakly-developed axial planar crenulation cleavage that dips steeply, mainly to the southwest.



Fig. 22. Phyllite and siltstone of the Slocan Group, deformed by northwest plunging folds with axial planar crenulation cleavage (parallel to pencil), 400 m north of the east end of Spanish Lake. View is northwest; crenulation cleavage dips northeast, bedding and slaty cleavage dip mainly southwest.



Fig. 23. Platy argillite, assemblage one of the Nicola Group, 3.5 km northwest of Spanish Mountain. View is to the north; beds dip about 45° northeast and are presumed to be overturned, weak slaty cleavage is refracted, but dips about 20° northeast.

Steeply dipping, southwest-facing rocks in the western part of assemblage one pass southwestward, apparently conformably, into well-bedded rocks of assemblage two that dip mainly to the northeast, but are overturned. The transition, farther southwest, into assemblage three is also inferred to be a steeply dipping, southwest-younging stratigraphic contact (Fig. 4), although bedding was not observed in this unit.

The structure of the Nicola Group in the Spanish Lake area, comprising steeply dipping, in part overturned, west-younging beds cut by more gently northeast-dipping cleavage (seen only in assemblage one), indicates that it occupies the forelimb of a major southwest-verging fold. This structure was recognized by Rees (1987), who referred to the fold as the Spanish Lake anticline. It is suspected that the slaty cleavage related to this fold correlates with the well-developed, northeast-dipping S2 crenulation cleavage in the Slocan Group. Structures related to the older northeast-verging folds that are prevalent in the Slocan Group were not recognized in the Nicola Group, although vestiges of such structures might be present in poorly-understood mesoscopic folds rarely observed in assemblage one.

The contact between the Nicola Group (assemblage one) and Slocan Group is inferred to be a fault, because it juxtaposes two units of the same age, and also juxtaposes two contrasting structural domains. Rees (1987) thought that the contact was stratigraphic, and folded by the southwest-verging Spanish Lake anticline, whereas Struik (1988), recognizing that the two units were in part the same age, inferred that it was an east-directed thrust fault (Spanish thrust) that carried the Nicola Group above the Slocan Group. The Spanish thrust is apparently an important structure regionally (Struik, 1988; Bloodgood, 1990), but it is suspected, mainly due to the contrasting structural domains, that the contact in the Spanish Lake area is a younger structure. This fault records northeast-side-up displacement, such that the

older Spanish thrust was eroded on the northeast side of the fault, and is in the subsurface on the southwest side. It might be a northeast-dipping thrust or reverse fault that is younger than, but perhaps broadly related to, the southwest-verging folds in the area.

6. Discussion

6.1. Paleogeographic setting of assemblage one

Assemblage one of the Nicola Group consists, in large part, of siltstone and argillite, with local accumulations of pillowed basalt that has geochemical characteristics of mid-ocean ridge basalt. The main link to the Nicola Group is provided by fine- to coarse-grained volcanic sandstones that are intercalated with the finer-grained rocks and become more abundant at higher stratigraphic levels. These sandstones are lithologically similar to volcanic sandstones of assemblage two, a major component of the Nicola Group regionally, that conformably overlies western exposures of assemblage one. These characteristics, and its location on the east side of the Nicola arc, which was generated by eastward subduction, suggest that assemblage one preserves the remnant of a back-arc basin. The Middle Triassic age for most rocks of assemblage one indicates that the Nicola arc, although represented mainly by Late Triassic rocks, was initiated during, or before, the Middle Triassic.

The Slocan Group represents a siliciclastic basin, in part the same age as assemblage one, east of the Nicola Group. The relationship and proximity of this basin to the back-arc basin of assemblage one is uncertain. However, the presence of arc volcanic rocks in the Slocan Group suggests a possible link. Arc volcanism may have been initiated in the Slocan basin in the Middle Triassic, then migrated westward, with formation of the assemblage one back-arc basin, to its current position and main axis of Late Triassic arc magmatism. Evaluating this scenario will require more precise ages for specific sedimentary and volcanic units in the Nicola and Slocan groups.

6.2. Structural correlations

The Nicola Group in the Spanish Lake area occurs on the partially-preserved, southwest-younging forelimb of a large southwest-verging fold. The Slocan Group, to the northeast, includes northeast-verging folds that are deformed by a younger set of structures related to a northeast-dipping crenulation cleavage. It is suspected that this crenulation cleavage, and related folds, are the same age as the southwest-verging fold in the Nicola Group, and therefore that the southwest-verging structures postdate the northeast-verging structures. This pattern was recognized by Rees (1987), who interpreted the Slocan and Nicola groups as an intact, west-younging stratigraphic succession that had been carried eastward, on an Early Jurassic thrust fault at the base of the Crooked amphibolite, and then deformed by southwest verging folds in the Middle Jurassic.

The structural pattern recognized by Rees (1987) in the Spanish Lake area, comprising east-directed thrusting of Slide Mountain and Quesnel terranes above pericratonic rocks, followed by west-directed folding and thrusting of this

previously assembled thrust stack, has also been recognized elsewhere in the region (Ross et al., 1985; Brown et al., 1986; Schiarizza and Preto, 1987; Murphy et al., 1995). Commonly, most of the early stage east-directed convergence was inferred to have occurred along an Early Jurassic thrust fault at the base of the Crooked amphibolite (Ross et al., 1985; Brown et al., 1986). However, Struik (1988) noted that the Slocan Group and assemblage one of the Nicola Group are the same age, and he postulated that they were juxtaposed across an east-directed thrust fault (the Spanish thrust) that probably had significant displacement and regional extent. This interpretation suggested that a significant component of the convergence between Quesnel terrane and adjacent pericratonic rocks occurred along the Spanish thrust. Furthermore, McMullin et al. (1990) proposed that the thrust fault at the base of the Crooked amphibolite is a Permo-Triassic structure, suggesting that the thrust-stacking of Slide Mountain and Quesnel terranes above pericratonic rocks was a protracted event, with the Spanish thrust as the main post-Triassic structure.

The Spanish thrust is not exposed in the Spanish Lake map area, where it is inferred to have been offset by a younger structure that forms the contact between the Slocan Group and assemblage one of the Nicola Group. Nevertheless, the contrast in sandstone composition and basalt geochemistry between these two age-equivalent units suggests significant lateral displacement, and it is inferred, following Struik (1988), that this displacement occurred on the east-directed Spanish thrust. The east-verging folds within the Slocan Group formed in the footwall of this thrust fault and are probably related. They probably formed in the late Early Jurassic, based on age constraints for easterly-verging structures along and near the eastern margin of Quesnel terrane elsewhere in southern (Murphy et al., 1995) and central (Nixon et al., 1997) British Columbia.

The partially preserved southwest-verging fold in the Nicola Group is correlated with a set of prominent southwest-verging structures documented throughout the region, which deform pericratonic rocks and structurally overlying rocks of Slide Mountain and Quesnel terranes (Ross et al., 1985; Schiarizza and Preto, 1987; Ferri and Schiarizza, 2006). The fold in the Spanish Lake area is markedly similar to a large west-verging anticline that deforms the Fennell Formation (Slide Mountain terrane) and underlying pericratonic rocks in the Clearwater-Barriere area, 150 km southeast of Spanish Lake (Schiarizza and Preto, 1987). This fold postdates structural emplacement of the Fennell Formation above pericratonic rocks, and has a steeply-dipping, west-facing forelimb more than 10 km wide. At deeper structural levels, in pericratonic rocks, these folds are represented by large southwest-verging nappes with amplitudes of several tens of kilometres (Ferri and Schiarizza, 2006). The southwest-verging folds formed mainly in the early Middle Jurassic, based in part on a 174 ± 4 Ma U-Pb age for metamorphic titanite from near Quesnel Lake (Mortensen et al., 1987).

7. Conclusions

Assemblage one of the Nicola Group forms a northwest-trending belt of Middle Triassic rocks that dips steeply, young southwest, and is stratigraphically overlain to the southwest by younger, Late Triassic assemblages of the Nicola Group. It, and adjacent Nicola assemblages are on the partially preserved forelimb of a major southwest-verging fold that probably formed in the Middle Jurassic. Assemblage one is juxtaposed against Middle Triassic rocks of the Slocan Group to the northeast, across a fault that postdates the southwest-verging fold, and probably accommodated northeast-side-up displacement.

Assemblage one consists mainly of siltstone and argillite, but also includes pillowed basalt that has geochemical characteristics of mid-ocean ridge basalt, and volcanic sandstones, similar to sandstones elsewhere in the Nicola Group, that become more abundant at higher stratigraphic levels. It is inferred to comprise the remnants of a back-arc basin that formed on the east margin of the Nicola arc. The Middle Triassic age of the basin implies that the Nicola arc, represented mainly by Late Triassic rocks, was initiated during, or before, the Middle Triassic.

Acknowledgments

I thank Evan Hall for his assistance and geological contributions during fieldwork, Sharon and Skeed Borkowski, of Northern Lights Lodge, for providing accommodation on Quesnel Lake, and Lawrence Aspler for a thorough review that improved the paper.

References cited

- Bloodgood, M.A., 1990. Geology of the Eureka Peak and Spanish Lake map areas, British Columbia. British Columbia Ministry of Energy, Mines and Petroleum Resources, British Columbia Geological Survey Paper 1990-3, 36 p.
- Brown, R.L., Journeay, J.M., Lane, L.S., Murphy, D.C., and Rees, C.J., 1986. Obduction, backfolding and piggyback thrusting in the metamorphic hinterland of the southeastern Canadian Cordillera. *Journal of Structural Geology*, 8, 255-268.
- Campbell, R.B., 1978. Quesnel Lake, British Columbia. Geological Survey of Canada, Open File 574; scale 1: 125,000.
- Colpron, M., and Price, R.A., 1995. Tectonic significance of the Kootenay terrane, southeastern Canadian Cordillera: An alternative model. *Geology*, 23, 25-28.
- Ferri, F., and Schiarizza, P., 2006. Re-interpretation of Snowshoe Group stratigraphy across a southwest-verging nappe structure and its implications for regional correlations within the Kootenay terrane. In: Colpron, M., and Nelson, J., (Eds.), *Paleozoic Evolution and Metallogeny of Pericratonic Terranes at the Ancient Pacific Margin of North America, Canadian and Alaskan Cordillera*. Geological Association of Canada, Special Paper 45, pp. 415-432.
- Ferri, F., Höy, T., and Friedman, R.M., 1999. Description, U-Pb age and tectonic setting of the Quesnel Lake gneiss, east-central British Columbia. In: *Geological Fieldwork 1998*, British Columbia Ministry of Energy and Mines, British Columbia Geological Survey Paper 1999-1, pp. 69-80.
- Holland, S.S., 1976. Landforms of British Columbia, a physiographic outline. British Columbia Department of Mines and Petroleum Resources, British Columbia Geological Survey Bulletin 48, 138 p.
- Logan, J.M., and Bath, A.B., 2006. Geochemistry of Nicola Group basalt from the central Quesnel trough at the latitude of Mount Polley (NTS 093A/5, 6, 11, 12). In: *Geological Fieldwork 2005*, British Columbia Ministry of Energy and Mines, British Columbia Geological Survey Paper 2006-1, pp. 83-98.
- Logan, J.M., and Moynihan, D.P., 2009. Geology and mineral occurrences of the Quesnel River map area, central British Columbia (NTS 093B/16). In: *Geological Fieldwork 2008*, British Columbia Ministry of Energy, Mines and Petroleum Resources, British Columbia Geological Survey Paper 2009-1, pp. 127-152.
- Logan, J.M., Schiarizza, P., Struik, L.C., Barnett, C., Nelson, J.L., Kowalczyk, P., Ferri, F., Mihalynuk, M.G., Thomas, M.D., Gammon, P., Lett, R., Jackaman, W., and Ferbey, T., 2010. Bedrock geology of the QUEST map area, central British Columbia. British Columbia Ministry of Energy, Mines and Petroleum Resources, British Columbia Geological Survey Geoscience Map 2010-1; scale 1:500,000. Also published as Geoscience BC, Report 2010-5; and Geological Survey of Canada, Open File 6476.
- McMullin, D.W.A., Greenwood, H.J., and Ross, J.V., 1990. Pebbles from Barkerville and Slide Mountain terranes in a Quesnel terrane conglomerate: evidence for pre-Jurassic deformation of the Barkerville and Slide Mountain terranes. *Geology*, 18, 962-965.
- Mortensen, J.K., Montgomery, J.R., and Phillipone, J., 1987. U-Pb zircon, monazite and sphene ages for granitic orthogneiss of the Barkerville terrane, east-central British Columbia. *Canadian Journal of Earth Sciences*, 24, 1261-1266.
- Murphy, D.C., van der Heyden, P., Parrish, R.R., Klepacki, D.W., McMillan, W., Struik, L.C., and Gabites, J., 1995. New geochronological constraints on Jurassic deformation of the western edge of North America, southeastern Canadian Cordillera. In: Miller, D.M., and Busby, C., (Eds.), *Jurassic Magmatism and Tectonics of the North American Cordillera*. Geological Society of America, Special Paper 299, pp. 159-171.
- Nelson, J.L., Colpron, M., and Israel, S., 2013. The cordillera of British Columbia, Yukon and Alaska: tectonics and metallogeny. In: *Tectonics, Metallogeny and Discovery: the North American Cordillera and Similar Accretionary Settings*. Society of Economic Geologists, Special Publication 17, pp. 53-109.
- Nixon, G.T., Hammack, J.L., Ash, C.H., Cabri, L.J., Case, G., Connelly, J.N., Heaman, L.M., Laflamme, J.H.G., Nuttall, C., Paterson, W.P.E., and Wong, R.H., 1997. Geology and platinum-group-element mineralization of Alaskan-type ultramafic-mafic complexes in British Columbia. British Columbia Ministry of Employment and Investment, British Columbia Geological Survey Bulletin 93, 141 p.
- Panteleyev, A., Bailey, D.G., Bloodgood, M.A., and Hancock, K.D., 1996. Geology and mineral deposits of the Quesnel River-Horsefly map area, central Quesnel Trough, British Columbia. British Columbia Ministry of Employment and Investment, British Columbia Geological Survey Bulletin 97, 155 p.
- Paradis, S., Bailey, S.L., Creaser, R.A., Piercey, S.J., and Schiarizza, P., 2006. Paleozoic magmatism and syngenetic massive sulphide deposits of the Eagle Bay assemblage, Kootenay terrane, southern British Columbia. In: Colpron, M., and Nelson, J., (Eds.), *Paleozoic Evolution and Metallogeny of Pericratonic Terranes at the Ancient Pacific Margin of North America, Canadian and Alaskan Cordillera*. Geological Association of Canada, Special Paper 45, pp. 383-414.
- Rees, C.J., 1987. The Intermontane - Omineca belt boundary in the Quesnel Lake area, east-central British Columbia: Tectonic implications based on geology, structure and paleomagnetism. Ph.D. thesis, Carleton University, 421 p.

- Rhys, D.A., Mortensen, J.K., and Ross, K., 2009. Investigations of orogenic gold deposits in the Cariboo Gold District, east-central British Columbia (parts of NTS 093A, H): Progress report. In: Geoscience BC Summary of Activities 2008, Geoscience BC Report 2009-1, pp. 49-74.
- Ross, J.V., Phillipone, J., Montgomery, J.R., Elsby, D.C., and Bloodgood, M., 1985. Geometry of a convergent zone, central British Columbia, Canada. *Tectonophysics*, 119, 285-297.
- Schiarizza, P., 2016. Toward a regional stratigraphic framework for the Nicola Group: Preliminary results from the Bridge Lake-Quesnel River area. In: *Geological Fieldwork 2015*, British Columbia Ministry of Energy and Mines, British Columbia Geological Survey Paper 2016-1, pp. 13-30.
- Schiarizza, P., 2017. Ongoing stratigraphic studies in the Nicola Group: Stump Lake-Salmon River area, south-central British Columbia. In: *Geological Fieldwork 2016*, British Columbia Ministry of Energy and Mines, British Columbia Geological Survey Paper 2017-1, pp. 17-33.
- Schiarizza, P., and Preto, V.A., 1987. Geology of the Adams Plateau-Clearwater-Vavenby area. British Columbia Ministry of Energy, Mines and Petroleum Resources, British Columbia Geological Survey Paper 1987-2, 88 p.
- Schiarizza, P., Israel, S., Heffernan, S., Boulton, A., Bligh, J., Bell, K., Bayliss, S., Macauley, J., Bluemel, B., Zuber, J., Friedman, R.M., Orchard, M.J., and Poulton, T.P., 2013. Bedrock geology between Thuya and Woodjam creeks, south-central British Columbia, NTS 92P/7, 8, 9, 10, 14, 15, 16; 93A/2, 3, 6. British Columbia Ministry of Energy, Mines and Natural Gas, British Columbia Geological Survey Open File 2013-05; 4 sheets, scale 1:100,000.
- Struik, L.C., 1983. Bedrock geology, Spanish Lake and adjoining areas, British Columbia. Geological Survey of Canada, Open File 920; scale 1:50,000.
- Struik, L.C., 1988. Regional imbrication within Quesnel Terrane, central British Columbia, as suggested by conodont ages. *Canadian Journal of Earth Sciences*, 25, 1608-1617.
- Struik, L.C., and Orchard, M.J., 1985. Late Paleozoic conodonts from ribbon chert delineate imbricate thrusts within the Antler Formation of the Slide Mountain terrane, central British Columbia. *Geology*, 13, 794-798.

Eaglet property, southeastern British Columbia: Re-Os geochronology, sulphur isotopes, and thermobarometry



Z.D. Hora^{1, a}, H. Stein², K. Žák³, and P. Dobeš⁴

¹ British Columbia Geological Survey (retired)

² AIRE Program, Colorado State University, Fort Collins, USA

³ Institute of Geology of the Czech Academy of Sciences, Prague, Czech Republic

⁴ Czech Geological Survey, Prague, Czech Republic

^a corresponding author: zhora@telus.net

Recommended citation: Hora, Z.D., Stein, H., Žák, K., and Dobeš, P., 2018. Eaglet property, southeastern British Columbia: Re-Os geochronology, sulphur isotopes, and thermobarometry. In: Geological Fieldwork 2017, British Columbia Ministry of Energy, Mines and Petroleum Resources, British Columbia Geological Survey Paper 2018-1, pp. 157-166.

Abstract

New Re-Os age data from three molybdenite samples collected at the Eaglet property in southeastern British Columbia yielded model ages of 200.3, 233.8 and 251.6 Ma, but the significance of these multiple ages remains unclear. Sulphur values of $\delta^{34}\text{S} +6.00$ to $+12.91\text{‰}$ for celestite are outside the range of published values for sulphates of marine origin and indicate some other crustal source of sulphate. Galena intergrown with celestite shows an overlapping $\delta^{34}\text{S}$ of $+12.07\text{‰}$, but pyrite displays much lower $\delta^{34}\text{S}$ values: $+0.99$ to -4.84‰ . With $\delta^{34}\text{S}$ restricted to -3.93 to -5.04‰ , molybdenite suggests a single homogeneous sulphur source, in spite of the three significantly different model ages. Fluid inclusions in fluorite samples display varied fluid types corresponding to three types of fluorite identified macroscopically. This is consistent with the idea of multiphase mineralization described for this deposit in previous reports. The minimum trapping pressure, constrained by temperature and composition, is 2.1 to 2.6 Kbar.

Keywords: Eaglet deposit, MINFILE 093A 046, fluorite, celestite, molybdenite, sulphur isotopes, Re-Os geochronology, fluid inclusion microthermobarometry

1. Introduction

The Eaglet property (Fig. 1; MINFILE 093A 046) is a fluorite deposit with a reported resource of 24 Mt averaging 11.5% CaF_2 (Ball and Boggaram, 1985; NI 43-101 noncompliant). Hora et al. (2008, 2010) described the exploration history, petrography, and mineralogy of the deposit and concluded that mineralization was the product of two hydrothermal events: introduction of sulphide minerals with some fluorite into fractured, K-feldspar altered host rock, followed by cataclasis and main fluorite and celestite deposition. A pilot sulphur isotopic study (Hora et al., 2010) analyzed six sulphate samples (celestite, $\delta^{34}\text{S} +6.00$ to $+12.91\text{‰}$) and two sulphide samples (molybdenite and pyrite, both with $\delta^{34}\text{S}$ between -4.81 and $+4.84\text{‰}$). The sulphur isotope results were explained by either two independent hydrothermal events that tapped different crustal sulphur sources for sulphate and sulphide, or that high-temperature isotope exchange occurred between oxidized and reduced sulphur (Hora et al., 2010).

In this paper, we test the idea of superimposed mineralization pulses at Eaglet using Re-Os age determinations of molybdenite. We also expand the set of $\delta^{34}\text{S}$ determinations to a wider variety of sulphide minerals, and present composition and trapping-temperature data from fluid inclusions in fluorite to examine the possibility of high-temperature isotope exchange.

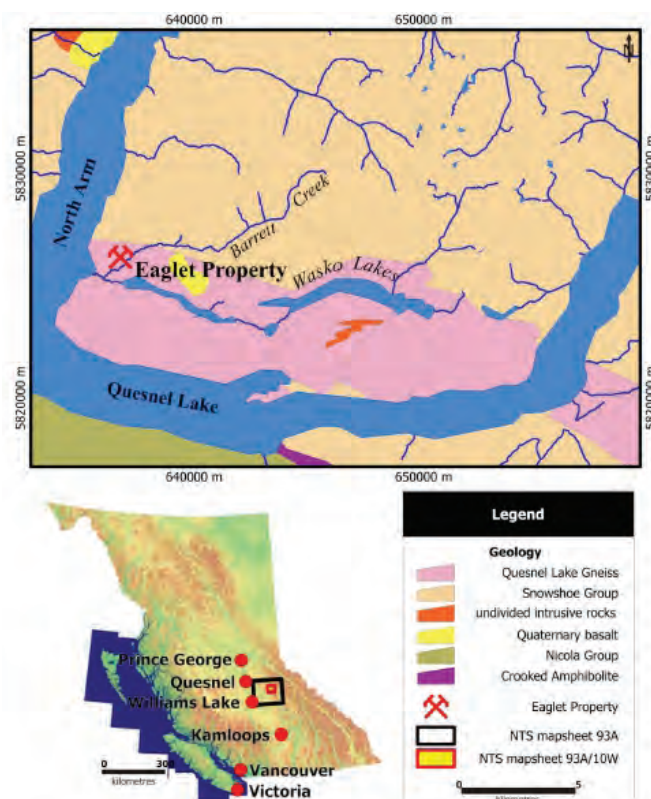


Fig. 1. Location of the study area (UTM Zone 10).

2. Regional geology

The Eaglet deposit is in the pericratonic Kootenay terrane near its border with the accreted Intermontaine superterrane. It is hosted by granitic rocks of the Quesnel Lake gneiss (Early Mississippian) which is part of the Barkerville subterrane. Orthogneiss compositions range from diorite to granite to syenite. U-Pb zircon geochronology indicates an age between 375 and 335 Ma (Ferri et al., 1999). Eaglet mineralization is in the East Quesnel Lake gneiss subunit. This subunit displays I-type characteristics with some assimilation of continental material. Although most geochemical characteristics of the East Quesnel Lake gneiss point to arc magmatism, its origins are not well understood. Ferri et al. (1999) considered that the gneiss is a relic of back-arc spreading during the Late Devonian to Early Mississippian along the western edge of ancestral North America. In this same area, rocks of oceanic character were thrust over the western margin of the Kootenay terrane during Mesozoic collision. Kootenay terrane rocks were metamorphosed from greenschist to amphibolite grade (see Ferri and Schiarizza, 2006 for details).

3. Property history

A summary of the property history can be found in MINFILE (093A 046) and Hora et al. (2008). From its discovery in 1946 until about 1980, Eaglet was considered only as a fluorite resource with silver as a potential byproduct and all samples were analyzed for fluorite only. In 1980, after Placer Development Ltd. examined the property, at that time under active exploration by Eaglet Mines Ltd., a bulk sample with visible molybdenite collected by Eaglet Mines Ltd. from the East Drift area of Adit 2 (Fig. 3) was tested for commercial Mo concentration. In 1985 the property was abandoned. Freeport Resources Inc. took over the property in 1994 and reanalyzed approximately 900 duplicate pulp samples from previous drilling and wall sampling of Adit 2 that had been stored on site by the previous owner (Hora, 2005). Analysis was by inductively coupled plasma mass spectrometry (ICP-MS), reporting either 31 or 34 elements. Results showed that Mo mineralization is more widespread than previously appreciated (Figs. 2, 3). The possibility of deep porphyry mineralization merited further investigation and provided the impetus for the present study.

4. Mineralization

The Eaglet Property, generally considered a fluorite deposit, was originally described as a stockwork of veins, pods, and irregular masses of fluorite-quartz-celestite containing minor Pb, Zn and Mo sulphides (McCammon, 1965). Calcite, pyrite, dickite, and allanite were also listed in the original description. Mineralogical and sulphur isotopic work on samples from drill core and dumps at Adits 1 and 2 (Fig. 2) were carried out by Hora et al. (2008, 2010).

The host rocks are commonly so heavily altered and recrystallized that their gneissic fabric is obscured, and the intensity of feldspar alteration makes distinguishing original

rock types uncertain. Hora et al. (2008, 2010) identified an alteration sequence of widespread albitization followed by K-feldspar alteration, with Nb, Th, Ti and REE mineralization including pyrochlore, REE carbonate (bastnesite?), thorite, and titanbetafite, none of which had been reported previously. XRD analysis revealed fluorapophyllite, also previously unknown. The Nb, Th, Ti and REE minerals exhibit extensive replacement reactions along their contacts, with silicification, albitization and then K-feldspar alteration products, and may have predated the albite-K feldspar alteration (Hora et al., 2010). Following K-feldspar alteration, introduction of some sulphide minerals (MoS_2 , FeS_2) may have occurred, before the oldest generation of fluorite. A period of cataclasis ensued, followed by carbonate alteration and addition of multiple generations of fluorite. Celestite is the last major addition to vein development. Low-temperature hydrothermal alteration superimposed on the mineralized zones introduced quartz, siderite, calcite, zeolite and clay minerals of the kaolinite group (Hora et al., 2008).

Molybdenite is common as a randomly distributed accessory mineral. It can be found along slickenside and gneissosity planes as groups of flakes (Figure 17 in Hora et al., 2008). Molybdenite also occurs as disseminated grains in quartz veinlets (sample MD-1040) and as grains in crosscutting veinlets of fluorite (samples MD 1311 and 1312). Approximately 25% of samples from 13 drill cores from 1983 exploration have Mo concentration ranging from 10s of ppm to 270 ppm (Fig. 2). More than 15% of 562 samples collected from the walls and roof of Adit 2 have between 100 ppm and 1143 ppm Mo (Fig. 3).

Celestite is the latest major hydrothermal component of mineralization. Locally in Adit 2, contents of celestite and fluorite are about equal. Celestite commonly replaces most other minerals (feldspar, quartz, calcite, and fluorite). Pyrite forms isolated crystals with molybdenite in quartz and fluorite but is less common. Sphalerite and galena are rare and spatially associated with calcite. Lead and zinc are usually elevated in the same samples, mainly in 10s of ppm and, locally, in the 100s of ppm (Hora, 2005). Quartz is common as veinlets and cement. Some veinlets contain local disseminated flakes of molybdenite and rare pyrite crystals.

5. Re-Os geochronology

The rhenium-osmium (Re-Os) chronometer is considered a reliable method for dating mineralization, particularly for molybdenite, which can be elevated in Re because it substitutes for Mo in the MoS_2 mineral structure. The Re-Os clock in molybdenite has been shown to withstand intense deformation and high-grade thermal metamorphism (e.g., Stein et al., 2001).

Two sets of samples were used for our laboratory studies. The first was selected from samples collected during a property visit in 2007. They were mainly collected from the dump below Adit 2 (sample prefix QLA) and the core storage facility (sample prefix QLC). Because of concerns of sample weathering, we also used a second set of samples, which was collected in 1984 from a 60 m-long, highly mineralized section of the East Drift

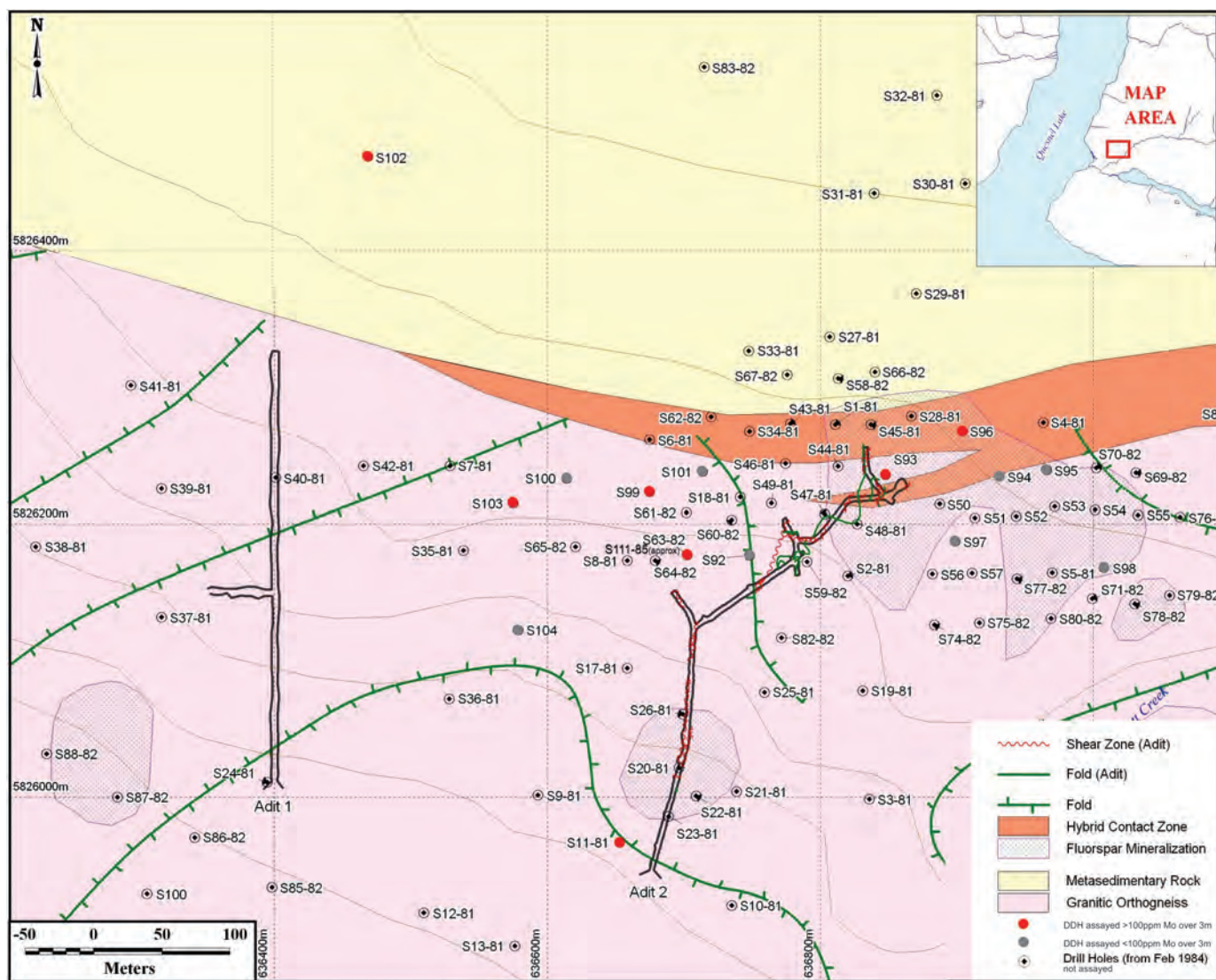


Fig. 2. Property map with adits and drill hole locations with Mo data. Courtesy of Freeport Resources Inc. (UTM Zone 10).

of Adit 2 (Fig. 3) and archived indoors at the British Columbia Geological Survey rock storage facility (designated Eaglet Adit 2, August 1984, East Drift mineral zone, Fig. 3).

Four samples collected from Adit 2 were submitted to the AIRIE program, Colorado State University for Re-Os isotopic determination of molybdenite. One sample contained molybdenite flakes in a quartz vein from a feldspathic gneiss that displayed incipient hydrothermal alteration, spotty rusty patches of iron oxide, veinlets of quartz with molybdenite, fluorite, and celestite (QLA 4; MD-1040). A second set of samples from the British Columbia Geological Survey archive collection were submitted for additional tests (Eaglet 0-1, MD-1311; and Eaglet 4, MD1312). The sample Eaglet 0-1 has molybdenite crystals in fluorite-celestite-quartz gangue and sample Eaglet 4 has molybdenite crystals in fluorite-calcite-celestite gangue with grains of siderite.

5.1. Re-Os methods

Re and Os isotopic measurements were obtained using negative thermal ionization mass spectrometry (NTIMS). Molybdenite separates were extracted from selected samples (Fig. 4) using a small hand-held drill. Molybdenite separates were 80-100% pure; sample weights ranged from 20-52 milligrams. Re-Os data were acquired using a Carius tube dissolution and a double Os spike; all samples were optimally spiked. All samples had less than 28 ppt common Os, of negligible consequence for the age calculation. Data are blank corrected, and corrected for Os isotope fractionation, and common Os. For MD-1040, blanks are Re=2.55 ± 0.04 pg, Os=0.44 ± 0.01 pg with $^{187}\text{Os}/^{188}\text{Os}=0.931 \pm 0.016$. For MD-1311 and MD-1312, blanks are Re=7.85 ± 1.48 pg, Os=1.86 ± 0.03 pg with $^{187}\text{Os}/^{188}\text{Os}=0.322 \pm 0.010$.

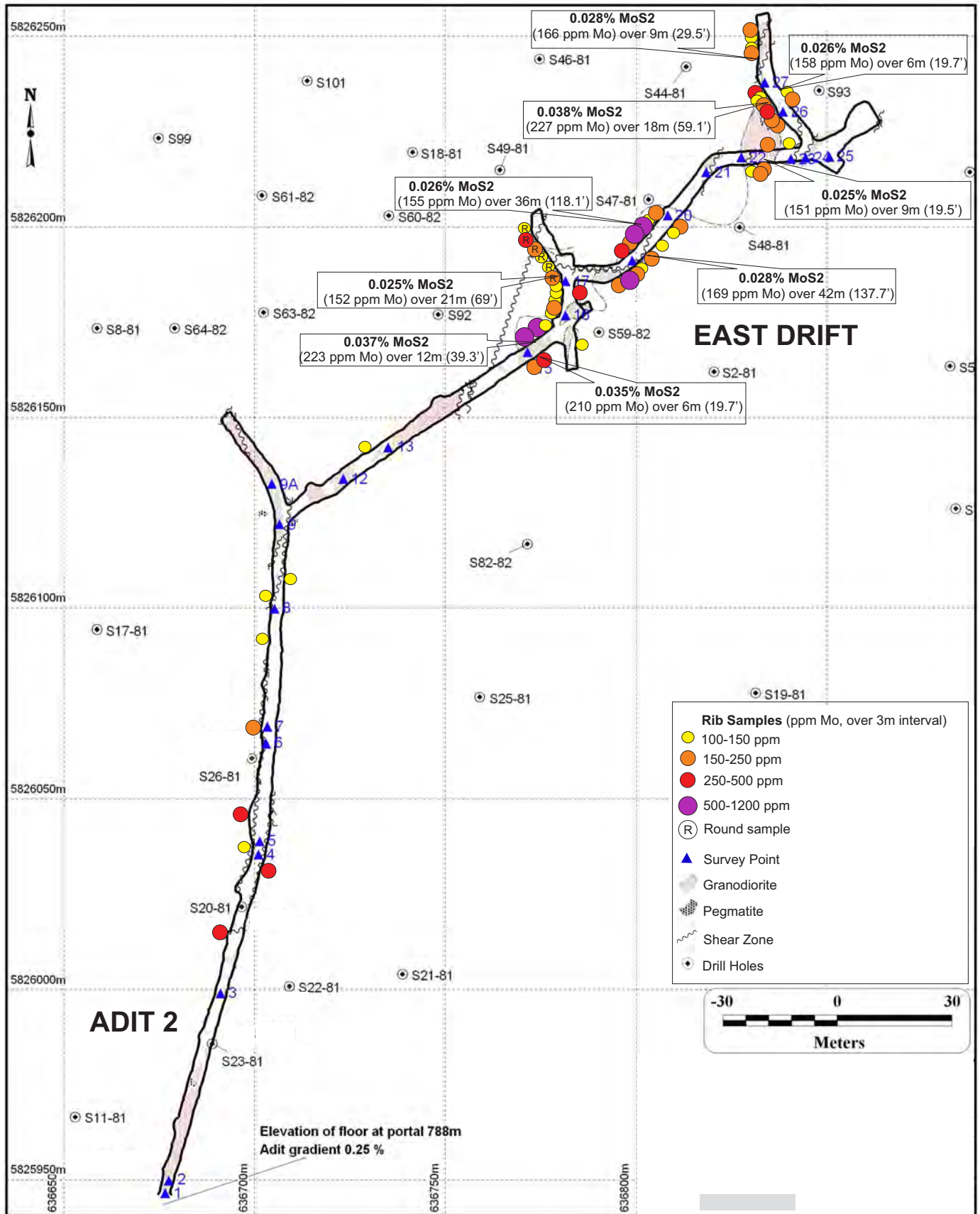


Fig. 3. Adit 2 with Mo results and East Drift mineralized zone (sample location). Courtesy of Freeport Resources Inc. (UTM Zone 10).

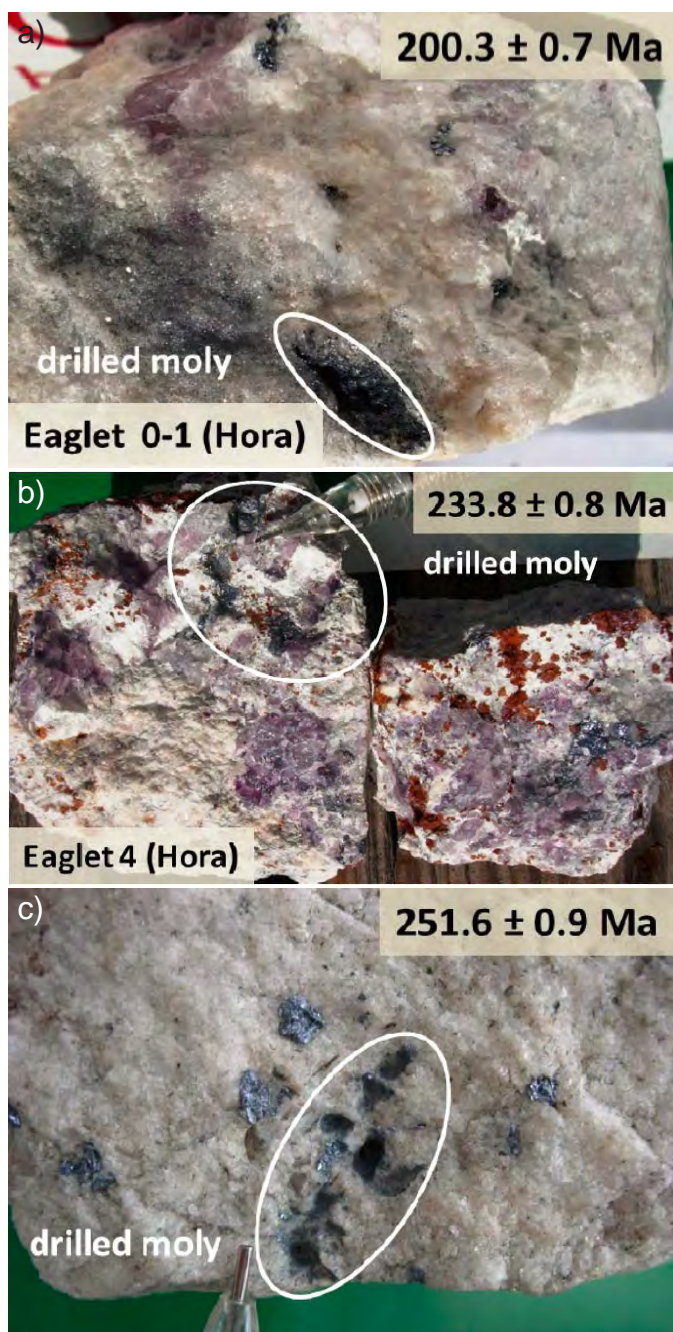


Fig. 4. Samples for Re-Os dating. **a)** MD-1311, molybdenite as small flakes in thin fluorite veinlets intersecting fluorite QL-1, spatially associated with celestite and quartz. **b)** MD-1312, molybdenite in thin fluorite veinlet in fluorite QLA-1, associated with celestite and siderite crystals. **c)** MD-1040, molybdenite in quartz vein from boulder, with celestite and fluorite QL-1 breccia veining.

5.2. Re-Os results

Re-Os data from the three Eaglet molybdenite samples from Adit 2 yielded three different model ages spanning 50 million years: 200.3 ± 0.7 Ma, 233.8 ± 0.8 Ma, and 251.6 ± 0.9 Ma (Table 1). The first sample is molybdenite in a quartz vein, whereas the other two are fissures in fluorite QL-1 and QLA-1. This type of age span is unexpected in a single deposit

and further work is warranted to assist interpreting the three disparate age results. Significant differences in molybdenite Re content from the same deposit are uncommon, but are known from other locations (Lawley and Selby, 2012) and do not affect the Re-Os results. Such differences may also reflect two polymorphous forms of molybdenite: 3R rhombohedral type, which usually carries higher Re with other impurities; and 2H hexagonal type, which is generally relatively pure (Newberry, 1979a, b). The XRD of the Eaglet molybdenite laboratory-scale concentrate sample tested in 2006 contained 33% of 3R and 22% of 2H types (Hora et al., 2008).

6. Sulphur isotope analyses

The analytical method used in this study is identical to that described in Hora et al. (2010). The initial sulphur isotope study of Hora et al. (2010) concentrated on celestite (five samples) with only two sulphide samples analyzed. Here we report eight additional $\delta^{34}\text{S}$ analyses of sulphide minerals from various mineral assemblages, including two pyrite-molybdenite pairs, i.e., minerals separated from the same samples (Table 2). The samples used for the Re-Os study were analyzed for sulphur isotopes as well.

Molybdenite in both sample sets demonstrates sulphur isotope homogeneity: $\delta^{34}\text{S}$ values fall in a narrow range between -3.93 and -5.04‰ , with variability slightly exceeding 1‰. This suggests deposition of molybdenite within a single mineralization process or singular source of sulphur. Pyrite $\delta^{34}\text{S}$ values range more widely, from -4.84 to $+2.42\text{‰}$. The analyzed mineral pair pyrite-molybdenite are not in isotopic equilibrium, indicating most probably that they did not crystallize from the same hydrothermal fluid. Celestite $\delta^{34}\text{S}$ also has a higher variability, between $+6.00$ and $+12.91$. Sulphur in galena is much heavier than the other sulphides, perhaps indicating a source through reduction of sulphate (i.e., celestite) sulphur, which has a similarly heavy isotopic composition.

7. Fluid inclusions in fluorite

Fluorite is plentiful in drill core and adit dump piles, providing abundant material for fluid inclusion study. Several different colours, grain sizes, and textures of fluorite are obvious and commonly occur together in hand samples. As described by Hora et al. (2008) dark purple fluorite is the oldest phase (Fluorite QLA-11). Next to form were varieties of light purple and light green to almost colourless fluorite in randomly distributed aggregates and veinlets (Fluorite QL-1). Last to form were intergrowths of medium purple, sugary aggregates together with calcite (Fluorite QLA-1). Locally altered siderite is the final phase. Samples of all three macroscopically distinct types of Eaglet fluorite were selected for fluid inclusion study.

7.1. Methods

Microthermometric investigations of fluid inclusions were done at the Czech Geological Survey in Prague using a CHAIXMECA heating and freezing stage operating from -180 to $+500^\circ\text{C}$ (Poty et al., 1976). The accuracy of temperature

Table 1. Re-Os data for molybdenite from the Eaglet F-Mo deposit.

AIRIE Run #	Sample Name	Re, ppm	Re err, abs (ppm)	¹⁸⁷ Os, ppb	¹⁸⁷ Os err, abs (ppb)	Age, Ma
MD-1040	#QLA-4	81.55	0.08	215.3	0.2	251.6 ±0.9
MD-1311	#0-1	5.641	0.009	11.86	0.01	200.3 ±0.7
MD-1312	#4	2.802	0.004	6.873	0.006	233.8 ±0.8

Molybdenite separates are 80-100% pure; dilution is silicate which does not affect Re-Os age calculation; sample weights ranged from 20 to 52 milligrams.

Re-Os analyses by NTIMS using a Carius tube dissolution and a double Os spike; all samples were optimally spiked.

All samples had less than 28 ppt common Os, negligible to the age calculation.

Data are blank corrected, and corrected for Os isotope fractionation, and common Os.

For MD-1040, blanks are Re = 2.55 ±0.04 pg, Os = 0.44 ±0.01 pg with ¹⁸⁷Os/¹⁸⁸Os = 0.931 ±0.016.

For MD-1311 and MD-1312, blanks are Re = 7.85 ±1.48 pg, Os = 1.86 ±0.03 pg with ¹⁸⁷Os/¹⁸⁸Os = 0.322 ±0.010.

Table 2. Sulphur isotope data on the celestite and sulphide minerals of the Eaglet Property. All δ³⁴S values are reported relative to CDT international standard. Overall analytical uncertainty is ±0.2‰.

Sample No.	Mineralogy	δ ³⁴ S celestite	δ ³⁴ S sulphide	Re-Os age of molybdenite, Ma
Hora et al. (2010)				
QL A-1	celestite, fluorite, quartz	+6.00		
QL A-2	celestite, quartz, fluorite	+7.06		
QL A-3	quartz, celestite, fluorite, feldspar	+12.91		
QLA-4, MD -1040	celestite, quartz, fluorite, molybdenite	+7.12	molybdenite -4.81	251.6 ±0.9
QL A-5	celestite, fluorite, quartz, feldspar	+6.87		
QL C-1	calcite, celestite, pyrite	+9.86	pyrite: -4.84	
Present study				
MD-1311 0-1	molybdenite with celestite, fluorite, quartz		molybdenite -4.34	200.3 ±0.7
0-2	molybdenite with celestite and fluorite		molybdenite - 5.04	
0-3	pyrite, close to molybdenite 0-2, in celestite and fluorite		pyrite +0.99	
MD- 1312 4	molybdenite, close to pyrite 4, in celestite and fluorite with siderite crystals		molybdenite -3.93	233.8 ±0.8
12	pyrite intergrown with fluorite and molybdenite		pyrite +2.42	
14	pyrite, pure in fluorite and celestite		pyrite -3.03	
16	galena, pure in fluorite, celestite and calcite		galena +12.07	

measurements is ±0.2°C at temperatures below 0°C and ±3°C at temperatures up to 400°C. The inclusions were classified according to Roedder's (1984) criteria for primary or secondary origins. Salinity (as wt.% NaCl equiv.) was calculated using the equations of Bodnar and Vityk (1995); the composition of the salt systems used the method described in Borisenko (1977).

V-T-X features of H₂O-CO₂ or H₂O-CH₄ inclusions were estimated according to Bakker and Diamond (2000) and Kerkhof and Thiery (2001). The density of CO₂ was calculated by the computer program FLUIDS (Bakker, 2003).

The fluid inclusion investigation began with characterizing fluid inclusion populations, also known as fluid inclusion

assemblages (FIAs). Petrographic description of fluid inclusions included the distribution of inclusions, their size, shape, liquid to vapour ratio, and their composition. Where fluid inclusion assemblages (FIAs) have uniform characteristics and occupy the same area of the sample, they are considered to have been trapped from the same hydrothermal fluid. Goldstein and Reynolds (1994) and Goldstein (2001) used the term 'fluid inclusion assemblages' as "the most finely discriminated, petrographically associated, group of inclusions".

The following phase transitions were measured in the inclusions.

- TmCO₂ - temperature of melting of solid CO₂
- TmclatCO₂ - temperature of melting of clathrate of CO₂
- ThCO₂ - temperature of homogenization of CO₂
- Tmice - temperature of melting of the last ice crystal
- Th - bulk homogenization temperature
- ThCH₄ - temperature of homogenization of CH₄
- LVR=L/(L+V) - liquid to vapour ratio

7.2. Results

7.2.1. Fluorite QLA-11

This sample is of dark purple fluorite considered the oldest variety in the Eaglet deposit (Hora et al., 2008). Primary inclusions in 3D distribution were found in the well-preserved parts of fluorite crystals and lack extensive trails of secondary inclusions. The inclusions measured have various shapes, range in long dimension from 5 to 80 μm, (Figs. 5 a, b) and have various compositions and numbers of contained phases.

H₂O, CO₂, or a mixture of these phases are common. H₂O inclusions have mostly consistent LVR=0.9, and are up to 20 μm in diameter. Tmice=-0.2 to -0.6°C, corresponding to salinities of an aqueous solution between 0.4 and 1.1 wt.% NaCl equivalent. Homogenization temperatures were measured only in inclusions with LVR=0.9, and ranged from 126 to 142°C.

H₂O-CO₂ inclusions are oval or fill space of crystal shape, up to 60 μm in diameter, and have LVR=0.4 to 0.7. TmCO₂ were measured between -56.3 and -57.5°C, which indicates very small amounts of CH₄ or N₂ in the vapour phase. TmclatCO₂=8.5 to 9.5°C, equal to the salinity of an aqueous solution from 1 to 3 wt.% NaCl equivalent. CO₂ homogenized to liquid at a temperature from 6.2 to 22.6°C. The density of CO₂=0.750-0.890 g/cm³. Homogenization temperatures were not observed because the inclusions consistently decrepitated, at about 230°C, before homogenization was achieved.

Several H₂O-CO₂ inclusions contain a small crystalline solid phase. Because the same isolated crystals can be found in solid fluorite, we believe that these crystals are not 'daughter crystals', i.e., crystallized from an oversaturated solution. Crystals are too small to identify (Fig. 5 b).

All inclusion types are observed together within one FIA indicating that they are contemporaneous. However, the inclusions can display variable composition, variable LVR, but a relatively narrow range of ThCO₂. Criteria supporting either a homogeneous or heterogeneous environment of inclusion trapping are ambiguous (Touret, 2001; Touret and Frezzotti,

2003). Measurements from pseudosecondary inclusions (see below) suggest that at least some of the H₂O-CO₂-rich inclusions were trapped in a homogeneous environment where H₂O-rich and CO₂-rich fluid phases were miscible (i.e., a single phase fluid that subsequently unmixed into immiscible CO₂ and H₂O phases; Fig. 5c).

A FIA containing H₂O-CO₂-rich fluid was found along short trails and are probably of pseudosecondary origin. These inclusions have a negative crystal shape and relatively consistent LVR=0.7. TmCO₂=-56.5°C, indicating pure CO₂ content in the vapour phase, TmclatCO₂=9.0 to 9.5°C, corresponding to the salinity of an aqueous solution between 1 and 2 wt.% NaCl equiv. The values of ThCO₂ (to liquid) ranged between 18.9 and 23.8°C, and the density of CO₂ was from 0.726 to 0.790 g/cm³. The bulk homogenization temperature ranged between 284 and 288°C.

An FIA with consistent LVR, ThCO₂ and Th within the narrow range can be considered as trapped in a homogeneous environment, where H₂O-rich and CO₂-rich phases are miscible. In such cases, bulk Th values are equal to the lowest temperatures of trapping of the inclusions (Fig. 5d). The minimum trapping pressure, constrained by temperature and composition, is about 2.1 to 2.6 Kb.

7.2.2. Fluorite QL-1

This sample represents the most abundant fluorite in the Eaglet deposit. It is usually massive and coarse grained, of lighter colours (purple or greenish to colourless). Primary H₂O-CO₂ inclusions were found along two distinct growth zones. The inclusions are oval to irregular shape, up to 40 μm in diameter (Fig. 5e), and have variable LVR. TmCO₂=-56.8 to -57.3°C, that indicate inclusions contain almost pure CO₂; Tmclat CO₂=8.7 to 9.2°C, corresponds to salinities between 1 and 3.5 wt.% NaCl equiv. CO₂ homogenized to liquid at temperatures from 6.5 to 8.5°C; the density of CO₂ was 0.874 to 0.887 g/cm³. Th values were not determined because the inclusions decrepitated before homogenization was attained.

7.2.3. Fluorite QLA-1

This fluorite is a later phase of intergrown medium purple fluorite, with calcite and highly altered siderite turned into rusty iron oxide. The fluorite contains primary oval inclusions up to 80 μm across (Fig. 5f), and variable LVR. This FIA is H₂O-rich. In some vapour-rich inclusions (LVR=0.1) methane was identified.

Homogenization temperatures of these H₂O-rich inclusions were measured for inclusions with LVR=0.8 to 0.9. Th values ranged from 108 to 159°C. Tmice was between -0.1 and -0.7°C, corresponding to salinities of 0.2 to 1.2 wt.% NaCl equivalent. CH₄ was identified only in several vapour-rich inclusions. CH₄ homogenized to liquid at temperature -85.6°C; it corresponds to a density of CH₄=0.217 g/cm³. H₂O and H₂O-CH₄ inclusions were probably trapped under conditions where the phases were immiscible.

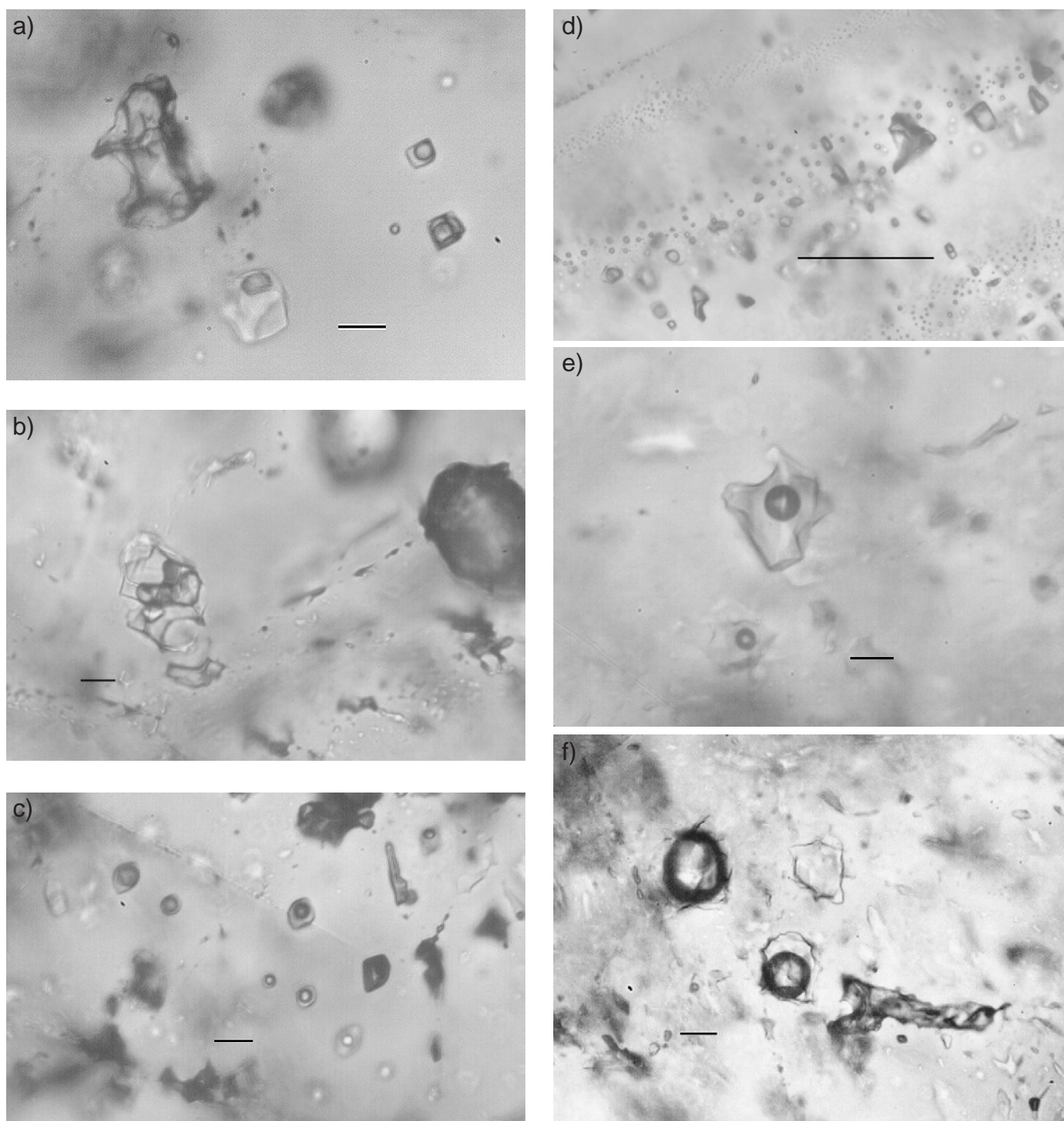


Fig. 5. Fluid inclusions. **a)** QLA-11 primary H₂O-CO₂ inclusions (scale 10µm). **b)** QLA-11 primary H₂O-CO₂ inclusions containing crystalline solid phase (scale 10µm). **c)** QLA-11 primary-secondary inclusions of H₂O-CO₂ type, consistent LVR (scale 10µm). **d)** QLA-11 secondary H₂O-CO₂ inclusions (scale 100µm). **e)** QLA-1 primary H₂O inclusions (scale 10µm). **f)** V>L primary H₂O-CH₄ inclusions (scale 10µm).

8. Discussion

Widespread distribution of molybdenite in reanalyzed drill core pulps and Adit 2 samples suggest that Mo could be a potential co-product should the deposit ever be mined. Re-Os molybdenite model ages appear to record molybdenite mineralization at 251.6 ± 0.9 Ma, 233.8 ± 0.8 Ma and

200.3 ± 0.7 Ma, spanning 50 million years. To our knowledge, such long-term episodicity is unknown in porphyry deposit settings. Especially surprising is that all three samples come from the same highly mineralized zone intersected in Adit 2 and all three samples plot in a narrow range of molybdenite $\delta^{34}\text{S}$ values, suggesting a uniform sulphur source.

With respect to sulphur sources, the data can be interpreted in two ways. Either the sulphate (celestite) oxidized sulphur and reduced sulphur were derived (recycled) from two different crustal sulphur sources, or the observed pattern resulted from a high-temperature isotope exchange between reduced and oxidized sulphur in the hydrothermal fluids (Ohmoto and Lasaga, 1982). With respect to sulphur isotope homogeneity of the molybdenite the first possibility is more probable. In molybdenite, the sulphur isotope data are very close whereas those in celestite vary more widely.

Macroscopic observations and limited microprobe data suggest that molybdenite growth was independent of celestite, which also supports independent sulphur sources and/or different fluid histories leading to growth of these two minerals (Hora et al., 2008). Some molybdenite may have recrystallized and thus reset the Re-Os geochronometer while retaining the same $\delta^{34}\text{S}$ composition (Suzuki et al., 2001). This process requires Re and Os decoupling and Os mobility within single molybdenite crystals (Stein et al., 2003; Košler et al., 2003; Aleinikoff et al., 2012). Further work will be required to test this possibility.

Complexity in mineralogy and chemical composition makes the Eaglet deposit difficult to assign to a specific mineral deposit type. Nevertheless, the style of mineralization at Eaglet is probably not unique. In a similar pericratonic location, some 150 km southeasterly from Eaglet, is the Rexspar fluorite deposit (also known as Birch Island; MINFILE 082M 007, 021, 022, 034 and 043). Sheared mineralized breccias reportedly contain a similar suite of associated minerals: molybdenite, celestite, strontianite, chalcopyrite, galena, niobian ilmenorutile, and a variety of uranium and thorium minerals in a pervasive potassium alteration halo (Pell, 1992). Unfortunately, Re-Os and sulphur isotope data are lacking and the mineralization at Rexspar is not sufficiently characterized to permit more detailed comparison.

9. Conclusions

Analytical work presented here further characterizes mineralization at the Eaglet property. Sulphur isotope data support work reported previously that indicated distinct and multiple phases of different types of mineralization, including Nb, REE and celestite. Most important is the peculiarity of three different Re-Os ages for molybdenite with consistent sulphur isotopic compositions suggesting derivation from a homogeneous sulphur isotope reservoir. In contrast, pyrite and celestite have much higher $\delta^{34}\text{S}$ variability. The significance of the multiple Re-Os ages remains unresolved and requires additional study.

The three distinct types of fluorite sampled from the Eaglet deposit have different FIA chemistries. Of the three samples, two contain FIAs with differing $\text{H}_2\text{O}-\text{CO}_2$ mixtures, or almost a pure CO_2 in some instances. The oldest, dark purple fluorite contained inclusions of a solid crystalline phase conspicuously absent in most common, pale coloured fluorite type. Fluid inclusions in a sample of youngest fluorite phase contained

significant methane component (CH_4).

A multiphase mineralizing history is suggested by the Re-Os geochronology; three different populations of fluorite with distinct fluid inclusion assemblage compositions; hydrothermal overprinting of early phase Nb-Th-Ti-REE mineralization (Hora et al., 2010), and an overall multi-stage stockwork character, with late emplacement of celestite. The economic potential of the Eaglet property is not established.

Acknowledgments

In memoriam of our colleague Edvin Pivec, who helped to coordinate several phases of the Eaglet property research. Due to his untimely death he could not participate in concluding work on the project. Initial support of this work was partly funded by the Beetle Impacted Zone project under the auspices of the British Columbia Geological Survey. Continued interest and support by Mitch Mihalynuk and Freeport Resources Inc. are appreciated. Review of an initial draft by Dave Lefebure and Mitch Mihalynuk significantly improved the final text. Participation of K. Žák was possible thanks to the support by the RVO67985831 program. I. Jačková prepared the samples and operated the mass spectrometer to obtain the sulphur isotope data. Kirk Hancock helped prepare the final draft. The final text was improved by reviewers L. Ootes and S.M. Rowins.

References cited

- Aleinikoff, J.N., Creaser, R.A., and Lowers, H.A., 2012. Multiple age components in individual molybdenite grains. *Chemical Geology*, 300-301, 55-60.
- Bakker, R.J., 2003. Package FLUIDS 1. Computer programs for analysis of fluid inclusion data and for modelling bulk fluid properties. *Chemical Geology*, 194, 3-23.
- Bakker, R.J., and Diamond, L.W., 2000. Determination of the composition and molar volume of $\text{H}_2\text{O}-\text{CO}_2$ fluid inclusions by microthermometry. *Geochimica et Cosmochimica Acta*, 64, 1753-1764.
- Ball, C.W., and Boggaram, G., 1985. Geological investigation of the Eaglet fluorspar deposit. *Mining Magazine*, 30, 506-509.
- Bodnar, R.J., and Vityk, M.O., 1995. Interpretation of microthermometric data for $\text{H}_2\text{O}-\text{NaCl}$ fluid inclusions. In: De Vivo, B., Frezzotti, M.L., (Eds.), *Fluid Inclusions in Minerals: Methods and Applications*. Short course of the working group Inclusions in Minerals. Blacksburg, VA, Virginia Polytechnic Institute, pp. 117-130.
- Borisenko, A.S., 1977. Cryotechnic methods for the determination of fluid inclusions salts in minerals. *Geologia i Geofizika*, 8, 16-27. (in Russian).
- Ferri, F., and Schiarizza, P., 2006. Reinterpretation of the Snowshoe Group stratigraphy across a southwest-verging nappe structure and its implications for regional correlations within the Kootenay terrane. In: Colpron, M., and Nelson, J.L., (Eds.), *Paleozoic Evolution and Metallogeny of Pericratonic Terranes at the Ancient Pacific Margin of North America*, Canadian and Alaskan Cordillera. Geological Association of Canada Special Paper 45, pp. 415-432.
- Ferri, F., Höy, T., and Friedman, R.M., 1999. Description, U-Pb age and tectonic setting of the Quesnel Lake gneiss, east-central British Columbia. In: *Geological Fieldwork 1998*, British Columbia Ministry of Energy and Mines, British Columbia Geological Survey Paper 1999-1, pp. 69-80.
- Goldstein, R.H., 2001. Fluid inclusions in sedimentary and

- diagenetic systems. *Lithos*, 55, 159-192.
- Goldstein, R.H., and Reynolds T.J., 1994. Systematics of fluid inclusions in diagenetic minerals. *SEPM Short Course*, 31, Tulsa, 199 p.
- Hora, Z.D., 2005. Analytical report on new assay data from 1980-1984 drill core samples, Q claims Cariboo Mining Division. British Columbia Ministry of Energy, Mines and Petroleum Resources, Assessment Report 27823.
- Hora, Z.D., Langrová A., and Pivec, E., 2008. Eaglet property revisited: Fluorite-molybdenite porphyry-like hydrothermal system, east-central British Columbia (NTS 093A/10W). In: *Geological Fieldwork 2007*, British Columbia Ministry of Energy, Mines and Petroleum Resources, British Columbia Geological Survey Paper 2008-1, pp. 17-30.
- Hora, Z.D., Langrová A., Pivec, E., and Žák, K., 2010. Niobium-thorium-strontium-rare earth element mineralogy and preliminary sulphur isotope geochemistry of the Eaglet property, east-central British Columbia (NTS 093A/10W). In: *Geological Fieldwork 2009*, British Columbia Ministry of Forests, Mines and Lands, British Columbia Geological Survey Paper 2010-1, pp. 93-96.
- Kerkhof van den, A., and Thiéry, R., 2001. Carbonic inclusions. *Lithos*, 55, 49-68.
- Košler, J., Simonetti, A., and Sylvester, P.J., 2003. Laser-ablation ICP-MS measurements of Re/Os in molybdenite and implications for Re-Os geochronology. *Canadian Mineralogist*, 41, 307-320.
- Lawley, C.J.M., and Selby, D., 2012. Re-Os geochronology of quartz-enclosed ultrafine molybdenite: implications for ore geochronology. *Economic Geology*, 107, 1499-1505.
- McCammon, J.W., 1965. Fluorite: Eaglet group. British Columbia Ministry of Mines, Annual Report 1965, 263-264.
- Newberry, R.J., 1979a. Polytypism in molybdenite (I): a non-equilibrium impurity-induced phenomenon. *American Mineralogist*, 64, 758-767.
- Newberry, R.J., 1979b. Polytypism in molybdenite (II): relationship between polytypism, ore deposition/alteration stages and rhenium contents. *American Mineralogist*, 64, 768-775.
- Ohmoto, H., and Lasaga, A.C., 1982. Kinetics of reactions between aqueous sulphates and sulphides in hydrothermal systems. *Geochimica et Cosmochimica Acta*, 46, 1727-1745.
- Pell, J., 1992. Fluorspar and fluorine in British Columbia. British Columbia Ministry of Energy, Mines and Petroleum Resources, British Columbia Geological Survey Open File 1992-16, 82 p.
- Poty, B., Leroy, J., and Jachimowicz, L., 1976. A new device for measuring the temperature under the microscope: the Chaixmeca microthermometry apparatus. *Bulletin de la Societe Francaise de Mineralogie et de Cristallographie*, 99, 182-186.
- Roedder, E., 1984. Fluid inclusions. *Reviews in Mineralogy*. Mineralogical Society of America, 644 p.
- Stein, H.J., Markey, R.J., Morgan, J.W., Hannah, J.L., and Schersten A., 2001. The remarkable Re-Os chronometer in molybdenite: how and why it works. *Terra Nova*, 13, 479-486.
- Stein, H.J., Schersten, A., Hannah, J., and Markey, R., 2003. Sub-grain scale decoupling Re and ¹⁸⁷Os and assessment of laser ablation ICP-MS spot dating in molybdenite. *Geochimica et Cosmochimica Acta*, 67, 3673-3686.
- Suzuki, K., Feely, M., and O'Reilly C., 2001. Disturbance of the Re-Os chronometer of molybdenite from the late-Caledonian Galway Granite, Ireland, by hydrothermal fluid circulation. *Geochemical Journal*, 35, 29-35.
- Touret, J.L.R., 2001. Fluids in metamorphic rocks. *Lithos*, 55, 1-25.
- Touret, J.L.R., and Frezzotti, M.L., 2003. Fluid inclusions in high pressure and ultrahigh pressure metamorphic rocks. In: Carswell, D.A., and Compagnoni, R., (Eds.), *Ultrahigh-Pressure Metamorphism*, E.M.U. Notes in Mineralogy, 5, pp. 467-487.

Rapid identification of sand-size mineral grains using portable XRF: A new method for indicator mineral surveys



Alexei S. Rukhlov^{1, a}, Mao Mao¹, and Christina Rippon²

¹ British Columbia Geological Survey, Ministry of Energy, Mines and Petroleum Resources, Victoria, BC, V8W 9N3

² School of Earth and Ocean Sciences, University of Victoria, Victoria, BC, V8P 5C2

^a corresponding author: Alexei.Rukhlov@gov.bc.ca

Recommended citation: Rukhlov, A.S., Mao, M., and Rippon, C., 2018. Rapid identification of sand-size mineral grains using portable XRF: A new method for indicator mineral surveys. In: Geological Fieldwork 2017, British Columbia Ministry of Energy, Mines and Petroleum Resources, British Columbia Geological Survey Paper 2018-1, pp. 167-182.

Abstract

Qualitative portable X-ray fluorescence (pXRF) offers a novel method of rapid, non-destructive identification of sand-size, single mineral grains. Using a (pXRF) instrument on 60 single-grain (0.5-1.0 mm) samples comprising 17 different rock-forming and accessory minerals, we detected essential constituents that readily identify ambiguous grains recovered from concentrates (e.g., Ca-P for apatite, Ca-Ti-Si for titanite, Ca-Nb-Ta for pyrochlore). Thus real-time readings (30-150 s) from a factory-calibrated instrument can help identify separated sand-sized single mineral grains in the field or laboratory. Considering the popularity of pXRF instruments, this simple method will be useful in mineral exploration and in other areas using mineral separates, such as industrial mineral, geochronologic, and provenance studies.

Keywords: Portable energy dispersive X-ray fluorescence (ED-XRF) spectrometry, pXRF, non-destructive analysis, X-ray emission spectra, indicator minerals, REE, Nb, Ta, Zr, Ti, apatite, olivine, zircon, titanite, ilmenite, pyrochlore, ferrocolumbite, zirconolite, alkali feldspar, amphibole, pyroxene, nepheline

1. Introduction

Geochemical surveys using dispersal of heavy (>2.8 g·cm⁻³) and indicator minerals in drainage and glacial sediments are long-established methods of mineral exploration in regions covered by extensive overburden (e.g., Averill, 2001; McClenaghan, 2005; Gent et al., 2011; Lett and Rukhlov, 2017). Generally resistant to abrasion during glacial transport and weathering, indicator minerals characteristic of a specific ore deposit or alteration type can be detected across a greater area than the source. Mineral fractions are recovered from rocks and sediments for prospecting and for geochronologic, detrital provenance, mineral chemistry, and tracer isotopic studies. Indicator minerals are typically identified and counted by hand-picking under a binocular microscope. Fractions (typically 0.25-0.50, 0.5-1.0, and 1-2 mm) are recovered by on-site screening and panning and by laboratory processing of bulk samples using shaking tables, magnetic separators, and heavy liquids (e.g., McClenaghan et al., 2014; Plouffe et al., 2014). Although modern automated techniques such as MLA (Mineral Liberation Analysis) and QEMSCAN® (Quantitative Evaluation of Materials by SCANNing electron microscopy; see Layton-Matthews et al., 2014 for an overview) allow rapid modal analysis of even finer-grained fractions (e.g., Mackay et al., 2016), many applications still use hand-picked mineral fractions.

Visually identifying small mineral grains can be a challenge, especially for worn detrital grains. Quantitative sorting of mineral grains thus requires more sophisticated methods,

either optical, using immersion liquids, or analytical, using for example, X-ray diffraction, scanning electron microscopy with energy-dispersive X-ray spectrometry (SEM-EDS) or reflectance spectroscopy. However, some of these methods destroy the sample, need additional sample preparation (e.g., grain mounts), and require costly laboratory equipment and time-consuming procedures. Having a rapid, in-field technique to confirm ambiguous mineral grains would be beneficial to prospecting and regional indicator mineral surveys.

Energy dispersive X-ray fluorescence (ED-XRF) spectrometry is a well-established method of rapid, non-destructive, multi-elemental analysis, whereby X-rays generated by an anode tube excite electrons in sample atoms, resulting in the emission of X-rays characteristic of specific elements (e.g., Piorek, 1994). Recent advances in the ED-XRF technology have made it field portable, and thus it has become an increasingly versatile technique for in situ geological, environmental, pedological, archaeological and other applications (e.g., Bishop et al., 2004; Glanzman and Closs, 2007; Potts and West, 2008; Palmer et al., 2009; Liritzis and Zacharias, 2011; Chen et al., 2013; Weindorf et al., 2013; Wiedenbeck, 2013; Simandl et al., 2014; Quye-Sawyer et al., 2015; Sarala et al., 2015; Chiari et al., 2016; Martín-Peinado and Rodríguez-Tovar, 2016; Young et al., 2016; Bull et al., 2017; Cohen et al., 2017; Ryan et al., 2017; Steiner et al., 2017; Zhang et al., 2017). Modern portable X-ray fluorescence (pXRF) spectrometers are capable of achieving accuracy and precision of multi-elemental determinations comparable to those of larger XRF instruments and other

laboratory methods (e.g., Knight et al., 2013; Rukhlov, 2013; Rouillon and Taylor, 2016; Ryan et al., 2017; Steiner et al., 2017). Although pXRF has been widely used in mineral exploration for in-field and laboratory analysis of different types of media such as rocks, drill cuttings, sediments, and pulverized samples (e.g., Wiedenbeck, 2013; Simandl et al., 2014; Sarala et al., 2015), we are unaware of reported pXRF applications to sand-size, single mineral grains.

In this paper we propose a novel method of rapid, non-destructive identification of <1 mm-size, single mineral grains by qualitative pXRF. Relative proportions of essential elements readily identify minerals (e.g., Ca-P for apatite, Fe-Nb for ferrocolumbite). Real-time readings (30-150 s) from a factory-calibrated instrument help identify ambiguous grains in the field or laboratory. Considering the popularity of pXRF instruments, this simple method will be useful in mineral exploration and in other areas that require mineral fractions be rapidly identified, such as geochronologic, provenance, and mineral chemistry studies.

2. Materials and methods

Samples for this study comprised individual grains (mostly 0.5-1.0 mm) of known rock-forming and accessory minerals separated from carbonatites and associated silicate rocks of the Blue River area, east-central British Columbia (Pell, 1994; Table 1). Rock samples were examined in thin sections, and mineral compositions were subsequently confirmed by wavelength-dispersion, electron-probe micro-analysis (EPMA). Sample preparation and pXRF analyses were carried out in the British Columbia Geological Survey (BCGS) laboratory. Rock samples were crushed to <3 mm-size using a steel mill, sieved to 0.5-1.0 and 1-2 mm-size fractions, and the ferromagnetic fraction separated using an MRM-1 hand magnet. The 0.5-1.0 mm-size fraction was washed and processed in bromoform (CHBr_3 ; $\text{SG}=2.85 \text{ g}\cdot\text{cm}^{-3}$) into the light and heavy fractions, followed by hand-picking under a binocular microscope. In the field, panning would replace the heavy liquid processing step.

All measurements were carried out on a self-contained Thermo Scientific Niton FXL 950 ED-XRF instrument (Fig. 1) equipped with 50 kV, 200 μA , 4W silver X-ray anode and a proprietary GOLDD (Geometrically Optimized Large Area Drift Detector) high-resolution detection system, capable of low detection limit, high-precision measurement of up to 42 elements (from $Z=12$ to 92). The instrument software includes fully automated data correction and reduction protocols optimized for determining elemental concentrations ranging ppm to ~100 wt.% in soils and rocks (Thermo Scientific, 2011). Real-time concentration results are displayed for each analysis and stored, along with the raw X-ray counts, in the internal memory for offline interpretation.

At each start up (~2 min) the system self-calibrated the energy resolution of the detector. The instrument detector resolution averaged $155 \pm 3 \text{ eV}$ (1σ) over three-year period ($n=76$). Each sample was analyzed in a plastic cup (2.45 cm diameter) with a bottom made of ultra-thin ($4 \mu\text{m}$) polypropylene film held by

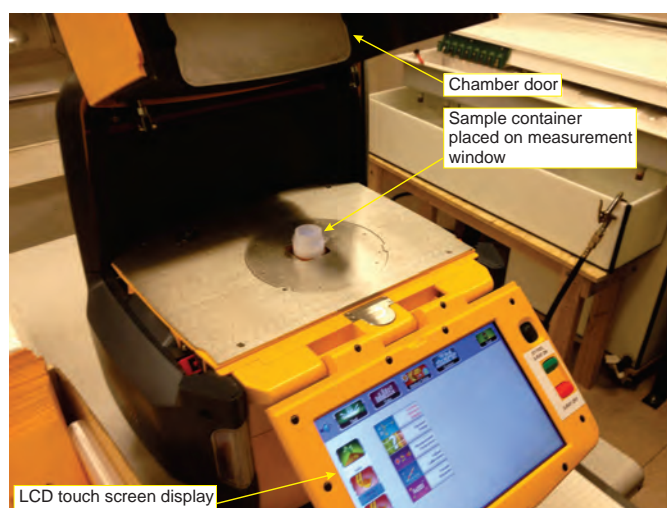


Fig. 1. Thermo Scientific Niton FXL 950 pXRF instrument and a sample container placed on the measurement window. A shielded sample chamber with an interlock system protects from X-ray radiation when the chamber door is closed and X-ray tube energized.

two concentric plastic rings (Fig. 2). The sample cup was placed onto the instrument measurement window so that mineral grain was centred above the 8 mm-diameter X-ray source (Fig. 1). For some measurements, air in the X-ray path was replaced with helium at a gas flow rate of $62.5 \text{ mL}\cdot\text{min}^{-1}$ to test if it would improve the detection of low atomic number elements such as Mg, Al, Si, P, S and Cl.

We used factory-calibrated 'Mining Cu/Zn or Ta/Hf' protocols based on fundamental parameters, because they measure a large number of elements with optimal sensitivity in different X-ray energy ranges via four excitation filters (Table 2; Thermo Scientific, 2011). Elements of the Main energy range were always measured, whereas the optional Low, High,

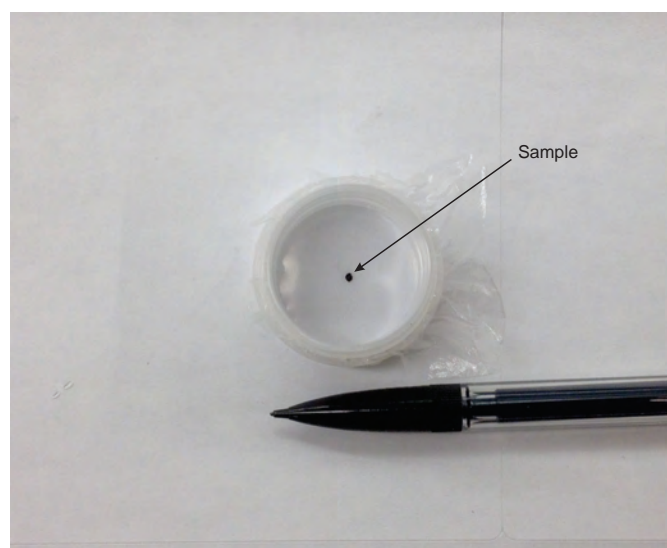


Fig. 2. Close-up of a sample holder (2.45 cm diameter) with a bottom made of ultra-thin ($4 \mu\text{m}$) polypropylene film held by two concentric plastic rings.

Table 1. Summary of minerals analyzed by pXRF as single grains. Essential elements detected are highlighted in bold.

Mineral	Source lithology	N ¹	Size fraction ²	General formula	Elements detected	Counting time ³
Albite	Fenites	5	0.5-1.0	(Na,Ca)[Al(Si,Al)Si ₂ O ₈]	Si, Ca ±Sr	105-150
Amphibole	Carbonatite	1	1.0	AB ₂ C ₅ [(Si,Al) ₈ O ₂₂](OH,F,Cl,O) ₂ A = Na, K; B = Li, Na, Mg, Fe, Mn, Ca; C = Li, Na, Mg, Fe, Mn, Al, Cr, Ti	Si, Fe, Ca, Mn	150
Apatite	Carbonatites, alkaline silicate rocks	13	0.5-1.0	A ₅ (BO ₄) ₃ (F,Cl,OH) A = Ca, Sr, Mn, Na, Y, REE ⁴ , Pb, Th, U; B = P, Si, S, As	P, Ca, Sr, Y ±S ±Ce ±Th	30-120
Calcite	Fenite	1	1.0	(Ca,Sr,Mg,Fe,Mn)CO ₃	Ca, Fe, Mn, Sr, Y	115
Dolomite	Carbonatites	2	0.5-1.0	(Ca,Sr)(Mg,Fe,Mn)(CO ₃) ₂	Ca, Fe, Mg, Mn, Sr	100
Fe sulphide	Carbonatite	1	1.0	Fe _{1-x} S – FeS ₂	Fe, S, Cu	100
Ferrocolumbite	Carbonatites	4	0.5-1.0	(Fe,Mn,Mg)(Nb,Ta) ₂ O ₆	Fe, Nb, Ta, Mn, Si, Zr, Y ±Hf ±U	115-130
Ilmenite	Carbonatites	8	0.5-1.0	(Fe,Mg,Mn,Zn)(Ti,Nb)O ₃	Fe≈Ti, Nb ±Mn ±Si ±Zr	50-150
Magnetite	Carbonatites	2	0.5-1.0	AB ₂ O ₄ A = Fe, Mn, Mg, Zn, Co, Ni, Cu; B = Fe, Cr, Al, V, Mn, Ti	Fe, Si ±Ti ±Mn ±Cr	100-115
Nepheline	Ijolite	2	0.5-1.0	(Na,K,Ca)[Al(Si,Al)O ₄]	Si, Al, K, Ca, Rb, Sr	120
Olivine	Carbonatites	7	0.5-1.0	(Mg,Fe,Mn,Ca) ₂ [SiO ₄]	Fe, Si, Mn ±Mg	35-115
Orthoclase	Granite	1	20 x 40	(K,Na,Ba)[Al(Si,Al)Si ₂ O ₈]	Si, Al, K, Ba, Fe, Ca, Sr, Mn, Rb, Ti,	150
Pyroxene	Carbonatites, fenite	4	0.5-1.0	AB[(Si,Al) ₂ O ₆] A = Li, Na, Ca, Mg, Fe, Mn; B = Mg, Fe, Mn, Al, Cr, V, Sc, Ti	Si, Ca, Fe ±Mn ±K	100-120
Pyrochlore	Carbonatites	3	0.5-1.0	A _{2-x} B ₂ O ₆ (F,OH,O) _{1-y} A = Na, Ca, U, Sr, Y, REE, Th, Ba; B = Nb, Ta, Ti, Zr, Si, Fe	Nb, Ca, Ta, U, Fe, Sr, Zr, Y ±Si ±S ±Ce ±Th	115-130
Titanite	Fenite, ijolite	2	0.5-1.0	AB[SiO ₃](O,F) A = Ca, Na, Y, REE, Sr, Mn, Mg; B = Ti, Sn, V, Al, Ta, Nb, Zr, Fe	Ca, Ti, Fe, Zr, Nb, Sr, Y, ±Si⁵	150
Zircon ⁵	Carbonatites	2	0.5-2.0	(Zr,Hf,U,Th,Y,REE)[SiO ₄]	Zr, Hf, Nb, Y	115-150
Zirconolite	Carbonatites	2	0.5-1.0	(Ca,Y,REE)Zr(Ti,Nb,Fe,Al) ₂ O ₇	Zr, Ti, Ca, Fe, Nb, Ta, Y, U, Hf, Sr ±Ce, ±Th	130-150

¹Number of analyzed grains. ²Grain size in millimetres. ³Total measurement time in seconds. ⁴Rare earth elements. ⁵Abundant Zr impedes Si detection due to spectral overlapping.

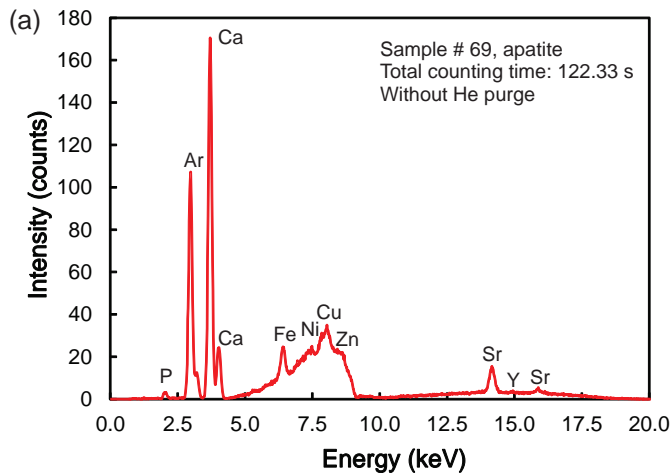
and Light energy filters were enabled to analyze samples containing these elements (Table 1). The measurements were 15-30 seconds each per energy range, except for the Light range elements, which were typically measured for 60 seconds. Although longer counting generally improves precision of the XRF analysis (e.g., Rukhlov, 2013), the total measurement time of 100-150 seconds provided acceptable counting statistics for detecting essential elements.

3. Results

We performed qualitative ED-XRF measurements on a total of 60 grains of different minerals (Table 1). An Ar peak was present in the X-ray spectra for all measurements (Figs. 3-9), except for a 2x4 cm orthoclase megacryst (larger than the instrument 8 mm sample spot; Fig. 7c). Although the pXRF detection system cannot resolve ArK α (2.958 keV) and AgL α (2.984 keV) energies, we attribute the Ar peak to the excitation

Table 2. Measurement conditions using Niton FXL “Mining” protocol in this study.

Filter ¹	Optional	Counting time (s)	Analyzed elements
Main	No	15-30	Mn, Fe, Co, Ni, Cu, Zn, As, Se, Rb, Sr, Y, Zr, Nb, Mo, Ag, Cd, Sn, Sb, Hf, Ta, W, Re, Au, Pb, Bi, Th, U
Low	Yes	15-30	K, Ca, Ti, V, Cr
High	Yes	0-30	Ag, Cd, Sn, Sb, Ba, La, Ce, Pr, Nd
Light	Yes	0-60	Mg, Al, Si, P, S, Cl

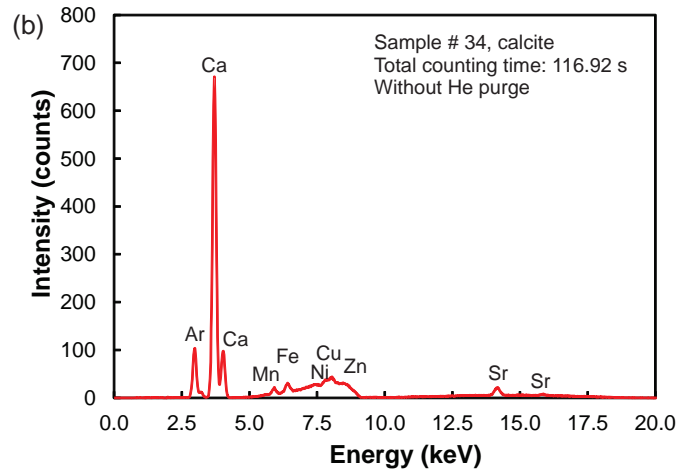
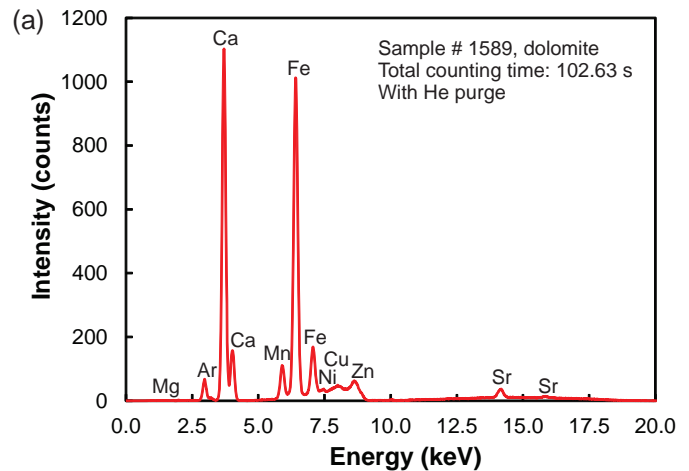
¹ X-ray energy range.

(b)

Elem	%	$\pm 2\sigma$
Al	< LOD	0.926
Si	3.071	0.284
P	10.327	0.428
S	< LOD	0.187
Cl	1.119	0.070
K	< LOD	0.227
Ca	27.390	1.093
Ti	< LOD	0.616
Mn	< LOD	0.248
Fe	0.264	0.083
Sr	0.747	0.044
Y	0.014	0.003

Fig. 3. Representative pXRF measurement on a single apatite grain (0.5 mm). **a)** Low-energy filter X-ray spectrum. **b)** Instrument read-out of the elemental abundances based on a factory-calibrated Mining protocol. Although the results are qualitative, relatively high Ca and P abundances, coupled with detectable Sr and Y, confirm apatite.

of air containing ~0.9% Ar in the X-ray path while measuring <1 mm-diameter samples on the instrument with 8 mm sample spot (K. Grattan, pers. comm. 2017). Due to using the Ag X-ray

**Fig. 4.** pXRF low energy filter X-ray spectra on single carbonate mineral grains (0.5-1.0 mm). **a)** Dolomite measured with He purge. **b)** Calcite measured with air in the X-ray path.

tube, all X-ray spectra had an elevated background or ‘hump’ in the region corresponding to the characteristic X-ray energies of Ni, Cu, and Zn (Figs. 3-9), thus yielding false minor abundances of these elements in most measurements. In addition, minor Cl detected in most measurements (Table 3) is likely due to unresolved spectral interferences in the low-energy range of the X-ray spectrum. Therefore, we will not further consider the results for Cl, Ar, Cu, Ni, and Zn.

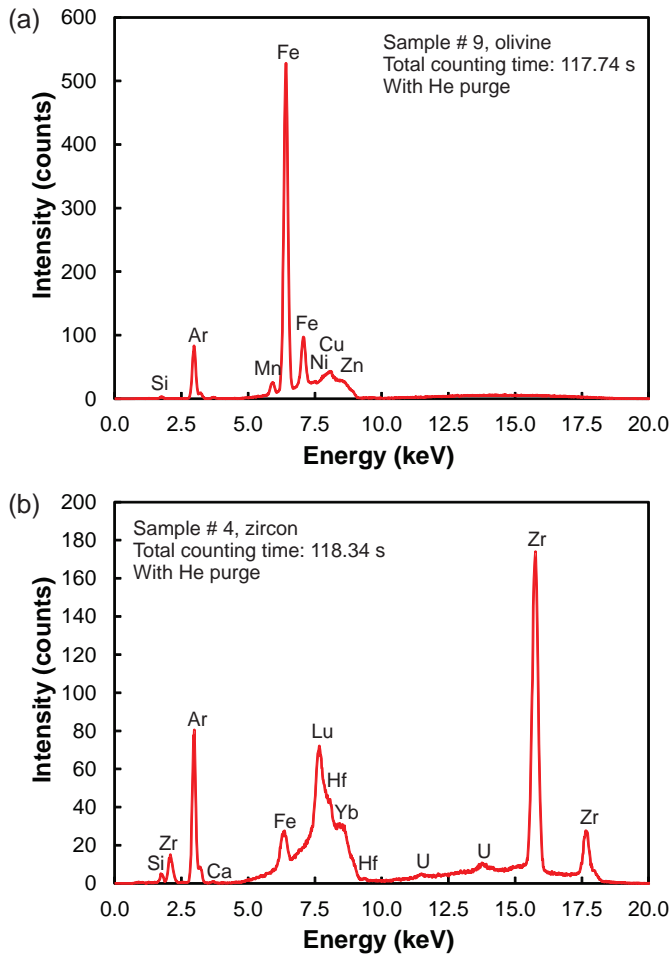


Fig. 5. pXRF low energy filter X-ray spectra on single silicate grains (0.5-2.0 mm) measured with He purge. a) Olivine. b) Zircon.

3.1. Apatite

We measured 13 apatite grains ranging from 0.5 to 1.0 mm. Two measurements were carried out with He in the X-ray path, which improved counting statistics only for Mg compared to those with air (Table 3). The pXRF measurements yielded essential Ca and P concentrations, as expected in apatite, along with relatively minor Si, Fe, Sr, and $Y \pm S \pm Ce \pm Th$ (Fig. 3), thus readily identifying the apatite grains.

3.2. Carbonate minerals

For two dolomite samples and one calcite sample (Table 1), the pXRF measurements yielded different proportions of the essential elements. Calcite yielded much higher Ca/(Fe, Mg, Mn) ratios than those of the dolomites, though Mg was detected only in measurements with He, which improved counting statistics on this element by an order of magnitude relative to the measurement with air in the X-ray path (Fig. 4; Table 3). The pXRF measurements also detected minor Sr and Si (Table 3).

3.3. Silicate minerals

3.3.1. Olivine

Six olivine samples from the Blue River carbonatites (Table 1) were measured with a He purge, whereas one sample was analyzed with air in the X-ray path. Main energy range elements were analyzed for 35 seconds. Counting statistics were similar to those for the longer measurements (100-115 seconds) using all four energy filters. All measurements showed essential Fe and Si abundances, coupled with relatively minor Mn and $Ca \pm S \pm Sr \pm Zr \pm Nb \pm Th$, with Mg detected only in one measurement made with He in the X-ray path (Fig. 5a; Table 3).

3.3.2. Zircon

Two pXRF measurements performed on zircon crystals from carbonatites (Table 1) yielded essential Zr abundances, coupled with relatively low Y, Nb, and Hf contents (Table 3; Fig. 5b). Other elements, including Si, were below the detection limits. Generally, the detection limits for low atomic number elements were much higher than those measured by pXRF on other minerals. Despite the poor counting statistics, the Si peak just visible in the X-ray spectrum, along with the prominent Zr peak at 15.78 keV (Fig. 5b), clearly identified zircon.

3.3.3. Titanite

Two titanite crystals from ijolite and fenite (Table 1) were measured for 150 seconds each using all four energy filters with air in the X-ray path. The pXRF measurements revealed essential Ti, Ca, and Si, along with minor Fe, Nb, Zr, Y, and Sr (Table 3), consistent with the available EPMA data on titanites from Blue River alkaline rocks (Mitchell et al., 2017). Similar to zircon, elevated Nb and Zr in titanite interfere with the low-energy range of the X-ray spectrum, resulting in elevated background for Si, Al and other elements (Table 3). However, the essential elements detected by pXRF (Fig. 6a) unambiguously identified titanites.

3.3.4. Pyroxenes and amphiboles

We measured four clinopyroxene (diopside to aegirine-augite) and one amphibole (actinolite-richterite) from carbonatites for 100-150 seconds (Table 1). Helium used in two measurements did not improve counting statistics relative to the analysis with air in the X-ray path. For diopside and amphibole, pXRF measurements detected essential Si, Ca, and Fe abundances, with diopsides showing much higher Si/Ca and Ca/Fe ratios than those of amphibole (Figs. 6b and d; Table 3). Minor $Mn \pm Sr \pm Zr \pm Nb \pm Th$ abundances indicate both substitutions (e.g., Mn) and inclusions (e.g., zircon and Nb-Ta oxides) in these minerals. Aegirine-augite yielded prominent Si and Fe abundances, along with detectable Mn, K and Rb. Calcium was not detected (Fig. 6c; Table 3), consistent with the mineral chemistry (Chudy, 2013; Mitchell et al., 2017). It should be noted that the Niton FXL instrument cannot detect elements with atomic number lower than Mg ($Z=12$), thereby limiting its application on Na-minerals. Although some modern

Table 3. Representative pXRF measurements on single grains of different minerals. All results are qualitative and provide only relative abundances of elements based on a factory-calibrated Mining protocol. LOD = Limit of detection based on the counting statistics (2σ error of the measurement); <LOD results are less than quoted 2σ values. NA = not analyzed; dash denotes missing values for elemental ratios owing to results <LOD or not determined.
¹Analysis also yielded 3.2 ± 0.2 wt.% Cu.

Mineral	Apatite		Dolomite		Calcite		Olivine		Diopside	
	wt.%	2σ	wt.%	2σ	wt.%	2σ	wt.%	2σ	wt.%	2σ
Sample No.	1584	8	1580	1589	34	1579	9	10		
Counting (s)	102.97	117.15	102.97	102.63	116.92	101.45	117.74	118.65		
He purge	No	Yes	No	Yes	No	No	Yes	Yes		
Element	wt.%	2σ	wt.%	2σ	wt.%	2σ	wt.%	2σ	wt.%	2σ
Si	1.122	0.137	2.340	0.157	0.786	0.096	0.542	0.040	0.994	0.119
Ti	<LOD	0.248	<LOD	0.406	<LOD	0.116	<LOD	0.097	<LOD	0.223
Al	<LOD	0.418	<LOD	0.288	<LOD	0.235	<LOD	0.064	<LOD	0.405
Fe	<LOD	0.058	0.096	0.053	0.716	0.042	4.815	0.087	0.115	0.037
Mn	<LOD	0.127	<LOD	0.172	0.079	0.050	0.573	0.043	0.229	0.077
Mg	<LOD	2.861	<LOD	0.649	<LOD	1.646	1.461	0.195	<LOD	2.483
Ca	22.101	0.525	24.825	0.640	10.587	0.240	17.969	0.236	31.882	0.589
K	<LOD	0.104	0.273	0.108	<LOD	0.066	<LOD	0.036	<LOD	0.081
P	10.161	0.082	13.162	0.319	<LOD	0.070	<LOD	0.024	<LOD	0.087
S	<LOD	0.082	0.325	0.067	<LOD	0.053	<LOD	0.021	<LOD	0.064
Cl	0.390	0.028	0.431	0.028	0.239	0.017	0.078	0.006	0.291	0.022
Rb	<LOD	0.002	<LOD	0.002	<LOD	0.002	<LOD	0.002	<LOD	0.002
Sr	0.075	0.004	0.168	0.007	0.024	0.001	0.206	0.004	0.292	0.009
Y	0.008	0.001	0.022	0.002	<LOD	0.002	<LOD	0.002	0.003	0.001
Zr	<LOD	0.002	<LOD	0.003	<LOD	0.002	<LOD	0.002	<LOD	0.003
Nb	<LOD	0.002	<LOD	0.002	<LOD	0.002	<LOD	0.002	<LOD	0.002
Ba	<LOD	0.023	<LOD	0.028	<LOD	0.014	<LOD	0.013	<LOD	0.023
Ce	<LOD	0.033	0.077	0.028	<LOD	0.019	<LOD	0.017	<LOD	0.031
Hf	NA	NA	0.060	0.018	NA	NA	NA	NA	NA	NA
Ta	NA	NA	0.293	0.033	NA	NA	NA	NA	NA	NA
Th	<LOD	0.005	<LOD	0.007	<LOD	0.003	<LOD	0.004	<LOD	0.006
U	<LOD	0.003	<LOD	0.003	<LOD	0.002	<LOD	0.002	<LOD	0.003
Cr	<LOD	0.086	<LOD	0.142	<LOD	0.039	<LOD	0.030	<LOD	0.072
Ca/Fe	-	259	14.8	3.73	277	-	-	-	-	11.6
Ca/Mn	-	-	134	31.4	139	-	-	-	-	-
Ca/Mg	-	-	-	12.3	-	-	-	-	-	-
Si/Ca	0.05	0.09	0.07	0.03	0.03	-	-	-	-	2.35

Table 3. Continued.

Mineral	Aegirine		Amphibole		Titanite		Zircon		Ilmenite		Magnetite		Fe sulphide ¹		
	wt.%	2σ	wt.%	2σ	wt.%	2σ	wt.%	2σ	wt.%	2σ	wt.%	2σ	wt.%	2σ	
Sample No.	1576	57	56	74	4	1586	1585	1578							
Counting (s)	101.92	152.10	150.04	153.29	118.34	104.05	101.09	101.39							
He purge	No	No	No	No	Yes	No	No	No	No	No	No	No	No	No	
Element	wt.%	2σ	wt.%	2σ	wt.%	2σ	wt.%	2σ	wt.%	2σ	wt.%	2σ	wt.%	2σ	
Si	4.568	0.190	13.710	0.426	6.755	0.370	17.97	<LOD	44.16	1.656	0.214	0.510	0.038	4.052	0.266
Ti	<LOD	0.138	<LOD	0.422	7.689	1.324	4.363	<LOD	0.085	6.617	1.336	<LOD	0.032	<LOD	0.193
Al	<LOD	0.250	<LOD	0.654	<LOD	0.495	1.762	<LOD	1.457	<LOD	0.507	<LOD	0.076	<LOD	0.734
Fe	1.965	0.061	12.930	0.407	0.235	0.072	0.185	<LOD	0.040	6.785	0.243	6.974	0.074	19.624	0.589
Mn	0.073	0.041	0.377	0.087	<LOD	0.256	0.313	<LOD	0.072	<LOD	0.370	0.041	0.022	<LOD	0.095
Mg	<LOD	1.635	<LOD	4.423	<LOD	3.686	15.32	<LOD	7.239	<LOD	3.867	<LOD	0.547	<LOD	5.301
Ca	<LOD	0.060	10.860	0.356	9.958	0.487	12.465	<LOD	0.019	<LOD	0.075	<LOD	0.010	<LOD	0.082
K	0.693	0.084	<LOD	0.132	<LOD	0.128	0.108	<LOD	0.047	<LOD	0.126	<LOD	0.021	<LOD	0.140
P	<LOD	0.074	<LOD	0.147	<LOD	0.144	89.160	<LOD	93.0	<LOD	0.155	<LOD	0.022	<LOD	0.146
S	<LOD	0.059	<LOD	0.112	<LOD	0.110	29.450	<LOD	50.21	<LOD	0.141	<LOD	0.017	8.086	0.271
Cl	0.261	0.020	0.606	0.039	0.605	0.044	0.487	<LOD	1.406	0.552	0.046	0.081	0.006	0.621	0.044
Rb	0.005	0.001	<LOD	0.002	<LOD	0.002	0.002	<LOD	0.002	<LOD	0.002	<LOD	0.002	<LOD	0.002
Sr	<LOD	0.002	0.003	0.001	0.003	0.001	0.059	0.027	<LOD	<LOD	0.002	<LOD	0.002	0.002	0.001
Y	<LOD	0.002	<LOD	0.002	0.010	0.001	0.026	0.012	0.014	<LOD	0.002	<LOD	0.002	<LOD	0.002
Zr	<LOD	0.002	0.002	0.001	0.024	0.002	0.169	0.079	4.764	0.004	0.001	<LOD	0.002	<LOD	0.002
Nb	<LOD	0.002	<LOD	0.002	0.011	0.001	0.244	0.115	0.008	0.056	0.004	<LOD	0.002	<LOD	0.002
Ba	<LOD	0.013	<LOD	0.036	<LOD	0.025	<LOD	0.026	<LOD	<LOD	0.029	<LOD	0.008	<LOD	0.039
Ce	<LOD	0.017	<LOD	0.048	<LOD	0.034	<LOD	0.048	<LOD	<LOD	0.041	<LOD	0.011	<LOD	0.056
Hf	NA	NA	NA	NA	NA	NA	0.194	0.119	NA	NA	NA	NA	NA	NA	NA
Ta	NA	NA	NA	NA	NA	NA	<LOD	0.027	NA	NA	NA	NA	NA	NA	NA
Th	<LOD	0.003	<LOD	0.007	<LOD	0.005	<LOD	0.009	<LOD	<LOD	0.007	0.003	0.001	<LOD	0.008
U	<LOD	0.002	<LOD	0.003	<LOD	0.002	<LOD	0.004	<LOD	<LOD	0.003	<LOD	0.002	<LOD	0.003
Cr	<LOD	0.043	<LOD	0.137	<LOD	0.744	<LOD	0.843	<LOD	<LOD	0.732	0.058	0.008	<LOD	0.073
Ca/Fe	-	-	0.84	-	42.4	-	34.2	-	-	-	-	-	-	-	-
Ca/Mn	-	-	28.8	-	-	-	-	-	-	-	-	-	-	-	-
Si/Ca	-	-	1.26	-	0.38	-	-	-	-	-	-	-	-	-	-
Fe/Ti	-	-	-	-	0.03	0.04	-	-	1.03	-	-	-	-	-	-

Table 3. Continued.

Mineral	Ferrocolumbite			Pyrochlore			Zirconolite			Albite			Orthoclase			Nepheline		
	48	46	47	1	45	66	59	51	71	wt. %	2 σ	No	wt. %	2 σ	No	wt. %	2 σ	No
Sample No.	131.63	133.7	134.92	117.37	133.00	153.41	107.49	151.94	120.11									
Counting (s)																		
He purge	No	No	No	Yes	No	No	No	No	No	No	No	No	No	No	No	No	No	No
Element	wt. %	2 σ	wt. %	2 σ	wt. %	2 σ	wt. %	2 σ	wt. %	2 σ	wt. %	2 σ	wt. %	2 σ	wt. %	2 σ	wt. %	2 σ
Si	2.214	0.228	1.970	0.168	2.121	0.131	5.343	0.260	<LOD	27.39	<LOD	30.24	16.99	0.875	23.45	0.116	14.76	0.429
Ti	<LOD	0.364	<LOD	0.346	<LOD	0.276	<LOD	0.631	4.243	2.500	3.677	2.078	<LOD	0.233	0.028	0.005	<LOD	0.183
Al	<LOD	0.515	<LOD	0.371	<LOD	0.237	<LOD	0.295	<LOD	3.497	<LOD	2.958	<LOD	1.458	7.388	0.106	6.402	0.641
Fe	3.437	0.100	3.233	0.086	0.086	0.018	1.281	0.083	1.439	0.835	1.113	0.582	<LOD	0.050	0.545	0.008	0.214	0.036
Mn	0.253	0.068	0.296	0.058	<LOD	0.083	<LOD	0.173	<LOD	0.186	<LOD	0.255	<LOD	0.108	0.047	0.004	<LOD	0.091
Mg	<LOD	3.491	<LOD	2.467	<LOD	1.489	<LOD	0.769	<LOD	28.77	<LOD	25.18	<LOD	6.631	<LOD	0.166	<LOD	2.733
Ca	<LOD	0.066	<LOD	0.031	1.554	0.083	3.904	0.246	3.001	1.662	4.282	2.182	1.418	0.128	0.151	0.007	0.228	0.086
K	<LOD	0.114	<LOD	0.083	<LOD	0.070	<LOD	0.138	<LOD	0.075	<LOD	0.089	<LOD	0.150	8.656	0.031	1.040	0.139
P	<LOD	0.311	<LOD	0.235	<LOD	0.167	<LOD	0.22	<LOD	93.87	<LOD	93.63	<LOD	0.356	<LOD	0.011	<LOD	0.136
S	<LOD	0.301	<LOD	0.231	<LOD	0.163	1.808	0.192	<LOD	56.94	<LOD	51.32	<LOD	0.295	0.021	0.006	<LOD	0.107
Cl	0.558	0.044	0.381	0.030	0.303	0.021	0.545	0.039	<LOD	0.341	0.424	0.261	0.724	0.095	<LOD	0.003	0.458	0.036
Rb	<LOD	0.002	<LOD	0.002	<LOD	0.004	<LOD	0.007	<LOD	0.002	<LOD	0.002	<LOD	0.002	0.033	0.001	0.005	0.001
Sr	0.003	0.001	<LOD	0.002	0.070	0.003	0.179	0.011	0.005	0.003	0.018	0.010	0.073	0.003	0.091	0.001	0.042	0.002
Y	0.002	0.001	0.003	0.001	0.006	0.001	0.005	0.003	0.064	0.037	0.168	0.092	<LOD	0.002	<LOD	0.002	<LOD	0.002
Zr	0.045	0.003	0.035	0.003	0.022	0.002	0.013	0.006	4.584	2.652	3.487	1.926	<LOD	0.002	0.007	0.0003	<LOD	0.002
Nb	5.815	0.201	5.584	0.177	4.409	0.113	8.963	0.564	0.827	0.479	0.199	0.111	0.002	0.001	<LOD	0.001	<LOD	0.002
Ba	<LOD	0.033	<LOD	0.030	<LOD	0.020	<LOD	0.059	<LOD	0.023	<LOD	0.025	<LOD	0.020	0.615	0.005	NA	NA
Ce	<LOD	0.046	<LOD	0.042	<LOD	0.028	<LOD	0.083	<LOD	0.078	0.213	0.128	<LOD	0.026	<LOD	0.007	NA	NA
Hf	0.026	0.016	<LOD	0.032	<LOD	0.027	<LOD	0.050	0.080	0.048	0.097	0.053	NA	NA	<LOD	0.014	NA	NA
Ta	1.075	0.046	2.650	0.074	3.710	0.078	5.100	0.233	0.349	0.204	0.172	0.093	NA	NA	<LOD	0.0002	NA	NA
Th	<LOD	0.027	<LOD	0.024	<LOD	0.021	<LOD	0.056	0.093	0.056	<LOD	0.015	<LOD	0.005	<LOD	0.003	<LOD	0.004
U	<LOD	0.005	0.004	0.003	1.351	0.037	1.522	0.097	0.129	0.074	0.015	0.009	<LOD	0.002	0.002	0.001	<LOD	0.003
Cr	<LOD	0.105	<LOD	0.099	<LOD	0.077	<LOD	0.181	<LOD	0.375	<LOD	0.389	<LOD	0.076	<LOD	0.105	<LOD	0.066
Ca/Fe	-	-	18.1	3.05	2.09	3.85	-	-	-	-	-	-	-	0.28	-	-	1.07	-
Si/Ca	-	-	1.37	1.37	-	-	-	-	-	-	-	-	12.0	156	-	-	64.7	-
Al/K	-	-	-	-	-	-	-	-	-	-	-	-	-	0.85	-	-	6.16	-
Si/K	-	-	-	-	-	-	-	-	-	-	-	-	-	2.71	-	-	14.2	-
Fe/Nb	0.59	0.58	0.02	0.14	1.74	5.59	-	-	-	-	-	-	-	-	-	-	-	-

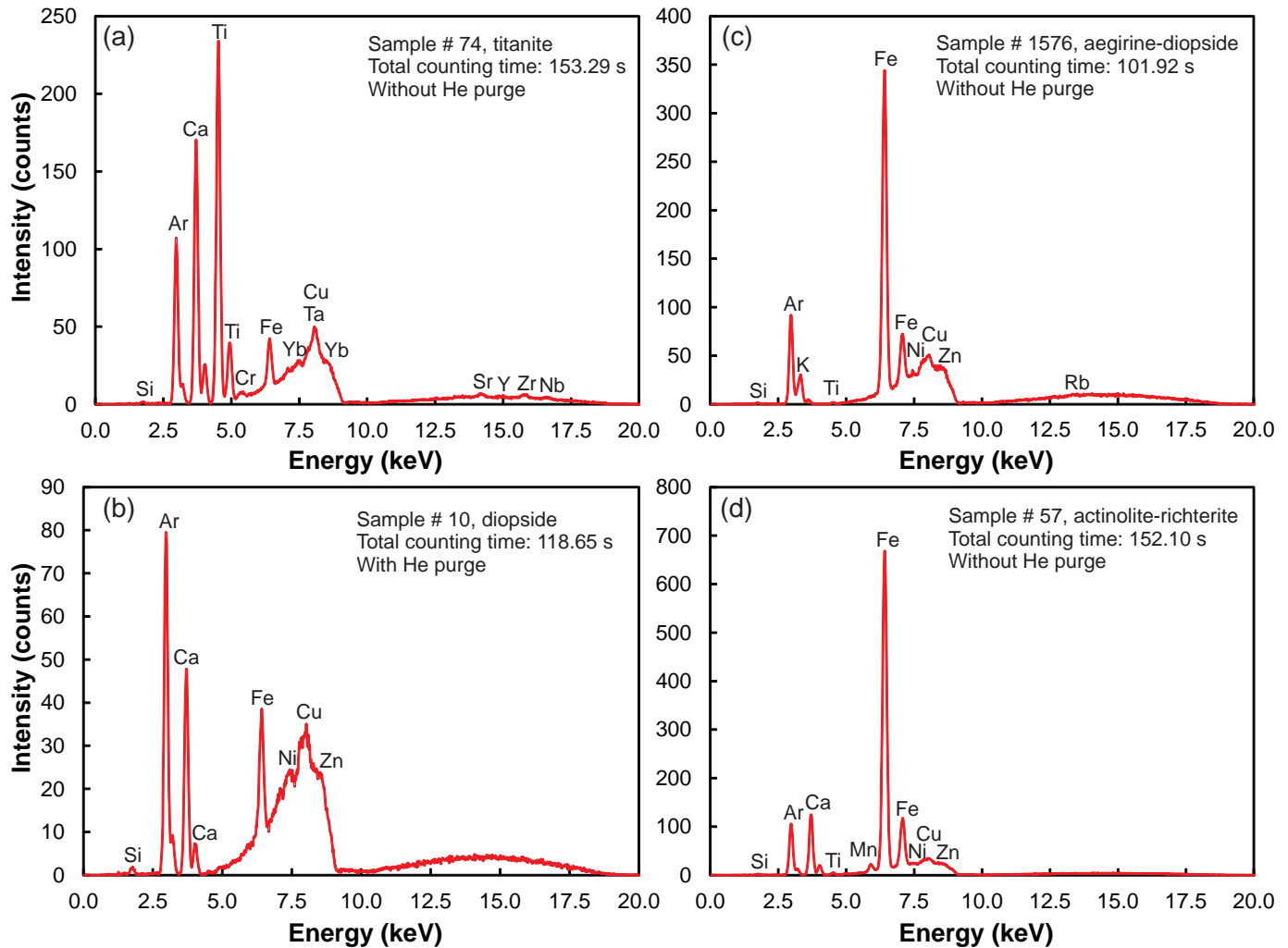


Fig. 6. pXRF low energy filter X-ray spectra on single silicate grains (0.5-1.0 mm). **a)** Titanite. **b)** Diopside. **c)** Aegirine-augite. **d)** Actinolite-richterite. All samples analyzed with air in the X-ray path, except (b) measured with He.

pXRF instruments capable of measuring Na and F (e.g., Bruker TRACER 5i) do not have this limitation, our results suggest that other elements in single-grain samples detected by pXRF readily identify pyroxenes and amphiboles.

3.3.5. Alkali feldspars and nepheline

We measured five albite ($\sim\text{An}_3$) and two nepheline single-grain (0.5-1.0 mm) samples from undersaturated alkaline rocks and fenites, and one orthoclase megacryst (2x4 cm; Table 1). All measurements, which were carried out for 105-150 seconds without He, yielded essential Si and minor Ca and $\text{Sr}\pm\text{Fe}\pm\text{Rb}\pm\text{Ba}$ abundances (Fig. 7; Table 3). Essential Al and K abundances were detected in orthoclase and nephelines but not in albites, with nephelines yielding much higher Al/K and Si/K ratios than those of orthoclase (Table 3). Although Na could not be measured using our pXRF instrument and hence alkali feldspars and feldspathoids cannot be unambiguously identified, our tests indicate that at least they can be distinguished from visually similar minerals (e.g., apatite) based on other essential elements (e.g., P).

3.4. Fe-Ti oxides

We performed pXRF measurements on two magnetite and eight ilmenite samples from carbonatites (Table 1). Total counting time was 50-150 seconds. Counting statistics for three ilmenites measured using He in the X-ray path did not improve compared to samples measured without He. The pXRF measurements readily distinguished between magnetites and ilmenites by different relative abundances of essential Fe and Ti in these minerals (Fig. 8). Minor elements detected by pXRF in the magnetites ($\text{Si}\pm\text{Mn}\pm\text{Cr}\pm\text{Nb}$) and ilmenites (Si , $\text{Nb}\pm\text{Mn}\pm\text{Ca}\pm\text{S}\pm\text{Sr}\pm\text{Zr}\pm\text{Ba}\pm\text{U}$) reflect common impurities in these minerals and possible inclusions (Table 3).

3.5. Rare-metal minerals

We analyzed single-grain samples of ferrocolumbite, pyrochlore, and zirconolite, which together with ilmenite, titanite, zircon and baddeleyite, are the principal hosts of Nb, Ta, Ti, Zr, Y, rare earth elements (REE), Th, and U in Blue River carbonatites and related rocks (Table 1).

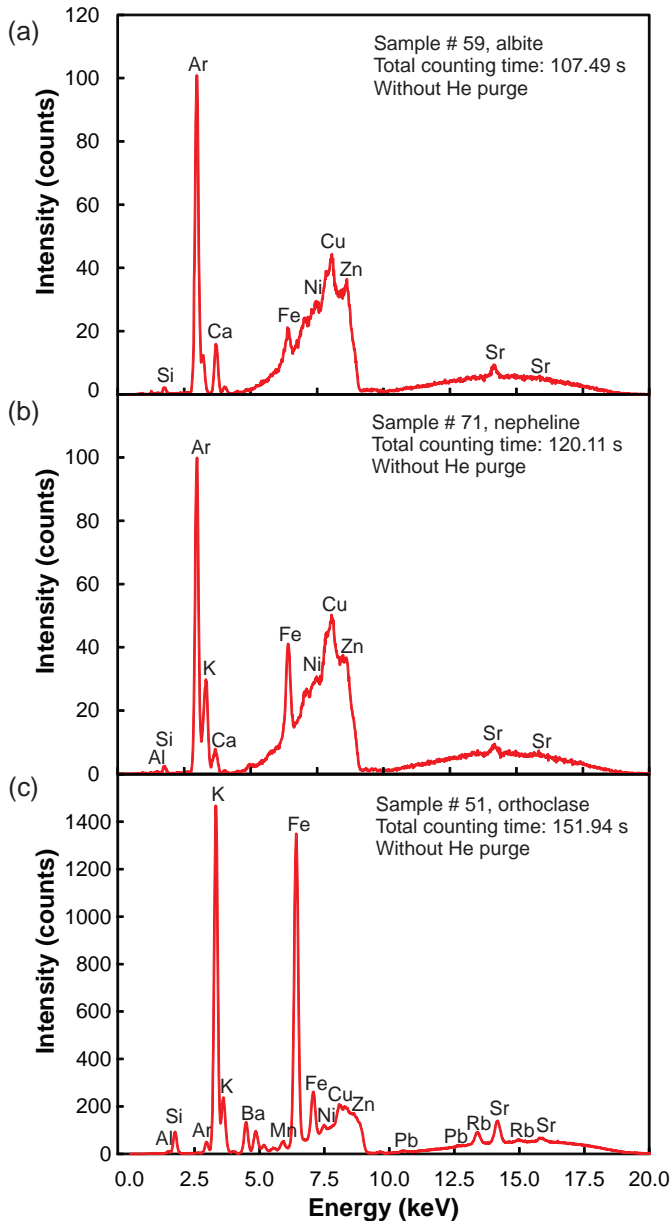


Fig. 7. pXRF low energy filter X-ray spectra on silicates measured with air in the X-ray path. **a)** Albite (~1 mm grain). **b)** Nepheline (~1 mm grain). **c)** Orthoclase megacryst (2x4 cm); note significant reduction of Ar peak compared with measurements on sand-size grains.

3.5.1. Ferrocolumbite

Four ferrocolumbite samples, measured 115-130 seconds each without He, yielded essential abundances of Fe and Nb, with minor Ta, Mn, Si, and Zr (Fig. 9a; Table 3). The qualitative pXRF results are generally consistent with ferrocolumbite compositions from Blue River carbonatites (Mariano, 1982; Chudy, 2013; Mackay and Simandl, 2015).

3.5.2. Pyrochlore

Measurements on three pyrochlore samples revealed essential Ca, Nb, Ta, and U abundances (Fig. 9b; Table 3), consistent with pyrochlore compositions from Blue River

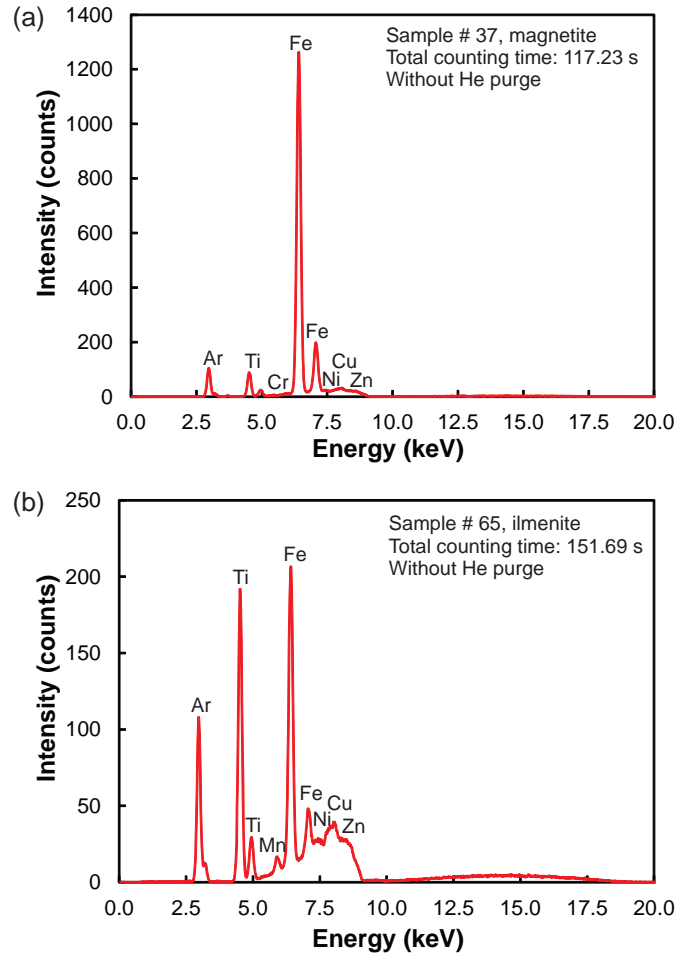


Fig. 8. pXRF low energy filter X-ray spectra on single Fe-Ti oxide grains (0.5-1.0 mm) measured with air in the X-ray path. **a)** Ti-magnetite. **b)** Ilmenite.

carbonatites (Mariano, 1982; Chudy, 2013; Mackay and Simandl, 2015). Minor elements detected by pXRF were Fe, Sr, Zr, Y±S±Ti±Ce±Th (Table 3). Although Si was also detected, we attribute it to Ta interference.

3.5.3. Zirconolite

pXRF measurements on two zirconolite samples (Table 1) readily detected essential Ti, Fe, Ca, Zr, and Nb, along with minor Sr, Y, Hf, Ta, and U±Ce±Th (Fig. 9c; Table 3). As with other Zr-rich minerals, spectral interference in the low-energy range of the X-ray spectrum rendered low-atomic number elements undetectable. Our qualitative pXRF results on single mineral grains are broadly consistent with the zirconolite chemistry (Mitchell et al., 2017) and thus demonstrate the effectiveness of pXRF for rapid identification of rare-metal minerals.

3.6. Other minerals

One pXRF measurement on a Fe sulphide grain (~0.5 mm) yielded essential Fe and S with less abundant Cu and Si

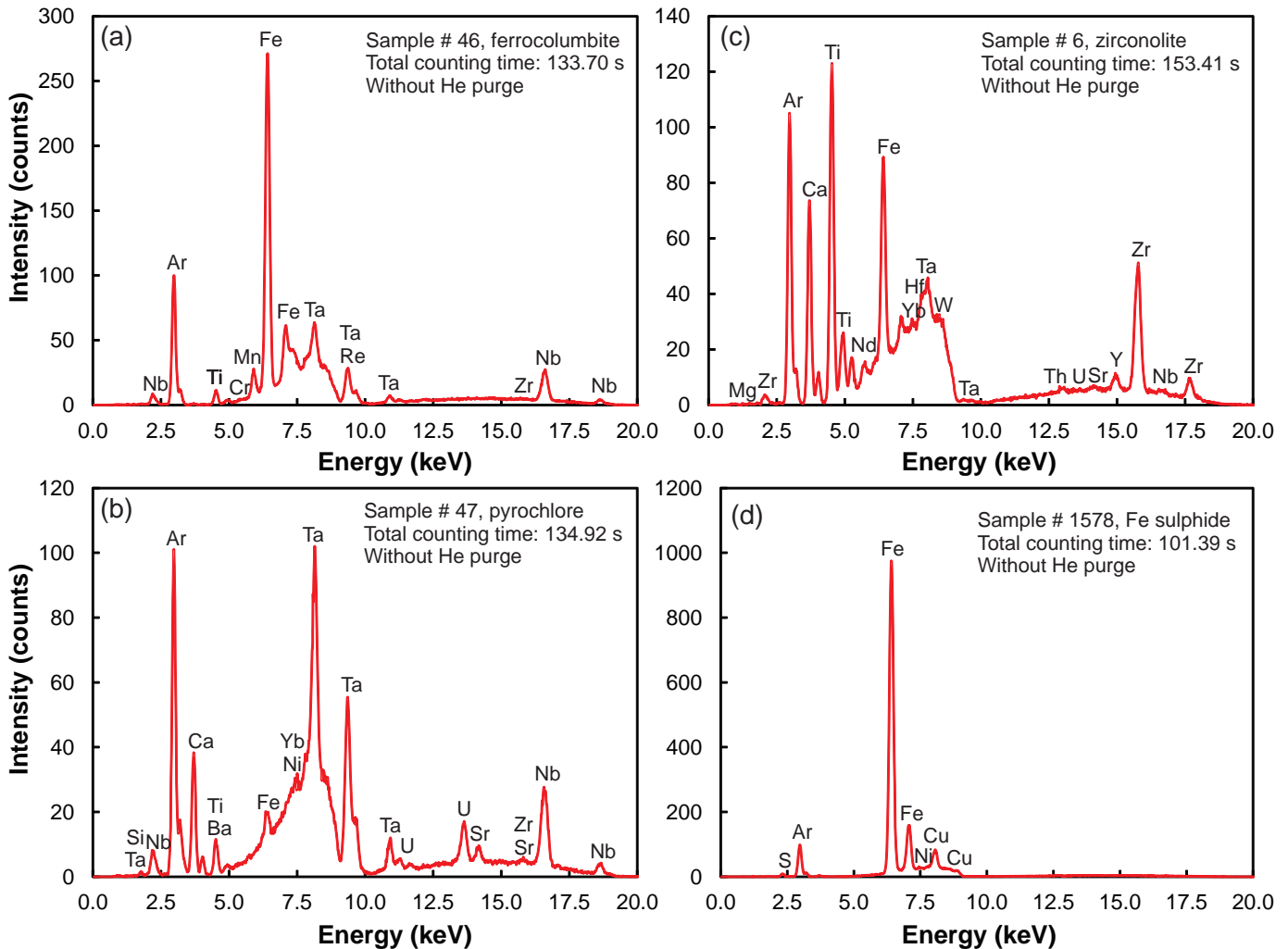


Fig. 9. pXRF low energy filter X-ray spectra on single grains of complex oxides and sulphide (0.5-1.0 mm) measured with air in the X-ray path. **a)** Ferrocolumbite. **b)** Pyrochlore. **c)** Zirconolite. **d)** Fe sulphide.

(Fig. 9c; Table 3), demonstrating the pXRF utility to confirm sulphides. Silicon likely reflects tiny amphiboles intergrown with the sulphide as suggested by petrographic examinations.

4. Discussion

Seventeen different minerals studied here, their general formulae, and essential and minor constituents detected by pXRF on single-grain (generally <1 mm) samples are summarized in Table 1. They include widespread rock-forming or accessory minerals that have a wide range of petrogenetic applications and are commonly recovered in indicator mineral surveys.

4.1. Significance of indicator minerals

Detrital dispersal of indicator minerals across a large area can be traced up the paleoflow direction to a much smaller source (Averill, 2001; McClenaghan, 2005; Gent et al., 2011; Lett and Rukhlov, 2018). Heavy (2.9-4.5 g·cm⁻³) and generally resistant to weathering, extensive solid-solution series within the

olivine, pyroxene and amphibole groups record crystallization conditions, and thus have a broad range of petrogenetic and mineral-exploration applications (e.g., Averill, 2001; Gent et al., 2011; Lett and Rukhlov, 2018). Although low-density (2.55-2.76 g·cm⁻³) feldspars and feldspathoids are usually not recovered in indicator mineral surveys, Williamson et al. (2016) suggested that plagioclase chemistry can be used as an exploration indicator for porphyry Cu deposits. Generally recessive for indicator mineral surveys, carbonates fix CO₂ and can concentrate Sr and REE, thereby making them important in stable and radiogenic isotopic applications among others (e.g., Rukhlov et al., 2015; Chakhmouradian et al., 2016).

Ubiquitous accessory or rock-forming minerals such as magnetite, ilmenite, titanite, zircon, and apatite have been widely used as indicator minerals and petrogenetic tools, because their chemistry fingerprints magmatic-hydrothermal processes and bedrock sources (Sha and Chappell, 1999; Hoskin and Ireland, 2000; Belousova et al., 2002a and b; Hayden et al., 2008; Bouzari et al., 2011, 2016; McLeod et al.,

2011; Gent et al., 2011; Carmody et al., 2014; Miles et al., 2014; Grimes et al., 2015; Bruand et al., 2016; Canil et al., 2016; Mao et al., 2016, 2017; Rukhlov et al., 2016, 2017; Smythe and Brennan, 2016). In addition, precise U-Pb ages and O-Hf-Nd isotopic compositions of detrital zircons provide insights into the Hadean crust-mantle evolution (e.g., Amelin et al., 1999; Wilde et al., 2001; Harrison et al., 2008).

Economic concentrations of minerals containing essential Nb±Ta±Ti±Zr±Hf±Y±U±Th±REE abundances are found mainly in carbonatites, related undersaturated rocks, and peralkaline complexes, with relatively minor production from granites, pegmatites and other sources (Mariano, 1989; Chakhmouradian, 2006; Chakhmouradian and Zaitsev, 2012; Mackay and Simandl, 2015; Mitchell, 2015). Burt (1989) listed about 190 minerals containing these elements as essential constituents. The most common minerals considered in this study are complex A-B oxides (A=Na, K, Ca, Fe²⁺, Mn, Mg, Sr, Ba, Pb, Y, REE, Th, and U; B=Al, Fe³⁺, V, Ti, Zr, Sn, Nb and Ta) such as pyrochlore (A_{2-x}B₂O₆(F,OH,O)_{1-y}·zH₂O), columbite (AB₂O₆), and zirconolite-zirkelite (AB₃O₇); zircon (ZrSiO₄); and titanite (ABSiO₃). Pyrochlore and ferrocolumbite are the major ore minerals in carbonatite-hosted Nb-Ta deposits in the Canadian Cordillera (Rowe, 1958; Mariano, 1982; Chudy, 2013; Chakhmouradian et al., 2015). Zirconolite was also found in Cordilleran carbonatites (A.N. Mariano, pers. comm., 1993, cited by Williams and Gieré, 1996) but analytical data were not available until recently. Millonig et al. (2012, 2013) reported accessory zirconolite (0.4-0.6 mm) associated with biotite, sulphides, magnetite, ilmenite, zircon, and baddeleyite in a carbonatite of the Blue River area. Mitchell et al. (2017) also noted rare zirconolite as inclusions in apatite and mantles (20-30 µm wide) on baddeleyite in some carbonatites and phoscoritic rocks at the Howard Creek locality mentioned by Williams and Gieré (1996). Because these minerals are resistant to physical and chemical weathering, they are useful indicators in exploration for Nb-Ta and REE deposits (Kogarko et al., 2013; Mackay and Simandl, 2015; Mackay et al., 2016).

4.2. Implications for mineral exploration

Regional geochemical surveys recovering heavy or indicator minerals from drainage and glacial deposits have been increasingly important for mineral exploration in regions covered by extensive overburden (e.g., Averill, 2001; McClenaghan, 2005; Gent et al., 2011; Lett and Rukhlov, 2018). Although bulk samples are usually processed for indicator minerals in the laboratory (McClenaghan et al., 2014; Plouffe et al., 2014), exploration companies and prospectors commonly examine the mineralogy of pan concentrates in the field (e.g., Gorham et al., 2009). However, visual identification and counting of worn detrital grains is challenging, because they lack crystal shape and may appear similar to other minerals. In our experience, 30-50% of grains hand-picked from 0.12-0.50 mm, 2.96-3.32 g·cm⁻³, non-paramagnetic (>1.2 A) fraction of granitic rocks were consistently rejected by EPMA as non-apatites (Mao et al., 2016). Though commercial laboratories

routinely check ambiguous mineral grains by SEM-EDS (e.g., Averill and Huneault, 2006), we applied the Niton FXL pXRF instrument in search of a rapid, in-field method of confirming ambiguous mineral grains.

Our qualitative pXRF measurements (30-150 seconds) on sand-size, single grains of different minerals demonstrate that essential constituents in minerals are readily detectable (Tables 1 and 3) using a factory-calibrated instrument, equipped with a standard 8 mm-wide sample spot, thereby providing a means to identify ambiguous grains. Although we used a benchtop pXRF instrument ideal for in-house applications, widely available hand-held pXRF instruments can be easily used in a benchtop mode with auxiliary test stands (Thermo Scientific, 2011). Instruments equipped with a smaller sample spot (e.g., 3 or 1 mm in diameter) and an XY control of the spot position (Thermo Scientific, 2011) would be optimal for measuring small samples such as single grains of sand.

4.3. Instrumental limitations

Unlike larger ED-XRF instruments and some newer pXRF analyzers, the Niton pXRF detection system does not determine Na (Z=11) and hence cannot unambiguously identify minerals containing essential Na concentrations. Despite this fundamental limitation, our pXRF measurements on single grains of such minerals (e.g., alkali feldspars, feldspathoids, clinopyroxenes and amphiboles) demonstrate that these minerals could be distinguished from visually similar minerals (e.g., apatite) on the basis of other essential elements detected by pXRF (Tables 1 and 3).

The 50 kV Ag X-ray target on the Niton FXL 950 pXRF instrument used in this study yields a broad peak in the low-energy range of the X-ray spectrum at ~8 keV, thus overlapping the region of the characteristic X-ray lines for Ni, Cu, Zn and other elements (e.g., Fig. 3a). Consequently, most pXRF measurements in this study had false minor abundances of these elements. Although factory-calibrated pXRF instruments are capable of precise and accurate determination of these elements on conventional samples such as soils and pulps (e.g., Knight et al., 2013; Rukhlov, 2013; Ryan et al., 2017; Steiner et al., 2017), these protocols may be inadequate for small-size samples such as <1 mm-diameter single mineral grains. However, our measurement on an Fe-sulphide grain indicated Cu content (Fig. 9d; Table 3). More measurements on small grains of minerals containing Ni, Cu, and Zn will help evaluate if they can be determined by pXRF.

4.4. Air interference with measuring small grains

All pXRF measurements on <1 mm-diameter samples in this study yielded an Ar peak in the X-ray spectra (Figs. 3-9) due to excitation of air (~0.9% Ar) in the X-ray path with an 8 mm-diameter sample spot (K. Grattan, pers. comm., 2017). Because the Ar peak size is inversely related to sample size, it may overlap adjacent low-energy lines of elements in the sample (e.g., Si, S, Cl, K, P, and Ca) with measurements on very small grains. However, Ar did not affect qualitative

detection of the essential elements for 0.5-1.0 mm-size single grains. Furthermore, our measurements to confirm ambiguous mineral grains in other studies (Rukhlov et al., 2017; Mao et al., 2018), on single grains as small as 0.12-0.25 mm, consistently detected P and Ca in apatite grains, suggesting that pXRF is a reliable, rapid method to confirm the identity of ambiguous grains.

4.5. Air versus helium in the X-ray path

Replacing air in the X-ray path with He is recommended for pXRF applications to low atomic number elements such as Mg, Al, Si, P, S and Cl (Thermo Scientific, 2011). Using He with the pXRF measurements in this study improved counting statistics (and hence detection limits) up to an order of magnitude only for Mg in some measurements on apatites, dolomites, and olivines (Table 3). However, He did not make a significant difference for detecting Mg in other minerals. Although Mg is an essential element in dolomites and olivines (Table 1), with the olivines from Blue River carbonatites containing 77-88 mol.% Mg_2SiO_4 end-member (Mariano, 1982; Mitchell et al., 2017), Mg was below the detection limit in these minerals measured with air in the X-ray path. These results illustrate the limitation of pXRF instruments for Mg determination on small samples. However, even with undetectable Mg, our pXRF measurements distinguished other essential elements in carbonate minerals (Ca-Fe-Mn) and olivine (Si-Fe-Mn). Helium did not significantly improve the detection limits for other low-atomic number elements, which were also generally detectable with air in the X-ray path in this study.

4.6. Spectral interferences

Magmatic carbonates and carbonatitic apatites are typically Sr-rich (Chakhmouradian et al., 2016, 2017; Mao et al., 2016). Although Si commonly substitutes into apatite via charge compensating reactions (see Mao et al., 2016 for an overview), minor Si detected by pXRF in apatites and carbonates in this study (Table 3) is likely due to Sr interference, because the pXRF detection system (~0.16 keV resolution) cannot resolve the $SiK\alpha$ (1.740 keV) and $SrL\alpha$ (1.807 keV) X-ray energies. Similarly, minor Si detected in Ta-rich pyrochlores is likely due to the Ta interference (Table 3).

Although Cl can be present in some mineral (e.g., apatites and amphiboles), minor Cl detected by pXRF for most samples in this study (Table 3) likely reflects unresolved spectral interferences in the low-energy range of the X-ray spectrum. Therefore, pXRF on small single grains cannot reliably determine Cl. Similarly, we attribute minor Hf and Ta detected in some apatites, olivines and diopsides (Table 3) to unresolved spectral interferences.

Detection limits for Mg, Al, Si, P, S and Cl in the pXRF measurements on Zr-rich minerals (zircon, titanite, zirconolite) were much higher than those on other minerals (Table 3). The poor counting statistics on these elements, due to the strong $Zr\pm Nb\pm Y$ interference on the low-energy range of the X-ray spectrum, thus somewhat limits pXRF application to identifying

Zr-bearing minerals. However, visual characteristics of these minerals, coupled with the robust detection of Ca, Ti, Fe, Y, Zr, Nb and other elements by pXRF (Figs. 5b, 6a and 9c), unambiguously identify these minerals.

4.7. Influence of inclusions in mineral grains

Relatively minor $Ca\pm Sr\pm Zr\pm Nb\pm Th$ detected by pXRF in some olivines, $Mn\pm Sr\pm Zr\pm Nb\pm Th$ in clinopyroxenes and amphibole, and Si in Fe-sulphide (Table 3) may reflect both inclusions of other minerals and chemical impurities (e.g., Ca in olivine and Mn in clinopyroxene and amphibole). However, traces of these elements could also be falsely detected by pXRF due to unresolved spectral interferences, especially in the low-energy range of X-ray spectrum as discussed above. As far as essential elemental abundances are concerned, the uncertain minor elements detected by pXRF will not impact the decision making with ambiguous mineral grains.

5. Future work

Our results demonstrate that qualitative pXRF is a powerful, rapid technique to identify sand-size, single mineral grains recovered in indicator mineral surveys. Although the pXRF measurements identified 17 different minerals in this study, future work is needed to test the technique on minerals containing essential Ni, Cu, Zn and other elements (e.g., As, Sb, REE). Systematic measurements on different minerals will help develop an algorithm that would improve the confidence of visual mineral identification using the qualitative pXRF element determinations. Low limits of detection for most elements determined by pXRF instruments permit first-order, in-field applications to distinguish indicator minerals based on mineral chemistry, such as for kimberlites (e.g., Cr-pyrope and Cr-diopside).

6. Conclusions

We tested pXRF instrument on single-grain (0.5-1.0 mm) samples of 17 different rock-forming and accessory minerals. Sixty qualitative measurements (30-150 seconds) using a factory-calibrated Mining mode based on fundamental parameters demonstrate that essential constituents detected by pXRF readily identify the minerals, thereby providing a new efficient, in-field technique for indicator mineral surveys and laboratory applications.

Acknowledgments

We thank Keith Grattan (Elemental Controls Limited) for discussion of the X-ray spectra and Ray Lett (British Columbia Geological Survey Emeritus Scientist), Ross Knight (Geological Survey of Canada) and Larry Aspler (British Columbia Geological Survey) for thorough reviews of the paper.

References cited

- Amelin, Y., Lee, D.C., Halliday, A.N., and Pidgeon, R.T., 1999. Nature of the Earth's earliest crust from hafnium isotopes in single detrital zircons. *Nature*, 399, 252-255.

- Averill, S.A., 2001. The application of heavy indicator mineralogy in mineral exploration with emphasis on base metal indicators in glaciated metamorphic and plutonic terrains. In: McClenaghan, M.B., Bobrowski, P.T., Hall, G.E.M., and Cook, S.J., (Eds.), *Drift Exploration in Glaciated Terrain*, Geological Society of London, Special Publication 185, pp. 49-82.
- Averill, S.A., and Huneault, R.G., 2006. Overburden Drilling Management Ltd: "Exploring Heavy Minerals". *Explore*, 133, 1-5.
- Belousova, E.A., Griffin, W.L., O'Reilly, S., and Fisher, N.I., 2002a. Apatite as an indicator mineral for mineral exploration: trace-element compositions and their relationship to host rock type. *Journal of Geochemical Exploration*, 76, 45-69.
- Belousova, E.A., Griffin, W.L., O'Reilly, S.Y., and Fisher, N.J., 2002b. Igneous zircon: trace element composition as an indicator of source rock type. *Contributions to Mineralogy and Petrology*, 143, 602-622.
- Bishop, J.L., Murad, E., Lane, M.D., and Mancinelli, R.L., 2004. Multiple techniques for mineral identification on Mars: A study of hydrothermal rocks as potential analogues for astrobiology sites on Mars. *Icarus*, 169, 311-323.
- Bouzari, F., Hart, C.J.R., Barker, S., and Bissig, T., 2011. Porphyry indicator minerals (PIMS): a new exploration tool for concealed deposits in south-central British Columbia. *Geoscience BC, Report 2011-17*, 31 p.
- Bouzari, F., Hart, C.J.R., Bissig, T., and Barker, S., 2016. Hydrothermal alteration revealed by apatite luminescence and chemistry: A potential indicator mineral for exploring covered porphyry copper deposits. *Economic Geology*, 111, 1397-1410.
- Bruand, E., Storey, C., and Fowler, M., 2016. An apatite for progress: Inclusions in zircon and titanite constrain petrogenesis and provenance. *Geology*, 44, 91-94.
- Bull, A., Brown, M.T., and Turner, A., 2017. Novel use of field-portable-XRF for the direct analysis of trace elements in marine macroalgae. *Environmental Pollution*, 220, 228-233.
- Burt, D.M., 1989. Compositional and phase relations among rare earth element minerals, Chapter 10. In: Lipin, B.R., and McKay, G.A., (Eds.), *Geochemistry and Mineralogy of Rare Earth Elements*, Mineralogical Society of America, *Reviews in Mineralogy*, 21, pp. 259-307.
- Canil, D., Grondahl, C., Lacourse, T., and Pisiak, L.K., 2016. Trace elements in magnetite from porphyry Cu-Mo-Au deposits in British Columbia, Canada. *Ore Geology Reviews*, 72, 1116-1128.
- Carmody, L., Taylor, L.A., Thaisen, K.G., Tychkov, N., Bodnar, R.J., Sobolev, N.V., Pokhilenko, L.N., and Pokhilenko, N.P., 2014. Ilmenite as a diamond indicator mineral in the Siberian craton: A tool to predict diamond potential. *Economic Geology*, 109, 775-783.
- Chakhmouradian, A.R., 2006. High-field-strength elements in carbonatitic rocks: geochemistry, crystal chemistry and significance for constraining the sources of carbonatites. *Chemical Geology*, 235, 138-160.
- Chakhmouradian, A.R., and Zaitsev, A.N., 2012. Rare earth mineralization in igneous rocks: sources and processes. *Elements*, 8, 347-353.
- Chakhmouradian, A.R., Reguir, E.P., Kressall, R.D., Crozier, J., Pisiak, L.K., Sidhu, R., and Yang, P., 2015. Carbonate-hosted niobium deposit at Aley, northern British Columbia (Canada): Mineralogy, geochemistry and petrogenesis. *Ore Geology Reviews*, 64, 642-666.
- Chakhmouradian, A.R., Reguir, E.P., and Zaitsev, A.N., 2016. Calcite and dolomite in intrusive carbonatites. I. Textural variations. *Mineralogy and Petrology*, 110, 333-360.
- Chakhmouradian, A.R., Reguir, E.P., Zaitsev, A.N., Couëslan, C., Xu, C., Kynický, J., Mumin, A., and Yang, P., 2017. Apatite in carbonatitic rocks: Compositional variation, zoning, element partitioning and petrogenetic significance. *Lithos*, 274-275, 188-213.
- Chen, Z., Williams, N., and Zhang, H., 2013. Rapid and nondestructive measurement of labile Mn, Cu, Zn, Pb and As in DGT by using field portable-XRF. *Environmental Science: Processes & Impacts*, 15, 1768-1774.
- Chiari, G., Sarrazin, P., and Heginbotham, A., 2016. Non-conventional applications of a noninvasive portable X-ray diffraction/fluorescence instrument. *Applied Physics A: Materials Science and Processing*, 122, 1-17.
- Chudy, T.C., 2013. The petrogenesis of the Ta-bearing Fir carbonatite system, east-central British Columbia, Canada. Unpublished Ph.D. thesis, University of British Columbia, Canada, 316 p.
- Cohen, D.R., Cohen, E.J., Graham, I.T., Soares, G.G., Hand, S.J., and Archer, M., 2017. Geochemical exploration for vertebrate fossils using field portable XRF. *Journal of Geochemical Exploration*, 181, 1-9.
- Gent, M., Menendez, M., Toraño, J., and Torno, S., 2011. A review of indicator minerals and sample processing methods for geochemical exploration. *Journal of Geochemical Exploration*, 110, 47-60.
- Glanzman, R.K., and Closs, L.G., 2007. Field portable X-ray fluorescence geochemical analysis – Its contribution to onsite real-time project evaluation. In: Milkereit, B., (Ed.), *Proceedings of Exploration 07: Fifth Decennial International Conference on Mineral Exploration*, pp. 291-301.
- Gorham, J., Ulry, B., and Brown, J., 2009. Commerce Resources Corp. 2008 diamond drilling and exploration at the Blue River property, north of Blue River, British Columbia. British Columbia Ministry of Energy, Mines and Petroleum Resources, British Columbia Geological Survey, Assessment Report 31174, 149 p., 21 appendices.
- Grimes, C.B., Wooden, J.L., Cheadle, M.J., and John, B.E., 2015. "Fingerprinting" tectono-magmatic provenance using trace elements in igneous zircon. *Contributions to Mineralogy and Petrology*, 170, 1-26.
- Harrison, T.M., Schmitt, A.K., McCulloch, M.T., and Lovera, O.M., 2008. Early (≥ 4.5 Ga) formation of terrestrial crust: Lu-Hf, $\delta^{18}\text{O}$, and Ti thermometry results for Hadean zircons. *Earth and Planetary Science Letters*, 268, 476-486.
- Hayden, L.A., Watson, E.B., and Wark, D.A., 2008. A thermobarometer for sphene (titanite). *Contributions to Mineralogy and Petrology*, 155, 529-540.
- Hoskin, P.W.O., and Ireland, T.R., 2000. Rare earth element chemistry of zircon and its use as a provenance indicator. *Geology*, 28, 627-630.
- Knight, R.D., Kjarsgaard, B.A., Plourde, A.P., and Moroz, M., 2013. Portable XRF spectrometry of reference materials with respect to precision, accuracy, instrument drift, dwell time optimization, and calibration. *Geological Survey of Canada, Open File 7358*, 45 p.
- Kogarko, L.N., Sorokhtina, N.V., Kononkova, N.N., and Klimovich, I.V., 2013. Uranium and thorium in carbonatitic minerals from the Guli massif, Polar Siberia. *Geochemistry International*, 51, 767-776.
- Layton-Matthews, D., Hamilton, C., and McClenaghan, M.B., 2014. Mineral chemistry: modern techniques and applications to exploration. In: McClenaghan, M.B., Plouffe, A., and Layton-Matthews, D., (Eds.), *Application of Indicator Mineral Methods to Mineral Exploration*, 26th International Applied Geochemistry Symposium, Short Course SC07, November 17, 2013, Rotarua, New Zealand. Geological Survey of Canada, Open File 7553, pp. 9-18.
- Lett, R., and Rukhlov, A.S., 2017. A review of methods for regional geochemical surveys (RGS) in the Canadian Cordillera. In: Ferbey, T., Plouffe, A., and Hickin, A.S., (Eds.), *Indicator Minerals in Till and Stream Sediments of the Canadian Cordillera*. Geological Association of Canada Special Paper Volume 50, and Mineralogical Association of Canada Topics in Mineral Sciences Volume 47, pp. 53-108.
- Liritzis, I., and Zacharias, N., 2011. Portable XRF of archaeological

- artifacts: current research, potentials and limitations. In: Shackley, M.S., (Ed.), *X-Ray Fluorescence Spectrometry (XRF) in Geoarchaeology*, Springer, New York, pp. 109-142.
- Mackay, D.A.R., and Simandl, G.J., 2015. Pyrochlore and columbite-tantalite as indicator minerals for specialty metal deposits. *Geochemistry: Exploration, Environment, Analysis*, 15, 167-178
- Mackay, D.A.R., Simandl, G.J., Ma, W., Redfearn, M., and Gravel, J., 2016. Indicator mineral-based exploration for carbonatites and related specialty metal deposits – a QEMSCAN® orientation survey, British Columbia, Canada. *Journal of Geochemical Exploration*, 165, 159-173.
- Mao, M., Rukhlov, A.S., Rowins, S.M., Spence, J., and Coogan, L.A., 2016. Apatite trace element compositions: A robust new tool for mineral exploration. *Economic Geology*, 111, 1187-1222.
- Mao, M., Rukhlov, A.S., Rowins, S.M., Hickin, A.S., Ferbey, T., Bustard, A., Spence, J., and Coogan, L.A., 2017. A novel approach using detrital apatite and till geochemistry to identify covered mineralization in the TREK area of the Nechako Plateau, British Columbia. In: Ferbey, T., Plouffe, A., and Hickin, A.S., (Eds.), *Indicator Minerals in Till and Stream Sediments of the Canadian Cordillera*, Geological Association of Canada Special Paper Volume 50, and Mineralogical Association of Canada Topics in Mineral Sciences Volume 47, pp. 191-243.
- Mariano, A.N., 1982. Petrology, mineralogy and geochemistry of the Blue River carbonatites. Confidential report for Anshultz (Canada) Mining Ltd., 130 p.
- Mariano, A.N., 1989. Economic geology of rare earth minerals, Chapter 11. In: Lipin, B.R., and McKay, G.A., (Eds.), *Geochemistry and Mineralogy of Rare Earth Elements*, Mineralogical Society of America, *Reviews in Mineralogy*, 21, pp. 309-337.
- Martín-Peinado, F.J., and Rodríguez-Tovar, F.J., 2016. Researching protected geosites: in situ and non-destructive analysis of mass-extinction bioevents. *Geoheritage*, 8, 351-357.
- McClenaghan, M.B., 2005. Indicator mineral methods in mineral exploration. *Geochemistry: Exploration, Environment, Analysis*, 5, 233-245.
- McClenaghan, M.B., Plouffe, A., McMartin, I. J., Campbell, J.E., Spirito, W.A., Paulen, R.C., Garrett, R.G., and Hall, G.E.M., 2014. Till sampling and geochemical analytical protocols used by the Geological Survey of Canada. *Geochemistry: Exploration, Environment, Analysis* 2013, 13, 285-301.
- McLeod, G.W., Dempster, T.J., and Faithfull, J.W., 2011. Deciphering magma-mixing processes using zoned titanite from the Ross of Mull Granite, Scotland. *Journal of Petrology*, 52, 55-82.
- Miles, A.J., Graham, C.M., Hawkesworth, C.J., Gillespie, M.R., Hinton, R.W., Bromiley, G.D., and EMMAC, 2014. Apatite: a new redox proxy for silicic magmas? *Geochimica et Cosmochimica Acta*, 132, 101-119.
- Millonig, L.J., Gerdes, A., and Groat, L.A., 2012. U-Th-Pb geochronology of meta-carbonatites and meta-alkaline rocks in the southern Canadian Cordillera: a geodynamic perspective. *Lithos*, 152, 202-217.
- Millonig, L.J., Gerdes, A., and Groat, L.A., 2013. The effect of amphibolite facies metamorphism on the U-Th-Pb geochronology of accessory minerals from meta-carbonatites and associated meta-alkaline rocks. *Chemical Geology*, 353, 199-209.
- Mitchell, R.H., 2015. Primary and secondary niobium mineral deposits associated with carbonatites. *Ore Geology Reviews*, 64, 626-641.
- Mitchell, R., Chudy, T., McFarlane, C.R.M., and Wu, F.-Y., 2017. Trace element and isotopic composition of apatite in carbonatites from the Blue River area (British Columbia, Canada) and mineralogy of associated silicate rocks. *Lithos*, 286-287, 75-91.
- Palmer, T., Jacobs, R., Baker, E., Ferguson, K., and Webber, S., 2009. Use of field-portable XRF analyzers for rapid screening of toxic elements in FDA-regulated products. *Journal of Agricultural and Food Chemistry*, 57, 2605-2613.
- Pell, J., 1994. Carbonatites, nepheline syenites, kimberlites and related rocks in B.C. British Columbia Ministry of Energy, Mines and Petroleum Resources, British Columbia Geological Survey, Bulletin 88, 136 p.
- Piorek, S., 1994. Principles and applications of man-portable X-ray fluorescence spectrometry. *Trends in Analytical Chemistry* 13, 281-286.
- Plouffe, A., McClenaghan, M.B., Paulen, R.C., McMartin, I., Campbell, J.E., and Spirito, W.A., 2014. Processing of glacial sediments for the recovery of indicator minerals: protocols used at the Geological Survey of Canada. *Geochemistry: Exploration, Environment, Analysis*, 13, 303-316.
- Potts, P.J., and West, M., (Eds.), 2008. *Portable X-ray Fluorescence Spectrometry: Capabilities for In Situ Analysis*. Royal Society of Chemistry, 291 p.
- Quye-Sawyer, J., Vandeginste, V., and Johnston, K.J., 2015. Application of handheld energy-dispersive X-ray fluorescence spectrometry to carbonate studies: opportunities and challenges. *Journal of Analytical Atomic Spectrometry*, 30, 1417-1680.
- Rouillon, M., and Taylor, M., 2016. Can field portable X-ray fluorescence (pXRF) produce high quality data for application in environmental contamination research? *Environmental Pollution*, 214, 225-264.
- Rowe, R.P., 1958. Niobium (Columbium) deposits of Canada. Geological Survey of Canada, *Economic Geology Series*, 18, 108 p.
- Rukhlov, A.S., 2013. Determination of major and trace element concentrations in Canadian sediment reference samples using portable energy-dispersive X-ray fluorescence (ED-XRF) spectrometer and implications for geochemical surveys. British Columbia Ministry of Energy, Mines and Natural Gas, British Columbia Geological Survey GeoFile 2013-6.
- Rukhlov, A.S., Bell, K., and Amelin, Y., 2015. Carbonatites, isotopes and evolution of the subcontinental mantle: An overview. In: Simandl, G.J. and Neetz, M., (Eds.), *Symposium on Strategic and Critical Materials Proceedings*, November 13-14, 2015, Victoria, British Columbia, British Columbia Ministry of Energy and Mines, British Columbia Geological Survey, Paper 2015-3, pp. 39-64.
- Rukhlov, A.S., Plouffe, A., Ferbey, T., Mao, M., and Spence, J., 2016. Application of trace-element compositions of detrital apatite to explore for porphyry deposits in central British Columbia. In: *Geological Fieldwork 2015*, British Columbia Ministry of Energy and Mines, British Columbia Geological Survey, Paper 2016-1, pp. 145-179.
- Rukhlov, A.S., Rowins, S.M., Mao, M., Coogan, L.A., and Spence, J., 2017. Apatite compositions as a proxy for the oxidation states of porphyry Cu-Mo-Au deposits. British Columbia Ministry of Energy and Mines, British Columbia Geological Survey GeoFile 2017-2.
- Ryan, J.G., Shervais, J.W., Li, Y., Reagan, M.K., Li, H.Y., Heaton, D., Godard, M., Kirchenbauer, M., Whattam, S.A., Pearce, J.A., Chapman, T., Nelson, W., Prytulak, J., Shimizu, K., Petronotis, K., the IODP Expedition 352 Scientific Team, 2017. Application of a handheld X-ray fluorescence spectrometer for real-time, high-density quantitative analysis of drilled igneous rocks and sediments during IODP Expedition 352. *Chemical Geology*, 451, 55-66.
- Sarala, P., Taivalkoski, A., and Valkama, J., 2015. Portable XRF: an advanced on-site analysis method in till geochemical exploration. In: Sarala, P., (Ed.), *Novel Technologies for Greenfield Exploration*, Geological Survey of Finland, Special Paper 57, pp. 63-86.
- Sha, L.-K., and Chappell, B.W., 1999. Apatite chemical composition, determined by electron microprobe and laser-ablation inductively coupled plasma mass spectrometry, as a probe into granite

- petrogenesis. *Geochimica et Cosmochimica Acta*, 63, 3861-3881.
- Simandl, G.J., Paradis, S., Stone, R.S., Fajber, R., Kressall, R., Grattan, K., Crozier, J., and Simandl, L.J., 2014. Applicability of handheld X-ray fluorescence spectrometry in the exploration and development of carbonatite-related niobium deposits: a case study of the Aley Carbonatite, British Columbia, Canada. *Geochemistry: Exploration, Environment, Analysis*, 17, 211-221.
- Smythe, D.J., and Brenan, J.M., 2016. Magmatic oxygen fugacity estimated using zircon-melt partitioning of cerium. *Earth and Planetary Science Letters*, 453, 260-266.
- Steiner, A.E., Conrey, R.M., and Wolff, J.A., 2017. PXRF calibrations for volcanic rocks and the application of in-field analysis to the geosciences. *Chemical Geology*, 453, 35-54.
- Thermo Scientific, 2011. Thermo Fisher Scientific Niton Analyzers: FXL Users Guide, Version 8.0, Revision A, March 2011, 106 p.
- Weindorf, D.C., Castañeda, J.H.C., Bakr, N., and Swanhart, S., 2013. Direct soil gypsum quantification via portable X-Ray fluorescence spectrometry. *Soil Science Society of America Journal*, 77, 2071-2077.
- Wiedenbeck, M., 2013. Field-portable XRF: A geochemist's dream? *Elements*, 9, 7-8.
- Wilde, S.A., Valley, J.W., Peck, W.H., and Graham, C.M., 2001. Evidence from detrital zircons for the existence of continental crust and oceans on the Earth 4.4 Gyr ago. *Nature*, 409, 175-178.
- Williams, C.T., and Gieré, R., 1996. Zirconolite: a review of localities worldwide, and a compilation of its chemical composition. *Bulletin of the Natural History Museum: Geology Series*, 52, 1-24.
- Williamson, B.J., Herrington, R.J., and Morris, A., 2016. Porphyry copper enrichment linked to excess aluminium in plagioclase. *Nature Geoscience*, 9, 237-241.
- Young, K.E., Evans, C.A., Hodges, K., Bleacher, J.E., and Graff, T.G., 2016. A review of the handheld X-ray fluorescence spectrometer as a tool for field geologic investigations on Earth and in planetary surface exploration. *Applied Geochemistry*, 72, 77-87.
- Zhang, W., Lentz, D.R., and Charnley, B.E., 2017. Petrogeochemical assessment of rock units and identification of alteration/mineralization indicators using portable X-ray fluorescence measurements: Applications to the Fire Tower Zone (W-Mo-Bi) and the North Zone (Sn-Zn-In), Mount Pleasant deposit, New Brunswick, Canada. *Journal of Geochemical Exploration*, 177, 61-72.

Development of MapPlace 2 geospatial web service to disseminate geoscience in British Columbia



Y. Cui^{1,a}, S. Zhao¹, G. Fortin¹, S. Meredith-Jones¹, and L.D. Jones¹

¹ British Columbia Geological Survey, Ministry of Energy, Mines and Petroleum Resources, Victoria, BC, V8W 9N3

^a corresponding author: Yao.Cui@gov.bc.ca

Recommended citation: Cui, Y., Zhao, S., Fortin, G., Meredith-Jones, S., and Jones, L.D., 2018. Development of MapPlace 2 geospatial web service to disseminate geoscience in British Columbia. In: Geological Fieldwork 2017, British Columbia Ministry of Energy, Mines and Petroleum Resources, British Columbia Geological Survey Paper 2018-1, pp. 183-195.

Abstract

MapPlace 2 is a geospatial web service developed in-house by the British Columbia Geological Survey. Based on user requirements determined from operating the original MapPlace for more than 20 years, MapPlace 2 has a modernized interface for visualization, and has improved performance. Through this interface, MapPlace 2 enables efficient browsing, displaying, searching, reporting, and analyzing data from multiple geoscience, mineral resource and tenure databases. It works on any web browser, requires no plug-ins, and can rapidly retrieve and display large volumes of data and third-party topographic maps and imagery, thus facilitating data mining by anyone interested in British Columbia geoscience. Built on open-source geospatial software, MapPlace 2 uses MapGuide Open Source as the web service platform, OpenLayers for rendering, and PostgreSQL/PostGIS for the application database. BCGS continues to add new data and databases and is developing a light version for mobile devices.

Keywords: MapPlace, geospatial web service, spatial database, geoscience

1. Introduction

MapPlace 2 (Fig. 1) is the geospatial web service developed by the British Columbia Geological Survey (BCGS) to serve the needs of the mineral exploration industry, environmental organizations, resource planners, public safety agencies, communities, First Nations, government, research organizations, and the general public. Developed entirely in-house, it builds on the success of MapPlace, which has been online since 1997 and has a proven record of helping decision makers reduce the costs of accessing and analyzing geoscience data. In contrast to the original, MapPlace 2 is easier to use and has much improved functionality and performance. It can be used on either a Mac or a PC, does not require plug-ins, and works on all web browsers. In addition, it allows visualizing and querying province-wide geoscience data at exceptional speed and provides applications to search, analyze, report, and download these data.

This paper provides a brief tour of MapPlace 2, highlighting how it has evolved, how it functions, what users can expect, key elements of its architecture and the development process, and plans for the future. For more detailed information how to use MapPlace 2, please refer to the workbook by Cui et al. (2017a).

2. History: from MapPlace to MapPlace 2

In 1995, BCGS geologist Ward Kilby started building MapPlace to make geoscience data from across the province accessible online. The initial version was based on Argus Technologies MapGuide, which was acquired by Autodesk in



Fig. 1. MapPlace 2 logo.

1996 and later released as Autodesk MapGuide (Bray, 2008). MapPlace was released to public in 1997, and has since evolved to include not only a comprehensive suite of geoscience and related data, maps, and satellite imagery, but also advanced web applications (Kilby, 1999; Tupper et al., 2001; Jones et al., 2002; Kilby et al., 2004). By 2003, an image analysis toolbox and enhanced satellite imagery were integrated into MapPlace, with online image processing capacity on multispectral and hyperspectral images (Kilby et al., 2004), an analytical technique typically only available through specialized software. Although MapPlace served the province well for more than 20 years, advances in technology made maintaining the service difficult.

MapPlace was built on a version of Autodesk MapGuide (6.5) that is now obsolete. Autodesk MapGuide required that users install a viewer plug-in that was built for early versions of the Microsoft Internet Explorer web browser and MapPlace could not work on other operating systems or browsers. Moreover, this version was last released in 2004 and vendor support ended in 2010, effectively ending upgrades to MapPlace. Keeping

MapPlace operational was also problematic. During its lifetime, most of the data products and applications in MapPlace were added as either ad hoc solutions or in response to requests from clients. Although this approach enabled MapPlace to be highly adaptable, it resulted in a difficult to maintain patchwork of inconsistent data models, multiple scripting languages, and obsolete database technologies, some of which needed to comply with government security policies. These challenges prompted BCGS to conduct a complete overhaul.

In 2012, after testing several platforms, we selected MapGuide Open Source to build a prototype. MapGuide Open Source gained a significant performance boost after incorporating a new version of OpenLayers (OpenLayers, 2017) as the rendering engine. By 2014, the first working prototype of MapPlace 2 was completed and made available to the public. We invited clients to test its performance and usability, and held a workshop to gather further feedback. Encouraged by early results, we continued to improve the functionality, culminating in a beta release as MapPlace 2 in 2016 (Cui et al., 2017a).

3. MapPlace 2 functional components and their applications

MapPlace 2 has two major functional components: 1) an application database for BCGS geoscience and related data from other government agencies; and 2) a web interface with tools and custom applications.

3.1. Geoscience and related data

MapPlace 2 disseminates geoscience data through a web interface that also provides other, land-related data such as mineral tenures, survey parcels, and topographic base maps and imagery. The geoscience data are organized in folders (Fig. 2) for easy discovery and browsing, and themed as map layers with styles, symbols, and legends (Fig. 3). Many of the data displayed in the map window are linked to databases and can be retrieved and downloaded.

The bedrock layer includes the current province-wide bedrock geology, with more than 33,000 units mapped at scales from 1:50,000 to 1:250,000 (Cui et al., 2017b). Other geological information, such as terranes, basins, physiographic areas, and tectonic assemblages are also available. MINFILE is British Columbia's mineral inventory of more than 14,600 metallic, industrial mineral, and coal occurrences. The Assessment Report Indexing System (ARIS) is a collection of more than 36,600 reports submitted to the Ministry summarizing exploration work on mineral claims. Similar to ARIS, COALFILE is a collection of close to 1000 coal assessment reports. Property File is a collection of more than 65,000 scanned and georeferenced documents donated to BCGS by government, university, industry, and individuals in the last 150 years.

MapPlace 2 hosts several geochemical and geophysical data sets. Geochemical data have been updated recently. The Regional Geochemical Survey (RGS) data contain multi-element analyses from stream, moss, and water samples collected from across the province since the 1970s (Han and

Rukhlov, 2017). The till geochemical data include analyses of nearly 10,500 samples from 39 till surveys (Bustard et al., 2017). Geophysical data include multisensor, airborne geophysical surveys of the entire province and targeted areas.

Several surficial geology layers are available. For example, one layer provides an index of available maps, with URLs to publication and data sources. Another layer includes ice-flow indicators (Arnold et al., 2016), themed by landforms that provide information on the flow directions of the Cordilleran Ice Sheet during the last glaciation.

The BCGS publication catalogue includes Papers, Open Files, GeoFiles, Geoscience Maps, Information Circulars, Mineral Deposit Profiles, and Bulletins published since 1874. These publications present the results of field-based projects conducted by the BCGS and the Geological Survey of Canada. MapPlace 2 offers footprints for many of these products allowing for rapid and efficient research.

Data sourced directly from the British Columbia Geographic Warehouse, include administrative boundaries, place names, topographic base maps, map grids, and public records of mineral, placer, and coal tenures from the Mineral Titles Office. Land use planning data include details such as community watersheds, habitat/wildlife management areas, protected areas, recreation and tourism areas, and settlements. Locations for climate, hydrometric and water quality stations are from Environment Canada. MapPlace 2 embeds access to a number of third party topographic base maps and imagery from external providers (Fig. 4), including Google Maps (transportation networks, imagery, and shaded relief), and OpenStreetMap (with transportation networks themed with topographic features).

3.2. MapPlace 2 functions and application highlights

MapPlace 2 provides tools very similar to typical desktop GIS software. It retains much of the functionality of the original MapPlace, but with improved performance, more advanced applications, and additional features.

3.2.1. Visualization

MapPlace 2 has a modernized user interface for visualization, and has improved performance in retrieving and displaying large volumes of province-wide data. In typical use, it takes less than one second to display maps of the entire province, which is significantly faster than similar services that handle this level of data. In addition, the new platform takes advantage of third-party developments. For example, Google StreetView has been embedded and can be used to view bedrock outcrops (Fig. 5), mineralization, mine sites, and even underground mines.

3.2.2. Basic functions and tools

MapPlace 2 has a set of basic tools to interact with the maps. A user can zoom and pan the maps by using the navigation control, the buttons on the menu bar, or a combination of click and drag (Fig. 2). Features on many of the map layers can be selected and descriptions viewed or reports generated by

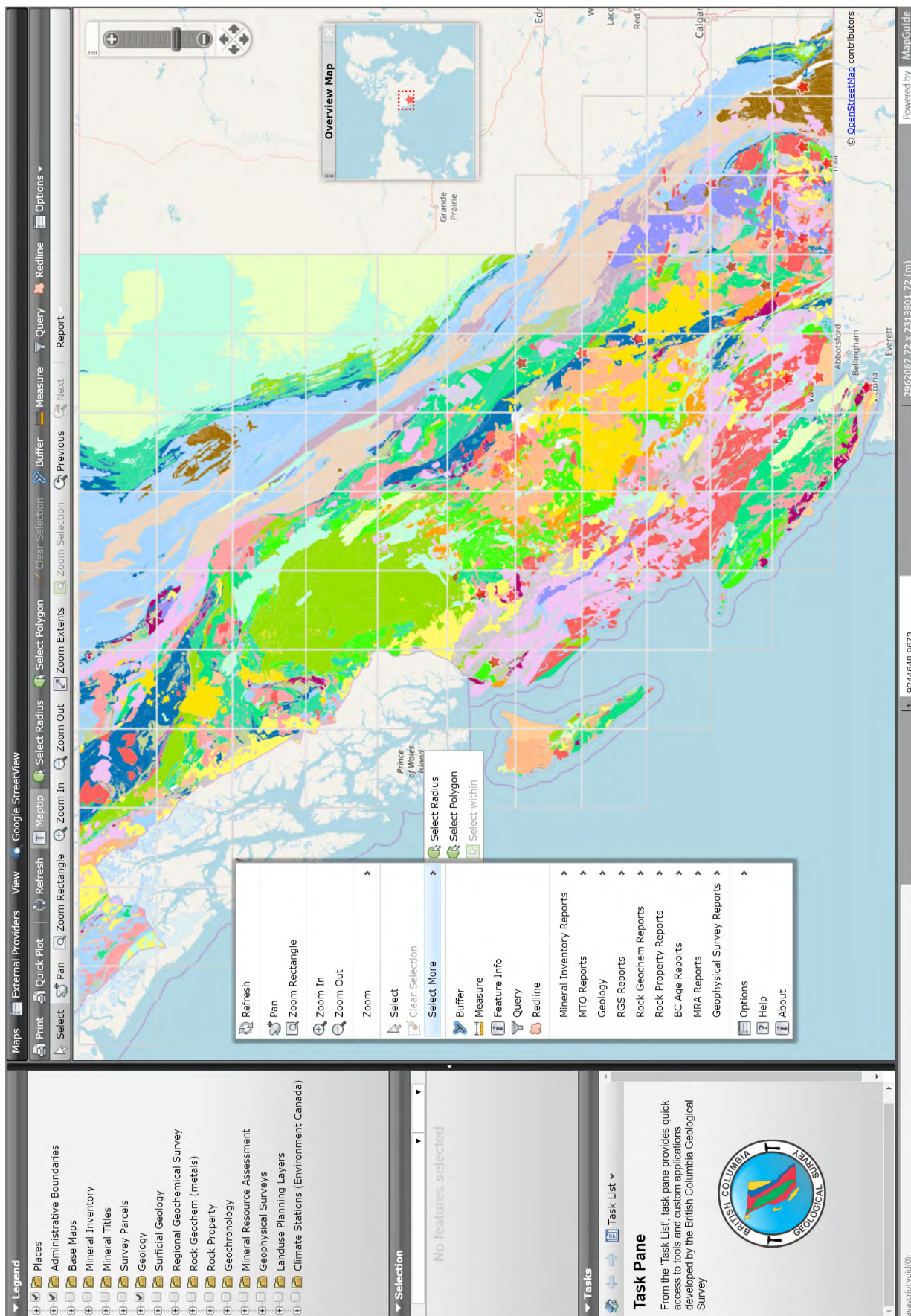


Fig. 2. MapPlace 2 interface.

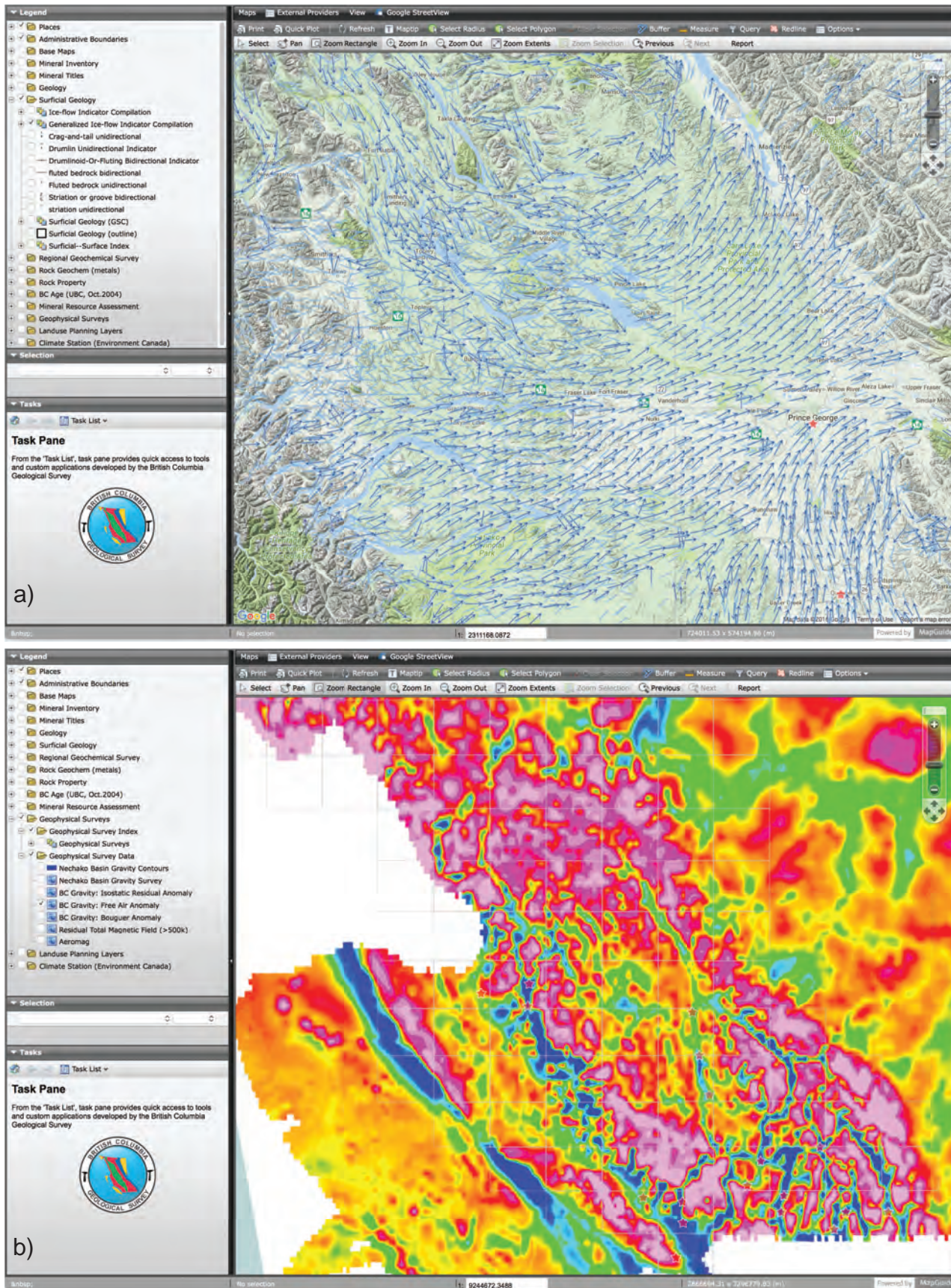


Fig. 3. Examples of geoscience data shown on MapPlace 2. a) Ice-flow indicators. b) Total residual magnetic field.

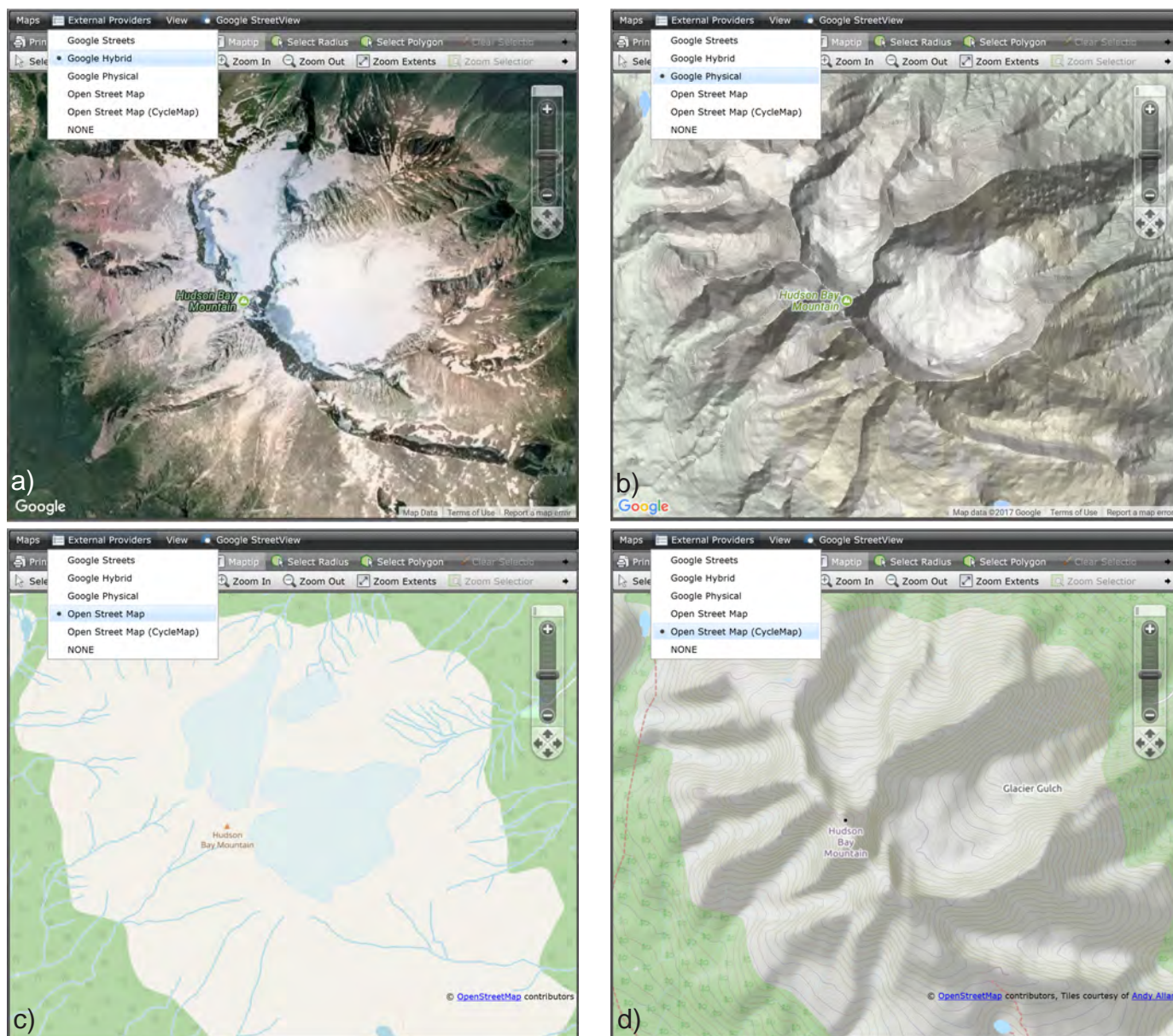


Fig. 4. Choices of different third-party basemaps and imagery. a) Google Hybrid, satellite imagery. b) Google Physical: shaded relief with contours. c) OpenStreetMap. d) OpenStreetMap-CycleMap.

mouse clicking or by outlining multiple features by drawing a selection rectangle, circle, or polygon. ‘Maptips’ is a tool that displays basic information about a feature when the cursor hovers over it, commonly with a hyperlink to pages with further details. The measurement tool gives the total length of continuous line segments and the total area the line segments enclose. The basic query tool allows selecting and interrogating many of the map features.

3.2.3. Custom query and report tools

We developed a suite of applications to conduct more advanced spatial and non-spatial queries and generate summary reports. These custom query tools are listed in the Tasks pane (Fig. 6a). Each of the custom query tools allows a user to

enter search criteria (Fig. 6b). Retrieved summary results are displayed in the Tasks pane (Fig. 6c). The summary can be saved as a Microsoft Excel spreadsheet. A general search tool is available to find named places, streets, rivers, lakes, and points of interest anywhere in the province.

Custom reporting tools are accessed using the ‘Report’ button on the top menu or by right-clicking in the map window (Fig. 7a). These tools retrieve data and generate summary reports of the selected features, and results are displayed in a webpage (Fig. 7b). The ID for each of the records has a link to full details in other BCGS geoscience databases. Most of the summary reports have a link to download a KML file that can display features on Google Earth.

MapPlace 2 allows users to combine these custom tools



Fig. 5. Google StreetView showing sedimentary rocks of the Allenby Formation (Princeton Group; Eocene), unconformably overlying volcanic rocks of the Nicola Group (Upper Triassic).

with a buffer and spatial overlay to carry out more complex spatial queries. Illustrated in Figure 8 is an example of a buffer being used as a spatial filter. Bedrock units with the potential for porphyry deposits are selected using the ‘Bedrock Geology Search’ tool (Figs. 6b and 6c), and all the mineral occurrences within the buffer are reported.

3.2.4. Custom map making: the ‘Redline’ tool

With the ‘Redline’ tool users can add text, points, lines, and polygons to a map (Fig. 9a) and generate cartographic features such as titles, legends, scale bars, north arrows, and coordinates (Fig. 9b). We have designed the map output to meet the requirements for submitting assessment reports. The final map can be printed or saved as a PDF file. The Redline tool also allows saving user-added data in Esri shapefile or Google KML format.

4. MapPlace 2 system components and their development

Hidden from the user interface are system components that make MapPlace 2 work. Our feasibility studies and prototyping led to a conceptual system design using available technical solutions specifically for the purpose of disseminating geoscience data. Below we provide a high-level overview of the system components and how we developed them.

4.1. System architecture

MapPlace 2 is built with a new system architecture (Fig. 10) based on ‘real-world’ cases and requirements gathered from operating the original MapPlace for more than two decades.

In other words, our system architecture has been developed through iterations that reflect requests, recommendations, and demands from clients that have long-used MapPlace. A system architecture is important to define the structure and behaviour of system components (e.g., geoscience databases and custom applications), their relationships, and dependency to external resources (e.g., external data sources and other web services).

MapPlace 2 depends on data sources that are external to the MapPlace 2 web server. These sources include the BCGS geoscience data that are maintained by a number of database management systems (loosely identified as part of the geoscience operational database environment), including digital geology in PostgreSQL/PostGIS, MINFILE and Property File in Microsoft SQL Server, ARIS in Microsoft FoxPro, and RGS in Microsoft Access. Other data products are available as Esri shapefile, Microsoft Access, and raster imagery format, including mineral resource assessment, ice flow indicators, and geophysical survey data. Mineral tenures, administrative boundaries, and topographic data are from the Oracle databases in the British Columbia Geographic Warehouse.

The core system components of MapPlace 2 are the geoscience application database environment (GADE), and the web services with custom applications.

4.2. Application database architecture and applications

MapPlace 2 requires an application database optimized to display maps quickly and support rapid spatial and non-spatial queries across all datasets. This application database must be built on a database architecture with consistent data models,

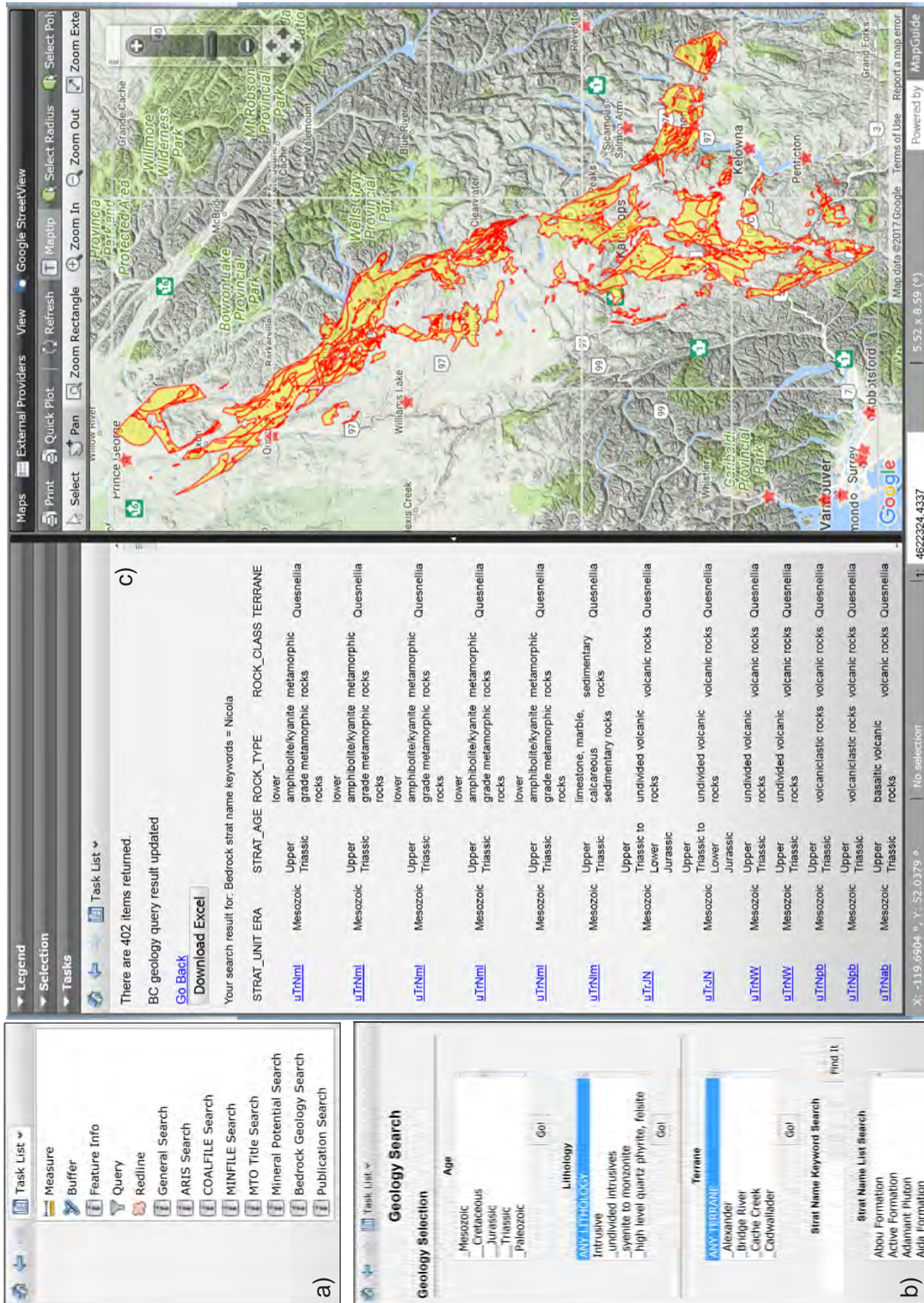
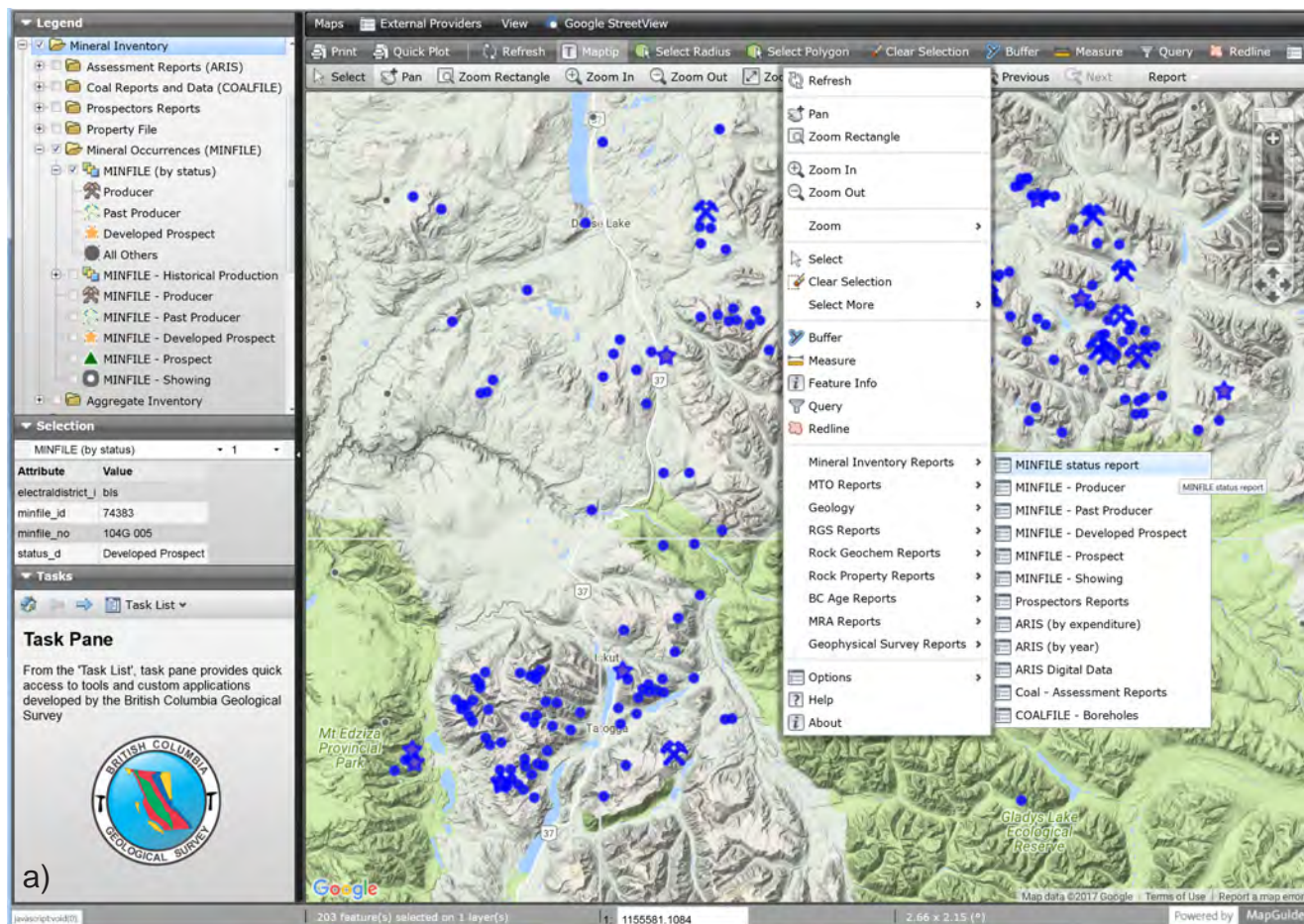


Fig. 6. MapPlace 2 custom search tools. a) List of tools. b) Bedrock geology search interface. c) Bedrock search results.



MapPlace

MINFILE Report

[Download to Excel](#)
 Click on [MINFILE Number link](#) for more details!
 Click on [Commodities](#) or [Deposit Type](#) label for definitions
 Click [GoogleEarth icons](#) to view individual occurrences in GoogleEarth™
 or click [GoogleEarth field header](#) to show all occurrences

MINFILE No.	Name	Status	Commodities	Deposit Type	Google Earth
104G 071	ART, AXE	Showing	CU	-	
104G 087	SUN	Showing	CU, AG	I06	
104G 160	QC - VEIN ZONE, VEIN, QC, UPPER GORDON, GORDON'S, MAIN, TOP, ANKERITE, OZ, A3, A4	Prospect	AU, ZN, CU, AG, PB	I05	
104G 163	VIOLET EAST, AXE, EAST VIOLET	Showing	AU, CU	I06, I01	
104G 164	VIOLET, AXE	Showing	AU, CU	I06, I01	
104G 165	PETAL, AXE	Showing	AU, AG, CU	I06, I01	
104G 166	PASS GOSSAN, AXE	Showing	PB, ZN, CU, AU	I05	
104G 167	CENTRAL, AXE	Showing	ZN, PB, CU, AU, AG	G06	
104G 168	GO/NO, AXE	Showing	AU, AG, CU, ZN, PB, AS	I05, I06	
104G 169	CURT, AXE	Showing	AU	I01	
104G 170	SOUTH SEESTOR, AXE, SEESTOR	Showing	CU, AU		
104G 172	WOLF WEST, AXE	Showing	AU, CU, ZN	L04	
104G 174	BEAUCHAMPS, AXE, SENTRA CREEK, FIRE CREEK	Showing	AU, AG, CU, PB, ZN	I05, I01, I06	
104G 175	BOND, BEAUCHAMPS, AXE	Showing	CU, AU	I06	
104G 176	HORN NORTH, C2, AXE	Showing	ZN, PB, AG, CU	I05	
104G 177	HORN EAST, AXE	Showing	AU	I01	
104G 005	HAWK, KLASTLINE, KONA, EAST CREEK	Developed Prospect	AU, AG, PB, ZN, CU	I05	
104G 033	QC, PORPHYRY ZONE, BOOT, HBA, CLIFF, KING HENRY II, ELEANOR OF AQUITAINE	Prospect	CU, AU	L04	
104G 035	HORN, SF, SILVER	Prospect	AG, AU, PB, ZN, CU, BA	I05, I10	
104G 044	AL, AXE	Prospect	CU, AU	L04	
104G 161	QUASH, QC, NORANDA QC, QUASH CREEK	Showing	ZN, PB, AU, AG, CU	I05	
104G 186	YT, GJ, KINASKAN	Showing	CU	L04	
104G 076	CASTLE, JO, CAS	Prospect	AU, AG, CU, MO, PB		
104H 017	NATION PEAK	Showing	BA, PB	I10	
104H 011	RAM, RAM 1-10	Showing	MO	L05	
104H 037	D1	Showing	CU, AU, AG	L03	
104H 031	GIN	Showing	CU, AU, AG, PB, ZN	L03	
104H 019	STIKINE RIVER LIMESTONE	Showing	LS	R09	

Fig. 7. MapPlace 2 custom report tools. a) List of tools and choices of mineral inventory reports. b) Report example for MINFILE.

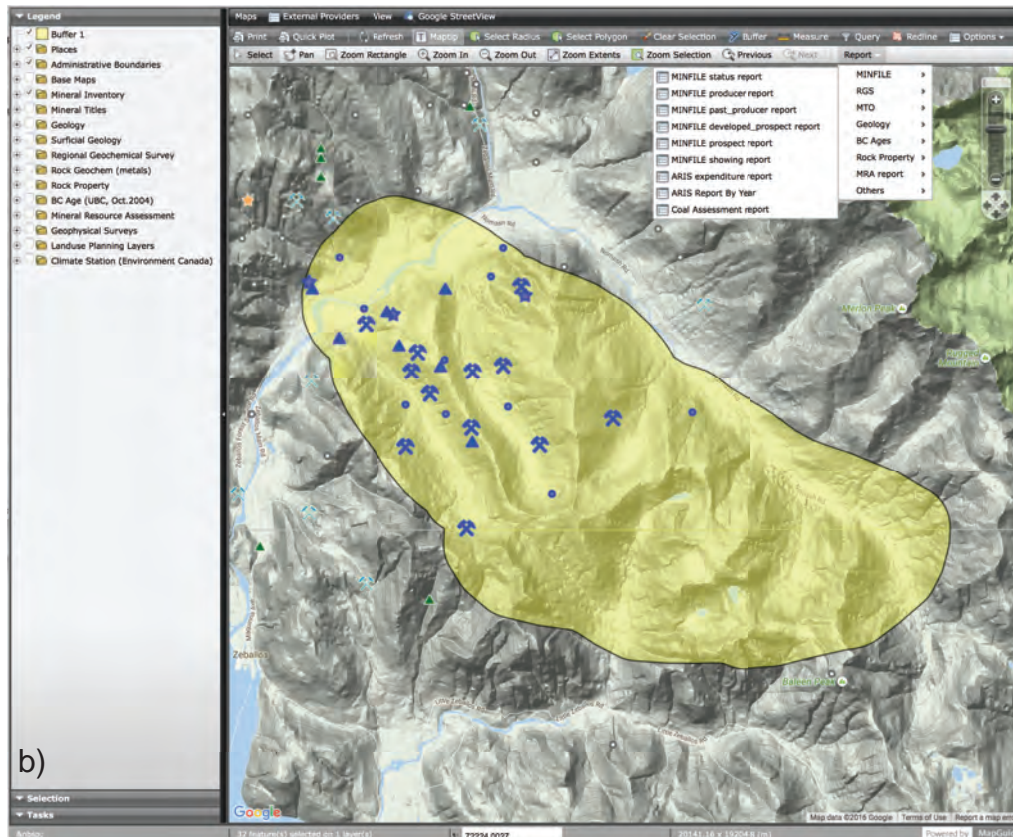
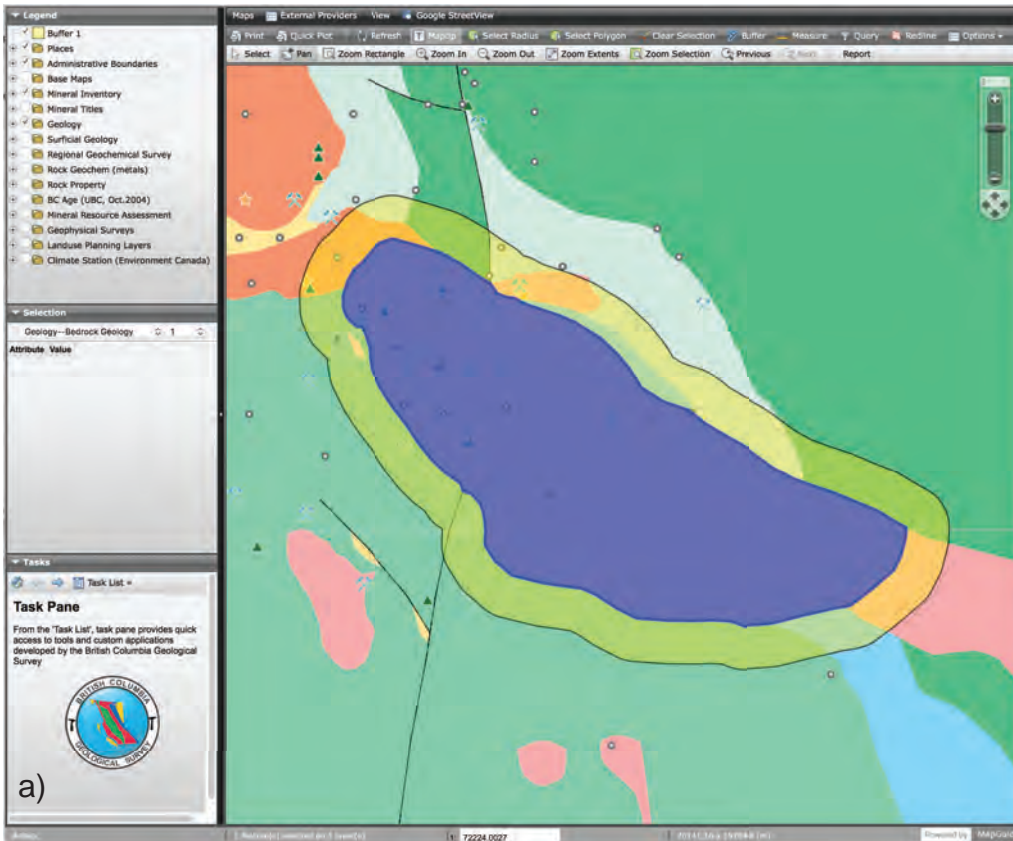
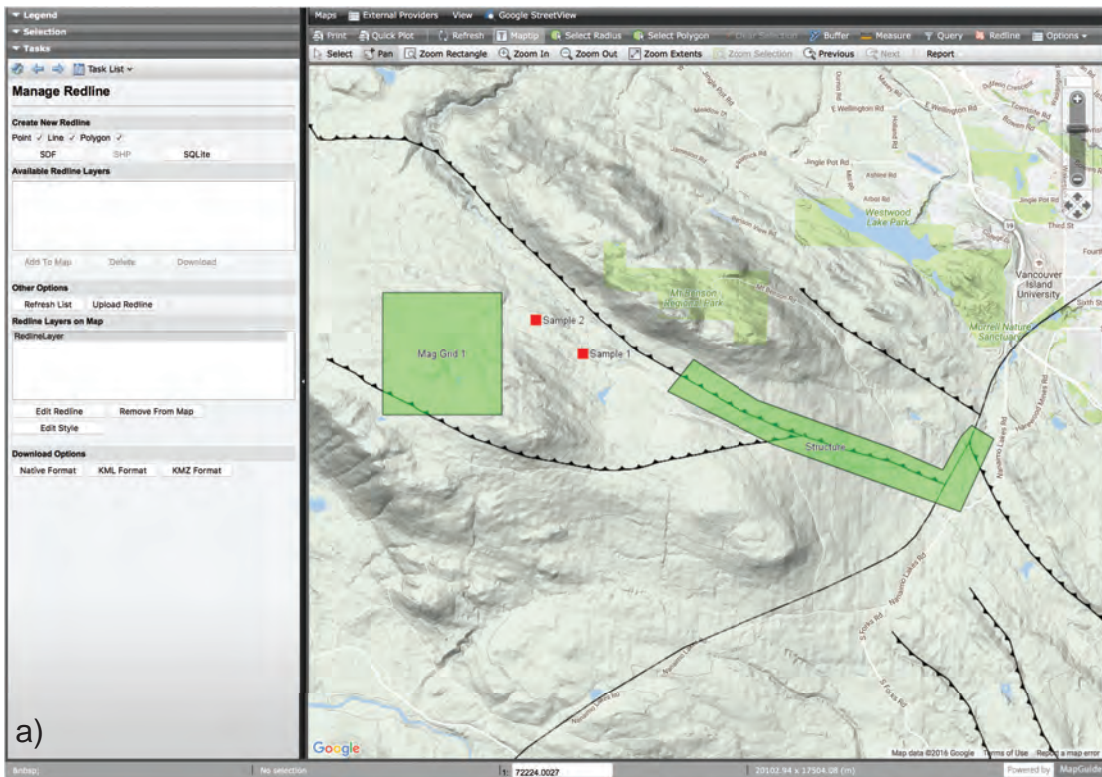


Fig. 8. Example of spatial overlay. **a)** A buffer (in yellow) is created on selected bedrock units (highlighted in blue). **b)** The buffer is used to select mineral occurrences (highlighted in blue) within the area (using Select within).



Property Map Work and Samples Locations

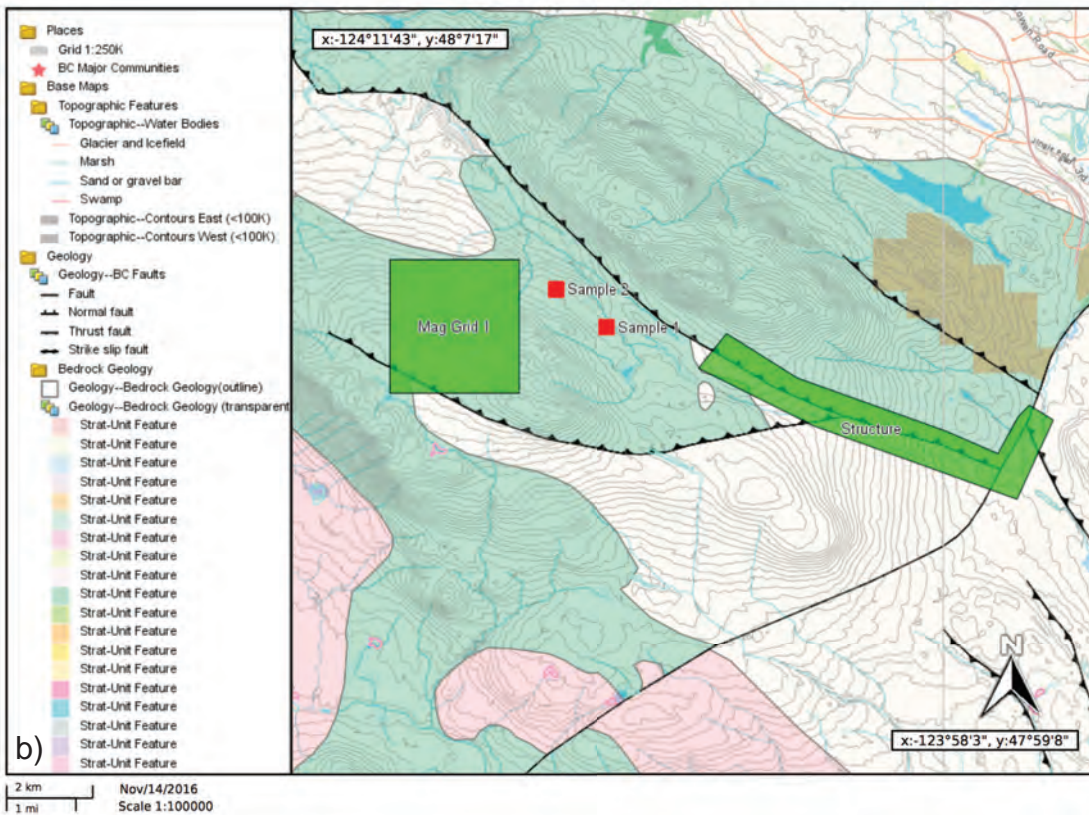


Fig. 9. Custom map making. **a)** Adding sample locations as points, survey areas as polygons, and text as labels using the Redline tool. **b)** Generating a map and saving it as PDF by the Quick Plot tool.

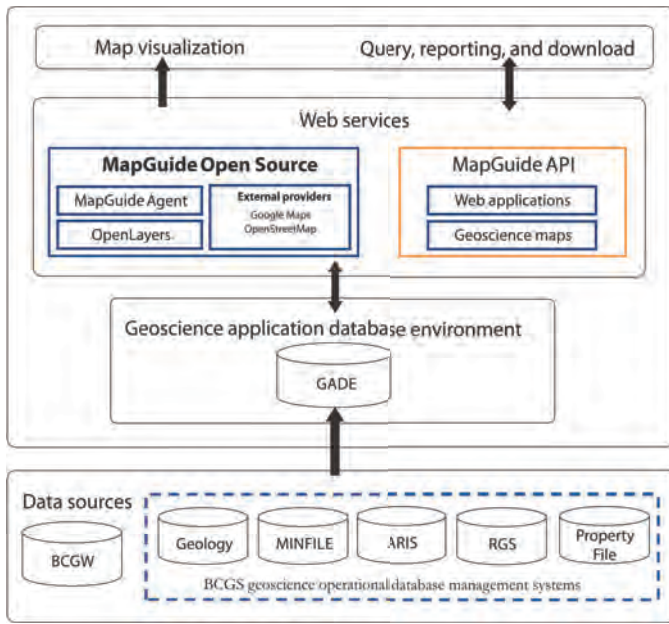


Fig. 10. MapPlace 2 system overview.

rules, and applications to streamline extracting, transforming, and loading (ETL) large volumes of province-wide geoscience and supporting data from different sources and in different formats, map projections, and database management systems (data silos). The new MapPlace 2 data models are designed to ensure consistency in data types, proper level of normalization, integrity of relationships, and naming conventions.

The application database architecture is deployed as a geoscience application database environment (GADE) in PostgreSQL/PostGIS that consists of a spatial database for geoscience data, rules, processes, and applications to manage the processes of ETL (Fig. 11). To break down the data silos, Foreign Data Wrapper is used to access remote data sources and

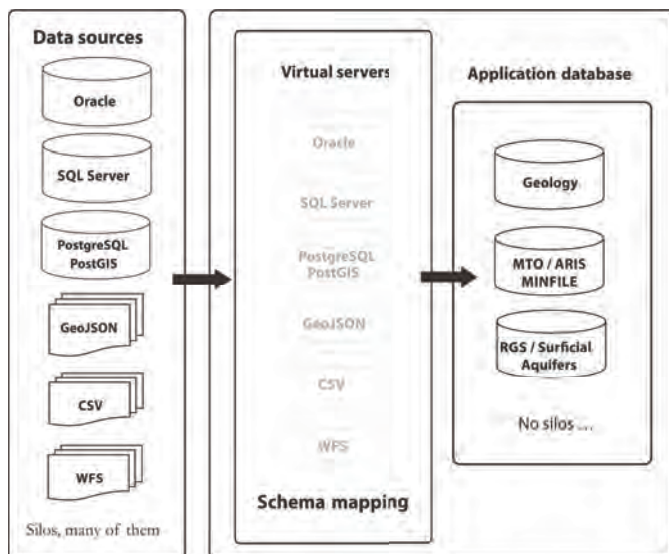


Fig. 11. MapPlace 2 application database architecture.

virtually integrate data through schema mapping. The result is the ability to execute queries on data from different remote sources, such as locating mineral occurrences (sourced from MINFILE in Microsoft SQL Server) within selected mineral tenures (sourced from BCGW in Oracle). The MapPlace 2 application database achieves further efficiency with a consistent query language, functions, triggers, and constraints by using a single spatial database in PostgreSQL/PostGIS.

4.3. Web services: custom applications

We developed MapPlace 2 web applications using MapGuide Open Source as the geospatial web service platform. We selected MapGuide Open Source because it is one of the most advanced open source geospatial web service platforms available, with great community support and the potential to extend and develop custom applications required for MapPlace 2. MapGuide Open Source has an open architecture in system configuration, data connections, and Application Programming Interface (API), and is independent of vendor-specific technology. Our decision to choose MapGuide Open Source was heavily based on the significant performance boost that resulted when a new version of OpenLayers was adopted as the rendering engine. OpenLayers is one of the most advanced rendering technologies in terms of performance, features, and installations.

We built most MapPlace 2 core web applications (custom query and reporting tools) in JavaScript, some with PHP code, to access the MapGuide Open Source API. MapPlace 2 extends to RESTful (Representational State Transfer) web services (Fielding, 2000; Richardson and Ruby, 2008) by forwarding selected features to 'get' and generate summary reports through scripts developed in Microsoft ASP.NET. An example of this RESTful extension is to view full details for a selected MINFILE record.

5. Future development

We are working on a light version of MapPlace 2 to support use on mobile devices (Fig. 12). This mobile version displays the same data as the desktop version, with similar appearance and performance. It is designed to work on small but high-resolution touch screens. Basic tools are available for navigation, selection, buffer creation, length and area measurement, querying, and Redline map customization. Users can retrieve further details by selecting and querying or through the hyperlinks in Maptips. We are soliciting feedback on an alpha version and are making it available upon request for user testing.

MapPlace 2 is slated to move to a better-configured web server in early 2018, which will provide a smoother user experience. The MapPlace 2 system architecture has evolved and been refined progressively and we continue adding to, and improving, the system components. As new data and databases become available, these are being added to MapPlace 2.

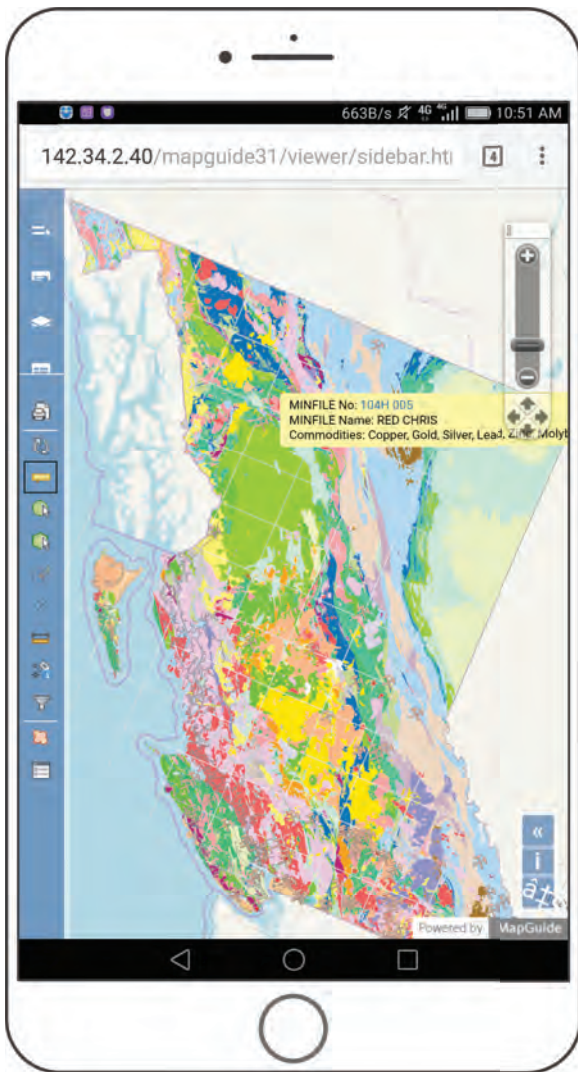


Fig. 12. MapPlace 2 mobile is available for alpha testing.

6. Conclusions

The British Columbia Geological Survey developed the MapPlace 2 geospatial web service to modernize disseminating public geoscience. With a completely new system architecture and interface, MapPlace 2 has improved performance and functionality and works in any web browser. It is of use to anyone interested in British Columbia geoscience, including the mineral industry, environmental organizations, resource planners, public safety agencies, communities, First Nations groups, government, research organizations, and the general public.

MapPlace 2 embraces the most appropriate free and open source software for rendering, integrating application databases, and developing new web applications. It differs from other geospatial web services in its ability to carry out advanced spatial and non-spatial queries and generate summary reports. The power of MapPlace 2 derives from an application database that integrates data from diverse external sources, enabling users to conduct queries and generate custom results across all

datasets. The British Columbia Geological Survey continues to improve MapPlace 2 with advanced applications and access to more geoscience data.

Acknowledgments

MapPlace 2 is the result of many years of teamwork. We thank previous BCGS staff, Pat Desjardins and Thomas Edgehill, for their contributions developing and testing early prototypes. The development of MapPlace 2 benefited enormously from user acceptance tests, workshops, and consultations with clients and with current staff, including Adrian Hickin, Jessica Norris, Deanna Miller, Holly Arnold, and Travis Ferbey. Travis Ferbey designed the new MapPlace logo.

References cited

- Arnold, H., Ferbey, T., and Hickin, A.S., 2016. Ice-flow indicator compilation, British Columbia and Yukon. British Columbia Ministry of Energy and Mines, British Columbia Geological Survey, Open File 2016-04, Geological Survey of Canada, Open File 8083, scale 1:750,000.
- Bray, R., 2008. Chapter 7, MapGuide Open Source. Open Source Approaches in Spatial Data Handling. *Advances in Geographic Information Science*, Volume 2, Springer, Berlin, Heidelberg, pp. 131-152.
- Bustard, A.L., Han, T., and Ferbey, T., 2017. Compiled till geochemical data for British Columbia. British Columbia Ministry of Energy, Mines, and Petroleum Resources, British Columbia Geological Survey, GeoFile 2017-09, 7 p.
- Cui, Y., Fortin, G., Meredith-Jones, S., Zhao, S., and Jones, L.D., 2017a. MapPlace 2 (beta) Workshop. British Columbia Ministry of Energy and Mines, British Columbia Geological Survey Information Circular 2017-3, 89 p.
- Cui, Y., Miller, D., Schiarizza, P., and Diakow, L.J., 2017b. British Columbia digital geology. British Columbia Ministry of Energy, Mines and Petroleum Resources, British Columbia Geological Survey Open File 2017-8, 9 p.
- Fielding, R.T., 2000. Architectural Styles and the Design of Network-based Software Architectures. Ph.D. dissertation, University of California, Irvine, 162 p.
- Han, T., and Rukhlov, A.S., 2017. Regional Geochemical Survey (RGS) data update and release using the newly developed RGS database. British Columbia Ministry of Energy, Mines and Petroleum Resources, British Columbia Geological Survey, GeoFile 2017-11, 7 p.
- Jones, L., MacIntyre, D., and Desjardins, P., 2002. The MapPlace-An internet-based mineral exploration tool. In: *Geological Fieldwork 2001*, British Columbia Ministry of Energy and Mines, British Columbia Geological Survey Paper 2002-1, pp. 409-420.
- Kilby, W.E., 1999. The MapPlace-Web-based GIS access to British Columbia mineral exploration information. *Proceedings of the Thirteenth International Conference on Applied Geologic Remote Sensing*, Vol. 1 (1999), pp. 204-212.
- Kilby, W.E., Jones, L.D., and Desjardins, P.J., 2004. MapPlace client-mapping tools. In: *Geological Fieldwork 2003*, British Columbia Ministry of Energy and Mines, British Columbia Geological Survey Paper 2004-1, pp. 217-218.
- Kilby, W.E., Kliparchuk, K., and McIntosh, A., 2004. Image analysis toolbox and enhanced satellite imagery integrated into the MapPlace. In: *Geological Fieldwork 2003*, British Columbia Ministry of Energy and Mines, British Columbia Geological Survey Paper 2004-1, pp. 209-215.
- OpenLayers, 2017. OpenLayers, <https://openlayers.org>. Last accessed November, 2017.

- OSGeo, 2017. MapGuide Open Source, <http://mapguide.osgeo.org>.
Last accessed November, 2017.
- Richardson, L., and Ruby, S., 2008. RESTful web services. O'Reilly Media, 448 p.
- Tupper, D., Jones, L., Kilby, W. and MacIntyre, D., 2001. The MapPlace, using web-based mineral exploration data as an environmental tool. Innovation June 2001, Volume 5, Number 5, 6 p.

Methods to update the digital geology of British Columbia and synopses of recently integrated mapping programs



Y. Cui^{1,a}, A.S. Hickin¹, P. Schiarizza¹, L.J. Diakow¹, D. Miller¹, G.T. Nixon¹, J.L. Nelson¹, and F. Ferri²

¹British Columbia Geological Survey, Ministry of Energy, Mines and Petroleum Resources, Victoria, BC, V8W 9N3

²Petroleum Geoscience, Tenure and Geoscience Branch, Ministry of Energy, Mines and Petroleum Resources, Victoria, BC, V8W 9N3

^acorresponding author: Yao.Cui@gov.bc.ca

Recommended citation: Cui, Y., Hickin, A.S., Schiarizza, P., Diakow, L.J., Miller, D., Nixon, G.T., Nelson, J.L., and Ferri, F., 2018. Methods to update the digital geology of British Columbia and synopses of recently integrated mapping programs. In: Geological Fieldwork 2017, British Columbia Ministry of Energy, Mines and Petroleum Resources, British Columbia Geological Survey Paper 2018-1, pp. 197-215.

Abstract

The British Columbia Geological Survey (BCGS) provides digital coverage of British Columbia's bedrock geology. The standardized stratigraphic nomenclature that BCGS uses for encoding bedrock across the province resembles that specified in the North American Stratigraphic Code and includes lithostratigraphic, lithodemic, and lithotectonic units. A spatial database handles the large volume of data, rapidly integrates new data, and allows multiple users to work at the same time. The bedrock geology integrates all details from compilations of field mapping at scales from 1:50,000 to 1:250,000, maintains consistent stratigraphic nomenclature, and is free of topological errors. A new 'geospatial frame data' model simplifies integration and reduces the time needed to move from field mapping to data delivery. The data, in shapefile format, are freely available for download from the BCGS web site. The geological map is available for display and query on MapPlace 2, the BCGS geospatial web service. The most recent edition of the digital geology includes updates to the Terrace, Kutcho, QUEST, North Coast, northern Vancouver Island, and Chilcotin-Bonaparte areas. It will soon include Bowser and Sustut basins and the southern Nicola arc area.

Keywords: Bedrock geology, integration, geospatial frame data model, digital map compilation, spatial database, British Columbia, BC

1. Introduction

The British Columbia Geological Survey (BCGS) provides digital coverage of British Columbia's bedrock geology (Fig. 1). In contrast to traditional hard-copy paper compilations, this digital geology is not just a static map at a single scale. The bedrock geology of the entire province is held in a database, and people can download shapefiles to conduct computations and generate customized products. People can work in GIS software or MapPlace 2, the Survey's geospatial web service (Cui et al., 2017a). Use of the database enables computations such as geological map rendering for visualization, spatial and non-spatial queries, statistical analysis, and producing custom maps. In addition, field observations too detailed to include in the original published sources are stored in the database, enabling people to access the highest level of detail possible. As Survey geologists carry out new field mapping, their data can be easily added to the database using novel in-house techniques. This leads to efficient integration and updating.

This paper is in two parts. We first describe the spatial database, the standardized stratigraphic nomenclature used for the entire province, and our 'geospatial frame data' model. This model resolves the problems encountered when attempting to update or merge maps by different geologists working at different scales using different map units or having different interpretations. We then summarize the geology of regional compilations that were recently integrated into the database

(Terrace, Kutcho, QUEST, North Coast, northern Vancouver Island, and Chilcotin-Bonaparte areas) and of areas soon to be included (Bowser and Sustut basins and southern Nicola arc). This second part emphasizes the primary sources that were used to create the database, underscoring that the digital geology of the province starts with field-based mapping.

2. A spatial database for British Columbia bedrock geology

The BCGS started compilation in the late 1980s, using Computer Aided Drafting (CAD) and, later, Geographic Information Systems (GIS) software. As part of mineral potential assessment projects from 1992 to 1996, the BCGS completed bedrock geology compilations of the entire province. Further updates led to a release in 2005 of the first province-wide digital geological map of British Columbia (Massey et al., 2005).

In 2008, the BCGS implemented a spatial database to handle the large volume of data, rapidly integrate new data, and allow multiple users to work from the database at the same time. This led to deployment of the 'Geoscience Operational Database Environment' (GODE), which consists of an operational database in PostgreSQL/PostGIS, data quality rules, desktop GIS, and a set of database applications for data quality assurance (Cui, 2011). Using GODE enables efficient data quality assurance, including detecting and fixing inconsistencies in stratigraphic nomenclature and erroneous

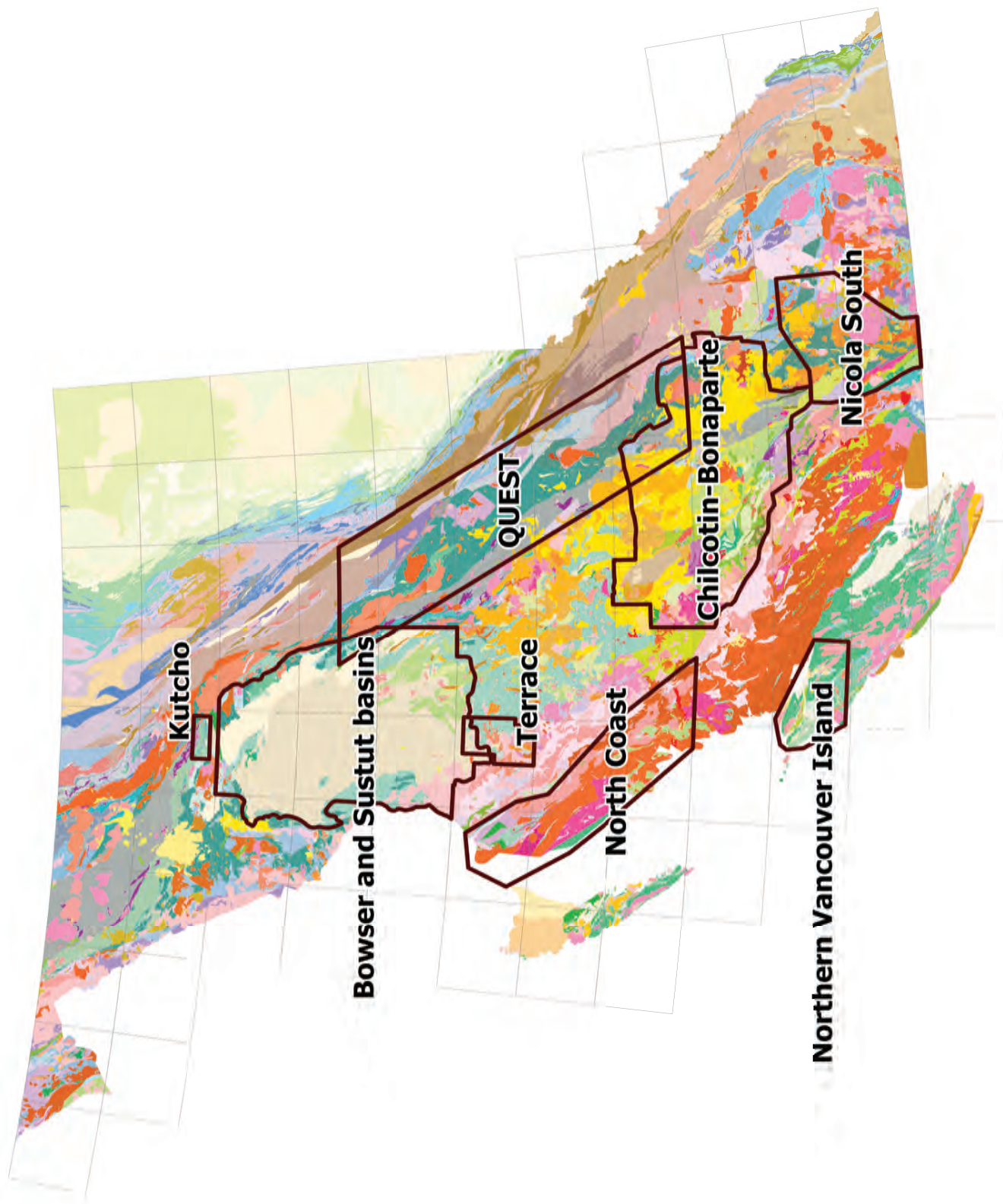


Fig. 1. Regional bedrock geology programs summarized herein.

geometries in geological contacts. Based on GODE, we developed a new way to eliminate topological errors such as overlaps, gaps, discontinuities, and slivers when maps are compiled and integrated ('geospatial frame data' model; see section 4 below).

3. Stratigraphic nomenclature and encoding

Needing a consistent scheme for the entire province, the stratigraphic nomenclature that BCGS uses for encoding resembles that specified in the North American Stratigraphic Code (North American Commission on Stratigraphic Nomenclature, 2005; Rawson et al., 2002; Easton et al., 2014). Ages are adopted from the International Commission on Stratigraphy (Cohen et al., 2013; International Commission on Stratigraphy, 2017). Listings of formally named geological units in the province are available from WEBLEX Canada at (<http://weblex.nrcan.gc.ca>).

We distinguish three lithological categories in the British Columbia digital geology database: lithostratigraphic, lithodemic, and lithotectonic. Lithostratigraphic units are material bodies of sedimentary, volcanic, metasedimentary, or metavolcanic strata that generally conform to the Law of Superposition and are distinguished on the basis of lithic characteristics and stratigraphic position (North American Commission on Stratigraphic Nomenclature, 2005). Although formation and lithodeme are the most common fundamental map units in British Columbia, informal terms comparable to formation in rank (succession, sequence, assemblage) have also been used. Lithodemic units are material bodies of predominantly intrusive, highly deformed, and/or highly metamorphosed rocks that generally do not conform to the Law of Superposition and are distinguished on the basis of lithic characteristics (North American Commission on Stratigraphic Nomenclature, 2005). Lithotectonic units are not included in the North American Stratigraphic Code. This term is used to define units on basis of structural features, mutual relations, origin or historical evolution (North American Geologic Map Data Model Steering Committee 2004; Neuendorf, et al., 2011; European Commission, 2017). Use of the term 'assemblage' in the lithotectonic category is interchangeable with the term 'tectonostratigraphic assemblage' or 'tectonic assemblage'.

The primary goals of encoding stratigraphy in digital geology are to help maintain data in the database and to support computation, which includes: 1) creating geological maps by assigning and updating styles and symbols (e.g., line types for geological boundaries, bedrock unit colours, legends, and age symbol fonts); 2) simplifying the rendering and visualization of derived geological maps; 3) carrying out spatial and non-spatial queries to search by stratigraphic unit name, rank, age, rock type, map area, compilation, and geologist; 4) statistical analysis; and 5) generalizing bedrock units and creating custom maps at a specific scale or with a specific theme (for example all bedrock units in a specified area with high potential for porphyry deposits).

Generalized stratigraphic age and lithology are captured

at the level of detail dictated by the scale of mapping. For example, a bedrock unit may simply be mapped as Triassic 'volcanic rocks' at reconnaissance scale, but referred to as 'mafic volcanic rocks' or, 'plagioclase-phyric basalts' at more detailed scales. With geochronology, petrography, and chemical analysis, the unit may be more precisely identified as Late Triassic calc-alkaline basalt.

4. Geospatial frame data model to integrate bedrock geology

Two major hurdles cause unnecessary complexity and topological errors in digital compilation. First, bedrock maps commonly depict the surface expression of quasi-planar features such as faults and unconformities using lines, and three-dimensional rock bodies using polygons. Geometric and topological errors may be inadvertently introduced along shared boundaries when such maps are revised. For example, gaps and overlaps can occur between adjacent polygons after bedrock units are subdivided and polygon geometries split. In addition, linework representing faults may be shared with polygon segments in cases where units are in fault contact, and the geometries for these shared boundaries can diverge, introducing topological errors. Second, in polygon-based maps, geometric and topological errors occur when maps are updated and merged. Commonly known as edge matching, errors occur where polygons are not aligned, resulting in overlaps, gaps, slivers, fictitious map boundary faults, and other discontinuities at map boundaries.

To reduce shared boundary problems and eliminate topological errors from updating polygons and in edge matching, the BCGS developed a geospatial frame data (GFD) model (Cui, 2014). It consists of three components: 1) centroids (points) that represent the geological units and their attributes; 2) lines that delineate the geological boundaries; and 3) data quality specifications (e.g., data consistency and integrity with respect to lines, points, and stratigraphic encoding). When updates are available or data quality issues detected, changes are applied only to the affected GFD lines and centroids. Polygons representing bedrock are not part of GFD but are generated in the finished data products.

In short, although the use of polygons to capture, theme, and display bedrock geology is attractive, it can lead to editing and merging problems that, in turn, lead to large costs when trying to integrate original source maps at the provincial level. The geospatial frame data model dispenses with polygons, resolving many of these problems.

5. Synopses of recent regional compilations

The most recent edition of the digital geology data for British Columbia (Cui et al., 2017b) includes updated compilations of the Terrace, North Coast, northern Vancouver Island, Kutcho, QUEST, and Chilcotin-Bonaparte areas (Fig. 1). The southern Nicola area and Bowser and Sustut basins will be integrated by early 2018. Emphasizing the primary sources where readers can find details, the following treatments summarize these compilations. For each area we consider the map or compilation

extent, historical mapping, the rationale and sources of support for the mapping projects, geologic overviews, products delivered, and significant results, particularly those of economic importance.

5.1. Terrace

The Terrace regional mapping project (Fig. 1), in western British Columbia, was completed between 2005 and 2009. The region, includes the towns of Usk, Terrace, and Kitimat, in NTS map sheets 103I/09, southern half of 103I/16, eastern half of 103I/10 and 103I/08. Reconnaissance mapping was also completed in map sheets 103I/07 and 103I/02. The Terrace data were integrated into the digital geology in 2013.

Coastal and northwestern British Columbia have relatively poor coverage of 1:50,000 scale mapping and before this project, no 1:50,000-scale mapping was available for 103I, except in unpublished theses (i.e., Mihalynuk, 1987; Heah, 1991). The project was initiated to address this knowledge gap and stimulate exploration interest. The project was a cooperative effort between the British Columbia Geological Survey and the Resource Management Department of the Kitselas First Nation.

The area is in western Stikinia, one of the Intermontane terranes recording mainly Paleozoic through mid-Jurassic island arc magmatism (Monger et al., 1991). The area also includes the eastern fringes of the Coast Plutonic complex, a linear belt of mainly granitoid and metamorphic rocks that occupies most of coastal British Columbia. The Coast Plutonic complex is the deeply eroded and tectonically denuded roots of the mid-Jurassic to Eocene continental successor arc, which developed along the western margin of North America following accretion of the Intermontane and Insular terranes (van der Heyden, 1992; Nelson et al., 2013b).

The oldest stratified unit recognized in the map area is upper Paleozoic volcanogenic rocks and limestones, correlative with younger strata in the Stikine assemblage in the Iskut-Stikine area (Logan et al., 2000, Brown et al., 1996). Nelson et al. (2006a) proposed these rocks to be referred to as the Zymoetz Group, divided into a lower volcanic complex (Mt. Attree Formation) and an overlying, Lower Permian limestone equivalent to the Ambition Formation (Gunning et al., 1994). Above these rocks are marine strata, equivalent to the Stuhini Group (Triassic), that are in turn unconformably overlain by intermediate to felsic volcanogenic rocks in the lower part of the Hazelton Group, equivalent to the Telkwa Formation (Lower Jurassic; Tipper and Richards, 1976; Gagnon et al., 2012). The upper Hazelton Group is represented by the Smithers and Quock formations (Middle Jurassic).

Much of the map area is underlain by intrusive rocks that range from late Paleozoic to Eocene. The late Paleozoic suite was emplaced before accretion and is deformed. The Early Jurassic intrusions are mainly represented by the Kleanza suite (Nelson, 2009). Cretaceous to Paleocene plutons that are part of the Coast Plutonic complex are predominantly represented by the Kitsumkalum suit of granite, granodiorite and diorite (early

Cenozoic; Nelson and Kennedy, 2007). Eocene intrusions are represented mainly by the Carpenter Creek suite of granite and granodiorite.

Three Open File maps were released from the project, including: Usk (Nelson et al., 2006a), Terrace (Nelson et al., 2007), and Chist Creek (Nelson et al., 2008a). Boudreau (2007) released her undergraduate thesis as a British Columbia Geological Survey Open File. The project produced seven British Columbia Geological Survey Geological Fieldwork articles (Barresi and Nelson, 2006; Nelson et al., 2006b; Nelson and Kennedy, 2007; McKeown et al., 2008; Nelson et al., 2008b; Angen, 2009; Nelson, 2009) and a Ph.D. thesis (Barresi, 2015) and a related journal article (Barresi et al., 2015).

The project resulted in several revelations. An extensive Paleozoic metavolcanic unit stratigraphically underlies Lower Permian limestone from Zymoetz River to Chist Creek. There is exploration potential in local occurrences of volcanogenic sulphide. Three base metal sulphide mineral showings northwest of Kitimat display characteristics of volcanogenic massive sulphide (VMS) feeder zone systems, suggesting a single belt of VMS-style mineralization, probably controlled by a penecontemporaneous seafloor structure. Two felsic marker units were identified and served to help resolve the stratigraphy of the Telkwa Formation. The Skeena River detachment fault system (Eocene) likely continues into the lowest elevations along Williams Creek, Chist Creek and the Kitimat River. The Paleozoic metavolcanic unit and its stratigraphically overlying discontinuous Lower Permian limestone extend west and southwest into the Coast Mountains in the core of a broad regional northeast-trending anticline. This anticlinal structure predates northwest-striking, northeast-side down normal faults that in turn are truncated by more northerly faults of the Kitsumkalum-Kitimat graben.

5.2. North Coast

The North Coast project (Fig. 1), also referred to as the Edges Multiple Metals-NW Canadian Cordillera project, or simply Edges, was a mapping program that ran from 2009 to 2011. The program, a contribution to Natural Resources Canada's (NRCan) first Geo-mapping for Energy and Minerals (GEM) program, encompassed an area that extends along the coast of British Columbia from north of Bella Bella to south of Prince Rupert that includes the communities of Klemtu and Hartley Bay. Mapping was completed at 1:20,000-1:50,000 and compiled to 1:150,000 in portions of NTS map sheets 103A, G, H, and J. The North Coast project data were included in the provincial digital geology in 2013.

Although the mineral potential of the northern coastal area of British Columbia had been assessed as high (Kilby, 1995), active mineral exploration was limited and the Edges project was directed at further assessing metallic mineral potential of the far-travelled terranes that make up the outer accreted margin of the Canadian Cordillera. The project was a collaboration among the Geological Survey of Canada, the British Columbia Geological Survey, and Yukon Geological

Survey, with participation by the United States Geological Survey and Canadian and American universities.

The northern coastal area was first mapped systematically as part of the Geological Survey of Canada's regional assessment of the Coast Mountains batholith and enclosed metamorphic rocks (Roddick, 1970; Baer, 1973; Hutchison, 1982). These studies concentrated on the plutonic rather than supracrustal rocks. More recent geological work focused on the structural and igneous history of the Coast Mountains (e.g., Chardon et al., 1999; Gehrels and Boghossian, 2000; Gehrels, 2001; Chardon, 2003; Butler et al., 2006; Gehrels et al., 2009).

Alexander terrane (Wheeler et al., 1991), which formed the principal focus of this project, is flanked by metamorphosed and deformed meta-sedimentary-volcanic rock units of the Gravina belt and Yukon-Tanana terrane (e.g., Gehrels and Saleeby, 1987; Gehrels et al., 1996; Rubin and Saleeby, 1992, Saleeby, 2000; Gehrels, 2001). The oldest successions mapped in project area are greenschist grade volcanic and sedimentary rocks of the Descon Formation (Early Ordovician to Late Silurian), which stratigraphically overlie the Wales Group, the oldest rocks recognized in Alexander terrane (Late Proterozoic to Cambrian) in Alaska. Plutons that are coeval (and probably cogenetic) with volcanic rocks of the Descon Formation are widespread, and range from diorite to granite. The Mathieson Channel sedimentary rocks, marble and volcanic rocks unconformably overlie the Descon Formation, the basal conglomerate of which is interpreted to represent a major phase of uplift and erosion from the Klakas orogeny (Gehrels and Saleeby, 1987). Rocks of Alexander terrane are overlain by Upper Jurassic to Upper Cretaceous turbidites and subordinate mafic volcanic rocks of the Gravina belt. These rocks can be traced, generally along the inboard margin of Alexander terrane, for the length of southeastern Alaska (Berg et al., 1972) and into northern coastal British Columbia.

Yukon-Tanana terrane underlies the western margin of the Coast Mountains and consists of high metamorphic grade marbles, quartzites, pelitic schists, and orthogneisses and greenschist to amphibolite grade metavolcanic rocks, pelitic schists, and minor marble. In northwestern British Columbia, the Ecstall belt (Gareau and Woodsworth, 2000; Alldrick, 2001; Alldrick et al., 2001), with its enclosed Devonian volcanogenic deposits, is also assigned to Yukon-Tanana terrane.

Tonalitic to granodioritic plutons of the Coast Plutonic complex, form isolated bodies in northern and western portions of the northern coastal British Columbia, and increase in extent southeastward to form continuous bodies of plutonic rock (Gehrels et al., 2009). The depth of emplacement of plutons increases eastward across the Coast Mountains. Late Jurassic bodies were emplaced at depths of ~15 km whereas the Early Cretaceous plutons were slightly deeper (~20 km) and, farther east, mid-Cretaceous plutons of the Ecstall belt were emplaced at significantly greater depths, perhaps 25-30 km (Butler et al., 2006). This increase in depth of emplacement correlates well with the eastward increase in metamorphic grade.

The two main map publications that resulted from this

project include Nelson et al. (2011a; NTS 103A/8, 9, 15, and 16) and Nelson et al. (2014; parts of NTS 103-A, -G, -H, -I, and -J). These maps were augmented by five Geological Fieldwork papers (Nelson et al., 2010; Nelson et al., 2011b; Nelson et al., 2012; Angen et al., 2012; Nelson et al., 2013b), a M.Sc. thesis (Angen, 2013), and several journal articles (e.g., Colpron and Nelson, 2009, 2011; Tochilin et al., 2014.).

This project established that the southern part of Alexander terrane contains an Ordovician volcanic-sedimentary-intrusive suite of probable back-arc affinity. The Pitt VMS occurrence on Pitt Island is aligned along a major shear zone that marks the southwestern limit of mid-Cretaceous ductile shearing along the Grenville Channel fault. Chalcopyrite and sphalerite from the main Pitt showing yield lead isotopic ratios significantly lower than those of Cretaceous syngenetic and epigenetic deposits elsewhere in the Coast belt and are thus incompatible with an epigenetic origin linked to the Grenville Channel fault. Instead, they closely match lead isotopic ratios from Ordovician volcanogenic deposits of New Brunswick, Newfoundland, Quebec, and Norway. Current tectonic models place Alexander terrane near the northern end of the Caledonide chain in the early to mid-Paleozoic, implying that Ordovician volcanogenic massive sulphides in Alexander terrane may link to deposits originating in back arcs that constituted a circum-Iapetus ocean ring of fire. Mapping identified some new small sulphide occurrences within and adjacent to Ordovician rhyolites and rhyolite breccias. A suite of samples of meta-igneous rocks east of northern Grenville and Telegraph channels are Permian and represent a previously unknown, late Paleozoic volcanic-sedimentary unit with related dikes in intrusive contact with the Alexander terrane. A large tract of Late Silurian to Early Devonian orthogneiss on Porcher Island was intruded during a Caledonian-age deformational event that probably marked the amalgamation of pericratonic and primitive arc elements in the composite Alexander terrane. And finally, the mapping traced out the Grenville Channel fault for 300 km along strike with Early to mid-Cretaceous sinistral motion.

5.3. Northern Vancouver Island

The northern Vancouver Island mapping project (Fig. 1) encompassed the entire northern tip of Vancouver Island. Geological mapping was completed at 1:50,000 scale and included parts of NTS sheets 92L/03, 05, 06, 07, 10, 11, 12, and 13 as well as 102I/08, 09, and 16. Mapping began in 1992 as part of a multiyear project jointly funded by the Canada-British Columbia Mineral Development Agreement (MDA) aimed at improving the understanding of the geology and mineral potential of northern Vancouver Island (Nixon et al., 1993a, b). The project later evolved into the northern Vancouver Island integrated project that included: bedrock and surficial geological mapping; water, till and bedrock geochemistry; and alteration and mineral deposits studies (Panteleyev et al., 1996). A major focus was to provide a clearer understanding of the Bonanza volcanic rocks, and their geochemical expression and mineral potential. Final Geoscience Maps for northern

Vancouver Island (Nixon et al., 2011a-e) were included in British Columbia's integrated digital geology in 2015.

The first geological investigations of northern Vancouver Island were made by Dawson (1887) who examined Cretaceous coal-bearing strata on the north and south shores of Quatsino Sound. Subsequent studies include those of Dolmage (1919), Gunning (1930, 1932), Jeffrey (1962) and Northcote (1969, 1971). Detailed descriptions of shoreline exposures were summarized by Jeletzky (1976) who made extensive fossil collections partially identified by Tozer (1967). The regional geology of northern Vancouver Island was provided by Muller et al. (1974) and Muller and Roddick (1983). A regional geological reconnaissance mapping program in the Quatsino Sound area was initiated in 1990 by Massey and Melville (1991).

Vancouver Island is mainly underlain by Late Paleozoic to Early Mesozoic rocks of Wrangell terrane (Jones et al., 1977), which extends northwards through Haida Gwaii into southern Alaska (Wheeler and McFeely, 1991). Wrangellia was amalgamated with Alexander terrane to form the Insular superterrane as early as the Late Carboniferous (Gardner et al., 1988), and was accreted to inboard terranes of the Coast and Intermontane belts as late as the mid-Cretaceous (Monger et al., 1982) or as early as the Middle Jurassic (van der Heyden, 1992; Monger and Journeay, 1994). On northern Vancouver Island, Wrangellia is intruded to the east by granitoid rocks of the Coast Plutonic complex and fault bounded to the west by the Pacific Rim terrane and metamorphosed and intrusive rocks of the West Coast crystalline complex (Wheeler and McFeely, 1991). On Vancouver Island the Sicker and Buttle Lake groups (Devonian to Early Permian) form the basement to Wrangellia (Massey, 1995a-c).

The stratigraphy of northern Vancouver Island consists of the Vancouver and Bonanza groups, as redefined by Nixon and Orr (2007). The Vancouver Group (Middle to Late Triassic) includes the calcareous shale informally known as the 'Daonella beds' at its base, overlain by Karmutsen flood basalt (Carnian) and Quatsino limestone (Carnian to Early Norian). The basal unit of the overlying Bonanza Group (Late Triassic to Middle Jurassic) is represented by the Parson Bay Formation (Norian to Rhaetian), a mixed carbonate-siliciclastic-volcanic succession. The Parson Bay Formation is succeeded by volcanoclastic-sedimentary strata (latest Triassic to earliest Jurassic) and the main volcanic phases of the Bonanza Group, LeMare Lake (Early Jurassic; Hettangian-Sinemurian) and Holberg (Middle Jurassic; Aalenian-Bajocian) volcanic units. Coeval granitoid intrusions of the Island Plutonic suite form the plutonic component of the Bonanza magmatic arc (Northcote and Muller, 1972; DeBari et al., 1999). The distribution of Neogene volcanic centres appear to be strongly influenced by high-angle faults. The northeasterly trending Brooks Peninsula fault zone appears to coincide with the southern limit of Neogene volcanism in the region and delineate the southern boundary of an extensional regime in the Queen Charlotte basin (Armstrong et al., 1985; Lewis et al., 1997).

The project resulted in an initial compilation in 1997 (Nixon et al., 1997) and included preliminary Open File maps of Mahatta Creek (NTS 92L/5; Nixon et al., 1993b), Quatsino-Port McNeill (NTS 92L/12 and 11 west; Hammack et al., 1994), and Quatsino-Cape Scott (NTS 92L/12 west and 102I/ 8,9; Hammack et al., 1995), supported by papers in Geological Fieldwork (Nixon et al., 1993a, 1994, 1995; Archibald and Nixon, 1995). Mapping and follow-up studies on northern Vancouver Island continued with release of Geoscience Maps for Quatsino-Port McNeill (Nixon et al., 2000a, 2006b), Alice Lake (Nixon et al., 2000b, 2006f), Mahatta Creek (Nixon et al., 1993b, 2006a), Nimpkish-Telegraph Cove (Nixon et al., 2006d, 2009), and Holberg-Winter Harbour (Nixon et al., 2006c). The final set of Geoscience Maps for northern Vancouver Island capture new stratigraphic, paleontological, geochronological, geochemical, and metamorphic data (Nixon et al., 2011a-e). Several papers complementing these studies were published in Geological Fieldwork and in refereed journal articles (Nixon and Orr, 2007; Nixon et al., 2006e, 2008; Ferri et al., 2008; Greene et al., 2006, 2009, 2010).

The work on northern Vancouver Island has significant economic implications. The evolution of the Bonanza Group, as currently defined, comprises three distinct stages: an incipient arc-building phase of submarine to locally emergent, mainly basaltic to andesitic volcanism in the Late Triassic (Parson Bay Formation); the main phase of largely subaerial basaltic to rhyolitic volcanism (LeMare Lake volcanics) in the earliest Jurassic (Hettangian-Sinemurian); and the final phase of subaerial basaltic to rhyolitic arc construction (Holberg volcanics) in the early Middle Jurassic (Aalenian-Bajocian). The latter two phases of Bonanza volcanism are accompanied by coeval plutonic rocks (predominantly diorite-granodiorite) of the Island Plutonic suite. The prime Cu-Au-Mo porphyry deposits along the Island Copper-Red Dog trend are associated with the Middle Jurassic Bonanza magmatic arc north of a major fault (Holberg fault) trending through Holberg and Rupert inlets. The metallogenic potential of northern Vancouver Island is further underscored by a young suite of Late Miocene-Pliocene plutons, spatially associated with the Brooks Peninsula fault zone, that carry Cu-Mo porphyry-style mineralization; and the discovery of high-Mg basalts (Keogh Lake picrites) in the Karmutsen flood basalt succession (Late Triassic) which raises their prospectivity for magmatic Ni-Cu-PGE sulphide deposits.

5.4. Kutcho

The Kutcho update area includes about 600 km² of northern British Columbia, in the southeast part of NTS map sheet 104I, extending from 50 to 115 km east-southeast of the community of Dease Lake (Fig. 1). The Kutcho mapping project was carried out by the British Columbia Geological Survey in 2010 and 2011. The main goals of the program were to gain a better understanding of, and provide more detailed geological maps for, the Kutcho assemblage (Permo-Triassic) in the area where it hosts the Kutcho Creek VMS deposit (MINFILE 092I 060).

This mapping was also a contribution to the NRCan-led Edges project. The project was co-funded by the British Columbia Geological Survey, a private-public partnership agreement with Kutcho Copper Corporation, and the Geological Survey of Canada. The Kutcho data were included in British Columbia's integrated digital geology in 2013.

The regional geology of the Kutcho area is summarized by Gabrielse (1998), incorporating work carried out by the Geological Survey of Canada and British Columbia Geological Survey from 1956 to 1991, including studies of the Kutcho assemblage by Thorstad (1984) and Thorstad and Gabrielse (1986). Studies of the Kutcho Creek deposit and surrounding rocks (mainly Kutcho assemblage) are presented by Bridge et al. (1986), Barrett et al. (1996), and Childe and Thompson (1997).

The Kutcho assemblage is in the King Salmon allochthon, a narrow belt of penetratively deformed, greenschist-grade metamorphic rocks that also includes slivers of the Cache Creek complex and a Triassic-Jurassic metasedimentary succession, the Whitehorse trough, that unconformably overlies both Kutcho and Cache Creek rocks. The allochthon is separated from the main exposures of the Cache Creek complex, to the north, by the Nahlin fault and from Stikine terrane and overlying Bowser basin to the south, by the King Salmon thrust fault, which dips north. The Kutcho dextral strike-slip fault, which strikes northwest, truncates the King Salmon allochthon, and juxtaposes it against Mesozoic volcanic and plutonic rocks of Quesnel terrane.

Preliminary results from the Kutcho mapping program were presented by Schiarizza (2011a, b). The final results featured new subdivisions of the Kutcho assemblage and new radiometric ages and documented relationships with adjacent geological units (Schiarizza (2012a, b).

5.5. QUEST

The Quesnellia Exploration Strategy, or QUEST, was a collaboration of the British Columbia Geological Survey, Geological Survey of Canada and Geoscience BC. This work was also a contribution to the Edges Project of the Natural Resources Canada that, with funding from Geoscience BC, supported a number of airborne geophysical and geochemical surveys. One of the major contributions of the project was a revised bedrock geology map for the poorly exposed region from Williams Lake north through Prince George to Williston Lake (Fig. 1). The QUEST area included portions of, or complete 1:250,000 map sheets for NTS 93A, B, G, H, I, J, K, O, N and 94B, C, and D. The QUEST data were included in British Columbia's integrated digital geology in 2010.

The objectives of the project were to: 1) stimulate mineral exploration in British Columbia, particularly in the Mountain Pine Beetle infested areas of central British Columbia; and 2) provide a framework of exploration datasets for any follow-up mineral exploration work in the drift-covered areas of Quesnellia. Driven mainly by new geophysical and geochemical data acquired by Geoscience BC, the bedrock

map integrated existing geological maps from the British Columbia Geological Survey and the Geological Survey of Canada, with interpretations from the geophysics. The purpose of the map revision and geophysical integration was to provide a context for porphyry mineral exploration in these covered areas. QUEST was initiated in 2007 and focused on Quesnel terrane, with the release of the hardcopy map in 2010 (Logan et al., 2010). Much of the mapping was based on the Massey et al. (2005) compilation with modifications that reflected geophysical interpretation and geological updates from Ferri and O'Brien (2003), Logan et al. (2007, 2008), Schiarizza and Macauley (2007), and Schiarizza et al. (2009).

Like Stikinia, Quesnel terrane is an island arc complex that is part of the Intermontane superterrane. The arc initiated in Late Devonian on Paleozoic basement outboard of the ancestral North American (Laurentian) margin on the eastern edge of the Panthalassa ocean (Nelson et al., 2013a; Logan and Mihalynuk, 2014). Arc construction was prolific during the Late Triassic, a particularly important period in which many Canadian Cordilleran porphyry deposits formed (Logan and Mihalynuk, 2014). By the Late Jurassic, Stikine and Quesnel arcs were accreted to the margin of ancestral North America.

5.6. Chilcotin-Bonaparte

The Chilcotin-Bonaparte compilation extends across about 73,000 km² of south-central British Columbia, encompassing parts of the Coast Mountains, the Interior Plateau, and the Quesnel and Shuswap highlands, and includes all or parts of NTS map sheets 92/I, J, N, O, P, and 93A, B, C (Fig. 1). It includes Paleozoic and Mesozoic rocks of Kootenay, Slide Mountain, Quesnel, Cache Creek, Cadwallader, Stikine, and Bridge River terranes, as well as metamorphic rocks, in the Coast belt, that may correlate with Yukon-Tanana terrane. The Chilcotin-Bonaparte data were included in British Columbia's integrated digital geology in 2017.

Before this compilation, the digital geology of the Chilcotin-Bonaparte area was based on the first-generation digital compilations prepared for the Mineral Potential project in the early to mid-1990s (Schiarizza et al., 1994; Schiarizza and Church, 1996). Subsequent studies in the region include several single- to multi-year mapping programs carried out by the British Columbia Geological Survey, as well as studies by the British Columbia Ministry of Energy and Mines, Oil and Gas Division, the Geological Survey of Canada, and as graduate thesis projects, mainly at the University of British Columbia. These studies introduced many substantial modifications to the original digital geology, providing motivation to undertake a new compilation.

Mesozoic rocks include late Middle Jurassic through Upper Cretaceous sedimentary successions of the Tyaughton-Methow basin in the eastern Coast Mountains, as well as Middle to Late Jurassic, Early Cretaceous, and Late Cretaceous arc volcanic successions. Eocene volcanic and local sedimentary rocks (including the Kamloops, Ootsa Lake and Endako groups), together with Neogene basalts of the Chilcotin Group, occur

across most of the compilation area, and are the predominant bedrock component in many parts of the Interior Plateau. Miocene-Pleistocene volcanic rocks of the Anahim volcanic belt (Ilgachuz and Itcha groups) occur in the northwestern part of the compilation area, whereas Pleistocene and Holocene basalt related to the Wells Gray volcanic field crop out near the eastern edge of the area. Plutonic rocks include Permian, Triassic and Early Jurassic suites that are integral components of Cache Creek, Cadwallader and Quesnel terranes. Younger plutons include Late Jurassic through Eocene granitic suites that are a predominant component of the Coast Mountains, less common dioritic to granitic rocks with a similar age range scattered through the adjacent Interior Plateau, and late Early Cretaceous granite and granodiorite (Bayonne suite) that intrude Kootenay, Slide Mountain and Quesnel terranes near the eastern edge of the compilation area.

The geology of Quesnel terrane, in the eastern part of the Chilcotin-Bonaparte area, is based mainly on the maps of Schiarizza et al. (2013), which summarize six years of fieldwork, conducted between 2000 and 2008. This work introduced new, regionally significant subdivisions of the Nicola Group (Upper Triassic) and recognized several different Late Triassic-Early Jurassic plutonic suites, some with characteristic Cu-Au or Cu-Mo mineralization. The geology of the Quesnel belt also incorporates studies by Anderson et al. (2010) who recognized Early Jurassic and Middle Jurassic subdivisions of the Thuya batholith, Logan and Schiarizza (2014) who looked at the geology of the Rayfield River pluton, and Friedman et al. (2014) who provided isotopic ages for Early and Middle Jurassic intrusive rocks mapped by Beaton (2011) at the Bonaparte mine, near the southeast margin of the compilation area. In addition, the compilation incorporates the study of Schiarizza (2015), showing that the Granite Mountain batholith, host to the Gibraltar Cu-Mo porphyry deposit, is part of Quesnel terrane (rather than Cache Creek terrane, as previously inferred).

Revisions to the geology of the Interior Plateau west of the Quesnel belt are based on a geological compilation of the Taseko Lakes (92O) map area by Mahoney et al. (2013), studies west of Williams Lake by Mihalynuk and Harker (2007) and Schiarizza (2013), geologic maps covering the SE part of the Anahim Lake (93C) map area (Mihalynuk et al., 2009), an M.Sc. thesis study of the Newton Au-Ag deposit by McClenaghan (2013), and isotopic ages presented by Riddell (2010). The pre-Cenozoic geology includes: a north-south belt of rocks comprising Cache Creek terrane; a substantial area of Triassic-Jurassic Cadwallader terrane rocks to the west, locally underlain by Upper Permian bimodal volcanic and volcanoclastic rocks that correlate with the Kutcho assemblage of northern British Columbia; a large area underlain by poorly exposed mid-Cretaceous volcanic rocks, locally associated with Jurassic volcanic rocks and Upper Cretaceous sedimentary and volcanic successions, including probable correlatives of the Upper Cretaceous host to the Blackwater-Davidson epithermal Au deposit; and, in the west, a belt of Jurassic volcanic and

sedimentary rocks that may, in part, correlate with upper Hazelton Group rocks of Stikine terrane.

A narrow fault-bounded belt of bimodal volcanic rocks and associated dioritic and tonalitic intrusions occurs in the eastern part of the Cache Creek belt, west and south of the town of Cache Creek. These rocks were previously assigned to the western belt of the Nicola Group (Upper Triassic), but were shown to be older, and correlated with the Kutcho assemblage (Childe et al., 1997). The Chilcotin-Bonaparte compilation was extended southward to encompass this belt, and show the revised interpretation.

Major revisions to the geology of the eastern Coast Mountains and adjacent Interior Plateau, in the southwestern part of the compilation area, are based on the geology presented by Schiarizza et al. (2002) for the Taseko Lakes-Tatlayoko Lake area. This area is underlain mainly by Middle Triassic to Middle Jurassic volcanic, plutonic and sedimentary units of Cadwallader terrane, and late Middle Jurassic to mid-Cretaceous rocks of the Tyaughton-Methow basin, and plays a prominent role in the regional definition and understanding of this terrane and basin. This improved understanding prompted revisions (mainly nomenclature and groupings of units) to the geology of the Taseko Bridge River area to the southeast, and this geology (Schiarizza et al., 1997) is also included in the compilation.

The geology of the Coast Mountains near the southwest limit of the compilation area, southwest of the Tchaikazan fault, includes Triassic rocks tentatively assigned to Stikine terrane, together with Lower and Upper Cretaceous volcanic and sedimentary rocks, structurally interleaved within the northeast-vergent eastern Waddington thrust belt (Rusmore and Woodsworth, 1993). Revisions to the geology in the southeast part of this belt are based on the thesis studies of Israel (2001), Blevings (2008), and Hollis (2009). Revisions to the northwest part of the belt are from Mustard et al. (1994).

The western end of the Chilcotin-Bonaparte compilation area incorporates major revisions to the geology of the Coast Mountains, based on maps by van der Heyden et al. (1994), Israel and van der Heyden (2006), and Israel et al. (2006). The geology of this area features undated metavolcanic and metasedimentary rocks of the Atnarko assemblage, associated migmatitic orthogneiss and amphibolite, and several distinct plutonic suites ranging from Early Jurassic to Paleocene.

The distribution of Eocene volcanic rocks was revised using maps by Mihalynuk and Harker (2007), Mihalynuk et al. (2009), Schiarizza et al. (2013), and Mahoney et al. (2013). These sources also provided updates on the distribution of the Neogene Chilcotin Group, augmenting the study of Dohaney et al. (2010), which shows the distribution of the group in the Taseko Lakes (92O) and Bonaparte Lake (92P) map areas. The northwestern part of the compilation incorporates the detailed study by Souther and Souther (1994) of the Ilgachuz Range (Anahim volcanic belt), and the eastern part shows previously unmapped outliers of Pleistocene basalt (Wells Gray volcanic field) after Schiarizza et al. (2013).

5.7. Bowser and Sustut basins

The Bowser and Sustut basins are in north-central British Columbia and include the lowlands of the Interior Plateaus and the Skeena Mountains (Fig. 1). The Sustut basin, with its relatively gently dipping strata, defines the Spatsizi Plateau (Mathews, 1986). The communities of Smithers, Hazelton and Kitwanga are along the southern margin of the Bowser basin. The Bowser and Sustut basin regional geology compilation was released by the Geological Survey of Canada in 2009 (Evenchick et al., 2009) and incorporates two decades of mapping, mainly by the Geological Survey of Canada. The mapping is slated for inclusion in the provincial digital geology in 2018.

Systematic mapping of the area underlain by the Bowser and Sustut basins began in the early 1950s as part of the Geological Survey of Canada's Operation Stikine. Although coal was known at Klappan since the 1890s (Dupont, 1900), it was only during this mapping project that these two large sedimentary basins were delineated (Geological Survey of Canada, 1957). Thematic and mapping studies were carried out in the 1970s and 1980s (e.g., Eisbacher, 1974a, b; Richards and Gilchrest, 1979; Gabrielse and Tipper, 1984; Evenchick, 1986, 1987, 1988, 1989) and continued through the 1990s and into the mid-2000s (e.g., Evenchick, 1991a,b, 1996a, b, 1997a, b, 2001, 2004, 2005; Evenchick and Green, 1990, 1995a-d, 2004a-c; Ricketts and Evenchick, 1991, 1999; Ricketts et al., 1992; Greig and Evenchick, 1993; Evenchick and McNicoll, 1993a, b; Evenchick and Porter, 1993; Evenchick and Thorkelson, 1993a, b, 1994a-c, 1995, 2004a-f, 2005; Evenchick and Parsons, 1997; Evenchick et al., 2000, 2001; Evenchick and Ritcey, 2005a, b). Mapping in the early to mid-2000s was undertaken as a federal-provincial program (Evenchick et al., 2002, 2003, 2004b, 2006, 2007a-k, 2008a-h; Hayes et al., 2004; Ferri and Boddy, 2005; Ferri et al., 2005; O'Sullivan et al., 2005; Waldron et al., 2006; Evenchick and Ferri, 2007; McMechan et al., 2007; Ricketts and Evenchick, 2007). The most recent regional compilation was completed by Evenchick et al. (2004a, 2009).

The Bowser Basin is on the northern half of Stikinia and contains greater than 5000 m of Middle Jurassic to Upper Cretaceous siliciclastic and minor volcanic rocks assigned to the Bowser Lake and Skeena groups. These sedimentary rocks were derived from erosion of mainly uplifted Cache Creek terrane rocks along the northeastern margin of the basin during and after amalgamation of Stikinia to the margin of ancestral North American (Evenchick and Thorkelson, 2005). The Bowser Lake Group represents a Middle Jurassic to earliest Cretaceous southwesterly prograding deltaic to deep-water succession that is overlain by predominantly Early Cretaceous fluvial siliciclastic rocks (Evenchick et al., 2001; Evenchick and Thorkelson, 2005). Fluvial Skeena Group (Cretaceous) siliciclastic rocks are found in southern Bowser. Both the Bowser Lake Group and Skeena Group (Cretaceous) contain significant coal deposits. The Sustut Basin, along the northeast margin of the Bowser Basin, preserves a Late Cretaceous fluvial section more than 2000 m thick that was sourced from cratonic

rocks of the Omineca Mountains to the east, and eroded Bowser Lake Group rocks that were being uplifted in the emergent Skeena Fold belt. The Sustut Group was deposited as a foreland basin ahead of the Skeena Fold belt and was deformed by the advancing thrust front.

The predominant structural elements in the Bowser and Sustut basins are a series of Cretaceous northeast verging folds and thrusts that comprise the Skeena Fold belt. The southern portion of the Bowser Basin is also cut by steep normal faults, likely Cretaceous, and is cut by numerous Late Cretaceous to Paleogene intrusions. Cretaceous to Paleogene plutons of the Coast Plutonic complex intrude the western margin of the Bowser Basin.

5.8. Southern Nicola arc

This compilation integrates results from a number of regional mapping studies by the Geological Survey of Canada, and the British Columbia Department of Mines (which later became the British Columbia Geological Survey), as well as university theses and company reports (Fig. 1). Regional-scale surveys conducted by the Geological Survey of Canada include adjoining maps by Rice (1947) and Cockfield (1948), both incorporated by Monger (1989) and Monger and McMillan (1989) in the Hope (92H) and Ashcroft (92I) map sheets, respectively. Schau (1968) made the first effort to establish a stratigraphy for the Nicola Group and obtained an Early Norian fossil age in rocks mapped in the area between Iron Mountain and Nicola Lake. From 1968 to 1974 systematic mapping undertaken by geologists from the British Columbia Geological Survey moved northward from Copper Mountain (Preto, 1972), to the Aspen Grove and Nicola Mountain areas (Christopher, 1973; Christopher et al., 1974). Preto (1979) synthesized results from this program, providing the most comprehensive lithologic subdivision of Nicola rocks in southern Quesnellia. He emphasized the importance of regional faults and their influence localizing magmatism and mineralization. Furthermore, he highlighted their role in segmenting the arc and subdivided Triassic strata into three parallel structural belts, each featuring distinctive rock types. Mapping north to Nicola Lake and west to Iron Mountain (McMillan, 1981) overlapped, in part, earlier work by Schau (1968), expanding adjacent lithologic units of the Nicola Group and adding notable felsic volcanic and limestone units, containing Early Norian fossils, features that distinguish the Western belt.

The Nicola Group in southern Quesnel terrane is the focus of a compilation nearing completion that will be available as an upgrade to the British Columbia integrated digital geology in spring, 2018. The compilation area extends across 14,000 km² and includes the southwestern extent of Quesnel terrane.

A new perspective on the Nicola Group and evolution of the Nicola arc stems from recent British Columbia Geological Survey studies whose boundaries largely overlap the region of earlier survey work in a representative region between Merritt and Princeton (Diakow and Barrios, 2008; Southern Nicola Arc Project - 2012-2014; Mihalyuk et al., 2016). Mapping

studies augmented by U-Pb isotopic ages from volcanic and sedimentary units, some of which are calibrated to conodont zones, give conclusive evidence for a two stage evolution of the Nicola arc spanning 36 million years of the Triassic. The compilation geology incorporates a revised stratigraphic framework for the Nicola Group that reflects its sequential development in southern Quesnellia. These revisions also serve as a foundation for comparison to other parts of Quesnellia.

Rocks in the Quesnel terrane record a Mesozoic history of east-directed plate subduction which generated a magmatic island arc system that presently extends as a fault-bounded belt, several thousand km long through British Columbia, north into the Yukon and south into the United States. The arc system in British Columbia is defined mainly by the Nicola Group, and co-magmatic calc-alkaline and alkalic intrusions that host economically significant porphyry Cu-Ag-Au±Mo deposits, and fewer spaced Alaskan-type ultramafic-mafic complexes that have potential for platinum metals as well as chrome, nickel, cobalt and jade.

6. Conclusions

The British Columbia Geological Survey updates the digital bedrock geology of the province and makes products available as data downloads and online on MapPlace 2. The province-wide bedrock geology uses a consistent stratigraphic nomenclature to accommodate the bedrock geology in British Columbia. The integration includes all details of maps from 1:50,000 to 1:250,000 scales. Using a 'geospatial frame data' model, which dispenses with polygons, and its implementation in a spatial database, the time required for map integration is reduced. This model and techniques eliminate topological errors typically associated with maps using polygons. Since the first generation of the province-wide digital map was released in 2005, large parts of the province's geology have been updated, including the Terrace, North Coast, northern Vancouver Island, Kutcho, QUEST, and Chilcotin-Bonaparte areas.

Acknowledgments

The integrated bedrock geology of British Columbia is the result of mapping by previous and current British Columbia Geological Survey geologists, including Dani Alldrick, Chris Ash, Kim Bellefontaine, Jim Britton, Derek Brown, Peter A. Christopher, Neil Church, John Cunningham, D.J. Dawson, Pat Desjardins, Larry Diakow, Kathryn Dunne, Travis Ferbey, Fil Ferri, Bob Gaba, Gordon Gibson, Keith Glover, Brian Grant, Jan Hammack, Trygve Höy, Wayne Jackaman, Victor Koyanagi, Andrew Legun, Ray Lett, Vic Levson, Jim Logan, Nick Massey, Don MacIntyre, Bill McMillan, Mitch Mihalyuk, JoAnne Nelson, Graham Nixon, Andre Panteleyev, Garry Payie, Vic Preto, Gerry Ray, Janet Riddell, Paul Schiarizza, and Ian Webster. Invaluable contributions were made by Geological Survey of Canada geologists including Bob Anderson, Carol Evenchick, Jim Haggart, Murray Journeay, P. McFeely, Peter S. Mustard, Andy Okulitch, Michael J. Orchard, Terry P. Poulton, Peter B. Read, Jim Roddick, Margaret E. Rusmore, Jack

Souther, Don F. Stott, Bert Struik, Howard W. Tipper, Edward Tim Tozer, John Wheeler, Glen Woodsworth, Chris J. Yorath, and Alex Zagorevski, by the University of British Columbia geologists Richard M. Friedman, Steve Israel, Peter Lewis, Jim Mortensen, and Peter van der Heyden, and colleagues from the United States, George Gehrels, Brian Mahoney, and Lori Snyder. We apologize to those who we inadvertently failed to thank.

References cited

- Alldrick, D.J., 2001. Geology and mineral deposits of the Ecstall belt, northwest B.C. In: Geological Fieldwork 1999, British Columbia. Ministry of Energy and Mines, British Columbia Geological Survey Paper 2000-1, pp. 279-306.
- Alldrick, D.J., Friedman, R.M., and Childe, F.C., 2001. Age and geologic history of the Ecstall greenstone belt, northwest B.C. In: Geological Fieldwork 1999, British Columbia. Ministry of Energy and Mines, British Columbia Geological Survey Paper 2000-1, pp. 269-278.
- Anderson, R.G., Schiarizza, P., Andrews, G., Breitsprecher, K., Davis, W., Dunne, C.E., Plouffe, A., and Thomas, M.D., 2010. Bedrock, surficial, geophysical, and geochemical mapping reveals exploration targets in the Thuya batholith, southern Nicola arc. In: Geological Association of Canada, Targeted Geoscience Initiative 3 Workshop, March 2010, Vancouver.
- Angen, J.J., 2009. Geospatial structural analysis of the Terrace area, west-central British Columbia (NTS 103I/08, 09, 10, 16). In: Geological Fieldwork 2008, British Columbia Ministry of Energy, Mines and Petroleum Resources, British Columbia Geological Survey Paper 2009-1, pp. 21-33.
- Angen, J.J., 2013. Structural and geochronological investigation of the southern Alexander terrane in the vicinity of Porcher Island, northwestern British Columbia. Unpublished M.Sc. thesis, University of Waterloo, 121 p.
- Angen, J.J., van Staal, C.R., and Lin, S., 2012. Structural geology of the Alexander Terrane in the vicinity of Porcher Island, northwestern British Columbia. In: Geological Fieldwork 2011, British Columbia Ministry of Energy and Mines, British Columbia Geological Survey Paper 2012-01, pp. 135-147.
- Archibald, D.A., and Nixon, G.T., 1995. ⁴⁰Ar/³⁹Ar Geochronometry of igneous rocks in the Quatsino-Port McNeill map area, northern Vancouver Island. In: Geological Fieldwork 1994, British Columbia Ministry of Energy, Mines, and Petroleum Resources, British Columbia Geological Survey Paper 1995-1, pp. 49-59.
- Armstrong, R.L., Muller, J.E., Harakal, J.E., and Muehlenbachs, K., 1985. The Neogene Alert Bay volcanic belt of northern Vancouver Island, Canada: descending-plate-edge volcanism in the arc-trench gap. *Journal of Volcanology and Geothermal Research*, 26, 75-97.
- Baer, A.J., 1973. Bella Coola-Laredo Sound map-areas, British Columbia. Geological Survey of Canada, Memoir 372, 122 p.
- Barresi, T., 2015. Tectono-magmatic and metallogenic evolution of the late Triassic to middle Jurassic Hazelton Group in northwest British Columbia. Unpublished Ph.D., thesis, Dalhousie University, 333 p.
- Barresi, T., and Nelson, J.L., 2006. Usk Map Area (NTS 103I/9), near Terrace, B.C.: Cross-sections and volcanic facies interpretation. In: Geological Fieldwork 2005, British Columbia Ministry of Energy, Mines and Petroleum Resources, British Columbia Geological Survey Paper 2006-1, pp. 21-28.
- Barresi, T., Nelson, J.L., Dostal, J., and Friedman, R., 2015. Evolution of the Hazelton arc near Terrace, British Columbia: Stratigraphic, geochronological and geochemical constraints on a Late Triassic-Early Jurassic arc and Cu-Au porphyry belt. *Canadian Journal of Earth Sciences* 52, 466-494.
- Barrett, T.J., Thompson, J.F.H., and Sherlock, R.L., 1996.

- Stratigraphic, lithogeochemical and tectonic setting of the Kutcho Creek massive sulphide deposit, northern British Columbia. *Exploration and Mining Geology*, 5, 309-338.
- Beaton, A.J., 2011. Bonaparte Gold underground decline and surface trench bulk sample project, April 01, 2009 to Sept 30, 2010. British Columbia Ministry of Energy and Mines, Assessment Report 32930, 382 p.
- Berg, H.C., Jones, D.L., and Richter, D.H., 1972. Gravina-Nutzotin belt-tectonic significance of an upper Mesozoic sedimentary and volcanic sequence in southern and southeastern Alaska. U.S. Geological Survey, Professional Paper 800-D, D1-D24.
- Blevings, S.K., 2008. Geologic framework for Late Cretaceous magmatic-hydrothermal mineralization in the Taseko Lakes region, southwestern B.C. Unpublished M.Sc. thesis, The University of British Columbia, 229 p.
- Boudreau, N.T., 2007. Volcanology, petrography, and geochemistry of the Kitselas volcanic rocks compared to rocks of the Telkwa Formation. British Columbia Ministry of Energy, Mines, and Petroleum Resource, British Columbia Geological Survey Open File 2007-5, 77 p.
- Bridge, D.A., Marr, J.M., Hashimoto, K., Obara, M., and Suzuki, R., 1986. Geology of the Kutcho Creek volcanogenic massive sulphide deposits, northern British Columbia. In: Morin, J.A., (Ed.), *Mineral Deposits of Northern Cordillera*, The Canadian Institute of Mining and Metallurgy, Special Volume 37, pp. 115-128.
- Brown, D.A., Gunning, M.H., and Greig, C.J., 1996. The Stikine Project: Geology of western Telegraph Creek map area, northwestern British Columbia. British Columbia Ministry of Energy and Mines, British Columbia Geological Survey, Bulletin 95, 176 p.
- Butler, R.F., Gehrels, G.E., Hart, W., Davidson, C., and Crawford, M.L., 2006. Paleomagnetism of Late Jurassic to mid-Cretaceous plutons near Prince Rupert, British Columbia. In: Haggart, J.W., Enkin, R.J., and Monger, J.W.H., (Eds.), *Paleogeography of the North American Cordillera: Evidence for and against large-scale displacements*: Geological Association of Canada, Special Paper 46, pp. 171-200.
- Chardon, D., 2003. Strain partitioning and batholith emplacement at the root of a transpressive magmatic arc. *Journal of Structural Geology*, 25, 91-108.
- Chardon, D., Andronicos, C.L., and Hollister, L.S., 1999. Large-scale transpressive shear zone patterns and displacements within magmatic arcs: the Coast Plutonic complex, British Columbia. *Tectonics*, 18, 278-292.
- Childe, F.C., and Thompson, J.F.H., 1997. Geological setting, U-Pb geochronology, and radiogenic isotopic characteristics of the Permo-Triassic Kutcho assemblage, north-central British Columbia. *Canadian Journal of Earth Sciences*, 34, 1310-1324.
- Childe, F.C., Friedman, R.M., Mortensen, J.K., and Thompson, J.F.H., 1997. Evidence for Early Triassic felsic magmatism in the Ashcroft (92I) map area, British Columbia. In: *Geological Fieldwork 1996*, British Columbia Ministry of Energy, Mines and Petroleum Resources, British Columbia Geological Survey Paper 1997-1, pp. 117-123.
- Christopher, P.A., 1973. Preliminary geological map of the Aspen Grove area, British Columbia. British Columbia Department of Mines and Petroleum Resources, British Columbia Geological Survey Preliminary Map No. 10 (092H/15E), scale 1:100,000.
- Christopher, P. A., Coombes, D., Preto, V.A., Kalnins, T.E., Thomsen, N.A., and Nebocat, J., 1974. Geology of Aspen Grove area, British Columbia. British Columbia Ministry of Energy Mines and Petroleum Resources, Preliminary Map 15 (5 Sheets), scale 1:50,000.
- Cockfield, W.E., 1948. Geology and mineral deposits of Nicola map-area, British Columbia. Geological Survey of Canada, Memoir 249, 164 p.
- Cohen, K.M., Finney, S.C., Gibbard, P.L., and Fan, J.-X., 2013 (updated). The ICS International Chronostratigraphic Chart. *Episodes*, 36, 199-204.
- Colpron, M., and Nelson, J. L., 2009. A Palaeozoic Northwest Passage: Incursion of Caledonian, Baltican and Siberian terranes into eastern Panthalassa, and the early evolution of the North American Cordillera. In: Cawood, P. A. & Kröner, A., (Eds.), *Earth Accretionary Systems through Space and Time*. Geological Society of London, Special Publications, 318, pp. 273-307.
- Colpron, M., and Nelson, J.L., 2011. A Palaeozoic NW Passage and the Timanian, Caledonian and Uralian connections of some exotic terranes in the North American Cordillera. *Geological Society of London, Memoirs*, 35, 463-484.
- Cui, Y., 2011. Improving the efficiency in the maintenance of the provincial geological database. In: *Geological Fieldwork 2010*, British Columbia Ministry of Forest, Mines and Lands, British Columbia Geological Survey Paper 2011-1, pp. 159-168.
- Cui, Y., 2014. Integration and delivery of British Columbia digital geology. British Columbia Ministry of Energy and Mines, British Columbia Geological Survey GeoFile 2014-9.
- Cui, Y., Fortin, G., Meredith-Jones, S., Zhao, S., and Jones, L., 2017a. MapPlace 2 (beta) workshop. British Columbia Ministry of Energy and Mines, British Columbia Geological Survey Information Circular 2017-3, 89 p.
- Cui, Y., Miller, D., Schiarizza, P., and Diakow, L.J., 2017b. British Columbia digital geology. British Columbia Ministry of Energy, Mines and Petroleum Resources, British Columbia Geological Survey Open File 2017-8, 9 p.
- Dawson, G.M., 1887. Report on a geological examination of the northern part of Vancouver Island B.C. Geological Survey of Canada, Annual Report 1886, Part B, 129 p.
- Dolmage, V., 1919. Quatsino Sound and certain mineral deposits of the west coast of Vancouver Island, B.C. In: *Summary Report 1918*, Geological Survey of Canada, Part B, 30B-38B.
- DeBari, S.M., Anderson, R.G., and Mortensen, J.K., 1999. Correlation amongst lower to upper crustal components in an island arc: the Jurassic Bonanza arc, Vancouver Island, Canada. *Canadian Journal of Earth Sciences*, 36, 1371-1413.
- Diakow, L.J., and Barrios, A., 2008. Geology, Spences Bridge Group, southwest of Merritt, British Columbia (parts of NTS 092H/14, 15 and 092I/2, 3). British Columbia Ministry of Energy Mines and Petroleum Resources, British Columbia Geological Survey Open File 2008-8, scale 1:50,000.
- Dohaney, J., Andrews, G.D.M., Russell, J.K., and Anderson, R.G., 2010. Distribution of the Chilcotin Group, Taseko Lakes and Bonaparte Lake map areas, British Columbia. Geological Survey of Canada, Open File 6344 and Geoscience BC, Map 2010-02-1, scale 1:250,000.
- Dupont, V.H., 1900. Preliminary report of an exploration on the upper part of the Stikine River. Department of Railways and Canals, Canada, Annual Report, July 1, 1898 to June 30 1899, Part 1, pp. 181-182.
- Easton, R.M., Catuneanu, O., Donovan, A.D., Fluegeman, R.H., Hamblin, A.P.T., Harper, H., Lasca, N.P., Morrow, J.R., Orndorff, R.C., Sadler, P., Scott, R.W., and Tew, B.H.N., 2014. North American Commission on Stratigraphic Nomenclature, Note 66: Records of Stratigraphic Commission, 2003-2013. *Stratigraphy*, 11, pp. 143-157.
- Eisbacher, G.H., 1974a. Deltaic sedimentation in the northeastern Bowser Basin, British Columbia. Geological Survey of Canada, Paper 73-33, 13 p.
- Eisbacher, G.H., 1974b. Sedimentary history and tectonic evolution of the Sustut and Sifton basins, north-central British Columbia. Geological Survey of Canada, Paper 73-31, 57 p.
- European Commission, 2017. Infrastructure for spatial information in Europe, <http://inspire.ec.europa.eu>. Last accessed November, 2017.

- Evenchick, C.A., 1986. Structural Style of the Northeast Margin of the Bowser Basin, Spatsizi map area, northcentral British Columbia. In: Current Research, Part B, Geological Survey of Canada, Paper 86-1B, pp. 733-739.
- Evenchick, C.A., 1987. Stratigraphy and Structure of the Northeast Margin of the Bowser Basin, Spatsizi map area, north - central British Columbia. In: Current Research Part A, Geological Survey of Canada, Paper 87-1A, pp. 719-726.
- Evenchick, C.A., 1988. Structural style and stratigraphy in northeast Bowser and Sustut basins, north-central British Columbia. In: Current research part E: Cordillera and Pacific margin, Geological Survey of Canada, Paper 88-1E, pp. 91-95.
- Evenchick, C.A., 1989. Stratigraphy and Structure in East Spatsizi map area, North-Central British Columbia. In: Current Research Part E, Cordillera and Pacific, Geological Survey of Canada, Paper no. 89-1E, pp. 133-138.
- Evenchick, C.A., 1991a. Structural relationships of the Skeena Fold Belt west of the Bowser Basin, northwest British Columbia. *Canadian Journal of Earth Sciences*, 28, 973-983.
- Evenchick, C.A., 1991b. Geometry, evolution, and tectonic framework of the Skeena Fold Belt, north central British Columbia. *Tectonics*, 10, 527-546.
- Evenchick, C.A., 1992. Bowser Basin facies and map units in Southwest Toodoggonne map area, British Columbia. In: Current Research, Part A, Cordillera and Pacific, Geological Survey of Canada, Paper no. 92-1A, pp. 77-84.
- Evenchick, C.A., 1996a. Geology, Cranberry River, British Columbia. Geological Survey of Canada, Open File 3224, scale 1:50,000.
- Evenchick, C.A., 1996b. Geology, Brown Bear Lake, British Columbia. Geological Survey of Canada, Open File 3225, scale 1:50,000.
- Evenchick, C.A., 1997a. Geology, Skelhome Creek, British Columbia. Geological Survey of Canada, Open File 3528, scale 1:50,000.
- Evenchick, C.A., 1997b. Geology, Sturdee River (west half), British Columbia. Geological Survey of Canada, Open File 3516, scale 1:50,000.
- Evenchick, C.A., 2001. Northeast-trending folds in the western Skeena Fold Belt, northern Canadian Cordillera: a record of Early Cretaceous sinistral plate convergence. In: White, J.C., Bleeker, W., Elliott, C., Lin, S., van Staal, C.R., (Eds.), *Evolution of Structures in Deforming rocks: in honour of Paul F. Williams*, *Journal of Structural Geology*, 23, 1123-1140.
- Evenchick, C.A., 2004. Geology, Skelhome Creek, British Columbia. Geological Survey of Canada, Map 2039A, scale 1:50,000.
- Evenchick, C.A., 2005. Geology, Laalui Lakes, British Columbia. Geological Survey of Canada, Open File 4947, scale 1:50,000.
- Evenchick, C.A., and Ferri, F., 2007. Foreword-Thematic studies in Bowser and Sustut Basins: establishing a geoscience framework for future resource assessment and development. In: *Thematic studies in Bowser and Sustut Basins: establishing a geoscience framework for future resource assessment and development*, *Bulletin of Canadian Petroleum Geology*, 55, 237-241.
- Evenchick, C.A., and Green, G.M., 1990. Structural Style and Stratigraphy of Southwest Spatsizi map area, British Columbia. In: Current Research Part F, Frontier Geoscience Program, Cordilleran and Offshore Basins, British Columbia, Geological Survey of Canada, Paper 90-1F, pp. 135-144.
- Evenchick, C.A., and Green, G.M., 1995a. Geology, Kluea Lake, British Columbia. Geological Survey of Canada, Open File 3016, scale 1:50,000.
- Evenchick, C.A., and Green, G.M., 1995b. Geology, Little Klappan River, British Columbia. Geological Survey of Canada, Open File 3174, scale 1:50,000.
- Evenchick, C.A., and Green, G.M., 1995c. Geology, Maitland Creek, British Columbia. Geological Survey of Canada, Open File 3173, scale 1:50,000.
- Evenchick, C.A., and Green, G.M., 1995d. Geology, Tumeke Creek, British Columbia. Geological Survey of Canada, Open File 3172, scale 1:50,000.
- Evenchick, C.A., and Green, G.M., 2004a. Geology, Kluea Lake, British Columbia. Geological Survey of Canada, Map 2028A, scale 1:50,000.
- Evenchick, C.A., and Green, G.M., 2004b. Geology, Little Klappan River, British Columbia. Geological Survey of Canada, Map 2034A, scale 1:50,000.
- Evenchick, C.A., and Green, G.M., 2004c. Geology, Maitland Creek, British Columbia. Geological Survey of Canada, Map 2035A, scale 1:50,000.
- Evenchick, C.A., and McNicoll, V.J., 1993a. U-Pb age for the Jurassic McEwan Creek pluton, north-central British Columbia: regional setting and implications for the Toarcian stage boundary. In: *Radiogenic age and isotopic studies: report 7*, Geological Survey of Canada, Paper 93-2, pp. 91-97.
- Evenchick, C.A., and McNicoll, V.J., 1993b. U-Pb ages for Late Cretaceous and early Tertiary plutons in the Skeena Fold Belt, north-central British Columbia. In: *Radiogenic age and isotopic studies: report 7*, Geological Survey of Canada, Paper 93-2, pp. 99-106.
- Evenchick, C.A., and Parsons, H.J., 1997. Geology of Spatsizi Plateau Wilderness Provincial Park. Geological Survey of Canada, Miscellaneous Report 60, scale 1:275,000.
- Evenchick, C.A., and Porter, J.S., 1993. Geology of west McConnell Creek map area, British Columbia. In: Current Research, Part A, Cordillera and Pacific Margin, Geological Survey of Canada, Paper 93-1A, 47-55.
- Evenchick, C.A., and Ritcey, D., 2005a. Geology, Stalk Lakes, British Columbia. Geological Survey of Canada, Open File 4948, scale 1:50,000.
- Evenchick, C.A., and Ritcey, D., 2005b. Geology, Sturdee River, British Columbia. Geological Survey of Canada, Open File 4946, scale 1:50,000.
- Evenchick, C.A., and Thorkelson, D.J., 1993a. Geology, Tuaton Lake, British Columbia. Geological Survey of Canada, Open File 2694, scale 1:50,000.
- Evenchick, C.A., and Thorkelson, D.J., 1993b. Geology, Spatsizi River, British Columbia. Geological Survey of Canada, Open File 2719, scale 1:250,000.
- Evenchick, C.A., and Thorkelson, D.J., 1994a. Geology, Cold Fish Lake, British Columbia. Geological Survey of Canada, Open File 2961, scale 1:50,000.
- Evenchick, C.A., and Thorkelson, D.J., 1994b. Geology, Buckinghorse Creek, British Columbia. Geological Survey of Canada, Open File 2960, scale 1:50,000.
- Evenchick, C.A., and Thorkelson, D.J., 1994c. Geology, Dawson River, British Columbia. Geological Survey of Canada, Open File 2988, scale 1:50,000.
- Evenchick, C.A., and Thorkelson, D.J., 1995. Geology, Eaglenest Creek, British Columbia. Geological Survey of Canada, Open File 3013, scale 1:50,000.
- Evenchick, C.A., and Thorkelson, D.J., 2004a. Geology, Buckinghorse Creek, British Columbia. Geological Survey of Canada, Map 2033A, scale 1:50,000.
- Evenchick, C.A., and Thorkelson, D.J., 2004b. Geology, Cold Fish Lake, British Columbia. Geological Survey of Canada Map 2030A, scale 1:50,000.
- Evenchick, C.A., and Thorkelson, D.J., 2004c. Geology, Dawson River, British Columbia. Geological Survey of Canada, Map 2031A, scale 1:50,000.
- Evenchick, C.A., and Thorkelson, D.J., 2004d. Geology, Eaglenest Creek, British Columbia. Geological Survey of Canada Map 2029A, scale 1:50,000.
- Evenchick, C.A., and Thorkelson, D.J., 2004e. Geology, Spatsizi

- River, British Columbia. Geological Survey of Canada, Map 2040A, scale 1:250,000.
- Evenchick, C.A., and Thorkelson, D.J., 2004f. Geology, Tuaton Lake, British Columbia. Geological Survey of Canada, Map 2032A, scale 1:50,000.
- Evenchick, C.A., and Thorkelson, D.J., 2005. Geology of the Spatsizi River map area, north-central British Columbia. Geological Survey of Canada, Bulletin 577, 276 p.
- Evenchick, C.A., Ferri, F., McMechan, M.E., Mustard, P.S., Hadlari, T., Jakobs, G., and Porter, S., 2007a. Geology, South Pass Peak and western Moosevale Creek, British Columbia. Geological Survey of Canada, Open File 5565, scale 1:50,000.
- Evenchick, C.A., Ferri, F., Mustard, P.S., Hadlari, T., and McMechan, M.E., 2007b. Geology, Asitka River and southwest Carruthers Pass, British Columbia. Geological Survey of Canada, Open File 5566, scale 1:50,000.
- Evenchick, C.A., Ferri, F., Mustard, P.S., McMechan, M., Osadetz, K., Stasiuk, L., Wilson, N.S.F., Enkin, R., Hadlari, T., and McNicoll, V.J., 2003. Recent results and activities of the Integrated Petroleum Resources Potential and Geoscience Studies of the Bowser and Sustut basins project. Geological Survey of Canada, Current Research (Online), 2003-A13, 11 p.
- Evenchick, C.A., Ferri, F., Mustard, P.S., Porter, S., Greig, C.J., and Ritcey, D.H., 2008a. Geology, Mount Beirnes, British Columbia. Geological Survey of Canada, Open File 5735, scale 1:50,000.
- Evenchick, C.A., Hayes, M.C., Buddell, K.A., and Osadetz, K.G., 2002. Vitrinite and bitumen reflectance data and preliminary organic maturity model for the northern two-thirds of the Bowser and Sustut basins, north-central British Columbia. Geological Survey of Canada, Open File 4343, 1:250,000.
- Evenchick, C.A., McMechan, M.E., Ferri, F., Mustard, P.S., and Porter, S., 2007c. Geology, Tatlatui Lake, British Columbia. Geological Survey of Canada, Open File 5563, scale 1:50,000.
- Evenchick, C.A., McMechan, M.E., McNicoll, V.J., and Carr, S.D., 2007d. A synthesis of the Jurassic-Cretaceous tectonic evolution of the central and southeastern Canadian Cordillera: exploring links across the orogeny. In: Sears, J.W., Harms, T.A., Evenchick, C.A., (Eds.), *Whence The Mountains? Inquiries into the Evolution of Orogenic Systems: a volume in honor of Raymond A. Price*, Geological Society of America, Special Paper 433, pp. 117-145.
- Evenchick, C.A., McMechan, M.E., Mustard, P.S., Ferri, F., Ritcey, D.H., Porter, S., and Greig, C.J., 2008b. Geology, Konigus Creek, British Columbia. Geological Survey of Canada, Open File 5736, scale 1:50,000.
- Evenchick, C.A., McMechan, M.E., Mustard, P.S., Ritcey, D.H., Smith, G.T., Ferri, F., and Waldron, J.W.F., 2008c. Geology, Hazelton, British Columbia. Geological Survey of Canada, Open File 5704, scale 1:125,000.
- Evenchick, C.A., Mustard, P.S., Greig, C.J., Porter, J.S., and McNeill, P.D., 2000. Geology, Bowser Lake (NTS 104 A), British Columbia. Geological Survey of Canada, Open File 3918, scale 1:250,000.
- Evenchick, C.A., Mustard, P.S., Greig, C.J., McMechan, M.E., and Porter, S., 2008d. Geology, McEvoy Flats, British Columbia. Geological Survey of Canada, Open File 5734, scale 1:50,000.
- Evenchick, C.A., Mustard, P.S., Greig, C.J., McMechan, M.E., Ritcey, D.H., Smith, G.T., and Ferri, F., 2008e. Geology, Nass River, British Columbia. Geological Survey of Canada, Open File 5705, scale 1:125,000.
- Evenchick, C.A., Mustard, P.S., Hadlari, T., and McMechan, M.E., 2007e. Geology, Thorne Lake, British Columbia. Geological Survey of Canada, Open File 5562, 1:50,000.
- Evenchick, C.A., Mustard, P.S., and McMechan, M.E., 2007f. Geology, Salix Creek, British Columbia. Geological Survey of Canada, Open File 5567, scale 1:50,000.
- Evenchick, C.A., Mustard, P.S., McMechan, M.E., Ferri, F., Porter, S., Hadlari, T., and Jakobs, G., 2007g. Geology, McConnell Creek, British Columbia. Geological Survey of Canada, Open File 5571, scale 1:125,000.
- Evenchick, C.A., Mustard, P.S., McMechan, M.E., Ferri, F., Ritcey, D.H., Waldron, J.W.F., Porter, S., Greig, C.J., and Smith, G.T., 2008f. Geology, Bowser Lake, British Columbia. Geological Survey of Canada, Open File 5706, scale 1:125,000.
- Evenchick, C.A., Mustard, P.S., McMechan, M.E., Porter, S., and Hadlari, T., 2007h. Geology, Malloch Creek, British Columbia. Geological Survey of Canada, Open File 5564, scale 1:50,000.
- Evenchick, C.A., Mustard, P.S., McNicoll, V.J., Holm, K., and Alldrick, D.J., 2007i. Digital bedrock geology of Nass River, British Columbia (103 P/05, /06, /10, and /15) for GIS. Geological Survey of Canada, Open File 5581, scale 1:50,000.
- Evenchick, C.A., Mustard, P.S., McMechan, M.E., Greig, C.J., Ferri, F., Ritcey, D.H., Smith, G.T., Hadlari, T., and Waldron, J.W.F., 2009. Geological compilation of Bowser and Sustut basins draped on shaded relief map, north-central British Columbia. Geological Survey of Canada, Open File 5794, scale 1:500,000.
- Evenchick, C.A., Mustard, P.S., McMechan, M.E., Ritcey, D.H., and Smith, G.T., 2008g. Geology, northeast Terrace and northwest Smithers, British Columbia. Geological Survey of Canada, Open File 5895, scale 1:125,000.
- Evenchick, C.A., Mustard, P.S., Porter, S., Greig, C.J., Ferri, F., McMechan, M.E., Ritcey, D.H., and Waldron, J.W.F., 2008h. Geology, Mount Alger, British Columbia. Geological Survey of Canada, Open File 5737, scale 1:50,000.
- Evenchick, C.A., Mustard, P.S., Woodsworth, G.J., and Ferri, F., 2004a. Compilation of geology of Bowser and Sustut basins draped on shaded relief map, north-central British Columbia. Geological Survey of Canada, Open File 4638, scale 1:500,000.
- Evenchick, C.A., O'Sullivan, P.B., and Waldron, J.W.F., 2006. Targeted energy-resource studies in the Bowser and Sustut interior basins of British Columbia. In: *Geological Fieldwork 2005*, British Columbia Ministry of Energy, Mines and Petroleum Resources, British Columbia Geological Survey Paper 2006-1, pp. 281-285.
- Evenchick, C.A., Poulton, T.P., Tipper, H.W., and Braidek, I., 2001. Fossils and facies of the northern two-thirds of the Bowser Basin, British Columbia. Geological Survey of Canada, Open File 3956, 103 p.
- Evenchick, C.A., Ritcey, D.H., Mustard, P.S., and McMechan, M.E., 2007j. Geology, Toodoggone River, British Columbia. Geological Survey of Canada, Open File 5570, scale 1:125,000.
- Evenchick, C.A., Ritcey, D., Mustard, P.S., and McMechan, M.E., 2007k. Geology, Sturdee River and southwest Attycelley Creek, British Columbia. Geological Survey of Canada, Open File 5561, scale 1:50,000.
- Evenchick, C.A., Stasiuk, L.D., Osadetz, K.G., and Ferri, F., 2004b. New and revised vitrinite reflectance data for the Bowser and Sustut basins, British Columbia. Geological Survey of Canada, Open File 4669.
- Ferri, F., and Boddy, M., 2005. Geochemistry of Early to Middle Jurassic organic-rich shales, Intermontane basins, British Columbia. In: *Summary of Activities 2005*, British Columbia Ministry of Energy and Mines, pp. 132-151.
- Ferri, F., and O'Brian, B.H., 2003. Geology of the Cariboo Lake Area, Central British Columbia. British Columbia Ministry of Energy, Mines and Petroleum Resources, British Columbia Geological Survey Open File 2003-01, scale 1:50,000.
- Ferri, F., Mustard, P.S., McMechan, M.E., Ritcey, D., Smith, G.T., Evenchick, C.A., and Boddy, M., 2005. Skeena and Bowser Lake groups, west half Hazelton map area (93M). In: *Summary of Activities 2005*, British Columbia Ministry of Energy and Mines, pp. 113-131.
- Ferri, F., Nixon, G.T., and Reyes, J., 2008. Organic geochemistry of Late Triassic to Early Jurassic sedimentary rocks in northern Vancouver Island. British Columbia Ministry of Energy, Mines and Petroleum Resources, Oil and Gas Geoscience Reports 2008-3, pp.

- 13-23.
- Friedman, R.M., Gabites, J.E., and Logan, J.M., 2014. U-Pb and Ar/Ar ages from the Bonaparte mine, southern British Columbia: Late Middle Jurassic Au±Cu vein mineralization. In: Geological Fieldwork 2013, British Columbia Ministry of Energy and Mines, British Columbia Geological Survey Paper 2014-1, pp. 59-66.
- Gabrielse, H., 1998. Geology of Cry Lake and Dease Lake map areas, north-central British Columbia. Geological Survey of Canada, Bulletin 504, 147 p., scale 1:100,000 and 1:250,000.
- Gabrielse, H., and Tipper, H.W. 1984. Bedrock geology of Spatsizi map area (104H). Geological Survey of Canada, Open File 1005, scale 1:250,000.
- Gagnon, J.-F., Barresi, T., Waldron, J.W.F., Nelson, J.L., Poulton, T.P., and Cordey, F., 2012. Stratigraphy of the upper Hazelton Group and the Jurassic evolution of the Stikine terrane, British Columbia. *Canadian Journal of Earth Sciences*, 49, 1027-1052.
- Gardner, M.C., Bergman, S.C., Cushing, G.W., MacKevett, E.M., Jr., Plafker, G., Campbell, R.B., Dodds, C.J., McClelland, W.C., and Mueller, P.A., 1988. Pennsylvanian pluton stitching of Wrangellia and the Alexander terrane, Wrangell Mountains, Alaska. *Geology*, 16, 967-971.
- Gareau, S.A., and Woodsworth, G.J., 2000. Yukon-Tanana terrane in the Scotia-Quaal belt, Coast Plutonic Complex, central-western British Columbia. In: Stowell, H.H. and McClelland, W.C., (Eds.), *Tectonics of the Coast Mountains, Southeastern Alaska and British Columbia*, Geological Society of America, Special Paper 343, pp. 23-44.
- Gehrels, G.E., 2001. Geology of the Chatham Sound region, southeast Alaska and coastal British Columbia. *Canadian Journal of Earth Sciences*, 38, 1579-1599.
- Gehrels, G.E., and Saleeby, J.B., 1987. Geologic framework, tectonic evolution and displacement history of the Alexander terrane. *Tectonics*, 6, 151-174.
- Gehrels, G.E., and Boghossian, N.D., 2000. Reconnaissance geology and U-Pb geochronology of the west flank of the Coast Mountains between Bella Coola and Prince Rupert, coastal British Columbia. In: Stowell, H.H. and McClelland, W.C., (Eds.), *Tectonics of the Coast Mountains, Southeastern Alaska and British Columbia*. Geological Society of America, Special Paper 343, pp. 61-76.
- Gehrels, G.E., Butler, R.F., and Bazard, D.R., 1996. Detrital zircon geochronology of the Alexander terrane, southeastern Alaska. *Geological Society of America Bulletin*, 108, 722-734.
- Gehrels, G., Rusmore, M., Woodsworth, G., Crawford, M., Andronicos, C., Hollister, L., Patchett, J., Ducea, M., Butler, R., Klepeis, K., Davidson, C., Friedman, R., Haggart, J., Mahoney, B., Crawford, W., Pearson, D., and Girardi, J., 2009. U-Th-Pb geochronology of the Coast Mountains batholith in north-coastal British Columbia: Constraints on age and tectonic evolution. *Geological Society of America Bulletin*, 121, 1341-1361.
- Geological Survey of Canada. 1957. Stikine River area, Cassiar District, British Columbia. Geological Survey of Canada, Map 9-1957, scale 1:253,440.
- Greene, A.R., Scoates, J.S., Nixon, G.T. and Weis, D., 2006. Picritic lavas and basal sills in the Karmutsen flood basalt province, Wrangellia, northern Vancouver Island, B.C. British Columbia Ministry of Energy, Mines and Petroleum Resources, British Columbia Geological Survey Paper 2006-01-05, pp. 39-52.
- Greene, A.R., Scoates, J.S., Weis, D., Katvala, E.C., Israel S., and Nixon, G.T., 2010. The architecture of oceanic plateaus revealed by the volcanic stratigraphy of the accreted Wrangellia ocean plateau. *Geosphere*, 6, 47-73.
- Greene, A.R., Scoates, J.S., Weis, D., Nixon, G.T., and Kieffer, B., 2009. Melting history and magmatic evolution of basalts and picrites from the accreted Wrangellia oceanic plateau. *Journal of Petrology*, 50, 467-505.
- Greig, C.J., and Evenchick, C.A. 1993. Geology of Oweegee Dome (geochemistry and paleontology), Delta Peak (104A/12) and Taft Creek (104A/11W) map areas, northwestern British Columbia; Geological Survey of Canada, Open File 2688, scale 1:50,000.
- Gunning, H.C., 1930. Geology and mineral deposits of Quatsino-Nimkish area, Vancouver Island, British Columbia. In: Summary Report 1929, Geological Survey of Canada, Part A, 94A-143A.
- Gunning, H.C., 1932. Preliminary report on the Nimkish Lake quadrangle, Vancouver Island, British Columbia. In: Summary Report 1931, Geological Survey of Canada, Part A, 22-35.
- Gunning, M.H., Bamber, E.W., Brown, D.A., Rui, L., Mamet, B.L., and Orchard, M.J., 1994. The Permian Ambition Formation of Northwestern Stikinia, British Columbia. In: Embry, A.F., Beauchamp, B., and Glass, D.J., (Eds.), *Pangea: Global Environments and Resources*, Canadian Society of Petroleum Geologists, Memoir 17, pp. 589-619.
- Hammack, J.L., Nixon, G.T., Koyanagi, V.M., Payie, G.J., Panteleyev, A., Massey, N.W.D., Hamilton, J.V., and Haggart, J.W., 1994. Preliminary Geology of the Quatsino - Port McNeill area, northern Vancouver Island (NTS 92L/12, 11W). British Columbia Ministry of Energy, Mines, and Petroleum Resources, British Columbia Geological Survey Open File 1994-26, scale 1:50,000.
- Hammack, J.L., Nixon, G.T., Payie, G.J., Snyder, L.D., Haggart, J.W., Massey, N.W.D., and Barron, D., 1995. Preliminary Geology of the Quatsino-Cape Scott Area, northern Vancouver Island (NTS 92L/12W; 102I/8, 9). British Columbia Ministry of Energy, Mines and Petroleum Resources, British Columbia Geological Survey Open File 1995-09, scale 1:50,000.
- Hayes, M., Ferri, F., and Morii, S., 2004. Interior basin strategy. In: Summary of Activities 2004, Resource Development and Geoscience Branch, British Columbia Ministry of Energy and Mines, pp. 69-71.
- Heah, T.S.T., 1991. Mesozoic ductile shear and Paleogene extension along the eastern margin of the Central Gneiss complex, Coast belt, Shames River area, near Terrace, British Columbia. Unpublished M.Sc. thesis, University of British Columbia, 155 p.
- Hollis, L., 2009. Cretaceous porphyry magmatic-hydrothermal systems in the Tchaikazan River area, southwest B.C. Unpublished M.Sc. thesis, The University of British Columbia, 225 p.
- International Commission on Stratigraphy, 2017. International chronostratigraphic chart. Drafted by K.M. Cohen, S.C. Finney, and P.L. Gibbard, International Commission on Stratigraphy, v2017/02, available at <http://www.stratigraphy.org>. Last accessed November, 2017.
- Infrastructure for Spatial Information in Europe, 2017. European Commission. <http://inspire.ec.europa.eu>. Last accessed November, 2017.
- Israel, S.A., 2001. Structural and stratigraphic relationships within the Tchaikazan River area, southwestern British Columbia: Implications for the tectonic evolution of the southern Coast belt. M.Sc. thesis, The University of British Columbia, 129 p., scale 1:20,000.
- Israel, S., and van der Heyden, P., 2006. Geology, Atnarko (93C/05), British Columbia. Geological Survey of Canada, Open File 5389, scale 1:50,000.
- Israel, S., van der Heyden, P., Haggart, J.W., and Woodsworth, G.J., 2006. Geology, Junker Lake and part of Knot Lakes (93C/04 and 92N/13), British Columbia. Geological Survey of Canada, Open File 5388, scale 1:50,000.
- Jeffery, W.G., 1962. Preliminary geological map, Alice Lake-Benson Lake area. British Columbia Ministry of Energy, Mines, and Petroleum Resources, scale 1:63,360.
- Jeletzky, J.A., 1976. Mesozoic and Tertiary rocks of Quatsino Sound, Vancouver Island, British Columbia. Geological Survey of Canada, Bulletin 242, 243 p.
- Jones, D.L., Silberling, N.J., and Hillhouse, J., 1977. Wrangellia-a displaced terrane in northwestern North America. *Canadian Journal of Earth Sciences*, 14, 2565-2577.
- Kilby, W.E., 1995. Mineral potential project-overview. In: Geological

- Fieldwork 1994, British Columbia Ministry of Energy, Mines and Petroleum Resources, British Columbia Geological Survey Paper 1995-1, pp. 411-416.
- Hutchison, W.W., 1982. Geology of the Prince Rupert-Skeena map area, British Columbia. Geological Survey of Canada Memoir 394, 115 p., with Map 1427A, scale 1:250,000.
- Lewis, T.J., Lowe, C., and Hamilton, T.S., 1997. Continental signature of a ridge-trench-triple junction: northern Vancouver Island. *Journal of Geophysical Research*, 102, 7767-7781.
- Logan, J.M., and Mihalynuk, M.G., 2014. Tectonic controls on early Mesozoic paired alkaline porphyry deposits belts (Cu-Au ± Ag-Pt-Pd-Mo) within the Canadian Cordillera. *Economic Geology*, 109, 827-858.
- Logan, J.M., and Schiarizza, P., 2014. The Rayfield River pluton, south-central British Columbia (NTS 92P/6): Geologic setting and copper mineralization. In: *Geological Fieldwork 2013*, British Columbia Ministry of Energy and Mines, British Columbia Geological Survey Paper 2014-1, pp. 15-27.
- Logan, J.M., Bath, A.B., Mihalynuk, M.G., and Rees, C.J., 2007. Regional Geology of the Mount Polley area, Central British Columbia (part of NTS 93A/05, 06, 11 and 12). British Columbia Ministry of Energy, Mines, and Petroleum Resources, British Columbia Geological Survey Geoscience Map 2007-1, scale 1:50,000.
- Logan, J.M., Drobe, J.R., and McClelland, W.C., 2000. Geology of the Forrest Kerr-Mess Creek area, northwestern British Columbia. British Columbia Ministry of Energy and Mines, British Columbia Geological Survey Bulletin 104, 164 p.
- Logan, J.M., Leroux, G., and Able, L. 2008. Regional geology of the Cottonwood area, central British Columbia (NTS 93G/01). British Columbia Ministry of Energy, Mines, and Petroleum Resources, British Columbia Geological Survey, Open File 2008-6, scale 1:50,000.
- Logan, J.M., Schiarizza, P.A., Struik, L.C., Barnett, C., Nelson, J.L., Kowalczyk, P., Ferri, F., Mihalynuk, M.G., Thomas, M.D., Gammon, P., Lett, R.E., Jackaman, W., and Ferbey, T., 2010. Bedrock Geology of the QUEST Map Area, Central British Columbia. British Columbia Ministry of Energy, Mines, and Petroleum Resources, British Columbia Geological Survey Geoscience Map 2010-1, Geoscience BC Report 2010-5, Geological Survey of Canada, Open File 6476, scale 1:50,000.
- Mahoney, J.B., Hickson, C.J., Haggart, J.W., Schiarizza, P., Read, P.B., Enkin, R.J., van der Heyden, P., and Israel, S., 2013. Geology, Taseko Lakes, British Columbia. Geological Survey of Canada, Open File 6150, scale 1:250,000.
- Massey, N.W.D., 1995a. Geology and mineral resources of the Alberni-Nanaimo lakes sheet, Vancouver Island, 92F/1W, 92F/2E and part of 92F/7E. British Columbia Ministry of Energy, Mines and Petroleum Resources, British Columbia Geological Survey Paper 1992-2, 132 p.
- Massey, N.W.D., 1995b. Geology and mineral resources of the Cowichan Lake sheet, Vancouver Island, 92C/16. British Columbia Ministry of Energy, Mines and Petroleum Resources, British Columbia Geological Survey Paper 1992- 3, 112 p.
- Massey, N.W.D., 1995c. Geology and mineral resources of the Duncan sheet, Vancouver Island, 92B/13. British Columbia Ministry of Energy, Mines and Petroleum Resources, British Columbia Geological Survey Paper 1992-4, 112 p.
- Massey, N.W.D., and Melville, D.M., 1991. Quatsinao sound project. In: *Geological Fieldwork*, British Columbia Ministry of Energy, Mines, and Petroleum Resources, British Columbia Geological Survey Paper 1991-1, pp. 85-88.
- Massey, N.W.D., MacIntyre, D.G., Desjardins, P.J., and Cooney, R.T., 2005. Digital geology map of British Columbia. British Columbia Ministry Energy, Mines, Petroleum Resources, British Columbia Geological Survey Open File 2005-02, scale 1:250,000.
- Mathews, W.H. 1986. Physiography of the Canadian Cordillera. Geological Survey of Canada, Map 1701A, scale 1:5,000,000.
- McClenaghan, L., 2013. Geology and genesis of the Newton bulk-tonnage gold-silver deposit, central British Columbia. M.Sc. thesis, The University of British Columbia, 186 p.
- McKeown, M., Nelson, J.L., and Friedman, R., 2008. Newly discovered volcanic-hosted massive sulphide potential within Paleozoic volcanic rocks of the Stikine assemblage, Terrace area, north western British Columbia (NTS 103I/08). In: *Geological Fieldwork 2007*, British Columbia Ministry of Energy, Mines and Petroleum Resources, British Columbia Geological Survey Paper 2008-1, pp. 103-116.
- McMechan, M.E., Evenchick, C.A., Porter, S., and Ferri, F., 2007. Geology, Birdflat Creek, British Columbia. Geological Survey of Canada, Open File 5568, scale 1:50,000.
- McMillan, W.J., Weber, M., Buckley, T., Schaumberger, M., Broach, J., and Bartlett, S., 1981. Nicola Project-Merritt area. British Columbia Ministry of Energy Mines and Petroleum Resources, Preliminary Map 47, north and south sheets (NTS 92I/2), scale 1:25,000.
- Mihalynuk, M.G., 1987. Metamorphic, structural and stratigraphic evolution of the Telkwa Formation, Zymoetz River area (NTS 103I/08 and 93L/05), near Terrace British Columbia. Unpublished M.Sc. thesis, University of Calgary, 128 p.
- Mihalynuk, M.G., and Harker, L.L., 2007. Riske Creek Geology (92O/16W). British Columbia Ministry of Energy, Mines and Petroleum Resources, British Columbia Geological Survey Open File 2007-6, scale 1:50,000.
- Mihalynuk, M.G., Diakow, L.J., Friedman, R.M., and Logan, J.M., 2016. Chronology of southern Nicola arc stratigraphy and deformation. In: *Geological Fieldwork 2015*, British Columbia Ministry of Energy and Mines, British Columbia Geological Survey Paper 2016-1, pp. 31-63.
- Mihalynuk, M.G., Orovan, E.A., Larocque, J.P., Bachiu, T., and Wardle, J., 2009. Chilanko Forks area geology. British Columbia Ministry of Energy, Mines and Petroleum Resources, British Columbia Geological Survey Open File 2009-6, scale 1:50,000.
- Monger, J.W.H., 1989. Geology, Hope, British Columbia. Geological Survey of Canada, Map 41-1989, scale 1:250,000.
- Monger, J.W.H., and Journeay, J.M., 1994. Basement geology and tectonic evolution of the Vancouver region. In: Monger, J.W.H., (Ed.), *Geology and Geological Hazards of the Vancouver Region, Southwestern British Columbia*, Geological Survey of Canada, Bulletin 481, pp. 3-25.
- Monger, J.W.H., and McMillan, W.J., 1989. Geology, Ashcroft, British Columbia (92I). Geological Survey of Canada, Map 42-1989, scale 1:250,000.
- Monger, J.W.H., Price, R.A., and Tempelman-Kluit, D.J., 1982. Tectonic accretion and the origin of the two major metamorphic and tectonic belts in the Canadian Cordillera. *Geology*, 10, 70-75.
- Monger, J.W.H., Wheeler, J.O., Tipper, H.W., Gabrielse, Hubert, Harms, Tekla, Struik, L.C., Campbell, R.B., Dodds, C.J., Gehrels, G.E., and O'Brien, J.A., 1991. Upper Devonian to Middle Jurassic assemblages, part B., Cordilleran terranes. In: Gabrielse, H., and Yorath, C.J., (Eds.), *Geology of the Cordilleran Orogen in Canada*, v. 4, *The Geology of North America: Geological Society of America*, G-2, pp. 281-328.
- Muller, J.E., and Roddick, J.A., 1983. Geology, Alert Bay-Cape Scott, British Columbia. Geological Survey of Canada, Map 1552A, scale 1:,250,000.
- Muller, J.E., Northcote, K.E., and Carlisle, D., 1974. Geology and mineral deposits of Alert Bay-Cape Scott map-area, Vancouver Island, British Columbia. Geological Survey of Canada, Paper 74-8, 77 p.
- Mustard, P.S., van der Heyden, P., and Friedman, R., 1994. Preliminary geologic map, Tatla Lake-Bussel Creek (east half), British Columbia. Geological Survey of Canada, Open File 2957, scale 1:50,000.

- Nelson, J.L., 2009. Terrace regional mapping project, year 4: Extension of Paleozoic volcanic belt and indicators of volcanogenic massive sulphide-style mineralization near Kitimat, British Columbia (NTS 103I/02, 07). In: Geological Fieldwork 2008, British Columbia Ministry of Energy Mines and Petroleum Resources, British Columbia Geological Survey Paper 2009-1, pp. 7-20.
- Nelson, J., and Kennedy, R., 2007. Terrace regional mapping project year 2: New geological insights and exploration targets. In: Geological Fieldwork 2006, British Columbia Ministry of Energy Mines and Petroleum Resources, British Columbia Geological Survey Paper 2007-1, pp. 149-162.
- Nelson, J.L., Barresi, T., Knight, E., and Boudreau, N., 2006a. Geology of the Usk map area (193I/09). British Columbia Ministry of Energy, Mines and Petroleum Resources, British Columbia Geological Survey Open File 2006-3, scale 1:50,000.
- Nelson, J.L., Barresi, T., Knight, E., and Boudreau, N., 2006b. Geology and mineral potential of the Usk map area (NTS 103I/09), near Terrace, B.C. In: Geological Fieldwork 2005, British Columbia Ministry of Energy, Mines and Petroleum Resources, British Columbia Geological Survey Paper 2006-1, pp. 117-134.
- Nelson, J.L., Colpron, M., and Isreal, S., 2013a. The Cordillera of British Columbia, Yukon, and Alaska: Tectonics and Metallogeny. In: Colpron, M., Bissing, T., Rusk, B.G., and Thompson, J.F.H., (Eds.), Tectonics, Metallogeny, and Discovery: The North American Cordillera and similar accretionary settings. Society of Economic Geologists, Special Publication 17, pp. 53-109.
- Nelson, J.L., Diakow, L.J., Karl, S., Mahoney, J.B., Gehrels, G.E., Pecha, M., and van Staal, C., 2011a. Geology of the Mid-Coast Region of British Columbia near Klemtu (parts of Laredo Sound Map Area, 103A/08, 09, 15, 16). British Columbia Ministry of Forest, Mines and Lands, British Columbia Geological Survey Open File 2011-3, Geological Survey of Canada, Open File 6762, scale 1:100,000.
- Nelson, J.L., Diakow, L.J., Karl, S., Mahoney, J.B., Gehrels, G.E., Pecha, M., and van Staal, C., 2011b. Geology and mineral potential of the southern Alexander terrane and western Coast Plutonic complex near Klemtu, northwestern British Columbia. In: Geological Fieldwork 2010, British Columbia Ministry of Forest, Mines and Lands, British Columbia Geological Survey Paper 2011-1, pp. 73-97.
- Nelson, J.L., Diakow, L.J., Mahoney, J.B., Gehrels, G.E., van Staal, C.R., Karl, S., Pecha, M., and Angen, J.J., 2014. Geology of the north and mid-coast regions, British Columbia (Parts of NTS 103 -A, -G, -H, -I and -J). British Columbia Geological Survey, Geoscience Map 2014-03, Geological Survey of Canada, Open File 7604, 2 sheets, scale 1:150,000.
- Nelson, J.L., Diakow, L.J., Mahoney, J.B., van Staal, C., Pecha, M., Angen, J.J., Gehrels, G., and Lau, T., 2012. North coast project: Tectonics and metallogeny of the Alexander terrane, and Cretaceous sinistral shearing of the western Coast Belt. In: Geological Fieldwork 2011, British Columbia Ministry of Energy and Mines, British Columbia Geological Survey Paper 2012-01, pp. 157-179.
- Nelson, J.L., Diakow, L.J., van Staal, C., and Chipley, D., 2013b. Ordovician volcanogenic sulphides in the southern Alexander terrane, coastal NW British Columbia: Geology, Pb isotopic signature, and a case for correlation with Appalachian and Scandinavian deposits. In: Geological Fieldwork 2012, British Columbia Ministry of Energy, Mines and Natural Gas, British Columbia Geological Survey Paper 2013-1, pp. 13-33.
- Nelson, J.L., Kennedy, R., Angen, J., and Newman, S., 2007. Geology of Terrace area (NTS 103I/9,10,15,16). British Columbia Ministry of Energy, Mines and Petroleum Resources, British Columbia Geological Survey Open File 2007-4, scale 1:70,000.
- Nelson, J.L., Kyba, J., McKeown, M., and Angen, J., 2008a. Geology of the Chist Creek map area (NTS 103I/08). British Columbia Ministry of Energy, Mines and Petroleum Resources, British Columbia Geological Survey Open File 2008-3, scale 1:50,000.
- Nelson, J.L., Kyba, J., McKeown, M., and Angen, J., 2008b. Terrace regional mapping project, year 3: Contributions to stratigraphic, structural and exploration concepts, Zymoetz River to Kitimat River, east-central British Columbia (NTS 103I/08). In: Geological Fieldwork 2007, British Columbia Ministry of Energy, Mines, and Petroleum Resources, British Columbia Geological Survey Paper 2008-1, pp. 159-173.
- Nelson, J.L., Mahoney, J.B., Gehrels, G.E., van Staal, C., and Potter, J.J., 2010. Geology and mineral potential of Porcher Island, northern Grenville Channel and vicinity, northwestern British Columbia. In: Geological Fieldwork 2009, British Columbia Ministry of Energy, Mines and Petroleum Resources, British Columbia Geological Survey Paper 2010-1, pp. 19-41.
- Neuendorf, K.K.E., Mehl Jr., J.P., and Jackson, J.A., 2011. Glossary of geology 5th ed. American Geological Institute, Alexandria, VA, 800 p.
- Nixon, G.T., and Orr, A.J., 2007. Recent revisions to the Early Mesozoic stratigraphy of northern Vancouver Island and metallogenic implications. British Columbia Ministry of Energy, Mines and Petroleum Resources, British Columbia Geological Survey Paper 2007-1, pp. 163-178.
- Nixon, G.T., Hammack, J.L., Hamilton, J.V., and Jennings, H., 1993a. Preliminary geology of the Mahatta Creek area, northern Vancouver Island (92L/5). In: Geological Fieldwork 1992, British Columbia Ministry of Energy, Mines, and Petroleum Resources, British Columbia Geological Survey Paper 1993-1, pp. 17-35.
- Nixon, G.T., Hammack, J.L., Hamilton, J.V., and Jennings, H., 1993b. Preliminary geology of the Mahatta Creek area, northern Vancouver Island (NTS 92L/5). British Columbia Ministry of Energy, Mines, and Petroleum Resources, British Columbia Geological Survey Open File 1993-10, scale 1:50,000.
- Nixon, G.T., Hammack, J.L., Hamilton, J.V., Jennings, H., Larocque, J.P., Orr, A.J., Friedman, R.M., Archibald, D.A., Creaser, R.A., Orchard, M.J., Haggart, J.W., Tipper, H.W., Tozer, E.T., Cordey, F., and McRoberts, C.A. 2011a. Geology, geochronology, lithochemistry and metamorphism of the Mahatta Creek area, northern Vancouver Island (NTS 92L/05). British Columbia Ministry of Energy, Mines, and Petroleum Resources, British Columbia Geological Survey Geoscience Map 2011-3, scale 1:50,000.
- Nixon, G.T., Hammack, J.L., Hamilton, J.V., Jennings, H., Orchard, M.J., Haggart, J.W., Tipper, H.W., Friedman, R.M., Archibald, D.A., Cordey, F., and Johnston, K.A., 2006a. Geology of the Mahatta Creek area, northern Vancouver Island (NTS 92L/5). British Columbia Ministry of Energy, Mines and Petroleum Resources, British Columbia Geological Survey Geoscience Map 2006-4, scale 1:50,000.
- Nixon, G.T., Hammack, J.L., Koyanagi, V.M., Payie, G.J., Haggart, J.W., Orchard, M.J., Tozer, T., Archibald, D.A., Friedman, R.M., Palfy, J., and Cordey, F., 2000a. Geology of the Quatsino-Port MacNeill area, northern Vancouver Island (draft). British Columbia Ministry of Energy, Mines, and Petroleum Resources, British Columbia Geological Survey Geoscience Map 2000-6, scale 1:50,000.
- Nixon, G.T., Hammack, J.L., Koyanagi, V.M., Payie, G.J., Haggart, J.W., Orchard, M.J., Tozer, E.T., Friedman, R.M., Archibald, D.A., Palfy, J., and Cordey, F., 2006b. Geology of the Quatsino-Port MacNeill area, northern Vancouver Island. British Columbia Ministry of Energy, Mines and Petroleum Resources, British Columbia Geological Survey Geoscience Map 2006-2, scale 1:50,000.
- Nixon, G.T., Hammack, J.L., Koyanagi, V.M., Payie, G.J., Orr, A.J., Haggart, J.W., Orchard, M.J., Tozer, E.T., Friedman, R.M., Archibald, D.A., Palfy, J., and Cordey, F., 2011b. Geology, geochronology, lithochemistry and metamorphism of the

- Quatsino-Port McNeill Area, northern Vancouver Island (NTS 92L/11, and parts of 92L/05, 12 and 13). British Columbia Ministry of Energy, Mines and Petroleum Resources, British Columbia Geological Survey Geoscience Map 2011-02, scale 1:50,000.
- Nixon, G.T., Hammack, J.L., Koyanagi, V.M., Payie, G.J., Panteleyev, A., Massey, N.W.D., Hamilton, J.V., and Haggart, J.W., 1994. Preliminary geology of the Quatsino-Port McNeill map areas, northern Vancouver Island. In: *Geological Fieldwork, 1993*, British Columbia Ministry of Energy, Mines, and Petroleum Resources, British Columbia Geological Survey Paper 1994-1, pp. 63-85.
- Nixon, G.T., Hammack, J.L., Koyanagi, V.M., Payie, G.J., Snyder, L.D., Panteleyev, A., Massey, N.W.D., Archibald, D.A., Haggart, J.W., Orchard, M.J., Friedman, R.M., Tozer, E.T., Tipper, H.W., Poulton, T.P., Palfy, J., Cordey, F., and Barron, D.J., 2006c. Geology of the Holberg-Winter Harbour area, northern Vancouver Island. British Columbia Ministry of Energy, Mines and Petroleum Resources, British Columbia Geological Survey Geoscience Map 2006-3, scale 1:50,000.
- Nixon, G.T., Hammack, J.L., Koyanagi, V.M., Snyder, L.D., Payie, G.J., Panteleyev, A., Massey, N.W.D., Hamilton, J.V., Orr, A.J., Friedman, R.M., Archibald, D.A., Haggart, J.W., Orchard, M.J., Tozer, E.T., Tipper, H.W., Poulton, T.P., Palfy, J., and Cordey, F., 2011c. Geology, Geochronology, lithochemistry and metamorphism of the Holberg-Winter Harbour area, northern Vancouver Island (parts of NTS 92L/05, 12, 13; 102I/08, 09 and 16). British Columbia Ministry of Energy, Mines and Petroleum Resources, British Columbia Geological Survey Geoscience Map 2011-1, scale: 1:50,000.
- Nixon, G.T., Hammack, J.L., Payie, G.J., Snyder, L.D., Archibald, D.A., and Barron, D.J., 1995. Quatsino-San Josef map area, northern Vancouver Island: Geological overview. In: *Geological Fieldwork, 1994*, British Columbia Ministry of Energy, Mines, and Petroleum Resources, British Columbia Geological Survey Paper 1995-1, pp. 9-21.
- Nixon, G.T., Hammack, J.L., Payie, G.J., Snyder, L.D., Koyanagi, V.M., Hamilton, J.V., Panteleyev, A., Massey, N.W.D., Haggart, J.W., and Archibald, D.A., 1997. Geology of northern Vancouver Island: preliminary compilation (NTS 92L/5, 6, 11, 12; 102I/8, 9). British Columbia Ministry of Energy, Mines and Petroleum Resources, British Columbia Geological Survey Open File 1997-13, scale 1:100,000.
- Nixon, G.T., Kelman, M.C., Larocque, J.P., Stevenson, D.B., Stokes, L.A., Pals, A., Styan, J., Johnston, K.A., Friedman, R.M., Mortensen, J.K., Orchard, M.J., and McRoberts, C.A., 2011d. Geology, geochronology, lithochemistry and metamorphism of the Nimpkish-Telegraph Cove area, northern Vancouver Island (NTS 92L/07 and part of 92L/10). British Columbia Ministry of Energy, Mines and Petroleum Resources, British Columbia Geological Survey Geoscience Map 2011-5, scale 1:50,000.
- Nixon, G.T., Kelman, M.C., Larocque, J.P., Stevenson, J.P., Stokes, L.A., Pals, A., Styan, J., Johnston, K.A., Orchard, M.J., and McRoberts, C.A., 2009. Geology of the Nimpkish-Telegraph Cove Area, northern Vancouver Island (NTS 92L/7, 10). British Columbia Ministry of Energy, Mines, and Petroleum Resources, British Columbia Geological Survey Geoscience Map 2009-2, scale 1:50,000.
- Nixon, G.T., Kelman, M.C., Stevenson, D., Stokes, L.A., and Johnston, K.A., 2006d. Preliminary geology of the Nimpkish map area, northern Vancouver Island (92L/07). British Columbia Ministry of Energy, Mines and Petroleum Resources Open File 2006-5, scale 1:50,000.
- Nixon, G.T., Kelman, M.C., Stevenson, D., Stokes, L.A., and Johnston, K.A., 2006e. Preliminary geology of the Nimpkish map area (NTS 92L/07), northern Vancouver Island, B.C. British Columbia Ministry of Energy, Mines and Petroleum Resources, British Columbia Geological Survey Paper 2006-1, pp. 135-152.
- Nixon, G.T., Larocque, J., Pals, A., Styan, J., Greene, A.R., and Scoates, J.S., 2008. High-Mg lavas in the Karmutsen flood basalts, northern Vancouver Island (NTS 92L): stratigraphic setting and metallogenic significance. British Columbia Ministry of Energy, Mines and Petroleum Resources, British Columbia Geological Survey Paper 2008-1, pp. 175-190.
- Nixon, G.T., Payie, G.J., Snyder, L.D., Long, S., Finnie, A., Friedman, R.M., Archibald, D.A., Orchard, M.J., Tozer, T., Poulton, T.P., and Haggart, J.W., 2000b. Geology of the Alice Lake area, northern Vancouver Island. British Columbia Ministry of Energy, Mines, and Petroleum Resources, British Columbia Geological Survey Geoscience Map 2000-7, scale 1:50,000.
- Nixon, G.T., Snyder, L.D., Payie, G.J., Long, S., Finnie, A., Friedman, R.M., Archibald, D.A., Orchard, M.J., Tozer, E.T., Poulton, T.P., and Haggart, J.W., 2006f. Geology of the Alice Lake area, northern Vancouver Island. British Columbia Ministry of Energy, Mines and Petroleum Resources, British Columbia Geological Survey, Geoscience Map 2006-1, scale 1:50,000.
- Nixon, G.T., Snyder, L.D., Payie, G.J., Long, S., Finnie, A., Orr, A.J., Friedman, R.M., Archibald, D.A., Orchard, M.J., Tozer, E.T., Poulton, T.P., and Haggart, J.W. 2011e. Geology, geochronology, lithochemistry and metamorphism of the Alice Lake Area, northern Vancouver Island (NTS 92L/06 and part of 92L/03). British Columbia Ministry of Energy, Mines, and Petroleum Resources, British Columbia Geological Survey Geoscience Map 2011-4, scale 1:50,000.
- North American Commission on Stratigraphic Nomenclature, 2005. North American Stratigraphic Code: American Association of Petroleum Geologists Bulletin, 89, pp. 1547-1591.
- North American Geologic Map Data Model Steering Committee, 2004. NADM Conceptual Model 1.0-A conceptual model for geologic map information. U.S. Geological Survey Open-File Report 2004-1334, 58 p., Geological Survey of Canada Open File 4737.
- Northcote, K.E., 1969. Geology of the Port Hardy-Coal Harbour area. In: *British Columbia Department of Mines Annual Report on Lode Metals, 1968*, pp. 84-87
- Northcote, K.E., 1971. Rupert Inlet-Cape Scott map area. In: *Geology, Exploration and Mining in B.C. 1970*, British Columbia Ministry of Energy, Mines and Petroleum Resources, pp. 254-258.
- Northcote, K.E., and Muller, J.E., 1972. Volcanism, plutonism, and mineralization: Vancouver Island. *Canadian Institute of Mining, Metallurgy and Petroleum, Bulletin* 65, 49-57.
- O'Sullivan, P.B., Donelick, R.A., Osadetz, K.G., Evenchick, C.A., Ferri, F. Wilson, N.S.F., and Hayes, M., 2005. Apatite fission-track data from seventy-one Bowser and Sustut basin rock samples. Geological Survey of Canada, Open File 4840, 500 p.
- Panteleyev, A., Bobrowsky, P.T., Nixon, G.T., and Sibbick, S.J., 1996. Northern Vancouver Island integrated project. In: *Geological Fieldwork 1995*, British Columbia Ministry of Energy, Mines, and Petroleum Resources, British Columbia Geological Survey Paper 1996-1, pp. 57-59.
- Preto, V.A., 1972. Geology of Copper Mountain. British Columbia Department Mines and Petroleum Resources, *Bulletin* 59, 87p.
- Preto, V.A., 1979. Geology of the Nicola Group between Merritt and Princeton. British Columbia Ministry of Energy, Mines and Petroleum Resources, British Columbia Geological Survey, *Bulletin* 69, 90 p.
- Rawson, P.F., Allen, P.M., Brenchley, P.J., Cope, J.C.W., Gale, A.S., Evans, J.A., Gibbard, P.L., Gregory, F.J., Hailwood, E.A., Hesselbo, S.P., Knox, R.W.O'B., Marshall, J.E.A., Oates, M., Riley, N.J., Smith, A.G., Trewin, N., and Zalasiewicz, J.A., 2002. Stratigraphical procedure. Geological Society, London, *Professional Handbook*, 57 p.
- Rice, H.M.A., 1947. Geology and mineral deposits of the Princeton map-area, British Columbia. Geological Survey of Canada,

- Memoir 243.
- Richards, T.A., and Gilchrist, R.D., 1979. Groundhog coal area, British Columbia. In: Current Research, Part B, Geological Survey of Canada, Paper 79-1B, pp. 411-414.
- Riddell, J.M., 2010. Summary of apatite fission-track analyses and radiometric dates from the Nechako region, British Columbia (NTS 92O, N; 93B, C, F, G, and L) and implications for oil and gas prospectivity. British Columbia Ministry of Energy, Mines and Petroleum Resources, Oil and Gas Geoscience Reports 2010, pp. 123-131.
- Ricketts, B.D., and Evenchick, C.A., 1991. Analysis of the Middle to Upper Jurassic Bowser Basin, northern British Columbia. In: Current Research, Part A, Cordillera and Pacific, Geological Survey of Canada, Paper 91-1A, pp. 65-73.
- Ricketts, B.D., and Evenchick, C.A., 1999. Shelfbreak gullies; products of sea-level lowstand and sediment failure: examples from Bowser Basin, northern British Columbia. *Journal of Sedimentary Research*, 69, 1232-1240.
- Ricketts, B.D., and Evenchick, C.A., 2007. Evidence of different contractional styles along foredeep margins provided by Gilbert deltas; examples from Bowser Basin, British Columbia, Canada. *Bulletin of Canadian Petroleum Geology*, 55, 243-261.
- Ricketts, B.D., Evenchick, C.A., Anderson, R.G., and Murphy, D.C., 1992. Bowser basin, northern British Columbia: constraints on the timing of initial subsidence and Stikinia-North America terrane interactions. *Geology*, 20, 1119-1122.
- Roddick, J.A., 1970. Douglas Channel-Hecate Strait map-area, British Columbia. Geological Survey of Canada, Paper 70-41, 70 p., with Map 23-1970, scale 1:250,000.
- Rubin, C.M., and Saleeby, J.B., 1992. Tectonic history of the eastern edge of the Alexander terrane, southeast Alaska. *Tectonics*, 11, 586-602.
- Rusmore, M.E., and Woodsworth, G.J., 1993. Geological maps of the Queen Bess (92N/7) and Razorback Mountain (92N/10) map areas, Coast Mountains, British Columbia. Geological Survey of Canada, Open File 2586, 2 sheets, scale 1:50,000.
- Saleeby, J.B., 2000. Geochronologic investigations along the Alexander-Taku terrane boundary, southern Revillagigedo Island to Cape Fox areas, southeast Alaska. In: Stowell, H.H. and McClelland, W.C., (Eds.), *Tectonics of the Coast Mountains, Southeastern Alaska and British Columbia*. Geological Society of America Special Paper 343, pp. 107-143.
- Schau, M.P., 1968. Geology of the Upper Triassic Nicola Group in south central British Columbia. Unpublished Ph.D. thesis, The University of British Columbia, 225 p.
- Schiarizza, P., 2011a. Geology of the Kutcho assemblage between Kutcho Creek and the Tucho River, northern British Columbia (NTS 104I/01). In: Geological Fieldwork 2010, British Columbia Ministry of Forests, Mines and Lands, British Columbia Geological Survey Paper 2011-1, pp. 99-117.
- Schiarizza, P., 2011b. Bedrock geology of the Andrea Creek area, part of NTS 104I/01. British Columbia Ministry of Energy and Mines, British Columbia Geological Survey Open File 2011-7, scale 1:25,000.
- Schiarizza, P., 2012a. Geology of the Kutcho assemblage between the Kehlechoa and Tucho rivers, northern British Columbia (NTS 104I/01, 02). In: Geological Fieldwork 2011, British Columbia Ministry of Energy and Mines, British Columbia Geological Survey Paper 2012-1, pp. 75-98.
- Schiarizza, P., 2012b. Bedrock geology of the upper Kutcho Creek area, parts of NTS 104I/01, 02. British Columbia Ministry of Energy and Mines, British Columbia Geological Survey Open File 2012-08, Geological Survey of Canada Open File 7234, scale 1:40,000.
- Schiarizza, P., 2013. The Wineglass assemblage, lower Chilcotin River, south-central British Columbia: Late Permian volcanic and plutonic rocks that correlate with the Kutcho assemblage of northern British Columbia. In: Geological Fieldwork 2012, British Columbia Ministry of Energy, Mines, and Natural Gas, British Columbia Geological Survey Paper 2013-1, pp. 53-70.
- Schiarizza, P., 2015. Geological setting of the Granite Mountain batholith, south-central British Columbia. In: Geological Fieldwork 2014, British Columbia Ministry of Energy and Mines, British Columbia Geological Survey Paper 2015-1, pp. 19-39.
- Schiarizza, P., and Church, N., 1996. Geological compilation of the Thompson-Okanagan area (82L, M; 83D; 92H, I, J, P; 93A). British Columbia Ministry of Employment and Investment, British Columbia Geological Survey Open File 1996-20.
- Schiarizza, P.A., and Macauley, J., 2007. Geology of the Hendrix Lake Area (NTS 093A/02). British Columbia Ministry of Energy, Mines and Petroleum Resources, British Columbia Geological Survey Open File 2007-03, scale 1:50,000.
- Schiarizza, P.A., Bell, K., and Bayliss, S., 2009. Geology of the Murphy Lake Area (NTS 93A/03). British Columbia Ministry of Energy, Mines and Petroleum Resources, British Columbia Geological Survey Open File 2009-03, scale 1:50,000.
- Schiarizza, P., Gaba, R.G., Glover, J.K., Garver, J.I., and Umhoefer, P.J., 1997. Geology and mineral occurrences of the Taseko - Bridge River area. British Columbia Ministry of Employment and Investment, British Columbia Geological Survey Bulletin 100, 291 p., scale 1:100,000.
- Schiarizza, P., Israel, S., Heffernan, S., Boulton, A., Bligh, J., Bell, K., Bayliss, S., Macauley, J., Bluemel, B., Zuber, J., Friedman, R.M., Orchard, M.J., and Poulton, T.P., 2013. Bedrock geology between Thuya and Woodjam creeks, south-central British Columbia, NTS 92P/7, 8, 9, 10, 14, 15, 16; 93A/2, 3, 6. British Columbia Ministry of Energy, Mines and Petroleum Resources, British Columbia Geological Survey Open File 2013-5, 4 sheets, scale 1:100,000.
- Schiarizza, P., Panteleyev, A., Gaba, R.G., Glover, J.K., Desjardins, P.J., and Cunningham, J., 1994. Geological compilation of the Cariboo-Chilcotin area (92J, K, N, O, P; 93A, B, C, F, G, H). British Columbia Ministry of Energy, Mines and Petroleum Resources, British Columbia Geological Survey Open File 1994-7, scale 1:250,000.
- Schiarizza, P., Riddell, J., Gaba, R.G., Melville, D.M., Umhoefer, P.J., Robinson, M.J., Jennings, B.K., and Hick, D., 2002. Geology of the Beece Creek - Niut Mountain area, British Columbia (NTS 92N/8, 9, 10; 92O/5, 6, 12). British Columbia Ministry of Energy and Mines, British Columbia Geological Survey Geoscience Map 2002-3, scale 1:100,000.
- Souther, J.G., and Souther, M.E.K., 1994. The Ilgachuz Range and adjacent parts of the Interior Plateau, British Columbia. Geological Survey of Canada, Bulletin 462, 75 p., scale 1:50,000.
- Thorstad, L.E., 1984. The Upper Triassic Kutcho Formation, Cassiar Mountains, north-central British Columbia. Unpublished M.Sc. thesis, The University of British Columbia, 271 p.
- Thorstad, L.E., and Gabrielse, H., 1986. The Upper Triassic Kutcho Formation, Cassiar Mountains, north-central British Columbia. Geological Survey of Canada, Paper 86-16, 53 p.
- Tipper, H.W., and Richards, T.A., 1976. Jurassic stratigraphy and history of north-central British Columbia. Geological Survey of Canada, Bulletin 270, 73 p.
- Tochilin, C.J., Gehrels, G., Nelson, J., and Mahoney, J.B., 2014. U-Pb and Hf isotope analysis of detrital zircons from the Banks Island assemblage (coastal British Columbia) and southern Alexander terrane (southeast Alaska). *Lithosphere*, 6, 200-215.
- Tozer, E.T., 1967. A standard for Triassic time. Geological Survey of Canada, Bulletin 156, 103p.
- van der Heyden, P., 1992. A Middle Jurassic to early Tertiary Andean-Sierran subduction model for the Coast belt of B.C. *Tectonics*, 11, 82-97.
- van der Heyden, P., Calderwood, A., and Huntley, D.H., 1994. Preliminary geological map, Charlotte Lake-Junker Lake (east

- half), British Columbia. Geological Survey of Canada, Open File 2984, scale 1:50,000.
- Waldron, J.W.F., Gagnon, J.-F., Loogman, W., and Evenchick, C.A., 2006. Initiation and deformation of the Jurassic-Cretaceous Bowser Basin: implications for hydrocarbon exploration in north-central British Columbia. In: Geological Fieldwork 2005, British Columbia Ministry of Energy, Mines and Petroleum Resources, British Columbia Geological Survey Paper 2006-1, pp. 349-360.
- Wheeler, J.O., and McFeely, P., 1991. Tectonic assemblage map of the Canadian Cordillera and adjacent parts of the United States of America. Geological Survey of Canada, Map1712A, scale 1:2,000,000.
- Wheeler, J.O., Brookfield, A.J., Gabrielse, H., Monger, J.W.H., Tipper, H.W., and Woodsworth, G.J., 1991. Terrane map of the Canadian Cordillera. Geological Survey of Canada, Map 1713A, scale 1:2,000,000.

Estimating the thickness of drift using a 3D depth-to-bedrock GOCAD model in the Ootsa Lake porphyry Cu-Mo-Au district of west-central British Columbia



Stephen M. Rowins^{1, a}, Deanna R. Miller¹, and Yao Cui¹

¹ British Columbia Geological Survey, Ministry of Energy, Mines and Petroleum Resources, Victoria, BC, V8W 9N3

^a corresponding author: Stephen.Rowins@gov.bc.ca

Recommended citation: Rowins, S.M., Miller, D.R., and Cui, Y., 2018. Estimating the thickness of drift using a 3D depth-to-bedrock GOCAD model in the Ootsa Lake porphyry Cu-Mo-Au district of west-central British Columbia. In: *Geological Fieldwork 2017*, Ministry of Energy, Mines and Petroleum Resources, British Columbia Geological Survey Paper 2018-1, pp. 217-227.

Abstract

Digital datasets were used to build a three-dimensional (3D) GOCAD model that estimates the thickness of unconsolidated Quaternary glacial and non-glacial sediments covering bedrock in the Ootsa Lake area of west-central British Columbia. The area hosts several porphyry Cu±Mo±Au deposits and the past-producing Huckleberry Cu-Mo mine. Estimates of drift thickness in the depth-to-bedrock model were based on interpolation between bedrock surfaces identified in diamond drillholes, outcrop, and surface topography derived from aerial Light Detection and Ranging survey (LiDAR) data. Where combined with geophysical data, structural (fault) data, and geochemical anomalies identified in soils from Regional Geochemical Survey (RGS) data, the depth-to-bedrock model is a useful aid in ranking exploration targets and understanding subsurface paleotopography. Most simply, geochemical anomalies in areas of shallow drift may be ranked higher than similar geochemical anomalies in areas of thicker drift because drilling is less costly and drillholes are easier to complete. However, not all areas of thick drift are necessarily low ranking targets in the present study. For example, anomalies that abruptly disappear or show decreased intensity upon crossing known post-mineralization faults and entering areas of thick drift may reflect transitions to grabens that contain deeper mineralized stratigraphy. Such geological interpretations, supported by geophysical data, may allow for a high-rank assignment to such grabens. The depth-to-bedrock map also may help identify previously undocumented faults, such as where abrupt changes in drift thickness define a strong linear feature with significant strike length. The construction of a 3D depth-to-bedrock GOCAD model on a mineral exploration property with sufficient existing digital data from drilling, mapping, and geochemical surveying is an inexpensive way to further interrogate the geology of a property and assess its exploration potential.

Keywords: Ootsa Lake, Seel deposit, Huckleberry mine, porphyry, bedrock, overburden, GOCAD modelling

1. Introduction

Approximately 64% of British Columbia is covered by unconsolidated Quaternary glacial and non-glacial sediments (commonly referred to as 'drift'), which creates significant challenges for grassroots mineral exploration (e.g., Levson, 2002). Exploration tools such as airborne geophysics and regional till surveys using indicators minerals (e.g., apatite, magnetite, epidote, tourmaline, chalcopyrite, and gold) and till geochemistry have proven effective for tracing up-ice sources of mineralization (Bustard and Ferbey, 2016, Hickin and Plouffe, 2017, Mao et al., 2017). Ultimately, however, covered exploration targets must be drilled to validate and, if warranted, advance to the next stage of development. Drilling through thick drift is expensive and technically challenging. It limits the number of grassroots exploration targets that may be evaluated and is a considerable deterrent to investment. One way to reduce the cost of drilling is to test exploration targets in areas where drift is minimal. On the other hand, some areas of deep drift may cover mineral deposits and represent excellent exploration opportunities, albeit with additional technical challenges presented by drilling through drift. In either case, knowledge of drift thickness is an important factor

in the design and execution of a mineral exploration program in covered terrane.

Subsurface modelling methods to determine bedrock topography and depth of sedimentary cover have been used for years in hydrogeological and geotechnical engineering projects (Tearpock and Bischke, 2002; Andrews et al., 2010). Similarly, 'isopach mapping' has been used for decades to estimate the thickness of sedimentary strata in a wide variety of geological studies, especially petroleum exploration (e.g., Levorsen, 1967). An isopach map displays contour lines (isopachs) of equal thickness over an area. Related bedrock topography maps have been developed for northeastern British Columbia by Hickin and Kerr (2005) and Hickin et al. (2008, 2016), where the geometry and depth of paleovalleys have important implications for shallow gas exploration, drilling safety, aquifer management, and seismic processing and interpretation (Levson et al., 2006).

In contrast to the Quaternary geology and sedimentological methods employed elsewhere, we have used GOCAD 3D modelling software from Mira Geoscience to build a 3D 'depth-to-bedrock' block model for the Ootsa Lake porphyry Cu-Mo-Au property (Fig. 1). This 3D modelling approach simply uses

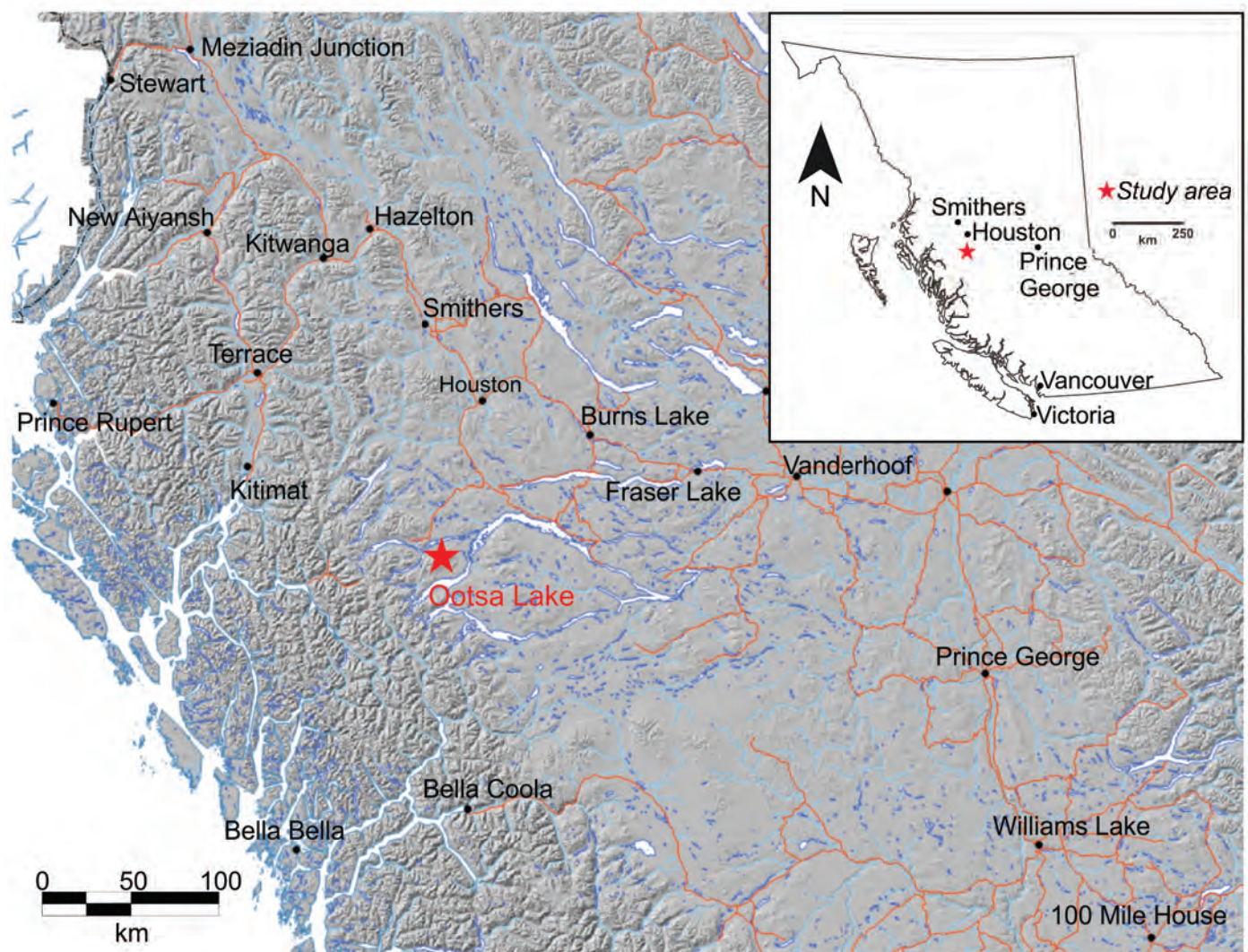


Fig. 1. Location map of the Ootsa Lake property in west-central British Columbia.

available digital data from drilling (bedrock-drift contacts, chemical assays), soil geochemistry surveys, property geology (faults and lithologies), and aerial Light Detection and Ranging survey (LiDAR) data (supplied by Gold Reach Resources Ltd.) to build a block model that includes an isopach map of drift thickness plus other relevant geological features. Where combined with existing company or public geophysical and geochemical data, the depth-to-bedrock block model allows for the ranking of geochemical anomalies and the identification of new exploration targets. The Ootsa Lake area has unpredictable and variable thicknesses of drift (e.g., Ferbey and Levson, 2001a, b; Ferbey, 2010), thus, knowledge on the approximate depth of drift is an important consideration prior to drilling a target. The exercise of ranking an exploration target (e.g., geochemical anomaly), however, is more complex than simply knowing the thickness of drift in an area. Rather, the ranking of a target and identification of new targets requires careful consideration of paleotopography, structural geology, bedrock lithologies and type(s) of mineral deposit under investigation.

Our GOCAD modelling method does not replace field exploration and the collection of geological, geochemical, and geophysical data. It simply relies upon results from previous and ongoing drill programs to create a depth-to-bedrock map that may be used by mineral exploration geologists to further interpret the geology of a property.

2. Geological setting of the Ootsa Lake area

The Ootsa Lake area is in west-central British Columbia approximately 140 km south of Smithers (Fig. 1). It is within Stikinia, a Paleozoic to Mesozoic oceanic arc terrane near the western margin of the Intermontane belt (Currie and Parrish, 1997). The porphyry deposits on the property form the southern end of a northwesterly trending belt of porphyry $\text{Cu}\pm\text{Mo}\pm\text{Au}$ deposits related to intrusive rocks of the Late Cretaceous (ca.70 to 88 Ma) Bulkley Intrusive suite. The intrusions are calc-alkaline with trace element characteristics suggestive of formation in a volcanic arc setting (MacIntyre, 1985; Petersen, 2014). Other significant porphyry deposits related to Bulkley

Suite intrusions in the region include the Huckleberry Cu-Mo mine, Whiting Creek, and Coles Creek (Carter, 1981; Friedman and Jordan, 1997; Lepitre et al., 1998).

The Ootsa property hosts the East Seel, West Seel, and Ox porphyry deposits in addition to a zone of high-grade Ag and Pb-Zn veins at Damascus. The property is road accessible and 7 km southeast of Imperial Metals' Huckleberry Cu-Mo mine (Fig. 2; Jackson and Illerbrun, 1996). The Seel deposit is hosted in Bulkley Suite intrusions and marine sedimentary rocks of the Smithers Formation, part of the Hazelton Group (Lower to Middle Jurassic; Diakow, 2006). It comprises two distinct porphyry systems. The East Seel deposit contains Cu-Au mineralization whereas the West Seel deposit contains Cu-Au-Mo-Ag mineralization. Mineralization at the East Seel deposit is hosted mainly in feldspar-phyric quartz monzonite and granodiorite porphyries whereas at the West Seel deposit, mineralization is hosted in feldspar-phyric quartz monzonite, granodiorite, quartz diorite and biotite hornfels (McDowell and Giroux, 2013; Petersen, 2014).

Extensional tectonics in the late Eocene produced basin-and-range style faults throughout Ootsa Lake area (e.g., MacIntyre, 1985). On the Ootsa property, northwest-trending horsts and grabens containing Eocene and younger strata are predominant. The Seel and Ox deposits are in the Sibola Creek graben, east of the Whiting-Huckleberry horst, which hosts the Huckleberry Cu-Mo mine and Whiting Creek deposit (Fig. 3; Diakow, 2006). Evidence of faults is found in diamond drill core from the Seel deposit. The two most significant faults identified are the North fault and the East fault, both bordering the East Seel deposit (McDowell and Giroux, 2013). The Ox and Damascus deposits are also adjacent to faults. All of these faults post-date the main episode of porphyry mineralization, but localize younger vein- and breccia-style mineralization. The faults dip steeply



Fig. 2. Photograph (view to the northwest) of the Ootsa Lake property (September 2017) showing low topographic relief and forest road infrastructure. The Seel exploration camp is in the bottom left corner of the photo and the Huckleberry Cu-Mo mine is in the upper left corner.

(McDowell and Giroux, 2013) but displacements are largely unconstrained. Porphyry-related alteration and mineralization do occur, however, on both sides of most structures.

The Seel deposit is beneath a gently sloped and forested area that is covered with extensive drift (Fig. 2). Detailed stratigraphic and sedimentological studies on the adjacent Huckleberry mine property indicates drift thickness ranges from a few m up to 27 m (Ferbey and Levson, 2001a, b). Development drilling undertaken on the fringes of the Huckleberry mine, within the proposed pit expansion area, identified even greater drift thicknesses indicating significant local variability (Imperial Metals, 2014). Quaternary geology studies in the Babine porphyry copper district to the north also revealed drift thicknesses up to 40 m (Levson, 2002). Collectively, these studies indicate that significant thicknesses of drift cover this entire part of west-central British Columbia.

3. Methods

3.1. Overview

The GOCAD technology is the mineral exploration industry standard for 3D modelling and visualizing geoscience data (e.g., McGaughy, 2003). Before visualization and interpretation, these data must be interpolated ('gridded') in 3D. GOCAD offers a suite of tools for interpolating both continuous variables (e.g., Cu concentrations) and categorical variables (e.g., lithologies).

The Ootsa Lake area was chosen as the study site for several reasons. First, extensive digital data are available from Gold Reach Resources Ltd. Second, the large mineral deposits (Seel and Ox) and the Huckleberry Cu-Mo mine approximately 7 km to the west attest to the high prospectivity of the area. Third, the area is covered by extensive drift (Ferbey and Levson, 2001a, b; Ferbey, 2010).

The following workflow was used to build the 3D GOCAD model.

1. Data compilation, assessing completeness of datasets, and preparation for modelling.
2. Interpretation of datasets to optimize use (i.e., removal of elements not used from geochemistry datasets; reduction in the point density of the LiDAR dataset to enable software processing).
3. Creation of a topographic surface, fault network, top of bedrock surface, and block model.
4. Physical property creation, i.e., the confidence map and the depth-to-bedrock map.
5. Generation of 2D and 3D products for visualization.

The final block model has a 10 x 10 x 10 m cell size that represents the estimated drift thickness, and a confidence map to assess the level of reliability of a thickness estimates for any given location on the map. Together with geochemical data (e.g., Cu, Au, Ag abundances from drill core and soil geochemistry) and mapped faults projected to depth from surface, several areas on the property were identified as favourable for further exploration.

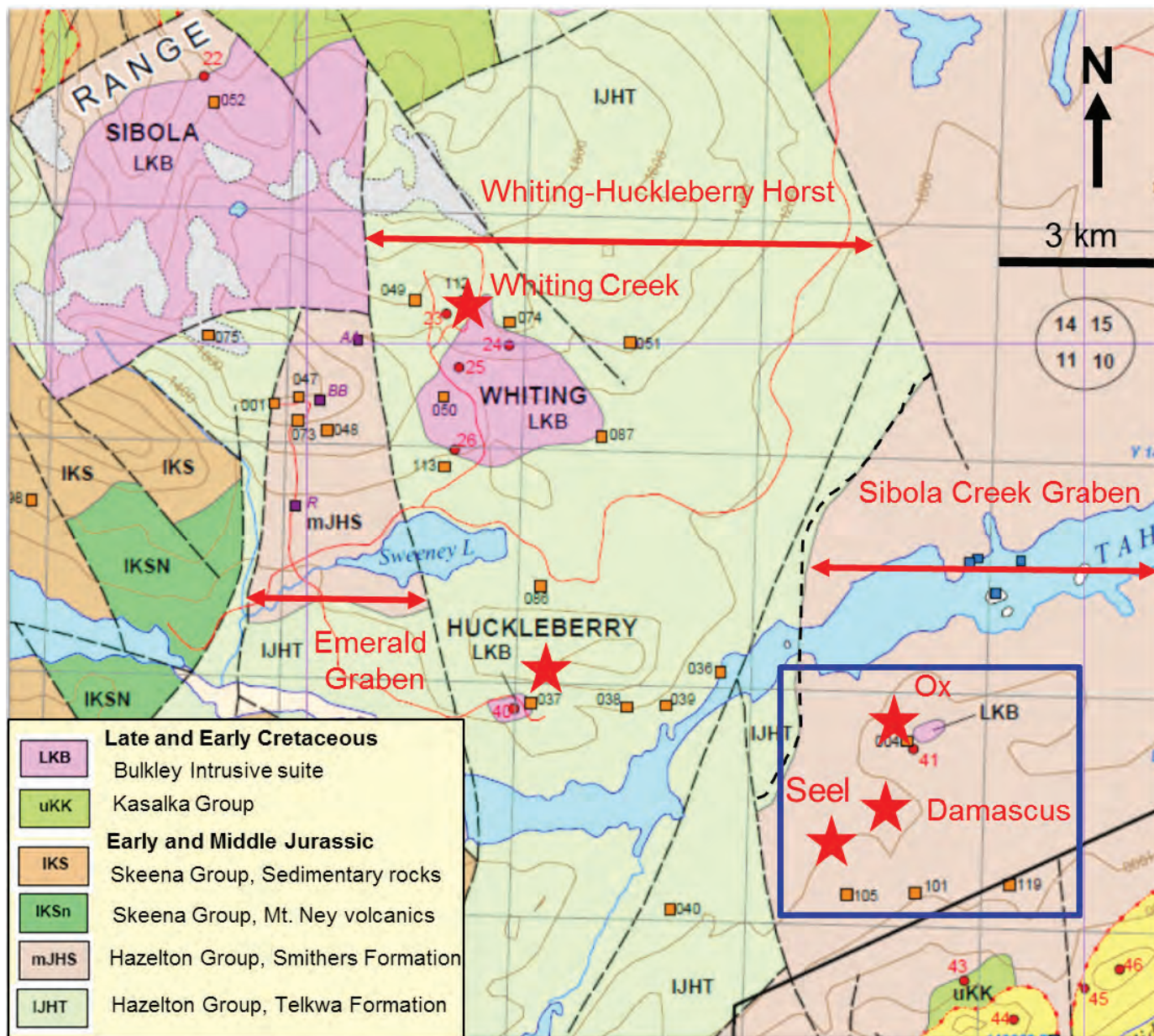


Fig. 3. Local geology of the Ootsa Lake property (modified from Diakow, 2006; McDowell and Giroux, 2013). The blue box outlines the study area and boundaries of the block model shown in Figures 4 to 10.

3.2. Data compilation, assessment and preparation for modelling

Compilation of all data into 3D modelling software required reformatting the original data into the GOCAD 3D format. Gold Reach Resources Ltd. provided all the digital datasets, which were also used for the resource estimate modelling of the Ootsa porphyry deposits as documented in a National Instrument (NI) 43-101 report by McDowell and Giroux (2013). All quality assessment and quality control (QA/QC) protocols regarding datasets are included in that report. The following datasets were provided by Gold Reach Resources Ltd and used in the modelling: 1) drillhole data; 2) property geology maps; 3) LiDAR and orthophotographs; 4) Bedrock exposure data (points and curves) and location of mineralized

zones. Drillhole datasets include assay, collar, lithology, soil geochemistry (not from drilling, but added to the file as accessory data), and survey data (Table 1). Data tables were reformatting for importation into the GOCAD 3D modelling software.

Two geology maps were used to build the 3D model. The first

Table 1. Drillhole datasets provided by Gold Reach Resources Ltd.

Collar	HoleID, X, Y, Z, Length_of_hole
Deviation (Survey)	HoleID, Depth, Azimuth, Dip
Geology	HoleID, From, To, Geology_unit
Property	HoleID, From, To, Property 1, Property 2

was a simplified 1: 50,000 scale geology map of the Ootsa Lake property compiled by Gold Reach Resources Ltd. The second was a regional 1:150,000 scale map of the Ootsa Lake property, also compiled by Gold Reach Resources Ltd., that provided claim boundaries, geology and topographic data.

3.2.1. LiDAR and orthophotographs

A topographic surface was created using 131 LiDAR point sets (called a 'PointSets' in GOCAD). Initial importation of the LiDAR data into GOCAD was difficult because it was too dense for the modelling software to process and manipulate. The area surveyed by Eagle Mapping in 2012 included 103 km² and the density of the survey was 7 points per square metre. These data were filtered to decrease point density from 8 million points to 250,000 points to create a single digital surface model (DSM) for the entire property. Finally, a 15,000 x 98,000 pixel orthophotograph mosaic with 1 m resolution of the Ootsa Lake area was imported into GOCAD and draped over the DSM.

3.2.2. Exposed bedrock data and mineralized zones

Included in the drilling database was a spreadsheet containing 35 X, Y, Z coordinates for point locations of exposed bedrock in the project area. These points were incorporated into the 3D model. Exposed bedrock was also represented by curves through digitization of exposures identified on the mosaic orthophotograph. Included with the property geology maps were GIS data including six polygons representing mineralized zones on the Ootsa property. These mineralized zones were imported into GOCAD to aid in geological interpretation.

4. 3D model build

4.1. Creation of surfaces and networks

The first step in building the model was the creation of an area of interest (AOI), which GOCAD uses to identify the area to be modelled. The AOI in the Ootsa project was based on the spatial extent of LiDAR, orthophotograph coverage, drillholes and exposed bedrock locations. A DSM surface was subsequently created from 131 LiDAR point sets and a mosaic orthophotograph at 1 m resolution was then draped over the topographic surface and bedrock exposures were digitized (curves) from the image (Fig. 4). The bedrock surface (typically covered under drift) was generated by creating drillhole 'markers' that populated a GOCAD points set. Markers represent bedrock-drift contacts in the drillholes. This points set was used subsequently to create the bedrock surface with the AOI curve acting as the constraining boundary (Fig. 5). Drillholes used to model the bedrock surface (green) are shown as red lines in Figure 5. Finally, a simplified property geology map was draped over the DSM and surface fault traces digitized. The fault curves were used to build a 'fault network' in GOCAD to the depth of the AOI assuming a vertical dip of 90 degrees (e.g., McDowell and Giroux, 2013). The depth of the AOI varies depending upon the depth of the bedrock surface at a particular location. The faults were used to aid geological interpretation of the block model (Fig. 6).

4.2. Block model

In GOCAD, a voxel (a regular 3D grid with constant cell sizes) was used to define the extent, depth, scale, and resolution of the 3D block model. The voxel cells in our model had X, Y, and Z axes of variable length to allow for flexibility in the model and resolution. The model was constructed using the NAD83 Zone 9N coordinate system to be consistent with data from Gold Reach Resources Ltd. The block modelling process involved adding the DSM surface and the bedrock surface to the voxel, building the voxel, and assigning rock-units (just 'drift' in our model) to the resulting volume of drift (Fig. 7). Essentially, the block model is a 3D isopach map of drift thickness.

4.3. Confidence map

A confidence map was made in GOCAD by creating a new attribute on the DSM. The term 'confidence' is defined as the averaged 'misfit' between the thickness of drift estimated at a particular location in the block model, and the distance of that location to its nearest bedrock 'control points' represented by drillhole 'markers' and surface exposures of bedrock. In other words, the bedrock-drift contact in a drillhole has zero misfit (perfect confidence) with confidence decreasing in the estimate of drift thickness with increasing distance from the bedrock control points (Fig. 8).

5. Results

The 3D depth-to-bedrock GOCAD model indicates that the known mineral deposits (i.e., West Seel, East Seel, Ox, and Damascus) in the Ootsa Lake area are overlain by shallow drift with significant geochemical anomalies (Fig. 9). We have only shown Cu in Figure 9, but other elements (i.e., Au, Mo) show similar behaviour to Cu with respect to anomalies and mineral deposits. Thin drift probably contains a significant component of local bedrock, and where the bedrock is mineralized, geochemical anomalies will develop in the drift. However, no attempt has been made to determine the location of up-ice sources of geochemical anomalies that cannot be ascribed to zones of known mineralization because ice-flow directions in the Ootsa Lake area are complicated by a reversal in ice-flow during the Late Wisconsinan glacial maximum (Ferbey, 2010). Nevertheless, the occurrence of geochemical anomalies directly overlying or partially covering the 4 mineral deposits is suggestive of limited glacial transport of till in the Ootsa Lake area by the latest glacial event, although it may also reflect the interplay between displacements of mineralized till by the ice-flow reversal (Ferbey, 2010).

Figure 9 reveals that the thickness of drift commonly changes dramatically across faults. Similarly, geochemical anomalies and mineralized zones abruptly disappear or show greatly diminished intensity where a fault is crossed. This behavior is especially apparent at the East Seel deposit, which is bounded by the East fault and North fault. The opposite sides of the Damascus and Ox faults also display very large changes in estimated thicknesses of drift. These abrupt increases in drift

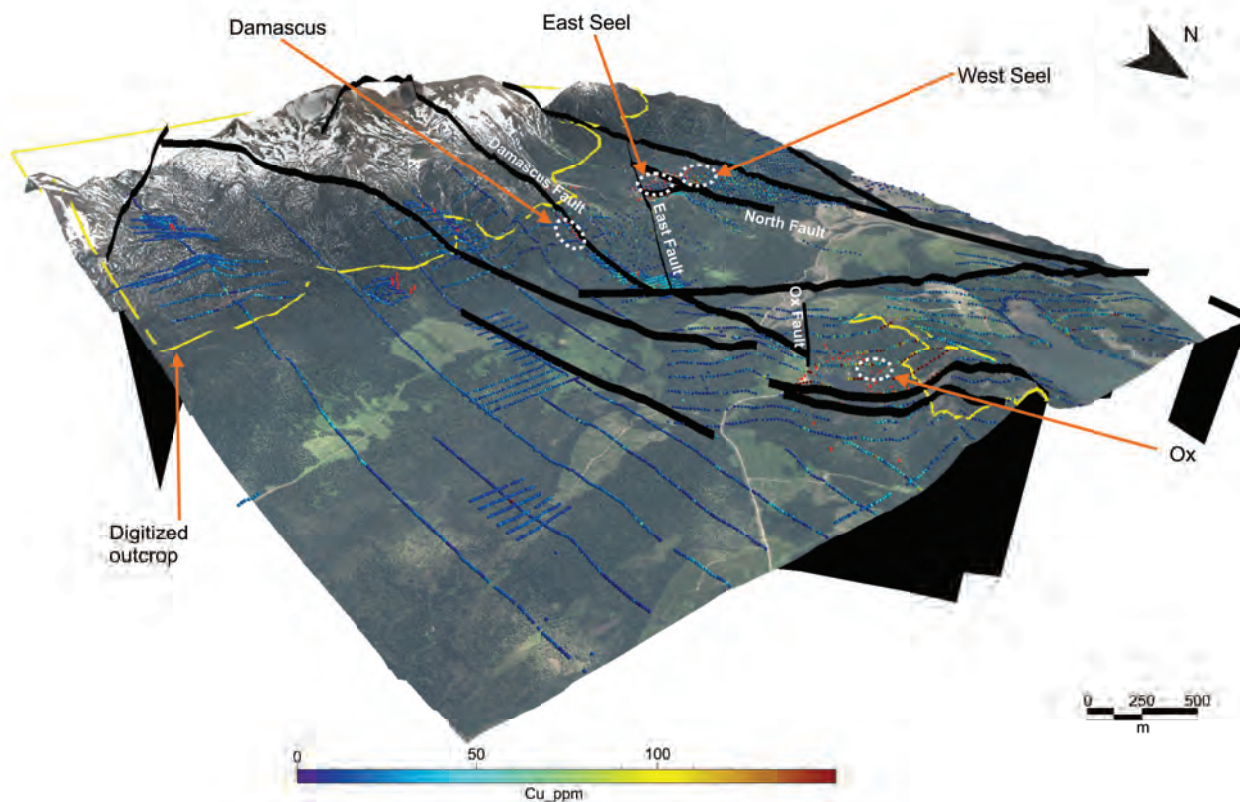


Fig. 4. Digital Surface Model (DSM) created from LiDAR data and a mosaic orthophotograph draped over the topographic surface. Also shown are mineral deposits (surface projection outlined by dotted white circles), faults (black lines), and Cu (ppm) in soils from gridded surveys (colour scale in ppm Cu at the bottom of the figure). The yellow lines enclose areas of digitized bedrock.

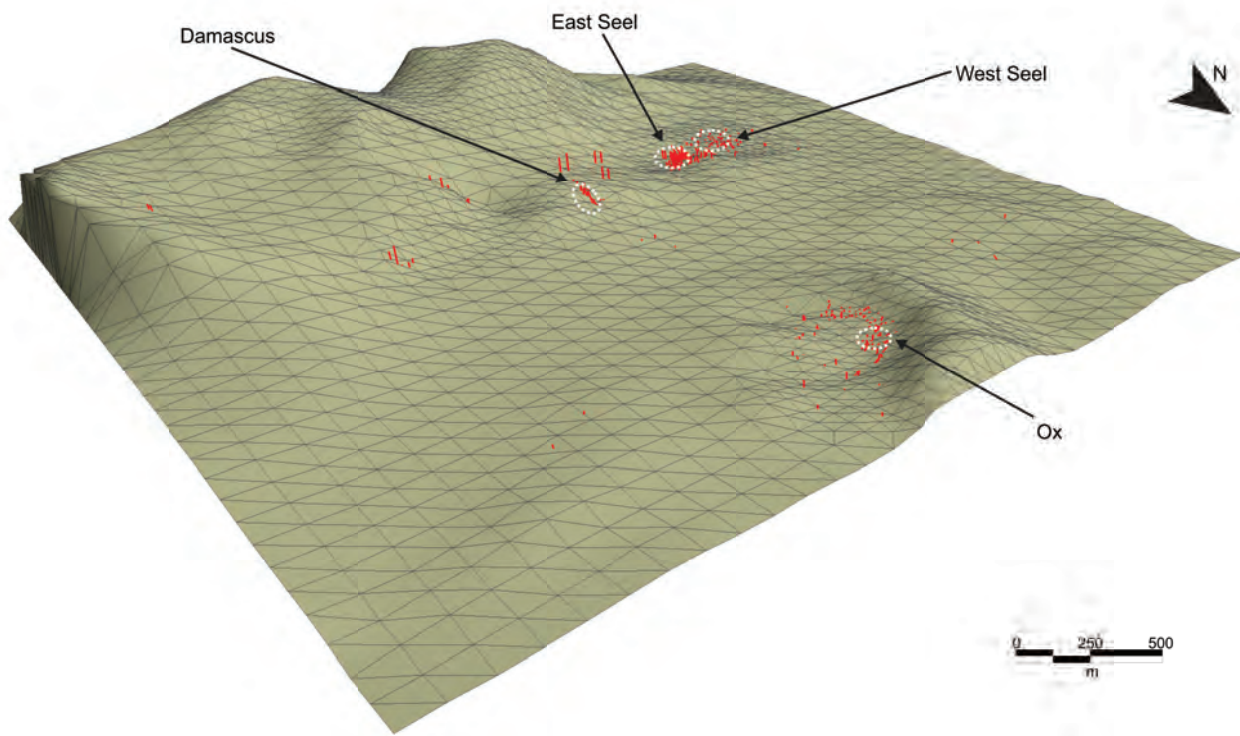


Fig. 5. Bedrock surface (green) modelled using bedrock control points, which comprise digitized bedrock exposures and bedrock-drift contacts (markers) in diamond drillholes (red lines). Also shown are mineral deposits (surface projection outlined by dotted white circles). The 3D view of the block model is the same as in Figure 4.

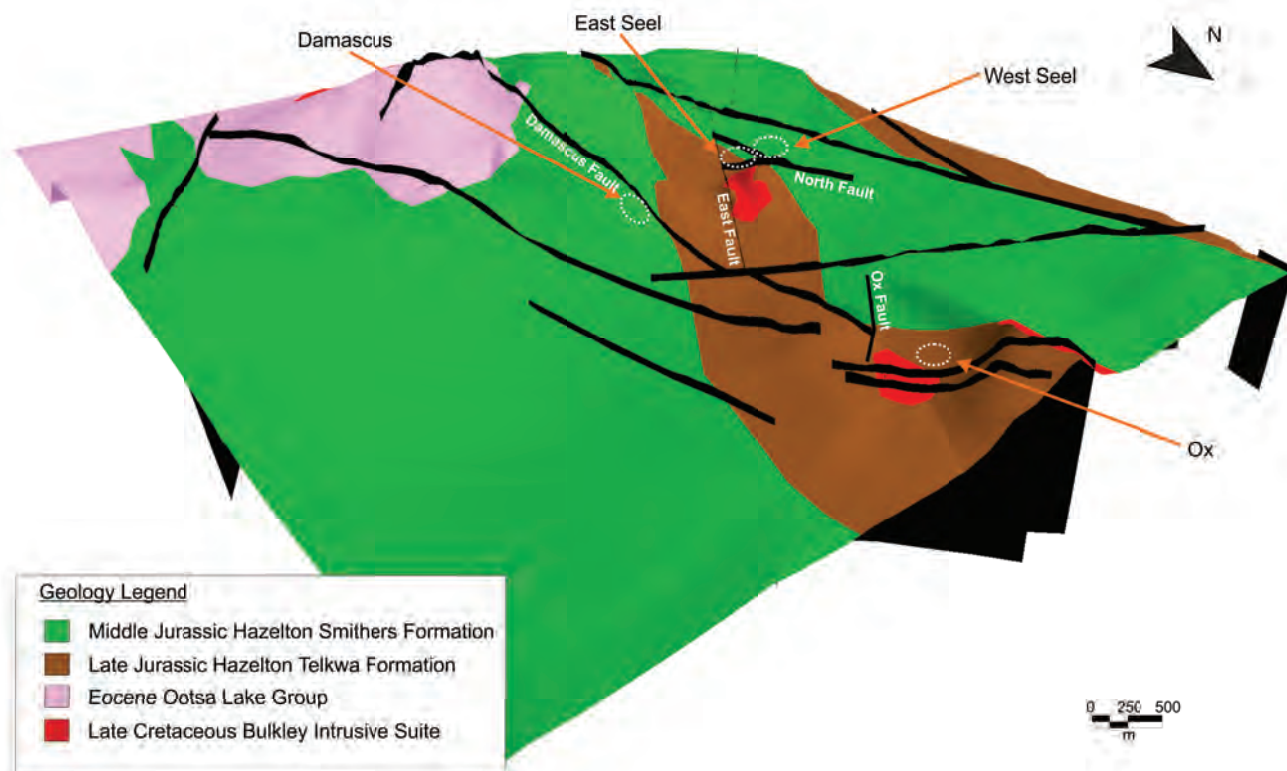


Fig. 6. Faults and local geology draped over the Digital Surface Model (DSM). Geology from the 1:150,000 scale map of Diakow (2006) modified by Gold Reach Resources Ltd. Also shown are mineral deposits (surface projection outlined by dotted white circles). The 3D view of the block model is the same as in Figure 4.

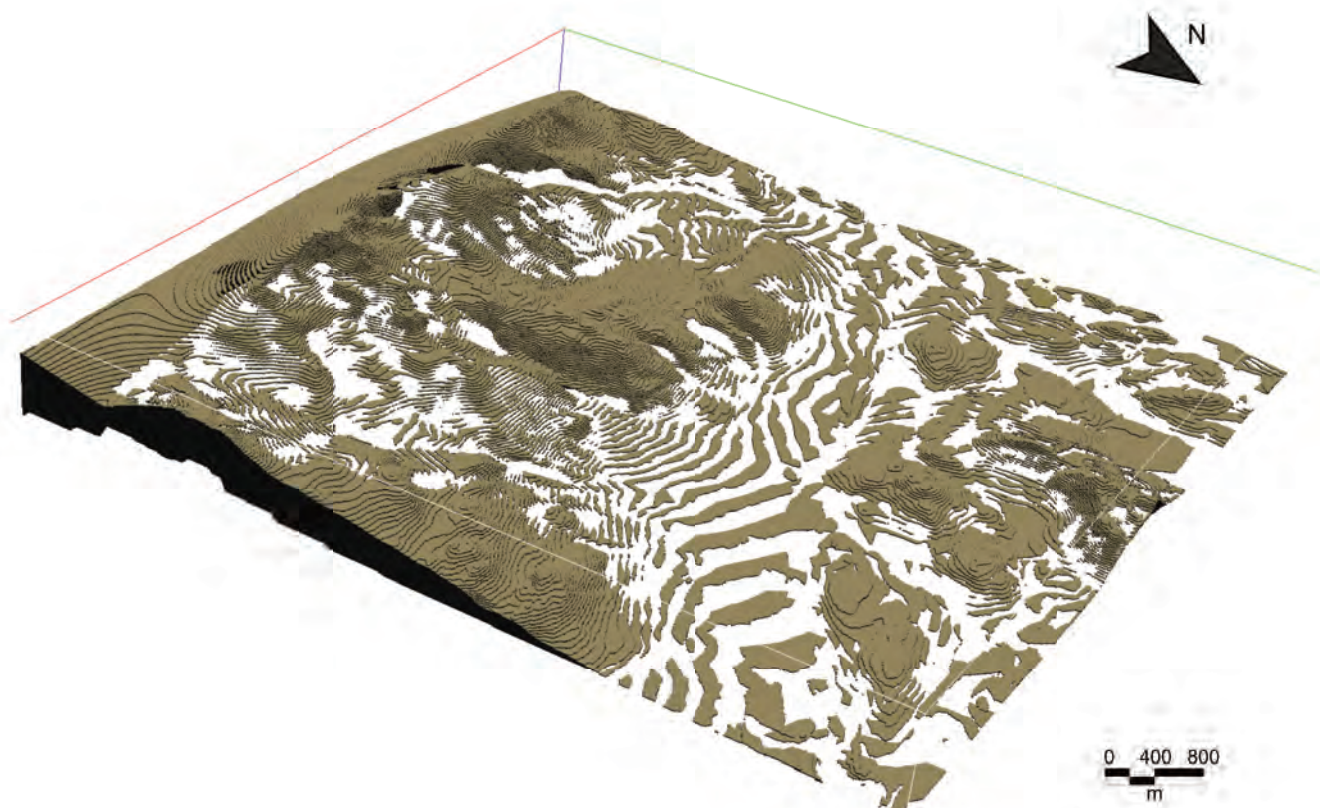


Fig. 7. Block model of drift volume (isopach map) for the Ootsa Lake property. Contour intervals are 10 m. Brown is the volume of drift. White represents areas of no drift. Top of the volume is the surface topography. Base of the volume is the bedrock surface. The 3D view of the block model is the same as in Figure 4.

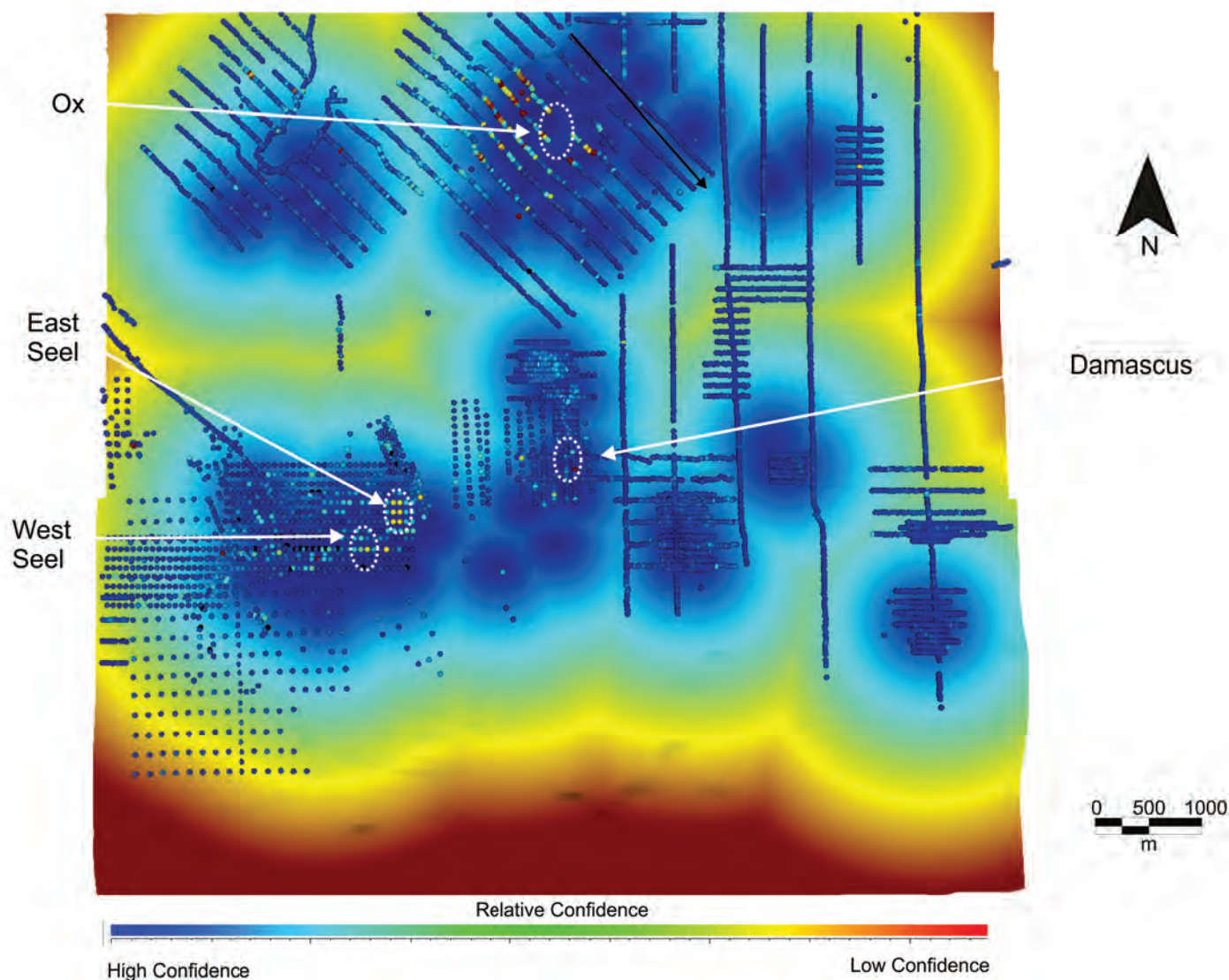


Fig. 8. Shaded confidence map based on the distance of the drift thickness estimate location from bedrock control points. Areas of relatively high confidence are represented by cold colours (blue) that grade to warmer colours (red - danger) in areas of lower confidence. Also shown are mineral deposits (surface projection outlined by dotted white circles), and Cu (ppm) in soils from gridded surveys (colour scale is the same as in Figure 4). The view of the study area is outlined in Figure 3, and is the same as the top of the GOCAD block diagrams shown in Figures 4 to 7.

thicknesses, decreases in intensity of geochemical anomalies, and disappearances of mineralized zones upon crossing a known fault suggest that thick sections of drift fill down-dropped fault blocks, which may contain mineralized stratigraphy. Such areas may be considered good exploration opportunities. The adjacent horsts with shallow drift and geochemical anomalies may indicate mineralized bedrock, potentially near the surface. These targets are easily tested by drilling and follow-up soil sampling (Fig. 9). The depth-to-bedrock map also may be used to identify previously undocumented faults where abrupt changes in drift thickness define a strong linear feature with significant strike length.

6. Limitations of the 3D GOCAD block model

This 3D depth-to-bedrock GOCAD modelling approach is not recommended for areas of rugged topography with highly

variable bedrock elevations because depths of drift can be significantly overestimated. This occurs due to interpolation between topographic surfaces at high elevation and bedrock surfaces with control points at relatively low elevations. The model works best in areas with relatively flat topography such as occur on the Interior Plateaus (e.g., Nechako and Chilcotin) of British Columbia.

A confidence map (Fig. 8) and drillhole location data such as shown on Figure 5 should be used in conjunction with the 3D depth-to-bedrock GOCAD model because it assigns a degree of reliability to the modelled drift estimates. This knowledge can be used to further rank exploration targets. For example, some caution might be advised to drilling a potential exploration target located in an area of shallow drift, but having very poor confidence in the thickness estimate.

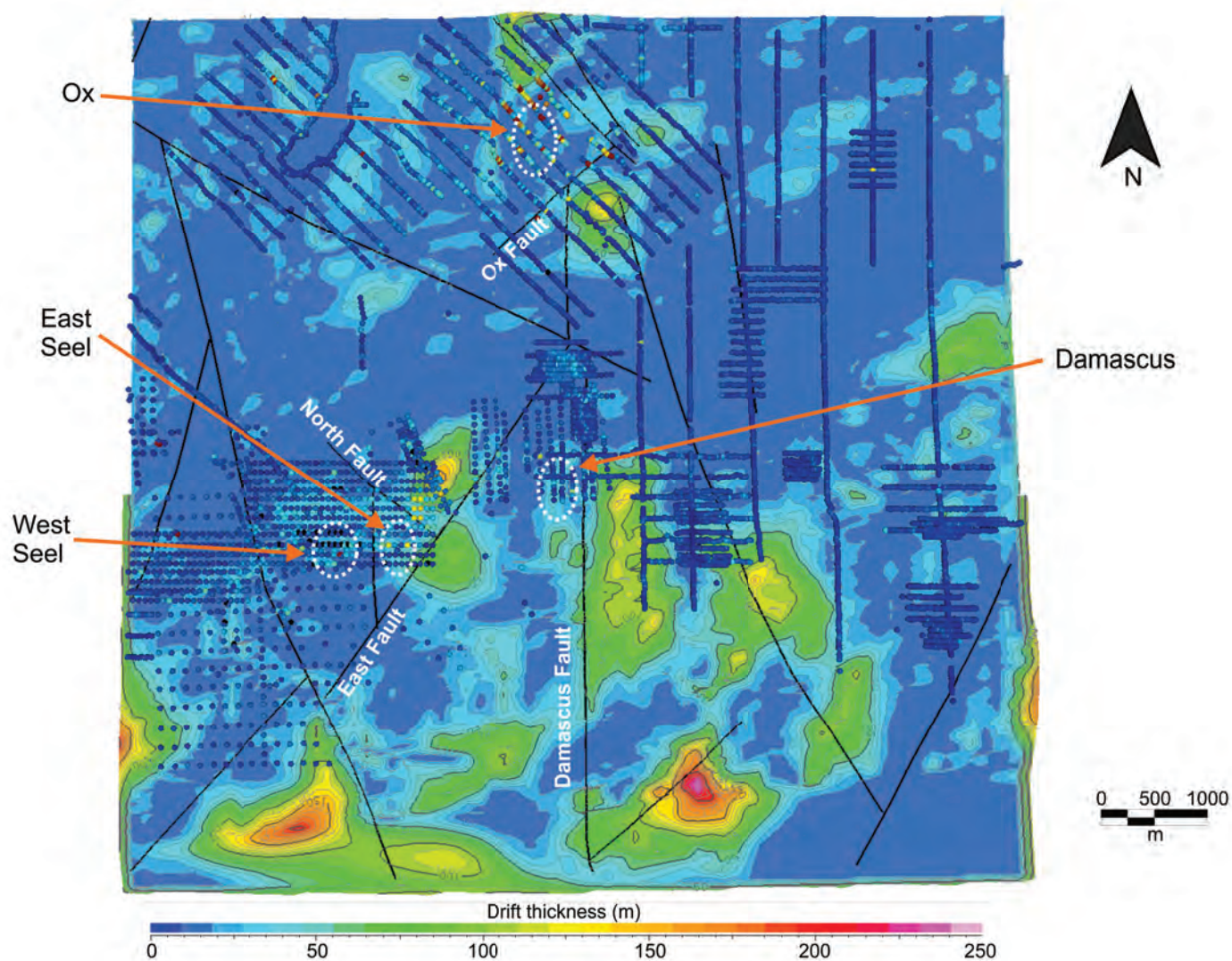


Fig. 9. 3D depth-to-bedrock GOCAD model for the Ootsa Lake project area with contoured thicknesses of drift (10 m intervals), major faults (black lines), locations of mineral deposits (dotted white circles), and Cu (ppm) in soils from gridded surveys (colour scale is the same as in Figure 4). The view of the study area is outlined in Figure 3, and is the same as Figure 8.

7. Conclusions

The 3D GOCAD modelling approach successfully created a depth-to-bedrock model of the Ootsa Lake area using company datasets. When combined with geophysical data (if available), the depth-to-bedrock model is a useful aid in assessing a property for both new and old targets. Specifically, geochemical anomalies in areas of shallow drift are less technically challenging targets and relatively inexpensive to drill. They may rank quite high if the confidence map indicates a high degree of reliability of the drift thickness estimate and are located near known mineralization. However, areas of thick drift with geochemical anomalies that disappear, or show decreased intensity upon crossing a known fault, may indicate down-dropped fault blocks with mineralized stratigraphy. Abrupt changes in drift thickness that define linear features with considerable strike length may signify previously undocumented faults. In summary, constructing a 3D depth-

to-bedrock GOCAD model for an exploration property with significant past and/or ongoing drilling, may provide sufficient digital data to produce an exploration aid at very little cost. It is essentially a data-mining exercise of existing datasets.

Expansion of the Ootsa 3D GOCAD model using data from the Huckleberry Cu-Mo mine to the northwest to build a regional model is possible. However, care will be needed to apply the model only to areas of low topographic relief. Other prospective areas in British Columbia that might benefit from 3D GOCAD modelling include the Woodjam area of south-central British Columbia. This area contains a cluster of large porphyry Cu-Mo-Au deposits in a region with extensive drift and low topographic relief (e.g., del Real et al., 2017). Except for the Southeast Zone porphyry Cu-Mo deposit, all the other porphyry deposits including Deerhorn, Megabuck, Takom and Three Firs (e.g., Vandekerkhove et al., 2014) are buried.

Finally, six potential areas were identified as favourable

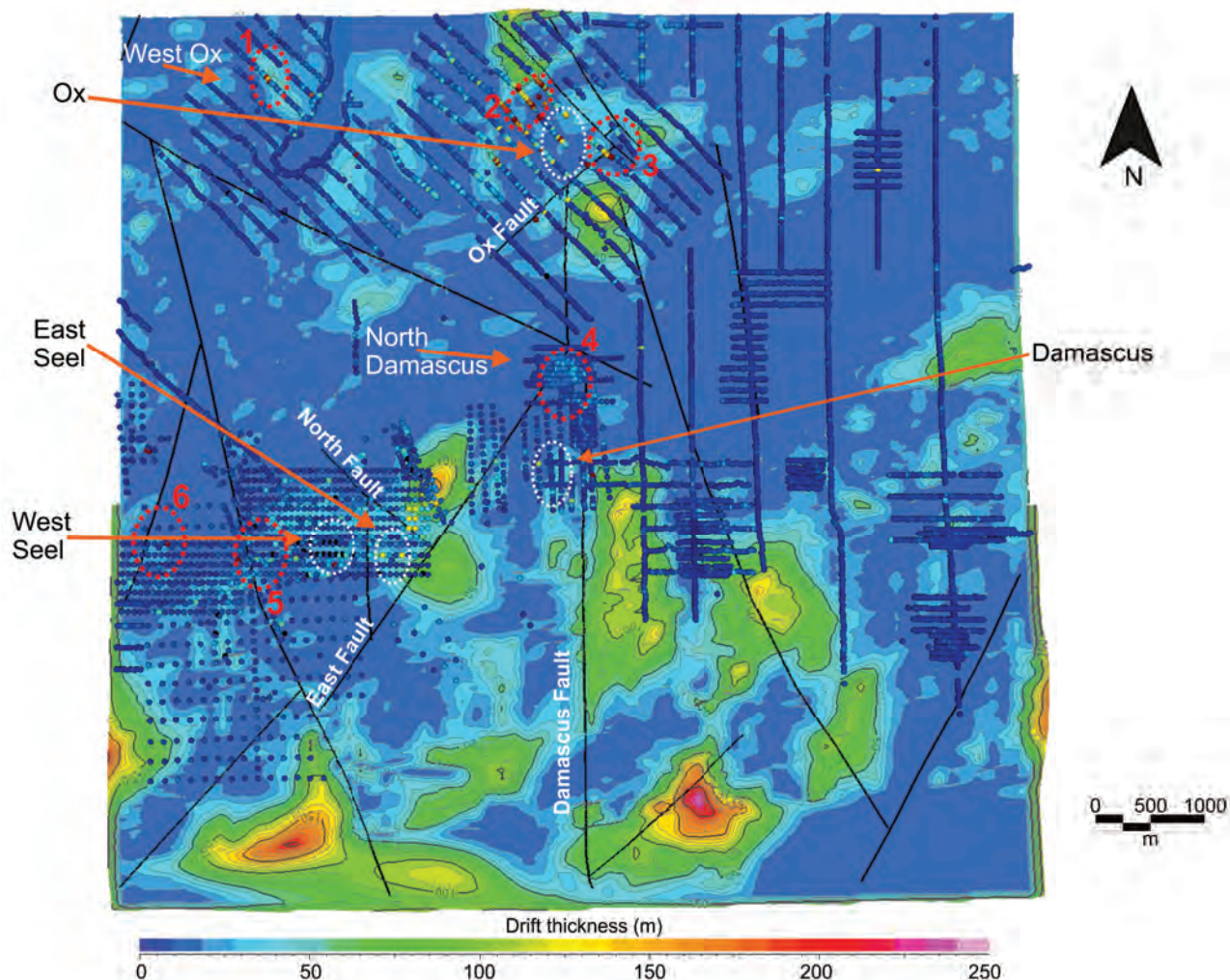


Fig. 10. 3D depth-to-bedrock GOCAD model for the Ootsa Lake project area with potential exploration targets (red circles labelled 1 to 6), contoured thicknesses of drift (10 m intervals), major faults (black lines), locations of mineral deposits (dotted white circles), and Cu (ppm) in soils from gridded surveys (colour scale is the same as in Figure 4). The view of the study area is outlined in Figure 3, and is the same as Figure 9.

targets for future exploration on the Ootsa Lake property (red circles in Fig. 10). For convenience, these selected areas are labelled 1 to 6 on Figure 10. They do not indicate a numerical rank. The selection of these targets was based solely on the data used to build the 3D depth-to-bedrock GOCAD model (i.e., drift thickness, geochemical anomalies, structures and confidence map). These exploration targets were previously identified by Gold Reach Resources Ltd. using soil geochemistry, field mapping, and additional geophysical data (e.g., West Ox and North Damascus). All of these activities are normal components of an advanced exploration project with ongoing regional exploration. We found it encouraging, however, that the 3D GOCAD model also identified these prospective areas and demonstrated that, in the absence of additional data, this simple digital approach has merit as a low-cost method to help evaluate an exploration property.

Acknowledgments

We thank Dr. Shane Ebert of Gold Reach Resources Ltd. for providing access to the Ootsa property, accommodation at the

Seel camp, and the exploration data used in the 3D modelling project. His knowledge of the geology of the Ootsa Lake region and advice on the 3D modelling project are greatly appreciated. Shannon Frey of Mira Geoscience is thanked for helping with GOCAD modelling of the data. Critical reviews by Adrian Hickin and Larry Aspler were very helpful in clarifying our ideas and presentation of the data.

References cited

- Andrews, G.D., Plouffe, A., Ferbey, T., Russell, J.K., Brown, S.R., and Anderson, R.G., 2011. The thickness of Neogene and Quaternary cover across the central Interior Plateau, British Columbia: analysis of water-well drill records and implications for mineral exploration potential. *Canadian Journal of Earth Sciences*, 48, 973-986.
- Bustard, A.L., and Ferbey, T., 2016. An index of base and precious metal regional- to property-scale subglacial till geochemical and mineralogical surveys in British Columbia. British Columbia Ministry of Energy and Mines, British Columbia Geological Survey, Open File 2016-2, scale 1:2,250,000.
- Carter, N.C., 1981. Porphyry copper and molybdenum deposits of west-central British Columbia. British Columbia Ministry of

- Energy, Mines and Petroleum Resources, Bulletin 64, 150 p.
- Currie, L., and Parrish, R., 1997. Paleozoic and Mesozoic rocks of Stikinia exposed in northwestern British Columbia: Implications for correlations in the northern Cordillera. *Geological Society of America Bulletin*, 109, 1402-1420.
- del Real, I., Bouzari, F., Rainbow, A., Bissig, T., Blackwell, J., Sherlock, R., Thompson, J.F.H., and Hart, C.J.R., 2017. Spatially and temporally associated porphyry deposits with distinct Cu/Au/Mo ratios, Woodjam district, central British Columbia. *Economic Geology*, 112, 1673-1717.
- Diakow, L.J., 2006. Geology of the Tahtsa Ranges between Eutsuk Laker and Morice Lake, Whitesail Lake map area, west-central British Columbia. British Columbia Ministry of Energy, Mines, and Petroleum Resources, British Columbia Geological Survey Geoscience Map 2006-5, scale 1:150,000.
- Ferbey, T., 2010. Quaternary geology and till geochemistry of the Nadina River map area (NTS 093E/15), west-central British Columbia. In: *Geological Fieldwork 2009*, British Columbia Ministry of Energy, Mines and Petroleum Resources, British Columbia Geological Survey Paper 2010-1, pp. 43-54.
- Ferbey, T., and Levson, V.M., 2001a. Ice-flow history of the Tahtsa Lake-Ootsa Lake region. British Columbia Ministry of Energy, Mines and Petroleum Resources, Open File 2001-8, scale 1:110,000.
- Ferbey, T., and Levson, V.M., 2001b. Quaternary geology and till geochemistry of the Huckleberry mine area. In: *Geological Fieldwork 2000*, British Columbia Ministry of Energy, Mines, and Petroleum Resources, British Columbia Geological Survey Paper 2001-1, pp. 397-410.
- Friedman, R.M., and Jordan, S., 1997. U-Pb ages for intrusive rocks at the Huckleberry porphyry copper deposit, Tahtsa Lake District, Whitesail Lake map area, west-central British Columbia (93E111). In: *Geological Fieldwork 1996*, British Columbia Ministry of Energy, Mines and Petroleum Resources, British Columbia Geological Survey Paper 1997-1, pp. 219-225.
- Hickin, A.S., and Kerr, B., 2005. Bedrock topography mapping and shallow gas in northeastern BC. In: *Summary of Activities 2004*, British Columbia Ministry of Energy, Mines and Petroleum Resources, Resource Development and Geoscience Branch, pp. 75-82.
- Hickin, A.S., and Plouffe, A., 2017. Sampling and interpreting stream, lake, and glacial sediments for mineral exploration in the Canadian Cordillera, a review. In: Ferbey, T., Plouffe, A., and Hickin, A.S., (Eds.), *Indicator Minerals in Till and Stream Sediments of the Canadian Cordillera*. Geological Association of Canada Special Paper Volume 50, and Mineralogical Association of Canada Topics in Mineral Sciences Volume 47, pp. 27-51.
- Hickin, A.S., Best, M.E., and Pugin, A., 2016. Geometry and valley-fill stratigraphic framework for aquifers in the Groundbirch paleovalley assessed through shallow seismic and ground-based electromagnetic surveys. British Columbia Ministry of Energy and Mines, British Columbia Geological Survey Open File 2016-5, 46 p.
- Hickin, A.S., Kerr, B., Turner, D.G., and Barchyn, T.E., 2008. Mapping Quaternary paleovalleys and drift thickness using petrophysical logs, northeast British Columbia, Fontas map sheet, NTS 941. *Canadian Journal of Earth Sciences*, 45, 577-591.
- Imperial Metals Corporation, 2014. Annual information form for the year ended December 31, 2013. Imperial Metals Corporation, pp. 16-20.
- Jackson, A., and Illerbrun, K., 1996. The Huckleberry porphyry copper deposit, Tahtsa Lake district, west-central British Columbia. In: T.G. Schroeter, (Ed.), *Porphyry Deposits of the Northwestern Cordillera of North America*. Canadian Institute of Mining, Metallurgy and Petroleum, 46, pp. 313-321.
- Lepit, M.E., Mortensen, J.K., Friedman, R.M., and Jordan, S.J., 1998. Geology and U-Pb geochronology of intrusive rocks associated with mineralization in the northern Tahtsa Lake District. In: *Geological Fieldwork 1997*, British Columbia Ministry of Energy, Mines and Petroleum Resources, British Columbia Geological Survey Paper 1998-1, pp. 321-329.
- Levorsen, A.I., 1967. *Geology of petroleum*, second edition. W.H. Freeman and Company, San Francisco, 724 p.
- Levson, V.M., 2002. Quaternary geology and till geochemistry of the Babine porphyry copper belt, B.C. (NTS 093L/9, 16; M/1, 2, 7 & 8). British Columbia Ministry of Energy and Mines, Bulletin 110, 273 p.
- Levson, V.M., Hickin, A.S., Ferbey, T., and Best, M., 2006. Mapping with high resistivity buried channel deposits with airborne electromagnetic surveys and other methods. In: *Proceedings of the 19th Annual Symposium on the Application of Geophysics to Engineering and Environmental Problems*, Seattle, Washington, pp. 152-161.
- MacIntyre, D., 1985. Geology and mineral deposits of the Tahtsa Lake district, west-central British Columbia. British Columbia Ministry of Energy, Mines and Petroleum Resources, Bulletin 75, 90 p.
- Mao, M., Rukhlov, A.S., Rowins, S.M., Hickin, A.S., Ferbey, T., Bustard, A., Spence, J., and Coogan, L.A., 2017. A novel approach using detrital apatite and till geochemistry to identify covered mineralization in the TREK area of the Nechako Plateau, British Columbia. In: Ferbey, T., Plouffe, A., and Hickin, A.S., (Eds.), *Indicator Minerals in Till and Stream Sediments of the Canadian Cordillera*. Geological Association of Canada Special Paper Volume 50, and Mineralogical Association of Canada Topics in Mineral Sciences Volume 47, pp. 191-243.
- McDowell, C., and Giroux, G., 2013. Mineral resources estimate update for the Seel and Ox deposits. NI-43-101 Technical Report for Gold Reach Resources Ltd., July, 2013, 168 p., <http://www.goldreachresources.com>.
- McGaughey, J., 2003. The application of GOCAD to geochemical interpretation in mineral exploration. *Explore*, 120, 17-18.
- Petersen, R.T., 2014. A petrographic and geochemical description and characterization of the Cu-Au East Seel and Cu-Au-Mo West Seel porphyry deposits, British Columbia, Canada. Unpublished M.Sc. thesis, Copenhagen University, 67 p.
- Tearpock, D.J., and Bischke, R.E., 2002. *Applied subsurface geological mapping with structural Methods (2nd Edition)*, Prentice-Hall, Englewood Cliffs, 822 p.
- Vandekerkhove, S., Rowins, S.M., and Johnston, S.T., 2014. Geology and physiochemical conditions of copper-gold mineralization at the Three Firs porphyry prospect, Woodjam district, south-central, British Columbia. In: *Geological Fieldwork 2013*, British Columbia Ministry of Energy, Mines and Petroleum Resources, British Columbia Geological Survey Paper 2014-1, pp. 67-94.

Appendix: British Columbia Geological Survey publications and peer-reviewed journal papers authored by BCGS staff and released in 2017

All BCGS publications are available for download, free of charge, from:

www.empr.gov.bc.ca/Mining/Geoscience/PublicationsCatalogue/Pages/default.aspx

To receive notification of our latest releases email:

Geological.Survey@gov.bc.ca



Papers

Paper 2017-1

Geological fieldwork 2016, a summary of field activities and current research, 234 p.

Hickin, A.S., Jones, L.D., and Clarke, G., 2017. British Columbia Geological Survey annual program review 2016-2017. In: Geological Fieldwork 2016, British Columbia Ministry of Energy and Mines, British Columbia Geological Survey Paper 2017-1, pp. 1-16.

Schiarizza, P., 2017. Ongoing stratigraphic studies in the Nicola Group: Stump Lake – Salmon River area, south-central British Columbia. In: Geological Fieldwork 2016, British Columbia Ministry of Energy and Mines, British Columbia Geological Survey Paper 2017-1, pp. 17-33.

Angen, J.J., Nelson, J.L., Rahimi, M. and Hart, C.J.R., 2017. Mapping in the Tatsi and Zymo ridge areas of west-central British Columbia: Implications for the origin and history of the Skeena Arch. In: Geological Fieldwork 2016, British Columbia Ministry of Energy and Mines, British Columbia Geological Survey Paper 2017-1, pp. 35-48.

Ootes, L., Elliott, J.M., and Rowins, S.M., 2017. Testing the relationship between the Llewellyn fault, gold mineralization, and Eocene volcanism in northwest British Columbia: A preliminary report. In: Geological Fieldwork 2016, British Columbia Ministry of Energy and Mines, British Columbia Geological Survey Paper 2017-1, pp. 49-59.

Nelson, J., 2017. Composite pericratonic basement of west-central Stikinia and its influence on Jurassic magma conduits: Examples from the Terrace-Ecstall and Anyox areas. In: Geological Fieldwork 2016, British Columbia Ministry of Energy and Mines, British Columbia Geological Survey Paper 2017-1, pp. 61-82.

van Straaten, B.I., and Gibson, R., 2017. Late Early to Middle Jurassic Hazelton Group volcanism and mineral occurrences in the McBride-Tanzilla area, northwest British Columbia. In: Geological Fieldwork 2016, British Columbia Ministry of Energy and Mines, British Columbia Geological Survey Paper 2017-1, pp. 83-115.

Milidragovic, D., Zagorevski, A., and Chapman, J.B., 2017. The Mount Hickman ultramafic complex: An Fe-rich Alaskan-type ultramafic intrusion. In: Geological Fieldwork 2016, British Columbia Ministry of Energy and Mines, British Columbia Geological Survey Paper 2017-1, pp. 117-132.

Zagorevski, A., Mihalyuk, M.G., Joyce, N., and Anderson, R.G., 2017. Late Cretaceous magmatism in the Atlin-Tagish area, northern British Columbia (104M, 104N). In: Geological Fieldwork 2016, British Columbia Ministry of Energy and Mines, British Columbia Geological Survey Paper 2017-1, pp. 133-152.

Mihalynuk, M.G., Zagorevski, A., English, J.M., Orchard, M.J., Bidgood, A.K., Joyce, N., and Friedman, R.M., 2017. Geology of the Sinwa Creek area (104K/14). In: Geological Fieldwork 2016, British Columbia Ministry of Energy and Mines, British Columbia Geological Survey Paper 2017-1, pp. 153-178.

Mihalynuk, M.G., Zagorevski, A., Devine, F.A.M., and Humphrey, E., 2017. A new lode gold discovery at Otter Creek: Another source for the Atlin placers. In: Geological Fieldwork 2016, British Columbia Ministry of Energy and Mines, British Columbia Geological Survey Paper 2017-1, pp. 179-193.

Green, C., Simandl, G.J., Paradis, S., Katay, F., Hoshino, M., Kon, Y., Kodama, S., and Graf, C., 2017. Geological setting of the Rock Canyon Creek REE-fluorite deposit, British Columbia, Canada In: Geological Fieldwork 2016, British Columbia Ministry of Energy and Mines, British Columbia Geological Survey Paper 2017-1, pp. 195-203.

Hoshino, M., Kon, Y., Kodama, S., Simandl, G.J., Paradis, S., Green, C., Namatame, C., Matsunaga, I., and Takagi, T., 2017. Mineralogy of the Rock Canyon Creek REE-fluorite deposit, British Columbia, Canada. In: Geological Fieldwork 2016, British Columbia Ministry of Energy and Mines, British Columbia Geological Survey Paper 2017-1, pp. 205-213.

Arnold, H., and Hickin, A.S., 2017. Using derived-stereo imagery to map macroscale ice-flow features. In: Geological Fieldwork 2016, British Columbia Ministry of Energy and Mines, British Columbia Geological Survey Paper 2017-1, pp. 215-229.

Appendix: British Columbia Geological Survey publications and peer-reviewed journal papers authored by BCGS staff and released in 2016, pp. 231-234.

Geoscience Maps

GM 2017-1

Nixon, G.T., Scheel, J.E., Friedman, R.M., Wall, C.J., Gabites, J., Miller, D., and Scoates, J.S., 2017. Geology and geochronology of the Turnagain ultramafic-mafic intrusion, British Columbia, 1:10,000 scale.

GM 2017-2

Boulanger, O., and Kiss, F., 2017. Aeromagnetic survey of the Llewellyn area, NTS 104-M/8 and parts of 104-M/1,2,6,7, British Columbia, residual total magnetic field, sheet 1 of 2, 1:100,000 scale and digital data (also published as Geological Survey of Canada, Open File 8287).

Boulanger, O., and Kiss, F., 2017. Aeromagnetic survey of the Llewellyn area, NTS 104-M/8 and parts of 104-M/1,2,6,7, British Columbia, first vertical derivative of the magnetic field, sheet 2 of 2, 1:100,000 scale and digital data (also published as Geological Survey of Canada, Open File 8290).

GM 2017-4

Boulanger, O., and Kiss, F., 2017. Aeromagnetic survey of the Llewellyn area, NTS 104-M/9,10,15,16 and parts of 104-M/11,14, British Columbia, residual total magnetic field. sheet 1 of 2, 1:100,000 scale and digital data (also published as Geological Survey of Canada, Open File 8288).

Boulanger, O., and Kiss, F., 2017. Aeromagnetic survey of the Llewellyn area, NTS 104-M/9,10,15,16 and parts of 104-M/11,14, British Columbia, first vertical derivative of the magnetic field, sheet 2 of 2, 1:100,000 scale and digital data (also published as Geological Survey of Canada, Open File 8291).

Open Files

OF 2017-1

Clarke, G., Britton, J., Jago, P., Katay, F., and Northcote, B., 2017. Selected exploration projects and operating mines in British Columbia, 2016.

OF 2017-2

Sacco, D., Arnold, H., Ferbey, T., and Jackaman, W., 2017. Basal till potential of the Anahim Lake map area (NTS 093C/06), British Columbia, 1:50,000 scale (also published as Geoscience BC Map 2017-02-01).

OF 2017-3

Sacco, D., Arnold, H., Ferbey, T., and Jackaman, W., 2017. Basal till potential of the Satah Mountain map area (NTS 093C/07), British Columbia, 1:50,000 scale (also published as Geoscience BC Map 2017-02-02).

OF 2017-4

Sacco, D., Arnold, H., Ferbey, T., and Jackaman, W., 2017. Basal till potential of the Downton Creek map area (NTS 093C/10), British Columbia, 1:50,000 scale (also published as Geoscience BC Map 2017-02-03).

OF 2017-5

Sacco, D., Arnold, H., Ferbey, T., and Jackaman, W., 2017. Basal till potential of the Christensen Creek map area (NTS 093C/11), British Columbia. 1:50,000 scale (also published as Geoscience BC Map 2017-02-04).

2017-6

Sacco, D., Arnold, H., Ferbey, T., and Jackaman, W., 2017. Basal till potential of the Carnlick Creek map area (NTS 093C/14), British Columbia, 1:50,000 scale (also published as Geoscience BC Map 2017-02-05).

2017-7

Sacco, D., Arnold, H., Ferbey, T., and Jackaman, W., 2017. Basal till potential of the Kushya River map area (NTS 093C/15), British Columbia, 1:50,000 scale (also published as Geoscience BC Map 2017-02-06).

OF 2017-8

Cui, Y., Miller, D., Schiarizza, P., and Diakow, L.J., 2017. British Columbia digital geology, 9 p.

OF 2017-9

van Straaten, B.I., Gibson, R., and Nelson, J., 2017. Preliminary bedrock geology of the Tanzilla and McBride area, 1:50,000 scale.

GeoFiles

GF 2017-1

Nelson, J.L. and Friedman, R. 2017. U-Pb and geochemical data from late Paleozoic and Jurassic rocks of western Stikinia and the Coast Mountains.

GF 2017-2

Rukhlov, A.S., Rowins, S.M., Mao, M., Coogan, L.A., and Spence, J. Apatite compositions as a proxy for the oxidation states of porphyry Cu-Mo-Au deposits. (Poster)

GF 2017-3

Cui, Y., Zhao, S., Jones, L., Fortin, G., and Meredith-Jones, S. Up to speed on MapPlace 2. (Poster)

GF 2017-4

Milidragovic, D., Zagorevski, A., and Chapman, J. The Mount Hickman ultramafic complex, northwestern British Columbia: An Fe-rich Alaskan-type intrusion. (Poster)

GF 2017-5

Bustard, A., Ferbey, T., and Levson, V.M. New till geochemical targets for potential porphyry Cu±Mo±Au mineralization in the Pendleton Bay area. (Poster)

GF 2017-6

Han, T., Rukhlov, A. S., Naziri, M., and Moy, A., New British Columbia litho-geochemical database: Development and preliminary data release. (Poster)

GF 2017-7

Green, C., Simandl, G.J., Paradis, S., Katay, F., Hoshino, M., Kon, Y., Kodama, S., and Graf, C. Geological Setting of the Rock Canyon Creek REE-Fluorite Deposit, BC, Canada. (Poster)

GF 2017-8

Hoshino, M., Kon, Y., Kodama, S., Simandl G.J., Namatame, C., Matsunaga, I., and Takagi, T. Mineralogy of the Rock Canyon Creek REE-fluorite deposit, British Columbia, Canada. (Poster)

GF 2017-10

Riddell, J., and Han, T., 2017. Ash chemistry database for British Columbia Rocky Mountain bituminous coals, 15 p.

GF 2017-11

Han, T. and Rukhlov, A.S., 2017. Regional Geochemical Survey (RGS) data update and release using the newly developed RGS database, 7 p.

GF 2017-12

Milidragovic, D., Zagorevski, A., Weis, D., 2017. Unravelling arc mantle using trace element and isotopic intelligence from the Middle-Late Triassic Stikine arc. (Poster)

Information Circulars

IC 2017-1

Clarke, G., Britton, J., Jago, P., Katay, F., and Northcote, B., 2017. Provincial overview of exploration and mining in British Columbia, 2016. British Columbia Ministry of Energy and Mines, British Columbia Geological Survey Information Circular 2017-1, 169 p.

Clarke, G., Britton, J., Jago, P., Katay, F., and Northcote, B., 2017. Exploration and Mining in British Columbia, 2016: A summary. In: Provincial Overview of Exploration and Mining in British Columbia, 2016. British Columbia Ministry of Energy and Mines, British Columbia Geological Survey, Information Circular 2017-1, pp. 1-29.

Northcote, B., 2017. Exploration and mining in the Southwest Region, British Columbia. In: Exploration and Mining in British Columbia, 2016. British Columbia Ministry of Energy and Mines, British Columbia Geological Survey, Information Circular 2017-1, pp. 133-147.

Mineral Development Office, 2017. Exploration and mining in the Northwest Region, British Columbia. In: Exploration and Mining in British Columbia, 2016. British Columbia Ministry of Energy and Mines, British Columbia Geological Survey, Information Circular 2017-1, pp. 149-169.

IC 2017-2

British Columbia Geological Survey, 2017. British Columbia Coal Industry Overview 2016, 14 p.

IC 2017-3

Cui, Y., Fortin, G., Meredith-Jones, S., Zhao, S., and Jones, L., 2017. MapPlace 2 (beta) workshop. British Columbia Ministry of Energy and Mines, British Columbia Geological Survey Information Circular 2017-3, 9 p.

IC 2017-4

British Columbia Geological Survey. (Brochure)

IC 2017-5

Online databases at the British Columbia Geological Survey. (Brochure)

IC 2017-6

Mineral Development Office. (Brochure)

Peer-reviewed journal publications

Ferbey, T., Plouffe, A., and Hickin, A.S. (Editors) 2017. Indicator Minerals in Till and Stream Sediments of the Canadian Cordillera. Geological Association of Canada Special Paper Volume 50, and Mineralogical Association of Canada Topics in Mineral Sciences Volume 47, 243 p.

Hickin, A.S., Ward, B.C., Plouffe, A., and Nelson, J., 2017. Introduction to the geology, physiography, and glacial history of the Canadian Cordillera in British Columbia and Yukon. In: Ferbey, T., Plouffe, A., and Hickin, A.S., (Eds.), Indicator Minerals in Till and Stream Sediments of the Canadian Cordillera. Geological Association of Canada Special Paper Volume 50, and Mineralogical Association of Canada Topics in Mineral Sciences Volume 47, pp. 1-25.

Hickin, A.S., and Plouffe, A., 2017. Sampling and interpreting stream, lake, and glacial sediments for mineral exploration in the Canadian Cordillera, a review. In: Ferbey, T., Plouffe, A., and Hickin, A.S., (Eds.), Indicator Minerals in Till and Stream Sediments of the Canadian Cordillera. Geological Association of Canada Special Paper Volume 50, and Mineralogical Association of Canada Topics in Mineral Sciences Volume 47, pp. 27-51.

- Lett, R., and Rukhlov, A.S., 2017. A review of analytical methods for regional geochemical survey (RGS) programs in the Canadian Cordillera. In: Ferbey, T., Plouffe, A., and Hickin, A.S., (Eds.), Indicator Minerals in Till and Stream Sediments of the Canadian Cordillera. Geological Association of Canada Special Paper Volume 50, and Mineralogical Association of Canada Topics in Mineral Sciences Volume 47, pp. 53-108.
- Lian, O.B., and Hickin, A.S., 2017. Origin and character of till and other diamictos and their applicability to mineral prospecting. In: Ferbey, T., Plouffe, A., and Hickin, A.S., (Eds.), Indicator Minerals in Till and Stream Sediments of the Canadian Cordillera. Geological Association of Canada Special Paper Volume 50, and Mineralogical Association of Canada Topics in Mineral Sciences Volume 47, pp. 109-127.
- Plouffe, A., and Ferbey, T., 2017. Porphyry Cu indicator minerals in till: A method to discover buried mineralization. In: Ferbey, T., Plouffe, A., and Hickin, A.S., (Eds.), Indicator Minerals in Till and Stream Sediments of the Canadian Cordillera. Geological Association of Canada Special Paper Volume 50, and Mineralogical Association of Canada Topics in Mineral Sciences Volume 47, pp. 129-159.
- Canil, D., Pisiak, L., Lacourse, T., Plouffe, A., Ferbey, T., and Grondahl, C., 2017. Magnetite as an indicator mineral in porphyry Cu±Au±Mo deposits of British Columbia, Canada. In: Ferbey, T., Plouffe, A., and Hickin, A.S., (Eds.), Indicator Minerals in Till and Stream Sediments of the Canadian Cordillera. Geological Association of Canada Special Paper Volume 50, and Mineralogical Association of Canada Topics in Mineral Sciences Volume 47, pp. 161-174.
- Simandl, G.J., Mackay, D.A.R., Ma, X., Luck, P., Gravel, J., and Akam, C., 2017. The direct indicator mineral concept and QEMSCAN® applied to exploration for carbonatite and carbonatite-related ore deposits. In: Ferbey, T., Plouffe, A., and Hickin, A.S., (Eds.), Indicator Minerals in Till and Stream Sediments of the Canadian Cordillera. Geological Association of Canada Special Paper Volume 50, and Mineralogical Association of Canada Topics in Mineral Sciences Volume 47, pp. 175-190.
- Mao, M., Rukhlov, A.S., Rowins, S.M., Hickin, A.S., Ferbey, T., Bustard, A., Spence, J., and Coogan, L.A., 2017. A novel approach using detrital apatite and till geochemistry to identify covered mineralization in the TREK area of the Nechako Plateau, British Columbia. In: Ferbey, T., Plouffe, A., and Hickin, A.S., (Eds.), Indicator Minerals in Till and Stream Sediments of the Canadian Cordillera. Geological Association of Canada Special Paper Volume 50, and Mineralogical Association of Canada Topics in Mineral Sciences Volume 47, pp. 191-243.
- Haugaard, R., Ootes, L., Heaman, L.M., Hamilton, M.A., Shaulis, B., and Konhauser, K., 2017. Depositional timing of Neoproterozoic turbidites of the Slave craton – recommended nomenclature and type localities. *Canadian Journal of Earth Sciences*, 54, 15-32.
- Haugaard, R., Ootes, L., and Konhauser, K., 2017. Neoproterozoic banded iron formation within a ~2620 Ma turbidite-dominated deep water basin, Slave craton, NW Canada. *Precambrian Research*, 292, 130-151.
- Huntley, D.H., Hickin, A.S., and Lian, O.B., 2017. The pattern and style of deglaciation at the Late Wisconsinan Laurentide and Cordilleran ice sheet limits in northeastern British Columbia. *Canadian Journal of Earth Sciences*, 54, 52-75.
- Manor, M.J., Scoates, J.S., Wall, C.J., Nixon, G.T., Friedman, R.M., Amini, M., and Ames, D.E., 2017. Age of the Late Cretaceous ultramafic-hosted Giant Mascot Ni-Cu-PGE deposit, southern Canadian Cordillera: Integrating CA-ID-TIMS and LA-ICP-MS U-Pb geochronology and trace element geochemistry of zircon. *Economic Geology*, 112, 1395-1418.
- Milidragovic, D., Beaudoin, G., Hamilton, M.A., and King, J.J., 2017. Corrigendum to “The Paleoproterozoic Otish Gabbro suite and coeval dyke swarms of the Superior Province: Probing the ca. 2.17 Ga mantle” [*Precambrian Res.* 278 (2016) 126-144]. *Precambrian Research* 301, 195-197.
- Nixon, G.T., Scheel, J.E., Friedman, R.M., Wall, C.J., Gabites, J., Jackson-Brown, S., and Scoates, J.S., 2017. Staged emplacement of the Turnagain Alaskan-type ultramafic-mafic intrusion, British Columbia, Canada: implications for Ni-Cu-PGE mineralization and the origin of zoned complexes. *Society for Geology Applied to Mineral Deposits*, 14th Biennial Meeting, v. 2, 555-558.
- Ootes, L., Jackson, V.A., Davis, W.J., Bennett, V., Smar, L., and Cousens, B.L., 2017. Parentage of Archean basement within a Paleoproterozoic orogen and implications for on-craton diamond preservation: Slave craton and Wopmay orogen, northwest Canada. *Canadian Journal of Earth Sciences*, 54, 203-232.

Ootes, L., Jackson, V.A., Davis, W.J., Bennett, V.C., Smar, L., and Cousens, B.C., 2017. Parentage of Archean basement within a Paleoproterozoic orogen and implications for on-craton diamond preservation: Slave craton and Wopmay orogen, NW Canada. *Canadian Journal of Earth Sciences*, 54,173-202.

Ootes, L., Snyder, D., Davis, W.J., Acosta-Góngora, P., Corriveau, L., Mumin, A.H., Gleeson, S.A., Samson, I.M., Montreuil, J.-F., Potter, E., and Jackson, V.A., 2017, A Paleoproterozoic Andean-type iron oxide copper-gold environment, the Great Bear magmatic zone, NW Canada. *Ore Geology Reviews*, 81, 123-139.

Pisiak, L.K., Canil, D., Plouffe, A., Ferbey, T., and Lacourse, T., 2017. Magnetite as an indicator mineral in the exploration of porphyry deposits: A case study in till near the Mount Polley Cu-Au Deposit, British Columbia, Canada. *Society of Economic Geologists, Special Publication 112*, 919-940.

Sigloch, K., and Mihalynuk, M.G., 2017. Mantle and geological evidence for a Late Jurassic–Cretaceous suture spanning North America. *Geological Society of America Bulletin*, 129, 1489-1520.
<https://ora.ox.ac.uk/objects/uuid:0edbd710-ba27-4aa4-a257-d79b43a84781>.

Contributions to partner publications

Castonguay, S., Ootes, L., Mercier-Langevin, P., Rowins, S.M., Devine, F., 2017. Orogenic gold along Cordilleran faults: key characteristics and analogies between Phanerozoic and Archean settings. In: Rogers, N., (Ed.), Targeted Geoscience Initiative, 2016 report of activities. Geological Survey of Canada, Open File 8199, pp. 35-37.

McClenaghan, M.B., McDonald, A., Leybourne, M.I., Beckett-Brown, C., Chapman, J.B., Layton-Matthews, D., Lougheed, H.D., Plouffe, A., and Ferbey, T., 2017. Controls on the fertility of porphyry mineralizing systems recorded in indicator minerals. In: Rogers, N., (Ed.), Targeted Geoscience Initiative, 2016 report of activities. Geological Survey of Canada, Open File 8199, pp. 87-89.

Ootes, L., Sandeman, H.A.I., and Jackson, V.A., 2017. Ultramafic intrusions (Wopmay pyroxenite pipes) in the southern metamorphic internal zone of the Wopmay orogen and the southwestern Slave craton, Northwest Territories. Northwest Territories Geological Survey, NWT Open Report, 2015-030, 31 p.

Plouffe, A., Ferbey, T., Kobylinski, C.H., Hattori, K., Grenier, A., McClenaghan, M.B., 2017. Deconvolution of complex spatial-temporal records of porphyry fertility recorded in till minerals. In: Rogers, N., (Ed.), Targeted Geoscience Initiative, 2016 report of activities. Geological Survey of Canada, Open File 8199, pp. 79-85.

Paradis, S., and Simandl, G.J., 2017. Is there a genetic link between the SEDEX and MVT deposits of the Canadian Cordillera? In: Rogers, N., (Ed.), Targeted Geoscience Initiative, 2016 Report of Activities, Geological Survey of Canada, Open File 8199, pp. 107-113.